



# Cycle biogéochimique du cobalt en domaines océaniques contrastés : l'Atlantique Ouest, la Mer Méditerranée et la Mer Noire

Gabriel Dulaquais

## ► To cite this version:

Gabriel Dulaquais. Cycle biogéochimique du cobalt en domaines océaniques contrastés : l'Atlantique Ouest, la Mer Méditerranée et la Mer Noire. Autre. Université de Bretagne occidentale - Brest, 2014. Français. NNT : 2014BRES0035 . tel-02147835

HAL Id: tel-02147835

<https://theses.hal.science/tel-02147835>

Submitted on 5 Jun 2019

**HAL** is a multi-disciplinary open access archive for the deposit and dissemination of scientific research documents, whether they are published or not. The documents may come from teaching and research institutions in France or abroad, or from public or private research centers.

L'archive ouverte pluridisciplinaire **HAL**, est destinée au dépôt et à la diffusion de documents scientifiques de niveau recherche, publiés ou non, émanant des établissements d'enseignement et de recherche français ou étrangers, des laboratoires publics ou privés.



université de bretagne  
occidentale



## THÈSE / UNIVERSITÉ DE BRETAGNE OCCIDENTALE

sous le sceau de l'Université Européenne de Bretagne

pour obtenir le titre de

DOCTEUR DE L'UNIVERSITÉ DE BRETAGNE OCCIDENTALE

Mention : Chimie Marine

École Doctorale (Ecole Doctorale des Sciences de la Mer)

présentée par

**Gabriel Dulaquais**

Préparée au Laboratoire des Sciences de  
l'Environnement Marin, IUEM

## Cycle biogéochimique du cobalt en domaines océaniques contrastés: L'Atlantique Ouest, la Mer Méditerranée et la Mer Noire



Thèse soutenue le 21/11/14

devant le jury composé de :

**Stéphane BLAIN**, Professeur UPMC, Laboratoire d'Océanographie  
Microbienne / Rapporteur

**Mak SAITO**, Associate Scientist, Woods Hole Oceanography  
Institution, Dept. of Marine Chemistry & Geochemistry / Rapporteur

**Ricardo RISO**, Professeur UBO, Laboratoire des Sciences de  
l'Environnement Marin / Président du jury

**Olivier ROUXEL**, Chargé de recherche IFREMER, REM, Laboratoire  
Géochimie et Métallogénie / Examinateur

**Marie BOYE**, Chargée de recherche CNRS, IUEM, Laboratoire des  
Sciences de l'Environnement Marin / Directrice de thèse

**Xavier CARTON**, Professeur UBO, Laboratoire de Physique des  
Océans / Co-encadrant de thèse



## Remerciements

Ce travail a été réalisé dans le cadre de projets soutenus par les programmes LEFE-CYBER (INSU-CNRS), LabEx-Mer (anciennement GIS-Mer), EU COST-Action ES801. La bourse de doctorat a été financée par l'Université de Bretagne Occidentale et la Région Bretagne

Merci à Mak Saito et Stéphane Blain pour avoir accepté de rapporter ces travaux de thèse, ainsi qu'à Olivier Rouxel pour les avoir examiné.

Merci à Ricardo Riso d'avoir examiné mes travaux de thèse, et aussi de m'avoir initié aux sciences de l'environnement marin tout au long de ma formation universitaire et de mes travaux de stage de fin d'étude.

Merci à Laurent Mémery et Olivier Ragueneau de m'avoir accueilli au sein du LEMAR.

Je tiens à remercier particulièrement Marie Boyé Directrice de ces travaux. Merci de m'avoir donné l'opportunité et les moyens d'entreprendre ce projet et de m'avoir aidé à mieux comprendre l'art subtil de la biogéochimie des éléments traces. Avec toi j'ai eu la chance d'être écouté, conseillé et de partager mes idées. Ce fut une expérience formidable!

Merci à Xavier Carton pour avoir co-encadré cette thèse et pour tes nombreux conseils utiles pour la réalisation de ses travaux.

Je remercie Mathieu Waeles, Jean François Maguer, Stéphane L'Helguen, Benoit Pernet-Coudrier et Hélène Planquette pour leur aide, leurs conseils et leur soutien au cours de ces quelques années passées au laboratoire.

Merci aux collègues de l'IUEM ainsi que de l'Ifremer grâce à qui l'institut n'était pas seulement un lieu de travail mais aussi un lieu de vie et d'échange : Nicolas, Alexis, Fabien, Rachel, Pierre, Camille, Jérôme, Thomas, Éric, Stefan, Marie, Manon, Arthur, Mélanie, ...

Merci à Micha Rijkenberg, Loes Guerringa et Hein de Baar du NIOZ (Royal Netherlands Institute for Sea Research) pour avoir entre autre organisé ces belles campagnes océanographiques grâce auxquelles j'ai découvert le goût du large !

Merci à l'UCC team et en particulier John Rolison et Joaquim Pampin.

Merci au Capitaine Pieter Kuijt ainsi qu'à l'ensemble de l'équipage de m'avoir accueilli à bord du *R.V. Pelagia*.

Et voilà ton tour Yohann Resnais, toujours présent depuis mon arrivée à Brest on aura été collègues de promo, de bureau, de labo et même colocataires. Tu auras eu toutes les casquettes! Merci pour ton soutien et ta bonne humeur.

Même si en doctorat on est souvent au laboratoire, parfois on s'en échappe! Un grand grand merci aux historiques : Valentin, Pierre-Louis, Amine, Ivan, Chacal, 2TA, Gaël, Yann, Mathieu ; au GzX crew : Clark, Gwen, David, JB, Thierry, Antoine, JG, Isma, Steph, Franck, Isa, Bab, Jean Paul ainsi qu'aux membres du navire amiral de la Capifornie: Allan, Marion, Pauline, Dylan et David.

Merci aux Dulaquais et aux Ségalen, à mon père, à ma mère et à tonton Cristobal pour votre soutien infaillible mais aussi pour votre patience.

Merci Morgane d'avoir été à mes côtés et (très) patiente.

Merci aux houles longues de l'Atlantique Nord de m'avoir permis de me vider l'esprit le temps d'une session entre deux analyses.



*« Le bon sens est la chose du monde la mieux partagée ; car chacun pense en être si bien pourvu, que ceux même qui sont les plus difficiles à contenter en toute autre chose n'ont point coutume d'en désirer plus qu'ils en ont.»*

René Descartes, Discours de la méthode, 1637



# SOMMAIRE

<b>Liste des tableaux</b>	<b>9</b>
<b>Liste des figures</b>	<b>11</b>
<b><u>Introduction générale</u></b>	<b>19</b>
<b>1 Le cobalt, propriétés chimiques et fonctions biochimiques</b>	<b>21</b>
1.1 Propriétés chimiques et réactionnelles	21
1.2 Fonctions biochimiques	21
<b>2 Le cobalt en milieu marin</b>	<b>22</b>
2.1 Distribution du cobalt en océan ouvert	23
2.1.1 Cobalt dissous	23
2.1.2 Spéciation physique	24
2.2 Etats rédox, géochimie oxydative et spéciation chimique du cobalt en milieu marin oxygéné	25
2.3 Paradoxe de la non-accumulation le long de circulation thermohaline	28
2.4 Le cobalt dans les eaux anoxiques et sulfidiques	29
2.5 Les corrélations Co-P: évidence du caractère nutritif du cobalt	30
2.6 Sources et puits de cobalt dissous en milieu océanique	31
2.6.1 Sources de DCo	31
2.6.2 Puits de DCo	32
2.6.3 L'apport atmosphérique	32
<b>3 Utilisation biologique et intérêt écologique en milieu marin</b>	<b>33</b>
3.1 Quotas cellulaires	33
3.2 Utilisation biologique	34
3.3 Intérêt écologique	37
<b>4 Transport à grande échelle dans le cycle du cobalt</b>	<b>37</b>
<b>5 Objectifs et zones d'études</b>	<b>39</b>
<b>6 Présentation des chapitres</b>	<b>41</b>
<b><u>Chapitre 1 - Méthodes analytiques</u></b>	<b>43</b>
<b>1 Propreté et qualité</b>	<b>45</b>
<b>2 Prélèvement</b>	<b>45</b>

<b>3 Filtration et spéciation physique</b>	<b>45</b>
<b>4 Conditionnement des échantillons</b>	<b>46</b>
<b>5 Méthode d'analyse du cobalt</b>	<b>47</b>
<b>6 Analyse de la spéciation organique du cobalt</b>	<b>54</b>
<b>7 Analyse des métaux particulaires</b>	<b>57</b>
<b>8 Analyse du carbone et de l'azote organique particulaire</b>	<b>60</b>

## **Chapitre 2 - Physical and remineralization processes govern**

### **the cobalt distribution in the deep western Atlantic Ocean**

<b>Abstract</b>	<b>61</b>
<b>1 Introduction</b>	<b>63</b>
<b>2 Methods</b>	<b>64</b>
2.1 Cruise track and sampling	64
2.2 Analytical method for cobalt analysis	65
2.2.1 Method	65
2.2.2 Analytical performance	66
2.3 Hydrography	66
2.4 Macronutrients analysis	66
<b>3 Results</b>	<b>66</b>
3.1 Circulation and dynamical stuctures	66
3.2 The nutrients distribution along the GEOTRACES-A02 section	67
3.3 The comprehensive distribution of cobalt in the western Atlantic	68
<b>4 Discussion</b>	<b>69</b>
4.1 Comparison of data sets of dissolved cobalt concentrations obtained at three crossover stations	70
4.2 Large-scale transportation of dissolved cobalt in the western Atlantic	72
4.2.1 Transportation in bottom waters within the core of AABW	72
4.2.2 Transportation within the core of the NADW	72
4.2.3 Temporal variation in the Subarctic gyre	74
4.2.4 The incursion of Atlantic Central Waters	75
4.3 Remineralization and decoupling of the cobalt and phosphate relationship in the intermediate western Atlantic	75
4.3.1 Remineralization of cobalt in the Atlantic Central Waters	75

4.3.2 Decoupling of the relationship between cobalt and phosphate	76
4.4 Physical processes impacting the distribution of dissolved cobalt in surface waters	77
4.4.1 Lateral advection in surface waters	77
4.4.2 The vertical diffusion	77
<b>5 Conclusions</b>	79
<b>Acknowledgments</b>	79
<b>References</b>	80

<b><u>Chapitre 3 - Contrasting biogeochemical cycles of cobalt in the surface western Atlantic Ocean</u></b>	83
<b>Abstract</b>	85
<b>1 Introduction</b>	85
<b>2 Methods</b>	86
2.1 Cruise track and sampling	86
2.2 Analytical method for cobalt analysis	87
2.2.1 Method	87
2.2.2 Analytical performance	88
2.3 Hydrography	88
2.4 Macronutrients analysis	88
<b>3 Results</b>	89
3.1 Dynamical features	89
3.2 Biogeochemical provinces	91
3.3 The distributions of cobalt in surface waters of the Western Atlantic	91
<b>4 Discussion</b>	94
4.1 Internal cycle of dissolved cobalt in the surface Western Atlantic	94
4.1.1 The dissolved cobalt and phosphate relationship	94
4.1.2 Biological uptake and regeneration rate of dissolved cobalt in surface waters as exemplified at the BATS station	96
4.1.3 Export of cobalt from the surface	98
4.2 External sources of dissolved cobalt in the Western Atlantic	99
4.2.1 The input by the Amazon	99

4.2.2 The atmospheric contribution	<b>100</b>
4.3 Residence time of cobalt in the upper 100 meters along the Western Atlantic	<b>102</b>
4.4 Comparative budgets and biogeochemical cycling of cobalt in the surface waters of the Western Atlantic	<b>104</b>
<b>5 Conclusions</b>	<b>107</b>
<b>Acknowledgments</b>	<b>107</b>
<b>References</b>	<b>107</b>

<b><u>Chapitre 4 – Atmospheric cobalt deposition along the surface western Atlantic and biogeochemical implications</u></b>	<b>112</b>
<b>Abstract</b>	<b>114</b>
<b>1 Introduction</b>	<b>115</b>
<b>2 Method</b>	<b>116</b>
2.1 Cruise track and sampling	116
2.2 Analytical method for cobalt analyses	117
<b>3 Results and Discussion</b>	<b>118</b>
3.1 Dynamical and biological specific features	118
3.2 Spatial distribution of cobalt	119
3.3 Atmospheric contribution to cobalt inventory in the mixed-layer	121
3.3.1 Dust deposition	121
3.3.2 Atmospheric deposition of cobalt	122
3.4 Relationship with the residence time of Co	123
3.5 Cumulative effect of the atmospheric input on the surface DCo inventories	125
3.6 Lithogenic and biogenic partitioning of particulate cobalt	126
3.7 Potential biological implications of the atmospheric deposition of cobalt	128
<b>4 Conclusions</b>	<b>131</b>
<b>Acknowledgments</b>	<b>132</b>
<b>References</b>	<b>132</b>

<b>Chapitre 5 – A Synoptic view of cobalt biogeochemistry in the Mediterranean and Black Seas</b>	<b>138</b>
<b>Abstract</b>	<b>140</b>
<b>1 Introduction</b>	<b>141</b>
<b>2 Method</b>	<b>145</b>
2.1 Cruise track and sampling	145
2.2 Hydrography	147
2.3 Macronutrients analysis	147
2.4 Analytical method for cobalt analyses in seawater	147
2.4.1Method	147
2.4.2 Analytical performance	148
2.5 Analytical method for the determination of particulate trace elements and phosphorus concentrations	149
2.5.1Method	149
2.5.2 Analytical performances	150
2.6 Analytical method for the determination of particulate organic nitrogen and carbon concentrations	150
<b>3 General circulation</b>	<b>151</b>
3.1 Eastern Atlantic and Gibraltar Strait	151
3.2 Mediterranean Sea	152
3.3 Black Sea	156
<b>4 Biogeochemical features</b>	<b>157</b>
4.1 Eastern Atlantic and Gibraltar Strait	157
4.2 Mediterranean Sea	159
4.3 Black Sea	166
<b>5 Cobalt biogeochemistry</b>	<b>169</b>
5.1 Overview of vertical distributions	169
5.2 Geochemistry of cobalt in the intermediate and deep waters	172

5.2.1 From the Eastern Atlantic to the Alboran Sea	172
5.2.2 Mediterranean Sea	175
5.2.3 Black Sea	185
5.3 Surface spatial distribution of DCo	187
5.3.1 From the Eastern Atlantic to Gibraltar strait	187
5.3.2 Mediterranean Sea	188
5.3.3 Black Sea	194
5.4 Atmospheric deposition of cobalt in the Mediterranean Sea	194
<b>6 Conclusions</b>	<b>201</b>
<b>Acknowledgments</b>	<b>203</b>
<b>References</b>	<b>203</b>
 <b><u>Conclusions générale</u></b>	<b>214</b>
<b>1 Efforts analytiques</b>	<b>216</b>
1.1 Exercices GEOTRACES d'inter-calibration et d'inter-comparaison	216
1.2 Une cartographie du cobalt dans les eaux marines	217
<b>2 Distribution et comportement du cobalt en eaux profondes</b>	<b>218</b>
2.1 Distribution verticale	218
2.2 Processus contrôlants la distribution verticale dans les eaux Intermédiaires et profondes	219
2.2.1 Océan Atlantique	220
2.2.2 Mer Méditerranée	221
2.2.3 Mer Noire	222
2.3 Minéralisation préférentielle	223
<b>3 Cycle biogéochimique de surface</b>	<b>223</b>
3.1 Océan Atlantique	223
3.2 Mer Méditerranée	225
3.3 Fractionnement en taille de DCo	226

<b>4 Apports atmosphériques</b>	<b>227</b>
4.1 Développement de nouveaux modèles	227
4.2 Apport atmosphérique de cobalt dissous	228
4.3 Interactions biogéochimiques	228
<b>5 Vue d'ensemble et perspectives</b>	<b>230</b>
5.1 Représentation 0D	230
5.2 Représentation 1D	231
5.3 Représentation 3D	231
5.4 Perspectives	233
<b>Références complémentaires</b>	<b>234</b>
<b><u>Annexes</u></b>	<b>242</b>
<b>1 Supplément au Chapitre 3</b>	<b>244</b>
<b>2 Performance analytiques relatives au chapitre 5</b>	<b>250</b>



## Liste des tables

### Introduction générale

<b>Table1</b>	<b>31</b>
Regression slopes of Co versus phosphates recorded in the upper water column in different biogeochemical domains	

<b>Table 2</b>	<b>35</b>
KMCo <sub>2+</sub> for different phytoplankton species determined by culture experiments.	

### Chapitre 1

<b>Table 1</b>	<b>50</b>
Comparison of dissolved cobalt analyses obtained in the UV-oxidized samples by the FIA-Chemiluminescence method used in the present study with consensus values reported by the Sampling and Analysis of iron (SAFe) and GEOTRACES programs	

### Chapitre 2

<b>Table1</b>	<b>66</b>
Comparison of dissolved cobalt analyses obtained in the UV-oxidized samples by the FIA-Chemiluminescence method used in the present study with consensus values reported by the Sampling and Analysis of iron (SAFe) and GEOTRACES programs	

<b>Table2</b>	<b>73</b>
Averaged dissolved cobalt concentration (DCo) and standard deviation (SD) obtained in the different water masses encountered along the western Atlantic GEOTRACES-A02 section	

<b>Table 3</b>	<b>77</b>
Mean dissolved cobalt concentration (DCo; pM), mean apparent particulate cobalt concentration (PCo; pM), and percentages of dissolved cobalt and phosphate produced by cumulative remineralization (respectively DCorem and Prem; %) calculated in the surface layer (0–150 m), the upper layer of Atlantic Central Waters (150–400 m) and the lower layer of Atlantic Central Waters (400–800 m) between 10° S and 10°N.	

<b>Table 4</b>	<b>78</b>
Lateral gradient of dissolved cobalt (Grad DCo <sub>150m</sub> ; 10–5 nmol m <sup>-3</sup> m <sup>-1</sup> ), and lateral advective fluxes of dissolved cobalt (FDCo <sub>adv</sub> ; nmol m <sup>-2</sup> d <sup>-1</sup> )	

<b>Table 5</b>	<b>78</b>
Vertical dissolved cobalt gradient ( $\Delta$ DCo/ $\Delta$ z 100–300 m; nmol m <sup>-3</sup> m <sup>-1</sup> ), mean Kz100–300m (cm <sup>2</sup> s <sup>-1</sup> ) and vertical dissolved cobalt fluxes from the mesopelagic layer to the euphotic layer (FDCo <sub>vertical diff.</sub> ; nmol m <sup>-2</sup> d <sup>-1</sup> )	

## **Chapitre 3**

### **Table 1**

**88**

Comparison of dissolved cobalt analyses obtained in the UV-oxidized samples by the FIA-Chemiluminescence method used in the present study with consensus values reported by the Sampling and Analysis of iron (SAFe) and GEOTRACES programs.

### **Table 2**

**97**

Cobalt to organic carbon ratio in particles at 100 meters ( $\text{PCo}_{>0.2\mu\text{m}}/\text{POC}_{>1\mu\text{m}}$ ), and the integrated export fluxes of Co on settling particles at 100 meters ( $\text{FCo}_{\text{export}}$ ).

### **Table 3**

**98**

Summary of dissolved cobalt ( $\text{FDCo}$ ) and phosphorus (FP) fluxes integrated for the upper 100 meters at the BATS station in the Sargasso Sea.

### **Table 4**

**103**

Stock and residence time of dissolved ( $\text{DCo}$ ) and particulate ( $\text{PCo}$ ) cobalt in the upper 100 meters for the different biogeochemical domains.

### **Table 5**

**104**

Summary of the dissolved ( $\text{DCo}$ ) and particulate ( $\text{PCo}$ ) cobalt fluxes for the upper 100 meters (averaging all stations of each biogeochemical domain) along the GEOTRACES-A02 section.

## **Chapitre 4**

### **Table 1**

**129**

Actual biogeochemical state of 760 the North-western Atlantic gyre and possible implications for a future 30% decrease of the dust deposition.

## **Chapitre 5**

### **Table 1**

**163**

Mean nutrients and cobalt stoichiometries in the particles collected in surface waters (0-100m) along the GA04-section.

### **Table 2**

**171**

Average surface concentrations and standards deviations of dissolved ( $\text{DCo}$ ), Soluble ( $\text{SCo}$ ), colloidal ( $\text{cCo}$ ) and particulate ( $\text{PCo}$ ) cobalt in the different reservoirs of the Mediterranean Sea. Numbers in brackets are ranges of concentrations

### **Table 3**

**181**

Vertical diffusive fluxes of  $\text{DCo}$  from the surface to the intermediate reservoirs ( $\text{FzDCo}$  at 200m), and from the intermediate to the deep reservoirs ( $\text{FzDCo}$  at 600m) in the different sub-basins of the Mediterranean Sea.

### **Table 4**

**194**

Biological Co-uptake fluxes ( $\text{Fuptake}$ ), and Co export fluxes on settling particles ( $\text{FCo}_{\text{export}}$ ) in the different sub-basins of the Mediterranean Sea.

### **Table 5**

**198**

Dust,  $\text{PCo}$  and  $\text{DCo}$  depositions and of the Co enrichment factor estimations in the different sub-basin of the Mediterranean Sea using the DIPA model.

### **Table 6**

**200**

Comparison of atmospheric inputs of  $\text{PCo}$  and  $\text{DCo}$  between the Western Atlantic (Dulaquais et al., 2014b) and the Mediterranean Sea (this study).

# Liste des figures

## Introduction générale

<b>Figure 1</b>	21
2D representation of the B <sub>12</sub> vitamin.	
<b>Figure 2</b>	22
Published DCo database before this work. Only studies including deep vertical distributions of DCo are indicated.	
<b>Figure 3</b>	23
Compilation of the 4 typical vertical distributions of DCo in oceanic waters.	
<b>Figure 4</b>	26
Vertical distribution of DCo in the Sargasso Sea (open dots) and in the central Pacific Ocean (dark dots)	
<b>Figure 5</b>	27
(a) Uptake of DCo (dark bars) and DMn (white bars) on particles as function of PAR in surface waters of Sargasso Sea (after Moffett and Ho, 1996). (b) Vertical distribution with depth of dissolved Co (DCo; open triangles), the organic ligands of DCo (LCo; dark dots) and DCo uptake on particles (dark squares) in surface waters of Sargasso Sea (adapted from Moffett and Ho, 1996; and Saito and Moffett, 2001).	
<b>Figure 6</b>	28
Vertical distributions of dissolved cobalt (DCo), labile cobalt, and inorganic cobalt (Co') in: (a) the central Pacific Ocean, (b) the North-Eastern Atlantic Ocean, (c) the Southern Ocean.	
<b>Figure 7</b>	29
Vertical distribution of DCo and its chemical speciation in open Black Sea.	
<b>Figure 8</b>	30
Conceptual representation of the Co-P surface relationship in surface oceanic waters.	
<b>Figure 9</b>	34
Cellular Co quota normalized to P (red bars) and to C (blue bars) in different phytoplankton species, obtain from culture or field measurements.	
<b>Figure 10</b>	34
Growth rate of <i>Emiliania huxleyi</i> as function of [Co <sup>2+</sup> ] in culture medium.	
<b>Figure 11</b>	35
3D representation of the carbonic anhydrase.	
<b>Figure 12</b>	36
Co-Zn inter-replacement effect on the growth rate of: (a) the coccolithophore <i>Emiliania huleyi</i> , (b) the diatom <i>Phaeocystis Antarctica</i>	
<b>Figure 13</b>	36
Absence of Co-Zn inter-replacement in: (a) the cyanobacteria <i>Prochlorococcus</i> (b) the cyanobacteria <i>Synechococcus</i>	
<b>Figure 14</b>	38
Schematic representation of relationship between local and large scale processes along the GEOTRACES A02 section (West Atlantic). (a) Downwelling of oxygenated	

waters in the North Atlantic Polar Regions impact the entire West Atlantic deep basin.  
**(b)** Cumulative remineralization along the large scale circulation impact the local phosphate vertical distribution.

**Figure 15** 38

Spatial and vertical distribution of DCo along : **(a)** the CoFeMUG section in the south Atlantic; **(b)** the BONUS-GoodHope section in the Atlantic sector of the Southern Ocean.

**Figure 16** 40

Cruise track of the GEOTRACES-A02 section.

**Figure 17** 41

Cruise track of the GEOTRACES-A04N section.

## **Chapitre 1**

**Figure 1** 45

Size partitioning of the different cobalt fractions analyzed in this work

**Figure 2** 48

Concentration of dissolved cobalt in deep (red squares) and surface (blue diamonds) South Atlantic seawater ( $40^{\circ}\text{S}$ ) as the function of the UV oxidation exposure time. Optimum exposure is 3h.

**Figure 3** 49

Evolution of the DCo concentration with time after the UV-digestion of a deep seawater sample

**Figure 4** 51

Intra laboratory comparison on the measurement of DCo between FIA-Chemiluminescent detection method on filtered acidified seawater (FIA-Chem / 0.01M) and Cathodic Stripping Voltammetry method on filtered frozen seawater for deep and surface seawater samples.

**Figure 5** 52

Intercomparison of DCo datasets at three cross-over stations

## **Chapitre 2**

**Figure 1** 65

GEOTRACES-A02 cruises track along the western Atlantic Ocean. Sampling locations of the four legs are shown

**Figure 2** 67

Interpolated vertical sections of **(a)** temperature (T), **(b)** salinity (S) and **(c)** dissolved oxygen (O<sub>2</sub>) along the GEOTRACES-A02 section in the western Atlantic, based on CTD data.

**Figure 3** 68

Interpolated vertical sections of **(a)** phosphate, **(b)** nitrate and **(c)** silicate based on 1440 analysis of water-column samples collected and measured by NIOZ along the Netherlands area of GEOTRACES-A02 section.

<b>Figure 4</b>	<b>69</b>
Interpolated vertical sections of <b>(a)</b> dissolved cobalt (DCo, pM) and <b>(b)</b> apparent particulate cobalt (PCo, pM) based on 675 analyses for DCo and 203 analyses for PCo along the GEOTRACES-A02 section in the western Atlantic.	
<b>Figure 5</b>	<b>70</b>
Typical vertical distribution of dissolved (DCo) and apparent particulate (PCo) cobalt against depth in the different biogeochemical domains.	
<b>Figure 6</b>	<b>71</b>
Intercomparison of DCo data sets at the crossover station BATS <b>(a, d)</b> between this study (blue diamonds) and ICP-MS method by Biller and Bruland (2008) (green triangles) and by R. Middag et al. (personal communication, 2014) (yellow dots=samples from the 2010 Dutch GEOTRACES-A02 cruise; red squares=samples from the 2011 American GEOTRACES-A03 cruise); at the crossover station located at 9° S <b>(b, e)</b> between this study (blue diamonds) and the CSV method by Noble et al. (2012) (green dots); and at the crossover station at 40° S <b>(c, f)</b> between this study (blue diamonds) with FIA-chemiluminescence method by M. C. Lohan et al. (personal communication, 2014) (orange dots=samples from the 2010 English GEOTRACES-A10 cruise).	
<b>Figure 7</b>	<b>73</b>
Conceptual schema of the DCo transportation along the large-scale circulation in the intermediate and deep western Atlantic Ocean.	
<b>Figure 8</b>	<b>75</b>
Relationship among the concentrations of dissolved cobalt (DCo) and the apparent oxygen utilization (AOU) in the intermediate waters of the equatorial area (150–750 m).	
 <b>Chapitre 3</b>	
<b>Figure 1</b>	<b>87</b>
Surface physical features and cruise track along the GEOTRACES-A02 section Sampling location of the different four Legs are shown.	
<b>Figure 2</b>	<b>89</b>
Interpolated vertical sections in the upper 1000 m of <b>(a)</b> Temperature (TMP), <b>(b)</b> Salinity (S) and <b>(c)</b> dissolved oxygen along the GA02 section, based on CTD data.	
<b>Figure 3</b>	<b>90</b>
Interpolated vertical sections in the upper 1000 m of <b>(a)</b> phosphate, <b>(b)</b> N:P ratio <b>(c)</b> Si/N ratio, based on 735 analyses of water-column samples collected along the GA02 section, and <b>(d)</b> Chl a distribution in the upper 250 meters derived from CTD data.	
<b>Figure 4</b>	<b>92</b>
Interpolated vertical section in the upper 1000 m of <b>(a)</b> dissolved cobalt concentration (DCo) with phosphate contours overlaid on the profile; <b>(b)</b> particulate cobalt concentrations (PCo); <b>(c)</b> DCo/P ratio with dissolved aluminium concentration (DAL) contours overlaid on the profile ( <i>Middagg et al., unpublished data</i> ).	

**Figure 5****93**

(a) Box plot representing the relative proportion of particulate cobalt (PCo) to total cobalt (TCo). Using all data for a given depth along the section. Dashed line represents the average (mean =  $12 \pm 12\%$ ; n = 76). (b) Box plot representing estimated Chl a (derived from CTD data) using all data, where PCo is available, for a given depth along the section.

**Figure 6****93**

Typical vertical distribution of dissolved (DCo) and particulate (PCo) cobalt against depth in the different biogeochemical domains.

**Figure 7****94**

General conceptual schema of the cobalt cycling in the upper 100 meters.

**Figure 8****95**

Scatter plots of the DCo data versus phosphate in the upper 250 meters, showing (a) the global DCo-P relationship (n = 228) along the section, and (b) the regional DCo-P relationships.

**Figure 9****99**

(a) Inverse linear correlation ( $R^2 > 0.97$ ) between dissolved cobalt (DCo) and the salinity in the waters influenced by the discharge of the Amazon (dark stars). (b) Percentage of the DCo stock in the mixed layer attributed to the input by the Amazon. The dashed line indicates 10% contribution of the Amazon to the DCo stock.

**Figure 10****101**

Estimation of the sea-surface atmospheric deposition of dry (dark circles, solid line) and soluble (open circles, dashed line) cobalt, along the section. The soluble Co deposition estimated by *Shelley et al.* [2012] and *Baker et al.* [2007] are shown for comparison.

**Figure 11****106**

Specific conceptual schema of cobalt cycling in the different biogeochemical domains along the section. Wideness of the arrows and boxes represent the relative intensity of the flux and the proportion of Co stock (at time of observation), respectively. The numeration is described in Figure 7.

**Chapitre 4****Figure 1****117**

Cruise track and surface physical features and cruise track along the GEOTRACE-A02 section.

**Figure 2****119**

Surface mixed layer depth (z), mean temperature (T), mean salinity (S) and mean Chlorophyll a (Chl a) derived from fluorescence distribution along the GEOTRACES-A02 section. The labels "c" locate the cyclonic eddies.

**Figure 3****120**

Surface mean dissolved cobalt (DCo, dark circles, solid line) and mean apparent particulate cobalt (PCo, open circles, dashed line) concentrations in the mixed layer along the GEOTRACES-A02 section. Stations sampled during summer 2012 are labelled in red.

<b>Figure 4</b>	<b>122</b>
Estimation of the sea-surface atmospheric deposition of dust (dots line), total Co (dark circles, solid line) and soluble Co (open circles, dashed line), along the GEOTRACES-A02 section.Brackets delimit the main air masses originated from: P: Patagonia; SWA: South Western Africa; S: Sahara; NA: North America; A: Arctic; E: Europe.	
<b>Figure 5</b>	<b>127</b>
Residence times of DCo (Atm. $\tau_{DCo}$ ; Dark line) and PCo (Atm. $\tau_{PCo}$ ; red line ) needed to recover the Co inventories in the mixed layer through atmospheric deposition. The residence times of DCo (dark dashed line) and PCo (red dashed line) determined by Dulaquais et al. ( 2014b) considering all the Co fluxes in the upper 100m are indicated.	
<b>Figure 6</b>	<b>126</b>
Cumulative atmospheric contribution to the DCo (dark bars) and PCo (red bars) inventories in the mixed layer	
 <b>Chapitre 5</b>	
<b>Figure 1</b>	<b>145</b>
Cruise track of the GEOTRACES-A04N section with the location of the stations sampled for cobalt and particulate elements analyses.	
<b>Figure 2</b>	<b>153</b>
Contour plots versus depth of (a) salinity; (b) dissolved oxygen; (c) apparent utilization of oxygen (AOU) between Stations 1a and 6a	
<b>Figure 3</b>	<b>154</b>
Spatial distribution of salinity at: (a) the subsurface (10 m); (b) 400 m depth; (c) 1000m depth, and (d) 2500 m depth along the GA04N section. Arrows indicate the simplistic surface (red) and deep (dark) circulations in the Mediterranean Sea. Dashed circles indicate location of physical quasi permanent instabilities. Crossed red circles indicate locations of deep convection	
<b>Figure 4</b>	<b>156</b>
(a) Spatial distribution at 10 m depth of the salinity in the Black Sea along the GA04N section. Arrows indicate the simplistic surface circulation of the Rim Current. The Batumi Eddy (BE) is also indicated. (b) Vertical distribution of the salinity from the Marmara Sea to the Batumi Eddy during the GA04N section. Arrows indicate the direction of outflow Black Sea Surface Waters (BSW) and of the Mediterranean Inflowing Waters (MIW).	
<b>Figure 5</b>	<b>158</b>
Vertical distributions of: (a) nitrate; (b) phosphate; (c) silicate concentrations between Stations 1a and 6a (labelled).	
<b>Figure 6</b>	<b>160</b>
Vertical distributions of (a) nitrate + nitrite; (b) phosphate; (c) silicate; (d) dissolved oxygen; (e) dissolved N/P ratio along the GA04N-section. Few stations numbers are labelled.	
<b>Figure 7</b>	<b>161</b>

Spatial distribution of integrated Chlorophyll a concentrations between 0 and 200 meters (data derived from fluorescence) along the GA04 section.

**Figure 8** 163

Scatter plots of: (a) nitrate + nitrite (Total N), (b) phosphate, (c) silicate concentrations versus the apparent utilization of oxygen (AOU). The color scale stands for the longitude of the sample ( $^{\circ}$ E).

**Figure 9** 164

Vertical distributions in the top-250 m of: (a) Chlorophyll a (fluorescence derived); (b) nitrite concentrations along the section. Few stations numbers are labelled.

**Figure 10** 167

Vertical distributions of: (a) phosphate, (b) dissolved oxygen, (c) sulfide concentrations in the Black Sea during the GA04 section. Anoxic-sulfidic transition layer and sulfidic reservoir are indicated. Few stations numbers are labelled.

**Figure 11** 168

Vertical distributions of: (a) phosphate, (b) nitrate (green line) and ammonium (black line), (c) silicate, (d) dissolved oxygen ( $O_2$ , blue line) and sulfides ( $HS^-$ , red line) in the central Black Sea (Station 5b).

**Figure 12** 170

Box plots of dissolved cobalt concentrations (DCo) versus depth in: (a) the Atlantic sector, (b) the Mediterranean Sea, (c) the Black Sea. Number of observations is indicated.

**Figure 13** 172

Comparison between the vertical distributions of dissolved cobalt (DCo) recorded in the Western Atlantic (section GA02; Dulaquais et al., 2014a) and in the Eastern Atlantic (section GA04N, this study), (a) at temperate latitudes, (b) in oligotrophic domains.

**Figure 14** 173

Vertical distributions of dissolved cobalt (DCo) between Stations 1a and 6a along the GA04N-section. Sampling stations for DCo are labelled.

**Figure 15** 174

Vertical distributions of: (a) dissolved cobalt (DCo), (b) particulate cobalt (PCo) in the area of the Gibraltar Strait.

**Figure 16** 176

Vertical distributions of: (a) dissolved cobalt (DCo); (b) Soluble cobalt (sCo); (c) colloidal cobalt (cCo) along the section.

**Figure 17** 178

Plot of particulate cobalt concentrations (PCo) versus particulate manganese concentrations (PMn) measured in the Mediterranean Sea. The different relationships and colors stand for the area and water-layers depths.

**Figure 18** 179

Particulate concentrations of: (a) cobalt (PCo), (b) manganese (PMn), (c) aluminum (PAL) measured along the section.

<b>Figure 19</b>	<b>182</b>
Vertical distributions of: (a) idealized diffusivity ( $K_z$ ) model after Wu and Haines (1998), (b) mean vertical diffusion flux of dissolved cobalt to the deep sea, (c) box-plots of vertical diffusion flux of dissolved cobalt to the deep sea estimated for the entire Mediterranean Sea.	
<b>Figure 20</b>	<b>186</b>
(a) Vertical distribution of dissolved cobalt (DCo) in the Black Sea. Bosphorus location and sampling stations for DCo are indicated; (b) vertical distribution of DCo and particulate cobalt (PCo) in the open Black Sea (at Station 5b). States of oxygenation of the water-column are indicated; (c) relationship between PCo and particulate manganese (PMn) in the suboxic layer, (d) relationship between PCo and particulate iron (PFe) in the sulfidic waters	
<b>Figure 21</b>	<b>190</b>
Spatial distribution of: (a) dissolved cobalt (DCo) at 10 meters depth along the GA04N-section, (b) integrated dissolved cobalt concentration ( $DCo_{\text{surface}}$ ), (c) integrated dissolved cobalt anomaly ( $\Delta DCo_{\text{surface}}$ , see text for calculation), in the top-200 meters in the Mediterranean Sea.	
<b>Figure 22</b>	<b>196</b>
Spatial distributions of: (a) dust deposition, (b) particulate cobalt deposition (PCo deposition) and (c) dissolved cobalt deposition (DCo deposition) fluxes to the surface waters along the GA04N-section.	
<b>Figure 23</b>	<b>199</b>
Spatial distribution of the enrichment factor of cobalt in aerosols ( $EF_{Co}$ ) estimated using the DIPA model (see text for the calculations). Air-flow directions from NOAA (Hysplit model) are reported for the 3-5 days before the sampling day.	
 <b>Conclusion générale</b>	
<b>Figure 1</b>	<b>219</b>
Typical vertical distributions of DCo observed during this study.	
<b>Figure 2</b>	<b>220</b>
Conceptual schema of the DCo transportation along the large-scale circulation in the western Atlantic.	
<b>Figure 3</b>	<b>220</b>
Scatter plot of DCo vs DMn in the West Atlantic. Colorbar as depth.	
<b>Figure 4</b>	<b>221</b>
Conceptual schema of the DCo transportation in the Mediterranean Sea.	
<b>Figure 5</b>	<b>223</b>
The vertical distribution of DCo and PCo in the Black Sea is function of the state of oxygenation (colorbar).	

<b>Figure 6</b>	<b>226</b>
Soluble cobalt (sCo) versus dissolved cobalt (SDCo) ( <b>a</b> ) in the surface North Atlantic Ocean; ( <b>b</b> ) in the Mediterranean Sea. (c) sCo–P correlation observed in the North Atlantic	
<b>Figure 7</b>	<b>227</b>
(a) Comparison of dust deposition estimation using modified MADCOW model and historical MADCOW model using the same dissolved aluminum concentration recorded along the GA02 section( Rob Middag, pers. comm.), ( <b>b</b> ) Actual most popular dust deposition model (Mahowald et al., 2005; Jickells et al., 2005).	
<b>Figure 8</b>	<b>228</b>
Actual surface available UV-DCo database. Orange arrows indicate natural dust input. Red arrows indicate anthropogenic dust inputs.	
<b>Figure 9</b>	<b>230</b>
Conceptual schema of the possible interaction between the phytoplankton and the DCo provide by dust dissolution	
<b>Figure 10</b>	<b>231</b>
0 dimensional conceptual schema of the interactions occurring between the different fractions in the cobalt biogeochemical cycle.	
<b>Figure 11</b>	<b>231</b>
Simplistic 1 dimensional conceptual schema of the interactions occurring between the DCo and PCo pools in a 3 layers marine system. Each layer is a 0 D model	
<b>Figure 12</b>	<b>232</b>
Distribution of dissolved cobalt in the Atlantic Ocean. Including data from Bown et al., 2011; Noble et al., 2012; Dulaquais et al., 2014a ; Lohan Laboratory (unpublished) and Saito laboratory (unpublished). Plot generated by Reiner Schlitzer.	
<b>Figure 13</b>	<b>232</b>
Vertical distribution of dissolved cobalt along the North Atlantic Drift (NAD). Dashed arrows indicate the direction of the vertical advection. Filled arrow indicates the pathway of the NAD.	

# **Introduction générale**



# Introduction générale et objectifs de l'étude

## 1 Le cobalt, propriétés chimiques et fonctions biochimiques

### 1.1 Propriétés chimiques et réactionnelles

Le cobalt ( $^{59}_{27}\text{Co}$ ) est un élément de transition de la première ligne, peu abondant dans l'écorce terrestre ( $17.3 \mu\text{g.g}^{-1}$ ). A l'état élémentaire sa configuration électronique est [Ar] 3d7 4s2. Le cobalt peut adopter différents états d'oxydation (-I à +IV), cependant il est généralement observé sous les formes réactives Co(II), ou inertes Co(III), dans lesquelles il est impliqué dans des complexes octaédriques ou en mailles *hcp* (hexagonal close packing). Le cobalt est un élément ferromagnétique, et son incorporation dans des alliages (CoPt) ou son couplage avec des éléments antiferromagnétiques (oxyde de manganèse) confèrent à ces matériaux une forte anisotropie magnétique. Par cette particularité, le cobalt peut être incorporé au sein d'aggrégats nanomériques qui sont utilisés dans les nouvelles technologies (enregistrement magnétique haute densité, évacuation de la chaleur), en médecine (traitement par hyperthermie magnétique), ou encore en synthèse chimique (réaction de surface).

### 1.2 Fonction biochimique

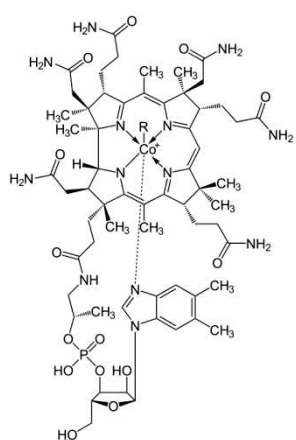


Figure 1 : 2D representation of the B<sub>12</sub> vitamin.  
(Wikipedia.fr)

Le cobalt est un micronutriments essentiel à la vie puisqu'il a de multiples fonctionnalités connues au sein des cellules. En étant l'atome central de la vitamine B<sub>12</sub> (ou cobalamine ; Figure 1), le cobalt est utilisé par une majeure partie des eucaryotes sous la forme de vitamine B<sub>12</sub> qui intervient, entre autre, dans la synthèse de la méthionine, un acide aminé essentiel. Lors de cette synthèse, le cobalt de la cobalamine agit en effet comme transporteur du groupement méthyl entre le méthyl-folate et l'homocystéine. La vitamine B<sub>12</sub> est aussi utilisée par les bactéries et les archaës anaérobiques pour des réactions de fermentation ou de dé-halogenation (Banerjee and Ragsdale, 2003).

Le cobalt peut aussi constituer l'atome central ou structurant de diverses enzymes, telles que la nitrile hydratase utilisée dans le métabolisme des amides, ou certaines anhydrases carboniques servant à l'assimilation de carbone inorganique.

## 2 Le cobalt en milieu marin

Les études reportant des concentrations de cobalt dissous (DCo; <0.2 µm) sur l'ensemble de la colonne d'eau de l'océan mondial restent, à l'heure actuelle, limitées (Figure 2).

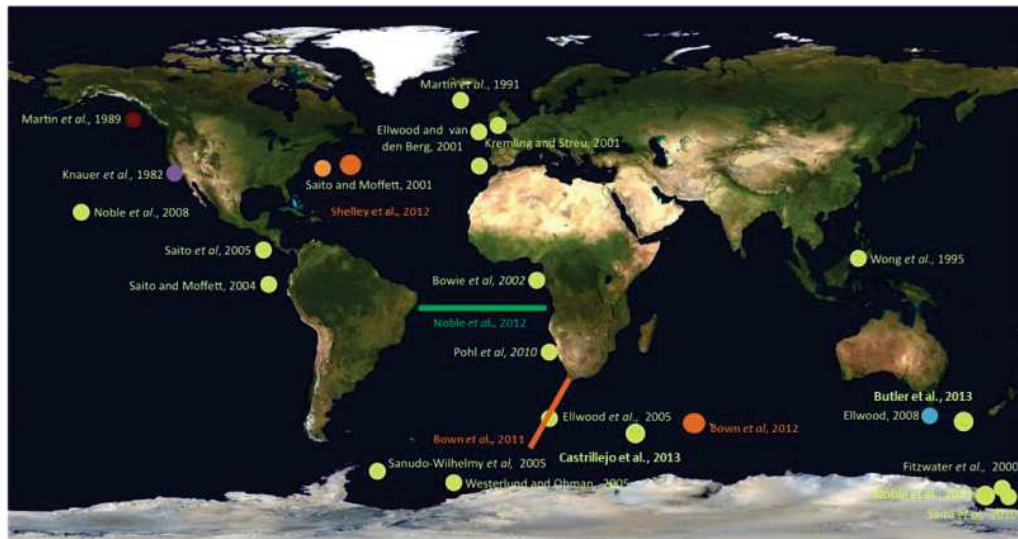


**Figure 2:** Published DCo database before this work. Only studies including deep vertical distributions of DCo are indicated.

De plus, la plupart de ces études ont été réalisées sans une étape d'oxydation des échantillons par les ultra-violets avant leur analyse. Or, il a été démontré très récemment que l'absence de traitement aux UV entraînait une sous-estimation des concentrations réelles en DCo, probablement en raison de sa spéciation chimique dans les eaux de mer (Saito and Moffett, 2001; Chapitre 1). Ainsi, une grande partie des études publiées dans la littérature, pourrait sous-estimer les concentrations en DCo.

Les concentrations en DCo dans les eaux océaniques varient entre 4 et 300 pM (avec 1 pM =  $10^{-12}$  mol.L<sup>-1</sup>), ce qui fait de cet élément l'un des moins abondants dans l'eau de mer. Les concentrations reportées dans les eaux de surface sont généralement faibles dans les domaines oligotrophes (Saito and Moffett, 2002 ; Noble et al., 2008 ; 2012 ; Bown et al. 2011 ; Shelley et al., 2012), intermédiaires dans les régions polaires (Saito et al., 2010 ; Bown et al., 2011), et plus élevées en milieu côtier ou proche des marges continentales (Knauer et al., 1982 ; Heimbürger et al., 2011 ; Noble et al., 2012 ; Bown et al., 2012b). Dans les eaux intermédiaires et profondes, les concentrations de DCo peuvent être particulièrement élevées dans les couches de minimum d'oxygène et les bassins anoxiques (Spencer and Brewer, 1971 ; Bown et al., 2011 ; Noble et al., 2012).

## 2.1 Distribution du cobalt en océan ouvert

### 2.1.1 Cobalt dissous

La distribution verticale du DCo n'est pas uniforme dans les océans, contrairement à d'autres métaux de transition (comme Zn, Cd, Mo). En effet, quatre distributions verticales type ont été observées pour le cobalt dissous : (i) une distribution de type nutritif décrite par de faibles concentrations dans la couche du maximum de chlorophylle-a et une augmentation des concentrations avec la profondeur. Cette distribution a été observée dans l'Atlantique Nord et dans l'Atlantique Sud subtropical (Figure 3a), (ii) une distribution de type « scavengé », comme en Méditerranée nord-occidentale, où les concentrations diminuent de la surface vers le fond (Figure 3b), (iii) une distribution de type conservatif avec des concentrations constantes le long de la colonne d'eau, comme celle des régions polaires (Figure 3c), (iv) une distribution hybride qui combine un comportement nutritif dans les eaux de surface et intermédiaires, et un comportement de type « scavengé » dans les eaux profondes, comme c'est le cas dans l'Atlantique Sud et l'Océan Pacifique (Figure 3d).

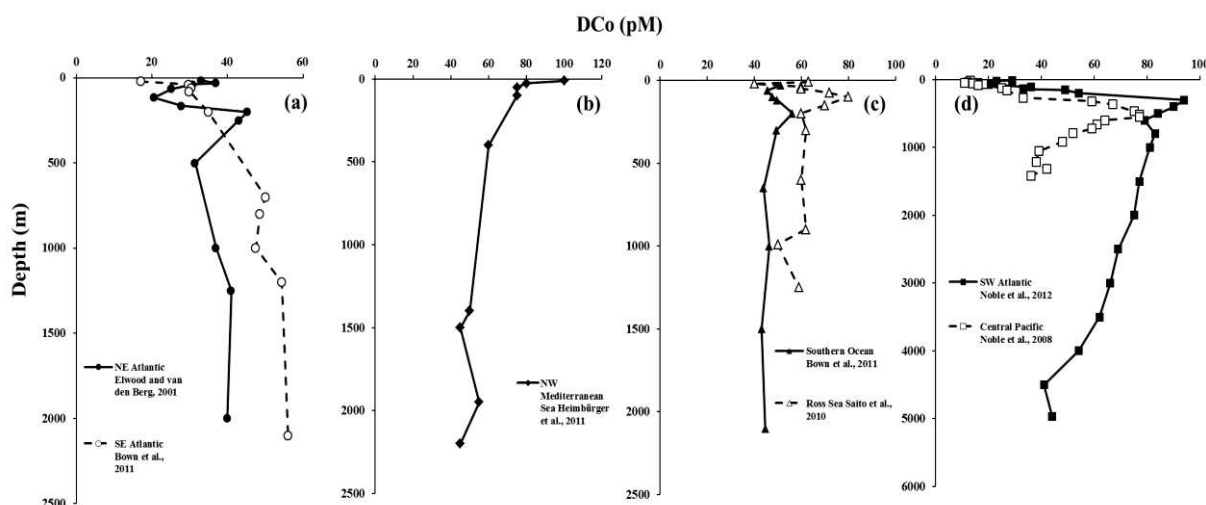


**Figure 3** Compilation of the 4 typical vertical distributions of DCo in oceanic waters: (a) Nutrient-like distribution; (b) Scavenged-like distribution; (c) Conservative distribution; (d) Hybrid distribution (Ellwood and van den Berg, 2001; Noble et al., 2008; 2012; Saito et al., 2010; Bown et al., 2011; Heimbürger et al., 2011).

La distribution verticale du DCo dans l'océan ouvert est majoritairement décrite comme étant de type hybride dans la littérature récente (Bruland and Lohan, 2003 ; Noble et al., 2008, 2012 ; Bown et al., 2011 ; 2012b). Les processus biologiques (assimilation et régénération) contrôleraient principalement la distribution du DCo dans les eaux de surface, conduisant à un profil de type nutritif. Dans les eaux intermédiaires (300-800 m), les processus de reminéralisation du cobalt assimilé en surface seraient principalement à l'origine

de l'augmentation des concentrations observée avec la profondeur, comme le suggère en effet les concentrations élevées de DCo détectées dans les zones de minimum d'oxygène à forte productivité en surface (Saito et al., 2004 ; 2005 ; Noble et al., 2012). Enfin, dans les eaux profondes, l'adsorption du cobalt par les particules et la précipitation du cobalt dissous avec les oxydes de manganèse pourraient être à l'origine de la diminution des concentrations avec la profondeur généralement observée en dessous de 1000 mètres (Saito and Moffett, 2002). Cette diminution des concentrations dans l'océan profond contraste avec le rôle de micro-nutritif du DCo.

### 2.1.2 Spéciation physique

En plus de la fraction dissoute, le cobalt peut exister sous forme particulaire (PCo;  $> 0.2 \mu\text{m}$ ). Dans la fraction dissoute, le cobalt peut également exister sous forme colloïdale ( $0.02 \mu\text{m} < \text{cCo} < 0.2 \mu\text{m}$ ), et sous forme soluble (sCo ;  $< 0.02 \mu\text{m}$ ).

La distribution du cobalt particulaire n'a encore été que très peu décrite dans les eaux océaniques. Dans les bassins oxygénés, les concentrations de PCo seraient plus faibles (0-10 pM) que celles de DCo, représentant généralement moins de 10% du cobalt total en surface et moins de 5% en profondeur (Noble et al., 2012 ; Bowie et al., 2010 ; Noble et al., 2011 ; Planquette et al., 2012 ; Bown et al., 2012b). Les maxima de concentrations en PCo ont généralement été observés dans la couche de surface ou dessus du plancher océanique, et associées, respectivement, à l'assimilation biologique et la resuspension sédimentaire (Bowie et al., 2010 ; Pohl et al., 2011 ; Noble et al., 2012 ; Bown et al., 2012b). Compte-tenu du peu de données existantes, le comportement du cobalt particulaire en milieu océanique est quasiment inconnu.

La répartition du cobalt dissous dans les fractions colloïdale et soluble est encore moins référencée. A l'heure actuelle, seule une publication scientifique reporte en effet ce fractionnement en taille et seulement dans des eaux de surface (Baeyens et al., 2011). Cette étude suggère que le DCo serait sous forme soluble dans le Pacifique nord-ouest, alors qu'il serait principalement sous forme colloïdale (à 70%) dans l'Océan Austral.

Alors que les questions sur l'assimilation biologique, la biodisponibilité ou les réactions de précipitation du cobalt dissous restent ouvertes, l'étude du fractionnement de taille du cobalt pourrait apporter des indications sur ces mécanismes de transfert de phases.

## 2.2 Etat redox, géochimie oxydative et spéciation chimique du cobalt en milieu marin oxygéné

En milieu marin, la forme inorganique du cobalt dissous la plus abondante est l'ion  $\text{Co}^{2+}$ , sous sa forme hydratée octaédrique  $(\text{Co}(\text{OH}_2)_6)^{2+}$  (Cozovic et al., 1982). Quant aux complexes  $\text{Co}(\text{II})\text{OH}_2$ , ils présentent une solubilité extrêmement faible ( $10^{-15}$  M) et n'apparaissent en solution que pour des potentiels d'hydrogène élevés ( $\text{pH} > 9$ ), supérieurs à ceux des eaux de mer ( $\text{pH} = 8.1$ ). Par ailleurs, les précipités  $\text{Co}(\text{III})\text{OH}_3$  se forment aux potentiels d'oxydo-réduction élevés au pH de l'eau de mer ( $> 0.7$  V ; Swanner et al., 2014). Ainsi, l'oxydation du Co(II) qui produit du Co(III) ne serait pas une réaction majeure dans les eaux océaniques oxygénées. Cependant, il a été suggéré que les oxydes de manganèse et de fer pourraient catalyser l'oxydation de Co(II) vers Co(III) en solution (Goldberg, 1961 ; Burns 1965 ; Murray et al., 1968). Le Co(II) hydraté serait en effet oxydé en Co(III) à l'interface solide-solution de ces oxydes (Murray and Dillar, 1979). Bien qu'effectivement il semblerait que le Co puisse exister sous forme de  $\text{Co}(\text{II})\text{OH}_2$  à la surface des oxydes de manganèse (Murray, 1975), le Co(III) produit par oxydation serait quant-à-lui incorporé sous forme octaédrique au sein de certains oxydes de manganèse. Le rayon ionique de l'octaèdre formé avec le Co(III) (0.0525 nm) suggère que le Co(III) pourrait préférentiellement se substituer à Mn(IV) (0.054 nm) dans les cristaux plutôt qu'à Mn(II) (0.82 nm) ou Mn (III) (0.065 nm) (Burns, 1976 ; Murray and Dillar, 1979). Le rayon ionique de l'octaèdre formé avec le Co(II) étant élevé (0.075 nm), son incorporation semble être physiquement limitée dans les oxydes de manganèse. L'adsorption de cobalt par les oxydes de manganèse serait rapide, linéairement fonction de la surface disponible à une concentration en Co fixée, et dépendante du pH. Ainsi, l'adsorption des complexes hydratés de Co(II) positivement chargés augmente avec le pH en raison de l'augmentation de la charge négative des oxydes (Murray, 1975). Néanmoins, ces études sont issues, pour la plupart, d'expérimentations en laboratoire où les concentrations de cobalt et d'oxydes de manganèse sont 100 à 1000 fois supérieures à celles enregistrées dans le milieu marin oxygéné. Elles ont également été réalisées dans des eaux de mer artificielles dans lesquelles l'adsorption du cobalt sur les oxydes de manganèse serait plus élevée que dans l'eau de mer naturelle (Murray et al., 1975). Enfin, ces expériences suggèrent que ces réactions oxydatives ne seraient significatives qu'à des concentrations élevées en manganèse particulière ( $> 100$  nM ; Murray 1975), lesquelles sont 1000 fois plus élevées qu'en milieu marin oxygéné (300-100 pM ; Noble et al., 2012).

La question de la précipitation du cobalt sur les oxydes de manganèse a une longue histoire dans la géochimie océanique du cobalt. Dans les nodules de manganèse, le cobalt est l'un des éléments les plus enrichis par rapport à la concentration de l'élément dans l'eau. Pour expliquer ce facteur d'enrichissement, l'adsorption du cobalt dissous sur des oxydes de manganèse (et/ou de fer) a ainsi été proposée (Goldberg, 1954). Cependant, les réactions chimiques d'adsorption du cobalt sur les oxydes de manganèse seraient, comme nous l'avons

précédemment suggéré, peu significatives dans les eaux de mer. Une autre voie d'oxydation du cobalt (sous forme inorganique) serait possible, catalysée par des bactéries, et facilitant ainsi son adsorption sur les oxydes (Moffett and Ho, 1996). Dans cette voie enzymatique, le cobalt serait un inhibiteur compétitif de l'oxydation du manganèse (Moffett and Ho, 1996). La précipitation du DCo après oxydation chimique (Goldberg, 1961 ; Burns 1965 ; Murray et al., 1968) ou oxydation biologique (Moffett and Ho, 1996) est souvent invoquée pour expliquer la diminution des concentrations de cobalt dissous avec la profondeur (Figure 3). Elle l'est aussi pour expliquer la non-accumulation de ce micro-nutritif le long de la circulation thermohaline (Figure 4 ; Moffett and Ho, 1996 ; Saito and Moffett, 2002).

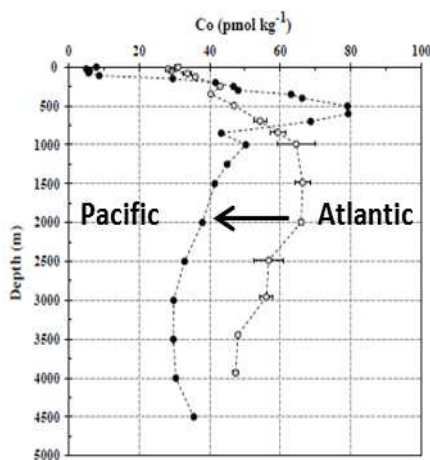


**Figure 4 :** Vertical distribution of DCo in the Sargasso Sea (open dots) and in the central Pacific Ocean (dark dots)  
(from Biller and Bruland, 2012)

Dans les eaux de surface de la Mer de Sargasses, il a été observé que l'adsorption du manganèse sur les particules est découpée de celle du cobalt aux différentes profondeurs d'activité photosynthétique (PAR ou Photosynthetically Active Radiation) (Figure 5a ; Moffett and Ho, 1996). En effet, l'adsorption du cobalt sur les particules est maximale vers 50-60 m puis diminue en profondeur, alors que celle du Mn augmente constamment avec la profondeur (Figure 5b). Dans ces eaux, le transfert du cobalt du dissous aux particules serait contrôlé par l'assimilation biologique, alors que celui du manganèse serait régi principalement par l'adsorption sur les particules (Moffett and Ho, 1996). D'autre part, le DCo existerait majoritairement sous forme complexée avec des ligands organiques (LCo) stables ( $\log K'_{LCO} > 15$ ) dans ces eaux, et la concentration cobalt organiquement lié augmenterait avec la profondeur (Saito et Moffett, 2001 ; Figure 5b). L'augmentation du cobalt organique concomitante à la diminution de l'adsorption particulaire du cobalt avec la profondeur

suggère que la complexation organique pourrait limiter l'adsorption passive du cobalt par les particules (Saito et Moffett, 2001). Cette complexation limiterait également l'oxydation bactérienne du cobalt (Saito et Moffett, 2001, 2002).

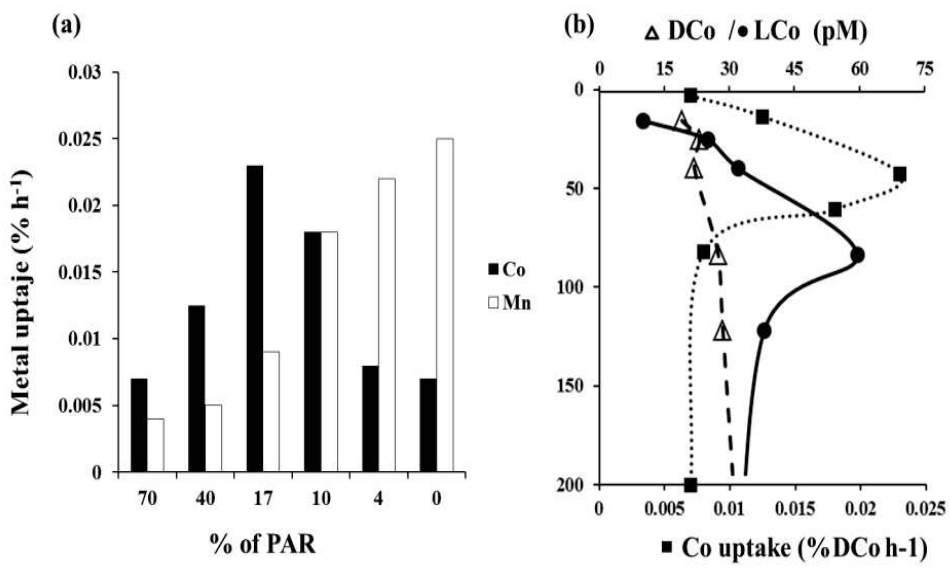


**Figure 5:** (a) Uptake of DCo (dark bars) and DMn (white bars) on particles as function of PAR in surface waters of Sargasso Sea (after Moffett and Ho, 1996). (b) Vertical distribution with depth of dissolved Co (DCo; open triangles), the organic ligands of DCo (LCo; dark dots) and DCo uptake on particles (dark squares) in surface waters of Sargasso Sea (adapted from Moffett and Ho, 1996; and Saito and Moffett, 2001).

Les études sur la spéciation organique du cobalt dissous en milieu marin ont montré que le cobalt dissous existerait majoritairement sous forme organique dans les eaux profondes (> 1000 m) de l'Atlantique Nord, du Pacifique, et de l'Océan Austral (Figure 6 ; Ellwood and van den Berg, 2001; Ellwood et al., 2005 ; Saito et al., 2001 ; Noble et al., 2008, 2012; Bown et al., 2012a). L'état rédox du cobalt organiquement lié n'a pas été déterminé pour le moment. Le cobalt organiquement lié pourrait être principalement sous forme Co(III) formant des complexes stables (Ellwood and van den Berg, 2001). Les ligands du cobalt, dont le cycle reste encore peu connu, pourraient être la vitamine B<sub>12</sub> ou un produit issu de sa dégradation, étant donnée la similitude de leur constante d'équilibre ( $\log K_{Co-B12} = 16.4$  ; Ellwood and van den Berg, 2001). Ces ligands seraient produits par les cyanobactéries dans les eaux de surface (Saito and Moffett, 2001 ; Saito et al., 2005 ; Bown et al., 2012a). Les cyanobactéries possèdent en effet le gène de synthèse de la vitamine B<sub>12</sub> et seraient capables de l'excréter en quantité importante (Bonnet et al., 2010). Dans les eaux intermédiaires, les ligands seraient minéralisés comme les macro-nutritifs (Bown et al., 2012a). Certains sédiments pourraient être également une source de ligands du cobalt (Bown et al., 2012a). Les processus d'oxydation et de précipitation du cobalt inorganique seraient ralentis par la complexation

organique (Saito and Moffett, 2001), favorisant ainsi le transport à grande échelle du DCo organiquement lié le long de la circulation thermohaline (Bown et al., 2012b).

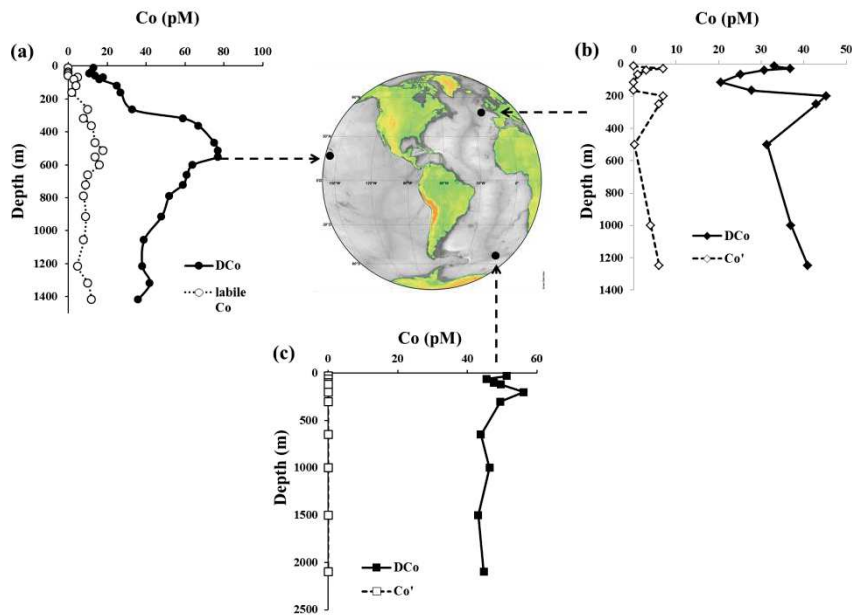


**Figure 6:** Vertical distributions of dissolved cobalt (DCo), labile cobalt, and inorganic cobalt ( $\text{Co}'$ ) in: (a) the central Pacific Ocean (Noble et al., 2008); (b) the North-Eastern Atlantic Ocean (Ellwood and van den Berg, 2001); (c) the Southern Ocean (Bown et al., 2012b)

### 2.3 Paradoxe de la non-accumulation le long de la circulation thermohaline

Des précédentes observations résulte un paradoxe : comment la diminution des concentrations en cobalt dissous entre les bassins profonds Atlantique et Pacifique le long de la circulation à grande échelle (Figure 4) pourrait-elle être provoquée par la précipitation de cobalt inorganique catalysée par des bactéries « manganèse-oxydantes » (Moffett and Ho, 1996), alors que ce même cobalt dissous est majoritairement lié à des ligands organiques qui le protège de ce processus oxydatif (Ellwood and van den Berg, 2001; Ellwood et al., 2005 ; Saito et al., 2001 ; Noble et al., 2008, 2012; Bown et al., 2012a)?

L’oxydation biologique du cobalt inorganique est en effet peu probable dans les eaux de fonds, puisque les bactéries dont la biochimie est basée sur l’oxydation du manganèse sont peu abondantes en milieu oxygéné, et sont généralement observées dans les eaux et les sédiments anoxiques ou près des sources hydrothermales (Tebo et al., 1984 ; Murray, 2007 ; Santelli et al., 2008). De plus, l’activité enzymatique de ces bactéries serait régie par la température et la teneur en manganèse (Saito et al., 2010 ; Noble et al., 2013). L’oxydation bactérienne du cobalt serait donc réduite dans l’océan profond pauvre en manganèse ( $[\text{Mn}]_{\text{moyenne}} = 0.3 \text{ nM}$ ; Bruland and Lohan, 2003) et froid ( $1^\circ\text{C} < T < 5^\circ\text{C}$ ).

Pour expliquer ce paradoxe, il a été proposé que la concentration en DCo dans les eaux soit contrôlée par la concentration en ligands organiques du cobalt, plutôt que par des réactions oxydatives (Bown, 2011).

#### 2.4 Le cobalt dans les eaux anoxiques et sulfidiques

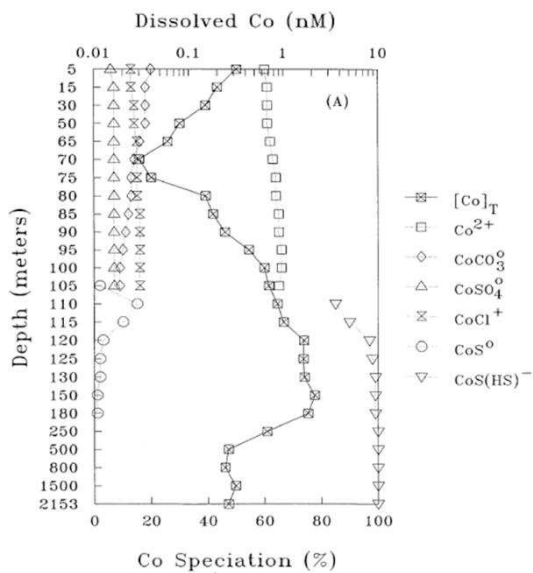


**Figure 7:** Vertical distribution of DCo and its chemical speciation in open Black Sea.

In Landing and Lewis (1991)

Dans les eaux anoxiques et sulfidiques telles qu'en Mer Noire, le cobalt a fait l'objet d'avantage d'investigations en raison des similitudes entre ces bassins et l'océan ancien. Ces eaux permettent aussi d'étudier les équilibres thermodynamiques du cobalt. Ainsi, il a été suggéré que les réactions d'oxydo-réduction et les échanges de cobalt entre les phases dissoute et particulaire seraient dépendantes de l'état d'oxygénéation du milieu (Spencer and Brewer ,1971; Spencer et al., 1972; Murray et al., 1975 ; Murray and Dillar, 1979 ; Kremling, 1983 ; Dryssen and Kremling, 1990; Murray and Dillar, 1979 ; Lewis and Landing, 1993 ; Viollier et al., 1995 ). L'approche

thermodynamique de Landing and Lewis (1991) de la spéciation chimique du cobalt dissous en Mer Noire en est une illustration (Figure 7). Les concentrations en DCo diminuent en effet de la couche oxique de surface jusqu'à la couche anoxique, puis augmentent d'un facteur 100 en dessous de l'interface O<sub>2</sub>-HS<sup>-</sup> dans la couche sulfidique supérieure (> 1 nM, Figure 7). Dans la couche sulfidique inférieure (en dessous de 500 m), les concentrations diminuent à nouveau (Figure 7). Par ailleurs, un maximum de concentration de cobalt particulaire a été rapporté dans la couche anoxique, avec une diminution dans la partie supérieure de la couche sulfidique (Haraldsson and Westerlund, 1991). Ces anti-correlations entre DCo et PCo suggèrent que les échanges entre les deux phases sont importants dans la couche de transition oxique-anoxique-sulfidique. Dans les bassins sulfidiques, le cobalt dissous serait principalement sous forme de complexes inorganiques soufrés (Figure 7). La complexation organique du cobalt ne serait pas significative selon ce modèle (Landing and Lewis, 1991), à moins que les ligands organiques ne soient présents à des concentrations extrêmement élevées (Swanner et al., 2014).

## 2.5 Les corrélations Co-P : évidence du caractère nutritif du cobalt

De manière similaire aux relations entre le cadmium et le phosphate (Cd-P), ou zinc-silicate (Zn-Si) enregistrées dans les eaux océaniques ; (Boyle et al., 1976 ; Bruland, 1980 ; Cullen et al., 2003 ; Baars et al., 2014 ; Wyatt et al., 2014), des corrélations entre le cobalt dissous et le phosphate (Co-P) ont été observées dans des eaux de surface de différents domaines biogéochimiques (Table 1), tels que le Golfe de l'Alaska, l'upwelling du Pérou, les océans Atlantique et Pacifique, la Mer de Ross et les eaux subantarctiques (Sunda and Huntsman, 1995 ; Saito and Moffett, 2002 ; Saito et al., 2004 ; Jakuba et al., 2008 ; Noble et al., 2008 ; Saito et al., 2010 ; Bown et al., 2011). Les corrélations Co-P indiquent un comportement du cobalt similaire à celui des phosphates en surface. Cependant, les corrélations relevées varient selon les domaines océaniques (Table 1). Ces variations peuvent résulter des différences d'intensité des processus mis en jeu dans le cycle de ces deux éléments, selon les domaines océaniques (Figure 8 ; Noble et al., 2008). Des différences d'assemblages phytoplanctoniques, ou de biodisponibilité du cobalt dissous entre les domaines peuvent aussi être invoquées (Saito and Moffett, 2002 ; Noble et al., 2008 ; Saito et al., 2010 ; Bown et al., 2011). Au premier ordre, l'assimilation biologique du DCo peut être considérée comme le processus contrôlant la valeur du rapport  $\Delta\text{Co} : \Delta\text{P}$  de chaque domaine (Table 1).

A la différence des relations Cd-P et Zn-Si, la corrélation Co-P n'est observable que dans les eaux de surface, suggérant que les cycles du Co et du P sont découplés dans les eaux intermédiaires et profondes. Ce découplage pourrait résulter du scavenging du cobalt dans les eaux profondes (Saito and Moffett, 2002 ; Noble et al., 2008), et/ou d'une minéralisation préférentielle du phosphate par rapport au cobalt (Bown et al., 2011).

De manière générale, la corrélation Co-P observée en surface dans différents domaines biogéochimiques confirme le caractère nutritif de cet élément.

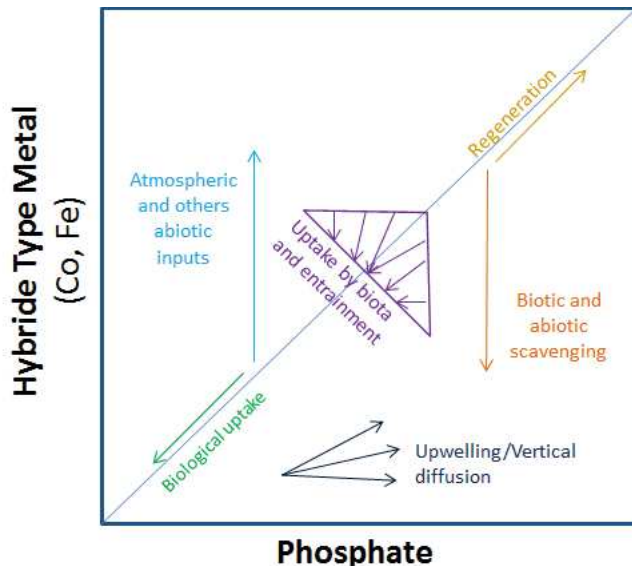


**Figure 8:** Conceptual representation of the Co-P surface relationship in surface oceanic waters. After Noble et al., 2008

**Table 1:** Regression slopes of Co versus phosphates recorded in the upper water column in different biogeochemical domains

Geographic location	Biogeochemical system	$\Delta\text{Co} : \Delta\text{P}$ ( $\mu\text{M} : \text{M}$ )	Reference
SE Atlantic	Oligotroph	49	Bown et al., 2011
NE Atlantic	Temperate	45	Martin et al., 1993
Equatorial Atlantic	Oligotroph	560	Saito and Moffett, 2002
Sargasso Sea	Oligotroph	137	Jakuba et al., 2008
NE Pacific	Subpolar	38	Martin et al., 1989
Peru Upwelling	Upwelling	248	Saito et al., 2005
Hawaï	Oligotroph	37	Noble et al., 2008
Southern Ocean	Subpolar	48	Bown et al., 2011
Ross Sea	Polar	38	Saito et al., 2010

## 2.6 Sources et puits de cobalt dissous en milieu océanique

### 2.6.1 Sources de DCo

Dans les eaux de surface, la source principale de DCo serait la régénération du cobalt biologiquement assimilé, cette source pouvant représenter 90% des pertes liées à son assimilation biologique (Bown et al., 2011). Ce flux de régénération peut augmenter dans les tourbillons cycloniques dans lesquels la biomasse détritique est piégée et minéralisée en surface (Noble et al., 2008). De plus, la diffusion dyapicnale et l'advection verticale peuvent être aussi des sources de DCo pour la couche de surface (Saito et al., 2005 ; Bown et al., 2011), en particulier dans les tourbillons (Noble et al., 2008 ; Shelley et al., 2012). Par ailleurs, les apports par les rivières peuvent drainer de fortes concentrations en cobalt (1.7 nM ; Martin and Window, 1991) au milieu côtier, et aussi à l'océan ouvert tel que l'Atlantique Ouest (Saito and Moffett, 2002 ; Tovar-Sánchez and Sañudo Wilhelmy, 2011).

Dans les eaux intermédiaires, la principale source de DCo pourrait être la minéralisation du matériel bio-détritique dans les couches de minimum d'oxygène (Bown et al., 2011 ; Noble et al., 2012). Dans les eaux profondes, la source sédimentaire semble être particulièrement importante (Sunby et al., 1985 ; Saito et al., 2005 ; Noble et al., 2012 ; Bown et al., 2012b) et ceci par diffusion sédimentaire de DCo depuis les eaux interstitielles lorsque l'interface eau-sédiment est faiblement oxygénée (Sunby et al., 1985 ; Saito et al., 2005), ou par dissolution du sédiment après sa resuspension près des marges ou plateaux continentaux en raison de forts courants de pente (Bown et al., 2012b). Ces apports benthiques peuvent

aussi être entraînés verticalement par upwelling (Saito et al., 2005 ; Noble et al., 2012) et/ou advectés latéralement à travers la circulation à grande échelle (Bown et al., 2012a ; 2012b).

### 2.6.2 Puits de DCo

Dans les eaux de surface, le puits principal de cobalt dissous serait l'assimilation biologique, plutôt que les processus d'oxydation/précipitation (Moffet an Ho, 1996 ; Saito and Moffett, 2001). L'assimilation biologique du DCo varie en fonction de chaque domaine biogéochimique, d'un facteur 1 à 5 entre les zones polaires et subtropicales respectivement (Bown et al., 2011). L'assimilation du cobalt dépendrait de chacun des groupes fonctionnels du phytoplancton (Sunda and Hunstmann, 1995, Saito et al., 2002). Par exemple, l'assimilation biologique importante observée dans les zones subtropicales serait liée au besoin absolu des cyanobactéries pour cet élément (Saito et al., 2002). Au contraire, la faible assimilation en zone polaire serait due aux faibles besoins en Co des diatomées (Sunda and Huntsmann, 1995), espèces prédominantes à ces latitudes.

Dans les eaux intermédiaires et profondes, l'adsorption et/ou la précipitation du DCo sur les particules seraient les puits principaux de cobalt dissous.

### 2.6.3 L'apport atmosphérique

Les sources atmosphériques de cobalt sont actuellement peu contraintes et peu comprises. Pour les métaux comme Fe, Al, Ti, les dépôts atmosphériques constituent une source importante à l'océan ouvert, alors qu'ils pourraient être un puits de DCo par adsorption sur les poussières (Aston et al., 1972). Plus récemment, il a été suggéré que les apports atmosphériques ne seraient pas une source significative de Co dans l'Atlantique Ouest tropical (Saito and Moffett, 2002), ainsi que dans l'Atlantique Sud-Est et le secteur atlantique de l'Océan Austral (Bown et al., 2011). En revanche, cette source pourrait être importante en Mer Méditerranée comme le suggère les concentrations élevées de DCo en surface (Figure 2b ; Ngoc and Whitehead, 1986 ; Heimbürger et al., 2011). Ces apports pourraient également significatifs au large des côtes Ouest-Africaines sous influence du panache saharien (Bowie et al., 2002).

Les dépôts atmosphériques de Co relativement faibles dans la Mer des Sargasses seraient jusqu'à 10 fois plus intenses à la fin de l'été qu'au printemps (Shelley et al., 2012). Une saisonnalité des dépôts atmosphériques de Co a aussi été observée en Méditerranée Nord

Occidentale (Heimbürger et al., 2011) entre l'hiver (faibles apports) et l'été (forts apports). Ces apports pourraient représenter près de la moitié des apports totaux en cobalt dissous en Méditerranéen Occidental durant l'été (Elbaz-Poulichet et al., 2001).

Une des principales difficultés dans la quantification du dépôt atmosphérique de cobalt est la variabilité des propriétés des aérosols. En effet, la concentration en cobalt dans les aérosols ainsi que la fraction susceptible de se dissoudre, varient largement selon l'origine des aérosols. L'abondance du cobalt dans les aérosols est définie comme mixte, variant selon les apports crustaux et ceux anthropogéniques liés aux émissions industrielles (Guieu et al., 1997 ; Gaiero et al., 2003; Reid et al., 2003; Baker et al., 2007; Trapp et al. 2010; Xia & Gao, 2010; Shelley et al., 2012). La proportion de cobalt contenu dans l'aérosol susceptible de se solubiliser dépend de l'origine des aérosols, de leurs tailles, et de leur temps de résidence dans l'eau de mer, et elle peut varier de 1 à 100 % (Guieu et al., 1997 ; Gaiero et al., 2003 ; Baker et al., 2007 ; Turoczy et al., 2010 ; Shelley et al., 2012).

### 3 Utilisation biologique et intérêt écologique en milieu marin

En étant à la fois l'atome centrale de la vitamine B<sub>12</sub>, indispensable à la croissance des cyanobactéries, et impliqué dans l'acquisition de carbone, le cobalt est l'un des rares éléments traces essentiels à la vie marine (Saito et al., 2002 ; Morel et al., 2003).

#### 3.1 Quotas cellulaires

La composition élémentaire des coccolithophores, des diatomées, des dinoflagellés et des cyanobactéries suggère de considérer le cobalt comme un élément essentiel utilisé par de nombreux groupes fonctionnels du phytoplancton (Figure 9 ; Sunda and Huntsmann, 1995 ; Kuss and Kremling, 1999 ; Cullen et al., 2003 ; Ho et al., 2003 ; Quigg et al., 2003 ; Tovar-Sanchez et al., 2006 ; Twinning et al., 2011). Les quotas cellulaires en cobalt varient en fonction des groupes fonctionnels, et au sein d'un même groupe d'espèces (Figure 9). En première approche, ces variations indiquent des besoins physiologiques en cobalt taxadépendants.

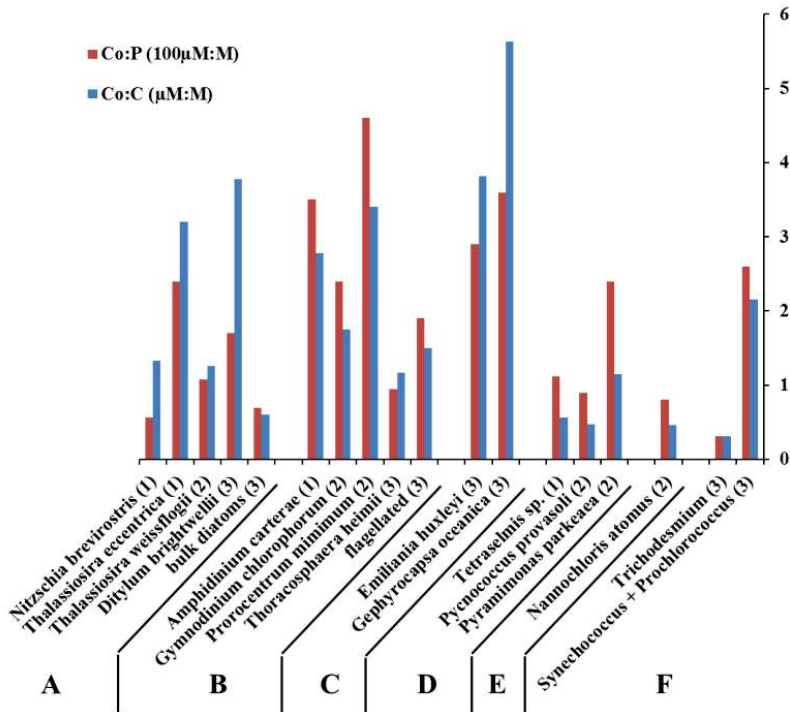


**Figure 9:** Cellular Co quota normalized to P (red bars) and to C (blue bars) in different phytoplankton species, obtained from culture or field measurements. Note the different scale between Co: P and Co:C. Letters indicate the taxa and numbers the environment, with A: Bacillariophyceae; B: Dinophyceae; C: Prymesiophyceae; D: Prasinophyceae; E: Chlorophyceae; F: Cyanophyceae. (1) estuarine; (2) Coastal; (3) Oceanic. (After Sunda and Hunstmann ; 1995 ; Kuss and Kremling, 1999 ; Cullen et al., 2003 ; Ho et al., 2003 ; Quigg et al., 2003 ; Tovar Sanchez et al., 2006 ; Twinning et al., 2011)

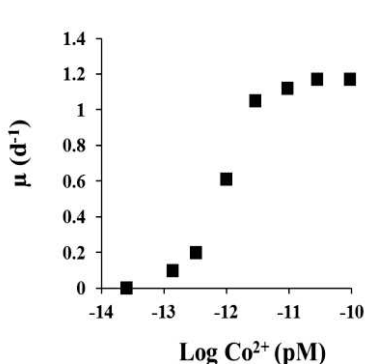


**Figure 10:** Growth rate of *Emiliania huxleyi* as function of [Co<sup>2+</sup>] in culture medium. After Sunda and Huntsmann, 1995

K<sub>MCo2+</sub>, la croissance de l'espèce considérée est limitée. Dépendamment des espèces considérées, différentes seuils de limitation en cobalt ont été enregistrées (Table 2). L'activité de l'anhydrase carbonique dépendrait aussi de la concentration en cobalt dissous (Price and Morel, 1990 ; Lane and Morel, 2000). La capacité du cobalt à limiter la croissance du

### 3.2 Utilisation biologique

L'impact du cobalt sur la croissance phytoplanctonique a été étudié lors d'expériences en culture (Figure 10). Ces expériences montrent que le taux de croissance ( $\mu$ ) suit une cinétique de type Michaëlienne en fonction de la concentration en cobalt inorganique (Co<sup>2+</sup>):  $\mu = \mu_{\max} * [\text{Co}^{2+}] / (\text{K}_{\text{MCo}2+} + [\text{Co}^{2+}])$ , où  $\mu_{\max}$  est le taux de croissance maximal de l'espèce, et K<sub>MCo2+</sub> la concentration en Co<sup>2+</sup> pour laquelle  $\mu = \mu_{\max} / 2$ . Lorsque [Co<sup>2+</sup>] <

phytoplancton et son implication dans l'assimilation de carbone en font un élément important dans la régulation du cycle global du carbone (Morel and Reinfelder, 1994).

**Table 2:**  $K_{MC_{O2+}}$  for different phytoplankton species determined by culture experiments.

Species	$K_{MC_{O2+}}$ (pM)	Study
<i>Prochlorococcus</i>	0.03	Saito et al., 2002
<i>Synechococcus</i>	0.1	Sunda and Huntsmann, 1995
<i>Emiliania huxleyi</i>	1	Sunda and Huntsmann, 1995
<i>Phaeocystis antarctica</i>	0.19	Saito and Goepfert, 2008
<i>Thalassiosira oceanica</i>	0.01	Sunda and Huntsmann, 1995
<i>Thalassiosira pseudonana</i>	3.6	Sunda and Huntsmann, 1995

L'utilisation biologique du cobalt par le phytoplancton se complique par l'introduction de deux concepts: i) la substitution cambialistique ; ii) la biodisponibilité.

i) La substitution cambialistique fait référence à la possibilité d'une entité biologique à remplacer un élément « x » par un élément « y » sans modifier la fonction, ni l'efficacité du processus pour lequel « x » est utilisé. Ainsi, la substitution dans une enzyme michaëlienne ne modifierait ni  $V_{max}$ , ni  $K_S$ . Dans la carbonique anhydrase, le cobalt et le cadmium pourraient se substituer au zinc qui est l'atome central de l'enzyme (Figure 11 ; Price and Morel, 1990 ; Lane and Morel, 2000 ; Lane et al., 2005 ; Xu et al., 2008).

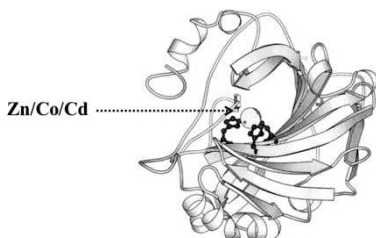


**Figure 11:** 3D representation of the carbonic anhydrase. The central metal atom could be Zn, Co or Cd and is bound by the imidazole functions of the 3 amino acid histidine

Cependant, il semble que de telles substitutions modifient l'efficacité des processus mis en jeu. Par exemple, le cobalt et le zinc peuvent se substituer pour la croissance d'*Emiliania huxleyi* mais la croissance maximale ne peut être atteinte qu'avec des concentrations en  $Co^{2+}$  supérieures à 10 pM (Figure 12a Sunda and Huntsmann, 1995 ; Saito et al., 2002).

La croissance de *Phaeocystis antarctica* n'est quant-à-elle maximale qu'en combinant des fortes concentrations en zinc et en cobalt (Figure 12b Saito and Goepfert, 2008).

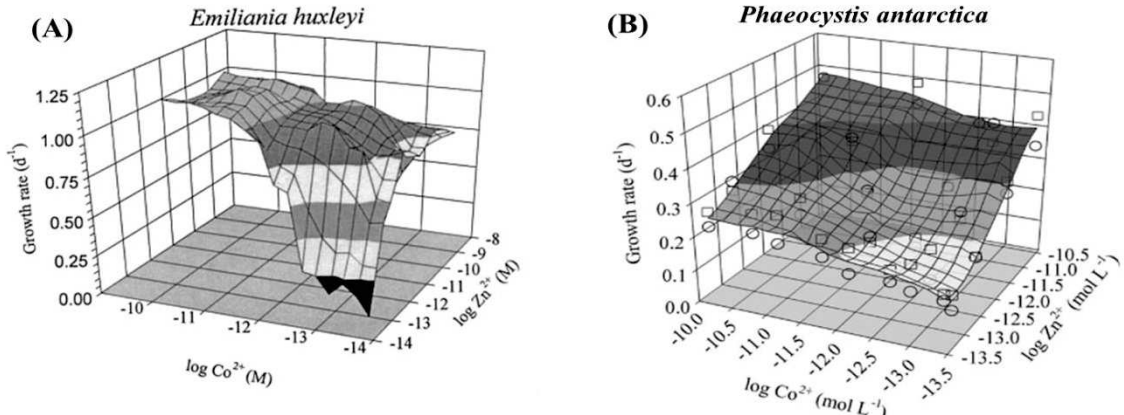


**Figure 12:** Co-Zn inter-replacement effect on the growth rate of: (a) the coccolithophore *Emiliania huxleyi*. In Saito et al., (2002) after Sunda and Hunstmann, (1995); (b) the diatom *Phaeocystis antarctica*. In Saito and Goepfert (2008). *Emiliania huxleyi* growth is optimum with high Co; *Phaeocystis antarctica* growth is enhanced with the combination of both high Co and Zn

Par ailleurs, ces substitutions ne s'opèrent pas chez les cyanobactéries de types *Prochlorococcus* et *Synechococcus*, puisqu'en l'absence de concentrations suffisamment élevées en Co<sup>2+</sup>, ces deux espèces ne se développent pas, même en présence de zinc (Figure 13a-b ; Saito et al., 2002). Ces procaryotes sont donc cobalt dépendants. Ce besoin absolu en Co serait une empreinte de l'environnement dans lequel les cyanobactéries seraient apparues, l'océan primitif archéen. Dans cet océan ferro-sulfidique, les concentrations en cobalt biologiquement disponible (Co<sup>2+</sup>) aurait, en effet, été significativement supérieures à celles en cuivre et cadmium, et dans une moindre mesure que celles en zinc (Saito et al., 2003 ; Robbins et al., 2013). Les cyanobactéries se seraient adaptées à cet environnement et auraient préféré le Co au Zn et Cd pour les processus biologiques (Saito et al., 2003). Ainsi, la dépendance au cobalt de ces organismes, qui ont peu évolué, serait un héritage de leur environnement historique (Saito et al., 2003).

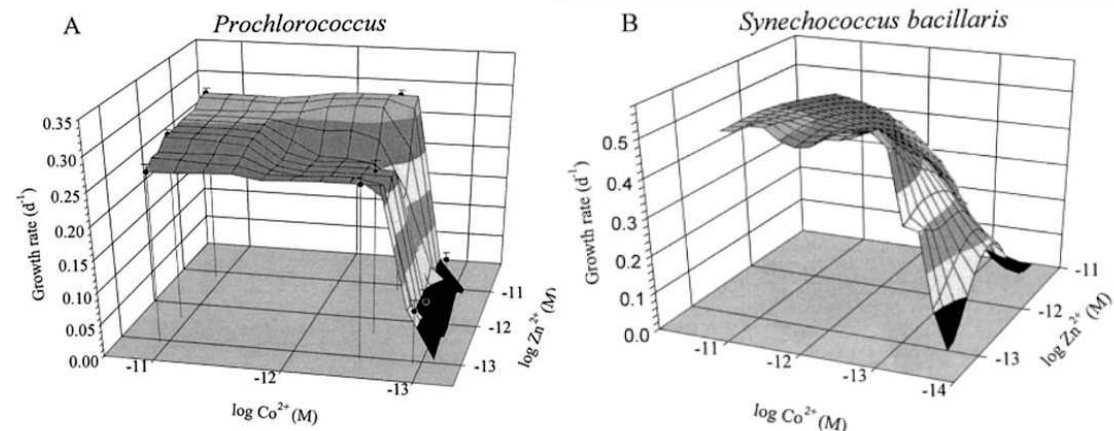


**Figure 13** Absence of Co-Zn inter-replacement in: (a) the cyanobacteria *Prochlorococcus* (b) the cyanobacteria *Synechococcus* (Saito et al. , 2002). Both species are Co dependents; Toxic effect of Zn is observed for *Synechococcus*

En considérant la prépondérance des cyanobactéries dans les domaines oligotrophes et l'étendue de ces zones à travers l'océan mondial, une partie importante de la production primaire des océans pourrait être considérée cobalt-dépendante.

ii) La biodisponibilité d'un élément fait référence à la fraction du cobalt disponible pour une entité biologique donnée. Les expériences de cultures précédemment citées ont été réalisées à l'aide de ligands synthétiques permettant de contrôler la proportion de cobalt inorganique ( $\text{Co}^{2+}$ ), qui est communément considérée comme la fraction bio-disponible pour le phytoplancton (Morel et al., 2003). Cependant, il a été observé que les cyanobactéries de type *Prochlorochoccus* sont effectivement capables d'assimiler le cobalt inorganique, mais pourraient aussi utiliser la fraction liée à des ligands organiques (Saito et al., 2002). Des « cobalophores », en référence aux sidérophores pour le fer, pourraient être en effet produits par les cyanobactéries pour faciliter l'assimilation du cobalt par ces espèces (Saito et al., 2002 ; Morel et al., 2003). La question sur la (ou les) fraction(s) biodisponible(s) du cobalt reste ouverte, et elle(s) pourrait varier en fonction des espèces phytoplanctoniques.

### 3.3 Intérêt écologique

Bien que certains eucaryotes n'utilisent pas la vitamine  $\text{B}_{12}$ , ils sont pour la plupart  $\text{B}_{12}$  dépendants puisqu'ils ne synthétisent pas cette molécule (Bertrand et al., 2007). La concentration en  $\text{B}_{12}$  peut ainsi limiter la croissance de ces organismes, comme en Mer de Ross où une co-limitation  $\text{B}_{12}$ -Fer a été observée (Bertrand et al., 2007). Cette vitamine impactera aussi la productivité et la biodiversité océanique (Sañudo-Wilhelmy et al., 2006; Panceza et al., 2006; Bertrand et al., 2007; Gobler et al., 2007).

De plus, il a récemment été mis en évidence que l'addition de cobalt à des eaux dont la concentration en cobalt dissous est faible ( $\sim 20 \text{ pM}$ ) augmente la synthèse de la vitamine  $\text{B}_{12}$ , ce qui suggère un rôle clef du cobalt dans la régulation de la voie de synthèse de cette vitamine (Panceza et al., 2008).

## **4 Transport à grande échelle dans le cycle du cobalt**

Dans l'océan, l'advection et la diffusion verticale et/ou latérale impactent les distributions des éléments chimiques. Ceci est observable dans la distribution des paramètres biogéochimiques, tel que l'oxygène ou les nutritifs, où des processus locaux peuvent impacter

leur distribution à grande échelle, et inversement des processus de grande échelle impactent des distributions locales (Figure 14).

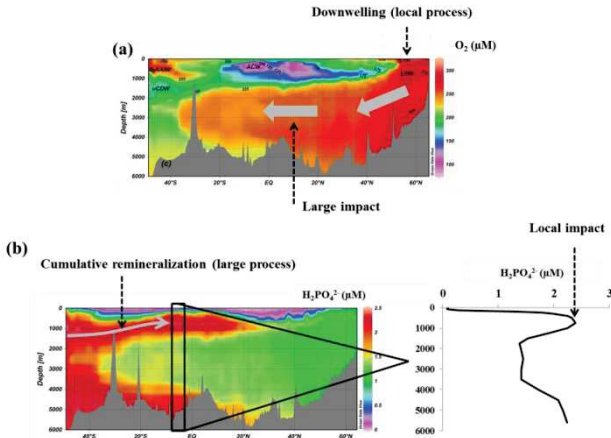


**Figure 14:** Schematic representation of relationship between local and large scale processes along the GEOTRACES A02 section (West Atlantic).

(a) Downwelling of oxygenated waters in the North Atlantic Polar Regions impact the entire West Atlantic deep basin.

(b) Cumulative remineralization along the large scale circulation impact the local phosphate vertical distribution.

(After Dulaquais et al., 2014)

Les récents efforts réalisés dans le cadre du programme international GEOTRACES ont permis de récolter, pour la première fois, des données de cobalt dissous le long de deux sections à l'échelle d'un bassin (Figure 15), dans le secteur austral de l'Atlantique (Bown et al., 2011), et dans l'Atlantique Sud (Noble et al., 2012). Ces deux premières études ont révélé l'importance du transport à grande échelle dans la distribution du cobalt. Ainsi, les fortes concentrations en cobalt dissous observées dans la couche du minimum d'oxygène au large des côtes Africaines dans l'Atlantique Sud seraient transportées d'un bord à l'autre de l'océan Atlantique (Figure 15a). De manière similaire, la section du secteur austral de l'Atlantique (Bown et al., 2011) a mis en évidence l'importance des remontées par upwelling d'eau intermédiaires enrichies en DC<sub>o</sub> au niveau du Front Polaire, et de l'advection d'eaux enrichies au Passage de Drake (Figure 15b).

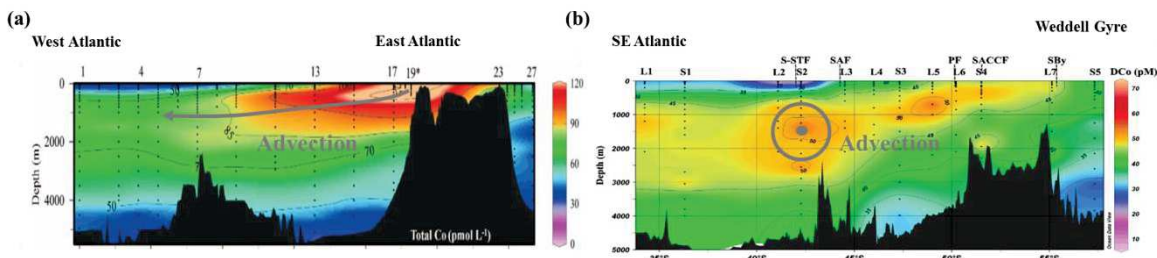


**Figure 15:** Spatial and vertical distribution of DC<sub>o</sub> along : (a) the CoFeMUG section in the south Atlantic (in Noble et al., 2012); (b) the BONUS-GoodHope section in the Atlantic sector of the Southern Ocean (Bown et al., 2011). Large scale transportation of DC<sub>o</sub> is evidenced

D'autre part, les échelles d'espace et de temps, ainsi que les échanges entre les phases dissoute et particulaire, sont aussi à prendre en compte dans les processus du cycle

biogéochimique du cobalt. Par exemple, l'enrichissement observé en cobalt dissous dans les eaux de surface au dessus du Plateau des Kerguelen serait du à une resuspension des sédiments dans le courant de pente qui est détecté par de fortes concentrations en cobalt particulaire, et à l'advection et la dissolution de ce PCo le long de la circulation au dessus du Plateau (Bown et al., 2012b).

En conclusion, la compréhension des processus gouvernants la distribution verticale du cobalt (dissous et particulaire) nécessite l'analyse des différentes fractions (spéciation physique et chimique), d'une stratégie de prélèvement, mais aussi l'utilisation de traceurs spécifiques adaptés à l'ordre de grandeur spatio-temporel du phénomène étudié.

## 5 Objectifs et zones d'études

Ce travail de doctorat est réalisé dans le cadre du programme international GEOTRACES, et vise à améliorer notre compréhension du cycle biogéochimique du cobalt dans l'océan. Il propose de répondre aux objectifs spécifiques suivants:

- Déterminer la faisabilité de comparer de larges jeux de données de cobalt dissous obtenues par différents laboratoires utilisant des techniques diverses.
- Améliorer la résolution spatiale de cet élément, indispensable à la compréhension des processus tridimensionnels de grande échelle impliqués dans le cycle biogéochimique du cobalt.
- Déterminer l'impact des processus physiques et géochimiques sur la distribution du cobalt dans l'océan, en tenant compte des échelles d'espace et de temps.
- Identifier et quantifier les termes sources et puits dans le cycle biogéochimique du cobalt en milieu marin à grande et petite échelles.
- Améliorer la compréhension des interactions entre le cobalt et les organismes phytoplanctoniques en milieu marin.

Pour répondre à ces objectifs, cette étude s'appuie sur l'observation en milieu naturel, par l'analyse d'échantillons d'eau de mer et de particules marines que nous avons collectés dans le cadre du programme international GEOTRACES le long de deux sections (GA02 et GA04), et provenant de domaines marins contrastés de par : i) leur géographie : océan ouvert (Atlantique), mers semi-fermées (Mer Méditerranée et Mer Noire) ; ii) leur niveau d'oxygénation (oxygéné, sub-oxique, anoxique, sulfidique) ; iii) leur système biogéochimique (subpolaire, oligotrophique, subantarctique). L'ensemble des zones

géographiques et domaines biogéochimiques étudiés dans ces travaux couvre une majeure partie des différents systèmes marins rencontrés dans l'océan.

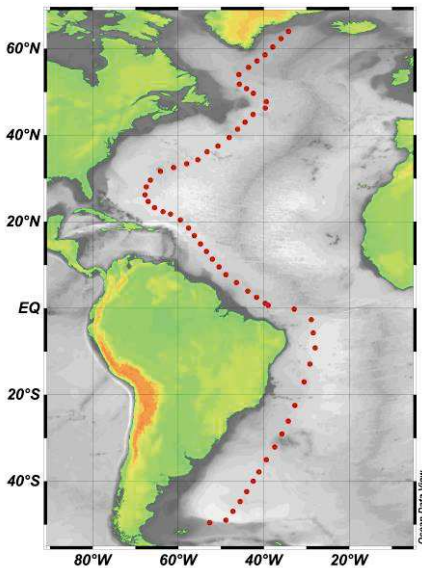


**Figure 16:** Cruise track of the GEOTRACES-A02 section

La section GEOTRACES-A02 dans l'Atlantique Ouest (Figure 16) s'étend de la mer d'Irminger au Plateau des Malouines, couvrant un large panel de domaines biogéochimiques différents. En effet, du gyre subpolaire où d'intenses efflorescences de coccolithophores peuvent être observées, aux eaux subantarctiques sujettes à des efflorescences de diatomées, en passant par les deux gyres subtropicaux oligotrophes, principalement peuplés de cyanobactéries, la section GEOTRACES-A02 traverse des domaines où les assemblages phytoplanctoniques diffèrent. Ces différentes conditions nous permettront d'améliorer notre compréhension de l'utilisation du cobalt

par les différentes espèces. D'autre part cette section traverse la zone équatoriale de l'Atlantique Ouest où les circulations horizontale et verticale, la déplétion en oxygène et les apports fluviaux (Amazone) sont intenses. Cette zone géographique se prête donc à l'étude des processus physique et de minéralisation, et des apports par les rivières, qui entrent en jeu dans le cycle du cobalt. De plus, cette section suit la circulation thermohaline à grande échelle, en particulier les Eaux Profondes Nord Atlantique. Elle permettra ainsi d'évaluer le rôle de la circulation à grande échelle sur la distribution du cobalt.

La section GEOTRACES-A04N couvre la Mer Méditerranée et la Mer Noire (Figure 17). Ces mers semi-fermées sont des sites idéaux pour l'étude de processus spécifiques du cycle biogéochimique du cobalt. La Mer Méditerranée reçoit en effet des apports atmosphériques intenses en raison de la proximité du plus grand désert sec au monde, le Sahara. Elle est donc idéale pour estimer le rôle de ces apports dans le cycle du cobalt. D'autre part, les processus oxydatifs impliqués dans le cycle du cobalt sont encore peu compris, ainsi la Mer Noire qui est le bassin anoxique le plus grand et le plus stable au monde est idéal pour étudier sur ces processus.

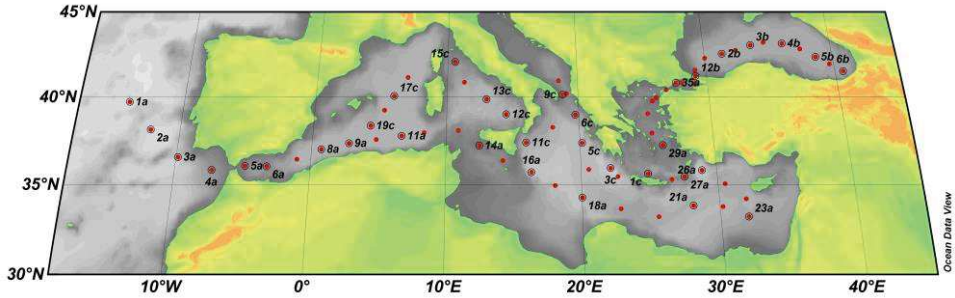


**Figure 17:** Cruise track of the GEOTRACES-A04N section

## 6 Présentation des chapitres

### Chapitre 1

Ce chapitre décrit les différentes méthodes analytiques utilisées au cours de cette étude. Ce chapitre inclut des tests analytiques réalisés préalablement à l'analyse des échantillons d'eau de mer. Il y est aussi discuté des exercices d'inter-calibration et d'inter-comparaison relatifs au programme international GEOTRACES auxquels nous avons participé. La question du mode de stockage des échantillons sur la préservation du cobalt y est aussi abordée.

Les chapitres 2, 3, 4 et 5 sont présentés sous le format d'articles. Ils sont rédigés en anglais.

### Chapitre 2

Ce chapitre s'intéresse à la distribution verticale du cobalt dissous et du particulaire apparent dans les eaux intermédiaires et profondes de l'Atlantique Ouest le long de la section GEOTRACES-A02 (64°N-50°S). Une attention particulière est portée sur le rôle des processus physiques, en particulier du mélange des masses d'eau, sur la distribution du cobalt dans l'océan profond. Le processus de minéralisation du matériel particulaire dans les Eaux Centrales Atlantiques peu oxygénées est également discuté. Ce travail fait l'objet d'un article publié :

Dulaquais, G., Boye, M., Rijkenberg, M. J. A., & Carton, X. (2014). Physical and remineralization processes govern the cobalt distribution in the deep western Atlantic ocean. *Biogeosciences*, 11(6), 1561-1580.

## **Chapitre 3**

Ce chapitre concerne l'étude du cycle biogéochimique du cobalt dans les eaux de surface de l'Atlantique Ouest le long de la section GEOTRACES-A02. Un effort particulier est apporté pour la quantification des différents puits et sources externes et internes. Des temps de résidence des phases dissoute et particulaire du cobalt ont été estimés, et un budget du cobalt est proposé à l'échelle du Bassin Atlantique Ouest. Ce travail fait l'objet d'un article accepté à la publication :

Dulaquais, G., Boye, M., Middag, R., Owens, S., Puigcorbe, V., Buesseler, K., de Baar, H. & Carton, X. (2014). Contrasting biogeochemical cycles of cobalt in the surface western Atlantic Ocean. *Global Biogeochemical Cycles*, 28(12), 1387-1412.

## **Chapitre 4**

Il présente une étude sur une source externe du cycle, l'apport atmosphérique en cobalt. Une étude fine a été réalisée sur la quantification de cet apport à l'Atlantique Ouest, et ses impacts biogéochimiques. Ce travail a été soumis pour publication:

Dulaquais G. and Boye M. (In review). Atmospheric cobalt deposition along the surface west Atlantic and biogeochemical implications. In review to *Marine Chemistry* (February 2015).

## **Chapitre 5**

Ce chapitre présente les résultats et discussions préliminaires de l'étude du cycle biogéochimique du cobalt en Mer Méditerranée et Mer Noire, le long de la section GEOTRACES-A04N. Ce chapitre propose de décrire et de quantifier les différents processus régissant la distribution du cobalt dissous et particulaire dans ces mers semi-fermées.

Par ailleurs il y est proposé une estimation pionnière, sous forme de modèle, de l'apport atmosphérique en se basant sur les concentrations de surface d'éléments traces dans la phase particulaire.

## **Conclusion générale**

Ce chapitre de conclusion générale présente la synthèse des travaux réalisés au cours de cette thèse de doctorat et les perspectives qu'ils ouvrent.

# Chapitre 1

## Méthodes analytiques



# Méthodes analytiques

## 1 Propreté et qualité

L'ensemble des expérimentations relatives à cette étude ont été réalisées sous condition d'hygiène ultra propre, en salle blanche (ISO 5) et sous hôte à flux laminaire (classe 100). L'eau utilisée pour les lavages et la préparation des réactifs est de l'eau de qualité ultra pure Milli-Q (résistivité = 18.2 MΩ) issue d'un système Millipore, Milli-Q® Element.

Les bouteilles et les filtres de prélèvements ainsi que la verrerie utilisée lors de cette étude ont été nettoyés, conditionnés et conservés selon les recommandations du programme GEOTRACES. L'ensemble des réactifs et des acides utilisés sont adaptés à la mesure des éléments traces (qualité ACS®, Suprapure®, TraceSelect®, ou Ultrapure®).

## 2 Prélèvements

L'ensemble des échantillons collectés, durant les campagnes à la mer, a été prélevé au moyen du système de prélèvement TITAN (*Rijkenberg et al.*, 2014) composé de 24 bouteilles de prélèvement (24.3 L) en PVDF. Les bouteilles sont placées dans un cadre composé exclusivement de titane (*de Baar et al.*, 2008) avec un système de fermeture automatisée et contrôlée depuis le pont par l'intermédiaire d'un hydro-câble de 17.7 mm de diamètre, lui-même composé de 7 câbles conducteurs (0.25 mm) recouverts d'une couche de kevlar (5 mm) et protégés par une couche extérieure de hydrel jacket.

## 3 Filtration et spéciation physique

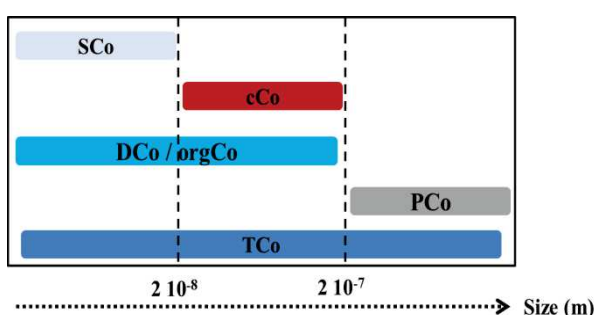


Figure 1: Size partitioning of the different cobalt fractions analyzed in this work (See text for abbreviations)

Après prélèvement l'ensemble du système TITAN est conduit dans un conteneur sous atmosphère protégée de prélèvement ultra propre ISO Class-7 (*de Baar et al.*, 2008). Les bouteilles de prélèvement sont ensuite connectées sous N<sub>2</sub> à pression 1 bar pour augmenter l'efficacité des filtrations. Les

filtrations ont été réalisées à bord, par connexion des cartouches de filtrations (ou des supports de filtres) directement à la bouteille de prélèvement par des connecteurs en HDPE.

Dans cette étude, différentes fractions de taille du cobalt (spéciation physique) sont étudiées (Figure 1). Sont définis le cobalt soluble (sCo) issus de la filtration à 0.02 µm (Sartorius, Virosart CPV capsule), les échantillons de cobalt dissous (DCo) sont issus d'une filtration à 0.2 µm (Sartobran® P 150) ainsi que ceux utilisés pour la détermination de la spéciation organique du cobalt (orgCo). Le cobalt total (TCo) correspond à des échantillons non-filtrés (analysés 6 mois après collecte). Le cobalt particulaire (PCo) a été collecté sur des filtres de 0.2 µm de porosité (PES, Milipore ®) via des supports de filtre en téflon,

La fraction colloïdale (cCo), et la fraction particulaire « apparente » (PCo) sont calculées selon les Equations (1) et (2), respectivement. Il est précisé, dans chaque étude, si le cobalt particulaire est issu d'une analyse des particules récoltées sur filtre, ou bien s'il s'agit de la fraction apparente résultant d'un calcul (Equation 2).

$$(1) \text{ cCo} = \text{DCo} - \text{sCo}$$

$$(2) \text{ PCo} = \text{TCo} - \text{DCo}$$

Les erreurs relatives de cCo et PCo sont calculées selon les Equations (3) et (4).

$$(3) \text{ SD}_{\text{cCo}} = (\text{SD}_{\text{DCo}}^2 + \text{SD}_{\text{sCo}}^2)^{0.5}$$

$$(4) \text{ SD}_{\text{PCo}} = (\text{SD}_{\text{TCo}}^2 + \text{SD}_{\text{DCo}}^2)^{0.5}$$

*Un test de Student est effectué afin de déterminer si la différence entre les deux fractions est significative (si  $P < 0.05$ , la différence est significative).*

## 4 Conditionnement des échantillons

Les échantillons ont été conditionnés à bord directement après leur prélèvement en vue d'analyse à terre, au laboratoire d'accueil. Les échantillons de sCo, DCo et TCo ont été acidifiés ( $\text{pH} = 2$ ), puis conservés dans l'obscurité et à température constante dans des sacs plastiques doublés. Les échantillons pour la détermination de orgCo ont été conservés au pH de l'eau de mer et congelés à -20°C dans des sacs plastiques doublés. Les filtres prélevés ont été conservés à -20°C dans des boites en PVC en sacs doublés.

## 5 Méthode d'analyse du cobalt

La mesure du cobalt (DCo, TCo, sCo) présent à des concentrations pico- ( $10^{-12}$  M) et sub-nanomolaires ( $10^{-10}$  M) dans les eaux océaniques nécessite l'emploi de techniques analytiques à la limite de détection basse, avec une forte reproductibilité de la mesure, et une faible incertitude. L'analyse semi-automatique par injection de flux associée à une détection par chimiluminescence (FIA-Chem.) a été utilisée car cette technique répond à ces exigences. Le principe de la méthode employée est décrite dans *Shelley et al.*, (2010), ainsi que dans *Bown et al.* (2011), seules les particularités et les performances relatives à cette étude sont brièvement rappelées ici.

### Analyse et propagation de l'erreur

Les différents mélanges de réactifs (mélange de pyrogallol, CTAB et H<sub>2</sub>O<sub>2</sub> en voie 1; et mélange de MeOH et NaOH en voie 2) sont injectés en flux continu dans un milieu réactionnel, et chauffé à 60°C en bain Marie. Dans ce milieu, le pyrogallol est oxydé par H<sub>2</sub>O<sub>2</sub> ce qui produit une réaction photochimique dont l'intensité est mesurée à l'aide d'un photomultiplicateur placé en sortie du milieu réactionnel. Sans introduction d'échantillon dans le milieu, la réaction est à l'équilibre et une ligne de base est observée. Lors de la phase de déposition, L'échantillon injecté (voie 3) est tamponné à pH 7 par injection en ligne d'une solution d'acétate d'ammonium (0.2 M) purifiée en ligne par son passage sur colonne de type Toyopearl® (voie 4), afin de déposer et concentrer le cobalt contenu dans l'échantillon sur une colonne de type Toyopearl®. Une solution HCl (pH 1) circule ensuite à travers la colonne (voie 5) afin d'éluer le cobalt, et de l'injecter dans le milieu réactionnel, ayant pour effet de catalyser la réaction photochimique de l'oxydation du pyrogallol par H<sub>2</sub>O<sub>2</sub>. Le pic de photon émis par cette réaction est proportionnel à la quantité de cobalt injecté dans le milieu. La hauteur de ce pic par rapport à la ligne de base est prise en compte pour la quantification. La concentration de cobalt est déterminée par calibration d'ajouts standards de cobalt dans une eau de mer artificielle. Les phases de déposition et d'injection sont gérées par des valves, elles-mêmes contrôlées par un logiciel de type Labview® 8.4 modifié (E. Duvieilbourg and M. Boye, LEMAR).

Chaque échantillon est analysé en triplicata. La concentration moyenne et son écart type sont calculés à partir des triplicatas, en tenant compte de la sensibilité (S<sub>n</sub>) relative de la méthode (pondération) au moment de l'analyse de l'échantillon et en la corrigeant du blanc

d'analyse ( $b_n$ ), selon les Equations 3-4-5-6. La concentration finale est calculée suivant l'Equation 7, et l'erreur sur la mesure est calculée à partir de la propagation des erreurs sur le blanc, de la calibration et de l'analyse en triplicata selon l'Equation 8.

$$(3) [Co]_n = (i_n) / S_n$$

$$(4) b_n = i b_n / S_n$$

$$(5) i b_n = i b_a + n * (i b_b - i b_a) / (b-a)$$

$$(6) S_n = S_a + n * (S_b - S_a) / (b-a)$$

$$(7) [Co]_n f = [Co]_n - b_n$$

$$(8) SD [Co]_n f = ((\{[(SD i_n / i_n)^2 + (SD S_n / S_n)^2]\}^{0.5} * [Co]_n)^2 + (\{[(SD i b_n / i b_n)^2 + (SD S_n / S_n)^2]\}^{0.5} * b_n)^2)^{0.5}$$

Note :  $a < n < b$

### Séquence d'analyse

Compte tenu de la variabilité des concentrations en cobalt dans les échantillons selon les zones d'études et les profondeurs, les échantillons ont été analysés, par station de prélèvement, des valeurs supposées les moins concentrées au plus concentrées (dans la mesure du possible), selon la séquence d'analyse suivante :

- i) Blanc (n= 1) ; ii) Calibration 1 (n = 5) ; iii) Eau de référence (n =1) ; iv) Blanc (n =1) ; v) Echantillons (n = 6-8 + 1 spiké à 20 pM) ; vi) Blanc ; vii) Eau de référence (n = 1) ; viii) Echantillons (n = 6-8 + 1 spiké à 20 pM) ; ix) Blanc (n =1) ; x) Calibration 2 (n = 5)

### Prétraitement UV

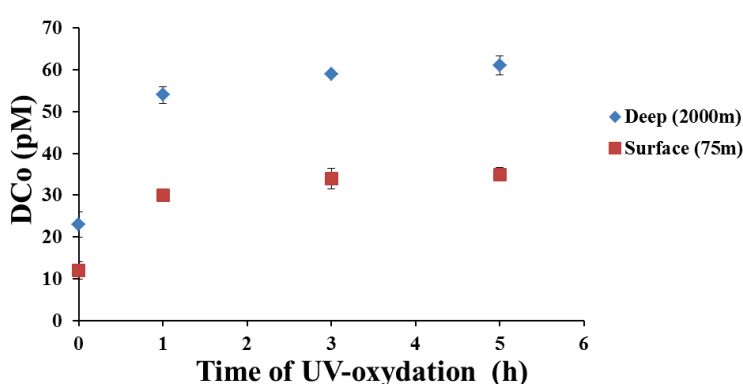


**Figure 2** : Concentration of dissolved cobalt in deep (red squares) and surface (blue diamonds) South Atlantic seawater (40°S) as the function of the UV oxidation exposure time. Optimum exposure is 3h.

Dans les eaux atlantiques, le cobalt dissous est majoritairement et fortement complexé à des ligands organiques (Saito and Moffett, 2001 ; Bown et al., 2012). Ces complexes très stables sont réfractaires au dépôt sur colonne de type Toyopearl® utilisée pour l'analyse par FIA-Chem. Une

dégradation de cette matière organique dissoute par traitement UV est donc préalablement nécessaire à l'analyse (Shelley *et al.*, 2010). L'échantillon est placé dans des tubes en verre borosilicaté avec un bouchon en téflon (préconisés par S. Van den Berg, Liverpool University, UK), puis placé sous rayon UV d'une lampe à vapeur de mercure de 600 W. Les tests que nous avons effectués sur deux eaux (surface et profonde) ont montré que les concentrations en cobalt dissous augmentent en fonction du temps d'exposition aux UV, jusqu'à 3 h d'exposition, où elles atteignent un plateau (Figure 2). Un traitement UV de 3 h a donc été appliqué à l'ensemble des échantillons dissous avant leur analyse. Les échantillons sont ensuite laissés à équilibration avant leur analyse.

#### Temps d'équilibration après exposition aux UVs

Après UV oxydation, les échantillons ont été conservés entre 12 h et 3 jours avant leur analyse. Afin d'estimer si des réactions de précipitations du cobalt inorganique intervenaient durant cette étape d'équilibration, nous avons réalisé des analyses du DCo dans le même échantillon jusqu'à 10 jours après son traitement UV (Figure 4).

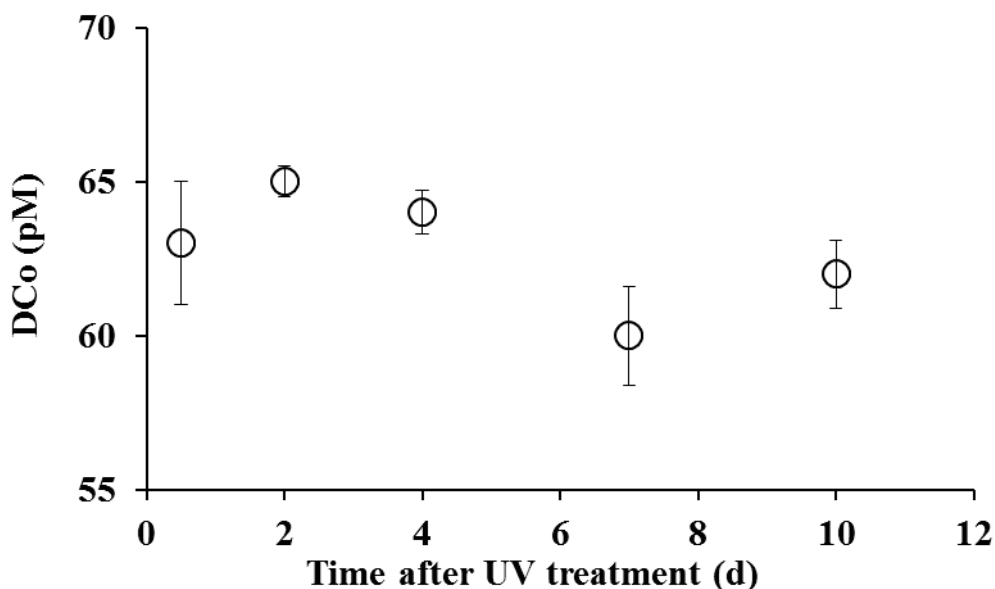


**Figure 3 :** Evolution of the DCo concentration with time after the UV-digestion of a deep seawater sample

Les résultats indiquent que la variation de la concentration de DCo n'est pas statistiquement significative jusqu'à 10 jours d'équilibration de l'échantillon passé aux UV (Figure 4). Notre protocole d'analyse dans les 12 h à 3 jours après traitement UV est donc validé.

### Reproductibilité

La reproductibilité a été déterminée par des analyses consécutives en triplicata chacune ( $n = 15 \times 3$ ) d'une eau de référence GEOTRACES. La reproductibilité de la méthode (reproductibilité =  $1 - (\text{SD } [X] / [\text{X}] \text{ moyenne})$ ) est de 96.2%.

### Blanc et limite de détection

Le blanc est mesuré dans de l'eau Mili-Q acidifiée à pH= 2. En considérant l'ensemble des blancs mesurés au cours de cette étude ( $n = 350$ ), la valeur moyenne du blanc d'analyse est de  $4.3 \pm 2.3 \text{ pM}$ . La limite de détection ( $\text{LD} = 3 \times \text{SD blanc}$ ) est ainsi de  $6.9 \text{ pM}$ , comparable avec les précédentes études (*Shelley et al., 2010 ; 2012 ; Bown et al., 2011*)

### Robustesse

La robustesse de la méthode a été évaluée par l'analyse d'eaux de références SAFe et GEOTRACES. Les valeurs de DCo mesurées dans les eaux de références sont en excellent accord avec les valeurs consensus actuelles (Table 1) il en est de même pour la valeur mesurée dans l'échantillon « Safe-S » dont la concentration est inférieure à notre limite de détection théorique. Nos résultats des analyses des eaux de références (Table 1) montrent que notre méthode analytique est validée permettant son utilisation pour l'analyse des échantillons d'eau de mer relatifs à cette étude.

**Table 1 :** Comparison of dissolved cobalt analyses obtained in the UV-oxidized samples by the FIA-Chemiluminescence method used in the present study with consensus values reported by the Sampling and Analysis of iron (SAFe) and GEOTRACES programs. Water samples provided by SAFe and GEOTRACES from surface waters (SAFe S and GEOTRACES S) and deep waters (SAFe D1 and D2, and GEOTRACES D) were analyzed. Errors are given as standard deviation from average values. *Dulaquais et al., 2014*

Sample	DCo measured	Consensus DCo Value
SAFe S	$5.1 \pm 2.2 \text{ (n=25)}$	$4.8 \pm 1.2$
SAFe D2	$44.2 \pm 1.7 \text{ (n=25)}$	$45.7 \pm 2.9$
SAFe D1	$42.3 \pm 1.4 \text{ (n = 15)}$	$45.4 \pm 4.7$
GEOTRACES S	$29.8 \pm 2 \text{ (n=35)}$	$31.8 \pm 1.1$
GEOTRACES D	$63.2 \pm 2.3 \text{ (n=25)}$	$65.2 \pm 1.2$

### Cas particulier des analyses dans les échantillons récoltés en Mer Noire

Dans le cas de la Mer Noire, les concentrations de DCo peuvent atteindre 7 nM, concentration 100 fois supérieure à celles généralement enregistrées dans les eaux océaniques. Afin de ne pas saturer la colonne d'extraction, des dilutions de ces échantillons ont donc été réalisées dans de l'eau MiliQ acidifiée à pH 2. Des dilutions de 5, 10 et 20 ont été effectuées selon la profondeur d'échantillonnage. Pour ne pas biaiser l'analyse, les calibrations ont été effectuées dans des matrices utilisant de l'eau de mer diluée dans de l'eau MiliQ selon la dilution correspondante aux échantillons analysés. La sensibilité ainsi que la reproductibilité de la méthode n'ont pas été altérées de manière significative par ces changements de matrice (< 2%).

### Intra-comparaison des méthodes d'analyse du DCo par FIA-Chem. et par voltamétrie et du mode de stockage de l'échantillon.

La concentration en DCo a été déterminée dans deux échantillons (surface et fond) prélevés en Atlantic Sud Ouest (42.5°W-40°S) par la méthode de FIA-Chemiluminescent detection et celle de cathodic stripping voltammetry (CSV). Ces deux techniques utilisées au laboratoire ont été préalablement validées par l'analyse d'eaux de références SAFe et GEOTRACES (*Bown et al., 2011 ; Bown et al., 2012*). L'analyse en voltamétrie a été réalisée sur des échantillons filtrés (0.2 µm), stockés congelés sans acidification (-20°C). L'analyse par FIA-Chimiluminescence a été réalisée sur des échantillons filtrés (0.2 µm), stockés acidifiés (0.01 M HCl ,Merck®), à température ambiante et à l'abri de la lumière. Pour un traitement similaire aux UV, la différence de concentration entre les deux méthodes n'est pas significative, en considérant l'erreur sur la mesure (Figure 4). Cette comparaison suggère aussi que le stockage de l'échantillon en condition acidifiée ou congelée ne modifie pas la concentration de DCo détectée.

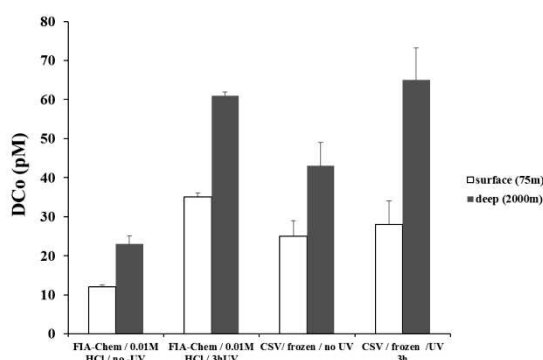


**Figure 4 :** Intra laboratory comparison on the measurement of DCo between FIA-Chemiluminescent detection method on filtered acidified seawater (FIA-Chem / 0.01M) and Cathodic Stripping Voltammetry method on filtered frozen seawater for deep and surface seawater samples. After 3h of UV oxydation no statistical difference between the two methods is observed

## Comparaison des concentrations en DCo aux stations conjointes des sections GEOTRACES

Nous avons effectué des exercices de comparaison des concentrations en cobalt dissous obtenues par différents laboratoires sur des échantillons récoltés indépendamment à trois stations communes à différentes sections GEOTRACES. Deux de ces « crossover » stations sont répertoriées dans le programme GEOTRACES (Station BATS ; et Station à 40°S). La troisième a été choisie à l'intersection de la section GA02 (cette étude, 10°S) et de la section CoFeMug (10°S ; Noble et al., 2012), en raison de leurs similitudes hydrographiques et biogeoquímiques (T, S, O<sub>2</sub>, nutriments). Il est important de noter que les échantillonnages à ces stations ont été effectués à des années et saisons différentes, sauf pour la série Middag *et al.*, 2010 (Figure 5a, carrés jaunes) à la station BATS, pour laquelle les mêmes échantillons ont été analysés entre le Bruland Laboratory et le Boye Laboratory.

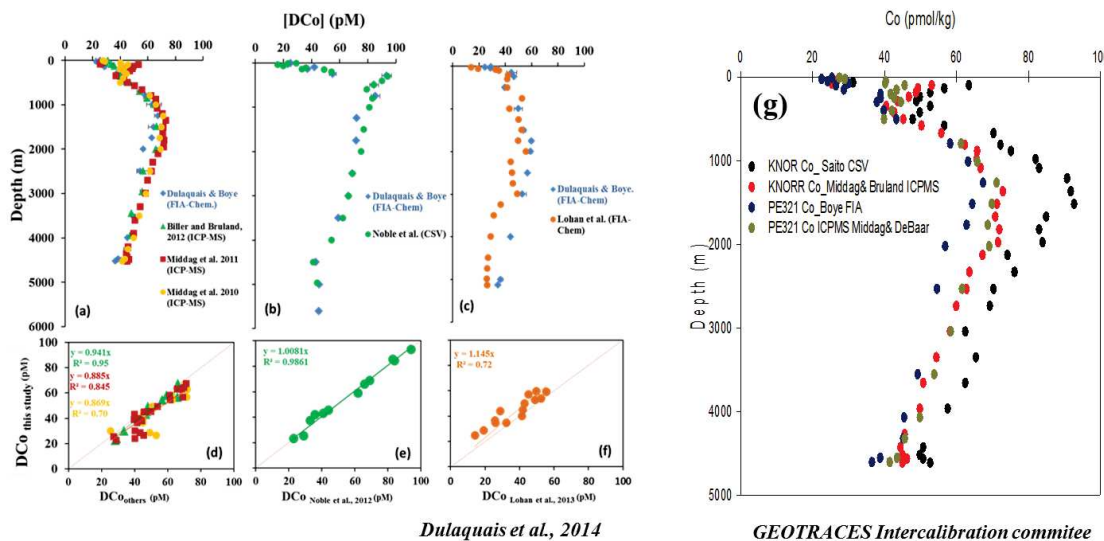


**Figure 5 :** Intercomparison of DCo datasets at the cross-over station BATS (a, d) between this study (blue diamonds) and ICP-MS method by Biller and Bruland [2008] (green triangles) and by Middag *et al.* [in prep.] (yellow dots= samples from the 2010 Dutch GEOTRACES-A02 cruise; red squares= samples from the 2011 American GEOTRACES-A03 cruise); at the cross-over station located at 9°S (b, e) between this study (blue diamonds) and the CSV method by Noble *et al.* [2012] (green dots); and at the cross-over station at 40°S (c, f) between this study (blue diamonds) with FIA-Chem. method by Lohan *et al.* [in prep.] (Orange dots=samples from the 2010 English GEOTRACES-A10 cruise). Figure published in Dulaquais *et al.*, 2014. (g) Intercomparison of DCo datasets at the cross-over station BATS between this study (blue dots), Middag *et al.* [in prep.] obtained by ICP-MS method (brown dots= samples from the 2010 Dutch GEOTRACES-A02 cruise; orange dots= samples from the 2011 American GEOTRACES-A03 cruise) and Saito Laboratory obtained by Cathodic Stripping Voltammetry method (dark dots). Figure provided by the GEOTRACES Intercalibration committee

Deux laboratoires en complément du nôtre, utilisant 2 techniques d'analyses différentes à la nôtre (Bruland Laboratory: ICP-MS ; Saito Laboratory : CSV ; Boye Laboratory: FIA-Chem.) ont participé à cet exercice de comparaison pour la station BATS. La comparaison à la station 40°S a été effectuée avec le Lohan Laboratory utilisant le même appareillage que le nôtre, et celle à la station 10°S a été effectuée avec le Saito Laboratory (méthode voltamétrique, CSV). Les résultats sont présentés Figure 5. A l'exception des données provenant du Saito Laboratory pour la station BATS (Figure 5g ; jeu de données non publié), les résultats de cette comparaison sont satisfaisants compte tenu des incertitudes sur la mesure, des différentes méthodes analytiques employées et des différents traitements des échantillons (notamment du type de résine lors de l'extraction), de la variabilité saisonnière (*Coale and Buck*, 2014), ainsi que des différents systèmes de prélèvement des échantillons. Les concentrations et les distributions de DCo sont en effet similaires entre les différents laboratoires, et les jeux de données sont statistiquement et significativement corrélés ( $0.7 < R^2 < 0.99$  ; Figure 5d, e, f).

Les récents travaux réalisés au sein du Saito Laboratory (Wood's Hole, MA, USA), rapportés par le comité d'intercalibration GEOTRACES, indiquent des concentrations significativement supérieures (+ 30%, Figure 5g) comparées à celles des autres laboratoires à la station BATS. Les échantillons analysés par le Saito Laboratory ont été désoxygénés immédiatement après leur prélèvement et stockés non-acidifiés (dans des sachets hermétiques et scellés à la chaleur), alors que ceux des autres laboratoires ont été stockés acidifiés sans désoxygénéation. Le Saito Laboratory propose ainsi que la présence d'oxygène dans les échantillons lors du stockage pourrait partiellement conduire à l'oxydation des complexes organiques du cobalt et à la précipitation du cobalt inorganique sous forme colloïdale, et donc à une sous-estimation de la concentration de DCo. (M. Saito, communication personnelle). Ces réactions seraient cependant mineures dans les eaux de l'Atlantique Sud-Ouest et inexistantes dans celles de l'Atlantique Sud-Est et des régions polaires.

A l'heure actuelle, nous ne connaissons pas les raisons qui mènent à ces différences, bien que l'acidification des échantillons non-désoxygénés pourrait jouer un rôle, au même titre que la désoxygénéation des échantillons non-acidifiés. Les différents conditionnements de l'échantillon (acidifié, désoxygéné, congelé), traitements (UV, acide), types d'extraction et de pré-concentration (résines, goutte suspendue de mercure), ainsi que les différentes méthodes analytiques et protocoles (FIA-Chem ; ICP-MS ; CSV) conduisent certainement à la détection de différentes fractions du cobalt dissous, dont il faudra lever les incertitudes. Un regard

critique doit être porté sur la fraction du cobalt dissous mise en jeux dans l'analyse, afin de mettre en relation les différents jeux de données.

## 6 Analyse de la spéciation organique du cobalt (orgCo)

La méthode utilisée pour déterminer la spéciation organique du cobalt est décrite dans *Bown et al.*, (2012). Nous rappelons ici brièvement la méthode et les performances relatives à cette étude.

### Cobalt dissous

Les concentrations en cobalt dissous (DCo) ont été déterminées selon la méthode FIA-et détection par Chimiluminescence décrite précédemment.

### Spéciation organique du cobalt

La spéciation organique du cobalt dissous a été déterminée par titration de la capacité complexante des ligands organiques du cobalt par voltammetrie (Competing Ligand Exchange-Adsortptive Cathodic Stripping Voltammetry CLE-AdCSV), à l'aide d'un équilibre compétitif avec les ligands synthétiques du cobalt, la nioxime, à pH 8.1. Cette méthode décrite dans *Zhang et al.* (1990) a été adaptée (selon *Bown et al.*;2012).

L'appareillage utilisé est constitué d'un stand polarographique (modèle VA 663, Metrohm®, Suisse) équipé d'une électrode de travail à goutte de mercure multimode positionné en mode SDME, d'une électrode de référence Ag/AgCl, KCl 3M avec un pont salin plongé dans une solution de KCl à 3M, et d'une contre-électrode en carbone vitreux. Elles sont reliées à un potentiostat  $\mu$ -autolab (Type II, Ecochemie®) et un auto-analyseur (Sample Processor 778, Metrohm®). Le potentiostat est connecté à un ordinateur. Le logiciel GPES 4.9 (General Purpose Electrochemical) permet de piloter la mesure et de traiter les résultats.

### Réactifs

Un tampon borate a été utilisé afin de fixer le pH à 8,1. Le tampon est préparé à partir d'acide borique ( $H_3BO_3$ , SigmaUltra®) et de soude ( $NaOH$  Merck® ultrapur). Les concentrations finales respectives dans le tampon sont 1 M et 0.3 M. Le tampon est ensuite purifié de toute trace de métaux en le passant à travers une colonne de type toyopearl (2

mL/min). La solution mère de nioxime est composée de 1,2-cyclohexanedione dioxime (0.1 M, Sigma Aldrich<sup>®</sup>) et de NaOH (0.2 M, Merck<sup>®</sup> ultrapur). La solution de cobalt servant aux ajouts de titration est à 10<sup>-8</sup> M, préparer à partir d'une solution mère à 0,979 µg.L<sup>-1</sup> (Sigma aldrich<sup>®</sup>), acidifiée avec de l'HCl ultra-pure (Fluka<sup>®</sup>) à 0,05% (v/v).

### Préparation des échantillons

Les échantillons sont préalablement décongelés à température ambiante. En salle blanche et sous hotte à flux laminaire, 220 mL d'échantillon sont mélangés au tampon (concentration finale à 10 mM) et à la nioxime (concentration final de 0,1 mM) dans une bouteille en téflon de 250 mL.. 11 x 20 mL de cette solution sont précautionneusement pipetés et placés dans 11 vials en téflon PTFA de 30 mL. Afin de titrer les échantillons, des concentrations connues de cobalt sont ajoutés à 9 de ces vials (de +10 à +200 pM), les deux vials restant sont sans ajout. Les vials contenant les échantillons et l'ensemble des réactifs et des additions standards sont ensuite laissés à équilibration, fermés, sous hotte à flux laminaire en salle blanche, 8 à 12h avant leur analyse.

### Analyse

Après équilibration, les échantillons sont disposés dans l'auto-sampler (dans l'ordre croissant des ajouts). Ils sont automatiquement injectés dans une cellule de mesure en téflon, les uns après les autres, selon la séquence suivante: i) purge de la cellule; ii) injection de 3 mL de la solution du vial n ; iii) purge de la cellule ; iv) injection de 15 mL de la solution du vial n. La cellule n'est pas rincée durant la titration mais nettoyée à l'eau acidifiée à la fin de chaque titration (HCl, 0,01 M).

Après introduction dans la cellule, l'échantillon subit 360 s de dégazage à l'azote (99,9999 %). S'en suit une phase de dépôt de 900 s à -0.7 V sur la goutte de mercure, puis le potentiel passe à -1V pendant 1 s, afin de diminuer les interférences avec les complexes nioxime-nickel. Après une équilibration de 10 s ; le potentiel est balayé de -0,9 à -1,2 V en mode voltammetrie impulsionale différentielle avec un pas de potentiel de 15 mV et une vitesse de balayage de 0,15 V.s<sup>-1</sup>. Le courant de réduction du complexe nioxime-cobalt est mesuré aux alentours de -1,05 V. Des triplicatas sont effectués pour chaque mesure. Les pics sont traités selon leur hauteur avec une ligne de base linéaire. La moyenne et l'écart type des trois mesures constituent la donnée et son incertitude.

### Détermination de $K'_{CoL}$ , $[Co']$ et $[CoL]$

La constante conditionnelle de stabilité pour les complexes organiques du cobalt ( $K'_{CoL}$ ) est définie par (1) :

$$K'_{CoL} = [CoL] / ([Co^{2+}] * [L']) \quad (1)$$

Avec  $[CoL]$  le cobalt organique,  $[Co^{2+}]$  le cobalt inorganique, et  $[L']$  les ligands « libres » (non liés au cobalt).

La concentration totale de ligands organiques du cobalt ( $[L]$ ) est définie selon (2) :

$$[L] = [CoL] + [L'] \quad (2)$$

En présence de nioxime et après équilibration, l'équilibre se réécrit selon (3) :

$$[Co_{labile}] / [CoL] = [Co_{labile}] / [L] + (\alpha_{Co'} + \alpha_{CoNioxime2}) / (K'_{CoL} \cdot [L]) \quad (3)$$

- Avec  $\alpha_{Co'}$ , le « side reaction coefficient » du cobalt inorganique dans l'eau de mer ( $\alpha_{Co'} = 1.74$ , selon Turner 1981), et  $\alpha_{CoNioxime2}$  ( $= 16.18$ ) celui du complexe cobalt-nioxime ( $\alpha_{CoNioxime2} = \beta'_{Co(Nioxime)2} * [Nioxime]^2$ , avec  $[nioxime] = 1.0.E^{-4}$  mol.L<sup>-1</sup> et  $\beta'_{Co(Nioxime)2} = 15.62$ ; Bown et al., 2012). Sous nos conditions expérimentales, la fenêtre de détection de la méthode est comprise entre  $10^{6.62}$  et  $10^{8.82}$  pour la détection de  $\alpha_{CoL}$  ( $\alpha_{CoL} = [L'] * K'_{CoL}$ ).

- Avec  $[Co_{labile}]$  la concentration de cobalt labile qui est mesurée selon (4) en fonction de la hauteur du pic mesuré (ip) et de la sensibilité S (pente de la partie linéaire de la titration, Figure 3b), et  $[CoL]$  celle du cobalt organique qui est à l'équilibre avec les complexes formés avec la nioxime, (déterminée selon (5)).

$$[Co_{labile}] = ip / S \quad (4)$$

$$[CoL] = [DCo] - [Co_{labile}] \quad (5)$$

$[L]$  et  $K'_{CoL}$  sont ensuite calculés à partir de la pente ( $1/[L]$ ) et l'ordonnée à l'origine correspond à  $((\alpha_{Co'} + \alpha_{CoNioxime2}) / (K'_{CoL} \cdot [L]))$  de la régression linéaire des moindres carrés de  $[Co_{labile}] / [CoL]$  en fonction de  $[Co_{labile}]$  selon l'Equation (3).

La concentration en ions cobalt  $[Co^{2+}]$  présente à l'origine dans l'échantillon est calculée selon (6) :

$$[Co^{2+}]^2 * \alpha_{Co'} * K'_{CoL} + [Co^{2+}] * \alpha_{Co'} + K'_{Co} * [L]K'_{Co} * [DCo] - [DCo] = 0 \quad (6)$$

La concentration de cobalt inorganique  $[Co']$  dans l'échantillon est calculée selon (7) :

$$[\text{Co}'] = \alpha \text{Co}' * [\text{Co}^{2+}] \quad (7)$$

La concentration de cobalt organique [CoL] présent dans l'échantillon est obtenue selon (8) :

$$[\text{CoL}] = [\text{DCo}] - [\text{Co}'] \quad (8)$$

La fraction organique du cobalt dissous (%) est définie par  $([\text{CoL}]/[\text{DCo}]) * 100$ .

## 7 Analyse des métaux particulaires

La méthode utilisée pour l'obtention des données en métaux particulaire en mers Méditerranée et Noire est décrite en détail dans *Planquette et al.* (2012). Seules les particularités et les performances relatives à cette étude sont brièvement rappelées ici.

### Filtration

Pour l'obtention du matériel particulaire, les échantillons d'eau de mer (de 4 à 15 L) ont été filtrés à 0.2 µm sur des filtres en polyéther sulfone (PES, Supor ®) de 47 mm de diamètre, lesquels étaient maintenus par des supports de filtre en téflon (Savillex ®) connectés en ligne aux bouteilles de prélèvement. Les filtrations ont été effectuées sous atmosphère protégée ISO Class-7 (*de Baar et al.*, 2008). Des blancs de filtration ont été collectés régulièrement (1 station sur 2) lors des prélèvements. Les blancs sont obtenus par re-filtration d'une eau de surface (50m) ou de fond (1500m) préalablement passée à travers une cartouche de filtration (0.2µm, Sartobran® P 150) en connectant en ligne le support contenant le filtre PES et la cartouche. Après filtration les filtres ont été placés à l'aide d'une pince en téflon dans des boites de pétris puis congelés à -20°C.

### Préparation des échantillons avant analyse

Au laboratoire, l'ensemble des manipulations a été effectué sous atmosphère ultra propre (Classe 100). Les filtres sont décongelés à température ambiante puis placés dans des bêchers en téflon PFA de 30 mL, dans lesquels 2 à 3 ml d'une solution acide (HNO<sub>3</sub> 8M, Merck Ultrapur® ; HF 2.9 M, Merck Suprapur®) sont introduits de manière à ce que le filtre et la solution ne soient pas en contact direct. Les bêchers sont chauffés à 130°C fermés (créant ainsi un reflux) pendant 4 h. La solution acide est ensuite évaporée à 110°C. Après évaporation totale, le résidu est dissous dans 6 mL d'une solution HNO<sub>3</sub> (0.8 M Merck ultrapur ®) doublement spiké à l'indium (1 ppb) ainsi qu'au rhénium (10 ppb) afin de suivre

la dérive lors de l'analyse par SF-ICP-MS. Les échantillons sont ensuite placés dans des tubes en polypropylène (Corning®) préalablement lavés et constituent les solutions archives. Des blancs chimiques d'attaque acide (bécher sans filtre) ont été réalisés selon le même protocole, à chaque série d'échantillons traités.

### Analyses

Les analyses ont été réalisées par un spectromètre de masse haute résolution à source plasma (SF-ICP-MS) Element-2 (ThermoFisher). Dans cette étude seule les résolutions basses (Cd, Pb) et moyennes (autres éléments) ont été utilisées. Le jour de l'analyse 500 µL de solution archive sont pipetés et dilués dans 3 mL de solution HNO<sub>3</sub> (0.8 M) dans des tubes en polypropylène (Corning®) préalablement lavés permettant ainsi de conserver assez d'échantillons pour effectuer des réplicas ainsi que de garder une archive de l'échantillon. Tous les 8 échantillons, un réplica est effectué ainsi qu'un blanc de tube. Compte tenu de la variabilité des rapports et des concentrations élémentaires dans le milieu naturel, deux solutions multi élémentaires ont été réalisées à partir de solutions mono élémentaires dans le but d'approcher ces rapports naturels. Pour prévenir d'éventuelles contaminations en mélangeant des concentrations faibles et élevées des différents standards, deux séries multi-élémentaires ont été réalisées. Une avec des fortes concentrations (Al, P, Fe, Ba) et une autre avec de faibles concentrations (Ti, V, Cr, Mn, Co, Ni, Cu, Zn, Cd, Mo, Pb, Zr). De ces solutions mères ont été réalisées deux séries de 10 points de calibration par dilution. Les 10 points couvrent des variations de concentration de deux ordres de grandeurs correspondant à la variabilité potentielle anticipée des concentrations dans les échantillons. Les droites de calibration ont été exécutées au début, en milieu et en fin de chaque séquence. Une séquence type comprend 8 blancs machine, 8 blancs de tubes, 3 droites de calibration, 72 échantillons (incluant des blancs chimiques), et 16 échantillons spikés par l'une des deux solutions multi élémentaires. L'erreur relative standard sur la mesure du signal est déterminée par le logiciel de l'ICP-MS.

### Reproductibilité

Pour tester la reproductibilité des mesures, des échantillons de concentrations variables ont été mesurés à plusieurs reprises lors d'une même séquence (tous les 8 échantillons). Les différences obtenues pour la totalité des échantillons sont inférieures à 5% sur l'ensemble des éléments (annexe 1)

### Blancs et limite de détection

Les résultats des analyses des blancs moyens de l'instrument, de digestion et chimiques sont présentés en Annexe 1. De manière générale, la digestion du filtre constitue la principale source potentielle de contamination (Annexe 1) comparée au blanc machine. Dans le cas du cobalt, l'étape de digestion plus que le filtre en lui-même semble être la plus grande source de contamination. Les limites de détection ( $LD = 3 \times SD$  blanc instrument) des différents éléments analysés sont indiquées en Annexe 1.

### Validation des données

En l'absence de matériel de référence pour les particules marines, l'analyse de matériel de référence de type BCR-414 (poudre de phytoplancton) a été utilisée afin de valider nos données. Le matériel a subi la même procédure de digestion que les filtres. Les résultats sont présentés Annexe 1. Compte-tenu des incertitudes de mesures et des valeurs consensus pour ce matériel, les résultats indiquent que la méthode et les données sont validées pour l'ensemble des éléments analysés, excepté pour le chrome ainsi que le zirconium pour lesquels aucune valeur consensus n'est connue pour ce matériel à l'heure actuelle.

## **8 Analyse du carbone et de l'azote organique particulaire**

La détermination du carbone et de l'azote organique particulaire a été effectuée selon le protocole décrit dans *L'Helguen et al.* (2014). Les échantillons d'eau (de 0.5 à 1 L) ont été filtrés sur des filtres en fibre de verre (Whatman GF/F de 47 mm de diamètre), préalablement grillés au four (4 h à 450°C) afin d'éliminer toute trace de matière organique. Après filtration à bord, les échantillons ont été placés dans des réceptacles préalablement traités au four (4 h à 450°C), empactés sous double sachets plastique (PE) et enfin congelés à -20°C. Au laboratoire, les filtres ont été décongelés en salle blanche puis placés dans un dessicateur sous HCl fumant durant 4 h afin d'éliminer la matière inorganique particulaire. Enfin, ils ont été placés à l'étuve (60°C) durant 24 h avant leur analyse. Les teneurs en carbone et azote particulaires collectés sur les filtres ont été obtenues par spectrométrie de masse de type Delta Plus ThermoFinnigan couplée via une interface type III à un analyseur élémentaire carbone-azote de type Thermo Finnigan CE Flash 1112. Les limites de détection ( $3\sigma$  Blanc) de la

méthode sont de  $0.51 \text{ }\mu\text{mol L}^{-1}$  et  $0.06 \text{ }\mu\text{mol L}^{-1}$  pour le carbone et l'azote organiques, respectivement.

## **Chapitre 2**

### **Physical and remineralization processes govern the cobalt distribution in the deep western Atlantic Ocean**





# Physical and remineralization processes govern the cobalt distribution in the deep western Atlantic Ocean

G. Dulaquais<sup>1</sup>, M. Boye<sup>1</sup>, M. J. A. Rijkenberg<sup>2,3</sup>, and X. Carton<sup>4</sup>

<sup>1</sup>Laboratoire des Sciences de l'Environnement Marin UMR6539, Institut Universitaire Européen de la Mer UMS3113, Technopôle Brest Iroise, Place Nicolas Copernic, 29280 Plouzané, France

<sup>2</sup>Department of Marine Biology, University of Groningen, P.O. Box 14, 9750 AA Haren, the Netherlands

<sup>3</sup>Department of Marine Chemistry and Geology, Royal Netherlands Institute for Sea Research, P.O. Box 59, 1790 AB Den Burg, the Netherlands

<sup>4</sup>Laboratoire de Physique des Océans, Université de Bretagne Occidentale – UFR Sciences, 6 avenue Le Gorgeu, C.S. 93837, 29238 Brest Cedex 3, France

Correspondence to: G. Dulaquais (gabriel.dulaquais@univ-brest.fr)

Received: 6 September 2013 – Published in Biogeosciences Discuss.: 16 October 2013

Revised: 23 January 2014 – Accepted: 28 January 2014 – Published: 24 March 2014

**Abstract.** The distributions of the bio-essential trace element dissolved cobalt (DCo) and the apparent particulate Co (PCo) are presented along the GEOTRACES-A02 deep section from 64° N to 50° S in the western Atlantic Ocean (longest section of international GEOTRACES marine environment program). PCo was determined as the difference between total cobalt (TCo, unfiltered samples) and DCo. DCo concentrations ranged from 14.7 pM to 94.3 pM, and PCo concentrations from undetectable values to 18.8 pM. The lowest DCo concentrations were observed in the subtropical domains, and the highest in the low-oxygenated Atlantic Central Waters (ACW), which appears to be the major reservoir of DCo in the western Atlantic. In the Antarctic Bottom Waters, the enrichment in DCo with aging of the water mass can be related to suspension and redissolution of bottom sediments as well as diffusion of DCo from abyssal sediments. Mixing and dilution of deep water masses, rather than scavenging of DCo onto settling particles, generated the meridional decrease of DCo along the southward large-scale circulation in the deep western Atlantic. Furthermore, the apparent scavenged profile of DCo observed in the deep waters likely resulted from the persistence of relatively high concentrations in intermediate waters and low DCo concentrations in underlying bottom waters. We suggest that the 2010 Icelandic volcanic eruption could have been a source of DCo that could have been transported into the core of the Northeast Atlantic Deep Waters. At intermediate depths, the high

concentrations of DCo recorded in the ACW linearly correlated with the apparent utilization of oxygen (AOU), indicating that remineralization of DCo could be significant (representing up to 37% of the DCo present). Furthermore, the preferential remineralization of phosphate (P) compared to Co in these low-oxygenated waters suggests a decoupling between the deep cycles of P and Co. The vertical diffusion of DCo from the ACW appears to be a significant source of DCo into the surface waters of the equatorial domain. Summarizing, the dilution due to mixing processes rather than scavenging of DCo and the above-mentioned remineralization could be the two major pathways controlling the cycling of DCo into the intermediate and deep western Atlantic.

## 1 Introduction

In the context of the international GEOTRACES program, unprecedented efforts are underway to map the distribution of trace elements and isotopes in the global oceans. Cobalt (Co) is among the important micronutrients highlighted in this program. Dissolved cobalt (DCo) typically occurs at concentrations lower than 150 pM in the open ocean (Knauer et al., 1982; Martin et al., 1990; Fitzwater et al., 2000; Saito and Moffett, 2001; Saito et al., 2004; Ellwood, 2008; Noble et al., 2008; Pohl et al., 2011; Bown et al., 2011), requiring sensitive analytical techniques for its detection (Vega and van den

Berg, 1997; Cannizzaro et al., 2000; Saito and Moffett, 2001; Milne et al., 2010; Shelley et al., 2010). Previous studies have suggested that DCo could be an hybrid-type metal (Bruland and Lohan, 2003; Noble et al., 2008), with a nutrient-like distribution in surface waters (Martin et al., 1993; Saito and Moffett, 2002; Saito et al., 2004; Jakuba et al., 2008; Noble et al., 2008; Saito and Goepfert, 2008; Bown et al., 2011) and a scavenged-type distribution in the deep ocean (Knauer et al., 1982; Wong et al., 1995; Noble et al., 2008; Boyd and Elwood, 2010). Biological uptake by cyanobacteria (Saito et al., 2002), recycling, organic complexation, scavenging and regeneration processes are suspected to strongly impact the distribution of DCo in the surface ocean (Saito and Moffett, 2001, 2002; Noble et al., 2008, 2012; Bown et al., 2011, 2012a). In addition, other important sources of DCo to surface waters, such as river (Tovar-Sánchez et al., 2011) or atmospheric deposition (Shelley et al., 2012), may significantly impact its surface distribution.

In the water column, cobalt and manganese (Mn) often cycle together through a removal pathway of co-oxidation with manganese driven by microbes, but the biological assimilation of DCo can uncouple the Mn-Co relationship in surface waters (Moffett and Ho, 1996). Furthermore, previous studies showed high DCo concentrations in oxygen-depleted waters (Saito et al., 2004; Pohl et al., 2011; Noble et al., 2012) that can be partly related to slowed microbial oxidation of DCo decreasing its scavenging rate (Noble et al., 2012). On the other hand, the low solubility of inorganic Co in oxygenated waters and the affinity of DCo for particles have been invoked to explain why DCo does not seem to accumulate in the deep waters along the thermohaline circulation (Bruland and Lohan, 2003) and to interpret the apparent scavenged-type profile of DCo observed in the deep ocean (Aparicio-Gonzalez et al., 2012). In fact, the scavenging of DCo onto settling particles and its stabilization in solution by the complexation with organic binding ligands could be the two major pathways controlling the internal cycling of DCo in the deep ocean (Saito and Moffett, 2001, 2002). Those pathways might drive the residence time of DCo in the deep waters, estimated 40–120 years, which is more than two orders of magnitude longer than in surface waters (e.g., 0.32 year; Saito and Moffett, 2002). Hydrothermal vents (Bruland and Lohan, 2003) and sediment resuspension (Bown et al., 2012a) can be the prevailing external sources of DCo to the bottom ocean. In addition, advection of water masses enriched in DCo, following contact with continental margins, can be a significant source of DCo and locally imprints the vertical DCo distribution in intermediate and deep waters (Wong et al., 1995; Saito et al., 2004; Noble et al., 2008; Bown et al., 2011, 2012b). Furthermore, large and mesoscale transport of DCo-enriched waters through the intermediate oceanic circulation has recently been evidenced in the poor-oxygenated Atlantic Central Waters (Noble et al., 2012) and Upper Circumpolar Deep Waters (Bown et al., 2011), as well as close to the Kerguelen Plateau (Bown et al.,

2012b). Nevertheless, despite these major findings our understanding of the biogeochemical cycle of cobalt in the ocean is still limited, notably in the western Atlantic Ocean where observations of the deep distribution of DCo are scarce.

In this study the vertical and meridional distributions of DCo and apparent particulate cobalt (PCo) are presented along the GEOTRACES-A02 section in the western Atlantic Ocean from the east coast of the Greenland Plateau (64° N) to the Malvinas Plateau (50° S). The GEOTRACES-A02 transect is revisiting the Atlantic GEOSECS (Geochemical Ocean Sections) program's section of 1972, crossing distinct biogeochemical areas such as subtropical, equatorial or subpolar domains where different trophic chains are growing in each. Moreover, this section also encounters several water masses involved in the thermohaline circulation and surface jets, such as the North Atlantic Drift, known for its important role in climate regulation. The spatial distributions of DCo and its transportation across the entire deep western Atlantic Ocean are examined. Intercomparison between this data set and others, at three crossover stations located in different biogeochemical domains, are presented. The advection of DCo in the different intermediate and deep water masses flowing in the western Atlantic are studied to further understand its spatial distributions. In addition, the potential effect of the 2010 Icelandic volcano Eyjafjallajökull eruption on the distribution of DCo is investigated. We also investigate the role of the remineralization in the distribution of DCo at intermediate depths, and its relationship with phosphate. Finally, the roles of the dynamic structures and the vertical diffusion are considered as they may provide a link between the deep and surface distributions of DCo. However, the complete description of the cycling and budget of DCo in the surface waters along the GEOTRACES-A02 section will be discussed elsewhere (Dulaquais et al., 2014). This large and deep section together with the relatively high spatial resolution has given us the opportunity to present, for the first time, the largest comprehensive data set of cobalt in the western Atlantic Ocean.

## 2 Methods

### 2.1 Cruise track and sampling

The samples were collected from stations (St.) along the GEOTRACES-A02 section in the western Atlantic Ocean, the longest section of the international GEOTRACES program. Four expeditions conducted between 2010 and 2012 were necessary to complete this section spreading from 64° N to 50° S along the western Atlantic Ocean (Fig. 1). Three cruises were operated aboard the Dutch R/V *Pelagia* (legs 1, 2, 4) and one cruise aboard the British RRS *James Cook* (leg 3). The first cruise started in April 2010 from 64° N to Bermuda in the Sargasso Sea (St. 1–19), followed by the second leg from the station BATS to the Equator (St. 21–41).

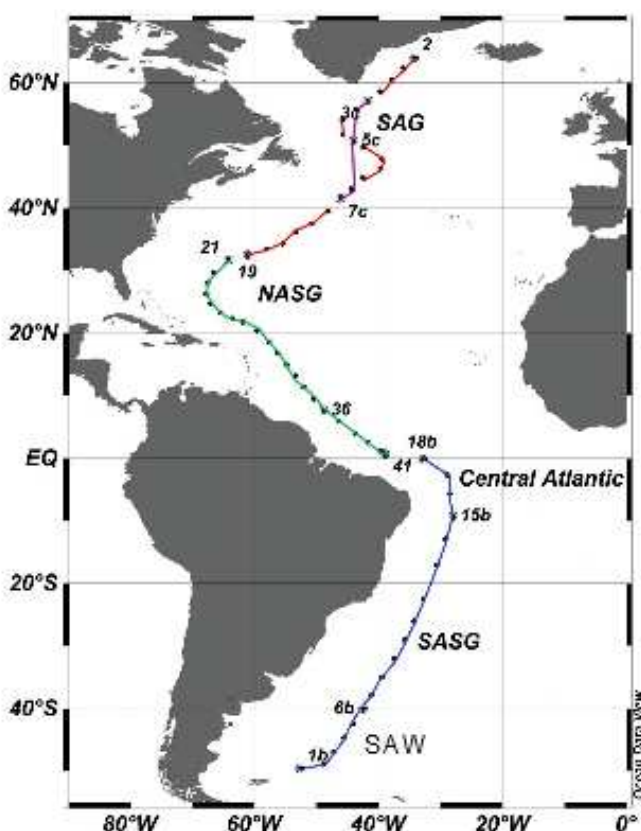


**Fig. 1.** GEOTRACES A02 cruises track along the western Atlantic Ocean. Sampling locations of the four legs are shown (leg 1 in red line from station 2 to station 19, leg 2 in green line from station 21 to station 41, leg 3 in blue line from station 1b to 18b and leg 4 in purple line from station 3c to 7c).

The section in the southwestern Atlantic (leg 3) from 50° S to the Equator was achieved in March 2011 (St. 1b–18b). An additional cruise (leg 4) was operated in August 2012 to complete the first leg that had been fragmented due to bad weather (St. 3c–7c).

A total of 47 stations with a vertical resolution of 12–16 depths between 9 m and 5930 m were sampled for dissolved cobalt analyses (DCo), and 15 stations for total (unfiltered) cobalt determinations (TCo). The apparent particulate cobalt concentrations (PCo) were calculated by subtraction of DCo from TCo. The complete data set of cobalt (dissolved, total, and apparent particulate) at all stations will be available at the international GEOTRACES data center (<http://www.bodc.ac.uk/geotrades/>).

Samples were taken using the TITAN-CTD frame of NIOZ (Netherlands), with 24 ultra-clean 24.4 L sampling bottles made of PVDF (polyvinylidene fluoride) plastic (de Baar et al., 2008). The frame was placed in a Class-100 container for sub-sampling (de Baar et al., 2008). Unfiltered samples were transferred into acid-cleaned 250 mL Nalgene™ LDPE (low-density polyethylene) bottles for

TCo analyses. The samples for DCo analyses were collected after filtration using 0.2 µm Sartobran™ 300 (Sartorius) cartridges under pure N<sub>2</sub> pressure (filtered 99.99 % N<sub>2</sub>, 0.7 atm) in acid-cleaned 250 mL or 500 mL Nalgene™ LDPE bottles. All samples were acidified at pH ~2 using ultrapure HCl (Merck) immediately after their collection. Then the acidified samples were dark-stored in double bags at ambient temperature in preparation of their analyses in the shore-based laboratory.

## 2.2 Analytical method for cobalt analyses

### 2.2.1 Method

Prior to the analyses, the samples were UV-digested (Saito and Moffet, 2002; Shelley et al., 2010) for 3 h in acid-cleaned silica tubes using a 600 W high-pressure mercury vapor lamp (Bown et al., 2011), and left for an equilibration time of 48 h. Preliminary tests indicated that 3 h of UV-digestion were required to fully recover Co in surface and deep samples (data not shown).

Dissolved and total cobalt concentrations were determined by flow-injection analysis (FIA) and chemiluminescence detection following the method adapted from Shelley et al. (2010), as described in Bown et al. (2011). In this method, cobalt catalyzes the oxidation reaction of pyrogallol with hydrogen peroxide in an alkaline solution in the presence of cetyltrimethylammonium bromide (CTAB) and methanol. A chemiluminescent emission in the visible wavelength proportional to the cobalt concentration is produced during this reaction. The system consists of one 10-port injection valve (VICI valves from VALCO instruments), which operates as an autosampler, and of two micro-electronically actuated injection valves (VICI valves from VALCO instruments) that use Tygon® tubes to inject the sample and the reagents. The flow injection is provided by a peristaltic pump (205 CA, Watson Marlow).

The reagents were prepared with trace metals quality reagents, as described in Bown et al. (2011). All reagents were prepared under a laminar flow hood (ADS Laminaire, ISO 5 class) in 1 L LDPE Nalgene® bottles with ultrapure water (MilliQ, 18.2 M) the day before the analysis and kept at room temperature for an overnight equilibration.

The sample was buffered online with ammonium acetate (0.3 M, ACS Reagents) and loaded onto an IDA-Toyopearl chelating resin to preconcentrate the cobalt contained in the sample. Then a HCl solution (0.1 M, Suprapur® Merck) was injected through the column to elute Co. The eluent was warmed in a 60 °C thermostatic bath to limit the interferences in the detection system due to bubbles (Shelley et al., 2010). The detection system consisted of a photomultiplier detector (Hamamatsu, H9319 series). The injection valves and the photomultiplier detector were operated on a laptop by a modified Labview® 8.4 interface (E. Duvelbourg and M. Boye,

LEMAR). The electrical devices were connected to a modulator of current (ELLIPSEMAX 600, MGE/UPS Systems).

The Co concentrations were calibrated against two calibration curves made with standard additions of cobalt of 0, 12.5, 25, 50, 75 and 100 pM to seawater, and performed before and after each series of 8 or 12 samples. TCo and DCo concentrations were based on triplicate analyses of each sample using the mean peak height of the chemiluminescent signal, and corrected with respect to blank analyses. Two to four reagent blanks, including the buffer blank, were analyzed per series of 8–12 samples at the beginning and at the end of the series in acidified MilliQ water instead of the sample (Bowie and Lohan, 2009; Bown et al., 2011).

The final standard deviation of the measurement was calculated by an error propagation using the error on blanks, the calibration curves and the deviation of the triplicate analyses. The paired two-tailed t test shows that the differences between TCo and DCo (e.g., equivalent to apparent particulate Co) are statistically significant at the 95 % confidence interval ( $P < 0.05$ ,  $t_{\text{critical}} = 2.84$ ,  $t_{\text{experimental}} = 12.83$ ,  $n = 203$ ), allowing reliable estimation of PCo concentration. The standard error on PCo was calculated by combining uncertainties of DCo and TCo measurements (e.g.,  $SD_{PCo} = (SD_{DCo}^2 + SD_{TCo}^2)^{0.5}$ ).

## 2.2.2 Analytical performance

The mean reagent blank (based on all blank determinations) was  $4.2 \pm 2.1$  pM ( $n = 180$ ) of Co in MilliQ ( $n = 180$ ). The limit of detection of the method estimated as three times the standard deviation of the mean reagent blank was 6.3 pM ( $n = 180$ ). Each series of samples was calibrated by running one or two samples collected during the "Sampling and Analysis of iron" (SAFe) program or GEOTRACES program. SAFe and GEOTRACES samples were UV-digested for 3 h prior to analysis and the results of DCo concentrations are reported in Table 1. The DCo concentrations we measured in the SAFe and GEOTRACES reference-samples are in excellent agreement with the consensus values (<http://www.geotraces.org/science/intercalibration/322-standards-and-reference-materials>). The DCo value obtained in the S-SAFe sample also falls in the consensus value despite the concentration being lower than the detection limit. The analytical precision of the method was determined from repeated analyses of the surface S-GEOTRACES reference sample, yielding an uncertainty of  $\pm 3.8\%$  expressed as relative standard deviation on the mean ( $n = 15$ ).

## 2.3 Hydrography

Hydrological parameters (S,  $T^*$ ,  $O_2$ , conductivity, fluorescence and turbidity) were measured using an SBE9+ underwater sensor, an SBE3+ thermometer ( $\pm 0.001^\circ\text{C}$ ), an SBE4 conductivity sensor ( $\pm 0.3 \text{ mS s}^{-1}$ ), an SBE43 dissolved oxygen sensor ( $\pm 2\%$ ), a Chelsea Aquatracka MKIII

**Table 1.** Comparison of dissolved cobalt analyses obtained in the UV-oxidized samples by the FIA-chemiluminescence method used in the present study with consensus values reported by the Sampling and Analysis of iron (SAFe) and GEOTRACES programs. Water samples provided by SAFe and GEOTRACES from surface waters (SAFe S and GEOTRACES S) and deep waters (SAFe D1 and D2, and GEOTRACES D) were analyzed. Errors are given as standard deviation from average values.

Sample	D Co measured (pM)	Consensus value (pM)
SAFe S	$5.1 \pm 2.2$ ( $n = 25$ )	$4.8 \pm 1.20$
SAFe D1	$42.3 \pm 1.4$ ( $n = 15$ )	$45.4 \pm 4.7$
SAFe D2	$44.2 \pm 1.7$ ( $n = 25$ )	$45.7 \pm 2.9$
GEOTRACES S	$29.8 \pm 2$ ( $n = 35$ )	$31.8 \pm 1.1$
GEOTRACES D	$63.2 \pm 2.3$ ( $n = 25$ )	$65.2 \pm 1.2$

fluorometer ( $\pm 0.2 \mu\text{g l}^{-1}$ ), and a Wetlabs C-Star transmissometer ( $\pm 0.02\% ^\circ\text{C}^{-1}$ ; 25 cm, deep, red).

## 2.4 Macronutrients analysis

Nutrient samples were collected in 125 mL polypropylene bottles using a CTD-rosette (Seabird®) equipped with Niskin bottles. The analyses were performed on board from surface to deep waters samples. All the nutrients were analyzed by colorimetric methods, following the methods of Murphy and Riley (1962) for phosphate ( $\text{HPO}_4^{2-}$ ), of Strickland and Parsons (1968) for silicate ( $\text{Si(OH)}_4^-$ ), and of Grasshoff et al. (1983) for nitrate ( $\text{NO}_3^-$ ) and nitrite ( $\text{NO}_2^-$ ).

## 3 Results

### 3.1 Circulation and dynamic structures

In the North Atlantic, the section crosses the subarctic gyre (SAG) between  $64^\circ\text{N}$  and  $50^\circ\text{N}$ , where the Labrador Sea Water (LSW) dives to form with the Arctic Bottom Water, the Western North Atlantic Deep Water (WNADW). Deeper, the Eastern North Atlantic Deep Water (ENADW) is also isolated in the SAG and forms, further south, with the WNADW the North Atlantic Deep Water (NADW) (Fig. 2). The well-oxygenated and dense waters of the subarctic gyre are separated, in the south, from relatively low-oxygenated, saline and warm waters of the North Atlantic subtropical gyre (NASG) by the North Atlantic subtropical front (NSTF) at  $\sim 45^\circ\text{N}$ . The NSTF is characterized by a high anomaly of temperature ( $+5^\circ\text{C}$ ) and by a strong eastward geostrophic current in surface waters (data not shown) which is likely to be the North Atlantic Drift (Reid, 1994).

In the NASG, low-density waters occur in the top 600 m due to relatively high salinity and temperature ( $T^* > 10^\circ\text{C}$ ;  $S > 35$ ) (Fig. 2). However, at  $15^\circ\text{N}$  and, to a lesser extent, at  $4^\circ\text{N}$  these saline waters are covered by relatively fresh

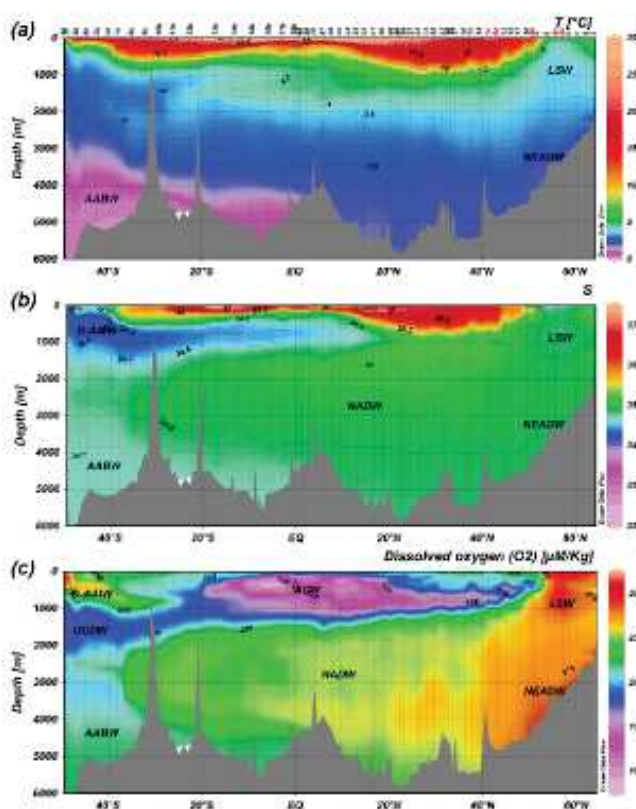


**Fig. 2.** Interpolated vertical sections of (a) temperature ( $T$ ), (b) salinity ( $S$ ) and (c) dissolved oxygen ( $O_2$ ) along the GEOTRACES-A02 section in the western Atlantic, based on CTD data. The different water masses – LSW, NEADW, NADW, ACW, AABW, D-AAIW and UCDW – are identified by their physical features and are indicated in the figure panels. Stations sampled during leg 4 are labeled in red.

waters (Fig. 2) originating from the Amazon plume. The waters influenced by the Amazon plume are characterized by a relatively high Si : N ratio and turbidity (data not shown).

Leaving the NASG southwards, the section enters into the equatorial area (EA). Here, the zonal geostrophic velocities indicate the presence of several jets near the surface, such as the North Equatorial Current (NEC, at 5–10° N), the North Equatorial Countercurrent (NECC, at ~3° N), the South Equatorial Current (SEC, at 5–10° S) and the South Equatorial Undercurrent (SEUC, at ~5° S, 200 m depth), as described by Peterson and Stramma (1991). The equatorial domain is bordered by the NEC in the north and by the SEC in the south, both of which are characterized by westward surface geostrophic propagating vectors of correlating speeds (respectively 0.2 and 0.15 m s<sup>-1</sup>). Below 100 m, the salinities and temperatures are lower than in the NASG, revealing denser waters. An oxygen minimum zone (OMZ;  $O_2 < 150 \mu\text{M}$ ) was also observed under these surface currents, between 150 and 600 m (Fig. 2c). Part of this low  $O_2$  signature was due to the advection of the poor-oxygenated

Atlantic Central Waters ( $O_2 < 50 \mu\text{M}$ ; Noble et al., 2012), flowing westward from the African border across the Atlantic basin.

Southward, the section enters into the South Atlantic subtropical gyre (SASG) characterized, like in the North Atlantic, by low-density waters associated with relatively high salinities and temperatures (Fig. 2a and b). Despite strong eddy activity in this area, clearly observed in the geostrophic current field, the Malvinas–Brazil confluence (MBC), an eastward jet resulting from the Brazil current flowing southward and the Malvinas current flowing northward, can be located in the Argentine basin around 40° S (e.g., at station 6b; data not shown). The MBC separates the SASG with saline and relative oxygen-poor waters from the subantarctic waters (SAW).

Several water masses involved in the large-scale ocean circulation were characterized by depth (Fig. 2). For instance, the LSW was characterized by  $34.9 < S > 34.8$  and  $O_2 > 275 \mu\text{mol kg}^{-1}$  in the subarctic gyre at 60° N (Fig. 2). The ENADW ( $S > 34.925$ ) circulates underneath the LSW, following the topography below 2500 m in the northern side of the section. The core of the ENADW is situated between 62° N and 45° N. The WNADW and the ENADW both form the NADW, spreading southward into the deep ocean from 60° N to 37° S (Tomczak and Godfrey, 2003). The Antarctic Bottom Water (AABW), characterized by  $S < 34.8$  and  $T^* < 1^\circ\text{C}$ , is formed in the Weddell Sea (Reid, 1989; Gladyshev et al., 2008) and spreads at the bottom of the ocean below 4000 m. The AABW enters the Atlantic Ocean by the south and follows the topography until 3° N. To the north the bottom waters are a mix between AABW, Arctic Bottom Waters (ABW) and NADW (Tomczak and Godfrey, 2003). In the Southern Hemisphere, the relatively fresh Antarctic Intermediate Waters entering from the Drake Passage (D-AAIW;  $S > 34.2$ ) are identified at intermediate depths between 500 and 1000 m. Finally, the oxygen distribution enables us to distinguish the different components of the Circumpolar Deep Waters (CDW; Whitworth and Nowlin, 1987), with its upper component (UCDW) at about 1500 m, marked by  $O_2 < 190 \mu\text{mol kg}^{-1}$ , and its intermediate component (ICDW) at about 2500 m with  $O_2 > 210 \mu\text{mol kg}^{-1}$  (Fig. 2c). The intermediate waters in the equatorial domain are formed by a mix of AAIW and UCDW that both flow northward and of the Atlantic Central Waters (ACW) originated from the east Atlantic basin (Poole and Tomczak, 1999). However, it has to be noted that the transitions between the different water masses vary with the latitude (Fig. 2).

### 3.2 The nutrients distribution along the GEOTRACES-A02 section

Different biogeochemical domains were characterized in surface waters along the GEOTRACES-A02 section (Fig. 3). The surface waters of the SAG were marked by relatively

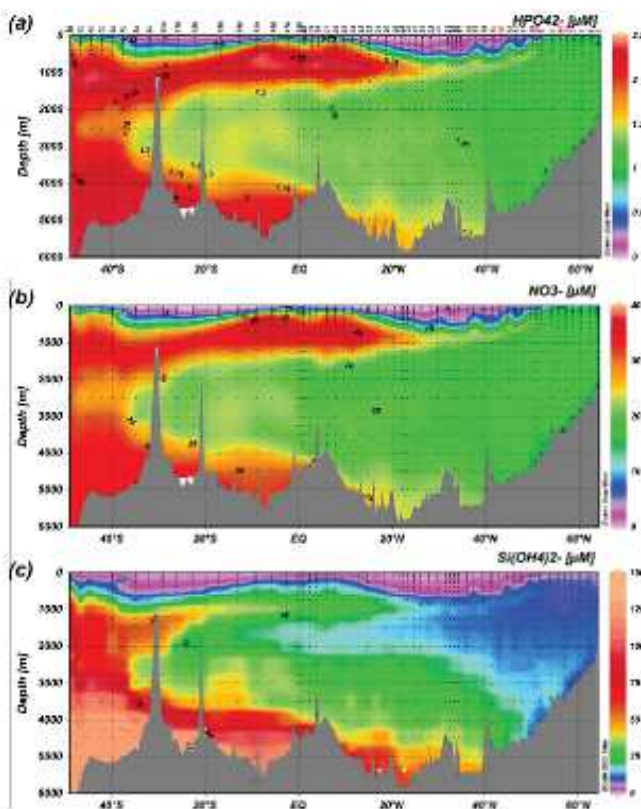


**Fig. 3.** Interpolated vertical sections of (a) phosphate, (b) nitrate and (c) silicate based on 1440 analysis of water-column samples collected and measured by NIOZ along the Netherlands area of GEOTRACES-A02 section. Stations sampled during leg 4 are labeled in red.

high phosphate and nitrate concentrations ( $\text{NO}_3 > 10 \mu\text{M}$ ;  $\text{PO}_4 > 0.8 \mu\text{M}$ ; Fig. 3). In the two subtropical domains, the extremely low nutrients concentrations (such as observed in the NASG where  $\text{PO}_4 < 0.5 \mu\text{M}$ ,  $\text{NO}_3 < 5 \mu\text{M}$ ,  $\text{Si} < 5 \mu\text{M}$ ) were characteristic of oligotrophic conditions. However, a greater depletion of nitrogen relative to phosphate was observed in the upper 300 m of the SASG ( $\text{N:P} < 10$ ) compared to the NASG ( $\text{N:P} > 25$ ), probably due to a greater proportion of  $\text{N}_2$  fixers, such as diazotrophic cyanobacteria, in the NASG than in the SASG (Mather et al., 2008). In the equatorial area, the intermediate waters were characterized by relatively high concentrations of nitrate and phosphate ( $\text{NO}_3 > 34 \mu\text{M}$ ,  $\text{PO}_4 > 2.3 \mu\text{M}$ ), whereas silicate concentrations were low ( $5 \mu\text{M} < \text{Si} < 15 \mu\text{M}$ ), suggesting the incursion of D-AAIW formed in the southwestern Atlantic. South of the south subtropical front, the nutrients distribution showed, as for oxygen, the influence of the AAIW and UCDW with relatively high nutrients concentration in the top 200 m depths ( $\text{NO}_3 > 20 \mu\text{M}$ ,  $\text{PO}_4 > 1.2 \mu\text{M}$ ). In the deep ocean the nutrients distribution reflected a combination of aging and advection of water masses (Fig. 3). The spreading of young NADW can be followed with the low-nutrients

signature ( $\text{Si} < 35 \mu\text{M}$ ;  $\text{NO}_3 < 20 \mu\text{M}$ ;  $\text{PO}_4 < 1.5 \mu\text{M}$ ). Phosphate and nitrate concentrations increased southward in the deep ocean (Fig. 3) due to mixing of Arctic waters (poor in nutrients) with nutrients-enriched Antarctic waters. The AABW was characterized by relatively high nutrients concentration ( $\text{Si} > 130 \mu\text{M}$ ;  $\text{NO}_3 > 30 \mu\text{M}$ ;  $\text{PO}_4 > 2 \mu\text{M}$ ), which decreased northward. The nutrients concentration in the Circumpolar Deep Waters was similar to those of AABW, but the concentrations in the ICDW were a little bit lower than those in the UCDW. The silicate levels are depleted in the AAIW compared to other Antarctic waters.

### 3.3 The comprehensive distribution of cobalt in the western Atlantic

The meridional and vertical distributions of DCo along the GEOTRACES-A02 section are presented in Fig. 4a. Dissolved cobalt concentrations range from  $14.72 \pm 1.43$  to  $93.27 \pm 3.31 \text{ pM}$  along the section. The lowest concentration was observed in surface waters of the SASG (e.g., at 9 m depth at St. 11b – 26° S), whereas the highest were recorded in the OMZ of the equatorial area (e.g., at St. 15b – 9° S at 290 m depth). The vertical distributions of the apparent particulate cobalt concentrations (PCo) are presented in Fig. 4b. The apparent particulate cobalt concentrations ranged from near undetectable values (e.g., the difference between unfiltered and filtered samples analyses is nearly null) to  $18.85 \pm 3.97 \text{ pM}$  (e.g., at St. 17 – 34.3° N at 5510 m depth). The PCo/DCo ratio ranged from 0.06% (St. 17; 2500 m) to 44% (St. 26, 25 m), with a mean of 7% ( $n = 192$ ).

Different vertical distributions of DCo were observed in each biogeochemical domain (Figs. 4 and 5). The distribution of DCo showed an apparent scavenged-like profile in the northern subarctic gyre (Figs. 4a–5a), with relatively higher concentrations in surface waters ( $\text{DCo}_{\text{upper } 200 \text{ m}} > 70 \text{ pM}$ ) compared to deeper waters ( $\text{DCo}_{\text{below } 2000 \text{ m}} < 60 \text{ pM}$ ). In this domain, lower surface DCo concentrations were recorded in 2012 during leg 4 (e.g.,  $42.1 \pm 2.15 \text{ pM}$  at St. 3c, and  $44.23 \pm 1.26 \text{ pM}$  at St. 4c, at 25 m depth) compared to those observed in 2010 during leg 1 (e.g., mean  $\text{DCo} = 64.56 \pm 5.25 \text{ pM}$  at 25 m ( $n = 4$ ), with a DCo maximum of  $68.2 \pm 1.08 \text{ pM}$  at St. 5). At intermediate depths (500–1000 m), the LSW was characterized by relatively high DCo concentrations ( $\text{DCo} \sim 70 \text{ pM}$ ) compared to those found in the ENADW ( $\text{DCo} \sim 55 \text{ pM}$  below 2000 m). In this domain, the apparent particulate cobalt distribution showed relative PCo maxima in the subsurface (ranging from  $5.9 \pm 1$  to  $10.4 \pm 1.96 \text{ pM}$ ), and decreasing concentrations with depth (until undetectable levels around 1500 m depth). Maxima of PCo ( $> 10 \text{ pM}$ ) were then observed near the bottom (at St. 2 and 11).

In contrast, DCo was depleted in the surface waters of the two subtropical domains and increased with depth below the nutricline, featuring a nutrient-like distribution

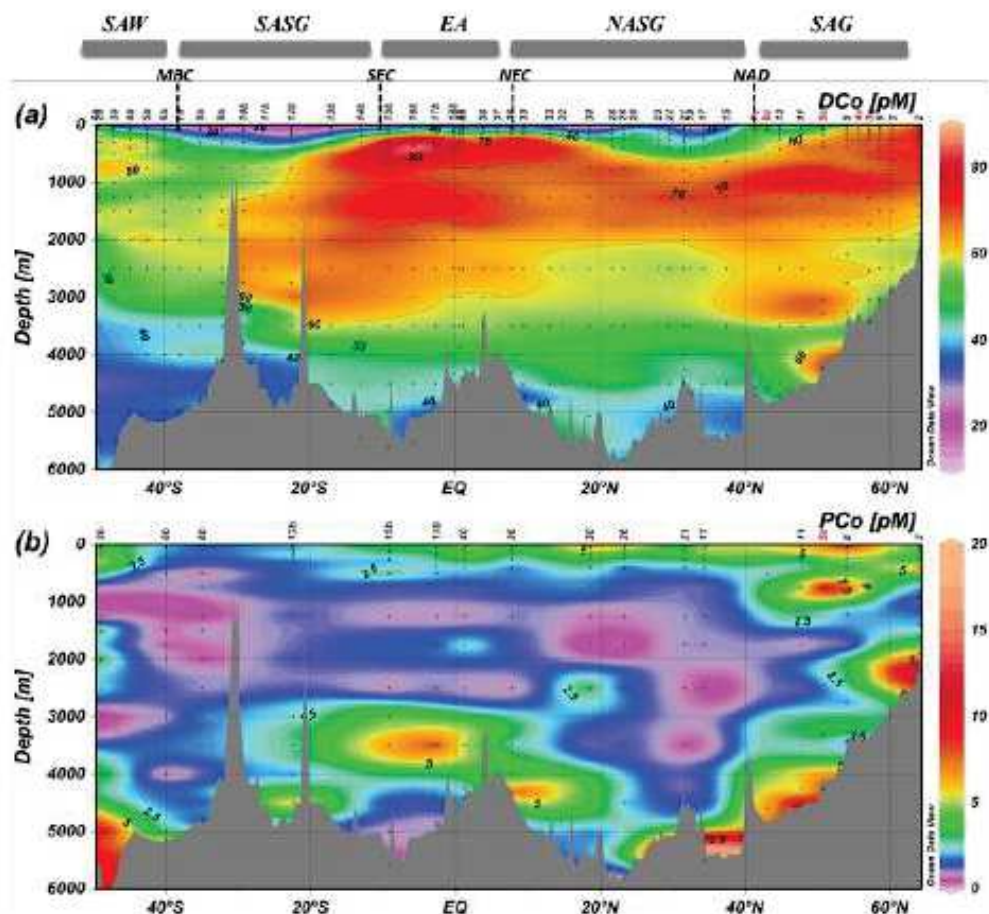


**Fig. 4.** Interpolated vertical sections of (a) dissolved cobalt ( $\text{DCo}$ , pM) and (b) apparent particulate cobalt ( $\text{PCo}$ , pM) based on 675 analyses for  $\text{DCo}$  and 203 analyses for  $\text{PCo}$  along the GEOTRACES-A02 section in the western Atlantic. Stations sampled during leg 4 are labeled in red. The domains of SAG, NASG, EA, SASG and SAW are characterized by the macronutrients concentrations and by the surface currents (e.g., NAD, NEC, SEC, and MBA).

(Figs. 4a–5b). However,  $\text{DCo}$  are slightly lower and shallower in the SASG (mean  $\text{DCo}$  value of  $23.01 \pm 4.17 \text{ pM}$ ,  $n = 9$ ) compared to those found in the NASG (mean  $\text{DCo}$  value of  $28.8 \pm 4.8 \text{ pM}$ ,  $n = 15$ ). Subsurface relative maxima of  $\text{DCo}$  were observed at about 10 m depth at a few stations in the NASG. Deep relative  $\text{DCo}$  maxima were also observed at around 1250–1750 m depth in the NASG, which are in the core of NADW and below the oxygen minima. On the contrary, relative  $\text{DCo}$  maxima and oxygen minima were often located at the same depth in the SASG, within the core of the mixed NADW. In the AABW of the SASG,  $\text{DCo}$  was on average equal to  $42.8 \pm 2.23 \text{ pM}$  ( $n = 15$ ). In the two subtropical gyres, the  $\text{PCo}$  concentrations ranged from undetectable value (e.g., at 2500 m of St. 17) to  $18.85 \pm 3.97 \text{ pM}$  (at 5510 m–34.3° N). Like in the northern latitudes, relatively high  $\text{PCo}$  concentrations were observed in the surface waters, decreasing with depth, and increasing again near the seafloor (Fig. 5e). The  $\text{PCo}$  distribution also showed, like  $\text{DCo}$ , relatively lower  $\text{PCo}$  concentrations in

the subsurface waters of the SASG (< 5 pM) compared to the NASG (> 5 pM).

In the equatorial area, the  $\text{DCo}$  distribution was characterized by low concentrations in the top 100 m (mean  $\text{DCo}_{100\text{m}} = 29.6 \pm 9 \text{ pM}$ ,  $n = 44$ ), a sharp increase between 100 and 250 m (mean  $\text{DCo}_{100-250\text{m}} = 61.7 \pm 13 \text{ pM}$ ,  $n = 10$ ), which continued to increase, reaching maximum values at about 400 m depth (mean  $\text{DCo}_{250-400\text{m}} = 73.2 \pm 10 \text{ pM}$ ,  $n = 19$ ) (Figs. 4–5c). These maximum concentrations were the highest values recorded along the section and reached values up to  $93.27 \pm 3.31 \text{ pM}$  (at 9° S). Furthermore, these  $\text{DCo}$  maxima strongly correlated with the oxygen depletion ( $\text{DCo} / \text{O}_2 = -0.28 \mu\text{M M}^{-1}, R^2 > 0.66$ ;  $n = 57$ ;  $P < 0.05$ ). Between 1000 and 2500 m depth, the  $\text{DCo}$  concentrations were in the same range as those observed at 100–250 m depths (mean  $\text{DCo}_{1000-2500\text{m}} = 67.6 \pm 5.8 \text{ pM}$ ,  $n = 33$ ). Deeper  $\text{DCo}$  concentrations decreased to a mean value of  $41 \pm 4 \text{ pM}$  ( $n = 15$ ) below 4000 m. The distribution of  $\text{PCo}$  in the equatorial domain

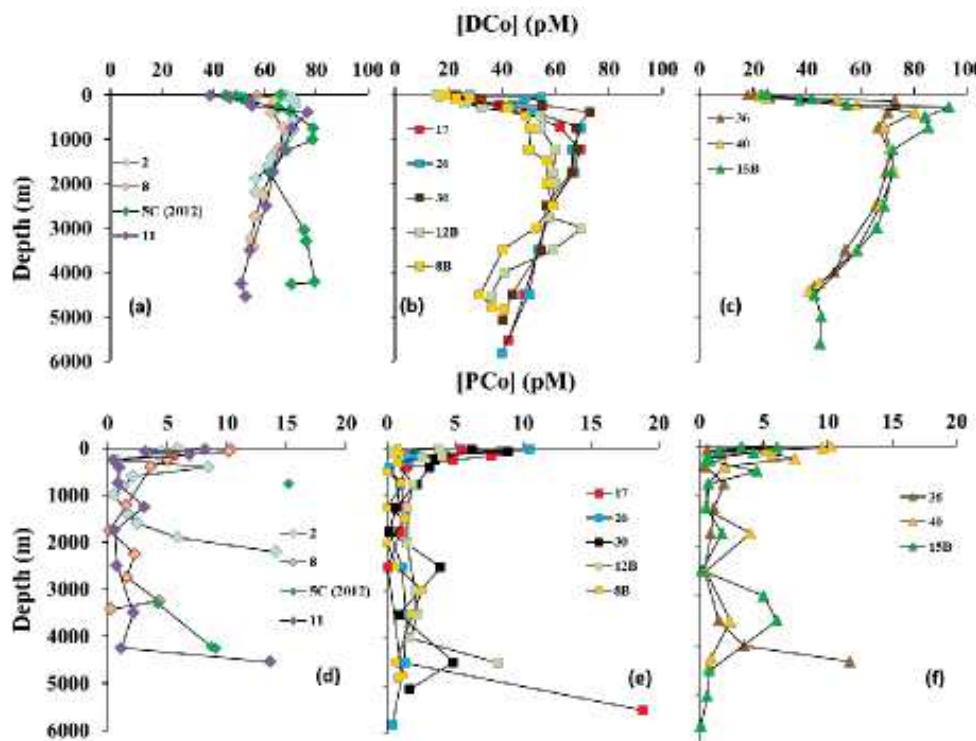


**Fig. 5.** Typical vertical distribution of dissolved (DCo) and apparent particulate (PCo) cobalt against depth in the different biogeochemical domains: in the SAG, DCo (**a**) and PCo (**d**) are shown for Station 2 ( $64^{\circ}$  N,  $34.25^{\circ}$  W), St. 8 ( $54^{\circ}$  N,  $45.84^{\circ}$  W), St. 5c ( $50^{\circ}$  N,  $44^{\circ}$  W) and St. 11 ( $48^{\circ}$  N,  $39.4^{\circ}$  W); in the north and south subtropical domains DCo (**b**) and PCo (**e**) are shown at St. 17 ( $34.3^{\circ}$  N,  $55.4^{\circ}$  W), St. 26 ( $23^{\circ}$  N,  $65.55^{\circ}$  W), St. 30 ( $18.5^{\circ}$  N,  $57.6^{\circ}$  W), St. 12b ( $22.47^{\circ}$  S,  $32.7^{\circ}$  W) and St. 8b ( $35^{\circ}$  S,  $39.4^{\circ}$  W); and in the equatorial area DCo (**c**) and PCo (**f**) are presented at St. 36 ( $7.8^{\circ}$  N,  $48.9^{\circ}$  W), St. 40 ( $1^{\circ}$  N,  $39.7^{\circ}$  W) and St. 15b ( $9^{\circ}$  S,  $28^{\circ}$  W).

was similar to that observed in the other domains, with several extremely low (undetectable) values in deep waters and relatively higher concentrations ( $\text{PCo} > 5 \text{ pM}$ ) in surface waters, up to a maximum value of  $10.24 \pm 2.1 \text{ pM}$  observed at 10 m at St. 40 ( $1.15^{\circ}$  N). A different pattern was, however, observed in the deep waters at  $8^{\circ}$  N (St. 36), where significant and increasing PCo concentrations were detected between 3500 m ( $1.52 \pm 0.7 \text{ pM}$ ) and 4315 m ( $11.73 \pm 1.9 \text{ pM}$ ), as well as at  $3^{\circ}$  S (St. 17b) where extremely high PCo concentrations were measured at 3500 m depth ( $12.53 \pm 2.4 \text{ pM}$ ). In the surface waters, high PCo concentration ( $\sim 10 \text{ pM}$ ) was detected at  $1^{\circ}$  N (St. 40) in the Amazon plume.

In the area of the Brazil–Malvinas confluence, DCo increased southward in the surface waters. The vertical distribution showed the highest DCo concentrations in the core of D-AAIW (100–600 m; Fig. 4a), whereas DCo levels decreased in deeper waters, generating an apparent scavenged-type distribution at latitudes of  $49\text{--}49.5^{\circ}$  S (St. 1b–2b). The DCo concentrations observed in the youngest AABW flowing in this area were the lowest values recorded in the core of the AABW along the section ( $\text{DCo}_{4000\text{--}6000\text{ m}} = 34.9 \pm 3 \text{ pM}$ ). Only one profile of PCo has been obtained in this area at  $49^{\circ}$  S (St. 2b). It showed relatively high PCo concentrations in the upper 300 m ( $\text{PCo} > 6 \text{ pM}$ ), and, as for

the other domains, undetectable PCo concentrations in deep-waters, except at 5000 m where PCo reached a maximum ( $11.8 \pm 3.4 \text{ pM}$ ).

## 4 Discussion

### 4.1 Comparison of data sets of dissolved cobalt concentrations obtained at three crossover stations

Three crossover stations were occupied along the GEOTRACES-A02 section, at the Bermuda Atlantic Time Series BATS station ( $64.17^{\circ}$  W,  $31.7^{\circ}$  N), at  $9^{\circ}$  S during the US CoFeMUG cruise in 2007, and at  $40^{\circ}$  S during the English GEOTRACES-A10 section in 2012 (Fig. 6).

Station BATS (St. 21) in the Sargasso Sea was occupied on 13 June 2010 during our GEOTRACES-A02 section sampling cruise. The DCo concentrations analyzed by the FIA-chemiluminescence method (this study, Fig. 6a and d; blue diamonds) are compared to those obtained by ICP-MS methods either in the same samples (Middag et al., 2014; Fig. 6a and d; yellow dots), or during other sampling cruises (Biller and Bruland, 2012; green triangles in Fig. 6a and d; Middag et al., 2014; red squares in Fig. 6a and d). All samples were

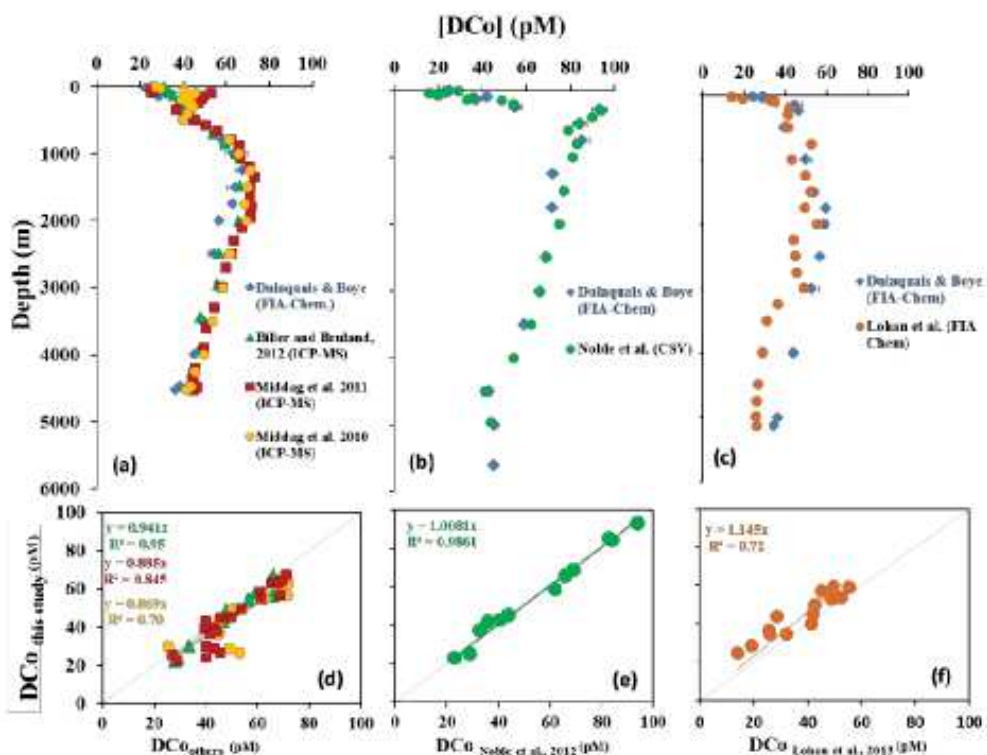


**Fig. 6.** Intercomparison of DCo data sets at the crossover station BATS (a, d) between this study (blue diamonds) and ICP-MS method by Biller and Bruland (2008) (green triangles) and by R. Middag et al. (personal communication, 2014) (yellow dots = samples from the 2010 Dutch GEOTRACES-A02 cruise; red squares = samples from the 2011 American GEOTRACES-A03 cruise); at the crossover station located at 9° S (b, e) between this study (blue diamonds) and the CSV method by Noble et al. (2012) (green dots); and at the crossover station at 40° S (c, f) between this study (blue diamonds) with FIA-chemiluminescence method by M. C. Lohan et al. (personal communication, 2014) (orange dots = samples from the 2010 English GEOTRACES-A10 cruise).

analyzed after UV treatment. In the deep waters, no significant differences were observed between the different data sets, even when samples were taken in different years. On the contrary, differences were observed in surface waters (25–200 m), with systematic higher DCo values using the ICP-MS compared to the FIA-chemiluminescence method. It is possible that seasonal variability, especially of the Co dust deposition – which widely varies in this area (Shelley et al., 2012), would cause those variations of DCo levels recorded in surface waters (Biller and Bruland, 2012; Middag et al., 2014; Fig. 6a and d; green triangles and red squares, respectively). However, further investigations are needed because differences are also observed in the same set of samples (this study; Middag et al., 2014; yellow dots in Fig. 6a and d), yielding an offset of 6–20 pM DCo in the top-100 m between the ICP-MS method and FIA-chemiluminescence analyses.

At 9° S, the DCo concentrations analyzed by FIA-chemiluminescence in the samples collected during the GEOTRACES-A02 section sampling cruise (23 March 2011, St. 15b, this study) were compared with data analyzed by cathodic stripping voltammetry after UV-treatment, but in non-acidified samples (Noble et al., 2012). Despite the fact that the two stations are not exactly at the same location and that

they were sampled in different years, the hydrography and the nutrient distributions were similar (data not shown), allowing the comparison of the DCo data sets. The comparison showed an excellent correlation ( $R^2 > 0.98$ ; Fig. 6e), suggesting that both analytical methods were in good agreement. Less temporal variability in this area due to lesser dust inputs or coastal influences potentially allowed for the good agreement when comparing the two methods at this station.

At 40° S, the two DCo data sets sampled during the GEOTRACES-A02 section cruise (10 March 2011, St. 6b, this study) and the GEOTRACES-A10 section cruise (January 2012; Lohan et al., 2014) were obtained using similar FIA-chemiluminescence methods after UV-digestion of the acidified sample. This method showed an overall good agreement between the two data sets in the upper 3000 m (Fig. 6c and f), and an offset of 8–15 pM in the deepest waters below 3000 m (Fig. 6c). The analytical methods and sample treatments were similar. However, this station was located on the Malvinas–Brazil confluence. Its position and intensity widely vary with season and with the incursion of subantarctic waters, notably of the Antarctic Intermediate Waters and Circumpolar Deep Waters. The seasonal variations can explain the differences of DCo observed at intermediate and

deeper depths between the two data sets. In the deepest waters, the difference observed in the nepheloid layer can be due to differences in the resuspension/dissolution of benthic sediments. Further investigation is needed to determine the sources of these differences.

#### 4.2 Large-scale transportation of dissolved cobalt in the western Atlantic

The behavior of DC<sub>O</sub> in the deep ocean is still poorly understood due to the lack of observations in the full water column, notably in the western Atlantic Ocean, as well as in the Indian and the central Pacific oceans. The few studies that report DC<sub>O</sub> concentrations in the deep ocean suggested a decrease of DC<sub>O</sub> levels in the deep waters from the Atlantic Ocean (80.8 pM), to the Southern Ocean (39.7 pM), and to the Pacific (28.8 pM) (Bown et al., 2011; Aparicio-Gonzalez et al., 2012). This observation has lead to the hypothesis that there is no accumulation or conservation of DC<sub>O</sub> along the thermohaline circulation, and to classify DC<sub>O</sub>, in the literature, among either the scavenged-type element like aluminium (Aparicio-Gonzalez et al., 2012) or the hybrid-type metals, those elements that have a nutrient behavior in surface waters and are strongly influenced by scavenging processes in the deep waters (Noble et al., 2008). However the scavenging of DC<sub>O</sub> invoked to interpret the deep inter-basins fractionation contrasts with DC<sub>O</sub> known to be stabilized in solution by strong complexation with organic ligands (conditional stability constant  $K_{CoL} > 10^{13}$ ) (Saito and Moffett, 2001; Saito et al., 2004, 2005, 2010; Bown et al., 2012a). On the other hand, other processes, such as mixing of water masses, have also been suggested to account for the decrease of DC<sub>O</sub> along the circulation in poor-oxygenated waters (Noble et al., 2012). We further investigated the behavior of DC<sub>O</sub> along the water-masses transportation in the deep and intermediate western Atlantic, which is conceptualized in Fig. 7.

##### 4.2.1 Transportation in bottom waters within the core of AABW

The Antarctic Bottom Waters spread northward with a transport of 3–5 Sv (where 1 Sv is equal to  $10^6 \text{ m}^3 \text{ s}^{-1}$ ) following the topography, in an opposite direction to the overlaying NADW (Tomczak and Godfrey, 2003). The mean DC<sub>O</sub> concentration in the AABW below 4000 m is  $41.75 \pm 5.3$  pM along the whole transect ( $n = 87$ ), but higher DC<sub>O</sub> levels are found in the older AABW flowing in the Northern Hemisphere than in the more recently formed AABW flowing in the Southern Hemisphere (mean values of  $44.52 \pm 4.8$  pM,  $n = 42$ ; and  $39.29 \pm 4.4$  pM,  $n = 45$ , respectively). At the same southern latitudes, DC<sub>O</sub> concentrations were similar to those reported in the core of the recently formed AABW, but in the eastern Atlantic Ocean (Bown et al., 2011; Table 2). Similar northward bottom enrichment of DC<sub>O</sub> in the core of AABW (see Supplement Fig. S1a), together with water mass

pathway and aging, has also been observed in the eastern Atlantic sector (Bown et al., 2011). Enrichment due to mixing of the AABW with the NADW in the subarctic basin is unlikely since DC<sub>O</sub> display similar concentrations in the cores of these two water masses (Table 2). Bottom enrichment due to resuspension of abyssal sediments and their dissolution during AABW transportation is more likely to account for the northward increase of DC<sub>O</sub>. Such enrichment of DC<sub>O</sub> in waters following contact with basaltic sediments has recently been highlighted in a study on the Kerguelen Plateau (Bown et al., 2012b). The significant increase of PC<sub>O</sub> observed close to the seafloor in the Northern Hemisphere (Fig. 5), rising up to 30 % of the total cobalt concentration at  $34^\circ \text{N}$ , also suggested that sediment resuspension could be significant. This is further supported by the strong signal of high dissolved aluminium concentrations observed in the bottom waters of the northern section ( $40\text{--}50^\circ \text{N}$ ) (R. Midagg, NIOZ, personal communication, 2014). Additionally, the concomitant increase of PC<sub>O</sub> and transmissometry near the seafloor (data not shown) strongly suggested benthic remobilization of cobalt. Finally, there was no record of high DC<sub>O</sub> at the bottom of the Mid-Atlantic Ridge (Fig. 4a), suggesting that hydrothermal activity may not be acting as a significant source of DC<sub>O</sub>, as previously thought (Bown et al., 2011).

##### 4.2.2 Transportation within the core of the NADW

Comparison of the DC<sub>O</sub> concentrations recorded in this study in the cores of the NEADW, NADW and D-AAIW with those reported in the southeastern Atlantic (Bown et al., 2011) shows an excellent agreement (Table 2). This comparison suggests that DC<sub>O</sub> may not be scavenged during zonal (eastward) transportation across the South Atlantic at intermediate and deep depths.

To investigate the meridional transportation of DC<sub>O</sub> across the deep western Atlantic Ocean in the core of the NADW, this water mass was characterized along its route southward with respect to its mean DC<sub>O</sub> concentrations at three different potential density anomaly, corresponding to its center ( $\sigma_0 = 27.85 \pm 0.02$ ), its upper-limit where the NADW interacts with intermediate waters (e.g.,  $\sigma_0 = 27.65 \pm 0.1$ ), and its lower-limit in contact with bottom waters (e.g.,  $\sigma_0 = 27.89 \pm 0.015$ ) (see Supplement Fig. S1b). No significant variations were observed along these isolines from the subarctic gyre to the equatorial area (e.g., DC<sub>O</sub> =  $68.7 \pm 6$  pM,  $n = 62$  at  $\sigma_0 = 27.65$ ;  $58.8 \pm 3$  pM,  $n = 19$  at  $\sigma_0 = 27.85$ ;  $56.9 \pm 7$  pM,  $n = 21$  at  $\sigma_0 = 27.89$ ), suggesting conservative behavior of DC<sub>O</sub> in the NADW. Around the Equator, DC<sub>O</sub> concentration increased at two potential densities ( $71.4 \pm 4.4$  pM,  $n = 10$  at  $\sigma_0 = 27.65$ ;  $62.6 \pm 5$  pM,  $n = 14$  at  $\sigma_0 = 27.85$ ) and decreased in the denser waters (DC<sub>O</sub> =  $51.9 \pm 8$  pM,  $n = 20$  at  $\sigma_0 = 27.89$ ). There was no variation of PC<sub>O</sub> in this area at  $\sigma_0 = 27.65$  and  $\sigma_0 = 27.85$ , and there was an increase of PC<sub>O</sub> at  $\sigma_0 = 27.89$  (by 4.6 pM), all suggesting that remineralization of PC<sub>O</sub> could not be

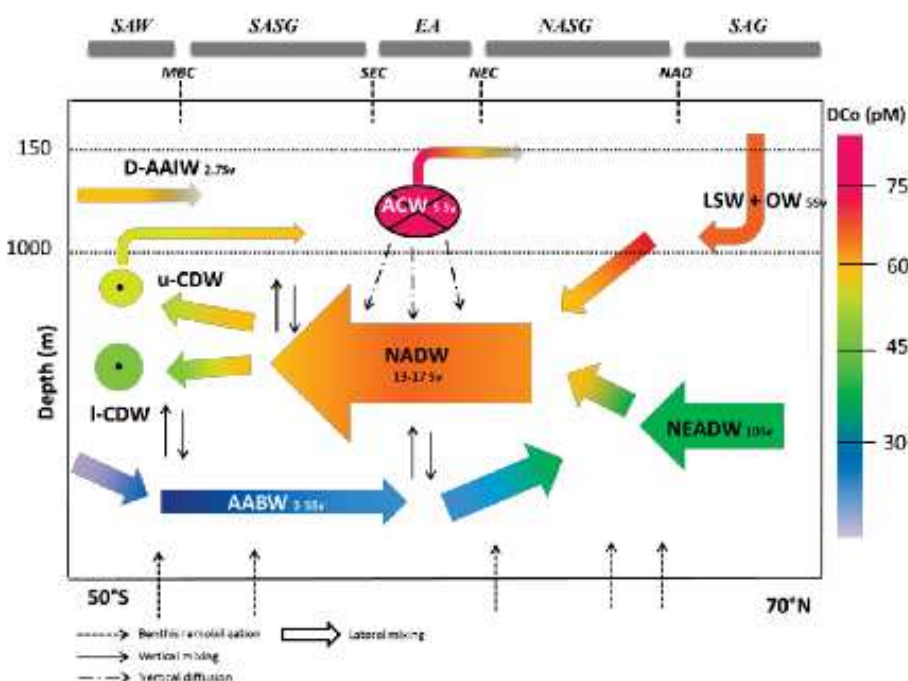


**Fig. 7.** Conceptual schema of the DCo transportation along the large-scale circulation in the intermediate and deep western Atlantic Ocean.

**Table 2.** Averaged dissolved cobalt concentration (DCo) and standard deviation (SD) obtained in the different water masses encountered along the western Atlantic GEOTRACES-A02 section: the Northeast Atlantic Deep Water (NEADW), Labrador Sea Water (LSW), North Atlantic Deep Water (NADW), Western Atlantic Central Waters (W-ACW), Northwest Antarctic Bottom Water (NW-AABW), Southwest Antarctic Bottom Water (SW-AABW), Upper Circumpolar Deep Water (UCDW) and Drake Antarctic Intermediate Water (D-AAIW).

Water mass	DCo (pM) (Others)	DCo (pM) (This study)	SD (pM) (This study)	n (This study)
NEADW	$53.9 \pm 3.3^a$	54.3	2.7	24
LSW		68.8	3.2	38
NADW	$59.2 \pm 2.05^a$ $70 \pm 11^b$	61.8	8.2	204
W-ACW	$79 \pm 11^b$	71	9	41
NW-AABW		44.52	4.8	42
SW-AABW	$40.0 \pm 2.49^a$ $42 \pm 12^b$	39.29	4.4	45
UCDW	$57.3 \pm 2.18^a$	58.7	3.9	4
D-AAIW	$55.8 \pm 3.68^a$	53.7	4.3	11

<sup>a</sup> from Bown et al. (2011). <sup>b</sup> from Noble et al. (2012).

directly related to the increases in DCo at those depths. Hence, the enrichment of DCo in the upper NADW may be more likely due to mixing with the overlaying Western Atlantic Central Waters (W-ACW), containing relatively high DCo concentrations ( $> 85$  pM).

Southward, the concentrations of DCo and PCo in the three layers were similar to those observed in the equatorial area until  $20^\circ$  S ( $\sigma_0 = 27.88$ ) or  $30^\circ$  S (along  $\sigma_0 = 27.65$  and  $\sigma_0 = 27.85$ ) (see Supplement Fig. S1b), again suggesting that DCo behaved conservatively at those southward latitudes. However, south of  $20^\circ$  S, a decrease of DCo

concentrations was observed along the three isoclines (see Supplement Fig. S1b). This decrease was more pronounced at the upper and lower limits than in the center of the NADW (e.g., the difference of concentrations between the North and the South Atlantic are  $D_{\text{Co}}\sigma_0 = 27.65 = -11.5$  pM;  $D_{\text{Co}}\sigma_0 = 27.85 = +1.5$  pM;  $D_{\text{Co}}\sigma_0 = 27.89 = -10.3$  pM). There was no variation in the PCo concentrations associated with the decreases in DCo at the three depths (Fig. 4b), again suggesting that scavenging of DCo onto particles is not likely. Mixing and dilution of the NADW with the overlaying waters (D-AAIW in the upper limit and AABW in the lower

layer) containing lower concentrations of DC<sub>O</sub> (Table 2) are thus more likely to explain the DC<sub>O</sub> decrease. Since mixing is stronger at the edges of the water masses, the center of the NADW would be less impacted by such mixing effect.

We further investigated the effect of water-masses mixing on the southward DC<sub>O</sub> gradients along the NADW by calculating the DC<sub>O</sub> concentrations resulting from the dilution of intermediate and deep water masses (Fig. 7). In the northern section, the NADW is formed by mixing 5 Sv of LSW with a mean DC<sub>O</sub> concentration of  $68.8 \pm 3.17 \text{ pM}$  ( $n = 38$ ; Table 2), with 10 Sv of NEADW with a mean DC<sub>O</sub> concentration of  $54.3 \pm 2.69 \text{ pM}$  ( $n = 24$ ; Table 2) (Tomczak and Godfrey, 2003). The resulting theoretical concentration of DC<sub>O</sub> of  $59.13 \text{ pM}$  compared perfectly with the mean DC<sub>O</sub> concentration observed in the NADW ( $61.4 \pm 7.8$ ,  $n = 204$ ; Table 2). In the equatorial area, the mixing of 15 Sv of the NADW with the 4 Sv of the W-ACW (Schmitz, 1995) leads to a theoretical DC<sub>O</sub> concentration of  $66.1 \text{ pM}$ , which is in excellent agreement with our measurements in this area ( $\text{DCo} = 65.3 \pm 7$ ,  $n = 43$ ). The slight increase observed in the DC<sub>O</sub> concentration of the NADW in this area can thus be due to mixing between the high DC<sub>O</sub> concentrations of the W-ACW and the NADW. The vertical mixing occurs through internal waves that can provide a mix of more than half of the NADW (up to 8 Sv) (Webb and Suginohara, 2001). Along the southward flow of the NADW in the Southern Hemisphere, the DC<sub>O</sub> concentrations are higher than in the north ( $\text{DCo} = 63.7 \pm 7 \text{ pM}$ ,  $n = 23$ ) until  $30^\circ \text{S}$ , beyond which a strong decrease is observed ( $\text{DCo} = 54.6 \pm 7 \text{ pM}$ ,  $n = 45$ ). Here, the penetration of the 2.7 Sv of D-AAIW (You, 2002) in the intermediate ocean, along with the 5 Sv of AABW in the deep sea (Tomczak and Godfrey, 2003), leads to a theoretical DC<sub>O</sub> concentration of  $54 \text{ pM}$  in the NADW, which is in excellent agreement with the concentration we measured in the NADW for this area ( $54.3 \pm 6.6 \text{ pM}$ ,  $n = 41$ ). Thus, mixing with overlaying water masses seems to control the concentrations of DC<sub>O</sub> along the circulation pathway of the NADW from the subarctic gyre to the south-western Atlantic, rather than scavenging processes. The lack of scavenging has previously been suggested in the central Atlantic (Noble et al., 2012) and in the Ross Sea (Saito et al., 2010). Here we further support that dissolved cobalt would behave conservatively in the deep western Atlantic Ocean along the thermohaline circulation. In turn, the apparent scavenged profile observed in the southern part of the section (SAW) resulted from the incursion of DC<sub>O</sub>-depleted waters at the bottom of the ocean (AABW) and D-AAIW in intermediate waters.

#### 4.2.3 Temporal variation in the Subarctic gyre

Resampling of the subarctic gyre after 2 years showed that the DC<sub>O</sub> concentration increased by  $20.5 \pm 5 \text{ pM}$  in the NEADW below 3000 m when comparing station 5c of leg 4 (2012) with the stations 8 and 11 of leg 1 (2010) at about  $51^\circ \text{N}$  (Fig. 4a). Integrated on the thickness of the

NEADW (1250 m), this increase corresponded to about  $25.6 \pm 6.3 \mu\text{mol m}^{-2}$ . Associated with these relatively high DC<sub>O</sub> concentrations, relatively high PC<sub>O</sub> concentrations were also observed below 3000 m depth ( $\text{PCo} > 5 \text{ pM}$ ; Figs. 4b and 5d). The transit time of the NEADW to the latitude where the increase of DC<sub>O</sub> was detected is estimated to be around 2 years (Fine et al., 2001). Two possible hypotheses could be invoked to explain this anomaly observed at this location: (i) intensive sediments input in the NEADW through resuspension and dissolution, and/or diffusive processes during its circulation above the seafloor; and (ii) strong external input of cobalt to the Arctic surface waters transferred to the deep ocean by the formation of the NADW and its transportation through the deep large scale circulation.

Considering an input of DC<sub>O</sub> from dissolution of basalt or granite rocks of  $0.054 \pm 0.014$  to  $2.00 \pm 0.22 \times 10^{-11} \text{ mol m}^{-2} \text{ d}^{-1}$  (Hausmann et al., 2009) and assuming this input would be continuous during the transit of the NEADW, the maximum cumulative input after two years of transit would be  $14.6 \text{ nmol m}^{-2}$ , which is three orders of magnitude lower than the excess observed. On the other hand, when considering a diffusive flux of Co from basalt of  $31.1 \text{ nmol m}^{-2} \text{ d}^{-1}$  estimated on the eastern Kerguelen Plateau (Bown et al., 2012a) and assuming a cumulative effect along the transportation of the water masses, the input would be  $22.7 \mu\text{mol m}^{-2}$ , in the range of the excess in DC<sub>O</sub> observed at station 5c. However, the relatively poor oxygenated waters ( $\text{O}_2 < 200 \mu\text{M}$ ) flowing along the Kerguelen eastern slope coupled to a relative high slope current ( $0.08 \text{ cm s}^{-1}$ ) could have enhanced sediment resuspension (Bown et al., 2012b) and makes the comparison with our rather well ventilated bottom waters ( $\text{O}_2 > 270 \mu\text{M}$ ) difficult. Furthermore, if sediment resuspension and dissolution would have caused the DC<sub>O</sub> anomaly, an increase in DC<sub>O</sub> along the pathway of the NEADW would be expected; however, this was not observed (Fig. 4a). Therefore, it is unlikely that the benthic input of DC<sub>O</sub> would cause the enhanced DC<sub>O</sub> concentrations that we observed in the core of the NEADW in 2012.

In April–May 2010 the Icelandic volcano Eyjafjallajökull erupted in the Arctic. The NEADW that forms in the Arctic transited for 2 years to reach the latitude where the excess of DC<sub>O</sub> was observed two years after the eruption in 2012 (Fine et al., 2002). It is thus conceivable that the DC<sub>O</sub> enrichment could be related to the input of these volcanic ashes and its advection by the NEADW. Volcanic ash emissions and subsequent deposition to the surface ocean have been reported to be a source of Co to the ocean (Froger et al., 2001). Most of the ash deposition occurred close to the vent, with 98 % of the tephra being transported less than 600–700 km from the source, and then decreasing exponentially (Gudmundsson et al., 2012). Using an ash deposition model and the mean bulk density determined by Gudmundsson et al. (2012), we estimated an ash input of  $1.68 \pm 0.7 \times 10^{14} \text{ g}$  of tephra in the first

$9 \times 10^4 \text{ km}^2$  around Iceland, where the NEADW is formed. Using this input and a cumulative release of  $8.76 \text{ nmol}$  of DCo per gram of similar Iceland tephra (calculated after 1.5 h of release from Frogner, 2001), the input of DCo is thus estimated at around  $16.3 \pm 6.3 \mu\text{mol m}^{-2}$  DCo in this area. Reported to the top 100 m, it represents an input of DCo of  $163 \pm 63 \text{ pM}$ , which is at least 1.5 and up to 2.5 times the concentration observed in upper 100 m at similar latitudes in the western subarctic gyre ( $[\text{DCo}]_{100 \text{ m}} = 67.2 \pm 2 \text{ pM}$ ), and much higher than the excess of DCo observed southward two years later ( $20.5 \pm 5 \text{ pmol}$ ). Similarly, it has been shown that the 2010 Icelandic eruption had significantly enhanced iron concentrations in surface waters of the Arctic Sea, locally increasing by a factor 2.5 the iron concentration in solution even 6 days after the ash deposition (Achterberg et al., 2013). Furthermore, the mean input of DCo we estimated from the volcanic ashes ( $16.3 \pm 6.3 \mu\text{mol m}^{-2}$ ) was in the same order of magnitude than the excess of DCo we measured two years later ( $25.6 \pm 6.3 \mu\text{mol m}^{-2}$ ). These observations strongly suggested that the volcanic eruption was a source of DCo that has been advected in the core of the NADW. Because of the quick release of Co from the ash (Frogner et al., 2001), and probably because of the short residence time of these particles in the surface waters, it is possible that most of the input of DCo occurred under the ash plume. Its advection by the NADW then enhanced the concentration of DCo far away from the eruption, similarly to the advection of DCo from continental margins (Bown et al., 2011).

#### 4.2.4 The incursion of the Atlantic Central Waters

The highest concentrations of DCo observed at intermediate depths in the equatorial area of the section were found in the core of the Atlantic Central Waters (ACW) that originate from the eastern Atlantic (Poole and Tomczak, 1999), and those DCo maxima correlated with the O<sub>2</sub> minimum (Figs. 2c, 4a and 5c). Actually, the incursion of the ACW constituted the major reservoir of DCo in the western Atlantic between the equatorial domain and the Caribbean basin (Fig. 4a). At these latitudes but in the eastern Atlantic, the O<sub>2</sub> depletion (Tomczak and Godfrey, 2003) and the DCo concentrations ( $> 150 \text{ pM}$ ; Noble et al., 2012) are even higher in the ACW compared to the western Atlantic, suggesting zonal westward transportation and decrease of DCo across the central Atlantic ocean. Reductive dissolution in the poor-oxygenated waters, resuspension of particulate matter in the sediments along the shelves of the eastern Atlantic, and remineralization processes were suspected to cause the DCo enrichment in the ACW observed in the eastern Atlantic (Noble et al., 2012). A decrease in DCo concentrations was also observed along the transit of the ACW in the eastern basin, where scavenging could not be discerned from water masses mixing (Noble et al., 2012). Once reaching our meridian section, the concentration of DCo continued to decrease

northward in the flow of the ACW (from  $93 \pm 1.3 \text{ pM}$  at 290 m, St. 15b to  $73 \pm 0.6 \text{ pM}$  at 150 m, St. 36). Accompanying these decreases, there was no significant enrichment in PCo (Figs. 4b and 5f), suggesting that scavenging was negligible compared to mixing and vertical diffusion. As discussed above, mixing processes with the NADW can contribute to the decrease in the DCo concentrations along the westward transportation of the ACW. Furthermore, using the mean decrease of  $15 \text{ nmol m}^{-3}$  of DCo concentrations integrated into the W-ACW from St. 15b ( $9^\circ \text{ S } 28^\circ \text{ W}$ ) to St. 36 ( $8^\circ \text{ N } 49^\circ \text{ W}$ ) and considering the 4 Sv introduced by the ACW in this area (Schmitz, 1995), we estimated a decrease rate of DCo of about  $5.2 \pm 0.5 \times 10^3 \text{ mol d}^{-1}$  due to the spread of the ACW northward. Reported to the surface of  $2 \times 10^6 \text{ km}^2$  occupied by the ACW between  $9^\circ \text{ S}$  and  $8^\circ \text{ N}$  in the western Atlantic, this decrease rate corresponded to  $2.6 \pm 0.25 \text{ nmol m}^{-2} \text{ d}^{-1}$ . This zonal decrease rate compared well with the one we estimated between  $10^\circ \text{ E}$  and  $30^\circ \text{ W}$  using published DCo values for the eastern area (Noble et al., 2012). Indeed, we estimated a decrease in DCo concentrations of  $56 \pm 14.8 \text{ nmol m}^{-3}$  across the central Atlantic Ocean ( $10 \times 10^6 \text{ km}^2$ ), which corresponded to a decrease rate of  $1.93 \pm 0.5 \text{ nmol m}^{-2} \text{ d}^{-1}$  when considering the ACW flow rate. In addition to dilution of the ACW, we suggest hereafter that the decreases of DCo can also be partially caused by vertical diffusion and advection of DCo to the surface waters, especially close to the equatorial currents where frontal systems and high turbulence were observed.

### 4.3 Remineralization and decoupling of the cobalt and phosphate relationship in the intermediate western Atlantic

#### 4.3.1 Remineralization of cobalt in the Atlantic Central Waters

The highest DCo concentrations recorded along the section were observed in the ACW (Fig. 4a marked by the lowest concentrations of O<sub>2</sub> (Fig. 2c)). Hence, we estimated the portion of DCo resulting from cumulative remineralization in the ACW by using the apparent oxygen utilization (AOU). The AOu represents the integrated oxygen consumption by heterotrophic bacteria in the breakdown of organic matter and it is computed as the difference between the oxygen saturation concentration, which depends on thermohaline properties (Weiss, 1970), and the observed oxygen concentration. The significant correlation between AOu and DCo recorded in these waters (Fig. 8) strongly suggests that remineralization was driving the internal cycle of cobalt in these intermediate waters. Other studies have also reported relatively high DCo concentrations in low-oxygenated waters (Saito et al., 2004; Pohl et al., 2011; Noble et al., 2012). This relationship is used to estimate the concentration of DCo due to the cumulative remineralization in the ACW ( $[\text{DCo}]_{\text{remineralization}}$ , Eq. 1), and its proportion compared

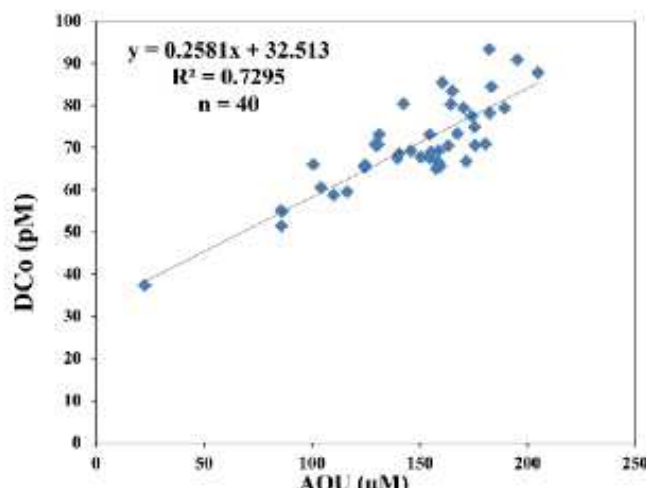


Fig. 8. Relationship among the concentrations of dissolved cobalt (DCo) and the apparent oxygen utilization (AOU) in the intermediate waters of the equatorial area (150–750 m).

to the recorded concentration of DCo (%DCo<sub>remineralized</sub>, Eq. 2), as follows:

$$[\text{DCo}]_{\text{remineralization}} = (\text{R}_{\text{Co:P}} \times \text{R}_{\text{P:O}_2} \times \text{AOU}) \quad (1)$$

$$\% \text{DCo}_{\text{remineralized}} = 100 \times [\text{DCo}]_{\text{remineralization}} / [\text{DCo}]_{\text{observed}}, \quad (2)$$

where  $\text{R}_{\text{Co:P}}$  is the stoichiometric Co : P ratio recorded in the surface waters of the equatorial area (with an average value of  $27 \times 10^{-6} \text{ M M}^{-1}$ ; Dulaquais et al., 2014), and  $\text{R}_{\text{P:O}_2}$  is the stoichiometric ratio between phosphate production and oxygen consumption (e.g.,  $\text{R}_{\text{P:O}_2} = 1/170 \text{ M M}^{-1}$ ; Matear and Hirst, 2003; Oschlies et al., 2008; Krishna-Murty et al., 2009).

The concentration of DCo due to remineralization was thus estimated at about  $23 \pm 5 \text{ pM}$  in the western ACW between 150 and 800 m, representing 32 % of the DCo measured ( $\text{DCo}_{150-800 \text{ m}} = 71 \pm 9 \text{ pM}$ ). In its layer fed by the central South Equatorial Current (CSEC, 400–800 m), the cumulative remineralized DCo could be even higher, representing up to 37 % of DCo (Table 3). If this remineralized DCo was only supplied by the transportation through the CSEC from the eastern basin, this proportion should be greater in the eastern central Atlantic where dilution with NADW does not affect this water mass yet. But we estimated a similar proportion in the eastern Atlantic (%DCo<sub>remineralized</sub> = 38 ± 5 %) by using the DCo data set of Noble et al. (2012). This result suggested that the DCo provided by remineralization in the west equatorial Atlantic is likely a combination of a westward transportation of the DCo remineralized in the eastern Atlantic basin, the cumulative remineralization along the transportation of ACW in these O<sub>2</sub> depleted waters, and the mixing between NADW and ACW across the equatorial Atlantic and in the western basin.

#### 4.3.2 Decoupling of the relationship between cobalt and phosphate

Several studies have shown that the biological utilization of DCo can be proportional to that of phosphate (P) in the surface waters of oligotrophic provinces (Saito et al., 2004, 2010; Jakuba et al., 2008; Noble et al., 2008; Bown et al., 2011). However, the lower apparent remineralization of DCo compared to P in intermediate and deep waters described by Bown et al. (2011) can suggest a decoupling between DCo and P in deeper waters. In our study, the absence of a significant correlation between DCo and P in intermediate and deep waters along the section ( $R^2 < 0.1$ ,  $n = 446$ ) further supported a decoupling between DCo and P in deep waters. Furthermore, the overall lower DCo : P ratios observed in deep waters compared to the surface (data not shown) and the increase with depth of the Co : P ratio in the particles (Sherrell and Boyle, 1992; Table 3) both suggested that the decoupling can be either due to the preferential remineralization of P relative to Co, or to the preferential scavenging of DCo. However, our measurements showed that P<sub>Co</sub> concentrations were not increasing with depth but instead they were rather decreasing (Table 3), strongly suggesting that scavenging of DCo could be negligible. Hence, we further investigated the impact of the remineralization on the decoupling between DCo and P in the equatorial area where the OMZ was located and where ACW dispatched the highest DCo concentrations recorded along the section. The proportion of P due to the cumulative remineralization (%P<sub>remineralized</sub>) was thus estimated according to

$$\% \text{P}_{\text{remineralized}} = 100 \times (\text{R}_{\text{P:O}_2} \times \text{AOU}) / [\text{P}]_{\text{observed}}. \quad (3)$$

In this area, the proportion of P and Co produced by the cumulative remineralization was estimated in the surface layer mainly impacted by the geostrophic currents (0–150 m), the upper layer of the ACW which was influenced by the North Brazil Undercurrent, the equatorial and central branches of the South Equatorial Current, all forming the North Brazil Current at these depths (150–400 m), and the lower layer of the ACW mostly fed by the CSEC (400–800 m). It is shown that the proportion of P provided by cumulative remineralization increased by a factor 7.4 between the surface layer and upper-ACW, whereas this increase was much lower for DCo (factor 1.5) (Table 3). This result suggested that the remineralization of P and DCo was not proportional in intermediate waters, and further supported the hypothesis that the preferential remineralization of P relative to DCo can largely cause the decoupling in deeper waters. Furthermore, the strongest remineralization of DCo that occurred deeper than that of P in the core of the lower-ACW (Table 3) may also lead to the decoupling between the deep cycles of DCo and P. Determination of the particles composition in Co and P would further help in understanding the processes involved in this decoupling.

**Table 3.** Mean dissolved cobalt concentration ( $D_{Co}$ ; pM), mean apparent particulate cobalt concentration ( $P_{Co}$ ; pM), and percentages of dissolved cobalt and phosphate produced by cumulative remineralization (respectively  $D_{Co_{rem}}$  and  $P_{rem}$ ; %) calculated in the surface layer (0–150 m), the upper layer of Atlantic Central Waters (150–400 m) and the lower layer of Atlantic Central Waters (400–800 m) between  $10^{\circ}$  S and  $10^{\circ}$  N (see text for definitions and calculation). The particulate ratios of  $Co:P$  ( $(Co/P)_{in\ particles}$ ;  $\mu M M^{-1}$ ) recorded in the western Atlantic (Sherrell and Boyle, 1992) are also indicated for comparison. Errors are given as standard deviation from averaged values.

Depth (m)	$D_{Co_0}$ (pM)	$P_{Co_0}$ (pM)	$D_{Co_{rem}}$ (%)	$P_{rem}$ (%)	$(Co/P)_{in\ particles}$ ( $\mu M M^{-1}$ )
0–150	$32 \pm 12$ (n = 37)	$4 \pm 3$ (n = 13)	$22 \pm 5$	$7 \pm 1$	$403 \pm 128$
150–400	$70 \pm 11$ (n = 28)	$2 \pm 2$ (n = 9)	$32 \pm 6$	$51 \pm 6$	$2718 \pm 1180$
400–800	$72 \pm 6$ (n = 19)	$2 \pm 1$ (n = 8)	$37 \pm 3$	$40 \pm 2$	$5420 \pm 2440$

#### 4.4 Physical processes impacting the distribution of dissolved cobalt in surface waters

##### 4.4.1 Lateral advection in surface waters

The lateral advection from continental margin is thought to be a source of  $D_{Co}$  in the open surface ocean (Bown et al., 2011, 2012b; Noble et al., 2012), but this source is still largely uncharacterized. Therefore, we estimated the lateral advective  $D_{Co}$  supply in the surface waters of the section ( $F D_{Co_{adv}}$ ; Eq. 4) by calculating the local geostrophic velocities ( $u, v$ ; referenced 1000 dbars) based on sea level anomalies (SLA, [www.aviso.oceanobs.com](http://www.aviso.oceanobs.com)), and using the lateral  $D_{Co}$  gradients ( $x, y$ ) integrated in the upper 150 m ( $z$ ) between two nearby stations (a, b; Eq. 5), using the following equations:

$$F D_{Co_{adv}}(a) = \text{Grad} D_{Co(x,y)} \times \text{velocity}_a \times z \quad (4)$$

$$\text{Grad} D_{Co(x,y)} = [(D_{Co_b} \int_{150\text{ m}}) - (D_{Co_a} \int_{150\text{ m}})] / d_{a-b}, \quad (5)$$

where  $D_{Co} \int_{150\text{ m}}$  is the mean  $D_{Co}$  concentration integrated over the upper 150 m at station (i);  $\text{velocity}_i$  is the lateral geostrophic velocity at station (i) integrated over the upper 150 m;  $z$  is equal to 150 m; and  $d_{a-b}$  is the distance between stations (a) and (b). A positive velocity is associated with a positive SLA and represents an advection from the considered station, and inversely for a negative velocity.

The dynamic structures with high lateral geostrophic velocities were generally observed in the frontal zones along the section (Table 4) and were associated with strong local currents (up to  $20\text{ cm s}^{-1}$ , as observed at  $5^{\circ}$  N), whereas relatively low velocities were estimated in the center of each oceanic domain ( $< 2\text{ cm s}^{-1}$ ). However, isolated events such as eddies were also identified in the center of the NASG (Table 4). The estimations of the lateral advective fluxes of  $D_{Co}$  in surface waters showed variations of more than two orders of magnitude between the different areas (Table 4). For instance, in the center of the domains like at

the station BATS, the geostrophic velocities and lateral  $D_{Co}$  gradients were smooth, resulting in negligible lateral fluxes of  $D_{Co}$  ( $-1\text{ nmol m}^{-2}\text{ d}^{-1} < F D_{Co_{adv}} < 1\text{ nmol m}^{-2}\text{ d}^{-1}$ ). On the contrary, in the frontal zones where turbulence and significant lateral  $D_{Co}$  gradients can be observed, the lateral advection fluxes of  $D_{Co}$  were relatively high in surface waters (from  $-61\text{ nmol m}^{-2}\text{ d}^{-1}$  to  $55\text{ nmol m}^{-2}\text{ d}^{-1}$ , Table 4).

The  $D_{Co}$  fluxes from lateral advection in surface waters can be important at a given station, but at the scale of a domain the impact was relatively limited, especially in the SASG. Indeed, at this scale the sum of the fluxes was low ( $-3\text{ nmol m}^{-2}\text{ d}^{-1} < F D_{Co} < 3\text{ nmol m}^{-2}\text{ d}^{-1}$ ). Nevertheless, the lateral advection within mesoscale structures, such as eddies, can be particularly important for the transportation of  $D_{Co}$  to interior basins, as it has been previously observed in the oligotrophic domain of the southeastern Atlantic where inputs of  $D_{Co}$  from continental margins were carried by Agulhas rings (Bown et al., 2011). Moreover, eddies can allow exchanges of  $D_{Co}$  between the different domains along the section, especially between the central Atlantic and the NASG through the equatorial current system, and between the SASG and the ECC through the MBC. Local turbulence associated with eddies can also induce local vertical advection (such as upwelling in the core of cyclonic eddies) as well as diffusion of  $D_{Co}$  from the intermediate waters. It has been shown that such physical processes can affect the vertical distribution of  $D_{Co}$  in surface waters (Noble et al., 2008; Shelley et al., 2012). All these direct and indirect effects make these dynamical structures sources or sinks of  $D_{Co}$  to the surface layer.

##### 4.4.2 The vertical diffusion

The vertical diffusion has been described as an important source of iron (Fe) and other nutrients to the euphotic layer, sustaining phytoplankton development in Fe-depleted areas (Law et al., 2003; Croot et al., 2005; Blain et al., 2008). In the equatorial Atlantic this internal source of Fe may be even greater than the input of Fe from Saharan dust deposition

**Table 4.** Lateral gradient of dissolved cobalt ( $\text{Grad DC}_{\text{Co}} \text{ of } 150\text{m}$ ;  $10^{-5} \text{ nmol m}^{-3} \text{ m}^{-1}$ ), and lateral advective fluxes of dissolved cobalt ( $\text{FD Co}_{\text{adv}}$ ;  $\text{nmol m}^{-2} \text{ d}^{-1}$ ) generated by local geostrophic lateral advection ( $\text{FW}_{\text{Geo}}$ ;  $\text{cm s}^{-1}$ ) are given in the upper 150 m for several sampling stations corresponding to key dynamical structures or domains.

Location	Structure	$\text{Grad DC}_{\text{Co}} \text{ of } 150\text{m}$	$\text{FW}_{\text{Geo}}$	$\text{FD Co}_{\text{adv}}$
St. 5 (37° W, 60° N)	Center of SAG	+ 0.39	- 0.23	- 0.11
St. 15 (50° W, 37.5° N)	Anti-cyclonic eddy	+ 1.37	- 9.73	- 17.28
St. 21 (BATS)	Center of NASG	- 0.39	- 0.16	0.08
St. 25 (67° W, 25° N)	Cyclonic eddy	- 0.15	+ 13.28	- 2.54
St. 36 (48.9° W, 7.8° N)	NEC	- 3.21	+ 10.03	- 41.67
Btw St. 37–38 (45° W, 5° N)	ECC	- 2.08	- 19.99	54.82
Btw St. 16b–17b (28.5° W, 5° S)	SEC	- 0.61	+ 3.92	3.19
St. 12b (32.7° W, 22.5° S)	Center S ASG	+ 0.62	+ 1.15	+ 0.92
St. 6b (42.5° W, 40° S)	MBC	- 1.58	- 7.76	15.85
Btw St. 2b–3b (48° W, 48° S)	Malvinas current	+ 0.02	- 7.54	- 0.23

(Rijkenberg et al., 2012). However, the importance of this supply for DC<sub>Co</sub> still has to be determined in the ocean. In the Southern Ocean and above the Kerguelen Islands the supply of DC<sub>Co</sub> to surface waters by vertical diffusion has been estimated to be negligible due to the small gradient in DC<sub>Co</sub> concentrations between the euphotic and mesopelagic layers caused by low biological assimilation of DC<sub>Co</sub> in these diatom-dominated waters (Bown et al., 2011, 2012b). By contrast, strong vertical gradients in DC<sub>Co</sub> concentrations between the surface and the nutricline were observed along the section in the western Atlantic Ocean, especially in the equatorial area (Fig. 5), allowing us to estimate this supply.

Briefly, the diffusion depends on the vertical gradient of DC<sub>Co</sub> concentrations, the diffusion coefficient ( $D_T$ ) and the turbulent diffusivity coefficient ( $K_z$ ). Whereas  $D_T$  is a physico-chemical property of the component within water (molecular property), the turbulent diffusivity coefficient is solely a property of the turbulent fluid. If the vertical gradient of concentrations ( $\partial \text{DCo} / \partial z$ ) is much higher than the lateral gradients ( $\partial \text{DCo} / \partial x \approx \partial \text{DCo} / \partial y$ ), the lateral diffusion is considered negligible (see Tables 4 and 5). Furthermore, the values of  $K_z$  estimated along the section (M. Rijkenberg, NIOZ, personal communication, 2013) were three to six orders of magnitude higher than  $D_T$ ; hence, the molecular diffusivity was considered negligible. The highest values of  $K_z$  were found near frontal zones (M. Rijkenberg, NIOZ, personal communication, 2013) where strong geostrophic velocities were observed. One to two orders of magnitude lower turbulent diffusivities were found in the subtropical domains, coherent with lower turbulence of the water column and lower wind stress.

The intrusion of the ACW in the southern side of the equatorial area and its northward flow along the coast of South America through the Guyana and Caribbean Currents (Poole and Tomczak, 1999) transported relatively high DC<sub>Co</sub> within the mesopelagic layer and at the bottom of the euphotic layer (100–250 m) between 10° S and 10° N (Fig. 4a). Due

**Table 5.** Vertical dissolved cobalt gradient ( $\text{DCo} / z \text{ of } 100\text{--}300\text{m}$ ;  $10^{-5} \text{ nmol m}^{-3} \text{ m}^{-1}$ ), mean  $K_z \text{ of } 100\text{--}300\text{m}$  ( $\text{cm}^2 \text{ s}^{-1}$ ) and vertical dissolved cobalt fluxes from the mesopelagic layer to the euphotic layer ( $\text{FD Co}_{\text{vertical diff}}$ ;  $10^{-5} \text{ nmol m}^{-2} \text{ d}^{-1}$ ) at few stations representative of the different areas crossed along the section (see text for the details of the calculations).

Location	$\text{DCo} / z \text{ of } 100\text{--}300\text{m}$	$z$	$\text{FD Co}_{\text{vertical diff}}$
St. 15 (50° W; 37.5° N)	0.115	7.03	+ 6.96
St. 21 (BATS)	0.069	0.08	+ 0.05
St. 26 (65.5° W; 23.3° N)	0.121	0.07	+ 0.07
St. 36 (48.9° W; 7.8° N)	0.291	2.44	+ 6.13
St. 15b (28° W; 9° S)	0.305	1.23	+ 3.16
St. 12b (32.7° W; 22.5° S)	0.062	0.11	+ 0.06
St. 6b (42.5° W; 40° S)	0.084	3.72	+ 2.69

to relatively high DC<sub>Co</sub> assimilation in surface waters at these latitudes (Dulaquais et al., 2014), strong DC<sub>Co</sub> vertical gradients were generated between the surface and intermediate waters (Figs. 4a and 5). For instance, the DC<sub>Co</sub> vertical gradient can be as high as  $0.31 \text{ nmol m}^{-3} \text{ m}^{-1}$  in the equatorial area at 9° S. By contrast, the vertical gradients are generally smooth in the subtropical domains and in the subarctic gyre ( $< 0.07 \text{ nmol m}^{-3} \text{ m}^{-1}$ ). Combining the vertical gradients with the  $K_z$  pattern, it is obvious that the vertical diffusion DC<sub>Co</sub> supply was expected to be higher in the frontal zones of the equatorial area than in the other domains. To further assess the role of the vertical diffusion on the distribution of DC<sub>Co</sub> in surface waters, we estimated the DC<sub>Co</sub> vertical diffusion flux ( $\text{FD Co}_{\text{diffusion}}$ ) in the different domains using the following equation:

$$\text{FD Co}_{\text{diffusion}} = - (K_z + D_T) \times (\partial \text{DCo} / \partial z) \quad (6)$$

with  $10^3 < (K_z / D_T) < 10^6$ .

The DC<sub>Co</sub> supply to the euphotic layer by vertical diffusion (Table 5) varies by two orders of magnitude between the frontal zones (e.g.,  $7 \text{ nmol m}^{-2} \text{ d}^{-1}$  in the north subtropical

frontal zone) and the center of the subtropical domains (e.g.,  $> 0.07 \text{ nmol m}^{-2} \text{ d}^{-1}$  in the oligotrophic domains). In the frontal systems, the highest turbulence (Table 5) combined with a significant vertical gradient of DC<sub>O</sub> concentrations caused high vertical diffusion fluxes of DC<sub>O</sub> into the surface waters. In the equatorial area the high diffusive input of DC<sub>O</sub> was mainly due to high vertical gradients of DC<sub>O</sub> induced by the incursion of the eastern south ACW enriched in DC<sub>O</sub>. This input may well sustain the growth of the cyanobacteria present in the equatorial domain towards 15° N (Tovar-Sánchez et al., 2006). By contrast, this input kept relatively low in the oligotrophic domains mainly due to lower turbulent fluids. Therefore, the vertical diffusion did not appear to be the dominant flux to sustain the cyanobacteria population in the oligotrophic domains of the western Atlantic. However, in these subtropical areas, eddies that locally increase the turbulence and thus vertical advection/diffusion (Noble et al., 2008) added to external sources such as dust deposition or rivers discharge (Tovar-Sánchez et al., 2006; Dulaquais et al., 2014) may rather be invoked than isopycnal diffusion to respond to the absolute requirement of the dominant cyanobacteria for cobalt (Saito and Moffett, 2001).

## 5 Conclusions

Large-scale observation of the deep distribution of dissolved cobalt as first assessed in this work allowed to further understand the role of physical and remineralization processes in the deep cycle of cobalt. In deep waters, DC<sub>O</sub> behaves conservatively along water masses transportation through the western Atlantic. Mixing and dilution of deep water masses, rather than scavenging of DC<sub>O</sub> onto settling particles, generate the meridional decrease of DC<sub>O</sub> along the southward large-scale circulation in the deep western Atlantic. This finding contrasted with previous interpretations which suggested that DC<sub>O</sub> is scavenged along the thermohaline circulation explaining the deep inter-basins fractionation (Bruland and Lohan, 2003). In addition, the conservative behavior of DC<sub>O</sub> allowed the persistence of relatively high concentrations in the core of the LSW and low concentrations in the underlaying AABW, hence generating the apparent scavenged profile of DC<sub>O</sub> observed in the deep waters of the western Atlantic. It also allowed large-scale transportation of external cobalt sources to interior basins, such as the 2010 Icelandic volcanic eruption, which was depicted by relatively high DC<sub>O</sub> concentrations in the core of the NEADW at 51° S. In addition, the DC<sub>O</sub> enriched intermediate waters can act as internal inputs of DC<sub>O</sub> into the surface waters through dynamic processes. Eddies and dynamical structures such as equatorial surface jets could play a major role in the fertilization of surface water in DC<sub>O</sub> through vertical diffusion and lateral advection. The input of DC<sub>O</sub> by the vertical diffusion is particularly enhanced in the equatorial domain where the incursion of the Atlantic Central Waters at intermediate

depths that transports high DC<sub>O</sub> concentrations compared to the surface, generating a strong vertical DC<sub>O</sub> gradient. However, these processes are still poorly constrained and may act as sinks as well; further work is required to better constrain these fluxes.

Next to physical processes, reductive processes – notably those linked to the oxygenation of the water masses – also play a major role in the deep cycle of DC<sub>O</sub>. The ACW characterized by relatively low O<sub>2</sub> indeed exhibited the highest DC<sub>O</sub> concentrations encountered along the section, hence constituting the major reservoir of DC<sub>O</sub> in the western Atlantic. The relatively low oxygenation of these waters may have promoted the stabilization of DC<sub>O</sub> in the westward flow of the ACW across the Atlantic Ocean, whereas physical processes did not prevent DC<sub>O</sub> to decrease along the route of these waters due to mixing and dilution with other water masses containing less DC<sub>O</sub> and to vertical diffusion to surface waters. In addition, the significant correlation between DC<sub>O</sub> concentrations and the apparent oxygen utilization found in these waters further indicated that remineralization (abiotic and biotic) was driving the internal cycle of cobalt in these intermediate waters. The remineralization of DC<sub>O</sub> was not proportional to that of phosphate in these intermediate waters, unlike the biological uptake of both DC<sub>O</sub> and P previously reported in oligotrophic surface waters (e.g., Saito et al., 2002; Noble et al., 2008; Bown et al., 2011). This decoupling leads to an enrichment of Co relative to P in the settling particles, mainly due to the preferential remineralization of P rather than a preferential scavenging of Co. Records of truly particulate cobalt will further help in revealing the role of particles in the deep cycle of cobalt.

Supplementary material related to this article is available online at <http://www.biogeosciences.net/11/1561/2014/bg-11-1561-2014-supplement.pdf>.

**Acknowledgements.** We are indebted to the captains, officers and crew members of the R/V *Pelagia* and RRS *James Cook*: without their exceptional support, this large ocean section would not have been possible. We are most grateful to H. J. W. de Baar, the Coordinator of the Dutch Project, and to Loes Gerrings and Micha Rijkenberg, the Chief Scientists of the cruises. We warmly thank Jan van Ooijen, K. Balken, E. van Weerlee, S. Ossebaar for the analyses of nutrients, as well as S. Ober, Martin Laan, Steven van Heuven, S. Asjes and L. Wuis for providing high quality CTD data. This investigation was supported by the GEOTRACES-GEOS ECS revisited in the western Atlantic project coordinated by Marie Boye and funded by the French LEFE-CYBER National Program of the Institut National des Sciences de l'Univers (INSU). We also acknowledge the European COST Action ES801 for funding a Short Term Scientific Mission to Gabriel Dulaquais to join the last cruise. The Université de Bretagne Occidentale (UBO) and the Région Bretagne are supporting the PhD fellowship of G. Dulaquais. This

investigation is a contribution to the international GEOTRACES program. The two referees, Johann Bown and Abigail Noble, are warmly acknowledged for their constructive remarks, which improved the manuscript.

Edited by: G. Herndl

## References

- Achterberg, E. P., Mark Moore, C., Henson, S. A., Steigenberger, S., Stohl, A., Eckhardt, S., Avendano, L. C., Cassidy, M., Hembury, D., Klar, J. K., Lucas, M. I., Macey, A. I., Marsay, C. M., and Ryan-Keogh, T. J.: Natural iron fertilization by the Eyjafjallajökull volcanic eruption, *Geophys. Res. Lett.*, 40, 921–926, 2013.
- Aparicio-Gonzalez A., Duarte C. M., Tovar-Sánchez A.: Trace metals in deep ocean waters: A review, *J. Mar. Systems*, 100, 26–33, 2012.
- Biller, D. V. and Bruland, K. W.: Analysis of Mn, Fe, Co, Ni, Cu, Zn, Cd, and Pb in seawater using the Nobias-chelate PA1 resin and magnetic sector inductively coupled plasma mass spectrometry (ICP-MS), *Mar. Chem.*, 130–131, 12–20, 2012.
- Blain, S., Quéguiner, B., Armand, L., Belviso, S., Bomblé, B., Bopp, L., Bowie, A., Brunet, C., Brussaard, C., Carlotti, F., Christaki, U., Corbière, A., Durand, I., Ebersbach, F., Fuda, J.-L., García, N., Gerringa, L., Griffiths, B., Guiguer, C., Guillerm, C., Jacquet, S., Jeandel, C., Laan, P., Lefèvre, D., Lo Monaco, C., Malits, A., Mossner, J., Obernosterer, I., Park, Y.-H., Picheral, M., Pondaven, P., Remenyi, T., Sandroni, V., Sarthou, G., Savoye, N., Scouarnec, L., Souhaut, M., Thiviller, D., Timmermans, K., Trull, T., Uitz, J., van Beek, P., Veldhuis, M., Vincent, D., Viollier, E., Vong, L., and Wagener, T.: Effect of natural iron fertilization on carbon sequestration in the Southern Ocean, *Nature*, 446, 1070–1074, 2007.
- Bowie, A. R. and Lohan, M. C.: Analysis of iron in seawater, in: *Practical Guidelines for the Analysis of Seawater*, edited by: Wurl, O., chapter 12, 235–257, Taylor and Francis, Boca Raton, Fla., ISBN:978-1-4200-7306-5, 2009.
- Bown, J., Boye, M., Baker, A., Duvieilbourg, E., Lacan, F., Le Moigne, F., Planchon, F., Speich, S., and Nelson, D. M.: The biogeochemical cycle of dissolved cobalt in the Atlantic and the Southern Ocean south off the coast of South Africa, *Mar. Chem.*, 126, 193–206, doi:10.1016/j.marchem.2011.03.008, 2011.
- Bown, J., Boye, M., and Nelson, D. M.: New insights on the role of organic speciation in the biogeochemical cycle of dissolved cobalt in the southeastern Atlantic and the Southern Ocean, *Biogeosciences*, 9, 2719–2736, doi:10.5194/bg-9-2719-2012, 2012a.
- Bown, J., Boye, M., Laan, P., Bowie, A. R., Park, Y.-H., Jeandel, C., and Nelson, D. M.: Imprint of a dissolved cobalt basaltic source on the Kerguelen Plateau, *Biogeosciences*, 9, 5279–5290, doi:10.5194/bg-9-5279-2012, 2012b.
- Boyd, P. W. and Ellwood, M. J.: The biogeochemical cycle of iron in the ocean, *Nat. Geosci.*, 3, 675–682, 2010.
- Bruland, K. W. and Lohan, M. C.: The control of trace metals in seawater, in: *The Oceans and Marine Geochemistry*, Treatise on Geochemistry, Vol. 6., edited by: Elderfield, H., Elsevier, 2003.
- Cannizzaro, V., Bowie, A. R., Sax, A., Achterberg, E. P., and Worsfold, P. J.: Determination of cobalt and iron in estuarine and coastal waters using flow injection with chemiluminescence detection, *The Analyst*, 125, 51–57, 2000.
- Croot, P. L., Laan, P., Nishioka, J., Strass, V., Cisewski, B., Boye, M., Timmermans, K. R., Bellerby, R. G., Goldson, L., Nightingale, P. L., de Baar, H. J. W.: Spatial and temporal distribution of Fe (II) and H<sub>2</sub>O<sub>2</sub> during EisenEx, an open ocean mesoscale iron enrichment, *Marine Chem.*, 95, 65–88, 2005.
- De Baar, H. J. W., Timmermans, K. R., Laan, P., De Porto, H. H., Ober, S., Blom, J. J., Baldker, M. C., Schilling, J., Sarthou, G., Smit, M. G., and Klunder, M.: Titan: A new facility for ultraclean sampling of trace elements and isotopes in the deep oceans in the international GEOTRACES program, *Mar. Chem.*, 111, 4–21, 2008.
- Dulaquais G., Boye M., Middag R., Owens S., Puigcorbé V., Masqué P., Buesseler K., de Baar, H., and Carton, X.: How to constrain the biogeochemical cycle of cobalt in the surface West Atlantic Ocean?, *Global Biogeochem. Cy.*, in preparation, 2014.
- Ellwood, M. J.: Wintertime trace metal (Zn, Cu, Ni, Cd, Pb and Co) and nutrient distributions in the subantarctic zone between 40–52° S; 155–160° E., *Mar. Chem.*, 112, 107–117, 2008.
- Fine, R. A., Rhein, M., and Andrie, C.: Using a CFC effective age to estimate propagation and storage of climate anomalies in the deep western North Atlantic Ocean, *Geophys. Res. Lett.*, 29, 2227–2230, 2002.
- Fitzwater, S. E., Johnson, K. S., Gordon, R. M., Coale, K. H., and Smith, W. O.: Trace metal concentrations in the Ross Sea and their relationship with nutrients and phytoplankton growth, *Deep-Sea Res. Pt II*, 47, 3159–3179, 2000.
- Frogner, P., Gislason, S. R., and Oskarsson, N.: Fertilizing potential of volcanic ash in ocean surface water, *Geology*, 29, 487–490, 2001.
- Gislason, S. R., Hassenkam, T., Nedel, S., Bovet, N., Eiriksdottir, E. S., Alfredsson, H. A., Hem, C. P., Balogh, Z. I., Dideriksen, K., Oskarsson, N., Sigfusson, B., Larsen, G., and Stipp, S. L. S.: Characterization of Eyjafjallajökull volcanic ash particles and a protocol for rapid risk assessment, *Proc. Nat. Acad. Sci.*, 108, 7307–7312, 2011.
- Gladyshev, S., Arhan, M., Sokov, A., and Speich, S.: A hydrographic section from South Africa to the southern limit of the Antarctic Circumpolar Current at the Greenwich meridian, *Deep-Sea Res. Pt. I*, 55, 1284–1303, 2008.
- Grasshoff, K., Ehrhardt, M., and Kremling, K.: Methods of seawater analysis., Verlag Chemie GmbH, Weinheim, 419 pp., 1983.
- Gudmundsson, M. T., Thordarson, T., Höskuldsson, A., Larsen, G., Björnsson, H., Prata, F. J., Oddsson, B., Magnusson, E., Högnadóttir, T., Petersen, G. N., Hayward, C. L., Stevenson, J. A., and Jónsdóttir, I.: Ash generation and distribution from the April–May 2010 eruption of Eyjafjallajökull, Iceland, *Nature Scientific Reports*, 2, 572, doi:10.1038/srep00572, 2012.
- Hausrath, E. M., Neaman, A., and Brantley, S. L.: Elemental release rates from dissolving basalt and granite with and without organic ligands, *Am. J. Sci.*, 309, 633–660, doi:10.2475/08.2009.01, 2009.
- Jakuba, R. W., Moffett, J. W., and Dyhrman, S. T.: Evidence for the linked biogeochemical cycling of zinc, cobalt, and phosphorus in the western North Atlantic Ocean, *Global Biogeochem. Cy.*, 22, GB4012, doi: 10.1029/2007GB003119, 2008.
- Knauer, G. A., Martin, J. H., and Gordon, R. M.: Cobalt in Northeast Pacific Waters, *Nature*, 297, 49–51, 1982.

- Krishnamurthy, A., Moore, J., Mahowald, N., Luo, C., Doney, S., Lindsay, K., and Zender, C.: Impacts of increasing anthropogenic soluble iron and nitrogen deposition on ocean chemistry, *Global Biogeochem. Cy.*, 23, GB3016, doi:10.1029/2008GB003440, 2009.
- Law, C. S., Abraham, E. R., Watson, A. J., and Liddicoat, M.: Vertical diffusion and nutrient supply to the surface mixed layer of the Antarctic Circumpolar Current, *J. Geophys. Res.*, 108, 3272, doi:10.1029/2002JC001604, 2003.
- Martin, J. H., Gordon, R. M., and Fitzwater, S. E.: Iron in Antarctic waters, *Nature*, 345, 156–158, 1990.
- Martin, J. H., Fitzwater, S. E., Gordon, R. M., Hunter, C. N., and Tanner, S. J.: Iron, primary production and carbon nitrogen flux studies during the JGOFS North-Atlantic Bloom Experiment, *Deep-Sea Res. Pt. I*, 40, 115–134, 1993.
- Matear, R. and Hirst, A.: Long-term changes in dissolved oxygen concentrations in the ocean caused by protracted global warming, *Global Biogeochem. Cy.*, 17, 12427, doi:10.1029/2002GB001997, 2003.
- Mather, R., Reynolds, S., Wolff, G., Williams, R. G., Torres-Valdes, S., Woodward, E. M. S., Landolfi, A., Pan, X., Sanders, R. W., and Achterberg, E.: Phosphorus cycling in the North and South Atlantic Ocean subtropical gyres, *Nat. Geosci.*, 1, 439–443, 2008.
- Milne, A., Landing, W., Bizimis, M., and Morton, P.: Determination of Mn, Fe, Co, Ni, Cu, Zn, Cd and Pb in seawater using high resolution magnetic sector inductively coupled mass spectrometry (HR-ICP-MS), *Analyt. Chim. Acta*, 665, 200–207, 2010.
- Moffett, J. W. and Ho, J.: Oxidation of cobalt and manganese in seawater via a common microbially catalyzed pathway, *Geochim. Cosmochim. Acta*, 60, 3415–3424, 1996.
- Murphy, J. and Riley, J. P.: A modified single solution method for the determination of phosphate in natural waters, *Analyt. Chim. Acta*, 27, 31–36, 1962.
- Noble, A. E., Saito, M. A., Maiti, K., and Benitez-Nelson, C. R.: Cobalt, manganese, and iron near the Hawaiian Islands: A potential concentrating mechanism for cobalt within a cyclonic eddy and implications for the hybrid-type trace metals, *Deep-Sea Res. Pt. II*, 55, 1473–1490, doi:10.1016/j.dsr2.2008.02.010, 2008.
- Noble, A. E., Lamborg, C. H., Ohnemus, D. C., Lam, P. J., Goepfert, T. J., Measures, C. L., Frame, C. H., Casciotti, K. L., DiTullio, G. R., Jennings, J., and Saito, M. A.: Basin scale inputs of cobalt, iron, and manganese from the Benguela-Angola front to the South Atlantic Ocean, *Limnol. Oceanogr.*, 57, 989–1010, 2012.
- Oschlies, A., Schulz, K., Riebesell, U., and Schmittner, A.: Simulated 21st century's increase in oceanic suboxia by CO<sub>2</sub>-enhanced biotic carbon export, *Global Biogeochem. Cy.*, 22, GB4008, doi:10.1029/2007GB003147, 2008.
- Peterson, R. G. and Stramma, L.: Upper-level circulation in the South Atlantic Ocean, *Prog. Oceanogr.*, 26, 1–73, doi:10.1016/0079-6611(91)90006-8, 1991.
- Pohl, C., Croot, P. L., Hennings, U., Daberkow, T., Budeus, G., and von der Loeff, M. R.: Synoptic transects on the distribution of trace elements (Hg, Pb, Cd, Cu, Ni, Zn, Co, Mn, Fe, and Al) in surface waters of the Northern- and Southern East Atlantic, *J. Mar. Systems*, 84, 28–41, 2011.
- Poole, R. and Tomeczak, M.: Optimum multiparameter analysis of the water mass structure in the Atlantic Ocean thermocline, *Deep Sea Res. Pt. I*, 46, 1895–1921, 1999.
- Reid, J. L.: On the total geostrophic circulation of the South-Atlantic Ocean – flow patterns, tracers, and transports, *Progr. Oceanogr.*, 23, 149–244, 1989.
- Reid, J. L.: On the total geostrophic circulation of the North Atlantic Ocean: Flow patterns, tracers and transports, *Progr. Oceanogr.*, 33, 1–92, 1994.
- Rijkenberg, M. J. A., Steigenberger, S., Powell, C. F., van Haren, H., Patey, M. D., Baker, A. R., and Achterberg, E. P.: Fluxes and distribution of dissolved iron in the eastern (sub-) tropical North Atlantic Ocean, *Global Biogeochem. Cy.*, 26, GB3004, doi:10.1029/2011gb004264, 2012.
- Saito, M. A. and Goepfert, T. J.: Zinc–cobalt colimitation of *Phaeocystis antarctica*, *Limnol. Oceanogr.*, 53, 266–275, 2008.
- Saito, M. A. and Moffett, J. W.: Complexation of cobalt by natural organic ligands in the Sargasso Sea as determined by a new high-sensitivity electrochemical cobalt speciation method suitable for open ocean work, *Mar. Chem.*, 75, 49–68, 2001.
- Saito, M. A. and Moffett, J. W.: Temporal and spatial variability of cobalt in the Atlantic Ocean, *Geochim. Cosmochim. Acta*, 66, 1943–1953, 2002.
- Saito, M. A., Moffett, J. W., and DiTullio, G. R.: Cobalt and nickel in the Peru upwelling region: A major flux of labile cobalt utilized as a micronutrient, *Global Biogeochem. Cy.*, 18, GB4030, doi:10.1029/2003GB002216, 2004.
- Saito, M. A., Moffett, J. W., Chrisholm, S. W., and Wetherbury, J. B.: Cobalt limitation and uptake in Prochlorococcus, *Limnol. Oceanogr.*, 47, 1629–1636, 2002.
- Saito, M. A., Goepfert, T. J., Noble, A. E., Bertrand, E. M., Sedwick, P. N., and DiTullio, G. R.: A seasonal study of dissolved cobalt in the Ross Sea, Antarctica: micronutrient behavior, absence of scavenging, and relationships with Zn, Cd, and P, *Biogeosciences*, 7, 4059–4082, doi:10.5194/bg-7-4059-2010, 2010.
- Shelley, R. U., Zachhuber, B., Sedwick, P. N., Worsfold, P. J., and Lohan, M. C.: Determination of total dissolved cobalt in UV-irradiated seawater using flow injection with chemiluminescence detection, *Limnol. Oceanogr.*, 8, 352–362, doi:10.1029/2009JC005880, 2010.
- Shelley, R. U., Sedwick, P. N., Bibby, T. S., Cabedo-Sanz, P., Church, T. M., Johnson, R. J., Macey, A. L., Masay, C. M., Sholkovitz, E. R., Ussher, S. J., Worsfold, P. J., and Lohan, M. C.: Controls on dissolved cobalt in surface waters of the Sargasso Sea: Comparisons with iron and aluminum, *Global Biogeochem. Cy.*, 26, GB2020, doi:10.1029/2011GB004155, 2012.
- Sherrell, R. M. and Boyle, E. A.: The trace metal composition of suspended particles in the oceanic water column near Bermuda, *Earth Planet. Sci. Lett.*, 111, 155–174, 1992.
- Schmitz Jr., W. J.: On the interbasin-scale thermocline circulation, *Rev. Geophys.*, 33, 151–173, 1995.
- Strickland, J. D. H. and Parsons, T. R.: A practical handbook of seawater analysis, 1st Edn., Fisheries Research Board of Canada, Bulletin No 167, p. 65, 1968.
- Tomeczak, M. and Godfrey, J. S.: Regional Oceanography: an Introduction, 2nd Edn., Pergamon, Oxford, 422 pp., 2003.
- Tovar-Sánchez, A., Sanudo-Wilhelmy, S. A., Kustka, A. B., Agustí, S., Dachs, J., Hutchins, D. A., Capone, D. G., and Duarte, C. M.: Effects of dust deposition and river discharges on trace metal

- composition of *Trichodesmium spp.* in the tropical and subtropical North Atlantic Ocean, Limnol. Oceanogr., 51, 1755–1761, 2006.
- Tovar-Sánchez, A. and Sanudo-Wilhelmy, S. A.: Influence of the Amazon River on dissolved and intra-cellular metal concentrations in *Trichodesmium* colonies along the western boundary of the sub-tropical North Atlantic Ocean, Biogeosciences, 8, 217–225, doi:10.5194/bg-8-217-2011, 2011.
- Vega, M. and van den Berg, C. M. G.: Determination of cobalt in seawater by catalytic adsorptive cathodic stripping voltammetry, Anal. Chem., 69, 874–881, 1997.
- Webb, D. J. and Sugino-hara, N.: Oceanography: Vertical mixing in the ocean, Nature, 409, 6816, doi:10.1038/3505117, 2001.
- Weiss, R.: The solubility of nitrogen, oxygen, and argon in water and seawater, Deep Sea Re. Oceanogr. Abstr., 17, 721–756, 1970.
- Whitworth III, T. and Nowlin Jr, W. D.: Water masses and currents of the Southern Ocean at the Greenwich Meridian, J. Geophys. Res., 92, 6462–6476, 1987.
- Wong, G. T. F., Pai, S. C., and Chung, S. W.: Cobalt in the western Philippine Sea, Oceanologica Acta, 18, 631–638, 1995.
- You, Y.: Quantitative estimate of Antarctic Intermediate Water contributions from the Drake Passage and the southwest Indian Ocean to the South Atlantic, J. Geophys. Res., 107, 3031, doi:10.1029/2001JC000880, 2002.

# **Chapitre 3**

## **Contrasting biogeochemical cycles of cobalt in the surface western Atlantic Ocean.**





# Global Biogeochemical Cycles

## RESEARCH ARTICLE

10.1002/2014GB004903

### Key Points:

- Surface biogeochemical cycle of cobalt assessed in the western Atlantic Ocean
- Recycling sustains the biological requirement for cobalt in subtropical domains
- The atmospheric and Amazon inputs affect the cobalt distribution

### Supporting Information:

- Readme
- Table S1
- Figure S1
- Figure S2
- Text S1

### Correspondence to:

G. Dulaquais,  
gabriel.dulaquais@univ-brest.fr

### Citation:

Dulaquais, G., M. Boye, R. Middag, S. Owens, V. Puigcorbe, K. Buesseler, P. Masqué, H. J. W. de Baar, and X. Carton (2014), Contrasting biogeochemical cycles of cobalt in the surface western Atlantic Ocean, *Global Biogeochem. Cycles*, 28, doi:10.1002/2014GB004903.

Received 24 MAY 2014

Accepted 28 OCT 2014

Accepted article online 29 OCT 2014

## Contrasting biogeochemical cycles of cobalt in the surface western Atlantic Ocean

Gabriel Dulaquais<sup>1</sup>, Marie Boye<sup>1</sup>, Rob Middag<sup>2,3</sup>, Stephanis Owens<sup>4</sup>, Viena Puigcorbe<sup>5</sup>, Ken Buesseler<sup>4</sup>, Pere Masqué<sup>6,8,7</sup>, Hein J. W. de Baar<sup>2</sup>, and Xavier Carton<sup>8</sup>

<sup>1</sup>Laboratoire des Sciences de l'Environnement Marin UMR6539, Institut Universitaire Européen de la Mer, Technopôle Brest Iroise, Plouzané, France, <sup>2</sup>Department of Marine Chemistry and Geology, Royal Netherlands Institute for Sea Research, Den Burg, Netherlands, <sup>3</sup>Department of Chemistry, University of Otago, Dunedin, New Zealand, <sup>4</sup>Woods Hole Oceanographic Institution, Woods Hole, Massachusetts, USA, <sup>5</sup>Institut de Ciència i Tecnologia Ambientals and Department of Physics, Universitat Autònoma de Barcelona, Bellaterra, Spain, <sup>6</sup>Oceans Institute and School of Physics, University of Western Australia, Crawley, Western Australia, Australia, <sup>7</sup>School of Natural Sciences and Centre for Marine Ecosystems Research, Edith Cowan University, Joondalup, Western Australia, Australia, <sup>8</sup>Laboratoire de Physique des Océans, Université de Bretagne Occidentale-UFR Sciences, Brest, France

**Abstract** Dissolved cobalt (DCo; < 0.2 μm; 14 to 93 pM) and the apparent particulate cobalt (PCo; > 0.2 μm; < 1 to 15 pM) were determined in the upper water column (< 1000 m) of the western Atlantic Ocean along the GEOTRACES-A02 section (64°N to 50°S). The lowest DCo concentrations, typical of a nutrient-type distribution, were observed in surface waters of the subtropical domains. Strong linear relationships between DCo and phosphate (P) as well as meridional gradients of decreasing DCo from high latitudes were characterized and both linked to the Co biological requirement. External sources such as the Amazon and the atmospheric deposition were found to contribute significantly (> 10%) to the DCo stock of the mixed layer in the equatorial and north subtropical domains. Biotic and abiotic processes as well as the physical terms involved in the biogeochemical cycle of Co were defined and estimated. This allowed establishing the first global budget of DCo for the upper 100 m in the western Atlantic. The biological DCo uptake flux was the dominant sink along the section, as reflected by the overall nutrient-type behavior of DCo. The regeneration varied widely within the different biogeochemical domains, accounting for 10% of the DCo uptake rate in the subarctic gyre and for up to 85% in southern subtropical domain. These findings demonstrated that the regeneration is likely the prevailing source of DCo in the surface waters of the western Atlantic, except in the subpolar domains where physically driven sources can sustain the DCo biological requirement.

### 1. Introduction

Cobalt (Co) is an essential trace nutrient required as the central atom of vitamin B<sub>12</sub> (cobalamin) [Bertrand et al., 2007]. Cobalt can also substitute for zinc involved as a cofactor in the carbonic anhydrase and the alkaline phosphatase that are essential for the acquisition of inorganic carbon and dissolved organic phosphorus by phytoplankton, respectively [Lane and Morel, 2000; Gong et al., 2005]. Cobalamin is also used by bacteria and archaea for anaerobic processes such as fermentation or dehalogenation [Swanner et al., 2014, and reference therein]. Moreover, cyanobacteria like Prochlorococcus sp., which often dominate the picophytoplankton assemblage and account for a significant proportion of the primary production in oligotrophic regions, have an absolute requirement for Co [Campbell et al., 1994; Sunda and Huntsman, 1995; Saito et al., 2002]. The elemental compositions of phytoplankton also suggest that Co is an important micronutrient for the coccolithophorids, diatoms, and dinoflagellates [Ho et al., 2003].

Previous studies have reported a nutrient-type distribution of dissolved cobalt (DCo) in surface waters of oligotrophic and temperate domains [Martin et al., 1993; Saito and Moffett, 2002; Jakuba et al., 2008; Noble et al., 2008], which is related to its biological uptake by cyanobacteria [Saito et al., 2002; Saito and Moffett, 2002; Bown et al., 2011]. Other surface distribution patterns have been observed, notably a nearly conservative-type behavior in the Southern Ocean associated with a low biological uptake of DCo by the Antarctic diatoms [Bown et al., 2011].

Previous field studies have reported a correlation between DCo and the macronutrient phosphate (P) in surface waters of different biogeochemical domains, indicative of their proportional biological uptake [Saito et al., 2004;

Noble et al., 2008; Saito et al., 2010; Bown et al., 2011]. Those studies also showed that the DCo/P depletion ratio varied between the oceanic domains, potentially reflecting differences in the phytoplankton assemblage and productivity, as well as regional variations in the input of DCo (and/or P). Thus, this comprehensive survey of DCo distributions across oceanic provinces will also increase our understanding of the coupling between DCo and P in the surface waters.

Previous estimates suggested that biological uptake is the prevailing sink of DCo in oligotrophic waters [Saito et al., 2002; Bown et al., 2011]. Indeed, biological uptake can be significantly higher than other removal mechanisms of DCo from surface waters such as cooxidation with manganese through microbial oxidation [Moffett and Ho, 1996; Saito et al., 2004] or export by adsorption (scavenging) on settling particles [Bown et al., 2011]. An indirect estimate suggested that recycling of Co in surface waters due to abiotic processes, microbial loop, cell lysis, and grazing, could sustain up to 70–90% of the DCo biological uptake in the subtropics of the southeastern Atlantic [Bown et al., 2011]. However, the terms that drive the internal cycle of DCo in the upper ocean need to be better assessed, notably the regeneration flux of DCo in surface waters, considering its potential importance in the Co cycle.

Among the external sources, the deposition of dust from the Patagonian and the Sahara deserts has been shown to be an important source of Co in the surface waters of the southwestern Atlantic and the central northern Atlantic, respectively [Gaiero et al., 2003; Baker et al., 2007]. For example, the relative DCo maximum observed in subsurface waters of the Sargasso Sea has been related to significant atmospheric Co input during the late summer [Shelley et al., 2012]. In other regions, the atmospheric deposition is likely negligible, such as the southeastern Atlantic [Bown et al., 2011] and southcentral Atlantic [Noble et al., 2012]. However, there are still large uncertainties in estimates of the atmospheric deposition of Co in the surface waters, due to the limited data on the fractional solubility of Co in aerosols and on the elemental compositions of the dust that vary depending on their provenance. By taking into account some of this spatial variability, our study reassesses the atmospheric deposition of Co in the western Atlantic.

The observation of an inverse linear relationship between DCo and salinity in the northwestern Atlantic [Saito and Moffett, 2002] and the western equatorial Atlantic [Tovar-Sánchez and Sañudo-Wilhelmy, 2011] suggest that freshwater may be another external source of DCo in the surface western Atlantic. For instance, the Amazon River represents a significant source of many elements to the western equatorial Atlantic [Boyle et al., 1982]; however, its importance to DCo needs to be better constrained. Recent work has also hinted at the importance of lateral advection of water masses enriched in DCo following contact with continental margins in the southeastern Atlantic [Bown et al., 2011] and of the diffusion from intermediate waters in the frontal areas of the western Atlantic [Dulaquais et al., 2014]. With only a first, tentative budget made for the southeastern Atlantic and the Southern Ocean [Bown et al., 2011], the sources and biogeochemical cycle of Co are still poorly constrained in the surface waters.

Despite these major advances, the oceanic behavior of DCo in the surface waters is still not well understood, with little data on DCo distribution in the global ocean. In this respect, a survey along a large radial in the entire western Atlantic Ocean was considered to be an ideal scheme to observe the changes in the surface vertical distribution of DCo across contrasting biogeochemical domains. In this study we investigate the meridional distributions of DCo and the apparent particulate cobalt (PCo) in the upper 1000 m along a section in the western Atlantic Ocean. Spanning from the East coast of Greenland ( $64^{\circ}\text{N}$ ) to the Malvinas Plateau ( $50^{\circ}\text{S}$ ) the radial encountered several biogeochemical domains. Two oligotrophic subtropical areas, the equatorial zone, and the subpolar and subantarctic latitudes in the extremities of the section were crossed. The distribution of Co is discussed in the context of the biogeochemical and physical features of the domains and the external inputs from the atmosphere and the Amazon in order to determine the various sources and sinks of Co. The coupling of Co with the macronutrient P and the potentially significant role of Co regeneration in surface waters of the western Atlantic are also discussed. By parameterizing the different processes involved in the Co cycle, a tentative budget for Co in the upper 100 m is presented on the scale of the individual domains and the western Atlantic basin.

## 2. Method

### 2.1. Cruise Track and Sampling

Seawater samples were collected during four cruises along the GEOTRACES-A02 section spreading from  $64^{\circ}\text{N}$  to  $50^{\circ}\text{S}$  in the western Atlantic Ocean that were conducted between 2010 and 2012 (Figure 1). A total

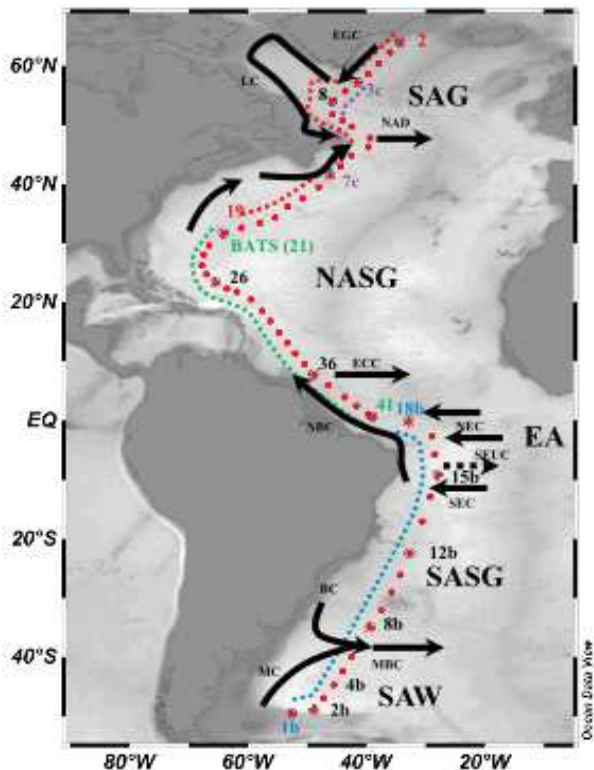


Figure 1. (a) Surface physical features and cruise track along the GEOTRACES A02 section. (b) Sampling location of the different four Legs are shown. (Leg 1 in red dashed line from station 2 to station 7c, Leg 2 in green dashed line from station 21 to station 41, Leg 3 in blue dashed line from station 1b to 18b, and Leg 4 in purple dashed line from station 3c to 7c).

0.01 M) immediately after their collection. Then the acidified samples were stored in double bags in the dark and at ambient temperature, before later analyses in the shore-based laboratory.

## 2.2. Analytical Method for Cobalt Analyses

### 2.2.1. Method

Prior to the analyses, the samples were UV digested [Saito and Moffett, 2002; Shelley et al., 2010] for 3 h in acid clean silicatubes using a 600 W high-pressure mercury vapor lamp [Bown et al., 2011; Dulaquais et al., 2014], and left for an equilibration time of 48 h. Dissolved and total cobalt concentrations were determined by Flow-Injection Analysis (FIA) and chemiluminescence detection following the method adapted from Shelley et al. [2010], as described in Bown et al. [2011] and Dulaquais et al. [2014]. The system consists of one 10-ports injection valve (MCI valves from VALCO instruments) which operates as an autosampler, and of two microelectronically actuated injection valves (VICI valves from VALCO instruments) to inject the sample and the reagents using Tygon® tubes. The flow injection is provided by a peristaltic pump (205 CA, Watson Marlow).

The reagents are prepared with trace metals quality reagents under a laminar flow hood (ADS Laminaire, International Organization for Standardization 5 class) with ultrapure water (MilliQ, 18.2 MΩ) the day before the analysis and kept at room temperature for an overnight equilibration [Dulaquais et al., 2014].

The samples were buffered online with ammonium acetate (0.3 M, American Chemical Society (ACS) Reagents), and loaded on an IDA-Toyopearl chelating resin to preconcentrate the cobalt contained in each sample. Then a HCl solution (0.1 M, Suprapur® Merck) was injected through the column to elute Co. The eluate was warmed in a 60°C thermostatic bath. The detection system consists of a photomultiplier detector (Hamamatsu, H9319 Series). The injection valves and the photomultiplier detector are operated on a laptop computer by

of 47 stations with a vertical resolution of 6–10 depths between 9 m and 1000 m were sampled for dissolved cobalt analyses (DCo), and 15 stations for total (unfiltered) cobalt determinations (TCo). The apparent particulate cobalt concentrations (PCo) were calculated by subtraction of DCo from TCo. The complete data set of cobalt (dissolved, total, and apparent particulate) at all stations is available at the international GEOTRACES data center (<http://www.bodc.ac.uk/geotrades/>).

Samples were collected using the TITAN-CTD frame [de Baar et al., 2008] of Nederlands Instituut voor Onderzoek der Zee (Netherlands), with 24 ultraclean sampling bottles of 24.4 L each made of (polyvinylidene fluoride) PVDF plastic [Rijkenberg et al., 2014]. The frame was placed in a Class-100 container for subsampling [de Baar et al., 2008]. Unfiltered samples were transferred into acid cleaned 250 ml Nalgene® Low-Density Polyethylene (LDPE) bottles for TCo analyses. The samples for DCo analyses were collected after filtration using 0.2 µm Sartobran® 300 (Sartorius) cartridges under pure N<sub>2</sub> pressure (filtered 99.99% N<sub>2</sub>, 0.7 atm) in acid cleaned 250 ml or 500 ml Nalgene® LDPE bottles. All samples were acidified using ultrapure HCl (Merck,

**Table 1.** Comparison of Dissolved Cobalt Analyses Obtained in the UV-Oxidized Samples by the FIA-Chemiluminescence Method Used in the Present Study With Consensus Values Reported by the Sampling and Analysis of Iron (SAFe) and GEOTRACES Programs

Sample	DCo Measured (pM)	Consensus Value (pM)
SAFe S	5.1 ± 2.2 (n = 25)	4.8 ± 1.2
SAFe D1	42.3 ± 1.4 (n = 15)	45.4 ± 4.7
SAFe D2	44.2 ± 1.7 (n = 25)	45.7 ± 2.9
GEOTRACES S	29.8 ± 2.0 (n = 35)	31.8 ± 1.1
GEOTRACES D	63.2 ± 2.3 (n = 25)	65.2 ± 1.2

modified Labview®8.4 interface (E. Duvieilbourg and M. Boye, Laboratoire des Sciences de l'Environnement Marin (LEMAR). The electrical devices

are connected to a modulator of current (ELIPSEM AX 600, MGE/UPS Systems).

The Co concentrations were calibrated against two calibration lines made with

standard additions of cobalt of 0, 12.5, 25, 50, 75, and 100 pM to seawater, and performed before and after each series of 8 or 12 samples. TCo and DCo concentrations are based on triplicate analyses of each sample using the mean peak height of the chemiluminescent signal, and they are corrected with respect to blank analyses. Two to four reagent blanks including the buffer blank were analyzed per series of 8–12 samples at the beginning and at the end of the series, in acidified MilliQ water instead of the sample [Bowie and Lohan, 2009; Bown et al., 2011].

The final standard deviation of the measurement is calculated by propagating the uncertainties on blanks, the calibration curves and the deviation of the triplicate analyses. A t test was applied to verify that the difference between TCo and DCo is significant to allow reliable estimation of PCo concentration. The standard error on PCo is calculated by combining uncertainties of DCo and TCo measurements ( $SD_{PCo} = (SD_{DCo}^2 + SD_{TCo}^2)^{0.5}$ ).

### 2.2.2. Analytical Performance

The mean reagent blank (based on all blank determinations) was  $4.2 \pm 2.1$  pM of Co in MilliQ ( $n = 180$ ). The limit of detection of the method estimated as three times the standard deviation of the mean reagent blank was thus 6.3 pM of Co ( $n = 180$ ). Each series of samples was validated by running samples previously collected during the Sampling and Analysis of Iron (SAFe) program or the GEOTRACES program, following the same procedure as described above. The DCo concentrations we measured in the SAFe and GEOTRACES reference samples were in excellent agreement with the consensus values (Table 1, [www.geotrades.org](http://www.geotrades.org)). The analytical precision of the method was determined from repeated analyses of the surface GEOTRACES (GS) reference sample, yielding an uncertainty of  $\pm 3.8\%$  expressed as relative standard deviation on the mean ( $n = 15$ ). Despite our agreement with the consensus values, some new concerns have recently emerged regarding possible losses of DCo due to storage protocol. Some underestimation of DCo could indeed result from storage of nonacidified samples collected in low O<sub>2</sub> and/or high-dust environments; this effect should be minor for samples from the South Atlantic and similar regions, but may be more pronounced for North Atlantic samples due to the very high dust loads (M. Saito, WHOI, personal communication, 2014). Additional work should be done to further assess this potential storage artifact, especially when the samples are acidified before storage as we have done for our samples and the GEOTRACES and SAFe reference samples.

### 2.3. Hydrography

Hydrological parameters (salinity (S), temperature (T), dissolved oxygen (O<sub>2</sub>), conductivity, fluorescence, and turbidity) were measured using a SBE9+ underwater sensor, a SBE3+ thermometer ( $\pm 0.001^\circ\text{C}$ ), a SBE4 conductivity sensor ( $\pm 0.3 \text{ mS}^{-1}$ ), a SBE43 dissolved oxygen sensor ( $\pm 2\%$ ), a Chelsea Aquatrack a MKII fluorometer ( $\pm 0.2 \mu\text{g L}^{-1}$ ), and a Wetlabs C-Star transmissometer ( $\pm 0.02\% \text{ }^\circ\text{C}^{-1}$ ).

### 2.4. Macronutrients Analysis

Seawater samples for nutrient analysis were collected the ultraclean sampling bottles (PVDF) described above and transferred to 125 ml polypropylene bottles. All the nutrients were analyzed onboard by colorimetric methods following the methods of Murphy and Riley [1962] for phosphate (PO<sub>4</sub><sup>3-</sup>), Strickland and Parsons [1968] for silicate (Si(OH)<sub>4</sub><sup>A</sup>), and Grasshoff et al. [1983] for nitrate (NO<sub>3</sub><sup>A</sup>) and nitrite (NO<sub>2</sub><sup>A</sup>). The detection limits of the methods (3σ after 24 analyses of the same sample) were 18 nM for phosphate, 252 nM for silicate, 190 nM for nitrate, and 3 nM for nitrite [van Ooijen, 2010].

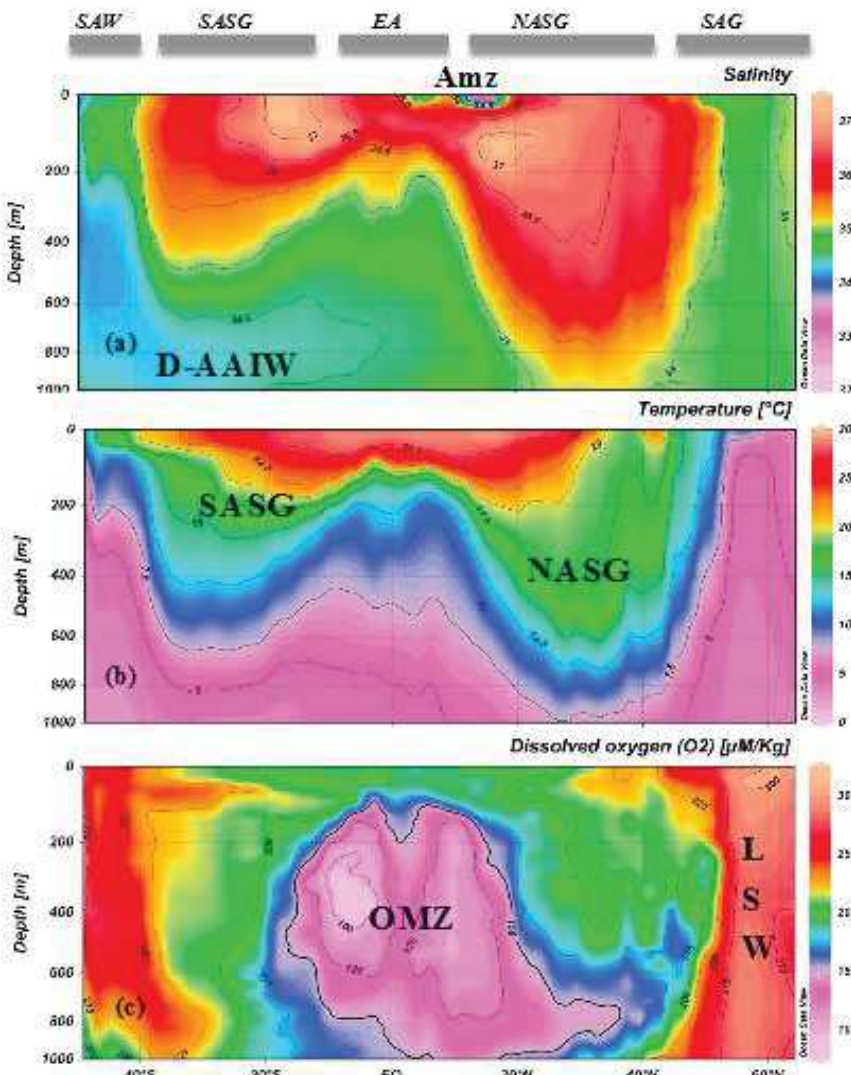


Figure 2. Interpolated vertical sections in the upper 1000 m of (a) temperature (TMP), (b) salinity (S), and (c) dissolved oxygen along the GA02 section, based on CTD data. Drake Antarctic Intermediate Waters (D-AAIW), Amazon River influence (Amz), South Atlantic Subtropical Gyre (SASG), North Atlantic Subtropical Gyre (NASG), Labrador Sea Waters (LSW) and Oxygen Minimum Zone (OMZ) are indicated.

### 3. Results

#### 3.1. Dynamical Features

The different surface physical features along the section are presented on Figure 1. In the North, the section crossed the subarctic Gyre (SAG) between 64°N and 50°N, where the Labrador Sea Water (LSW) dives to form, with the Arctic Bottom Water, the Western North Atlantic Deep Water. In this area, the surface currents (East Greenland Current and Labrador Current induce a mean southward flow. The well oxygenated and dense waters of the subarctic gyre are separated, in the south, by the North Subtropical Front (NSTF) at ~45°N from the relatively low-oxygenated, saline, and warm waters of the North Atlantic Subtropical Gyre (NASG). The NSTF is characterized by high-temperature anomaly (+5°C) and by a strong eastward geostrophic current in surface waters (data not shown), likely the North Atlantic Drift [Red, 1994], known for its important role on climate regulation [Minobe et al., 2010].

In the NASG, low-density waters occur in the top 600 m due to relatively high salinity and temperature ( $S > 35$ ,  $T > 10^{\circ}\text{C}$ ; Figure 2). However, at 15°N and to a lesser extent at 4°N these saline waters were covered

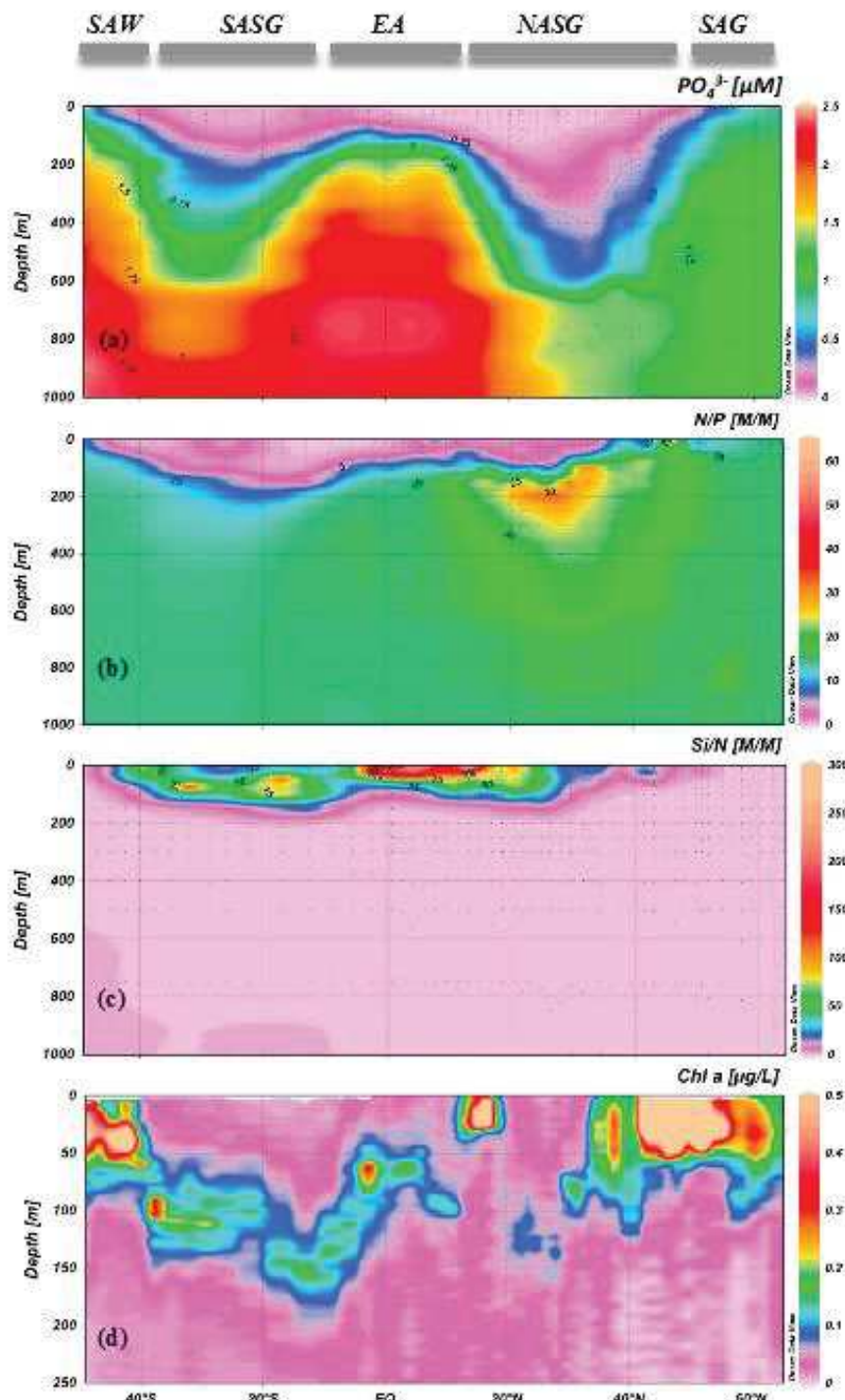


Figure 3. Interpolated vertical sections in the upper 1000 m of (a) phosphate; (b) N:P ratio; (c) Si:N ratio, based on 735 analyses of water column samples collected along the GA02 section, and (d) Chl a distribution in the upper 250 m derived from CTD data.

by relatively fresh waters (Figure 2,  $32.1 < \text{S} < 34.9$ ), originating from the Amazon plume. The waters influenced by the Amazon plume were also characterized by high Si:N ratio (Figure 3c).

Leaving the NASG southward, the section enters the equatorial area. Here the zonal geostrophic velocities (not shown) indicate the presence of several surface and subsurface jets (Figure 1). The North Equatorial

Current (NEC, at 5–10°N), the North Equatorial Countercurrent (NECC, at ~3°N; 0.2 m s<sup>-1</sup>), the South Equatorial Current (SEC, at 5–10°S) and the South Equatorial Undercurrent (SEUC, at ~5°S; 0.12 m s<sup>-1</sup> 200 m depth) [Peterson and Stramma, 1991; Stramma and England, 1999] can thus be located. The equatorial domain is bordered by the NEC in the North and by the SEC in the South, both of which were characterized by westward surface geostrophic propagating vectors and similar speed (respectively, 0.15 and 0.2 m s<sup>-1</sup>). A mean flow toward the northwest, the north Brazil current (NBC), results from these equatorial surface currents. This equatorial current system supplies eddies to the northern subtropical domain [Oschlies and Garçon, 1998]. Additionally, under these surface currents, an oxygen minimum zone (OMZ; O<sub>2</sub> < 150 μM) was also observed between 150 and 600 m (Figure 2c). Part of this low O<sub>2</sub> signature was due to the advection of the poorly oxygenated Atlantic Central Waters (O<sub>2</sub> < 50 μM) [Noble et al., 2012], flowing westward from the African shelf across the Atlantic basin.

Southward the section enters into the South Atlantic Subtropical Gyre (SASG). South of the SASG, in addition to strong eddy activity in this area as observed in the geostrophic current field, the Malvinas-Brazil confluence (MBC), an eastward jet resulting from the Brazil current (BC) flowing southward and the Malvinas Current (MC) flowing northward, can be located in the Argentine basin at around 40°S (e.g., at station 6b; geostrophic data not shown). The saline and relatively oxygen-poor waters of the MBC separate the SASG from the subantarctic Waters (SAW). At depth the Drake Antarctic intermediate waters (D-AAW) are flowing northward in the southern part of the section.

### 3.2. Biogeochemical Provinces

The different biogeochemical domains characterized along the section (Figure 3) were mostly delineated by the frontal and jet systems described above (Figure 1). The surface waters of the SAG were marked by relatively high-phosphate and nitrate concentrations (NO<sub>3</sub><sup>A</sup> > 10 μM, data not shown; PO<sub>4</sub><sup>3A</sup> > 0.8 μM). Furthermore, the Chlorophyll a levels observed in the southern side of the SAG and lower nutrients concentrations (e.g., Chl a = 1.9 μg L<sup>-1</sup>, NO<sub>3</sub><sup>A</sup> < 1 μM, PO<sub>4</sub><sup>3A</sup> < 0.2 μM at station 10–49°N, 24 m depth, Figure 3) suggested the occurrence of a phytoplankton bloom. In the upper 100 m of the two subtropical domains the extremely low nutrients concentrations (such as observed in the NASG: PO<sub>4</sub><sup>3A</sup> < 0.5 μM; NO<sub>3</sub><sup>A</sup> < 5 μM, Si < 5 μM) and the subsurface Chlorophyll a values (Chl a < 0.03 μg/L, Figure 3d) were characteristic of oligotrophic conditions. In these domains, the N/P ratios were generally below the Redfield ratio in the upper 100 m waters (Figure 3b) suggesting that nitrogen might be more limiting than phosphorus. However, a greater depletion of nitrogen relative to phosphate was observed in the upper 300 m of the SASG (N:P < 10) compared to the NASG (N:P > 25; Figure 3b) [Dulaquais et al., 2014] likely due to a greater proportion of N<sub>2</sub> fixers, such as diazotrophic cyanobacteria, in the NASG than in the SASG [Mather et al., 2008]. In the equatorial area, low nutrients concentrations were observed in the upper 100 m (NO<sub>3</sub><sup>A</sup> < 0.8 μM; PO<sub>4</sub><sup>3A</sup> < 0.1 μM; Si < 1.3 μM), whereas high concentrations of nitrate and phosphate (NO<sub>3</sub><sup>A</sup> > 34 μM; PO<sub>4</sub><sup>3A</sup> > 2.3 μM) and low levels of silicate (5 μM < Si < 15 μM) were recorded at intermediate depths due to the incursion of the Atlantic Central Waters [Dulaquais et al., 2014]. In this area, the Chl a levels were similar to those recorded in the oligotrophic domains. South of the MBC, the influence of the AAW and upper circum polar deep waters (UCDW) generated a southward gradient of nutrients in the top 1000 m layer (Figure 3a) with increasing concentrations southward. Relatively high-nutrient concentrations were generally observed in the top 200 m depths (NO<sub>3</sub><sup>A</sup> > 20 μM; PO<sub>4</sub><sup>3A</sup> > 1.2 μM; Si > 15 μM). In the southern latitudes of the section, the Chl a concentrations > 0.5 μg L<sup>-1</sup> and the high levels of nitrite (NO<sub>2</sub><sup>A</sup> > 0.16 μM) observed in the upper 100 m layer, associated with the depletion of silicate levels (Si < 1.2 μM) and the low Si:N ratio (< 0.2) (Figure 3c), hinted at the final stages of a diatom bloom.

### 3.3. The Distributions of Cobalt in Surface Waters of the Western Atlantic

The meridional and vertical distributions of DCo and PCo are presented in the upper 1000 m along the section in Figure 4. Dissolved cobalt concentrations ranged from 14.7 ± 1.4 to 93.3 ± 3.3 pM along the section and mostly follow a nutrient-like behavior in the upper 1000 m (Figure 4a). The lowest concentration was observed in surface waters of the SASG (e.g., at 9 m depth at station 11b-26°S), whereas the highest were recorded in the OMZ of the equatorial area (e.g., at station 15b-9°S at 290 m depth). The vertical distributions of PCo generally exhibited higher concentrations in the subsurface and decreasing concentrations with depth (Figure 4b). PCo concentrations ranged from near undetectable values to 15.2 ± 2.3 pM (e.g., at station

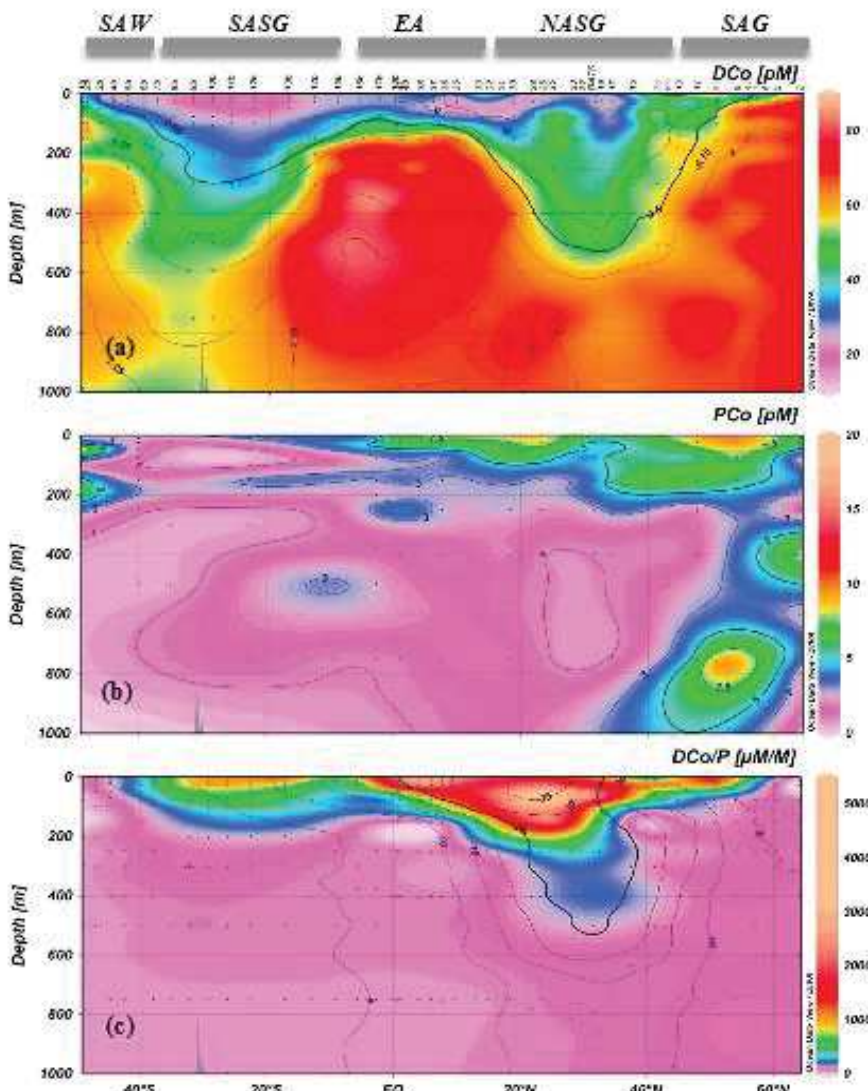


Figure 4. Interpolated vertical section in the upper 1000 m of (a) dissolved cobalt concentration (DCo) with phosphate contours overlaid on the profile, (b) particulate cobalt concentrations (PCo), and (c) DCo/Pratio with dissolved aluminium concentration (DAI) contours overlaid on the profile (Middag et al., unpublished data).

5°–50.8°N at 761 m depth). The relative proportion of PCo to TCo (Figure 5a) ranged from less than 5% at several stations in the intermediate waters (250–1000 m) to up to 34% (at station 26–25 m depth), with a mean of  $12 \pm 12\%$  ( $n = 76$ ), indicating that cobalt was primarily present in the dissolved fraction. Furthermore, the relative proportion of PCo covaried with the Chl a distribution (Figures 5a and 5b).

Distinct vertical distributions of DCo were observed in the surface waters of the different biogeochemical domains (Figures 6). At the highest latitudes of the northern subarctic gyre, high DCo concentrations were measured (about 60–70 pM; Figures 4a and 6a). Here the particulate cobalt was shown similar in terms of concentration and vertical distribution to those observed by Weinstein and Moran [2004], with relative PCo maxima in the subsurface (ranging from  $5.9 \pm 1.0$  to  $10.4 \pm 2.0$  pM), and decreasing concentrations with depth (Figure 6f). In the southern side of the SAG, high PCo concentrations were observed in the Chl a maximum (at station 11; 25 m PCo = 8.2 pM). Lower DCo concentrations were detected in surface waters of this region (Figure 6a) in August 2012 during Leg-4 (e.g., mean  $\text{DCo}_{25\text{m}} = 43.2 \pm 1.6$  pM  $n = 2$ ) compared to measurements in samples collected in April 2010 during Leg-1 (e.g., mean  $\text{DCo}_{25\text{m}} = 64.6 \pm 5.4$  pM at 25 m  $n = 4$ ).

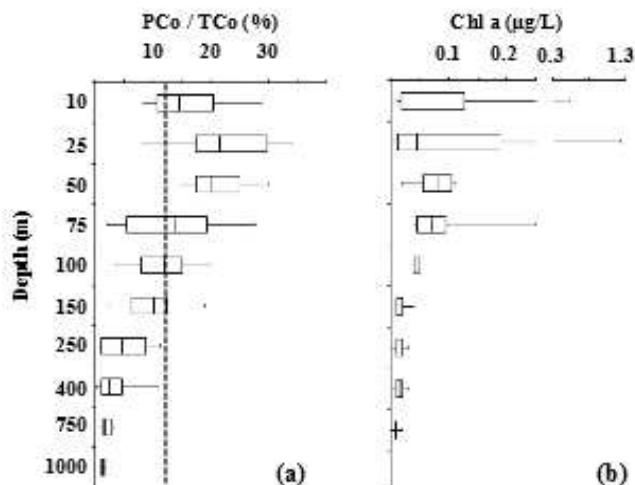


Figure 5. (a) Box plot representing the relative proportion of particulate cobalt (PCo) to total cobalt (TCo) using all data for a given depth along the section. Dashed line represents the average (mean = 12 ± 12%; n = 78). (b) Box plot representing estimated Chl a (derived from CTD data) using all data, where PCo is available, for a given depth along the section.

DCo was depleted in the surface waters of both subtropical domains and its concentration increased with depth below the nutricline, featuring a nutrient-like distribution (Figures 4a, 6b, and 6d). The concentrations of DCo were slightly lower in the SASG (mean  $DCo_{100m} = 24 \pm 5$  pM) compared to those recorded in the NASG (mean  $DCo_{100m} = 33 \pm 8$  pM). Furthermore, the PCo distribution also showed, like DCo, lower concentrations in the subsurface waters of the SASG (< 5 pM; Figure 6i) compared to the NASG (> 5 pM; Figure 6g). Additionally, relative maxima of DCo were observed at about 10 m depth at a few stations in the NASG (as exemplified for station 26, Figure 6b).

In the equatorial area, the DCo distribution was characterized by low concentrations in the top 100 m (mean  $DCo_{100m} = 30 \pm 9$  pM,  $n = 44$ ) and a

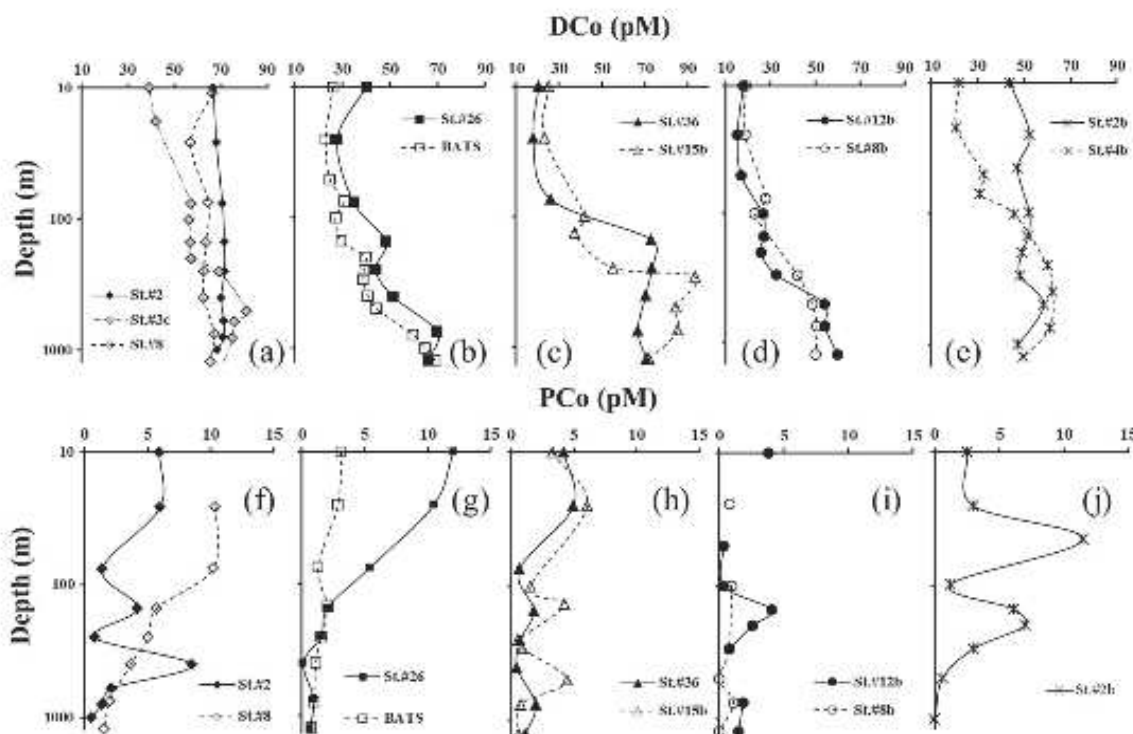


Figure 6. Typical vertical distribution of dissolved (DCo) and particulate (PCo) cobalt against depth in the different biogeochemical domains. In the SAG (a) DCo and (f) PCo are shown for station 2 (Leg-1; 64°N 34.25°W), station 8 (Leg-1; 54°N 45.84°W), and station 3c (Leg-4; 57°N 44°W). In the northern subtropical domain, (b) DCo and (g) PCo are shown at station 28 (Leg-2; 23°N 66.55°W) and at the BATS station (Leg-2; 31.7°N 64.2°W). In the equatorial area, (c) DCo and (h) PCo are presented at station 38 (Leg-2; 7.8°N 48.9°W) and station 15b (Leg-3; 9°S 28°W). In the southern subtropical domain, (d) DCo and (i) PCo are shown for station 12b (Leg-3; 22.47°S 32.7°W) and station 8b (Leg-3; 35°S 39.4°W). In the subantarctic area (e) DCo and (j) PCo are shown at station 12b (Leg-3; 49°S 48.9°W) and station 4b (Leg-3; 44.7°S 45.6°W).

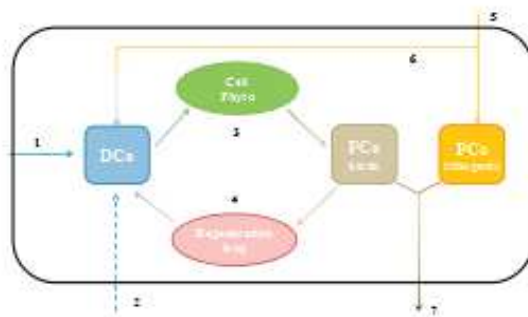


Figure 7. Simplistic conceptual schema of the cobalt cycling in the upper 100 m. Arrows represent the fluxes as follows: 1: lateral advection; 2: vertical diffusion; 3: uptake; 4: regeneration; 5: Co deposition; 6: dust dissolution; and 7: export. Here scavenging could not be discerned from biological uptake and is considered negligible.

South of the Brazil-Malvinas confluence, in the subantarctic waters, a surface southward increasing gradient of DCo was observed (Figure 4a), and the vertical distribution of DCo showed nutrient distribution in the upper 200 m, below which the concentrations were relatively constant. At these latitudes, the highest DCo concentrations were recorded in the core of D-AAIW (100–600 m; Figure 6e).

#### 4. Discussion

With the aim to better constraining the biogeochemical cycle of cobalt in the surface western Atlantic, regional variability in the DCo:P relationship is discussed and key fluxes, conceptualized in Figure 7, are estimated. We propose an estimate of the regeneration rate of DCo in surface waters due to a combination of abiotic processes, the microbial loop, cell lysis, and grazing. We also evaluate the external inputs of Co from the atmosphere and the Amazon River to the surface western Atlantic. Surface (100 m) Co budgets are proposed the different biogeochemical domains of the western Atlantic.

##### 4.1. Internal Cycle of Dissolved Cobalt in the Surface Western Atlantic

###### 4.1.1. The Dissolved Cobalt and Phosphate Relationship

The vertical distribution of DCo was nutrient-like, akin to the macronutrient phosphate (P) in the oligotrophic and tropical surface waters (Figure 4a). Strong linear correlations between DCo and P have been previously reported in the surface waters of subtropical regions in the South Pacific [Ellwood, 2008], the northeast Pacific [Sunda and Huntsman, 1995], the North Atlantic [Martin et al., 1993], and the Sargasso Sea [Saito and Moffett, 2002; Jakuba et al., 2008], as well as in other oligotrophic systems [Saito and Moffett, 2002; Bown et al., 2011], or in upwelling [Saito et al., 2004], in eddies near islands [Noble et al., 2008], and in Antarctic waters of the Ross Sea [Saito et al., 2010]. These correlations suggested that the biological uptake of DCo is proportional to that of P in the surface waters [Jakuba et al., 2008; Noble et al., 2008; Bown et al., 2011]. Along the section sampled here, when all the data are considered, a linear relationship between DCo and P concentrations was also obtained in the surface layer (0–250 m) providing a mean DCo:P slope of  $23.1 \mu\text{M M}^{-1}$  ( $R^2 > 0.53$ ,  $n = 231$ ; Figure 8a). However, the slopes of DCo:P correlations varied across the different biogeochemical domains crossed along the section (Figure 8b), with the highest DCo:P slopes observed in the two subtropical domains ( $> 50 \mu\text{M M}^{-1}$ ). These regional differences in DCo:P could reflect differences in phytoplankton assemblages between the domains, since a wide range of internal Co:P cellular quota have been reported for different phytoplankton species [Ho et al., 2003; Cullen et al., 2003; Tovar-Sánchez et al., 2006; Twining et al., 2011; Twining and Baines, 2013]. Other factors could account for the regional differences in DCo:P ratios, including differences in the surface regeneration rate, external sources, and/or physical processes [Noble et al., 2008].

A mean DCo:P slope of  $31.2 \mu\text{M M}^{-1}$  ( $R^2 = 0.78$ ,  $n = 28$ ) was found in the surface subarctic gyre (Figure 7b), which is similar to the slope previously observed at high latitudes, as exemplified in the Ross Sea (e.g.,  $37.6 \mu\text{M M}^{-1}$ ) [Saito et al., 2010]. The DCo:P slopes did not vary significantly in surface waters of the SAG despite a southward decrease of DCo concentrations (Figures 4a and 8b). Diatoms may dominate the phytoplankton assemblage at the highest latitudes of the SAG [Parsons and Lalli, 1988], whereas coccolithophorids

sharp increase between 100 and 250 m (mean  $\text{DCo}_{100-250\text{m}} = 62 \pm 13 \mu\text{M}$ ,  $n = 10$ ), that continued to increase to reach maximum values at about 400 m depth (mean  $\text{DCo}_{250-400\text{m}} = 73 \pm 10 \mu\text{M}$ ,  $n = 19$ ) (Figures 4 and 6c). These maximum concentrations were the highest values recorded along the section, reaching values up to  $93.3 \pm 3.3 \mu\text{M}$  (at  $9^\circ\text{S}$ ), and strongly correlated with the oxygen depletion ( $\Delta\text{DCo}/\Delta\text{O}_2 = 0.28 \mu\text{M/M}$ ,  $R^2 > 0.66$ ) as reported by Dulaquais et al. [2014]. The distribution of PCo in this equatorial domain was similar to that observed in the other domains, with relatively high concentrations in surface waters ( $\text{PCo} > 5 \mu\text{M}$ , Figure 6h), reaching a maximum value of  $10.2 \pm 2.1 \mu\text{M}$  observed at 10 m at station 40 ( $1.15^\circ\text{N}$ ).

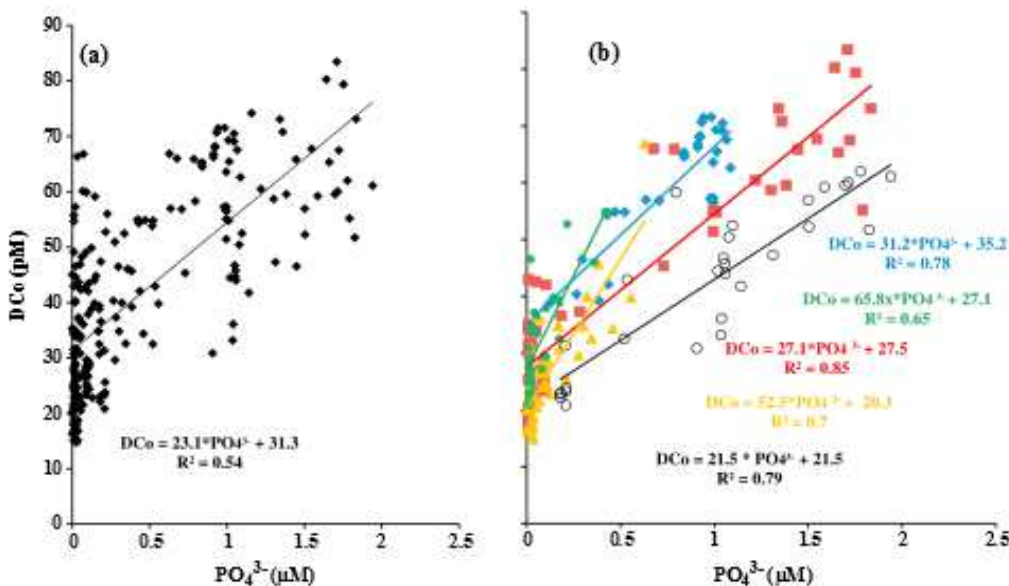


Figure 8. Scatter plots of the DCo data versus phosphate in the upper 250 m, showing (a) the global DCo-P relationship ( $n = 228$ ) along the section and (b) the regional DCo-P relationships obtained in the SAG ( $n = 28$ ; blue diamonds), the NASG ( $n = 32$ ; green dots), the equatorial area ( $n = 53$ ; red squares), the SAG ( $n = 51$ ; yellow triangles), and the SAW ( $n = 22$ ; white dots).

were probably blooming in the southern side of this domain during spring [Okada and McIntyre, 1979; Head et al., 2000; Gregg and Casey, 2007]. Diatoms have a lower cellular Co:P quota ( $60\text{--}150 \mu\text{M M}^{-1}$ ) compared to coccolithophorids ( $300\text{--}360 \mu\text{M M}^{-1}$ ) [Ho et al., 2003; Cullen et al., 2003; Tang and Morel, 2006; Twining et al., 2011] that have an higher biological requirement for Co [Sunda and Huntsman, 1995]. In turn, it is possible that strong biological uptake of DCo (and P) by blooming coccolithophores could have caused the depletion of DCo observed in the southern section of the SAG. The invariance of the DCo:P slope in this domain suggests that additional processes such as the lateral advection, may account for the observed correlation. The seasonal decrease of the DCo surface concentrations observed in this area between April 2010 ( $\text{DCo}_{\text{upper 250m}} = 66 \text{ pM}$  at station  $6\text{--}58.6^\circ\text{N}$ ) and August 2012 ( $\text{DCo}_{\text{upper 250m}} = 55.1 \text{ pM}$  at station  $30\text{--}57.2^\circ\text{N}$ , Figure 6a) fits with the observed formation of the shallow pycnocline or thermocline at the end of spring which can promote the coccolithophorid bloom [Head et al., 2000].

At the high latitudes of the Southern Hemisphere, the lowest DCo:P slope of  $21.5 \mu\text{M M}^{-1}$  ( $R^2 = 0.79$ ;  $n = 22$ ; Figure 8b) was observed in the subantarctic waters. This slope might reflect the low Co:P cellular quota of diatoms [Twining et al., 2011] which probably dominate in this area [Ferreira et al., 2013; Browning et al., 2014]. In addition, the high productivity of this area [Field et al., 1998] may have significantly reduced the DCo stock close to the MBC (Figure 4a), in spite of a low Co biological requirement by diatoms [Sunda and Huntsman, 1995]. A southward shift between the surface gradient of DCo and dissolved zinc (DZn) in subantarctic waters [Croot et al., 2011; Middag et al., unpublished data, 2014] suggests a southward decrease of DCo uptake by diatoms when DZn becomes nonlimiting. Indeed, diatoms are known to preferentially assimilate Zn compared to Co [Sunda and Huntsman, 1995].

The equatorial domain was characterized by a low DCo:P slope of  $\sim 27 \mu\text{M M}^{-1}$  ( $R^2 > 0.87$ ;  $n = 51$ ; Figure 8b). It contrasts with the extremely high DCo:P slope ( $> 560 \mu\text{M M}^{-1}$ ) reported at similar latitudes but in the central Atlantic [Saito and Moffett, 2002]. However, it may be difficult to compare these ratios since the latter was obtained with subsurface samples (5 m depth only), and close to the African coast. In that area, DCo probably accumulated at the subsurface notably due to dust dissolution, which would increase the DCo:P slope. In the western equatorial region, the plankton assemblage could be dominated by both the cyanobacteria *Richelia intracellularis* and the diatom *Pseudonitzschia* during summer (June and July) [Tovar-Sánchez et al., 2006]. The DCo:P slope recorded in this area ( $27.1 \mu\text{M M}^{-1}$ ) was similar to the cellular Co:P mean quota determined for the bulk of these species ( $31 \mu\text{M M}^{-1}$ ) [Tovar-Sánchez et al., 2006].

suggesting that the biological uptake of DCo and P by cyanobacteria and diatoms can drive their concentrations and ratio. The low DCo:P observed in the surface waters of the equatorial domain may also be accounted for by vertical diffusion fluxes from intermediate waters of relatively low DCo:P ( $23.1 \mu\text{M M}^{-1}$  between 250 and 600 m depths) [Dulaquais et al., 2014].

The highest DCo:P slopes were observed in the subtropical areas (Figure 8b), with the highest mean value being observed in the Sargasso Sea ( $\text{DCo:P} > 65.8 \mu\text{M M}^{-1}$ ;  $R^2 > 0.65$ ;  $n = 32$ ; Figure 8b). Combined with the low DCo concentrations recorded (Figure 4a), it suggests strong biological uptake of DCo in the subtropical provinces. The ratios observed in this study were in the same range, although slightly higher, than those previously reported in other oligotrophic regions [Saito and Moffett, 2002; Noble et al., 2008; Jakuba et al., 2008; Bown et al., 2011; Twining and Baines, 2013]. The cyanobacteria *Prochlorococcus* sp. and *Synechococcus* sp., which dominate the picophytoplankton assemblage in oligotrophic regions, have an absolute cobalt requirement for growth [Saito et al., 2002] and thus assimilate Co leading to the low DCo concentrations recorded in these domains (Figure 4a). Furthermore, the high DCo:P observed in these oligotrophic waters are consistent with the high Co:P cellular ratios reported in phytoplankton bulk dominated by *Prochlorococcus* sp. and *Synechococcus* sp. from the eastern Atlantic (e.g.,  $260 \mu\text{M M}^{-1}$ ) [Tovar-Sánchez et al., 2006].

Significantly lower P concentrations were recorded in the NASG (mean  $0.07 \mu\text{M}$ ) compared to the SASG (mean  $0.19 \mu\text{M}$ ) in the upper 250 m. The alkaline phosphatase activity of the biota could be enhanced at nanomolar concentrations of P [Ji and Sherrell, 2008], as reported in the Sargasso Sea, and thus, the biological uptake of DCo would also be higher [Sunda and Huntsman, 1995; Jakuba et al., 2008]. Thus, it is possible that Co was used more intensely in the NASG, likely contributing to the higher DCo:P there ( $65.8 \mu\text{M M}^{-1}$ ) compared to the SASG ( $52.5 \mu\text{M M}^{-1}$ ). The higher atmospheric input of Co in the Northern Hemisphere (Figure 10) also likely caused an accumulation of DCo relative to P in the NASG (Figure 4c) and thus higher DCo:P ratios.

Overall, the regional DCo:P slopes were generally lower than Co:P cellular ratios of the dominant phytoplankton species suggesting that other processes were occurring in addition to biological uptake in surface waters.

#### 4.1.2. Biological Uptake and Regeneration Rate of Dissolved Cobalt in Surface Waters as Exemplified at the Bermuda Atlantic Time-Series Study Station

The cellular quotas of Co:P reported for the dominant phytoplankton functional groups potentially present in the different biogeochemical domains along the section were significantly higher than the corresponding DCo:P slopes we measured in the surface waters except in the equatorial region (Figure 8b) [Ho et al., 2003; Cullen et al., 2003; Tang and Morel, 2006; Tovar-Sánchez et al., 2006; Twining et al., 2011; Twining and Baines, 2013]. For instance, DCo:P in the upper 250 m of the Sargasso Sea ( $65.8 \mu\text{M M}^{-1}$ ) was 4 times lower than the cellular Co:P quota of the predominant cyanobacteria (e.g.,  $260 \mu\text{M M}^{-1}$ ; as reported in a bulk of *Prochlorococcus* sp. and *Synechococcus* sp. in the eastern Atlantic; Tovar-Sánchez et al. [2006]). Because the apparent biological use of DCo relative to P did not match the cellular quotas, the stoichiometric DCo:P slopes should thus reflect a combination of the several sinks and sources terms, such as regeneration in surface waters, in addition to the biological uptake. Hence, the DCo:P measured in the Sargasso Sea was used to discriminate the terms and to estimate the regeneration rate of DCo. The biological uptake rate of DCo by the cyanobacteria, that presumably dominate the phytoplankton assemblage in these waters, was estimated in the top 100 m (Table 2). The biomass was derived from the *in situ* Chl a (fluorescence) measurements, and literature values were used for growth rate of cyanobacteria in the Sargasso Sea and their Co/C cellular quota (equation (1) and references therein). We estimated a Co:C cellular quota of  $2.16 \pm 0.7 \mu\text{M M}^{-1}$  for cyanobacteria, which is in agreement, considering the relative error, with the Co:C ratio reported in particulate matter of Sargasso Sea ( $1.5 \pm 0.6 \mu\text{M M}^{-1}$ ) [Sherrell and Boyle, 1992] and the Co:C cellular quota of *Synechococcus* sp. ( $1.43 \mu\text{M M}^{-1}$ ) [Sunda and Huntsman, 1995] grown in zinc-depleted conditions similarly to surface waters of the Sargasso Sea [Bruland and Frank, 1983]. In our approach, the scavenging process could not be discerned from the biological uptake. The covariation between the relative proportion of PCo and the Chl a concentration we observed in the upper 1000 m along the section (Figure 5) strongly suggests that the transfer of DCo to PCo could be mainly driven by biological processes rather than by scavenging onto particles. Thus, the scavenging rate of DCo ( $F_{DCo\text{scavenging}}$ ) was assumed negligible in

Table 2. Summary of Dissolved Cobalt (FDCo) and Phosphorus (FP) Fluxes Integrated for the Upper 100 m at the BATS Station in the Sargasso Sea<sup>a</sup>

Atmospheric Deposition <sup>b</sup>	River Input	Lateral Advection <sup>c</sup>	Vertical Diffusion <sup>c</sup>	Scavenging <sup>d</sup>	Uptake	Regeneration
FDCo (nmol m <sup>-2</sup> d <sup>-1</sup> )	+ 0.7 ± 0.1	Negligible	+ 0.08 ± 0.01	+ 0.05 ± 0.01	Negligible	~ 45 ± 15
FP (μmol m <sup>-2</sup> d <sup>-1</sup> )	+ 0.14 ± 0.03	Negligible	+ 0.02 ± 0.01	+ 0.72 ± 0.1)	Negligible	~ 175 ± 53

<sup>a</sup>Standards errors are indicated in brackets.<sup>b</sup>See section 4.2.2 for the calculation.<sup>c</sup>From and following the method of Dulaquais et al. [2014] with the following: FDCo<sub>diffusion</sub> =  $\frac{1}{2} (K_z + D_T) \times (\partial DCo / \partial z)$  and FDCo<sub>adv</sub> =  $G_{adv} DCo(x,y) \times \text{velocity}_z \times z$ .<sup>d</sup>Scavenging could not be discerned from biological uptake.

the surface waters. This assumption is further supported by a previous study that also suggests absence of scavenging in the upper waters column of Sargasso Sea [Moffett and Ho, 1996].

$$FDCo_{\text{uptake}} \approx \delta Co = Chl_{\text{cyano}} \cdot \delta C = Chl \approx 1 = M_C \cdot \% Chl \approx 100m \cdot \mu \quad (1)$$

where  $(Co/C)_{\text{cyano}} = 2.16 \mu\text{mol mol}^{-1}$  using  $(Co/P)_{\text{cyano}} = 260 \mu\text{mol mol}^{-1}$  [Tovar-Sánchez et al., 2006] and  $(P/C)_{\text{cyano}} = 8.3 \pm 2.6 \text{ mmol mol}^{-1}$  (after the review by Bertilsson et al. [2003]);  $\mu$  is the growth rate of cyanobacteria in the Sargasso Sea and it is equal to  $0.4 \text{ day}^{-1}$  [Mann, 2000];  $C/\text{Chl} = 75 \text{ g g}^{-1}$  [Amigo et al., 1998]; and  $M_C$  is the carbon molar mass ( $12 \text{ g mol}^{-1}$ ).

These calculations lead to an uptake flux of DCo of  $45 \pm 15 \text{ nmol DCo m}^{-2} \text{ d}^{-1}$  by the cyanobacteria at the Bermuda Atlantic Time-series Study (BATS) station (Table 3), which is in agreement with an estimate by Saito et al. [2002] for the upper 100 m of the Sargasso Sea ( $30 \pm 12 \text{ nmol DCo m}^{-2} \text{ d}^{-1}$ ). The apparent slope of DCo versus P ( $\Delta DCo / \Delta P_{\text{app}}$ ) reflects the sum of the fluxes  $F$  (sources and sinks) of DCo relative to that of P in equation (2):

$$\delta \Delta DCo = \Delta P_{\text{app}} \cdot \frac{X}{F_{DCo}} = \frac{X}{F_P} \quad (2)$$

The DCo fluxes were estimated in the top 100 m at the BATS station (Table 2). The P fluxes were estimated using the same parameterization as for DCo, but using the P concentrations data (Table 2). In the Sargasso Sea, the regeneration rate of P ( $F_{P,\text{reg}}$ ) was determined using a relationship between regeneration and uptake fluxes of P ( $F_{P,\text{reg}} = 0.35 \times F_{P,\text{uptake}}$ ) [McLaughlin et al., 2013]. Then using equation (2), the regeneration flux of DCo can thus be written as

$$F_{Co,\text{reg}} \approx \frac{\Delta DCo}{\Delta P_{\text{app}}} \cdot \frac{X}{F_P} = \frac{\Delta DCo_{\text{diffusion}} + DCo_{\text{advection}} + DCo_{\text{atmosphere}} + DCo_{\text{uptake}} + DCo_{\text{scavenging}}}{\Delta P_{\text{app}}} \quad (3)$$

ADCo regeneration rate of  $37 \pm 15 \text{ nmol m}^{-2} \text{ d}^{-1}$  was estimated at BATS (Table 2), using the measured DCo:P slope at BATS of  $69.2 \mu\text{M M}^{-1}$ . This regeneration flux represented about 80% of the Co uptake rate by cyanobacteria (e.g.,  $F_{Co,\text{reg}} / F_{Co,\text{uptake}} = 0.8$ ), indicating that most of the biogenic cobalt can be recycled in these surface waters. A different approach resulted in similar estimates of 70–90% regeneration for oligotrophic waters of the southeastern Atlantic [Bown et al., 2011]. From these calculations, we estimate a corresponding turnover of Co in cyanobacteria cell ( $T_{Co,\text{cell}} = F_{Co,\text{uptake}} / F_{Co,\text{reg}}$ ) of 1.3 days at BATS.

In Sargasso Sea, the regeneration rate of P represented only 35% of its biological uptake in these waters (Table 2). The twofold difference in regeneration rates of P and DCo suggests non-Redfieldian regeneration of P and DCo and is probably the cause of the mismatch between the DCo:P slope and the Co:P cellular ratio in these waters. These estimates of biological DCo fluxes are based on estimated Co:C ratio in cyanobacteria; large uncertainty exists on this term, and further determinations will be required to improve such calculation of the bioassimilation and regeneration rate of DCo. The organic speciation of DCo also needs to be taken into account since it too can impact the bioavailability of DCo [Saito et al., 2002; Bown et al., 2012]. For instance, it has been suggested that Prochlorococcus sp. are able to assimilate organically bounded DCo [Saito et al., 2002] and that cyanobacteria might produce organic binding-DCo ligands in oligotrophic waters [Bown et al., 2012].

Table 3. Cobalt to Organic Carbon Ratio in Particles at 100 m Derived From Measurements ( $\text{PCo}_{>0.2\mu\text{m}}/\text{POC}_{>1\mu\text{m}}$ ), and the Integrated Export Fluxes of Co on Large Particles ( $>53\mu\text{m}$ ) at 100 m ( $\text{FCo}_{\text{export}}$ )<sup>a</sup>

	Domain					
	SAG	NASG	N-EA	S-EA	SASG	SAW
$\text{PCo}_{>0.2\mu\text{m}}/\text{POC}_{>1\mu\text{m}} (\mu\text{M M}^{-1})$	$2.1 \pm 0.6$	$6.9 \pm 1.4$	$1.5 \pm 0.4$	$1.5 \pm 0.4$	$2.16^b$	$0.4^b$
$\text{FCo}_{\text{export}} (\text{nmol m}^{-2} \text{d}^{-1})$	$4.2 \pm 3.4$	$12.9 \pm 32.4$	$3.6 \pm 2.0$	$5.5 \pm 1.5$	$4.9 \pm 1.2$	$2.3 \pm 0.5$

<sup>a</sup>N-EA: North Equatorial area; S-EA: South Equatorial area.

<sup>b</sup>Data from Bown et al. [2011].

#### 4.1.3. Export of Cobalt From the Surface Waters

The export flux of cobalt on settling particles from the surface waters was estimated using the export fluxes of the particulate organic carbon (POC) at 100 m depth ( $C_{\text{export}}$ , equation (4)) inferred from  $^{234}\text{Th}/^{238}\text{U}$  measurements ( $^{234}\text{Th}_{\text{flux}}$ ) in the water column and the POC/ $^{234}\text{Th}$  ratio measured in large particles  $>53\mu\text{m}$  [Owens et al., 2014; V. Puigcorbé et al., manuscript in preparation, 2014]. The Co:C ratio was found to covary in large and total particles ( $n = 5$ ) in the north western Atlantic (at  $35.4^\circ\text{N}$ – $66.5^\circ$  and  $39.7^\circ\text{N}$ – $69.8^\circ\text{W}$ ) during the GEOTRACES-A03 cruise (Phoebe Lam, personal communication, 2014). This allows us to use equation (5) and to calculate the export fluxes of Co by the large settling particles ( $>53\mu\text{m}$ ) at 100 m ( $\text{FCo}_{\text{export}}$ , equation (6)).

$$C_{\text{export}} \propto \frac{1}{4} \frac{^{234}\text{Th}_{\text{flux}}}{\text{POC}_{>53\mu\text{m}}} \propto \frac{1}{4} \frac{^{234}\text{Th}}{\text{POC}_{>1\mu\text{m}}} \quad (4)$$

$$\text{PCo}_{>53\mu\text{m}} = \text{POC}_{>53\mu\text{m}} \times \frac{1}{4} \frac{\text{PCo}_{>0.2\mu\text{m}}}{\text{POC}_{>1\mu\text{m}}} = \text{POC}_{>53\mu\text{m}} \quad (5)$$

$$\text{FCo}_{\text{export}} \propto \frac{1}{4} \frac{C_{\text{export}}}{\text{POC}_{>53\mu\text{m}}} \propto \text{POC}_{>53\mu\text{m}} \quad (6)$$

In the Northern Hemisphere, the carbon export fluxes were available at date for 14 stations at 100 m depth (Puigcorbé et al., manuscript in preparation), and mean values of the Co:POC ratios were estimated in the SAG, the NASG, and the Equatorial Area (EA) (Table 3). In the Southern Hemisphere, the carbon export fluxes were available at 18 stations at 100 m depth [Owens et al., 2014] but there was no POC data available in the SASG and the SAW. For these domains, PCo/POC ratios recorded in similar biogeochemical conditions in surface waters (e.g., T, Chl a, DCo) but in the southeastern Atlantic [Bown et al., 2011] were used (Table 3).

In the subarctic gyre and the equatorial area, the PCo/POC ratios were, respectively, equal to  $2.1 \pm 0.6$  and  $1.5 \pm 0.4 \mu\text{M M}^{-1}$  at 100 m depth. These values are in excellent agreement with the Co/C cellular quota of coccolithophorids in nonlimiting conditions ( $1.4$ – $3.6 \mu\text{M M}^{-1}$ ) [Sunda and Huntsman, 1995; Ho et al., 2003] but much higher than those measured in oceanic diatoms ( $0.3 \mu\text{M M}^{-1}$ ) [Twining et al., 2011]. At  $23^\circ\text{N}$ , the PCo/POC ratio ( $6.9 \pm 1.3 \mu\text{M M}^{-1}$ ) was 3 times higher than the cellular quota of the predominant cyanobacteria ( $1.43$ – $2.16 \mu\text{M M}^{-1}$ ) [Sunda and Huntsman, 1995; Tovar-Sánchez et al., 2006] and than the PCo/POC ratio obtained in particulate material collected with *in situ* pumps in oligotrophic conditions ( $1.5 \pm 0.6 \mu\text{M M}^{-1}$ ) [Sherrell and Boyle, 1992], suggesting an additional (lithogenic) source of PCo in these waters probably from the atmosphere as shown below. In the SASG, the PCo/POC ratio used ( $2.15 \mu\text{M M}^{-1}$ ) [Bown et al., 2011] was in the range of the cellular quota of cyanobacteria [Sunda and Huntsman, 1995; Tovar-Sánchez et al., 2006]. South of the Southern Subtropical Front, the PCo/POC ratio of  $0.4 \mu\text{M M}^{-1}$  (derived from Bown et al. [2011]) was in agreement with the cellular quota of diatoms [Twining et al., 2011] that probably dominate the phytoplankton assemblage in this area [Browning et al., 2014].

The estimated export flux of Co varied within the different biogeochemical domains (Table 3), with the lowest in the SAW ( $2.3 \pm 0.5 \text{ nmol m}^{-2} \text{ d}^{-1}$ ;  $n = 6$ ) and the highest in the NASG ( $13 \pm 32 \text{ nmol m}^{-2} \text{ d}^{-1}$ ;  $n = 6$ ). Interestingly, relatively lower Co export fluxes were estimated in domains with potentially higher particulate sinking rates such as the SAW and the north EA, due to the predominance of diatoms, compared to areas like the NASG that are dominated by cyanobacteria and have nominally lower particulate sinking rates (Table 3). This suggests that the export of Co by particles might not be directly proportional to the primary productivity, and that other parameters should be taken into account such as the biological requirement and uptake of Co by the dominant functional groups that can drive the Co

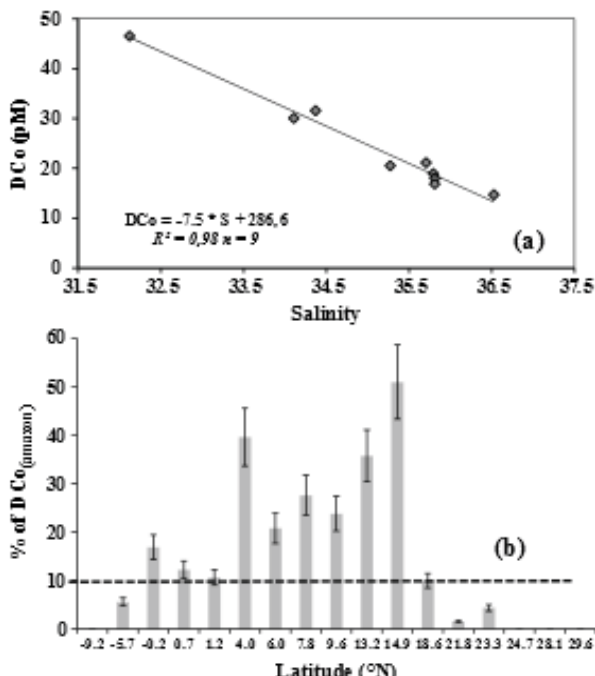


Figure 9. (a) Inverse linear correlation ( $R^2 > 0.97$ ) between dissolved cobalt (DCo) and the salinity in the waters influenced by the discharge of the Amazon (dark stars). (b) Percentage of the DCo stock in the mixed layer attributed to the input by the Amazon. The dashed line indicates 10% contribution of the Amazon to the DCo stock.

elements to the western equatorial Atlantic [Boyle et al., 1982; Aucour et al., 2003; Seyler and Boaventura, 2003] and its influence has been traced as far as the Caribbean basin [Moore et al., 1986]. In contrast, it has a little impact on regions south of the equator and east of 47°W [Moller et al., 2010] due to the direction of its plume. However, retroflection of the North Brazil Current and the equatorial countercurrent can transport signatures of the plume southeastwards of its mouth [Moller et al., 2010].

A strong linear correlation between DCo concentrations and salinity of 32 to 36.5 was found in the plume of the Amazon ( $R^2 > 0.97, n = 9$ ; this study; Figure 9a). At the extrapolated zero salinity, the DCo concentration was thus estimated at 287 pM (Figure 9a). This end-member estimate is significantly lower than the DCo concentration of 0.64–1.87 nM reported for the upper Amazon [Seyler and Boaventura, 2003]. Similarly, underestimation of the DCo end-member for a North American estuary has already been reported [Saito and Moffett, 2002]. Transfer from dissolved to particulate fractions through chemical flocculation [Church, 1986; Moffett and Ho, 1996] can explain the difference between the reported and estimated end-members. The Co discharge to the estuary of the Amazon has been shown to predominantly occur as particulate cobalt, representing up to 95% of the total Co discharge [Seyler and Boaventura, 2003]. It is thus conceivable that the increase of the ionic strength across the saline gradient would cause flocculation and particles precipitation that would trap much of the riverine input in the delta sediments [Smoak et al., 2006]. On the other hand, sediments are subjected to constant reworking, such as sediment resuspension and dissolution that would increase the DCo input from the estuary. Additional data are clearly needed across the saline gradient to understand the behavior of DCo in the Amazon plume. Biological drawdown, in addition to such flocculation processes and to the dilution of the plume, can also account for the decrease of DCo along the pathway of the plume. For instance, higher intracellular Co-quotas of bacteria growing in the plume of the Amazon were reported compared to those of species growing outside it [Tovar-Sánchez and Sañudo-Wilhelmy, 2011], suggesting higher biological uptake of DCo in the Amazon plume.

abundance in the exported biogenic particles. This result contrasts with previous assumptions suggesting that the POC export could be rather small in oceanic domains dominated by the picoplankton and nanoplankton [Takahashi and Benfang, 1983; Silver et al., 1986; Goldman, 1988, 1993]. However, it is in line with recent findings showing that *Synechococcus* sp., *Prochlorococcus* sp., and nanoplankton can represent a significant portion of the POC downward flux especially in the oligotrophic regions, contributing to up to 33 ± 16% of the POC export flux in the Sargasso Sea [Lomas and Moran, 2011]. In turn, the absolute requirement of cyanobacteria for Co associated with the atmospheric deposition, as discussed in the following section, below could account for the enrichment of large particles in Co and therefore for the high export flux of Co estimated in the NASG.

#### 4.2. External Sources of Dissolved Cobalt in the Western Atlantic

##### 4.2.1. The Input by the Amazon

With a mean water flux of  $172\,000\text{ m}^3\text{ s}^{-1}$  [Moller et al., 2010], the Amazon River represents an important source of many

In order to estimate the input of DCo from the Amazon to our study region, we used the first-order DCo-salinity relationship (Figure 9a;  $\Delta\text{DCo}/\Delta S = 7.5 \text{ pM}$ ). Then we normalized the relationship assuming the Amazon influence is null for  $S \geq 36.5$  (equation (7)), since no plume was observed along the section at  $S$  above this value. The Amazon plume was depicted by its low salinities and its relatively high Si:N ratios observed in the mixed layer, consistent with previous observations [Hellweger and Gordon, 2002]. We estimated the concentration of DCo brought by the Amazon ( $\text{DCo}_{\text{Amazon}}$ ) and its relative contribution (%  $\text{DCo}_{\text{Amazon}}$ , Figure 9b) to the mean DCo concentration recorded in the mixed layer ( $\text{DCo}_z$ ), according to

$$\text{DCo}_{\text{Amazon}} \propto \delta S_{\text{obs}} \text{ for } S \leq 36.5 \quad (7)$$

$$\% \text{DCo}_{\text{Amazon}} = \frac{\text{DCo}_{\text{Amazon}}}{\text{DCo}_z} \times 100 \quad (8)$$

Where  $S_{\text{obs}}$  is the observed salinity and varies from 32 to 36.5;  $z$  varied between 15 and 60 m.

The input of DCo by the Amazon was significant ( $> 10\%$ ) for 10 stations ( $\text{DCo}_{\text{Amazon}} > 10\%$  of  $\text{DCo}_z$ ; Figure 9b), and varied between  $2.2 \pm 0.5 \text{ pM}$  at  $18^\circ\text{N}$  (station 30) and up to  $14.3 \pm 2.9 \text{ pM}$  at  $15^\circ\text{N}$  (station 32) where it accounted for 51% of the  $\text{DCo}_z$ . The advection of DCo by the plume of the Amazon River was detectable until  $18^\circ\text{N}$  (between station 18b and 30; Figure 9b), whereas northward, it was considered negligible as it represented less than 10% of the  $\text{DCo}_z$ . The contribution southward of the Amazon mouth was also found to be negligible. These estimates suggested that the DCo inputs by the Amazon discharge can be significant in the north western tropical Atlantic between the equator and  $18^\circ\text{N}$  (Figure 9b).

In fact, the inputs of nutrients by the Amazon River might significantly promote the diazotrophy in the central western Atlantic, as it has been previously suggested [Subramaniam et al., 2008]. It has been shown that up to 100% of the cellular metal content (including Co) of the diazotroph *Trichodesmium* sp. growing in the Amazon plume of the central Atlantic may actually originate from the Amazon discharge [Tovar-Sánchez et al., 2006]. These cyanobacteria are producers of  $\text{B}_{12}$ -vitamin that requires Co as the central atom [Bonnet et al., 2010] and  $\text{B}_{12}$  production could be enhanced by input of DCo [Panceza et al., 2008]. The production of  $\text{B}_{12}$ -vitamin may also promote the development of several other phytoplankton species limited by this vitamin [Bertrand et al., 2007; Bonnet et al., 2010], when iron is not limiting as likely it was the case in these waters [Rijkenberg et al., 2014]. In turn, the input of DCo by the Amazon in the north equatorial area could have ecological implications through an Amazon-DCo- $\text{B}_{12}$  cascade.

#### 4.2.2. The Atmospheric Contribution

Several subsurface DCo maxima ( $\text{DCo}_{10\text{m}} > \text{DCo}_{25\text{m}}$ ) were observed along the section in the Northern Hemisphere, especially in the NASG and in the northern equatorial area (Figures 6b and 6c). Moreover, relative maxima of PCo were generally observed in the upper 50 m along the transect (Figure 4b). The highest surface concentrations of PCo were recorded in the NASG, representing 10–20% of the TCo in subsurface, and up to 34% at  $26^\circ\text{N}$  (e.g.,  $\text{PCo} = 10.3 \pm 2.6 \text{ pM}$  at 25 m), whereas this fraction only represented generally less than 2% of the TCo concentration below 400 m. These observations suggested a possible atmospheric deposition of PCo in the NASG that produced subsurface DCo maxima after dissolution. In addition, anomalies of high DCo:P ratios (up to  $> 5.4 \text{ mM M}^{-1}$ ) were observed in the surface waters of the NASG centered at  $23^\circ\text{N}$  and the equatorial area (Figure 4c), likely resulting from an accumulation of DCo versus P. Indeed, the Co:P ratio in aerosols is significantly higher than in seawater ( $\text{Co:P}_{\text{seawater}} < 10^{A3} \text{ M.M}^{-1}$ , this study;  $\text{Co:P}_{\text{aerosols}} > 10^{A2} \text{ M.M}^{-1}$ , Reid et al. [2003]). Therefore, dissolution of aerosols might have caused these high DCo:P ratio. Additionally, the relative accumulation of DCo (versus P) was associated with an enrichment of dissolved aluminium (DAI) (Middag et al., unpublished data) in these surface waters (Figure 4c), further suggesting dust inputs in this region, far away from other potential external sources. Previous observations have shown that dust can be transported from North Africa to the entire tropical Atlantic all yearlong [Prospero and Lamb, 2003]. Using a modified dust deposition MADCOW model based on DAI as proxy for the dust input [Measures and Brown, 1996; Measures and Vink, 2000; Vink and Measures, 2001; de Jong et al., 2007] and the surface DAI concentrations recorded along the section (Middag et al., unpublished data), we estimated dust deposition rates in the western Atlantic. Improvements in this model are inclusion of variable

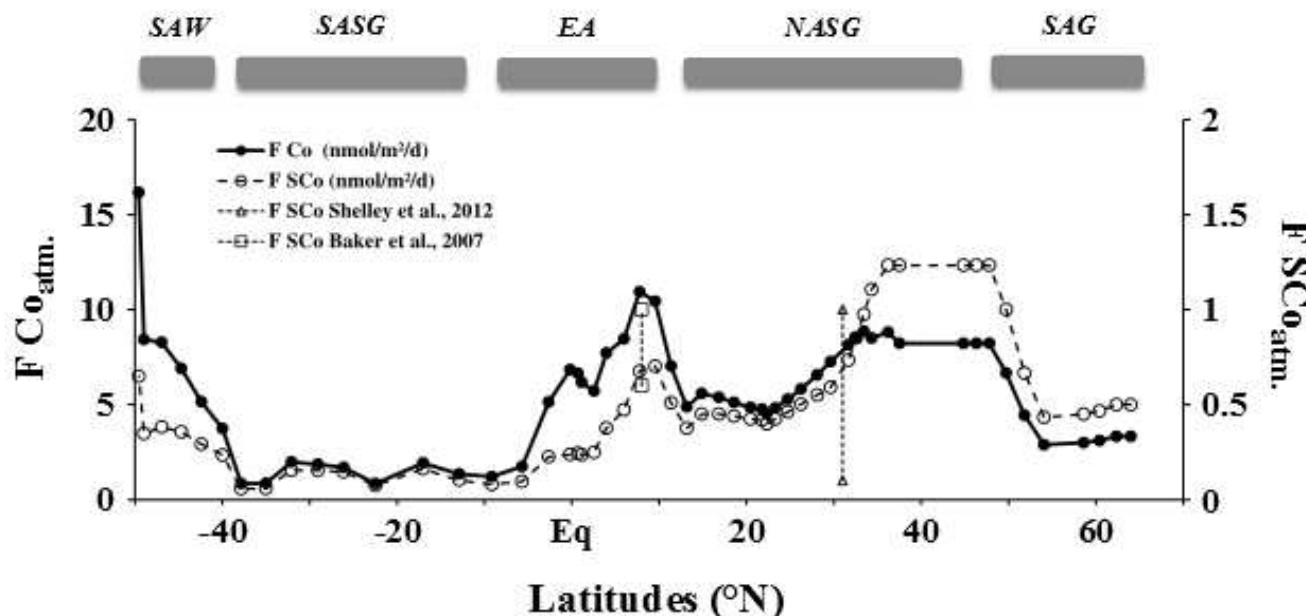


Figure 10. Estimation of the sea surface atmospheric deposition of dry (dark circles, solid line) and soluble (open circles, dashed line) cobalt, along the section. The soluble Co deposition estimated by Shelley et al. [2012] and Baker et al. [2007] are shown for comparison.

mixed layer depth, variable Al solubility of aerosols, and variable DAI residence times. The residence time of DAI in surface waters was assessed from its scavenging flux (equation (9); see supporting information for the parameterizations and coefficients). Dust deposition fluxes ranged from less than  $0.20 \pm 0.04 \text{ g m}^{-2} \text{ yr}^{-1}$  at several stations in the SASG (stations 7, 8, 9, and 10) to up to  $5.4 \pm 1.1 \text{ g m}^{-2} \text{ yr}^{-1}$  at about  $8^\circ\text{N}$  (station #36).

Despite the difficulties and limitations to use DAI as a dust proxy [Dammshäuser et al., 2011], especially due to its removal through biogenic particles [Moran and Moore, 1988; Middag et al., 2009], our estimations are consistent with previous studies showing that the atmospheric input can be 10 times higher in the NASG than in the SASG [Tegen et al., 2004; Jickells et al., 2005], and with model predictions of dust deposition in the Atlantic Ocean [Ginoux et al., 2001; Tegen et al., 2004; Mahowald et al., 2005; van Hulten et al., 2013] (see supporting information).

$$\text{Dust deposition rate } \frac{1}{4} \text{ DAI } \text{ Å } z \text{ Å } M \text{ Al } \text{ Å } \delta \text{ Ab Al } \text{ Å } \text{ SAI } \text{ Å } \tau \text{ Al } \text{ Å }^2 \text{ yr}^{-1} \quad (9)$$

where DAI is the mean dissolved aluminum (Al) concentration in the mixed layer,  $z$  is the mixed layer depth,  $M \text{ Al}$  is the molar mass of aluminum,  $\delta \text{ Ab Al}$  is the crustal abundance of Al, SAI is the solubility of Al in aerosols [from Baker et al., 2013],  $\tau \text{ Al}$  is the residence time of Al in the mixed layer (see supporting information for parameterizations and coefficients).

Considering these estimated rates of dust deposition, and the concentrations of Co in dust ( $[\text{Co}]_{\text{dust}}$ ) that varied from 17 to  $170 \mu\text{g g}^{-1}$  in aerosols of the West Atlantic depending on their origins [Gaiero et al., 2003; Reid et al., 2003; Rudnick and Gao, 2003; Baker et al., 2007; Trapp et al., 2010; Xia and Gao, 2010; Shelley et al., 2012; R. Shelley, personal communication, 2014] (see supporting information), we estimated the atmospheric Co deposition flux (Flux  $\text{Co}_{\text{atm}}$ ) along the section, according to equation (10):

$$\text{Flux Co}_{\text{atm}}: \frac{1}{4} \text{ Dust deposition rate } \text{ Å } \text{ Co}_{\text{dust}} \quad (10)$$

The estimates of Co deposition rates varied from  $0.9 \text{ nmol m}^{-2} \text{ d}^{-1}$  in the center of the SASG to up to  $17.4 \text{ nmol m}^{-2} \text{ d}^{-1}$  close to Patagonia (station 1b) (Figure 10). The strongest deposition of dust was centered on the EA (see supporting information), whereas the relatively high atmospheric inputs of Co were located in the temperate latitudes of the Northern Hemisphere ( $35^\circ\text{N}$ – $50^\circ\text{N}$ ; mean Flux  $\text{Co}_{\text{atm}} = 8 \pm 1 \text{ nmol m}^{-2} \text{ d}^{-1}$ ).

the northern equatorial area (mean Flux Co<sub>atm</sub> = 8 ± 2 nmol m<sup>-2</sup> d<sup>-1</sup>) and away from Patagonia in the SAW (mean Flux Co<sub>atm</sub> = 9 ± 4 nmol m<sup>-2</sup> d<sup>-1</sup>). Much lower Co atmospheric depositions were found in the SASG (mean Flux Co<sub>atm</sub> = 1.5 ± 0.5 nmol m<sup>-2</sup> d<sup>-1</sup>) and the SAG (mean Flux Co<sub>atm</sub> = 3 ± 1 nmol m<sup>-2</sup> d<sup>-1</sup>). The high atmospheric deposition of Co in the EA was linked to the high dust deposition, and those estimated in the SAW and at temperate latitudes of the North Atlantic to the Co enrichment of, respectively, the Patagonian aerosols [Gaiero et al., 2003] and the North American aerosols (R. Shelley, personal communication). Low Co atmospheric inputs were mainly caused by low dust depositions.

The atmospheric input of soluble Co (Flux SCo<sub>atm</sub>) was then estimated using solubility coefficients of Co from dust, following equation (11).

$$\text{Flux SCo}_{\text{atm}} \approx F_{\text{Co}_{\text{atm}}} \cdot S_{\text{Co}} \quad (11)$$

where S<sub>Co</sub> is the dissolution coefficient of cobalt from atmospheric particles in seawater and varies from 3% to 15% depending on the origin of the aerosol (see supporting information for the coefficients).

The modeled atmospheric deposition of soluble Co showed a different pattern compared to the estimated input of TCo (Figure 10). The highest input of soluble Co was indeed located in the temperate northern Atlantic, where 10 times higher inputs of soluble Co were estimated compared to the SASG (Figure 10). The model also showed a strong asymmetry of the soluble Co inputs between the two hemispheres with higher F<sub>SCo<sub>atm</sub></sub> in the north with the exception of the SAW where inputs from Patagonia are detected (Figure 10).

Despite consistent trends, these estimations have to be taken carefully due to the lack of available data on the different parameters, especially on the solubility of aerosols in seawater. Moreover, seasonal differences in the intensity of the dust deposition and in the air masses regimes likely introduce seasonal differences in Co inputs. For instance, lower dust deposition can occur during fall than in summer [Prospero and Lamb, 2003]. We compared the accuracy of our estimates in the West Atlantic with the only two direct measurements of the atmospheric inputs of soluble Co available in the literature at date. At the BATS station (31°N), our estimate of soluble Co deposition (0.7 nmol m<sup>-2</sup> d<sup>-1</sup>) is in the range of the atmospheric DCo input previously measured during the FeATMIS-1 and FeAST-6 cruises (1.1 (late summer) and 0.1 nmol (early summer) m<sup>-2</sup> d<sup>-1</sup>, respectively; Figure 10) [Shelley et al., 2012]. At about 8°N, our estimation (0.7 nmol m<sup>-2</sup> d<sup>-1</sup>; Figure 10) was in agreement with the atmospheric inputs of soluble Co recorded in this area during fall by Baker et al. [2007] (0.6–1.1 nmol m<sup>-2</sup> d<sup>-1</sup>). Overall, our estimations strongly suggested that the atmospheric input can be a main external source of DCo in the subtropical and equatorial areas of the northwestern Atlantic. The asymmetry of SCo<sub>atm</sub> inputs between the two hemispheres may be due to the westward trade winds that are strongest at the equator and 30°N compared to the south, and to the North American aerosols that can be enriched in Co at temperate latitudes (R. Shelley, personal communication). The higher inputs of soluble Co in the Northern Hemisphere can account for the relative accumulation of DCo (versus P) observed in the surface waters of the NASG (Figure 4c). Without the atmospheric input, the concentrations of DCo in the surface waters of the NASG would be similar to those recorded in areas receiving far less atmospheric inputs, such as in the SASG (e.g., 24 ± 5 pm) and in another oligotrophic gyre like in the Central Pacific [Noble et al., 2008] and the South Central Atlantic [Noble et al., 2012]. The biogeochemical implications of the atmospheric source of DCo are discussed in details elsewhere (G. Dulaquais and M. Boye, Atmospheric cobalt deposition along the surface western Atlantic and biogeochemical implications, in review for publication in Earth and Planetary Sciences Letters).

#### 4.3. Residence Time of Cobalt in the Upper 100 m Along the Western Atlantic

The residence time of dissolved (DCo) and particulate (PCo) cobalt in the upper 100 m of the different domains were inferred using the stocks measurements and estimates of sources and sinks/fluxes we estimated (Table 4). It is conceptualized in a simplistic scheme of the Co cycling shown in Figure 7. The particulate export flux of Co (Table 2) was used to estimate the residence time of PCo in surface waters (equation (12)).

$$t_{\text{PCo}} \approx \frac{\text{PCo stock}}{\text{PCo export rate}} \quad (12)$$

The residence time of DCo due to biogeochemical processes ( $t_{\text{DCo biogeo}}$ , Table 4) was estimated considering the loss of DCo from the upper 100 m due to the export of the biogenic fraction of PCo (equation (13)).

Table 4. Stock and Residence Time of Dissolved (DCo) and Particulate (PCo) Cobalt in the Upper 100 m for the Different Biogeochemical Domains<sup>a</sup>

	SAG	NASG	N-BA	SEA	SASG	SAW
PCo stock ( $\mu\text{mol m}^{-2}$ )	$0.93 \pm 0.47$	$0.80 \pm 0.34$	$0.52 \pm 0.34$	$0.27 \pm 0.17$	$0.11 \pm 0.03$	$0.31 \pm 0.19$
$\tau_{\text{PCo}}$ (year)	$0.6 \pm 0.5$	$< 0.1 \pm 0.1$	$0.4 \pm 0.2$	$0.1 \pm 0.1$	$< 0.1 \pm 0.1$	$0.3 \pm 0.2$
DCo stock ( $\mu\text{mol m}^{-2}$ )	$5.9 \pm 1$	$3.3 \pm 0.8$	$3 \pm 1$	$3.4 \pm 1.0$	$2.4 \pm 0.5$	$3.8 \pm 0.8$
$\tau_{\text{DCo biogeo.}}$ (year)	$12.1 \pm 6.1$	$1.4 \pm 1.2$	$=$	$3.4 \pm 0.5$	$1.7 \pm 0.5$	$=$
$\tau_{\text{DCo phy.}}$ (year)	$0.7 \pm 0.2$	$9.0 \pm 2.2$	$1.0 \pm 0.3$	$0.9 \pm 0.3$	$6.6 \pm 1.4$	$0.7 \pm 0.2$
$\tau_{\text{DCo bio.}}$ (year) <sup>b</sup>	0.2	0.1	0.3	0.3	0.1	0.5

<sup>a</sup>The residence times of DCo are given considering biogeochemical processes ( $\tau_{\text{DCo biogeo.}}$ ) and physical processes ( $\tau_{\text{DCo phy.}}$ ) (see text for the explanation and calculation). The biological transfer time of the DCo stock ( $\tau_{\text{DCo bio.}}$ ) is also indicated.

<sup>b</sup>Estimated by  $\tau_{\text{DCo bio.}} = \text{DCo stock}/\text{DCo uptake}$  (using DCo uptake from Table 5).

For the calculations, we assumed that the atmosphere was the only source of lithogenic PCo and that scavenging does not occur in the upper 100 m. In a steady state regime, the export of the biogenic fraction of PCo can then be determined using equations (14) and (15).

$$\tau_{\text{DCo biogeo.}} \approx \text{DCo stock} / \text{Co biotic export rate}^{\text{A1}} \quad (13)$$

$$\text{Co biotic export rate} \approx \text{Co export rate} / \text{Co lithogenic export rate} \quad (14)$$

$$\text{Co lithogenic export rate} \approx F_{\text{Co atm}} / F_{\text{Co sol}} \quad (15)$$

The residence time of DCo due to physical processes ( $\tau_{\text{DCo phy.}}$ , Table 4) was also estimated following equation (16). The smaller of the two estimations will be considered as the residence time of DCo.

$$\tau_{\text{DCo phy.}} \approx \text{DCo stock} / (F_{\text{DCo advection}} + F_{\text{DCo diffusion}})^{\text{A1}} \quad (16)$$

The residence times of particulate cobalt in the surface waters were generally much lower than those of the dissolved cobalt in the different domains, up to 28 times lower in the SASG (Table 4). Particulate cobalt resided shortly in the two oligotrophic domains ( $\tau_{\text{PCo}} \sim 20$  days), whereas at high latitudes and near the equator, longer PCo residence times were estimated, up to 200 days in the SAG. In this latter domain, the residence time of PCo was probably overestimated, as we assumed a steady state, whereas an intensive bloom occurring during our period of sampling (spring) may have increased the PCo stock by the assimilation of DCo. This would result in the apparent high stock of PCo ( $\sim 1 \mu\text{mol m}^{-2}$ ) that might not be representative of the annual average PCo stock.

The longer residence times of DCo were estimated in the two oligotrophic domains ( $\sim 1.5$  years). In these high-regeneration systems, the residence times of DCo were driven by biogeochemical processes rather than by the physical processes ( $3 < \tau_{\text{DCo phy.}}/\tau_{\text{DCo biogeo.}} < 7$ ). On the contrary, at high latitudes the physical processes may drive the DCo residence time ( $0 < \tau_{\text{DCo phy.}}/\tau_{\text{DCo biogeo.}} < 0.06$ ). Similar low-DCo residence times were estimated in the two hemispheres at high latitudes (0.7 year). Advection of DCo-enriched waters by the Labrador Current in the north and by the Malvinas Current in the south and strong seasonal biological Co uptake may explain the short residence time at those high latitudes. On either sides of the equator, we estimated an intermediate residence time of  $\sim 1$  year. Like at the high latitudes, the physics could drive the DCo residence time there, notably due to high-DCo input through diffusion caused by sharp vertical DCo gradients and by the equatorial current system that increases the diffusivity [Dulaquais et al., 2014]. Furthermore, the organic complexation of DCo in surface waters could slow down its scavenging onto particles [Saito and Moffett, 2001, 2002], further increasing its residence time in surface waters. The abundance of cyanobacteria in oligotrophic waters combined with their capacity to produce DCo organic ligands [Saito et al., 2005] would both account for the longer residence time of DCo estimated in these regions. Determination of the organic complexation of DCo in these waters is required to further confirm this hypothesis.

Table 5. Summary of the Dissolved (PCo) and Particulate (PCo) Cobalt Fluxes for the Upper 100 m (Averaging All Stations of Each Biogeochemical Domain) Along the GEOTRACES A02 Section<sup>a</sup>

Domain	SAG	NASG	SASG	SAW			
Period of Sampling	Spring	Dry Season	Dry Season	Summer			
Fluxes (nmol m <sup>-2</sup> d <sup>-1</sup> )							
PCo (Å) or DCo (+)	(1) Scavenging <sup>b</sup> (2) Uptake <sup>c</sup> (3) Regeneration <sup>d</sup> (4) Dust dissolution	Negl. (Å) 106 [20–220] 10 [2–60] 0.5 [0.4–0.6]	Negl. (Å) 64 [18–197] 51 [14–130] 1.0 [0.3–1.3]	Negl. (Å) 27 [21–30] 21 [16–23] 0.5 [0.2–0.7]	Negl. (Å) 31 [15–47] 11 [5–20] Negl. [0.1–0.3]	Negl. (Å) 33 [14–51] 28 [10–40] Negl. [0–0.2]	Negl. (Å) 22 [7–30] 7 [2–10] 0.5 [0.3–0.7]
PCo	(5) Dust (6) Export $\Sigma$ PCo	(+) 3 [3–4] (+) 4 [3–5] (+) 94.5	(+) 7 [5–8] (+) 13 [0–30] (+) 6.5	(+) 8 [6–10] (+) 4 [2–6] (+) 9.5	(+) 4 [1–7] (+) 6 [5–8] (+) 18	(+) 1.5 [0.8–2] (+) 5 [3–7] (+) 1.5	(+) 9 [5–16] (+) 2 [1–3] (+) 21.5
DCo	(7) Amazon <sup>e</sup> (8) Vertical diffusion <sup>f</sup> (9) Lateral advection <sup>g</sup> $\Sigma$ DCo	Negl. (+) 7 [Å] 2–10 (+) 15 (Å) 73.5	Negl. (+) 1 [0–2] Negl. (Å) 11.5	(+) 1 [0–4] (+) 7 [2–10] (+) 2 (+) 4.5	Negl. (+) 7 [3–10] (+) 4 (Å) 9	Negl. (+) 1 [0–2] Negl. (Å) 4	Negl. (+) 9 [4–15] (+) 7 (+) 2
PCo + DCo	Sum <sup>h</sup>	(+) 380	(Å) 970	(+) 330	(+) 190	(Å) 160	(+) 280

<sup>a</sup>In italic and brackets = range; in bold = sum.

<sup>b</sup>Scavenging is assumed negligible.

<sup>c</sup>Using equations (1) and (3) with CoCof  $2.1 \pm 0.6 \mu\text{M M}^{-1}$  in the SAG (this study);  $2.16 \pm 0.7 \mu\text{M M}^{-1}$  in the NASG and the SASG [after Tovar-Sánchez et al., 2008; Berthelson et al., 2003];  $1.48 \pm 0.4 \mu\text{M M}^{-1}$  in the N-BA and S-BA (this study);  $0.4 \mu\text{M M}^{-1}$  in the SAW [Bown et al., 2011].

<sup>d</sup>The Amazon flux of DCo is determined using  $\text{FDCo}_{\text{Amazon}} = (\text{DCo}_{\text{Amazon}} \times z/100)/\tau_{\text{DCo}}$ .

<sup>e</sup>The diffusion fluxes are estimated as described in Dulaquais et al. [2014] and Table 3.

<sup>f</sup>The lateral advection of DCo is estimated in the SAG from  $\Delta$ DCo concentrations between stations 2 and 13, an area of  $8.4 \times 10^5 \text{ km}^2$  and a mean water flow of  $5.9 \text{ Sv}$  in the upper 100 m [Reid, 1994; Ratau et al., 2003]. In the SAW it is estimated from  $\Delta$ DCo concentrations between stations 1b and 6b, an area of  $5.5 \times 10^5 \text{ km}^2$  and a mean water flow of  $2.5–35 \text{ Sv}$  in the upper 100 m [Peterson et al., 1998]. In the N-BA, it is estimated from  $\Delta$ DCo concentrations between stations 41 and 35, an area of  $1 \times 10^6 \text{ km}^2$  and a mean water flow of  $5.9 \text{ Sv}$  in the upper 100 m [Tomczak and Godfrey, 2003]. In the S-BA, it is estimated from  $\Delta$ DCo concentrations between stations 15b and 41 an area of  $1.1 \times 10^6 \text{ km}^2$  and a mean water flow of  $5.3 \text{ Sv}$  in the upper 100 m [Tomczak and Godfrey, 2003].

<sup>g</sup>This sum is calculated using  $(\text{Sum DCo} + \text{Sum PCo}) \times S$ , where  $S$  is the surface of the different domain ( $0.84 \cdot 10^{12} \text{ m}^2$  for SAG,  $9.10^{12} \text{ m}^2$  for NASG,  $1.110^{12} \text{ m}^2$  for N-BA,  $1.10^{12} \text{ m}^2$  for S-BA,  $3.10^{12} \text{ m}^2$  for SASG, and  $0.55 \cdot 10^{12} \text{ m}^2$  for SAW).

In the northern subtropical domain, the residence time of DCo is 4 times higher than that previously estimated in the same area (e.g., 0.32 year) [Saito and Moffett, 2002]. However, it might be difficult to compare both values, since the latter was estimated without taking into account the regeneration process. Indeed, it was calculated as the quotient between the DCo stock and a mean annual new production of carbon at BATS [Jenkins and Goldman, 1985] that relies on a mean particulate Co:C ratio in the Sargasso Sea [Sherrell and Boyle, 1992]. On the other hand, our estimate of the biological transfer time of the DCo stock ( $\tau_{\text{DCo,bio}} = \text{DCo}_{\text{stock}}/\text{FDCo}_{\text{uptake}}$ ) at BATS ( $0.2 \pm 0.1$  year; Table 4) is in the range of the previous estimate of Saito and Moffett [2002]. In turn, the regeneration process increases the residence time of DCo in surface waters of Sargasso Sea.

Overall, these first assessments of the residence time of Co showed interesting features in the different domains. Longer PCo residence times were found in areas with shorter residence times of DCo and inversely, suggesting exchange processes between the two fractions. However, additional studies will be needed to better constrain these terms.

#### 4.4. Comparative Budgets and Biogeochemical Cycling of Cobalt in the Surface Waters of the Western Atlantic

The Co budgets in the upper 100 m water layer of each biogeochemical province are presented in Table 5 for PCo and DCo and shown conceptually for the entire western Atlantic in Figure 11. These budgets represent the state of the system at the time of the observations, hence, they only integrate fluxes and processes operating with a timescale that allows their observations. The aim of this exercise is to compare the characteristics of the different domains and the order of magnitude of the different terms rather than determine absolute values. The budgets are based on the full data sets available during the cruises (chemical, biological, geochemical, and hydrographic parameters), but some fluxes had to be estimated using parameters from the literature when cruise data were lacking.

Biological assimilation was the dominant flux in the different biogeochemical domains (Table 5). This is in line with the observations showing an overall nutrient-like distribution of DCo in the surface waters (Figures 4 and 6). The biological uptake flux of DCo was estimated as mentioned above, using Chl *a* values derived from the in situ fluorescence measurements obtained during the cruises and reported values of cellular quotas of Co/C in the phytoplankton species (Table 5) dominating in the different biogeochemical provinces [Sunda and Huntsman, 1995; Ho et al., 2003; Tovar-Sánchez et al., 2006; Twining et al., 2011; Twining and Baines, 2013]. The lowest uptake was estimated for the SAW ( $22 \text{ nmol m}^{-2} \text{ d}^{-1}$ ) and the highest in the SAG ( $106 \text{ nmol m}^{-2} \text{ d}^{-1}$ ). In the latter domain a bloom of coccolithophorids was likely occurring during our period of sampling in 2010 as suggested by the relatively high Chl *a* and PCo levels (Figures 3d and 4b) and potentially accounting for this extremely high uptake rate of DCo. The reoccupation of the SAG at a different season showed a decrease of the DCo stock by  $1.4 \mu\text{mol m}^{-2}$  (~25% of DCo stock) between April 2010 (station 8) and July 2012 (station 3c) at  $57^{\circ}\text{--}58.6^{\circ}\text{N}$  (Figure 6a). Considering the daily uptake of DCo estimated in the SAG during spring ( $106 \text{ nmol m}^{-2} \text{ d}^{-1}$ , Table 5), the observed DCo decrease ( $1.4 \mu\text{mol m}^{-2}$ ) would correspond to 13 days of biological uptake. This fits with the timescale of a coccolithophorid bloom [Brown and Yoder, 1994], further supporting the idea that the surface DCo depletion observed in summer was related to a coccolithophorid spring bloom. The regeneration rate of DCo in the surface waters ( $\text{Co}_{\text{reg}}$ ) was the second most important flux and represented between 10 and 85% of the Co uptake flux ( $\text{Co}_{\text{uptake}}$ ; Table 5). The highest regeneration fluxes of DCo were estimated in the subtropical domains ( $\text{Co}_{\text{reg}}/\text{Co}_{\text{uptake}} > 0.75$ ), consistent with the concept of oligotrophic areas being regenerated systems. At the high latitudes, the regeneration fluxes were low ( $\text{Co}_{\text{reg}}/\text{Co}_{\text{uptake}} < 0.25$ ), with the lowest flux estimated in the SAG (10%). The equatorial area was marked by an intermediate regeneration rate, representing about 50% of the Co uptake flux. Hence, the regeneration can be the dominant internal source of DCo in the surface waters, especially in the subtropical domains.

The removal fluxes of Co by export via settling particles to deeper waters were 5 (in the NASG) to 25 (in the SAG) times lower than the biological uptake of DCo (Table 5), reinforcing the importance of surface recycling of biogenic Co in oligotrophic surface waters. Among the external sources to the surface waters, the inputs of DCo by the Amazon can be considered significant only in the northern equatorial area ( $> 1 \text{ nmol m}^{-2} \text{ d}^{-1}$ ), and to a lower extent in the southern side of the NASG. The atmospheric inputs of soluble Co were considered as significant in three areas, the SAW, the EA, and the NASG. However, the atmospheric source was relatively small compared to the other fluxes (Table 5), probably because low solubility of aerosols that can limit their impact.

Lateral advection by mesoscale structures can be an important term of the DCo budget at a local scale [Dulaquais et al., 2014]. These eddies can act either as intensive source or sink of DCo depending on whether they are cyclonic or anticyclonic [Dulaquais et al., 2014]. Nevertheless, the lateral input of DCo by these eddies would be negligible at the scale of a basin, such as in the subtropical domains (Table 5). By contrast, the advection of DCo-enriched surface waters like from the eastern Atlantic by the equatorial currents and from the Amazon plume entrained by the equatorial countercurrent, can represent a significant source of DCo at low latitudes (Dulaquais et al. [2014] and Table 5, respectively). Similarly, the lateral transport of DCo-enriched surface waters from high latitudes to DCo-depleted temperate waters by the Labrador Current in the North and by the Malvinas Current in the South can also represent important source terms in the DCo surface budgets (Table 5). At frontal systems, turbulence, and diffusivity could also account for a significant input of DCo from deep waters into the surface [Dulaquais et al., 2014] (Table 5).

The nearly conservative behavior of DCo observed at high latitudes in the north associated with the high DCo concentrations recorded in these surface waters are in line with the budget estimations that indicated strong inputs of DCo into the surface layer due to lateral advection of DCo-enriched waters from higher latitudes and comparatively low biological uptake (Table 5). It is possible that melting of Arctic ice enriched in DCo (e.g.,  $\text{DCo}_{\text{ice}}/\text{DCo}_{\text{seawater}} > 15$ ) [Tovar-Sánchez et al., 2010], as well as continental shelf enrichment along the surface waters circulation were significant sources of DCo at these high latitudes. Additionally, the estimated DCo uptake flux by phytoplankton increased southward from these high latitudes and this is in line with the observations that DCo showed a nearly conservative behavior that gradually changed to a nutrient-like vertical distribution in the southern side of the SAG (Figure 4a). It is conceivable that this seasonal biological removal of DCo would be partially resupplied by regeneration of DCo at the end of summer.

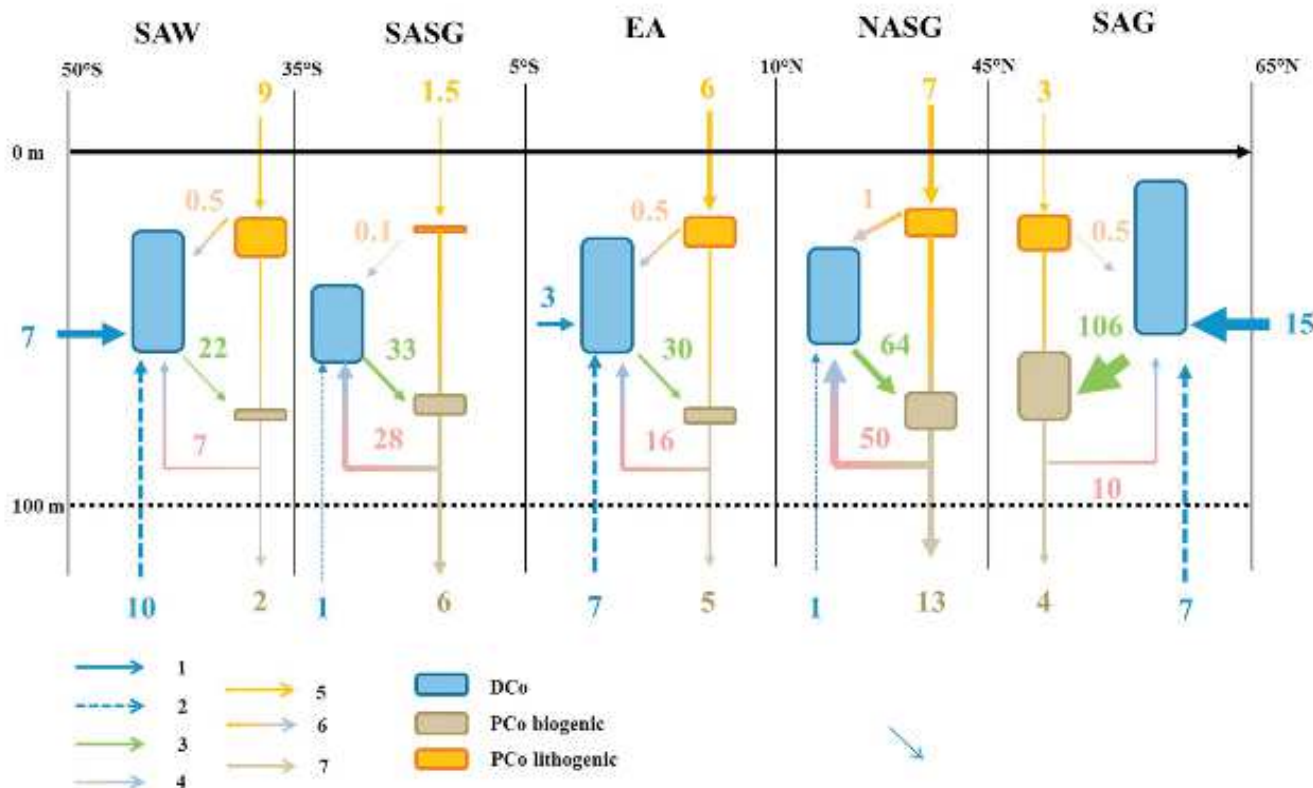


Figure 11. Conceptual schema of cobalt cycling in the different biogeochemical domains along the section. Wideness of the boxes represents the relative proportion of Co stock (at time of observation). Intensities of the fluxes are indicated and the numeration is described in Figure 7.

and by the mixing from wind-stress turbulence during late fall and winter times. In the subtropics, the nutrient-like P distributions of DCo (Figure 4a) fitted with the high biological uptake and extremely high regeneration rate (> 80%) of DCo estimated for the oligotrophic gyres (Table 5). Prochlorococcus and Synechococcus sp. dominated the phytoplankton assemblage in those domains, and their high biological requirement for cobalt probably generated the surface DCo depletion. This nutrient-like distribution was recorded at different seasons [Saito and Moffett, 2002]; hence, it could be a permanent feature of the Co cycle in the oligotrophic systems. However, higher external inputs were detected in the northern gyre, especially due to the dust deposition during the dry season and to the Amazon River discharge during the wet season, and they generated an asymmetry between the two hemispheres (Figures 9b and 10 and Table 5). In the equatorial area, the physical processes can sustain the biological uptake of DCo both sides of the equator (Table 5). Relatively high vertical diffusion DCo fluxes due to the incursion of DCo-enriched Atlantic Central Waters [Dulaquais et al., 2014] may indeed constitute a substantial source of DCo there (Table 5), in addition to the westward lateral advection of DCo-enriched waters by the equatorial currents system [Dulaquais et al., 2014]. The inputs by the physical dynamics can actually sustain up to 40% of the DCo drawdown due to biological uptake on both sides of the equator.

The global budget (DCo + PCo) at the scale of the western Atlantic (Table 5) clearly showed that the subtropical domains are acting as sink of Co (approximately  $\sim 1100$  t of Co/year), especially in the NASG. In contrast, high latitudes and equatorial Atlantic constituted sources of Co into the surface western Atlantic, balancing the sink determined in the subtropics (approximately  $\sim 1200$  t of Co/year). This mass balance suggests exchanges between the different domains probably through circulation of intermediate waters and transport by eddies. The MBC and the equatorial current system indeed supply eddies to the south and north subtropics, respectively. These dynamic structures can then supply in DCo the subtropics by advection of enriched surface waters, as well as by vertical advection/diffusion of DCo from intermediate waters wherein concentrations are higher. Like dust events, blooms, and export flux, eddy events can vary

seasonally. Thus, the seasonal variability within the different domains must be taken into account to understand the biogeochemical cycle of cobalt in the surface western Atlantic.

## 5. Conclusions

Significant regional correlations were observed between DCo and P across the different biological domains of the western Atlantic Ocean in part due to differences in the phytoplankton community composition. For instance, the highest DCo:P depletion ratios recorded in the two subtropical domains were related to an absolute requirement for DCo of the dominant cyanobacteria species, whereas the low DCo:P recorded in the subantarctic waters could reflect the low Co requirement of diatoms.

Biological uptake was the main sink of DCo in the surface waters of the western Atlantic, resulting in the overall nutrient-like distribution of DCo. The covariation of biogenic PCo and Chl a further supports the micronutritive behavior of Co. The higher biological assimilation rates of DCo by cyanobacteria at tropical latitudes compared to subpolar and subantarctic domains, can lead to the decreasing gradients of surface DCo observed from the high to the low latitudes along the western Atlantic. Regeneration that includes abiotic processes, microbial loop, cell lysis, and grazing was the prevailing internal source of DCo in oligotrophic surface waters, sustaining up to 85% of the biological DCo drawdown. Overall, the internal cycle of DCo was primarily driven by the two processes of biological uptake and regeneration.

The atmospheric input was a significant source of DCo to the Northern Hemisphere and generated an asymmetry in DCo concentrations between the north and south subtropical domains. The Amazon River accounted for up to 50% of the DCo inventory of the mixed layer in the tropical northwestern Atlantic, but its impact rapidly decreased away from the mouth. Together, these external sources can sustain the higher biological demand of DCo estimated in the northern subtropical gyre compared to the southern gyre.

Advection of DCo-enriched waters from the high latitudes can be source of DCo especially to the subpolar Atlantic, a region characterized by a low Co regeneration rate. Moreover, lateral advection and vertical diffusion can sustain the biological demand of DCo in the equatorial area.

Constraining the different sources and sinks has also allowed estimation of the DCo residence time in the upper 100 m. Short residence times driven by physical processes were determined at high northern latitudes (~0.7 year), whereas residence times were more than 2 times longer in the regenerated systems of the subtropics (~1.5 years).

Tentative budgets of Co in surface waters were assessed and they suggested non steady state regimes at the scale of each biogeochemical domain. At the scale of the western Atlantic basin, the loss of Co (dissolved plus particulate) in the subtropics could be balanced by the gain at the high latitudes and in the equatorial area. Exchanges and transportation from source regions (high latitudes) to sink regions (subtropics) through dynamic features (surface jets, eddies, and circulation at intermediate depths) could balance the Co budget in the western Atlantic basin.

This study has demonstrated the importance of variability in internal cycling and external sources of DCo across biogeochemical domains to regional and basin-scale Co budgets. This work also provides new keys to the parameterization of cobalt biogeochemistry in marine systems, which can be implemented in future three-dimensional global models of the oceanic cobalt cycle.

## References

- Arrigo, K. R., D. Worthen, A. Schell, and M. P. Lizotte (1998), Primary production in Southern Ocean waters, *J. Geophys. Res.*, 103(C8), 15,587–15,600, doi:10.1029/98JC00930.
- Aucour, A. M., F. X. Tao, P. Moreira-Turcq, P. Seyler, S. Sheppard, and M. F. Benedetti (2003), The Amazon River: Behaviour of metals (Fe, Al, Mn) and dissolved organic matter in the initial mixing at the Rio Negro/Solimoes confluence, *Chem. Geol.*, 197(1), 271–285.
- Baker, A. R., K. Weston, S. D. Kelly, M. Voss, P. Streu, and J. N. Cape (2007), Dry and wet deposition of nutrients from the tropical Atlantic atmosphere: Links to primary productivity and nitrogen fixation, *Deep Sea Res., Part I*, 54, 1704–1720.
- Baker, A. R., C. Adams, T. G. Bell, T. D. Jokalis, and L. Ganzeveld (2013), Estimation of atmospheric nutrient inputs to the Atlantic Ocean from 50°N to 50°S based on large-scale field sampling: Iron and other dust-associated elements, *Global Biogeochem. Cycles*, 27, 755–767, doi:10.1002/gbc.20062.
- Bertilsson, S., O. Berglund, D. M. Karl, and S. W. Chisholm (2003), Elemental composition of marine Prochlorococcus and Synechococcus: Implications for the ecological stoichiometry of the sea, *Limnol. Oceanogr.*, 48, 1721–1731.

## Acknowledgments

The complete data set of cobalt (dissolved, total, and apparent particulate) at all stations is available at the international GEOTRACES data center (<http://www.bodc.ac.uk/geotrades>). We are indebted to the Captains, officers, and crew members of the RV *Relâgia* and RSS *James Cook*: without their exceptional support, this large ocean section would not have been possible. We are most grateful to Loes Gerrings and Micha Rijkenberg, the chief scientists of the cruises. We warmly thank Jan van Coijen, K. Bakker, E. van Weerlee, and S. Ossabar for the analyses of nutrients, as well as S. Ober, Martin Laan, Steven van Heuven, S. Asjes, and L. Wuis for providing high-quality CTD data. We are much grateful to M. Rutgers van der Loeff for providing the particulate carbon data in the west northern Atlantic, R. Shelley for communication on cobalt concentrations in North Atlantic aerosols, and P.J. Lant for communication on cobalt/carbon ratio in the different size class of west northern Atlantic marine particles. This investigation was supported by the GEOTRACES-GEOSECS revisited in the West Atlantic project coordinated by M. Boye and funded by the French LEFE-CYBER National Program of the Institut National des Sciences de l'Univers (INSU). We also acknowledge the European COST Action E9801 for funding a short-term Scientific Mission to G. Dulaquais to join the last cruise of the GEOTRACES-A02 section. The Université de Bretagne Occidentale (UBO) and the Région Bretagne (AREB) are supporting the PhD fellowship of G. Dulaquais. P.M. was supported in part by a Geddes Visiting Fellowship awarded by the Institute of Advanced Studies at The University of Western Australia. This investigation is a contribution to the international GEOTRACES program. We warmly thank the two referees Mak Saio and Johann Bönni for their comments and constructive remarks.

- Bertrand, E. M., M. A. Saito, J. M. Rose, C. R. Rieselman, M. C. Lohan, A. E. Noble, P. A. Lee, and G. R. DiTullio (2007), Vitamin B12 and iron co-limitation of phytoplankton growth in the Ross Sea, *Limnol. Oceanogr.*, 52, 1079–1093.
- Babinet, S., E. A. Webb, C. Panzica, D. M. Karl, D. G. Capone, and S. A. Sañudo-Wilhelmy (2010), Vitamin B12 excretion by cultures of the marine cyanobacteria *Crocospheara* and *Synechococcus*, *Limnol. Oceanogr.*, 55(5), 1959–1964.
- Bowie, A. R., and M. C. Lohan (2009), Analysis of iron in seawater, in *Practical Guidelines for the Analysis of Seawater*, chap. 12, edited by O. Wurl, pp. 235–257, Taylor and Francis, Boca Raton, Ra.
- Brown, J., M. Boye, A. Baker, E. Duweilbourg, F. Lacan, F. Le Moigne, F. Planchon, S. Speich, and D. M. Nelson (2011), The biogeochemical cycle of dissolved cobalt in the Atlantic and the Southern Ocean south off the coast of South Africa, *Mar. Chem.*, 126, 193–206, doi:10.1016/j.marchem.2011.03.008.
- Brown, J., M. Boye, and D. M. Nelson (2012), New insights on the role of organic speciation in the biogeochemical cycle of dissolved cobalt in the southeastern Atlantic and the Southern Ocean, *Biogeosciences*, 9, 2719–2736.
- Boyle, E. A., S. S. Hustedt, and B. Grant (1982), The chemical mass balance of the Amazon River II. Copper, nickel, and cadmium, *Deep Sea Res. Part A*, 29(11), 1355–1364.
- Brown, C. W., and J. A. Yoder (1994), Coccolithophorid blooms in the global ocean, *J. Geophys. Res.*, 99(C4), 7487–7482, doi:10.1029/93JC02156.
- Browning, T. J., H. A. Bouman, C. M. Moore, C. Schlosser, G. A. Tairan, E. M. S. Woodward, and G. M. Henderson (2014), Nutrient regimes control phytoplankton ecophysiology in the South Atlantic, *Biogeosciences*, 11(2), 463–479.
- Brunland, K. W., and R. P. Franks (1983), Mn, Ni, Cu, Zn and Cd in the western North Atlantic, in *Trace Metals in Sea Water*, edited by C. S. Wong et al., pp. 395–414, Springer, New York.
- Campbell, L., H. A. Nolla, and D. Vaultot (1994), The importance of Prochlorococcus to community structure in the central North Pacific Ocean, *Limnol. Oceanogr.*, 39, 954–961, doi:10.4319/lo.1994.39.4.0954.
- Church, T. M. (1986), Biogeochemical factors influencing the residence time of microconstituents in a large tidal estuary, Delaware Bay, *Mar. Chem.*, 18(2), 393–403.
- Ooot, P. L., O. Baars, and P. Streu (2011), The distribution of dissolved zinc in the Atlantic sector of the Southern Ocean, *Deep Sea Res. Part II*, 58(25), 2707–2719.
- Cullen, J. T., Z. Chae, K. H. Coale, S. E. Fitzwater, and R. M. Sherrell (2003), Effect of iron limitation on the cadmium to phosphorus ratio of natural phytoplankton assemblages from the Southern Ocean, *Limnol. Oceanogr.*, 48, 1079–1087.
- Dammshäuser, A., T. Wagener, and P. L. Croat (2011), Surface water dissolved aluminum and titanium: Tracers for specific time scales of dust deposition to the Atlantic?, *Geophys. Res. Lett.*, 38, L24601, doi:10.1029/2011GL049847.
- de Baar, H. J. W., et al. (2008), Titan: A new facility for ultra-clean sampling of trace elements and isotopes in the deep oceans in the international GEOTRACES program, *Mar. Chem.*, 111(1–2), 4–21.
- de Jong, J. T. M., M. Boye, M. D. Gelado-Caballero, K. R. Timmermans, M. J. W. Veldhuis, R. F. Nolting, C. M. G. van den Berg, and H. J. W. de Baar (2007), Inputs of iron, manganese and aluminium to surface waters of the Northeast Atlantic Ocean and the European continental shelf, *Mar. Chem.*, 107, 120–142.
- Dulaquais, G., M. Boye, M. J. A. Rijkenberg, and X. Carton (2014), Physical and remineralization processes govern the cobalt distribution in the deep western Atlantic Ocean, *Biogeosciences*, 11(8), 1581–1580.
- Elwood, M. J. (2008), Wintertime trace metal (Zn, Cu, Ni, Cd, Pb and Co) and nutrient distributions in the subantarctic zone between 40–52°S, 155–180°E, *Mar. Chem.*, 112(1), 107–117.
- Ferreira, A., D. Stramski, C. A. Garcia, V. M. Garcia, A. M. Ootti, and C. R. Mendes (2013), Variability in light absorption and scattering of phytoplankton in Patagonian waters: Role of community size structure and pigment composition, *J. Geophys. Res. Oceans*, 118, 698–714, doi:10.1002/jgrc.20082.
- Feld, C. B., M. J. Behrenfeld, J. T. Panderson, and P. Falkowski (1998), Primary production of the biosphere: Integrating terrestrial and oceanic components, *Science*, 281(5374), 237–240.
- Ratau, M. K., L. Talley, and P. P. Niiler (2003), The North Atlantic Oscillation, surface current velocities, and SST changes in the subpolar North Atlantic, *J. Clim.*, 16(14), 2355–2369.
- Gaiero, D. M., J.-L. Probst, P. J. Depetris, S. M. Bdart, and L. Leleyter (2003), Iron and other transition metals in Patagonian riverborne and windborne materials: Geochemical control and transport to the southern South Atlantic Ocean, *Geochim. Cosmochim. Acta*, 67(19), 3603–3623.
- Ghoux, P., M. Chin, I. Tegen, J. M. Prospero, B. Holben, O. Dubovik, and S. J. Lin (2001), Sources and distributions of dust aerosols simulated with the GOCART model, *J. Geophys. Res.*, 106(D17), 20,255–20,273, doi:10.1029/2000JD000053.
- Goldman, J. C. (1988), Spatial and temporal discontinuities of biological processes in pelagic surface waters, in *Toward a Theory on Biological-Physical Interactions in the World Ocean*, edited by B. J. Rothschild, pp. 273–296, Kluwer Acad., Dordrecht, Netherlands.
- Goldman, J. C. (1993), Potential role of large oceanic diatoms in new primary production, *Deep Sea Res. Part I*, 40, 159–168.
- Gong, N., C. Chen, X. Liping, H. Chen, X. Lin, and R. Zhang (2005), Characterization of a thermostable alkaline phosphatase from a novel species *Thermus yunnanensis* sp. nov. and investigation of its cobalt activation at high temperature, *Biochim. Biophys. Acta, Proteins Proteomics*, 1750, 103–111.
- Grasshoff, K., M. Ehrhardt, and K. Kremling (1983), *Method of Seawater Analysis*, pp. 419, Verlag Chemie GmbH, Weinheim, Germany.
- Gregg, W. W., and N. W. Caey (2007), Modeling coccolithophores in the global oceans, *Deep Sea Res. Part II*, 54, 447–477.
- Head, E. J. H., L. R. Harris, and R. W. Campbell (2000), Investigations on the ecology of *Calanus* spp. in the Labrador Sea. I. Relationship between the phytoplankton bloom and reproduction and development of *Calanus finmarchicus* spring, *Mar. Ecol. Prog. Ser.*, 193, 53–73.
- Hellweger, F. L., and A. L. Gordon (2002), Tracing Amazon River water into the Caribbean Sea, *J. Mar. Res.*, 60, 537–549.
- Ho, T. Y., A. Quigg, Z. V. Rinke, A. J. Milligan, K. Wyman, P. G. Falkowski, and F. M. M. Morel (2003), The elemental composition of some marine phytoplankton, *J. Phycol.*, 39(8), 1145–1159.
- Jakuba, R. W., J. W. Moffett, and S. T. Dyrham (2008), Evidence for the linked biogeochemical cycling of zinc, cobalt, and phosphorus in the western North Atlantic Ocean, *Global Biogeochem. Cycles*, 22, GB4012, doi:10.1029/2007GB003119.
- Jenkins, W. J., and J. C. Goldman (1985), Seasonal oxygen cycling and primary production in the Sargasso Sea, *J. Mar. Res.*, 43(2), 485–491.
- Ji, Y., and R. M. Sherrell (2008), Differential effects of phosphorus limitation on cellular metals in *Chlorella* and *Microcystis*, *Limnol. Oceanogr.*, 53, 1790–1804.
- Jokela, T. S., et al. (2005), Global iron connections between desert dust, ocean biogeochemistry and climate, *Science*, 308, 67–71.
- Lane, T. W., and F. M. M. Morel (2000), Regulation of carbonic anhydrase expression by zinc, cobalt, and carbon dioxide in the marine diatom *Thalassiosira weissflogii*, *Rant Physiol.*, 123, 345–352, doi:10.1104/pp.123.1.345.

- Lomas, M. W., and S. B. Moran (2011), Evidence for aggregation and export of cyanobacteria and nano-eukaryotes from the Sargasso Sea euphotic zone, *Biogeoosciences*, 8(1), 203–216, doi:10.5194/bg-8-203-2011.
- Mahowald, N. M., A. R. Baker, G. Bergametti, N. Brooks, R. A. Duce, T. D. Jokela, N. Kubilay, J. M. Prospero, and I. Tegen (2005), Atmospheric global dust cycle and iron inputs to the ocean, *Global Biogeochem. Cycles*, 19, GB4025, doi:10.1029/2004GB002402.
- Mann, E. L. (2000), Trace metals and the ecology of marine cyanobacteria, PhD thesis, MIT/WHOI Joint Program in Oceanography, Cambridge, Mass.
- Martin, J. H., S. E. Fitzwater, R. M. Gordon, C. N. Hunter, and S. J. Tanner (1993), Iron, primary production and carbon nitrogen flux studies during the JGOFS North-Atlantic bloom experiment, *Deep Sea Res., Part I*, 40(1–2), 115–134.
- Mather, R., S. Reynolds, G. Wolff, R. G. Williams, S. Torres-Valdes, E. M. S. Woodward, A. Landolfi, X. Pan, R. W. Sanders, and E. Achterberg (2009), Phosphorus cycling in the North and South Atlantic Ocean subtropical gyres, *Nat. Geosci.*, 1, 438–443.
- McLaughlin, K., J. A. Sohm, G. A. Cutter, M. W. Lomas, and A. Paytan (2013), Phosphorus cycling in the Sargasso Sea: Investigation using the oxygen isotopic composition of phosphate, enzyme-labeled fluorescence, and turnover times, *Global Biogeochem. Cycles*, 27, 375–387, doi:10.1002/gbc.20037.
- Measures, C. I., and E. T. Brown (1998), Estimating dust input to the Atlantic Ocean using surface water Al concentrations, in *The Impact of African Dust Across the Mediterranean*, edited by S. Guerzoni and R. Chester, pp. 389, Kluwer Acad., Dordrecht, Netherlands.
- Measures, C. I., and S. Virk (2000), On the use of dissolved aluminium in surface waters to estimate dust deposition to the ocean, *Global Biogeochem. Cycles*, 14, 317–327, doi:10.1029/1999GB001188.
- Middag, R., H. J. W. de Baar, P. Laan, and K. Bakker (2009), Dissolved aluminium and the silicon cycle in the Arctic Ocean, *Mar. Chem.*, 115, 176–186, doi:10.1016/j.marchem.2009.08.002.
- Minobe, S., M. Miyashita, A. Kuwayano-Yoshida, H. Tokinaga, and S. P. Xie (2010), Atmospheric response to the Gulf Stream: Seasonal variations, *J. Clim.*, 23(13), 3699–3719, doi:10.1175/2010JCLI3359.1.
- Moffett, J. W., and J. H. (1998), Oxidation of cobalt and manganese in seawater via a common microbially catalyzed pathway, *Geochim. Cosmochim. Acta*, 62(18), 3415–3424.
- Moller, G. S. F., E. M. L. de M. Novo, and M. Kampel (2010), Space-time variability of the Amazon River plume based on satellite ocean color, *Cont. Shelf Res.*, 30, 342–352.
- Moore, W. S., J. L. Sarmiento, and R. M. Key (1988), Tracing the Amazon component of surface Atlantic water using  $^{228}\text{Ra}$ , salinity and silica, *J. Geophys. Res.*, 91(C2), 2574–2580, doi:10.1029/JC091iC02p02574.
- Moran, S. B., and R. M. Moore (1988), Evidence from mesocosm studies for biological removal of dissolved aluminum from seawater, *Nature*, 335, 706–708, doi:10.1038/335706a0.
- Murphy, J., and J. P. Riley (1962), A modified single solution method for the determination of phosphate in natural waters, *Anal. Chim. Acta*, 27, 31–38.
- Noble, A. E., M. A. Saito, K. Maiti, and C. R. Benitez-Nelson (2008), Cobalt, manganese, and iron near the Hawaiian Islands: A potential concentrating mechanism for cobalt within a cyclonic eddy and implications for the hybrid-type trace metals, *Deep Sea Res., Part II*, 55, 1473–1490, doi:10.1016/j.dsr2.2008.02.010.
- Noble, A. E., et al. (2012), Basin scale inputs of cobalt, iron, and manganese from the Benguela–Angola front to the South Atlantic Ocean, *Limnol. Oceanogr.*, 57, 989–1010.
- Okada, H., and A. McIntyre (1979), Seasonal distribution of modern coccolithophores in the western North Atlantic Ocean, *Mar. Biol.*, 54, 319–328.
- Oshiba, A., and V. Garçon (1998), Eddy-induced enhancement of primary production in a model of the North Atlantic Ocean, *Nature*, 394, 266–269.
- Owens, S. A., Pike, S., and K. O. Buesseler (2014), Thorium-234 as a tracer of particle dynamics and upper-ocean export in the Atlantic Ocean, *Deep Sea Res., Part II*, in press.
- Panzica, C. A., J. Beck, K. Leblanc, G. T. Taylor, D. A. Hutchins, and S. A. Sañudo-Wilhelmy (2008), Potential cobalt limitation of vitamin B12 synthesis in the North Atlantic Ocean, *Global Biogeochem. Cycles*, 22, GB2029, doi:10.1029/2007GB003124.
- Parsons, T. R., and C. M. Lalli (1988), Comparative oceanic ecology of the plankton communities of the subarctic Atlantic and Pacific Oceans, *Oceanogr. Mar. Biol. Annu. Rev.*, 26, 317–359.
- Peterson, R. G., and L. Stramma (1991), Upper-level circulation in the South Atlantic Ocean, *Prog. Oceanogr.*, 28, 1–73, doi:10.1016/0079-6411(91)90008-8.
- Peterson, R. G., C. S. Johnson, W. Krauss, and R. E. Davis (1998), Lagrangian measurements in the Malvinas Current, in *The South Atlantic Present and Past Circulation*, edited by G. Wefer et al., pp. 239–247, Springer, New York.
- Prospero, J. M., and P. J. Lamb (2003), African droughts and dust transport to the Caribbean: Climate change implications, *Science*, 302, 1024–1027.
- Reid, J. J. (1994), On the total geostrophic circulation of the North Atlantic Ocean: Flow patterns, tracers and transports, *Prog. Oceanogr.*, 33, 1–92.
- Reid, E. A., J. S. Reid, M. M. Meier, M. R. Dunlap, S. S. Cliff, A. Broumas, K. Perry, and H. Maring (2003), Characterization of African dust transported to Puerto Rico by individual particle and size aggregated bulk analysis, *J. Geophys. Res.*, 108(D19), 8591, doi:10.1029/2002JD002935.
- Rijkenberg, M. J., R. Middag, P. Laan, L. J. Gerringa, H. M. van Aken, V. Schoemann, J. T. M. de Jong, and H. J. de Baar (2014), The distribution of dissolved iron in the West Atlantic Ocean, *PLoS One*, 9(8), e101323, doi:10.1371/journal.pone.0101323.
- Rudnick, R. L., and S. Cao (2003), Composition of the continental crust, in *The Crust*, edited by R. L. Rudnick, pp. 1–70, Elsevier, Amsterdam.
- Saito, M. A., and J. W. Moffett (2001), Complexation of cobalt by natural organic ligands in the Sargasso Sea as determined by a new high sensitivity electrochemical cobalt speciation method suitable for open ocean work, *Mar. Chem.*, 75, 49–68.
- Saito, M. A., and J. W. Moffett (2002), Temporal and spatial variability of cobalt in the Atlantic Ocean, *Geochim. Cosmochim. Acta*, 66, 1943–1953.
- Saito, M. A., J. W. Moffett, S. W. Chisholm, and J. B. Waterbury (2002), Cobalt limitation and uptake in Prochlorococcus, *Limnol. Oceanogr.*, 47(8), 1629–1638.
- Saito, M. A., J. W. Moffett, and G. R. DiTullio (2004), Cobalt and nickel in the Peru upwelling region: A major flux of labile cobalt utilized as a micronutrient, *Global Biogeochem. Cycles*, 18, GB4030, doi:10.1029/2003GB002216.
- Saito, M. A., G. Rocap, and J. W. Moffett (2005), Production of cobalt binding ligands in a Synechococcus feature at the Costa Rica Upwelling Dome, *Limnol. Oceanogr.*, 50, 279–290, doi:10.4319/lo.2005.50.1.0279.
- Saito, M. A., T. J. Goepfert, A. E. Noble, E. M. Bertrand, P. N. Sedwick, and G. R. DiTullio (2010), A seasonal study of dissolved cobalt in the Ross Sea, Antarctica: Micronutrient behavior, absence of scavenging, and relationships with Zn, Cd, and P, *Biogeoosciences*, 7, 4059–4082, doi:10.5194/bg-7-4059-2010.
- Seyler, P., and G. R. Boaventura (2003), Trace elements in the mainstream Amazon River, in *The Biochemistry of the Amazon Basin*, edited by M. E. McCain, pp. 534, Oxford Univ. Press, Oxford, U.K.

- Shelley, R. U., B. Zachhuber, P. N. Sedwick, P. J. Worsfold, and M. C. Lohan (2010), Determination of total dissolved cobalt in UV-irradiated seawater using flow injection with chemiluminescence detection, *Limnol. Oceanogr.*, 55, 352–362, doi:10.4319/lom.2010.55.2.00352.
- Shelley, R. U., et al. (2012), Controls on dissolved cobalt in surface waters of the Sargasso Sea: Comparisons with iron and aluminum, *Global Biogeochem. Cycles*, 26, GB2020, doi:10.1029/2011GB004155.
- Sherrill, R. M., and E. A. Boyle (1992), The trace metal composition of suspended particles in the oceanic water column near Bermuda, *Earth Planet. Sci. Lett.*, 111, 155–174.
- Silver, M. W., M. M. Gowing, and P. J. Davoll (1986), The association of photosynthetic picoplankton and ultraplankton with pelagic detritus through the water column (0–2000 m), *Can. Bull. Fish. Aquat. Sci.*, 214, 311–341.
- Snoak, J. M., J. M. Krest, and P. W. Szwarczki (2006), Geochemistry of the Amazon estuary, in *Estuaries*, pp. 71–90, Springer, Berlin.
- Sstramma, L., and M. England (1999), On the water masses and mean circulation of the South Atlantic Ocean, *J. Geophys. Res.*, 104(C9), 20883–20883, doi:10.1029/1999JC000139.
- Strickland, J. D. H., and T. R. Parsons (1968), *A practical handbook of seawater analysis*, First Edition, Fisheries Research Board of Canada, Bulletin, No. 167, p. 85.
- Subramaniam, A., et al. (2008), Amazon River enhances diazotrophy and carbon sequestration in the tropical North Atlantic Ocean, *Proc Natl. Acad. Sci. USA*, 105(30), 10,460–10,465.
- Sunda, W. G., and S. A. Huntsman (1995), Cobalt and zinc inter-replacement in marine phytoplankton: Biological and geochemical implications, *Limnol. Oceanogr.*, 40, 1404–1417.
- Swanner, E. D., N. J. Planavsky, S. V. Lalonde, L. J. Robbins, A. Bekker, O. J. Rouxel, M. A. Saito, A. Kappler, S. J. Mojzsis, and K. O. Konhauser (2014), Cobalt and marine redox evolution, *Earth Planet. Sci. Lett.*, 390, 253–263.
- Takahashi, M., and P. K. Benfeng (1983), Size-structure of phytoplankton biomass and photosynthesis in subtropical Hawaiian waters, *Mar. Biol.*, 76, 203–211.
- Tang, D., and F. F. M. Morel (2006), Distinguishing between cellular and Fe-oxide-associated trace elements in phytoplankton, *Mar. Chem.*, 99(1), 18–30.
- Tegen, I., M. Werner, S. P. Harrison, and K. E. Kohfeld (2004), Relative importance of climate and land use in determining present and future global soil dust emission, *Geophys. Res. Lett.*, 31, L05105, doi:10.1029/2003GL019216.
- Tomczak, M., and J. S. Godfrey (2003), *Regional Oceanography: An Introduction*, 2nd ed., pp. 422, Pergamon, Oxford, U.K.
- Tovar-Sánchez, A., and S. A. Sañudo-Wilhelmy (2011), Influence of the Amazon River on dissolved and intra-cellular metal concentrations in *Trichodesmium* colonies along the western boundary of the sub-tropical North Atlantic Ocean, *Biogeosciences*, 8, 217–225, doi:10.5194/bg-8-217-2011.
- Tovar-Sánchez, A., S. A. Sañudo-Wilhelmy, A. B. Kustka, S. Agustí, J. Dachs, D. A. Hutchins, D. G. Capone, and C. M. Duarte (2008), Effects of dust deposition and river discharges on trace metal composition of *Trichodesmium* spp. in the tropical and subtropical North Atlantic Ocean, *Limnol. Oceanogr.*, 51(4), 1755–1761.
- Tovar-Sánchez, A., C. M. Duarte, J. C. Alonso, S. Lacorte, R. Tauler, and C. Galba-Malagon (2010), Impacts of metals and nutrients released from melting multiyear Arctic sea ice, *J. Geophys. Res.*, 115, C07003, doi:10.1029/2009JC005685.
- Trapp, J. M., F. J. Miller, and J. M. Prospero (2010), Temporal variability of the elemental composition of African dust measured in trade wind aerosols at Barbados and Miami, *Mar. Chem.*, 120(1–4), 71–82, doi:10.1016/j.marchem.2008.10.004.
- Twining, B. S., and S. B. Baines (2013), The trace metal composition of marine phytoplankton, *Annu. Rev. Mar. Sci.*, 5, 191–215.
- Twining, B. S., S. B. Baines, J. B. Bozard, S. Vogt, E. A. Walker, and D. M. Nelson (2011), Metal quotas of plankton in the equatorial Pacific Ocean, *Deep Sea Res., Part II*, 58(3), 325–341.
- van Hulten, M. M. P., A. Sterk, A. Tagliabue, J. C. Dutay, M. Gehlen, H. J. De Baar, and R. Middag (2013), Aluminium in an ocean general circulation model compared with the West Atlantic Geotraces cruises, *J. Mar. Syst.*, 126, 3–23.
- van Coijen, J. (2010), Nutrient measurements, Cruise Report 64PE319, 17–19.
- Vink, S., and C. I. Measures (2001), The role of dust deposition in determining surface water distributions of Al and Fe in the South West Atlantic Deep Sea Res., Part II, 48(13), 2787–2809.
- Weinstein, S. E., and S. B. Moran (2004), Distribution of size-fractionated particulate trace metals collected by bottles and in-situ pumps in the Gulf of Maine–Scotian Shelf and Labrador Sea, *Mar. Chem.*, 87(3), 121–135.
- Xia, L., and Y. Gao (2010), Chemical composition and size distributions of coastal aerosols observed on the US East Coast, *Mar. Chem.*, 119(1), 77–80.



# **Chapitre 4**

## **Atmospheric cobalt deposition along the surface Western Atlantic and biogeochemical implications**



# ATMOSPHERIC COBALT DEPOSITION ALONG THE SURFACE WESTERN ATLANTIC AND BIOGEOCHEMICAL IMPLICATIONS

Gabriel Dulaquais<sup>1\*</sup> and Marie Boye<sup>1</sup>

<sup>1</sup> Laboratoire des Sciences de l'Environnement Marin UMR 6539 (UBO/CNRS/IRD/Ifremer), Institut Universitaire Européen de la Mer, Université de Bretagne Occidentale. Place Nicolas Copernic - FR 29280 Plouzané

\* corresponding author : G. Dulaquais, LEMAR UMR6539, 29280, FRANCE  
(gabriel.dulaquais@univ-brest.fr)

## Abstract:

The potential links existing between the distribution of cobalt (Co), the phytoplankton productivity and diversity, and the atmospheric deposition in the surface ocean have still received little attention, despite indirect evidences. For exploring such relationships, we report the spatial distributions of dissolved (DCo) and apparent particulate (PCo) cobalt in the surface Western Atlantic, and we estimate the contribution of the atmospheric input to the DCo and PCo inventories in the mixed-layer by assessing the dust deposition over the Western Atlantic, as well as the atmospheric fluxes in Co and soluble Co, and the residence times of those particulate and dissolved Co inputs in the surface waters. The atmospheric input is shown to significantly (20%) account in the stock of DCo in the surface Western Atlantic, but it is not the prevailing source of DCo into the mixed-layer, apart in the North Atlantic subtropical gyre (> 60%). In this latter domain, this input could largely feed the biological requirement of the pico-phytoplankton assemblage dominated by cyanobacteria. The high biological uptake of DCo by cyanobacteria is further supported by the prevailing biogenic nature of PCo in those waters. By contrast, the growth of *Synechococcus* sp. could be rather limited by the low atmospheric input of Co and the low bioavailability of inorganic Co in the South Atlantic subtropical gyre, unlike *Prochlorococcus* sp. In the other domains, the investigation of the lithogenic and biogenic partitioning of PCo suggests that the inverse relationship observed between the DCo inventories and the atmospheric input of Co with the chlorophyll a contents could mainly be driven by the spatial distribution of phytoplankton communities, rather than by the magnitude of dust deposition. By providing new insights on the dust contribution to surface Co biogeochemistry, this study suggests to consider the dust dissolution as an essential process to support cyanobacteria growth in the tropical North Atlantic, with further ecological implications.

**Keywords:** cobalt, biogeochemistry, Atlantic Ocean, dust deposition

## 1 Introduction

The elemental composition of coccolithophorids, diatoms and dinoflagellates suggests cobalt (Co) can be a bioactive element used by a wide range of phytoplankton (Ho et al., 2003; Quigg et al., 2003; Twining and Baines, 2013). Indeed, Co is the central atom of the B<sub>12</sub> vitamin (cobalamin), a bio-molecule used in several biological pathways (Raux et al., 2000; Martens et al., 2002). Recently it has been evidenced that addition of inorganic Co to Co-depleted waters increased the biosynthesis of B<sub>12</sub> suggesting that Co availability could also regulate the synthesis of this vitamin (Panzeca et al., 2008). Since B<sub>12</sub> abundance is suspected to play a role in phytoplankton growth, productivity and diversity (Sañudo-Wilhelmy et al., 2006; Panzeca et al., 2006; Bertrand et al., 2007; Gobler et al., 2007), the ecological interest of cobalt has recently increased.

In addition, Co can substitute for zinc (Zn) or cadmium (Cd) as co-factor in the carbonic anhydrase and, to a lesser extent, in the alkaline phosphatase (Price and Morel, 1990; Sunda and Huntsman, 1995; Yee and Morel, 1996; Lane and Morel, 2000; Lane et al., 2005; Gong et al., 2005). Such metal interplays can promote biological uptake of Co in waters depleted in Zn and Cd like in the subtropical domains (Wyatt, 2014). The cyanobacteria that are abundant in those oligotrophic regions are furthermore known to primarily require Co for their growth (Sunda and Huntsman, 1995; Saito et al., 2002). The primary production can thus be significantly cobalt dependent in these regions.

The correlations between dissolved cobalt (DCo) and phosphate (P) observed in the surface waters of temperate and subtropical regions (Martin et al., 1993; Saito and Moffett, 2002; Jakuba et al., 2008; Noble et al., 2008; Dulaquais et al., 2014b) further indicate the removal of DCo in surface waters due to phytoplankton uptake. For instance, the extremely low DCo concentrations and the relatively high DCo/P depletion ratio recorded in the subtropical Atlantic (Saito and Moffett, 2002; Jakuba et al., 2008; Bown et al., 2011) evidence the enhanced biological utilization of DCo in these areas. This biological uptake can be especially high in the northern subtropical gyre of the Western Atlantic compared to the southern gyre (Dulaquais et al., 2014b). Because there was no evidence of an iron limitation in those domains (Rijkenberg et al., 2014), it further suggests the importance of DCo in the subtropical waters. Contrastingly, nearly conservative surface distributions were recorded in the subarctic gyre of the Atlantic (Dulaquais et al., 2014a) and in the Southern Ocean (Bown et al., 2011). In the latter area, the conservative distribution has been related to the low biological utilization of DCo by Antarctic diatoms (Bown et al., 2011) in these Zn-replete

waters (Croot et al., 2011), consistent with the relatively high Zn:Co elemental ratio found in diatoms (Ho et al., 2003). The biological removal of DCo can thus be taxa-dependent and potentially be controlled by the availability of other trace metals concentrations such as Zn.

Understanding the sources of DCo to surface waters is important regarding the biological implications of this micronutrient. Here lateral advection, eddies diffusion, transportation from shelf sediment, river discharge and recycling have been reported to be sources of DCo in the surface waters of several oceanic areas (Saito and Moffett, 2002; Noble et al., 2008; 2012; Bown et al., 2011; Tovar-Sanchez, Sañudo-Wilhelmy, 2011; Dulaquais et al., 2014a, 2014b). The atmospheric input of Co has not been considered to predominantly drive the residence time of DCo in surface waters (Saito and Moffett, 2002). Yet the actual scarcity of measurements and/or estimations of the Co atmospheric fluxes yield this source and its impact on the phytoplankton to be poorly known.

For instance, the deposition of dust originating from Patagonia in the South and from Sahara in the North has been described to be significant source of Co to the Western Atlantic (Gaiero et al., 2003; Baker et al., 2007). In the north-western Atlantic, this input could mainly occur during the late summer, as exemplified in the Sargasso Sea (Shelley et al., 2012). In addition, the relative surface enrichment of DCo observed in the tropical Atlantic was also thought to be due to atmospheric input (Bowie et al., 2002). On the contrary, this input could be negligible in the south-eastern Atlantic (Bown et al., 2011) and in the south-central Atlantic (Noble et al., 2012), these areas receiving poor deposition of dust (Mahowald et al., 2005). Recent studies have also evidenced a wide range in the Co fractional composition and solubility of aerosols, depending of their crustal, marine or anthropogenic origins (Gaiero et al., 2003; Reid et al., 2003; Rudnick and Gao, 2003; Baker et al., 2007; Thuroczy et al., 2010; Trapp et al. 2010; Xia and Gao, 2010; Shelley et al., 2012). Despite such investigations, the atmospheric inputs of DCo to the surface waters and their biological implications have still been hardly studied. For instance, a co-limitation of the growth of *Prochlorococcus* sp. by iron and cobalt has been suggested in the subtropical-southern Atlantic where the dust load is relatively low (Shelley, 2011). Additionally, the correlation between the concentration of Co in aerosols and the Co cellular content of *Trichodesmium* sp. reported in the Equatorial Atlantic (Tovar-Sanchez et al., 2006) further suggests a key role of the atmospheric input of Co in such cyanobacteria growth. There, the metals cellular quotas (including Co) of *Trichodesmium* sp. would actually almost entirely (for 83-100 %) originate from Saharan deposition (Tovar-Sánchez et al., 2006).

Despite these recent findings, the relationships between the dust deposition, the distribution of Co in seawater and the phytoplankton productivity and diversity are still poorly known. To investigate these potential links, this study presents the spatial distributions of DCo and the apparent particulate cobalt (PCo) in the surface waters of the Western Atlantic Ocean, and it proposes an estimation of the atmospheric deposition of the dust and Co along the radial. Hence, we quantified the contribution of the dust deposition to the cobalt (particulate and dissolved) inventories in the mixed layer from the East of Greenland ( $64^{\circ}\text{N}$ ) to the Subantarctic waters ( $50^{\circ}\text{S}$ ). Those results are then discussed in regards with the physical and biological features encountered along the radial. This study is a first attempt to investigate the potential links between the atmospheric input of Co and the phytoplankton assemblage in the surface waters of the Western Atlantic.

## 2 Method

### 2.1 Cruise track and sampling

Samples were collected along the GEOTRACES-A02 section spreading from  $64^{\circ}\text{N}$  to  $50^{\circ}\text{S}$  in the Western Atlantic Ocean conducted between 2010 and 2012 (Figure 1). A total of 47 stations were sampled for dissolved cobalt analyses (DCo), and 15 stations for total (unfiltered) cobalt determinations (TCo). The apparent particulate cobalt concentrations (PCo) were calculated by subtraction of DCo from TCo. The complete dataset of Co is available at the international GEOTRACES datacenter (<http://www.bodc.ac.uk/geotrades/>).

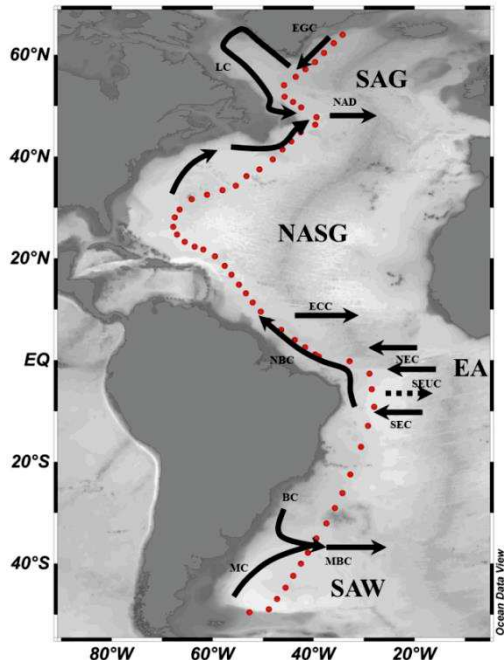


**Figure 2:** Cruise track and surface physical features and cruise track along the GEOTRACES-A02 section

All samples were collected using the TITAN-CTD frame of the Royal-NIOZ (Netherlands; de Baar et al., 2008; Rijkenberg et al., 2014). Unfiltered samples were transferred into acid cleaned 250 ml LDPE bottles (Nalgene) for TCo analyses. The samples for DCo analyses were collected after filtration using 0.2  $\mu\text{m}$  Sartobran 300 cartridges (Sartorius) under pure  $\text{N}_2$  pressure (filtered 99.99%  $\text{N}_2$ , 0.7 atm) in acid cleaned 250 ml or 500 ml LDPE (Nalgene) bottles. All samples were acidified using ultrapure HCl<sup>®</sup> at 0.01 M (Merck) immediately after their

collection. Then the acidified samples were stored in double bags at dark and ambient temperature before their analyses in the shore-based laboratory.

## 2.2 Method for cobalt analyses

Prior to the analyses, the seawater samples were UV-digested (Saito and Moffett, 2002; Shelley et al., 2010) for 3 h in acid clean silica tubes using a 600 W high-pressure mercury vapor lamp and left for an equilibration time of 48 h (Bown et al., 2011; Dulaquais et al., 2014a). Dissolved and total cobalt concentrations were determined by Flow-Injection Analysis (FIA) and chemiluminescence detection following the method described in Dulaquais et al. (2014a).

The mean reagent blank determined in acidified MilliQ water was  $4.2 \pm 2.1$  pM of Co in MilliQ ( $n = 180$ ). The standard deviation of the measurement is calculated by an error propagation using the error on blanks ( $\sigma$ ), the calibration curves and the deviation of the triplicate analyses (Dulaquais et al., 2014a). The limit of detection of the method ( $3\sigma$ ) was on average 6.3 pM of Co ( $n = 180$ ). Concentrations of DC<sub>o</sub> we measured in the reference SAFe and GEOTRACES samples were in excellent agreement with the consensus values (Dulaquais et al., 2014a). The analytical precision of the method was determined from repeated analyses of the surface GEOTRACES (GS) reference-sample, yielding an uncertainty of  $\pm 3.8\%$  ( $n = 15$ ).

## 3 Results and Discussion

### 3.1 Dynamical and biological specific features

The meridional mixed-layer depth ( $z$ ), as well as the mean salinity ( $S$ ), the temperature ( $T$ ), and the Chlorophyll a concentration (Chl a) derived from the fluorescence are presented, for the mixed layer along the section, in Figure 2. Five different domains are crossed along the radial, separated by surface jets as described in Dulaquais et al. (2014a). Briefly, the section starts at 64°N in the Subarctic gyre (SAG) which is limited to the south by the North Atlantic Subtropical Front (NASTF) at near 43-45°N. Then, the section enters in the North Atlantic subtropical gyre (NASG) separated to the Equatorial area (EA) by the North Equatorial Current (NEC). To the south, the section enters into the South Subtropical domain (SASG) by crossing the South Equatorial Current (SEC). Finally, the Subantarctic Waters (SAW) are reached south of the Malvinas-Brazil confluence (MBC). These surface jets can be located through, among others, their mixed-layer depth (Figure 2). The turbulence of these currents increases the mixed-layer depth. Furthermore, the surface temperature ( $T$ ) and salinity ( $S$ ) (Figure 2) are characteristic of the different domains along the section, and anomalies allow depicting specific features. For instance, the low salinities observed in surface between 4°N and 13°N are related to the Amazon River plume (Dulaquais et al., 2014a). Moreover, 3 cyclonic eddies were identified by their  $T$  and  $S$  signatures at 23°N, 29°S and 48.8°S (Figure 2), as well as by their sea level anomalies (data not shown). The spatial distribution of Chl a in surface furthermore indicates that SAG and SAW can be more biologically productive (mean Chl a  $> 0.3 \mu\text{g/L}$ ) than the Subtropical and Equatorial domains (mean Chl a  $< 0.1 \mu\text{g/L}$ ). Additionally, the biomass is higher in the NASG than in the SASG (Figure 2).

### 3.2 Spatial distribution of cobalt

The spatial distributions of the mean DC<sub>o</sub> and PC<sub>o</sub> concentrations in the mixed layer ( $z$ ) along the section are shown in Figure 3. Mean DC<sub>o</sub> concentrations range from 15.1 in the NASG (at 21.8°N) to 68.5 pM in the Denmark Strait (at 64°N). PC<sub>o</sub> inventories range from

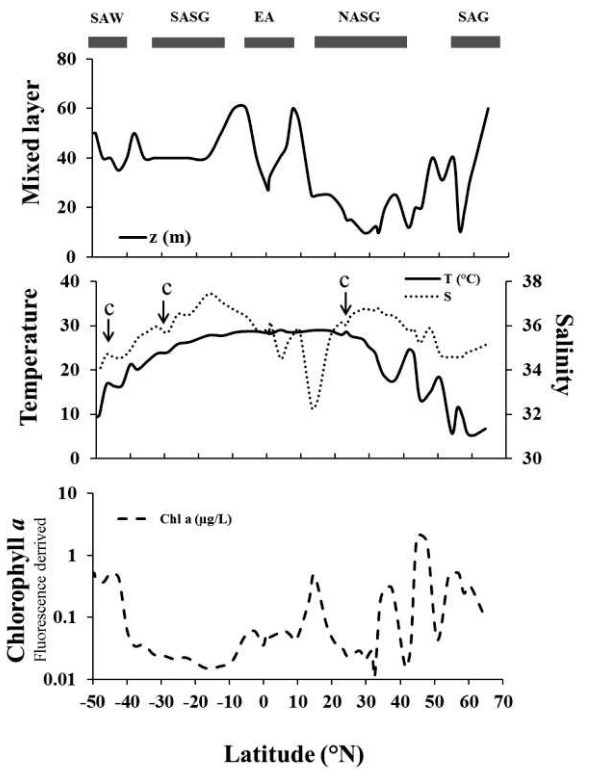


**Figure 2:** Surface mixed layer depth ( $z$ ), mean temperature ( $T$ ), mean salinity ( $S$ ) and mean Chlorophyll a (Chl a) derived from fluorescence distribution along the GEOTRACES-A02 section. The labels “c” locate the cyclonic eddies (see text for explanation).

The spatial distribution of Chl a in surface furthermore indicates that SAG and SAW can be more biologically productive (mean Chl a  $> 0.3 \mu\text{g/L}$ ) than the Subtropical and Equatorial domains (mean Chl a  $< 0.1 \mu\text{g/L}$ ). Additionally, the biomass is higher in the NASG than in the SASG (Figure 2).

0.8 pM in the SASG to 10.5 pM NASG, at 35°S and 23°N, respectively. The surface concentrations of PCo are marked by higher values in the northern hemisphere compared to the South (Figure 3). As described by Dulaquais et al. (2014a), cobalt occurs predominantly in the dissolved fraction in the Western Atlantic, thus the distribution of mean PCo in the mixed layer dispatches significantly lower concentrations than those of DCo, accounting for less than 3% (at 2.6°S) and up to 29 % (at 26°N) of the total cobalt concentrations (mean = $15 \pm 8$  %, n = 15). The physical features strongly impact the spatial distribution of DCo in the mixed layer (Dulaquais et al., 2014a). Indeed, high DCo concentrations are depicted in the frontal zones and surface jets (Figure 3), notably in the NASTF (around 43°N) and in the Equatorial

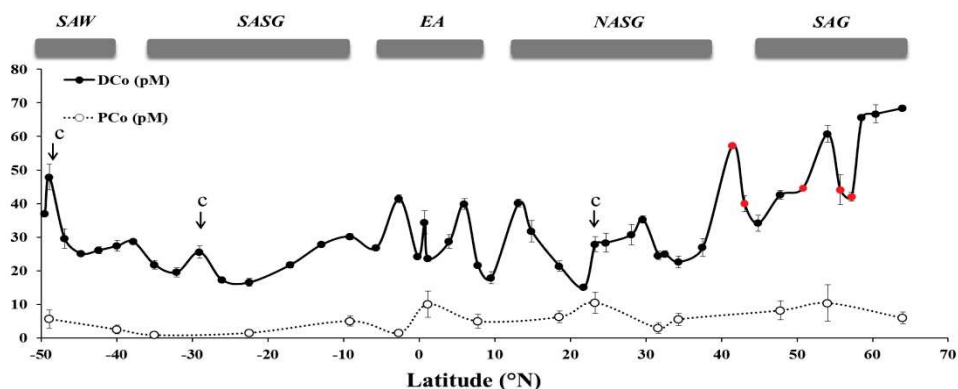


**Figure 3** Surface mean dissolved cobalt (DCo, dark circles, solid line) and mean apparent particulate cobalt (PCo, open circles, dashed line) concentrations in the mixed layer along the GEOTRACES-A02 section. Stations sampled during summer 2012 are labelled in red.

Current System (10°S-5°N). Furthermore, at locations where the section encounters cyclonic eddies (Figure 2), DCo also displays relatively high concentrations in the surface waters (Figure 3). Lateral advection of enriched-DCo waters by surface jets, as well as input from below through vertical advection and diffusion of intermediate and deep waters are thought to be main dynamical processes to increase the DCo concentration in surface waters (Noble et al., 2008; Bown et al., 2011; Shelley et al., 2012; Dulaquais et al., 2014a). On the contrary, the distribution of PCo is poorly impacted by the fronts, jets and eddies occurring in surface (Figure 3). The concentration of PCo indeed decreases with depth minimizing the input from below (Dulaquais et al., 2014a), and the residence time of PCo can be rather short compared to that of DCo lowering the input of PCo by lateral advection (Dulaquais et al., 2014b).

Interestingly, the lower DCo concentrations recorded in the subtropical domains, especially in the south, compared to High latitudes, are not associated with the highest Chl a concentrations, but actually it is with the lowest Chl a levels of  $< 0.1 \mu\text{g/L}$  that characterize the oligotrophic conditions of the subtropics (Figure 2). Similarly, the highest DCo levels are observed at the High latitudes where the Chl a concentrations are also the highest (Figure 2). Those patterns contrast fairly with the nutrient-like distribution of DCo observed in the surface waters of the Western Atlantic (Dulaquais et al., 2014), since an inverse correlation between DCo and Chl a concentrations would thus be expected. Hence, this result suggests that the intensity of the biological uptake that generates the nutrient-like profile of DCo could further depend from the phytoplankton assemblage rather than from the photosynthetic production. For instance, cyanobacteria dominate the pico-assemblage in the subtropics, and they have an absolute requirement for Co (Saito el al., 2002), whereas diatoms which are likely predominant at High latitudes do not preferentially assimilate Co for their growth (Sunda and Hunstmann, 1995). In turn, the strong assimilation of DCo by cyanobacteria in the low Chl a subtropical waters, and the relatively low assimilation by diatoms in the high Chl a waters of High latitudes likely account for the decreasing DCo gradient with latitude which does not fit with the decreasing Chl a concentrations (Dulaquais et al., 2014b). Nevertheless, higher DCo concentrations are recorded in the Subarctic gyre during the spring 2010 (65 pM; Figures 3) compared with the late summer 2012 (43.2 pM; Figure 3). There, the decrease of DCo concentrations over the springtime together with the increase of PCo (by up to  $10.4 \pm 4.44 \text{ pM}$ ) both fit with the development of the phytoplankton bloom occurring seasonally at those latitudes (Dulaquais et al., 2014b). Thus, the seasonality of the phytoplankton production might be superimposed to the composition of the phytoplankton assemblage to account for the extent of the biological uptake of DCo in the Western Atlantic.

The concentrations of DCo and PCo are furthermore generally lower in the southern than in the northern subtropical domain (Figure 3), in spite of similar predominance of cyanobacteria assemblage in both gyres. In this regard, it is conceivable that higher external sources in the North, such as the Amazon discharge crossed at  $4-13^\circ\text{N}$  (Figure 2), and potentially such as the dust deposition, would cause this asymmetry observed between the two hemispheres, in addition to differences between the northern and southern subtropics in the physical processes that are sources of Co in surface. Hereafter, we propose to characterize and quantify the contribution of the dust deposition to the cobalt concentrations in the mixed layer

along the radial, the other fluxes being described and quantified elsewhere in detail (Dulaquais et al., 2014b).

### **3.3 Atmospheric contribution to the cobalt inventory in the mixed-layer**

#### **3.3.1 Dust deposition**

To assess the dust deposition in the Western Atlantic, we use a modified version of the MADCOW model (Equation 1; Dulaquais et al., 2014b). Dissolved aluminum (DAI) is used as a proxy for the dust input in this model (Measures and Brown, 1996; Measures and Vink, 2000; Vink and Measures, 2001; de Jong et al., 2007), and we rely on the surface DAI concentrations recorded along the section (Middag et al., data not published). The major improvements of the model are the inclusion of a variable mixed-layer depth, a variable Al solubility in aerosols, and variable DAI residence times, depending on the biogeochemical province and the air-mass origin (Dulaquais et al., 2014b).

$$\text{Dust deposition rate} = \text{DAI} * z * M_{\text{Al}} * (A_{\text{Al}} * S_{\text{Al}} * \tau_{\text{Al}})^{-1} \quad \text{Equation (1)}$$

With  $z$  the mixed-layer depth ; DAI the mean concentration of DAI in  $z$  ;  $M_{\text{Al}}$  the molar mass of Al ;  $A_{\text{Al}}$  the crustal abundance of Al ;  $S_{\text{Al}}$  the solubility of Al in aerosols (Baker et al., 2013) ;  $\tau_{\text{Al}}$  the residence time of Al in  $z$  (Dulaquais et al., in rev.).

The dust deposition fluxes we estimate in this way vary from less than  $1 \pm 0.2 \text{ mg m}^{-2} \text{ d}^{-1}$  at several stations in the south-western Atlantic to up to  $15 \pm 0.3 \text{ mg m}^{-2} \text{ d}^{-1}$  near the Equator (Figure 4).

Despite the difficulties and limitations to use DAI as a dust proxy (Dammshäuser et al., 2011), especially due to its scavenging by biogenic particles (Moran and Moore, 1988; Middag et al., 2009), these estimations are in excellent agreement with previous predictions of the dust deposition fluxes in the Atlantic Ocean (Vink and Measures, 2001; Ginoux et al. 2001; Tegen et al. 2004; Mahowald et al., 2005; van Hulten et al., 2013).

#### **3.3.2 Atmospheric deposition of cobalt**

The atmospheric deposition fluxes of Co (Flux  $\text{Co}_{\text{atm}}$ ; Figure 4) are derived from the latter calculated dust deposition rates using Equation 2, in which the abundance of Co in aerosols ( $[\text{Co}]_{\text{dust}}$ ) vary between  $17$  and  $170 \mu\text{g g}^{-1}$  in the Western Atlantic depending on the air-mass origin (Gaiero et al., 2003; Reid et al., 2003; Rudnick and Gao, 2003; Baker et al., 2007; Trapp et al. 2010; Xia & Gao, 2010; Shelley et al., 2012; R. Shelley, personal communication). Then, the deposition rates of soluble Co (Flux  $\text{SCo}_{\text{atm}}$ ; Figure 4) are

estimated from the Co deposition fluxes and using reported solubility coefficients for Co in dust (Sol. Co), following Equation 3.

$$\text{Flux Co}_{\text{atm.}} = \text{Dust deposition rate} * [\text{Co}]_{\text{dust}} \quad \text{Equation (2)}$$

$$\text{Flux SCo}_{\text{atm.}} = F\text{Co}_{\text{atm.}} * \text{Sol. Co} \quad \text{Equation (3)}$$

with Sol. Co the solubility coefficient of Co from atmospheric particles in seawater (3%-15% depending on the origin of the aerosol; see details in Dulaquais et al., in rev.).

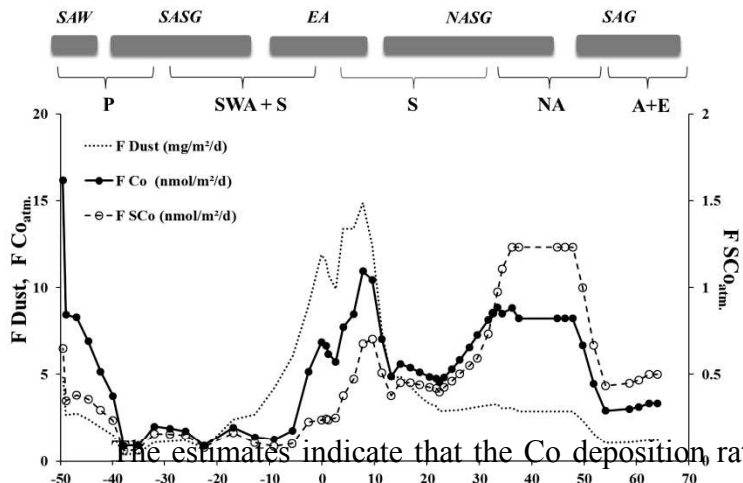


**Figure 4 :** Estimation of the sea-surface atmospheric deposition of dust (dots line), total Co (dark circles, solid line) and soluble Co (open circles, dashed line), along the GEOTRACES-A02 section. After Dulaquais et al., (2014b). Brackets delimit the main air-masses originated from: P: Patagonia; SWA: South Western Africa; S: Sahara; NA: North America; A: Arctic; E: Europe

The estimates indicate that the Co deposition rates vary from  $0.9 \text{ nmol.m}^{-2}.\text{d}^{-1}$  in the center of the SASG to up to  $16.2 \text{ nmol.m}^{-2}.\text{d}^{-1}$  close to Patagonia at St.#1b (Figure 4). The strongest mean atmospheric inputs of Co are located away from Patagonia in the SAW (mean Flux  $\text{Co}_{\text{atm}} = 9 \pm 4 \text{ nmol.m}^{-2}.\text{d}^{-1}$ ), at the temperate latitudes of the northern hemisphere ( $35^{\circ}\text{N}$ - $50^{\circ}\text{N}$ ; mean Flux  $\text{Co}_{\text{atm}} = 8 \pm 1 \text{ nmol.m}^{-2}.\text{d}^{-1}$ ) and in the northern-equatorial area (mean Flux  $\text{Co}_{\text{atm}} = 8 \pm 2 \text{ nmol.m}^{-2}.\text{d}^{-1}$ ). Those high atmospheric depositions of Co are clearly related to the high dust input at the EA (Figure 4), and to the high abundance of Co in the Patagonian dust (Gaiero et al., 2003) and in the North American aerosols (R. Shelley, personal communication) which settle in the SAW and at the temperate latitudes of the North Atlantic, respectively. Much lower atmospheric inputs of Co are found in the SASG (mean Flux  $\text{Co}_{\text{atm}} = 1.5 \pm 0.5 \text{ nmol.m}^{-2}.\text{d}^{-1}$ ), and in the SAG (mean Flux  $\text{Co}_{\text{atm}} = 3 \pm 1 \text{ nmol.m}^{-2}.\text{d}^{-1}$ ), likely due to the low input of dust we have estimated (Figure 4). Overall, an asymmetry of the Co deposition between the North and South hemispheres is designed, with higher Co deposition in the North ( $6.4 \text{ nmol of Co.m}^{-2}.\text{d}^{-1}$ ) than in the South ( $4.2 \text{ nmol of Co.m}^{-2}.\text{d}^{-1}$ ).

The modeled SCo input provided by dust dissolution shows a different pattern compared to the atmospheric flux of Co (Figure 4). Indeed, the highest input of soluble Co released from dust is found in the temperate North Atlantic ( $1.25 \text{ nmol.m}^{-2}.\text{d}^{-1}$ ), which is, respectively, 10 times and 2 times higher than that received by the SASG and close to

Patagonia by station 1b ( $0.65 \text{ nmol.m}^{-2}.\text{d}^{-1}$ ) (Figure 4). The model also shows a strong asymmetry of the soluble Co input between the two hemispheres, with high fluxes in the North compared to the South, at the exception of the relatively high values in the SAW due to the Patagonian input (Figure 4). The asymmetry in the atmospheric fluxes of Co and soluble Co fits with the distribution of PCo and DCo that shows higher concentrations in the North compared to the South. In a first order approach, the asymmetry in concentrations between the two hemispheres can thus be related to differences in the atmospheric inputs.

### 3.4 Relationship with the residence times of Co

In order to determine the influence of the atmospheric deposition on the Co distribution in the surface waters, the residence times needed to recover the Co inventories in the mixed-layer are estimated (Atm.  $\tau_{\text{Co}_z}$ ; Figure 5) as quotient between the Co inventory in the mixed-layer ( $\text{DCo}_z \text{ stock}$  or  $\text{PCo}_z \text{ stock}$ ; with  $\text{Co}_z \text{ stock} = \int_0^z \text{Co}$ ) and the net DCo or PCo atmospheric fluxes following Equations 4 and 5, respectively for DCo and PCo.

$$\text{Atm. } \tau_{\text{DCo}_z} = \text{DCo}_z \text{ stock} * \text{Flux SCo}_{\text{atm.}}^{-1} \quad \text{Equation (4)}$$

$$\text{Atm. } \tau_{\text{PCo}_z} = \text{PCo}_z \text{ stock} * (\text{Flux Co}_{\text{atm.}} - \text{Flux SCo}_{\text{atm.}})^{-1} \quad \text{Equation (5)}$$

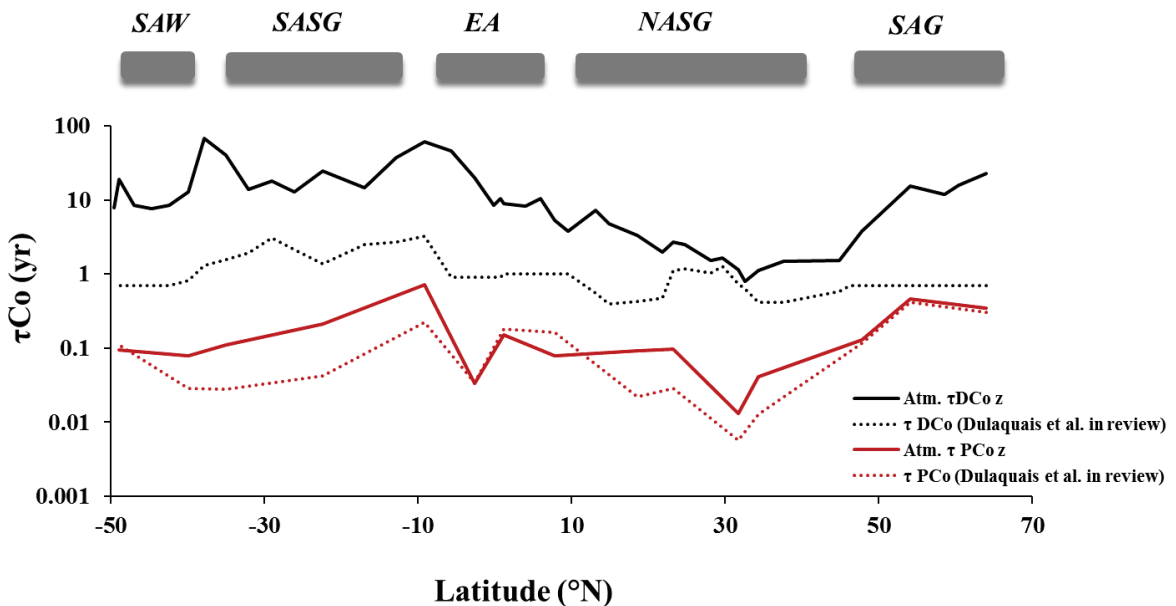


**Figure 5:** Residence times of DCo (Atm.  $\tau_{\text{DCo}_z}$ , Dark line) and PCo (Atm.  $\tau_{\text{PCo}_z}$ , red line) needed to recover the Co inventories in the mixed layer through atmospheric deposition. The residence times of DCo (dark dashed line) and PCo (red dashed line) determined by Dulaquais et al. (2014b) considering all the Co fluxes in the upper 100m are indicated. See text for explanation and calculation

In these conditions, the residence time needed to recover the DCo and PCo inventories in the mixed-layer shows to co-vary with the atmospheric inputs of SCo and Co respectively (Figures 4-5), suggesting the dust deposition strongly impacts the distributions of Co in the surface waters. Our estimations also describe residence time of PCo one to two orders of magnitude shorter than that of DCo in the mixed layer (Figure 5), indicating that PCo inventories could be more rapidly affected by dust event than DCo. This is in line with the common idea that particles react faster than dissolved compounds. Additionally, the shorter residence times are estimated in the central NASG for both fractions of Co (as low as 0.73 year for DCo, and 3-4 days for PCo; Figure 5). It suggests that the surface distribution of Co in the Sargasso Sea could be significantly more sensitive to atmospheric inputs than elsewhere in the Western Atlantic. The longest residence times are found close to the frontal zones, with Atm.  $\tau_{DCo_z}$  of up to 68 years at the MBC, and Atm.  $\tau_{PCo_z}$  of 0.7 year at the SEC (Figure 5). These latter estimations contrast fairly with expectation based on the physical and biological properties of these very dynamic areas where residences times are expected to be relatively short.

The comparison of the residence times of DCo and PCo obtained when considering only the atmospheric flux of Co to the mixed-layer (this study) with those estimated when all Co fluxes (e.g.; sources and sinks) are considered in the upper 100 m (Dulaquais et al., 2014b) indicates an overall longer residence times of DCo if the atmospheric deposition is the only one flux in surface waters ( $2 < \text{Atm. } \tau_{DCo_z} / \tau_{DCo_{100\text{ m}}} < 70$ , mean ratio = 13, n = 47; Figure 5). This result strongly suggests that the input of SCo from dust could not drive alone the residence time of DCo in surface waters. In turn, the impact of the atmospheric inputs could be rather small or less significant than the other fluxes in most of the biogeochemical domains. Nevertheless, in the central NASG, the two estimations for  $\tau_{DCo}$  are in the same order of magnitude (Figure 5), suggesting that dust deposition can drive the  $\tau_{DCo}$  there, and thus significantly impact the concentrations of DCo in the Sargasso Sea. The residence times of PCo estimated through the atmospheric Co deposition tightly follow the estimations based on all PCo fluxes in the surface waters (Figure 5; Dulaquais et al., 2014b). It indicates that the PCo inventories can be significantly driven by the atmospheric input of Co to the surface waters of the Western Atlantic. However, this is not the case in the two subtropical domains (Figure 5), where our  $\tau_{PCo}$  estimates are significantly higher than those considering all PCo fluxes (by a factor 3-5). Hence, other fluxes rather than the atmospheric input of Co likely govern the residence times of PCo in the subtropics, such as the biological assimilation and regeneration of Co by cyanobacteria (Dulaquais et al., 2014b).

### 3.5 Cumulative effect of the atmospheric input on the surface DCo inventories

To determine the contribution of the dust deposition to the Co concentrations in the mixed-layer, the cumulative effect of this flux is estimated by assuming that the dissolution of dust can only occur in the mixed-layer, and using the residence times that include all the fluxes of Co in the surface waters (Dulaquais et al., 2014b; Figure 5). In these conditions, the cumulative effect of atmospheric input to the mixed-layer DCo inventories (% Atm. DCo<sub>z</sub>) is estimated according to Equation 6.

$$\% \text{ Atm. DCo}_z = \text{Flux SCo} * \tau_{\text{DCo}} * \text{DCo}_{z \text{ stock}}^{-1} \quad \text{Equation (6)}$$

The results indicate that dissolution of aerosols in surface waters accounts for less than 10% of the DCo inventories in the Southern hemisphere, while it represents nearly 30% of this stock in the Northern hemisphere, even reaching 80% at 30°N (Figure 6). On the basin scale, the atmospheric input contributes for about 20% on average of the stock of DCo present in the mixed-layer of the Western Atlantic. Furthermore, the higher atmospheric input of SCo in the Northern hemisphere compared to the Southern one (Figure 4) is well reflected by the higher contribution of the atmospheric source to the DCo inventories in the North (Figure 6). However, the flux of SCo alone is too small to fully recover the DCo inventory in the mixed-layer in the Northern hemisphere (% Atm. DCo<sub>z</sub> ~ 30%; Figure 6). Thereby, the atmospheric inputs do not predominantly drive the DCo distribution in the mixed-layer of the Western Atlantic, apart in the north-western tropical Atlantic where the dust deposition and subsequent dissolution is the prevailing source of DCo to the surface waters of the NASG (% Atm. DCo<sub>z</sub> > 60%; Figure 6). In turn, other sources of DCo such as eddies (Noble et al., 2008; Dulaquais et al., 2014), lateral advection (Bown et al., 2011; Noble et al., 2012; Dulaquais et al., 2014), riverine inputs (Saito and Moffett, 2002; Dulaquais et al., 2014b), margin inputs (Bown et al., 2012b) have thus to be also considered in most of the Western Atlantic, as well as regeneration of Co in the surface waters (Dulaquais et al., 2014b).

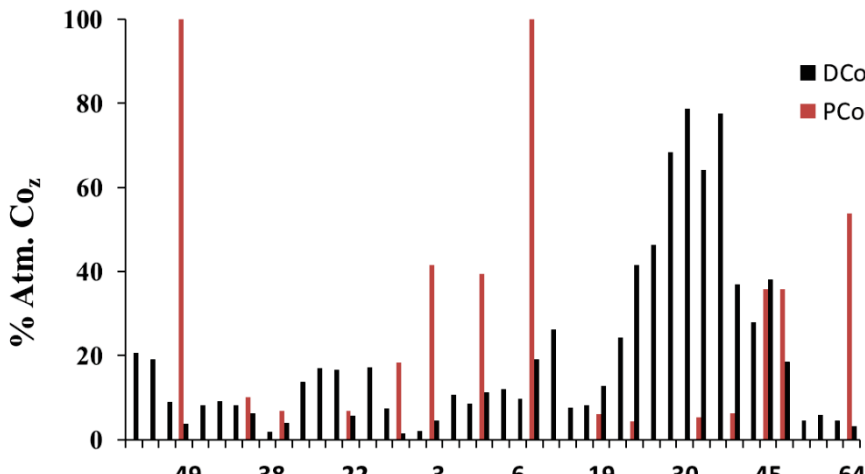


Figure 6: Cumulative atmospheric contribution to the DCo (dark bars) and PCo (red bars) inventories in the mixed layer.

### 3.6 Lithogenic and biogenic partitioning of particulate cobalt

Assuming the atmosphere is the only source of lithogenic PCo in the surface Western Atlantic, the estimation of the cumulative effect of the atmospheric input to the PCo inventories (Equation 7) provides a direct estimate of the lithogenic portion of PCo present in the mixed-layer (Equation 8). The portion of PCo from biogenic origin is then calculated according to Equation 9.

$$\% \text{ Atm. PCo}_z = (\text{Flux Co} - \text{Flux SCo}) * \tau_{\text{PCo}} * \text{PCo}_{z \text{ stock}}^{-1} \quad \text{Equation (7)}$$

$$\% \text{ Lithogenic PCo} = \% \text{ Atm. PCo}_z \quad \text{Equation (8)}$$

$$\% \text{ Biogenic PCo} = 1 - \% \text{ Atm. PCo}_z \quad \text{Equation (9)}$$

Interestingly, the partitioning suggests that PCo occurs predominantly as biogenic particles (> 90%) in the subtropical domains (Figure 6), whereas Chl a levels are extremely low in these areas (Figure 2). It suggests that biogeochemical processes can control the surface cycle of PCo in the subtropics, independently of the intensity of Co atmospheric deposition (Figures 4 and 6). Due to their essential requirement for Co to grow (Saito et al., 2002), the cyanobacteria that dominate the phytoplankton assemblage in the subtropics can indeed significantly increase the biogenic fraction of PCo. The strong uptake of DCo by cyanobacteria and the subsequent increase of biogenic PCo are further supported by the concomitant low DCo concentrations and the well-marked nutrient-like profiles of DCo recorded in these surface waters (Dulaquais et al., 2014).

On the contrary, PCo can be mainly of lithogenic origin at the High latitudes (up to 100% close to Patagonia; Figure 6), suggesting that PCo concentrations could be mainly driven by dust deposition at these latitudes. The lithogenic origin of PCo contrasts fairly with the relatively high photosynthetic biomass (Figure 2) and the rather small dust delivery in the subpolar domain (Figures 4 and 6). However, the diatoms that probably dominated the phytoplankton assemblage at the High latitudes at the season of sampling (Henson et al., 2006; Olgun and Alder, 2011) preferentially assimilate Zn (or Cd) rather than Co (Saito et al., 2008; and references therein), thus poorly contributing to increase biogenic PCo. The rather low biological uptake of Co is further supported by the nearly conservative distribution of DCo observed in subpolar surface waters (Dulaquais et al., 2014). Nevertheless, additional investigations on Zn (and Cd) bioavailability would be required to further confirm this hypothesis.

In the productive area of the temperate North Atlantic (45–50°N; Figure 2) that receives high Co deposition (Figure 4), the proportion of biogenic PCo keeps relatively high (65%; Figure 6). There, the coccolithophorids that likely bloom in this area at date of sampling (Dulaquais et al., 2014; and references therein) require Co to growth (Sunda and Huntsman, 1995) and have a relatively high Co cellular content (Ho et al., 2003; Quigg et al., 2003). Thus, the bloom could have temporarily generated the high PCo inventory (Figure 3), and significantly increased the biogenic PCo portion (Figure 6).

The Equatorial area is marked by intermediate proportions of lithogenic PCo (40%; Figure 6), and slightly higher biogenic origin (60%) of the particulate Co. Those estimates are in line with the strong biological uptake of Co by the cyanobacteria which represent a significant proportion of the pico-assemblage in this domain (Agusti, 2004; Tovar-Sanchez and Sanudo Wilhelmy, 2011), and with the high atmospheric Co deposition (Figure 4), that both increase the PCo inventories (Figure 3) in the biogenic and lithogenic fractions. Exception is found at 8°N, where surface PCo can originate entirely from the atmospheric deposition of lithogenic dust (Figure 6). This is in agreement with the extremely high atmospheric deposition of Co we estimated at this latitude ( $> 10 \text{ nmol.m}^{-2}.\text{d}^{-1}$ ; Figure 4), and with the low Chl a level recorded at this location at time of sampling (Figure 2).

### 3.7 Potential biological implications of the atmospheric deposition of cobalt

The dissolution of the aerosol in the north-western subtropical Atlantic which receives high dust deposition (Figure 4) significantly impacts the DCo in mixed-layer (Figure 6), accounting for 62% of the mean 29 pM measured in the center of the northern gyre (Figure 3). This prevailing source of DCo can actually feed the absolute requirement for Co of cyanobacteria that dominate the pico-assemblage in this domain (Treush et al., 2011). Indeed, the concentrations of inorganic DCo ( $\text{Co}^{2+}$ ) we determined in the Sargasso Sea at BATS station resting on our analyses of the organic complexation of DCo in these surface samples (e.g.; DCo = 27 pM; the organic Co-binding ligand concentration, L, is equal to 26.4 pM; and the conditional stability constant of the organic  $\text{Co}^{2+}\text{-L}$  complexes,  $\log K'_{\text{CoL}}$ , is equal to 18; n = 2) following the method published in Bown et al. (2012a), are equal to about 0.6 pM. These inorganic levels are 6 to 20 times higher than the half-saturation constants for  $\text{Co}^{2+}$  ( $K_{m\text{Co}2+}$ ; Table 1) of the cyanobacteria *Prochlorococcus* and *Synechococcus* (e.g.; 0.03 pM and 0.1 pM, respectively; Sunda and Huntsman, 1995; Saito et al., 2002). Consequently, the

atmospheric input of Co would be largely sufficient to sustain optimum growth of the cyanobacteria in the Sargasso Sea.

Interestingly, in the north-western subtropical Atlantic receiving high Co atmospheric deposition (Figure 4), *Synechococcus* abundances ( $10^7 \text{ cell.L}^{-1}$ ; Twining et al., 2010) are 10 to 40 times higher than those found in the south-western subtropical Atlantic ( $5-10 \times 10^5 \text{ cell.L}^{-1}$ ; Agusti, 2004) where atmospheric DCo fluxes are low (Figure 4). On the contrary, the cell densities of *Prochlorococcus* are similar in the North- and South-western subtropical domains ( $\sim 10^8 \text{ cell.L}^{-1}$ ; Agusti, 2004; Treush et al., 2011). These two subtropical domains also dispatch similar macro-nutrients concentrations (Dulaquais et al., 2014) and similar concentrations of organic Co-binding ligands (at 22°S: DCo = 24 pM L= 29 pM;  $\log K'_{\text{CoL}} = 18.4$ ; n =2), but the  $\text{Co}^{2+}$  concentrations we determined in the SASG ( $< 10^{-5} \text{ pM}$ ) are 4 orders of magnitude lower than those found in the NASG (0.6 pM). In turn, it is conceivable that *Synechococcus* growth ( $K_{m\text{Co}^{2+}} = 0.1 \text{ pM}$ ; Sunda and Huntsman, 1995) would be limited in the south-western Atlantic gyre by the low atmospheric input of Co and the low availability of  $\text{Co}^{2+}$  ( $< 10^{-5} \text{ pM}$ ), whereas *Prochlorococcus* which can rely on the organic cobalt to growth (Saito et al., 2002) will be fully replenished in DCo even in the southern area of low dust input (DCoSASG = 24 pM; % Atm. DCo<sub>z</sub> = 10%).

**Table1.** Actual biogeochemical state of the North-western Atlantic gyre and possible implications for a future 30% decrease of the dust deposition.

State of Atmospheric deposition intensity	Actual	70% of Actual
Mean Dust deposition ( $\text{mg.m}^{-2}.\text{d}^{-1}$ )	3.05	2.1
Mean Atmospheric Co flux ( $\text{nmol.m}^{-2}.\text{d}^{-1}$ )	6.6	4.8
Mean Atmospheric DCo flux ( $\text{nmol.m}^{-2}.\text{d}^{-1}$ )	0.57	0.4
Mean DCo <sub>z</sub> (pM)	29	23.5 <sup>a</sup>
Mean $\text{Co}^{2+}$ (pM)	0.6 <sup>b</sup>	$10^{-5}$ <sup>c</sup>
$K_{m\text{Co}^{2+}}$ <i>Synechococcus</i> (pM) <sup>d</sup>	0.1	0.1
<i>Synechococcus</i> abundance ( $\text{cell.I}^{-1}$ )	$10^7$ <sup>e</sup>	$5 \times 10^5$ <sup>f</sup>
<i>Synechococcus</i> B <sub>12</sub> production rate ( $\text{mol.cell}^{-1}$ ) <sup>g</sup>	$12 \times 10^{-20}$	$12 \times 10^{-20}$
B <sub>12</sub> seawater (pM) <sup>h</sup>	1.2	0.06

a Estimated considering that 62% of the actual DCo concentration in the mixed layer is provided by the atmospheric DCo flux

b Determined following the method of Bown et al., 2012a

c Estimated considering estimation of DCo and a constant ligand concentration between the two states

d From Sunda and Huntsman, 1995

e From Twining et al., 2010

f *Synechococcus* abundance from Agusti, 2004 in the  $\text{Co}^{2+}$  growth limiting waters of the south western subtropical waters

g For starved N-condition, from Bonnet et al., 2010

h Estimated as the *Synechococcus* abundance multiplied by the B12 production rate of these species

In a scenario of potential future decreasing of the dust deposition by 30% in the NASG (Mahowald et al., 2006), the atmospheric Co inputs would also decrease by 30%. In these conditions, we estimate that DCo concentration would drop from 29 to 23.5 pM in the center of the northern gyre (Table 1). Hence, the concentration of  $\text{Co}^{2+}$  would be as low as  $4 \times 10^{-6}$  pM (Table 1), if the concentrations and composition of the organic Co-binding ligand would not change compared with present conditions. At this level the growth rates of *Synechococcus* would be severely Co-limited and their cell densities would drop to abundances as low as those previously recorded in the SASG (Agusti, 2004; Table 1). Yet, *Prochlorococcus* sp. which can rely not only on  $\text{Co}^{2+}$ , but also on the organic Co complexes to growth (Saito et al., 2002) could be poorly affected by 30% decrease of the atmospheric Co-input, since DCo (23.5 pM) would still keep at levels about 2 orders of magnitude higher than the half-saturation constant for Co of these species (0.03 pM; Sunda and Huntsman, 1995).

The decrease of the *Synechococcus* abundance potentially induced by 30% decrease of the atmospheric input of Co in the North Atlantic gyre could impact the entire phytoplankton community, considering their determining role in the oceanic production of  $\text{B}_{12}$  vitamin.  $\text{B}_{12}$  is indeed a Co-containing organometallic compound involved in several vital enzymes of many phytoplankton species, such as in the methionine synthase (Raux et al., 2000; Martens et al., 2002). Its concentrations in seawater can influence the growth rate of several species and drive the spatial distribution of many taxa (Sañudo-Wilhelmy et al., 2006; Panzeca et al., 2006; Bertrand et al., 2007; Gobler et al., 2007; Koch et al., 2011). While most of eukaryotic phytoplankton are  $\text{B}_{12}$  consumers and required exogenous  $\text{B}_{12}$  vitamin, many bacteria including *Synechococcus* and *Prochlorococcus* possess the biosynthetic pathway to synthetize vitamin  $\text{B}_{12}$  (Rodionov, 2003). However, while *Synechococcus* are able to excrete large amount of this vitamin (Bonnet et al., 2010), there is no evidence at date that *Prochlorococcus* can synthesize such amount. Considering the typical abundance of the *Synechococcus* population in the North Atlantic gyre of  $10^4 \text{ cell.mL}^{-1}$  (Twining et al., 2010), and the  $\text{B}_{12}$  production rate by these species in non-limiting cultures of  $12 \times 10^{-20} \text{ mol.cell}^{-1}$  (Bonnet et al., 2010), the  $\text{B}_{12}$  concentration resulting from the production by *Synechococcus* would be of 1.2 pM in the NASG (Table 1). Thus, the subpicomolar to picomolar  $\text{B}_{12}$  levels of 0-2.5 pM recorded in the subtropical North Atlantic (Menzel and Spaeth, 1962; Panzeca et al., 2008) could be entirely attributed to the *Synechococcus* excretion. Thereby, a decrease of

*Synechococcus* abundance in the north-western subtropical Atlantic would directly diminish the production of B<sub>12</sub> vitamin available for the eukaryotes.

In turn, the dust deposition and its subsequent dissolution can be key points for the bioavailability of inorganic Co to *Synechococcus* in the subtropical North Atlantic, and indirectly for the bioavailability of B<sub>12</sub> vitamin which is essential for the entire phytoplankton community. Change in the dust deposition rates, for example due to changes in desert storm frequency, land use, and/or in the aerosols composition (pollution) has thus the potential to affect the entire subtropical North Atlantic phytoplankton ecosystem through, among others, a Co<sup>2+</sup>-*Synechococcus*-B<sub>12</sub> loop.

## 4 Conclusions

While significant in itself, the dust deposition is not the prevailing source of DCo into the mixed-layer of the Western Atlantic, apart in the North Atlantic subtropical gyre. This source can significantly impact the distributions of DCo and PCo in the mixed-layer, in addition to the physical features and the distribution of the phytoplankton species, respectively. For instance, the residence times required to replenish the DCo inventories in the mixed-layer through dissolution of dust, as first assessed in this work, largely exceed previous estimations based on all Co-fluxes in surface waters, apart in the subtropical North Atlantic. Thus, other sources also sustain the biological DCo demand that is the main sink of this micronutrient in the surface waters of the Western Atlantic.

Quantification of the cumulative effect of aerosol dissolution indicates a significant contribution of the atmospheric input (20%) to the mixed-layer DCo concentrations at basin scale. However, this contribution widely varies between the different biogeochemical domains, ranging from 2% to 80% of the DCo inventories in the mixed-layer. At the tropical and temperate latitudes of the Northern hemisphere, DCo is strongly impacted by this source (> 30% on average, and > 60% in the subtropical gyre), unlike the Southern hemisphere (< 10%), even close to Patagonia where the atmospheric deposition of Co is the most intensive estimated along the section.

The biogenic and lithogenic partitioning of PCo is mostly related to the distribution of phytoplankton communities in the different domains rather than to their productivity or the intensity of atmospheric inputs. In the subtropical domains, the predominance of cyanobacteria that require Co to grow indeed correlates with PCo being predominantly biogenic, despite low productivity of these domains and regardless the magnitude of the

atmospheric Co inputs. By contrast, the relatively high productivity and low Co atmospheric fluxes in the subpolar latitudes both do not fit with PCo being mainly lithogenic. However, it is in accordance with the predominance of diatoms at these latitudes, those species that do not preferentially assimilate Co to grow.

This work also shows that atmospheric input and aerosol dissolution can fully support the growth of cyanobacteria in the subtropical North Atlantic, and drive the abundance of *Synechococcus* sp. It also suggests that potential changes in atmospheric deposition would cause cascading effects on the production and distribution of the phytoplankton assemblage in the subtropical North Atlantic through, among other, a Co<sup>2+</sup>-*Synechococcus*-B<sub>12</sub> loop.

## Acknowledgement

We are indebted to the Captains, Officers and Crew Members of the *R.V. Pelagia* and *R.S.S. James Cook* for their exceptional support at sea. The Chief Scientists, L. Gerringa and M. Rijkenberg, are warmly acknowledged, and H. de Baar, the PI of the GEOTRACES-A02 section. We thank H. van Haken and S. Ober for providing high quality CTD data. This investigation was financed by a French LEFE-CYBER National Program of INSU-CNRS. The European COST-Action ES801 is acknowledged for supporting a STSM to G.D. The University of Western Brittany and the Brittany Region support the PhD fellowship of G.D. This investigation is a contribution to the international GEOTRACES program.

## References

- Agustí, S. (2004). Viability and niche segregation of *Prochlorococcus* and *Synechococcus* cells across the Central Atlantic Ocean. *Aquatic microbial ecology*, 36(1), 53-59.
- Baker, A.R., K. Weston, S.D. Kelly, M. Voss, P. Streu, J.N. Cape (2007) Dry and wet deposition of nutrients from the tropical Atlantic atmosphere: Links to primary productivity and nitrogen fixation. *Deep Sea Res. Part I*, 54, 1704 - 1720.
- Baker, A. R., Adams, C., Bell, T. G., Jickells, T. D., & Ganzeveld, L. (2013). Estimation of atmospheric nutrient inputs to the Atlantic Ocean from 50° N to 50° S based on large scale field sampling: Iron and other dust-associated elements. *Global Biogeochemical Cycles*, 27(3), 755-767.
- Bertrand, E.M., Saito, M.A., Rose, J.M., Lohan, M.C., Noble, A.E., Lee, P.A. & G.R., DiTullio (2007). Vitamin B<sub>12</sub> and iron co-limitation of phytoplankton growth in the Ross Sea. *Limnol. & Oceanogr.*, 52, 1079-1093.
- Bown, J., Boye, M., Baker, A., Duvieilbourg, E., Lacan, F., Le Moigne, F., Planchon, F., Speich, S., and Nelson, D. M. (2011), The biogeochemical cycle of dissolved cobalt in the Atlantic and the Southern Ocean south off the coast of South Africa. *Mar. Chem.*, 126, 193–206, doi:10.1016/j.marchem.2011.03.008, 2011.
- Bown, J., Boye, M., & Nelson, D. M. (2012a). New insights on the role of organic speciation in the biogeochemical cycle of dissolved cobalt in the southeastern Atlantic and the Southern Ocean. *Biogeosciences*, 9, 2719-2736.
- Bown, J., Boye, M., Laan, P., Bowie, A. R., Park, Y. H., Jeandel, C., & Nelson, D. M. (2012b). Imprint of a dissolved cobalt basaltic source on the Kerguelen Plateau. *Biogeosciences*, 9, 5279-5290.
- Bonnet, S., Webb, E. A., Panzeca, C., Karl, D. M., Capone, D. G., & Sañudo-Wilhelmy, S. A. (2010). Vitamin B12 excretion by cultures of the marine cyanobacteria *Crocospheara* and *Synechococcus*. *Limnol. & Oceanogr.*, 55(5), 1959.

- Bowie, A. R., Whitworth, D. J., Achterberg, E. P., Mantoura, R. F. C., & Worsfold, P. J. (2002). Biogeochemistry of Fe and other trace elements (Al, Co, Ni) in the upper Atlantic Ocean. *Deep Sea Research Part I: Oceanographic Research Papers*, 49(4), 605-636.
- Buat-Menard, P., & Chesselet, R. (1979). Variable influence of the atmospheric flux on the trace metal chemistry of oceanic suspended matter. *Earth and Planetary Science Letters*, 42(3), 399-411.
- Carpenter, E., Montoya, J.P., Burns, J., Mulholland, M., Subramaniam, A., Capone, D.G., (1999), Extensive bloom of a N<sub>2</sub> fixing symbiotic association in the tropical Atlantic ocean. *Marine Ecology: Progress Series* 188, 273–283.
- Croot, P. L., Baars, O., & Streu, P. (2011). The distribution of dissolved zinc in the Atlantic sector of the Southern Ocean. *Deep Sea Research Part II: Topical Studies in Oceanography*, 58(25), 2707-2719.
- De Baar, H.J.W., K.R. Timmermans, P. Laan , H.H. De Porto, S. Ober, J.J. Blom, M.C. Bakker, J. Schilling, G. Sarthou, M.G. Smit and M. Klunder (2008), Titan: A new facility for ultraclean sampling of trace elements and isotopes in the deep oceans in the international GEOTRACES program. *Mar. Chem.*, 111 (1-2).
- de Jong, J.T.M., Boye, M., Gelado-Caballero, M.D., Timmermans, K.R., Veldhuis, M.J.W., Nolting, R.F., van den Berg, C.M.G., de Baar, H.J.W., (2007), Inputs of iron, manganese and aluminium to surface waters of the Northeast Atlantic Ocean and the European continental shelf. *Mar. Chem.*, 107, 120–142.
- Dammshäuser, A., Wagener, T., & Croot, P. L. (2011). Surface water dissolved aluminum and titanium: Tracers for specific time scales of dust deposition to the Atlantic?. *Geophys. Res. Lett.*, 38(24), doi:10.1029/2011GL049847
- Duce, R. A., & Tindale, N. W. (1991). Atmospheric transport of iron and its deposition in the ocean. *Limnology & Oceanography*, 36(8), 1715–1726.
- Dulaquais, G., Boye, M., Rijkenberg, M. J. A., & Carton, X. (2014). Physical and remineralization processes govern the cobalt distribution in the deep western Atlantic Ocean. *Biogeosciences*, 11(6), 1561-1580.
- Dulaquais, G., Boye, M., Middag, R., Owens, S., Puigcorbe, V., Buesseler, K., de Baar, H. & Carton, X. (2014). Contrasting biogeochemical cycles of cobalt in the surface western Atlantic Ocean. *Global Biogeochemical Cycles*, 28(12), 1387-1412.
- Ellwood, M.J. and C.M.G. van den Berg, (2001). Determination of organic complexation of cobalt in seawater by cathodic stripping voltammetry, *Mar. Chem.*, 75, 33-47.
- Ellwood, M. J., van den Berg, C. M., Boye, M., Veldhuis, M., de Jong, J. T., de Baar, H. J., Croot, P.L. & Kattner, G. (2005). Organic complexation of cobalt across the Antarctic Polar Front in the Southern Ocean. *Marine and freshwater research*, 56(8), 1069-1075.
- Gaiero, D.M., Probst, J. -L., Depetris, P. J., Bidart, S. M. and Leleyter, L., (2003). Iron and other transition metals in Patagonian riverborne and windborne materials: geochemical control and transport to the southern South Atlantic Ocean. *Geochimica & Cosmochimica Acta*, 67 (19), 3603-3623.
- Ginoux, P., Chin, M., Tegen, I., Prospero, J.M., Holben, B., Dubovik, O., Lin, S.J., (2001). Sources and distributions of dust aerosol simulated with the GOCART model. *J. Geophys. Res.*, 106, 20,255–20,273.
- Gobler, C. J., Norman, C., Panzeca, C., Taylor, G. T., & Sañudo-Wilhelmy, S. A. (2007). Effect of B-vitamins (B1, B12) and inorganic nutrients on algal bloom dynamics in a coastal ecosystem. *Aquatic Microbial Ecology*, 49(2), 181-194.
- Gong, N., et al . (2005). Characterization of a thermostable alkaline phosphatase from a novel species *Thermusyunnanensis* sp. nov. and investigation of its cobalt activation at high temperature, *Biochim. Biophys. Acta*, 1750, 103-111.

- Henson, S. A., Sanders, R., Holeton, C., & Allen, J. T. (2006). Timing of nutrient depletion, diatom dominance and a lower-boundary estimate of export production for Irminger Basin, North Atlantic. *Marine Ecology Progress Series*, 313, 73-84.
- Ho, T. Y., A. Quigg, Z. V. Finkel, A. J. Milligan, K. Wyman, P. G. Falkowski, and F. M. Morel. (2003). The elemental composition of some marine phytoplankton. *J. Phycol.* 39: 1145–1159.
- Fung, I. Y., Meyn, S. K., Tegen, I., Doney, S. C., John, J. G., & Bishop, J. K. (2000). Iron supply and demand in the upper ocean. *Global Biogeochemical Cycles*, 14(1), 281–295.
- Jakuba, R.W., Moffett, J.W., Dyhrman, S.T. (2008), Evidence for the linked biogeochemical cycling of zinc, cobalt, and phosphorus in the western North Atlantic Ocean. *Global Biogeochem. Cycles*, 22 (4), doi: 10.1029/2007GB003119.
- Koch, F., Alejandra Marcoval, M., Panzeca, C., Bruland, K. W., Sanudo-Wilhelmy, S. A., & Gobler, C. J. (2011). The effect of vitamin B12 on phytoplankton growth and community structure in the Gulf of Alaska. *Limnology and oceanography*, 56(3), 1023-1034.
- Lane, T. W., and F. M. M. Morel (2000), Regulation of carbonic anhydrase expression by zinc, cobalt, and carbon dioxide in the marine diatom *Thalassiosira weissflogii*. *Plant Physiol.*, 123, 345–352, doi:10.1104/pp.123.1.345.
- Lane, T. W., Saito, M. A., George, G. N., Pickering, I. J., Prince, R. C., & Morel, F. M. (2005). Biochemistry: a cadmium enzyme from a marine diatom. *Nature*, 435(7038), 42-42.
- Mahowald, N.M., Baker, A.R., Bergametti, G., Brooks, N., Duce, R.A., Jickells, T.D., Kubilay, N., Prospero, J.M., Tegen, I., (2005), Atmospheric global dust cycle and iron inputs to the ocean. *Glob. Biogeochem. Cycles*, 19, GB4025. doi:10.1029/2004GB002402
- Mahowald, N. M., Muhs, D. R., Levis, S., Rasch, P. J., Yoshioka, M., Zender, C. S., & Luo, C. (2006). Change in atmospheric mineral aerosols in response to climate: Last glacial period, preindustrial, modern, and doubled carbon dioxide climates. *Journal of Geophysical Research: Atmospheres (1984–2012)*, 111(D10).
- Martens, J. H., Barg, H., Warren, M., & Jahn, D. (2002). Microbial production of vitamin B12. *Applied microbiology and biotechnology*, 58(3), 275-285.
- Martin, J.H., Fitzwater, S.E., Gordon, R.M., Hunter, C.N., Tanner, S.J., (1993). Iron, primary production and carbon nitrogen flux studies during the JGOFS North-Atlantic Bloom Experiment. *Deep-Sea Res. Part I- Topical Studies in Oceanography*, 40 (1–2), 115–134.
- Measures, C.I., Brown, E.T., (1996). Estimating dust input to the Atlantic Ocean using surfacewater Al concentrations. In: Guerzoni, S., Chester, R., (Eds.), *The impact of African Dust across the Mediterranean*, Kluwer, Dordrecht, 389 pp.
- Measures, C.I., Vink, S., (2000). On the use of dissolved aluminium in surface waters to estimate dust deposition to the ocean. *Global Biogeochem. Cycles*, 14, 317–327.
- Menzel, D. W., & Spaeth, J. P. (1962). Occurrence of vitamin B<sub>12</sub> in the Sargasso Sea. *Limnol. & Oceanogr.*, 7, 151-158.
- Middag, R., H. J. W. de Baar, P. Laan, and K. Bakker (2009). Dissolved aluminium and the silicon cycle in the Arctic Ocean. *Mar. Chem.*, 115, 176–195, doi:10.1016/j.marchem.2009.08.002.
- Moran, S. B., and R. M. Moore (1988). Evidence from mesocosm studies for biological removal of dissolved aluminum from sea water. *Nature*, 335, 706–708, doi:10.1038/335706a0

- Morel, F. M. M., & Price, N. M. (2003). The biogeochemical cycles of trace metals in the oceans. *Science*, 300(5621), 944-947.
- Noble, A. E., Saito, M. A., Maiti, K., and Benitez-Nelson, C. R. (2008). Cobalt, manganese, and iron near the Hawaiian Islands: A potential concentrating mechanism for cobalt within a cyclonic eddy and implications for the hybrid-type trace metals. *Deep-Sea Res. Part II*, 55, 1473-1490, doi:10.1016/j.dsr2.2008.02.010.
- Noble, A. E., Lamborg, C. H., Ohnemus, D. C., Lam, P. J., Goepfert, T. J., Measures, C. I., Frame, C. H., Casciotti, K. L., DiTullio, G. R., Jennings, J., and Saito, M. A. (2012). Basin scale inputs of cobalt, iron, and manganese from the Benguela-Angola front to the South Atlantic Ocean. *Limnol. & Oceanogr.*, 57, 989-1010.
- Olgún, H. F., & Alder, V. (2011). Species composition and biogeography of diatoms in antarctic and subantarctic (Argentine shelf) waters (37–76° S). *Deep Sea Research Part II: Topical Studies in Oceanography*, 58(1), 139-152.
- Panzeca, C., Tovar-Sánchez, A., Agustí, S., Reche, I., Duarte, C. M., Taylor, G. T., & Sañudo-Wilhelmy, S. A. (2006). B vitamins as regulators of phytoplankton dynamics. *Eos, Transactions American Geophysical Union*, 87(52), 593-596.
- Panzeca, C., Beck, A. J., Leblanc, K., Taylor, G. T., Hutchins, D. A., & Sañudo-Wilhelmy, S. A. (2008). Potential cobalt limitation of vitamin B12 synthesis in the North Atlantic Ocean. *Global Biogeochemical Cycles*, 22(2).
- Parsons, T. R., & Lalli, C. M. (1988). Comparative oceanic ecology of the plankton communities of the subarctic Atlantic and Pacific oceans. *Oceanogr. Mar. Biol. Ann. Rev.* 26, 317-359.
- Price, N. M., & Morel, F. M. M. (1990). Cadmium and cobalt substitution for zinc in a marine diatom. *Nature*, 344(6267), 658-660.
- Quigg, A., Finkel, Z. V., Irwin, A. J., Rosenthal, Y., Ho, T. Y., Reinfelder, J. R., Schofield O., Morel F.M.M. & Falkowski, P. G. (2003). The evolutionary inheritance of elemental stoichiometry in marine phytoplankton. *Nature*, 425(6955), 291-294.
- Raux, E., Schubert, H. L., & Warren, M. J. (2000). Biosynthesis of cobalamin (vitamin B12): a bacterial conundrum. *Cellular and Molecular Life Sciences CMLS*, 57(13-14), 1880-1893.
- Reid, E.A., Reid, J.S., Meier, M.M., Dunlap, M.R., Cliff, S.S., Broumas, A. (2003). Characterization of African dust transported to Puerto Rico by individual particle and size segregated bulk analysis. *J. Geophys. Res. D: Atmos.* 19, 108.
- Rudnick, R. L. & Gao, S. (2003). Composition of the continental crust. In: Rudnick, R. L. (ed.) *The Crust*. Amsterdam: Elsevier, pp. 1-70.
- Saito, M. A., & Moffett, J. W. (2002). Temporal and spatial variability of cobalt in the Atlantic Ocean. *Geochim. Cosmochim. Acta*, 66, 1943–1953.
- Saito, M. A., Moffett, J. W., Chisholm, S. W., & Waterbury, J. B. (2002). Cobalt limitation and uptake in *Prochlorococcus*. *Limnol. & Oceanogr.*, 47(6), 1629-1636.
- Saito, M. A., Goepfert, T. J., & Ritt, J. T. (2008). Some thoughts on the concept of colimitation: three definitions and the importance of bioavailability. *Limnology & Oceanography*, 53(1), 276.
- Sañudo-Wilhelmy, S. A., Gobler, C. J., Okbamichael, M., & Taylor, G. T. (2006). Regulation of phytoplankton dynamics by vitamin B12. *Geophysical Research Letters*, 33(4), L04604.
- Shelley, R. (2011). Cobalt biogeochemistry in the Atlantic Ocean using Flow Injection Chemiluminescence. *PhD Thesis*. University of Plymouth, 362pp.
- Shelley, R. U., Zachhuber, B., Sedwick, P. N., Worsfold, P. J., and Lohan, M. C. (2010). Determination of total dissolved cobalt in UV-irradiated seawater using flow injection

- with chemiluminescence detection. *Limnol. & Oceanogr.*, 8, 352–362, doi:10.1029/2009JC005880.
- Shelley, R. U., Sedwick, P. N., Bibby, T. S., Cabedo-Sanz, P., Church, T. M., Johnson, R. J., Macey, A. I., Marsay, C. M., Sholkovitz, E. R., Ussher, S. J., Worsfold, P. J., and Lohan, M. C. (2012). Controls on dissolved cobalt in surface waters of the Sargasso Sea: Comparisons with iron and aluminum. *Global Biogeochem. Cycles*, 26 (2) GB2020.
- Sunda, W.G., and S.A. Huntsman (1995). Cobalt and zinc inter-replacement in marine phytoplankton: biological and geochemical implications. *Limnol. & Oceanogr.*, 40, 1404-1417.
- Tegen, I., Werner, M., Harrison, S.P., Kohfeld, K.E. (2004). Relative importance of climate and land use in determining present and future global soil dust emission. *Geophys. Res. Lett.* 31 (5), L05105.doi:10.1029/2003GL019216.
- Tovar-Sanchez, A., Sanudo-Wilhelmy, S. A., Kustka, A. B., Agusti, S., Dachs, J., Hutchins, D. A., Capone, D. G., Duarte, C. M. (2006). Effects of dust deposition and river discharges on trace metal composition of *Trichodesmium spp.* in the tropical and subtropical North Atlantic Ocean. *Limnol. & Oceanogr.*, 51(4), 1755–1761.
- Tovar-Sanchez, A. and Sanudo-Wilhelmy, S. A. (2011). Influence of the Amazon River on dissolved and intra-cellular metal concentrations in *Trichodesmium* colonies along the western boundary of the sub-tropical North Atlantic Ocean. *Biogeosciences*, 8, 217–225, doi:10.5194/bg-8-217-2011.
- Trapp, J. M., F. J. Millero, and J. M. Prospero (2010). Temporal variability of the elemental composition of African dust measured in trade wind aerosols at Barbados and Miami, *Mar. Chem.*, 120(1–4), 71–82, doi:10.1016/j.marchem.2008.10.004
- Treusch, A. H., Demir-Hilton, E., Vergin, K. L., Worden, A. Z., Carlson, C. A., Donatz, M. G., Burton, R.M., & Giovannoni, S. J. (2011). Phytoplankton distribution patterns in the northwestern Sargasso Sea revealed by small subunit rRNA genes from plastids. *The ISME journal*, 6(3), 481-492.
- Thuróczy, C. E., Boye, M., & Losno, R. (2010). Dissolution of cobalt and zinc from natural and anthropogenic dusts in seawater. *Biogeosciences*, 7(6), 1927-1936.
- Twining, B. S., Nunez-Milland, D., Vogt, S., Johnson, R. S., & Sedwick, P. N. (2010). Variations in *Synechococcus* cell quotas of phosphorus, sulfur, manganese, iron, nickel, and zinc within mesoscale eddies in the Sargasso Sea. *Limnology and Oceanography*, 55(2), 492.
- Twining, B. S., & Baines, S. B. (2013). The trace metal composition of marine phytoplankton. *Annual review of marine science*, 5, 191-215.
- Van Hulten, M. M. P., Sterl, A., Tagliabue, A., Dutay, J. C., Gehlen, M., De Baar, H. J., & Middag, R. (2013). Aluminium in an ocean general circulation model compared with the West Atlantic Geotraces cruises. *Journal of Marine Systems*, 126, 3-23.
- Vink, S., & Measures, C.I. (2001). The role of dust deposition in determining surface water distributions of Al and Fe in the South West Atlantic. *Deep-Sea Res. Part II*, 48 (13), 2787–2809.
- Wyatt, N. (2014). The Biogeochemistry of iron, zinc and cobalt in the Atlantic Ocean: the Atlantic Meridional Transect and UK GEOTRACES sections. *PhD Thesis*, University of Plymouth, 260pp.
- Xia, L., & Gao, Y. (2010). Chemical composition and size distributions of coastal aerosols observed on the US East Coast. *Mar. Chem.*, 119(1), 77-90.
- Yee, D., & Morel, F. M. (1996). In vivo substitution of zinc by cobalt in carbonic anhydrase of a marine diatom. *Limnology & Oceanography*, 41(3), 573-577.



# **Chapitre 5**

## **A synoptic view of cobalt biogeochemistry in the Mediterranean and Black seas**



# A synoptic view of cobalt biogeochemistry in the Mediterranean and Black Seas

Gabriel Dulaquais<sup>1\*</sup> and Marie Boye<sup>1</sup>

In collaboration with Hélène Planquette<sup>1</sup>, Stéphane L'Helguen<sup>1</sup> and Micha J.A Rijkenberg<sup>2</sup>

<sup>1</sup> Laboratoire des Sciences de l'Environnement Marin UMR6539, Institut Universitaire Européen de la Mer, Technopôle Brest Iroise, Place Nicolas Copernic, 29280 Plouzané, France

<sup>2</sup> Department of Marine Chemistry and Geology, Royal Netherlands Institute for Sea Research, P.O. Box 59, 1790 AB Den Burg, The Netherlands

\* corresponding author : G. Dulaquais, LEMAR UMR6539, 29280, FRANCE  
(gabriel.dulaquais@univ-brest.fr)

**Foreword:** This chapter is a draft of paper(s) that will be submitted by the end of 2014.

**Keywords:** Mediterranean Sea, Black Sea, biogeochemistry, cobalt, trace elements, suspended particulate matter.

## Abstract :

We report the spatial and vertical distribution of cobalt (Co) along the GEOTRACES-A04 section spreading from the Eastern Atlantic to the Black Sea through the entire Mediterranean Sea. The dissolved (DCo) and the particulate (PCo) fractions of Co were investigated, as well as the particulate distributions of others trace elements. The vertical distributions of DCo and PCo varied in function of the different domains, depending on the prevailing biogeochemical processes. In the Eastern Atlantic, DCo displayed a nutrient-like distribution in surface, with depleted concentrations in surface waters (as low as 14 pM) that increased with depth. Its distribution in the deep Atlantic waters was governed by the circulation of North East Atlantic deep waters, North Atlantic Central Waters, Mediterranean Outflow and Lower deep waters. On the contrary, DCo distribution was scavenged like over the whole Mediterranean Sea. However, we suggested that this distribution mostly resulted from the decoupling between the surface and deep reservoirs rather than from scavenging processes. Indeed, our estimations of the biogeochemical fluxes indicated strong external inputs by the Gulf of Cadix system at Gibraltar strait and by the atmosphere, both combined with a low biological assimilation in the central Mediterranean sea ( $20\text{-}40\text{nmol.m}^{-2}\cdot\text{d}^{-1}$ ) lead to the accumulation of DCo in surface waters. On the contrary, the fast deep circulation, the extremely low export of PCo from the surface waters (generally  $< 5\text{nmol.m}^{-2}\cdot\text{d}^{-1}$ ) likely due to regeneration, and the absence of PCo remineralization in intermediate waters prevent the accumulation of DCo in the deep Mediterranean Sea. In the Black Sea, high surface DCo concentrations ( $> 500 \text{ pM}$ ) were recorded. Coastal inputs and regeneration combined with a low ventilation rate may have caused accumulation of DCo in surface. Deeper, the vertical

distribution of DCo was governed by competitive redox-processes. In the suboxic waters, the high surface DCo concentrations ( $> 500$  pM) dramatically decreased (as low as 28 pM) probably due to scavenging onto manganese oxide (MnO<sub>x</sub>). Below this layer, the reduction of MnO<sub>x</sub> released DCo in the upper sulfidic layer, where the highest DCo concentrations never encountered before in modern open marine systems were recorded (up to 6.6 nM). Deeper, DCo sharply decreased with depth, likely due to sorption of DCo onto ferrihydrite in the sulfidic environment.

## **Introduction:**

The Mediterranean and Black Seas are semi-enclosed seas surrounded by continents that make these marine systems particularly sensitive to anthropogenic forcing. Both seas are “miniature oceans”, wherein they display specific thermohaline circulations.

The Mediterranean Sea circulation is driven by the incursion of Atlantic waters, deep convection of surface waters and outflow of deep waters at the straits. In this sea, the residence time of the water-masses is very short (e.g. decades) compared to the ocean (e.g. centuries to millennium). The Atlantic waters penetrating in surface at the Strait of Gibraltar feed the surface Mediterranean basin. Rivers and the relatively fresh waters of the Black Sea also contribute to close the Mediterranean water budget. In the Black Sea, the surface waters that outflow through the Bosphorus have low salinities due to the influence of the surrounding rivers. These surface waters describe an overall counter clock pathway around the basin. The deep Mediterranean circulation is governed by deep convection of intermediate during the winter (Millot and Taupier-Letage, 2005a). In the deep Black Sea, the Mediterranean inflow that constitutes the main source of salt and the deep winter convection occurring in the center of the Black Sea mainly drive the deep circulation. Additionally, the geothermal activity generates a convective turnover of the deep waters at the bottom (Özoy et al., 1991). In turn, the deep Black Sea reservoir can be impacted by double diffusion with intermediate and bottom waters contribution.

In the Mediterranean Sea, the northern rivers provide most of the freshwater inputs that balance the strong evaporation and low precipitation. These runoffs also provide nutrients that increase the primary productivity at their mouth, and those inputs are source of nutrients to the whole oligotrophic basin. The Mediterranean is a “Low-Nutrient Low-Chlorophyll” (LNLC) system among the least productive of the world’s ocean. In this Sea, the oligotrophy intensifies eastward (Bethoux et al., 1998), as exemplified by the eastward decrease of the primary productivity and the surface nutrient concentrations. Exchanges at the straits, atmospheric depositions, and river discharges are controlling the distribution of nutrients

there. Furthermore, extreme events such as large river floods or Saharan dust pulses also supply the Mediterranean Sea in macro- and micro-nutrients (Mermex group, 2011).

The nutrients stoichiometry is similar in the Black Sea compared to other marine systems, while that of the Mediterranean Sea is unusual since it displays an excess of carbon, a deficiency of phosphorus (P) relative to nitrogen (N), and an occasional deficiency of silicate (Béthoux et al., 2002a). The stoichiometric anomaly of N/P increases eastward from 22/1 to 28/1 (M/M) (Krom et al., 1991; Kress and Herut, 2001; Kress et al., 2003). In this respect, the Mediterranean Sea is considered as phosphorus limited (Krom et al., 1991), whereas nitrogen is classically considered as the limiting macro-nutrient in much of the ocean (Codispoti, 1989).

The concentration of dissolved trace metals are elevated in the Mediterranean surface waters compared to similar oligotrophic waters such as the subtropical North Atlantic, and their distributions generally show a conservative behavior in the deep sea (Kremling and Petersen, 1981; Boyle et al., 1985; Sherell and Boyle, 1988; Bethoux et al., 1990; Ruiz-Pino et al., 1990, 1991; Saager et al., 1993; Achterberg and van den Berg, 1996; Morley et al., 1997). The surface enrichments of trace metals, notably those observed for zinc, copper, cadmium and nickel, have been related to natural and anthropogenic inputs (van Geen et al., 1988; van Geen and Boyle, 1990; Ruiz-Pino et al., 1990), from rivers, dust deposition and/or shelf exchanges (van Geen et al., 1988; van Geen and Boyle, 1990; Ruiz-Pino et al., 1990). For instance, the inputs of trace elements by inflow of Atlantic Waters at the Strait of Gibraltar can be considerable (Boyle et al., 1985). Actually, these inputs could account for more than 50% of the total inputs to the Western Mediterranean basin for certain trace elements (e.g.; Mn, Co, Pb) in summer (Elbaz-Poulichet et al., 2001b). Such high inputs can be related to the influence of the Gulf of Cadiz system, since its surface waters that partially feed the Atlantic Waters are enriched in trace metals due to releasing of the Odiel and Tinto Rivers that are extremely enriched in metals (Elbaz-Poulichet et al., 2001c). Indeed, this river is located in the watershed of the Iberian Pyrite Belt, one of the largest metal-rich sulfide deposits in the world (van Geen et al., 1991; van Geen et al., 1997).

Micro-nutrients are not depleted in surface waters of the Mediterranean Sea and do not significantly correlate with macro-nutrients in the surface layer (Kremling and Petersen, 1981; Saager et al., 1993), probably due to limitation by macro-nutrients that prevents strong biological removal of trace elements and to high inputs in surface waters. An eastward gradient has been described for surface concentrations of several trace elements including Co (Spivack et al., 1983; Achterberg and van den Berg, 1996; Morley et al., 1997; Bonnet et al.,

2013). It probably results from mixing processes, insignificant recycling (Morley et al., 1997), and high atmospheric inputs in surface (Chester et al., 1993). The deep concentrations of trace metals are generally uniform over the Mediterranean Sea (Boyle et al., 1985; Achterberg and van den Berg, 1996; Morley et al., 1997). Intense horizontal and vertical mixing (Béthoux et al., 1980) has been proposed to explain this quasi-conservative deep concentration of dissolved trace elements (Achterberg and van den Berg, 1996). Additionally, local enrichments of dissolved trace elements were observed near the bottom (Achterberg and van den Berg, 1996; Morley et al., 1997), likely due to remobilization of sediments and their subsequent dissolution (Achterberg and van den Berg, 1996).

Dissolved cobalt (DCo) is poorly referenced in the Mediterranean Sea, and the data available to date are issued from a few profiles in restricted areas (Ngoc and Whitehead, 1986; Zhang et al., 1989; Morley et al., 1997, Tankéré, 2000; Heimburger et al., 2011). These studies focused on the Western Basin and the Adriatic Sea, thus the distribution of DCo in the Eastern Basin is unknown. Furthermore, these previous DCo analyses were performed on non-UV digested samples; hence the dissolved concentrations of Co were most probably under-estimated. Indeed, the UV oxidation is required to release Co from its complexes with strong organic ligands (Vega and van den Berg, 1997). In the Western Mediterranean Sea, the vertical distribution of DCo is described by a scavenged-type profile, with high concentrations in surface decreasing in intermediate and deep waters, and eventually showing relative maxima near the bottom (Ngoc and Whitehead, 1986; Zhang et al., 1989; Morley et al., 1997, Tankéré, 2000; Heimburger et al., 2011). Surface DCo maxima were previously related to atmospheric crustal input (Heimburger, 2010), and the decreasing concentrations with depth to scavenging onto settling particles (Zhang and Wollast, 1990). Nevertheless, apart these few investigations, the biogeochemical cycle of Co remains unknown in the Mediterranean Sea.

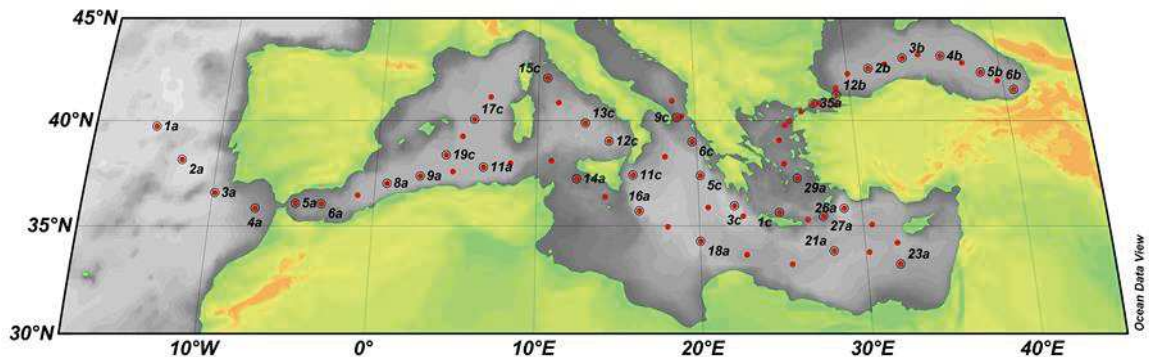
The Black Sea is the world's largest anoxic marine basin. Bosphorus provides 312 km<sup>3</sup>.yr<sup>-1</sup> to the Black Sea in quasi-steady exchange (Gregg et al., 1999). The residence time of the deep Black Sea is of the order of 1750 years, thus the anoxic layer is stable, in quasi steady state and allows studying the chemistry of trace elements in anoxic conditions at steady state. Combined with sedimentary records, understanding the biogeochemical processes affecting the vertical behavior of trace elements in the modern Black Sea is a pathway to assess the evolution of the trace elements composition of the ocean throughout geological timescales. Additionally, anoxic environments are spreading and intensifying in coastal areas

due to anthropogenic forcing, hence the study of heavy metals such as Co in the natural anoxic marine system of the Black Sea could provide answer to future environmental challenges. Cobalt is better referenced in the Black Sea than in the Mediterranean Sea (Spencer and Brewer, 1971; Spencer et al., 1972; Murray et al., 1975; Landing and Lewis, 1991; Haraldsson and Westerlund, 1991; Lewis and Landing, 1992; Guieu et al., 1998; Tankéré et al., 2001; Yiğiterhan et al., 2011). There, the vertical distribution of DCo mainly depends on the exchanges with particulate cobalt (PCo) that are impacted by the oxygenation states. The mechanisms potentially involved in these exchanges include scavenging-regeneration cycle of DCo with particulate Mn-oxyhydroxides (MnOx) across the oxic-sulfidic interface, and co-precipitation of DCo with iron (Fe) oxydes, such as ferrihydrite in the deep waters (Lewis and Landing, 1992). In this Sea, the solubility of DCo would poorly depend on the complexation with organic ligands (Landing and Lewis, 1991). Considering the adsorption of DCo onto MnOx, the Black Sea is thus a perfect playground to study scavenging processes of DCo.

The most efficient pathway to transfer trace elements from the continent to the open waters could be by atmospheric transport and dust deposition (Boutron et al., 1991; Jickells, 1995). However, the distribution of DCo in surface waters of the open ocean has been described to be poorly impacted by dust deposition (Saito and Moffett, 2002, Bown et al., 2011). The dust deposition could even be a sink of DCo in surface waters due to its adsorption onto sinking lithogenic particles (Aston et al., 1972). The Mediterranean Sea receives one of the highest fluxes of dust of any oceanic basin in the world (Chester et al., 1977). Together with its low trace metal recycling (Morley et al., 1997), the DCo concentrations should be thus much lower there than in other marine system, if the atmospheric particles act as a sink of DCo. On the contrary, much higher DCo concentrations are observed compared to other oligotrophic domains (Ngoc and Whitehead, 1986). Recent studies indicate a significant contribution of aerosols deposition to the Co surface distribution in the subtropical North Atlantic gyre (Dulaquais et al., 2014b). In this latter domain, DCo provided by dust dissolution could account up to 80% of the mean 29 pM recorded in the mixed layer (Dulaquais and Boye, in review). The high dust delivery and the low biological removal of bioactive trace metals due to oligotrophic conditions made the Mediterranean Sea particularly prone to study the impact of dust deposition on the DCo distribution and concentration. The dust deposition in the Mediterranean Sea has been described by a combination of Saharan

inputs and European anthropogenic emissions (Chester et al., 1997), those having different composition in Co (Gieu et al., 1997). Thus, in this basin an estimation of Co deposition should take into account the dust delivery flux and the origin of air-masses.

The purpose of this study is to investigate the spatial and vertical distribution of DCo and PCo in order to design a comprehensive biogeochemical cycle of Co in the Mediterranean and Black Seas. In this aim, we present along the section GEOTRACES-A04 the widest Co dataset obtained in these Seas, and a dataset of particulate key trace elements. The section is spreading from offshore Portugal in the eastern Atlantic to the Batumi eddy in the eastern Black Sea (Figure 1). Samples were collected in all the different sub-basins of the Mediterranean Sea apart in the North-western basin and the Adriatic Sea, and in the anoxic waters of the Black Sea. Main sources, sinks and processes that govern the deep and the surface distribution of cobalt are investigated. Tentative deep waters DCo budget is provided at basin scale of the Mediterranean Sea. A pioneer model of sea-surface dust deposition is also proposed based on particulate aluminum concentrations (PAI) recorded in surface waters. This study allows understanding the cycle of DCo in these two semi-enclosed marine systems.



(sCo) and colloidal (cCo) cobalt. Furthermore, 19 stations were sampled for particulate trace elements (101 analyses) and for particulate nutrient determination (26 analyses).

All samples were collected using the TITAN-CTD frame of NIOZ (Netherlands), with 24 ultra-clean sampling bottles of 24.4 L each made of PVDF plastic (Rijkenberg et al., 2014). The frame was placed in a Class-100 container for sub-sampling (de Baar et al., 2008). The samples for DCo analyses were collected after filtration using 0.2 µm Sartobran® 300 Sartorius® cartridges. sCo samples were collected after filtration using 0.02 µm virosart CPV MidiCaps Sartorius® cartridges, themselves connected online to the 0.2 µm Sartobran® 300 Sartorius®. All seawater filtrations were operated online to the sampling bottle under pure N<sub>2</sub> pressure (filtered 99.99% N<sub>2</sub>, 0.7 atm) in acid cleaned 250 ml and 60 mL Nalgene® LDPE bottles respectively for DCo and sCo. All seawater samples were acidified using ultrapure HCl® at 0.01M (Merck) immediately after their collection. Then the acidified samples were stored in double bags at dark and ambient temperature, before their analyses in the shore-based laboratory.

Particulate trace elements analyses were collected after filtration of 4 to 15 L of seawater on 47 mm polyether sulfone filters (PES, Supor®) placed in acid cleaned Teflon filter holders (47mm, Savilex®) connected inline to the PVDF ultra-cleaned sampling bottles under pure N<sub>2</sub> pressure (filtered 99.99% N<sub>2</sub>, 0.7 atm) using acid cleaned Teflon tubing. Immediately after filtration, filters were stored at -20°C in acid-cleaned plastic boxes double bagged. Before use, all filters were acid cleaned following the method of Planquette et al. (2012). Blank filters were also systematically collected at every sampling station as described in Planquette et al. (2012), at least in deep waters (typically 1500 m) and in the surface waters (50 m), by filtering seawater firstly through a 0.2 µm pore size capsule filter (Sartobran® 300) mounted on the outlet of the sampling bottle. So, the trace metal clean 0.2 µm filtered seawater passed through the particle sampling filter, which was attached inline to the capsule filter. The standard volumes for these flow-through blanks procedures were 10 L for deep waters and 5 L for surface waters.

Particulate carbon and nitrogen were sampled after filtration of seawater (0.5 to 1.2 L) onto 47 mm pre-combusted Whatman-GF/F-filters placed into acid-clean and 5 times MilliQ rinsed polyethylene sulfone filter holders connected inline to the sampling bottles under pure N<sub>2</sub> pressure (filtered 99.99% N<sub>2</sub>, 0.7 atm). Blank of filters were sampled typically at 1500 m and 50 m at each sampling station surface (50 m) by filtering seawater (1 L) through a 0.2 µm

pore size capsule filter (Sartobran® 300) before passing on the GF/F filter. The GF/F filters were stored at -20°C in pre-combusted receptacles.

## 2.2 Hydrography

The hydrological parameters (salinity (S), temperature (T), dissolved oxygen ( $O_2$ ), conductivity, fluorescence and turbidity) were measured using a SBE9+ underwater sensor, a SBE3+ thermometer ( $\pm 0.001^\circ C$ ), a SBE4 conductivity sensor ( $\pm 0.3 \text{ mS.s}^{-1}$ ), a SBE43 dissolved oxygen sensor ( $\pm 2\%$ ), a Chelsea Aquatracka MKIII fluorometer ( $\pm 0.2 \mu\text{g.l}^{-1}$ ), and a Wetlabs C-Star transmissiometer ( $\pm 0.02\%.^\circ C^{-1}$ ).

## 2.3 Macronutrients analysis

Nutrient samples were collected in 125 ml polypropylene bottles. The analyses were performed onboard from surface to deep waters samples. All the nutrients were analyzed onboard by colorimetric methods following the methods of Murphy and Riley (1962) for phosphate ( $HPO_4^{2-}$ ), Strickland and Parsons (1968) for silicate ( $Si(OH)_4$ ), and Grasshoff et al. (1983) for nitrate ( $NO_3^-$ ) and nitrite ( $NO_2$ ).

## 2.4 Analytical method for cobalt analyses in seawater

### 2.4.1 Method

Prior to the analyse, the samples for DCo and sCo analyses were UV-digested (Shelley et al., 2010) for 3 h in acid clean silica tubes using a 600 W high-pressure mercury vapor lamp (Bown et al., 2011; Dulaquais et al., 2014), and left for an equilibration time of 48 h. Dissolved and soluble cobalt concentrations were determined by Flow-Injection Analysis (FIA) and chemiluminescence detection following the method adapted from Shelley et al. (2010), as described in Dulaquais et al. (2014). The reagents are prepared with trace metals quality reagents, as described in Dulaquais et al. (2014). All reagents are prepared under a laminar flow hood (ADS Lamineaire, ISO 5 class) with ultrapure water (MiliQ, 18.2 mΩ) the day before the analysis and kept at room temperature for an overnight equilibration.

Procedures for the determination of DCo and sCo concentrations are described in Dulaquais et al. (2014). However, due to the wide difference of DCo concentrations between the bottom and top depths in the Mediterranean Sea (Lars-Eric Heimbürger, pers. comm.), samples from 1000 m depth to the bottom were calibrated against calibration curves

made with standard additions of 0, 20, 40, 60, 80 and 100 pM of cobalt to artificial and chelex-seawater, whereas the samples from the upper water-column to 950 m depth were calibrated against calibration curves made with standard additions of 0, 50, 100, 200, 300 and 400 pM of cobalt. The calibrations were performed before and after each series of 8 or 12 samples. Additionally, due to extremely high DCo concentrations expected in the Black Sea (Tankéré et al., 2001), the samples collected in the Black Sea were diluted in MilliQ water by a factor 2, 5, 10 or 20 depending of the depth, after the UV-digestion of the sample. For the surface samples of the Black Sea, calibration curves were constructed by dilution of artificial and chelex-seawater at the same dilution factor than that of the sample using MilliQ, and with standard additions of 0, 50, 100, 200, 300 and 400 pM. The DCo concentrations are based on triplicate analyses of each sample using the mean peak height of the chemiluminescent signal, and they are corrected with respect to blank analyses. Indeed, two to four reagent blanks including the buffer blank were analyzed per series of 8-12 samples at the beginning and at the end of the series, in acidified MilliQ water instead of the sample (Bown et al., 2011; Dulaquais et al, 2014). The final standard deviation of the measurement is calculated by an error propagation using the error on blanks, the calibration curves and the deviation of the triplicate analyses. Small colloidal Co concentrations (cCo) were calculated by difference between DCo and SCo. cCo was thus in the size-fraction >0.02 µm - <0.2 µm.. Standard deviation of cCo is determined through the following Equation 1:

$$SD\ cCo = \sqrt{SD\ DCo^2 + SD\ SCo^2} \quad (1)$$

#### 2.4.2 Analytical performance

The mean reagent blank (based on all blank determinations) was  $4.4 \pm 1.8$  pM of Co in MilliQ ( $n = 87$ ). The limit of detection of the method estimated as three times the standard deviation of the mean reagent blank is thus on average 5.7 pM of Co ( $n = 108$ ). Each series of samples was calibrated by running one reference sample collected during the Sampling and Analysis of Iron (SAFe) program or the GEOTRACES program. SAFe and GEOTRACES reference-samples were UV-digested for 3 h prior to analysis. The DCo concentrations we measured in the reference-samples are in excellent agreement with the consensus values (Appendix 2). The analytical precision of the method was determined from repeated analyses of the same sample collected at 1000 meters depth in the central Mediterranean Sea, yielding an uncertainty of  $\pm 2.1$  % expressed as relative standard deviation on the mean ( $DCo = 47.4 \pm 1$  pM;  $n = 10*3$ ).

## **2.5 Analytical method for the determination of particulate trace elements and phosphorus concentrations**

### **2.5.1 Method**

#### *Digestion procedure*

Trace metal grade Ultrapur® and Suprapur® acids (Merck) were used for the digestion of the PES filters that followed the procedure described in Cullen and Sherell (1999). Manipulations were performed within a class 100 clean hood. The filters were digested in flat bottom screw cap Teflon PFA vials (30 mL, Savillex®), as described in Planquette et al. (2012). Filters were placed in the vials where 2-3 mL of an acid solution was added ( $\text{HNO}_3$  8 M, Merck Ultrapur®; HF 2.9 M, Merck Suprapur®). Vials were then closed and heated at 130°C on a Teflon thermostated plate during 4 h in a laminar flow Class 100 all plastic fume hood. After a short cooling, vials were opened and heated at 110°C to evaporate the acid solution and dried the samples. After totally dryness, 6 mL of 0.8 M  $\text{HNO}_3$  solution spiked with indium (1 ppb) and rhenium (10 ppb), used as drift monitor, were introduced in the vials and then transferred into acid cleaned 15 mL polypropylene tubes (Corning®) for archiving before analysis.

#### *ICP-MS analysis*

Trace element analyses were performed on a Sector Field Inductively Coupled Plasma Mass Spectrometer (SF-ICP-MS) Element-2 (Thermofisher) with variable resolution ( $R = M/\Delta M$ ). In this study only the low ( $R \sim 300$ ) for Cd and Pb, and medium ( $R \sim 3000$ ) for other elements resolutions were used.

On the day of analysis, 500  $\mu\text{L}$  of archived solution were pipetted and diluted into 3 mL of  $\text{HNO}_3$  (0.8 M) solution in acid cleaned polypropylene tubes (Corning®). Every 8 samples a replicate as well as a tube blank are prepared.

Given the variability of concentration range and elemental ratios in the environment, two multi-elemental solutions were realized from single element primary standards solutions. All working solutions for calibration were prepared from 10 or 1000  $\text{mg}\cdot\text{L}^{-1}$  NIST traceable primary standards purchased from high purity standards and diluted to appropriated concentrations with 0.8 M  $\text{HNO}_3$ . To avoid potential cross contamination when mixing high and low concentration standards, two separate multi-element standard curves were constructed. One with high concentration for Al, P, Ca, Fe, Sr and Ba and another with low concentrations for Ti, V, Cr, Mn, Co, Ni, Cu, Zn, Cd, Mo, Pb and Zr. The two 10 points external standards curves were prepared by dilution of multi-element mixed standard stock

solution and spiked with indium (1 ppb) and rhenium (10 ppb). The calibration curves cover two orders of magnitude of potential concentration variation between the samples and were run at the beginning, the middle and the end of each sequence. A typical sequence contains 8 instrument blanks, 8 tube blanks, 72 samples (including process blanks) and 16 samples spiked with multi-element standards solution. Relative standards errors on the measurement are determined by the ICP-MS software.

### **2.5.2 Analytical performance**

The analytical performances are presented for the only 5 elements of interest in this study (Co, P, Al, Mn, Fe). Accuracy of the method was determined by running the same sample during the same sequence (each 8 samples). Analytical reproducibility was always < 10% for all elements. Results of mean instrument, digestion, process blanks are reported in Appendix 2 and show different patterns for the different elements. While the filter itself is the main contributor to the mean blank for Al, the filtration and the digestion procedure are the prevailing sources of contamination for P and Co respectively. As described in Planquette et al. (2012), instrument blanks were exceeded by a large factor by process and filter blanks. At date, there is no available CRM for marine suspended particles, hence we compare results for dried powder CRM of phytoplankton (BCR-414a). Regarding uncertainties of the method and certified values for this material, data are validated (Appendix 2).

### **2.6 Analytical method for the determination of particulate organic nitrogen and carbon concentrations**

As describe in L'Helguen et al., (2014), before analysis, filters were placed in a dessicator with fuming HCl Normapur® (10 N, Merck) during 4 hours to eliminate the inorganic phase, then filters were over dried for 24 h (60°C). Particulate organic carbon (POC) and particulate organic nitrogen (PON) concentrations were quantified with a mass spectrometer (Delta+, ThermoFisher Scientific) coupled with a C/N analyser (Flash EA, ThermoFisher Scientific) via a type III-interface. The limit of detections of the method estimated as three times the standard deviation of the mean reagent blank were, on average, 0.51 and 0.06 µmol L<sup>-1</sup> for POC and PON concentrations, respectively.

### 3 General circulation

#### 3.1 Eastern Atlantic and Gibraltar Strait

Briefly, the section started offshore of Portugal in the mid latitudes of the North-eastern Atlantic Ocean ( $14.2^{\circ}\text{W}$ ;  $39.7^{\circ}\text{N}$ ), followed a south-east transect (Figure 1) and entered into the Mediterranean Sea through the Strait of Gibraltar. In the Atlantic sector (Stations 1a to 4a), different water masses were characterized. The surface (0-250 m) was characterized by relatively salty and low dense waters (Figure 2a). Deeper, the North Atlantic Central Waters (NACW) mostly composed of Antarctic Intermediate Waters (AAIW) flowing northward across the Eastern Atlantic can be located between 400 and 750 meters. They dispatch lower salinities (Figure 2a; Tsuchiya et al., 1992) compared to the underlying Mediterranean Outflow Waters (MOW) centered at 1000 meters (Figure 2a). The high salinity signature of the MOW is entrained into the Atlantic Ocean from Gibraltar, by the AAIW (van Aken, 2000a). The upper MOW (750-1000 m) is mixed with the AAIW, and the lower MOW (1000-1250 m) with the Labrador Seawater (LSW). However, these latter ones could not be discerned at our latitudes (Tsuchiya et al., 1992). The North Eastern Atlantic Deep Waters (NEADW) are observed between 1500 and 2500 m. At this location, the NEADW are composed of MOW, LSW, Iceland Scotland Overflow Water (ISOW) and Lower Deep waters (LDW), accounting, respectively, for 5, 29, 17 and 49% (estimated after van Aken, 2000b). Below 2500 meters, the LDW are mixed with Antarctic Bottom Waters (AABW) flowing northward (Mantyla and Reid, 1983; McCartney, 1992; Schmitz and McCartney, 1993).

The water budget at Gibraltar varies widely depending on the different studies from simple to double (see review of Ribera d'Alcalà et al., 2003). The Gibraltar experiment by Bryden and Kinder (1991) on the dynamic of this strait indicated inflow of Atlantic Waters (AW) in the top 160 m above the isohaline 37, whereas the outflow of MOW occur below ( $> 160$  m depth). The inflow and outflow fluxes reported by Bryden et al. (1994) and Béthoux et al. (1980) vary by factor 2, but a relatively similar value of the net water inflow flux entering the Mediterranean Sea is estimated in both studies ( $\sim 0.06 \pm 0.02$  Sv, where  $1\text{ Sv} = 10^6 \text{ m}^3 \text{ s}^{-1}$ ). This average value is similar to the net inflow flux estimated over with the last 20 years records ( $0.057 \pm 0.009$  Sv; Boutov et al., 2014) and compensated the net evaporation of  $50\text{-}100 \text{ cm.yr}^{-1}$  in the Mediterranean Sea (Marrioti et al., 2002). In this study, we will use the historical water fluxes determined by Béthoux et al. (1980).

It is admitted that the outflow of MOW at Gibraltar mainly consists of modified Levantine Intermediate Waters (LIW; Millot, 1999). Inflowing Atlantic waters (AW) are a

mix of NACW, North Atlantic Surface Waters (NASW) and Waters from the Gulf of Cadix (GCW; Elbaz-Poulichet et al., 2001a). These inflowing AW are influenced, among others, by shelf exchanges, riverine inputs and anthropogenic sources (Boyle et al., 1985; van Geen et al., 1997, Elbaz-Poulichet et al., 2001a) that mainly occur in the Gulf of Cadix.

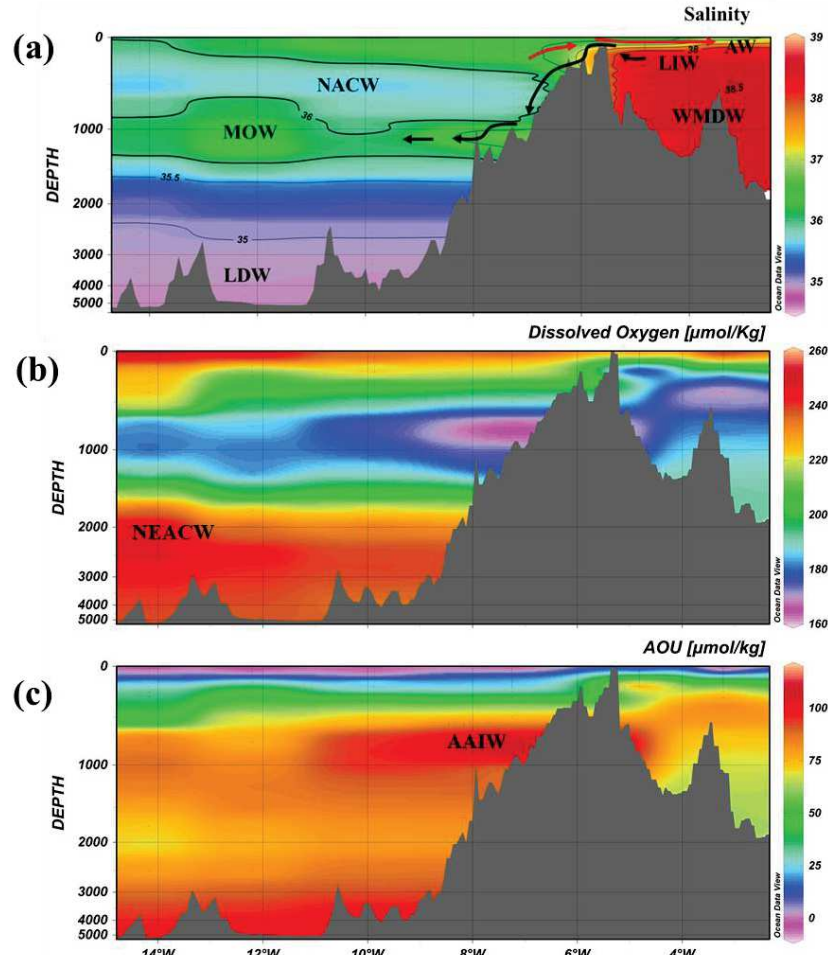


**Figure 2 :** Contour plots versus depth of a) salinity; b) dissolved oxygen; c) apparent utilization of oxygen (AOU) between Stations 1a and 6a. North Atlantic Central Waters (NACW); Mediterranean Outflow waters (MOW); Lower Deep Waters (LDW); Atlantic inflowing Waters (AW); Levantine Intermediate Waters (LIW); Western Mediterranean Deep Waters (WMDM); North East Atlantic Deep Waters and Antarctic Intermediate Waters (AAIW) are labeled. Arrows indicate the water-flow direction at the Gibraltar Strait.

### 3.2 Mediteranean Sea

Passing the Gibraltar Strait, the section enters into the Mediterranean Sea. The thermohaline circulation of this sea drives the transport of the water masses in and across the different sub-basins. Overall, an overturning circulation, specific circulations in the different basins, shelf-slope exchanges and meso-scale dynamics, all contribute to advection and

exchanges of nutrients and trace elements between the different sub-basins (MerMex group, 2011). Based on its stratification, the Mediterranean Sea could be defined as a three layers system (Ribera d'Alcalà et al., 2003), with the surface (0-200 m), intermediate (200-600 m) and the deep layer (600 m-bottom).

### *Surface circulation*

The Mediterranean Sea has a negative water budget due to strong evaporation (Millot, 1999). Indeed, fresh and rain water inputs do not compensate the evaporation, thus the inflow of surface AW through the Strait of Gibraltar is required to compensate this loss. Incursion of the less dense AW mainly drives the surface circulation of the entire Mediterranean Sea (Figure 3a), by following counterclockwise continental slopes. This circulation is mainly due to Coriolis effect (Millot & Taupier-Letage, 2005a), as well as to mesoscale instability, especially in the Algerian Gyre (Millot, 1999). Along the circulation in the Mediterranean Sea, AW are modified, among other, by mixing with the low dense Black Sea waters in the North Aegean Sea and with the fresh waters of the Pô River in the Adriatic. The strong evaporation in the eastern Mediterranean Basin also modifies AW during their transport, leading to the warmest and saltiest surface waters found in the Mediterranean Sea close to Rhodes Island (Figure 3a; Millot & Taupier-Letage, 2005a). Surface mesoscale instabilities can also modify the properties of AW by mixing with intermediate waters especially in the Eastern Algeria area, the Central Ionian Sea and close to the Lybio-Egyptian continental slope (Figure 3a; Millot & Taupier-Letage, 2005a). In the Mediterranean Sea, the surface inflow from the eastern basin to the western basin is limited. The AW, the fresh Black Sea and Pô river waters, as well as their modifications, can be tracked across the different basins with their sub-surface salinity signatures (Figure 3a).

The surface Mediterranean Sea is highly stratified from spring to late fall and the residence time of surface waters are short (20-50 years; MerMex group, 2011). Thus, hydrographic exchanges between surface and deeper waters are limited, and predominantly occur in the forming areas of intermediate and deep waters.

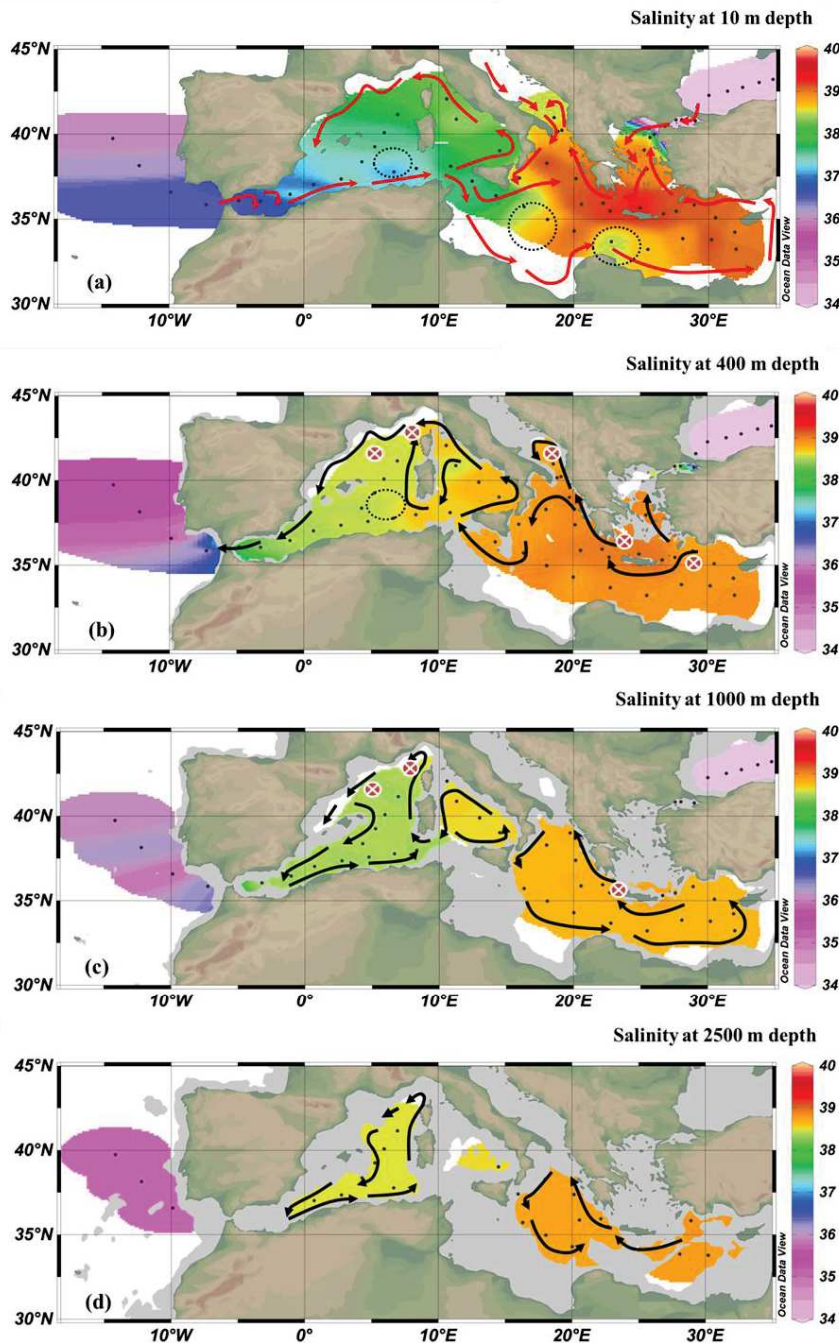


**Figure 3 :** Spatial distribution of salinity at: **a)** the subsurface (10 m); **b)** 400 m depth; **c)** 1000m depth, and **d)** 2500 m depth along the GA04N section. Arrows indicate the simplistic surface (red) and deep (dark) circulations in the Mediterranean Sea. Dashed circles indicate location of physical quasi permanent instabilities. Crossed red circles indicate locations of deep convection.

### *Intermediate circulation*

Both Eastern and Western north part of the Mediterranean Sea suffer intense dry and cold North winds during winter, generating dense waters prone to deep convection. Wind-stress is especially severed in the North Levantine basin, south-east of Rhodes Island (Millot and Taupier-Letage, 2005a). There the AW are the warmest and the saltiest of the Sea, the winter cooling of this area induces a convection of a large volume of waters to the intermediate depths that form the LIW and then spread in the wole basin at 200-600 m. Similarly to AW circulation, LIW are transported and modified along the entire Mediterranean Sea by Coriolis effect and by mesoscale instabilities (Millot, 1987; Millot & Taupier-Lepage, 2005b). Due to the topography LIW only penetrate into the Western Basin across the Sicilian Strait (Figure 3b). In the Western basin, modified LIW follow the northern continental slopes (Figure 3b), and finally outflow across the Gibraltar Strait (Millot & Taupier-Lepage, 2005b). Additionally to LIW, specific intermediate waters are also formed in the Cretan Sea, Adriatic Sea, the Gulf of Lion and the Ligurian Sea (Figure 3b; Millot, 1999). These waters can be tracked with the salinity recorded during the cruises at intermediate depths (Figure 3b).

### *Deep circulation*

The Eastern Mediterranean Deep Waters (EMDW) are formed in two distinct areas. In the Cretan Sea, the LIW mix with the dense Aegean deep waters (AeDW) formed in the south Aegean Sea. In the North Ionian Sea, the modified LIW mix with the Adriatic deep waters (AdDW) formed in the South Adriatic Sea. Due to their high density these two similar dense water-masses dive to form EMDW that circulate counterclockwise along the slopes below 600m depth. The denser EMDW waters are formed during winter and feed the greatest depth (> 2000m) of the Eastern Basin (Figure 3d).

In the Western Basin, the deep waters are composed of Western Mediterranean Deep Waters (WMDW) formed in the Gulf of Lion and of Tyrrhenian dense waters (TDW). TDW result from the mixing of EMDW, LIW and WMDW. The flow of the WMDW and TDW strongly depends of the Western Basin topography aditionally to their density. Indeed, the denser WMDW is trapped in the deep (> 2000m) western side of the basin (West of Sardinia Channel, Figure 3d). At shallower depths, (600-2000m) modified WMDW can enter into the Tyrrhenian Sea where they mix with TDW and then outflow from the Tyrrhenian Sea by the

Sicily Channel. Then these modified western deep waters flows along the Sardinia / Corsica slopes up to the Ligurian Sea (Figures 3c).

The residence time of deep water-masses is short in the Mediterranean Sea, ~25 yr in the Western Basin and ~50 yr in the Eastern basin (after Ruiz-Pino et al., 1990). In addition to the Coriolis effect which mainly drives the deep circulation in both Eastern and Western Basins, the Bernoulli effect at the Gibraltar (Kinder and Parilla, 1987) accounts for the shorter residence time and more intense conveyor belt recorded in the Western Basin compared to the Eastern Basin (Millot & Taupier-Letga, 2005a).

### 3.3 Black Sea

The Black Sea is a quasi-enclosed marine system connected to the Marmara Sea through the Bosphorus Strait (Figure 4a) itself connected to the Aegean Sea by the Dardanelles Strait. The discharge of the surrounding rivers decrease the salinity in the surface waters ( $S \sim 18$ , Figure 4b), whereas the Mediterranean salty inflow spreading at intermediate depth and then dive to the bottom ( $S \sim 22$ , Figure 4b). Both generate a sharp pycnocline at around 100-150 m depth (Figure 4b). The water flows across the Bosphorus Strait are balanced between the Black and Mediterranean Seas (Oguz, 2005). The inflow into the Black Sea is estimated to 0.01 Sv (Unlata et al., 1989).

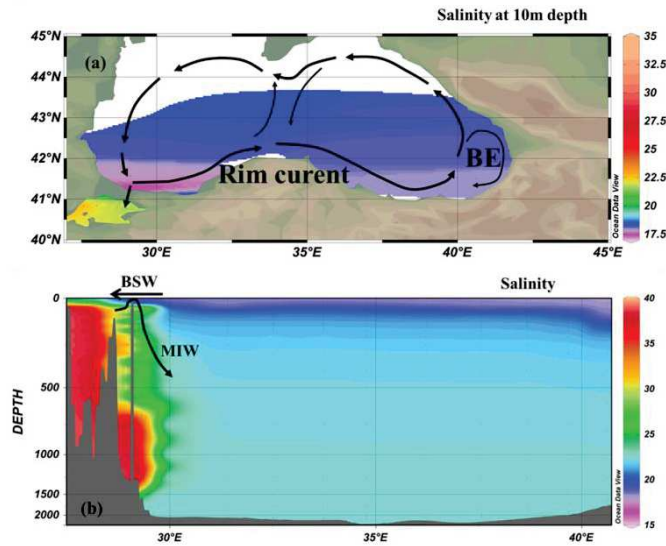


**Figure 4 :** (a) Spatial distribution at 10 m depth of the salinity in the Black Sea along the GA04N section. Arrows indicate the simplistic surface circulation of the Rim Current. The Batumi Eddy (BE) is also indicated. (b) Vertical distribution of the salinity from the Marmara Sea to the Batumi Eddy during the GA04N section. Arrows indicate the direction of outflow Black Sea Surface Waters (BSW) and of the Mediterranean Inflowing Waters (MIW).

### *Surface circulation*

A cyclonic boundary surface current (Figure 4a) flows along the continental slope, with a typical speed of 0.3-0.5 m.s<sup>-1</sup> that can be recorded as deep as 300-400 m (Oguz et al., 1993). Prone to strong wind stress, several mesoscale gyres are frequently observed in the Black Sea. Two predominant cyclonic gyres are observed, in the Western side and in the Eastern part of this Sea. A quasi-permanent anticyclonic eddy (called Batumi eddy) is also observed in the South-eastern side of the Black Sea (Figure 4a; Oguz et al., 1995).

### *Deep circulation*

The extremely rough meteorological conditions of this region during the wintertime (influenced by the continental weather) generate the formation of dense waters on the shelves and in the center of the two cyclonic gyres. There, the dense waters dive to the intermediate depths, where they form the cold intermediate layer (Shapiro, 2009). The Mediterranean inflow feeds the deep Black Sea in salts (Gregg et al., 1999). This inflow partly entrains the intermediate cold waters to the deep (Murray et al., 1990; Özsoy et al., 1993). The mixing of intermediate and deep waters is enhanced by mesoscale eddies and basin-scale circulation (Oguz et al., 1995; Shapiro, 2009).

## **4 Biogeochemical features**

### **4.1 Eastern Atlantic and Gibraltar Strait**

#### *Nutrients and oxygen distributions*

Nutrients concentrations recorded in the Atlantic sector are similar to those previously reported by van Haken et al. (2000 a,b). The low concentrations of nitrate, phosphate and silicate in surface waters that increase with depth (Figure 5) reflect their uptake in surface waters and accumulation in deep waters, likely due to cumulative remineralization along the deep circulation in the Mediterranean Sea. Stoichiometric N/P ratio was about 15.9/1 M/M below 250 m depth, similar to the Redfield Ratio (RR = 16/1 M/M; Redfield, 1963). The vertical and zonal distributions of oxygen and apparent utilization of oxygen (AOU) are reported on Figures 2b&c, respectively. The oxygen distribution showed a well oxygenated surface layer, a decrease with depth until an oxygen minimum depth (OMD) which was generally centered between 750 and 1250 meters depth. The OMD resulted from mixing between two poor oxygenated water-masses, the MOW and the AAIW. Below the OMD, oxygen levels increased to reach a deep maximum located at around 2000-2500 meters depth,

in the well oxygenated NEADW. Deeper oxygen slightly decreased. The AOU profiles allowed to better discern the recently formed NEADW with its significantly lower AOU values compared to the other water-masses (Figure 2c). Deeper older water-mass with a component of AABW displayed a relatively high AOU ( $98 \mu\text{M}$ ) resulting from cumulative remineralization as exemplified by the high nutrient concentrations recorded in this water mass (Figure 5).

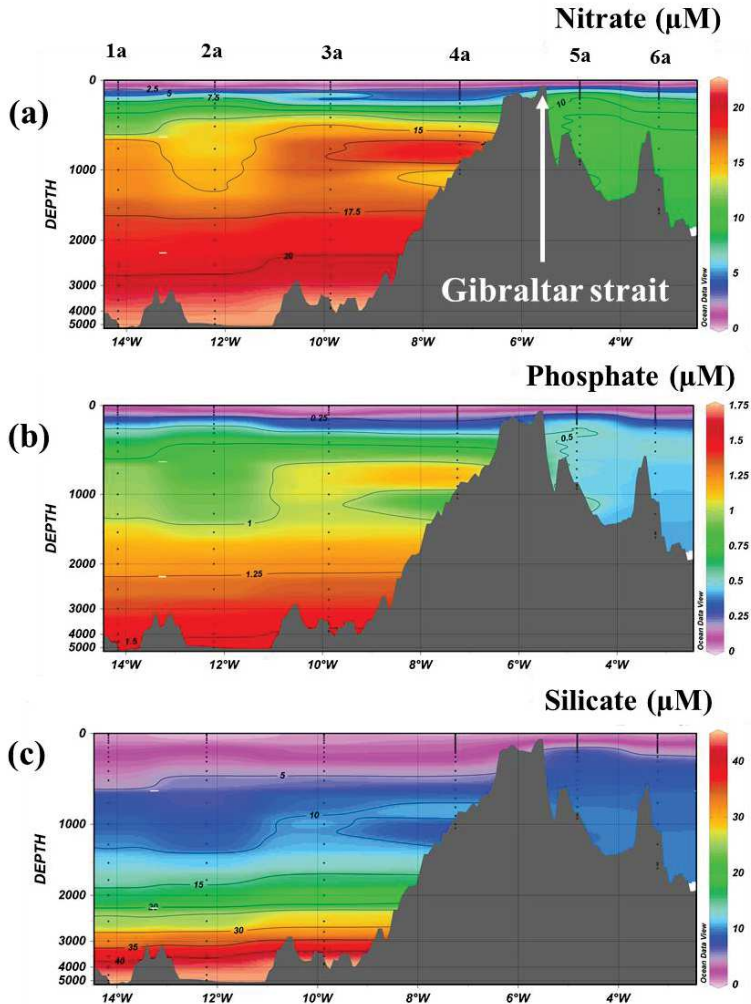


**Figure 5:** Vertical distributions of: **a)** nitrate; **b)** phosphate; **c)** silicate concentrations between Stations 1a and 6a (labelled).

An elevated AOU signal ( $> 100 \mu\text{M}$ ) was recorded near 800 meters depth close to Gibraltar (at Station 4). Anomalies of high concentrations were also observed there for nitrate and phosphate (Figure 5), and to a lesser extend for silicate. Those signals are significantly higher than those observed in the core of MOW (AOU  $\sim 90 \mu\text{M}$  which is likely flowing deeper ( $\sim 1000 \text{ m}$ ; Figure 2a). The intrusion of the old AAIW enriched in macro-nutrients and marked by a high AOU signal ( $100 \mu\text{M}$ ; van Haken 2000b), and/or high remineralization of terrestrial

matter discharged by Spanish Rivers in the Gulf of Cadix located north of this station, could both be invoked to explain those anomalies.

The budget of macro-nutrients reported at Gibraltar widely varied in the literature, but all studies are according to suggest that the Gibraltar circulation induce a net loss of nutrients to the Mediterranean (see review by Ribera d'Alcalà et al., 2003).

## 4.2 Mediterranean Sea

### *Nutrients and oxygen distributions*

The Mediterranean Sea is known to dispatch low nutrients concentrations in deep waters, peculiar stoichiometric N/P ratios compared to other oceanic domains (Figure 6), and oligotrophic conditions which increase eastward (Figure 7; Béthoux et al., 1998, 2005; Bosc et al., 2004). In this semi-enclosed sea, inputs by the atmosphere, groundwater and rivers, all forced by anthropogenic pressures, are major sources of phosphate and nitrogen, rather than basin exchanges. Indeed, nutrient inputs from the Atlantic to the Western Basin at Gibraltar and from the Black Sea to the Eastern Basin through Bosphorus account for less than 30% and 1% of the total nutrient inputs to the Western and Eastern Basin, respectively (Béthoux et al., 1998; Krom et al., 2004). The vertical distributions of nitrate, phosphate, silicate and oxygen concentrations, as well as apparent oxygen utilization (AOU) are presented for the different sub-basins of the Mediterranean Sea (Figure 6). The values reported are in excellent agreement with previous studies (see review of Ribera d'Alcalà et al., 2003).

In the Western Basin, the nutrients showed the lowest concentrations in surface, then an increase with depth (Figure 6), and they reached their maximum values at the OMD ( $O_2 < 180 \mu M$ ; Figure 6d) which is generally located near  $500 \pm 100$  meters depth. This OMD probably resulted from remineralization of biogenic material. A slight decrease of nutrients concentrations was observed below the OMD. The influence of the Eastern Basin to the Western Basin can be discerned in the Tyrrhenian Sea by the lower nutrients concentrations in the 500-1500 meters layer compared to the rest of the Western Basin (Figure 6). The Eastern Basin showed extremely low nutrients concentrations in surface waters (Figure 6), which featured ultra-oligotrophic conditions. The nutrients concentrations increased with depth, reaching their maximum concentrations at the OMD located deeper than in the western basin (~750 m). Below the OMD nutrient concentrations decreased with depth. The southern edge of the Adriatic (Station 7c, 8c, 9c; Figure 1) dispatched low nutrients concentrations (Figure 6), and oxygenated waters (Figure 6). In the shallow waters of Aegean and Cretan Seas,

nutrients levels were similar than those recorded in the South Adriatic. Hence, the EMDW which are formed in the south Adriatic and Cretan seas provide low preformed nutrients concentrations and oxygenated waters to the deep Eastern Basin.

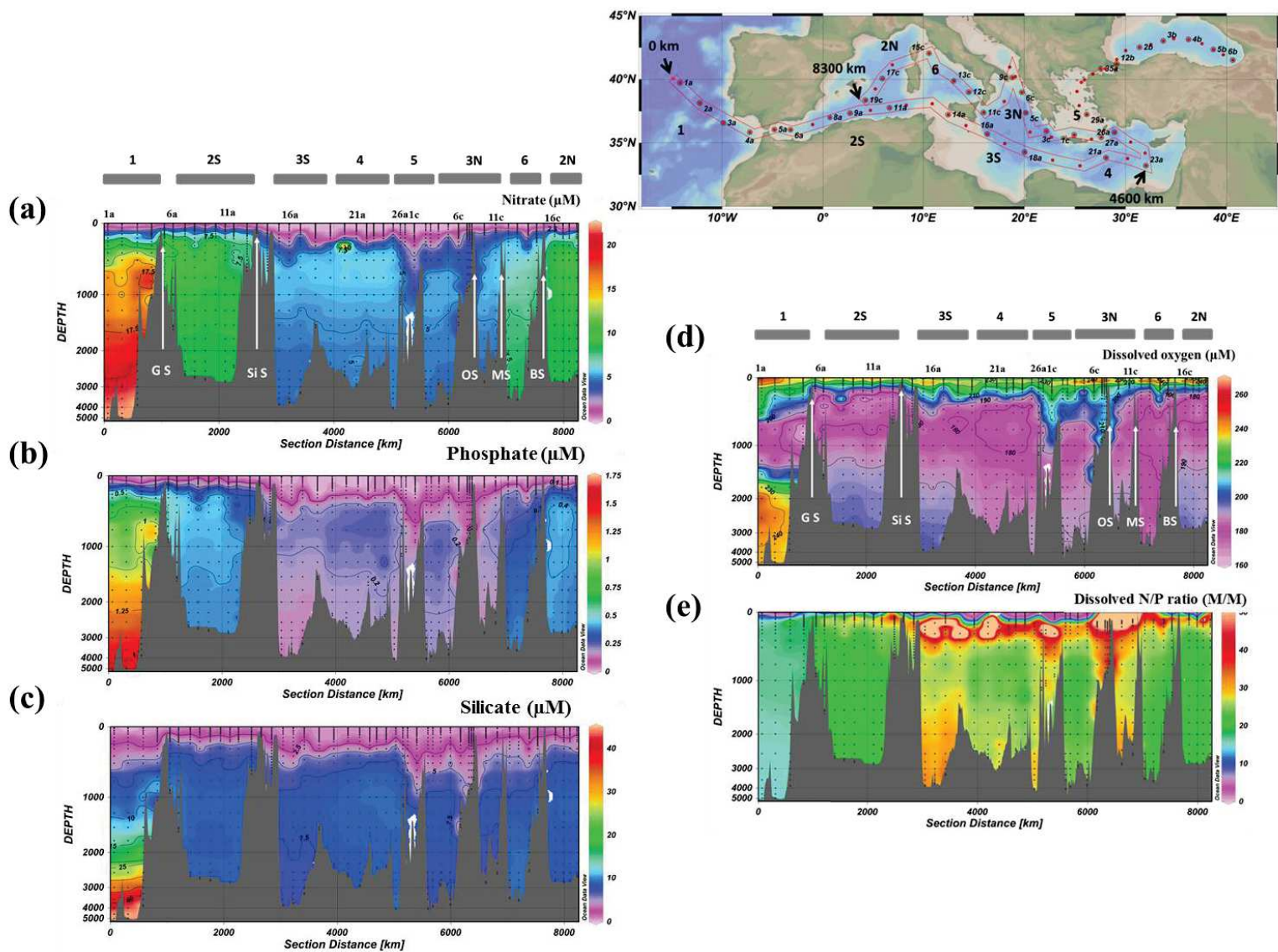


**Figure 6:** Vertical distributions of **a)** nitrate + nitrite; **b)** phosphate; **c)** silicate; **d)** dissolved oxygen; **e)** dissolved N/P ratio along the GA04N-section. Few stations numbers are labelled. The different sub-basins are labeled as following: 1) North Eastern Atlantic; 2S and 2N) South and North Western Mediterranean Basin, 3S and 3N) South and North Ionian Sea; 4) Levantine Basin; 5) Cretan Sea; 6) Tyrrenian Sea. The Gibraltar Strait (GS), Sicily Strait (Si S), Otranto Strait (OS), Messine Strait (MS) and Bonifacio Strait (BS) are indicated on panels **(a)** and **(d)**.

In both Western and Eastern Basins, the highest nutrients concentrations were recorded at depth in the OMD. The relationship observed between AOU and the nutrients concentrations indicated significant correlation in intermediate and deep waters (Figure 8), likely resulting from remineralization of organic matter into inorganic products by the consumption of oxygen. Tight correlations were observed in the Eastern Basin (Figures 8d-e-f), but different relationships were observed in the Western Basin in the core of the WMDW (Figures 8a-b-c). This different pattern might be related to a nutrients specific signature of the North-western Mediterranean Sea, where WDMW are formed.

The nutrient concentrations recorded along the GA04N section were higher in the Western compared to the Eastern basins, which contrasts fairly with remineralization processes that should increase the nutrients concentrations with ages of deep water masses, thus eastward. For instance, the Eastern deep water masses have a longer residence time compared to Western deep water masses (~ 50 and 25 yr, respectively), whereas nutrients deep concentrations and AOU were lower. The anti-estuarine circulation of the Eastern basin and the difference in the productivity between the two basins can both explain this anomaly. Indeed, the deep waters outflowing from the Eastern basin towards the Strait of Sicily are enriched in nutrients compared to the nutrients-depleted inflowing waters, inducing a net loss of nutrients for the Eastern basin (Béthoux et al., 1992; Ribera d'Alcalà et al., 2003; Krom et al., 2010). The higher productivity in the Western basin compared to the Eastern basin (Figure 7, Moutin and Rimbault, 2002; Bosc et al., 2004) could also be invoked. The higher downward flux of biogenic material, and its subsequent remineralization would also lead to higher nutrients concentrations and higher AOU in the West compared to the East (Ribera d'Alcalà et al., 2003).

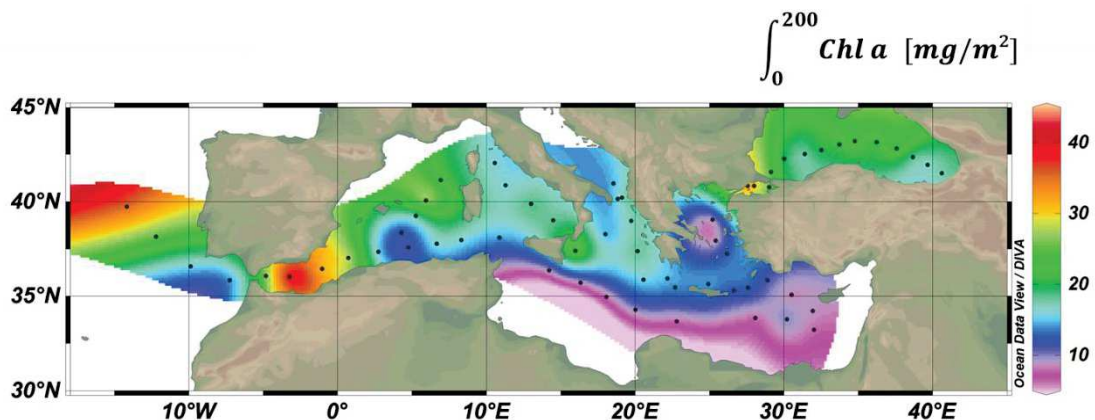


**Figure 7 :** Spatial distribution of integrated Chlorophyll a concentrations between 0 and 200 meters (data derived from fluorescence) along the GA04 section.

### *N/P stoichiometry*

Another characteristic of the Mediterranean Sea is the specific nutrients stoichiometry of the different basins as we observed. Indeed, while most of surface waters showed N/P ratios lower than the RR, the intermediate and deep waters displayed dissolved N/P ratios higher than the RR (Figure 6e). The RR describes a nutrient stoichiometry normalized to phosphate of 1/16/106/138 for P/N/Si/C/ $\Delta O_2$ , respectively (Redfield et al., 1963). These stoichiometric ratios have been revisited by Anderson and Sarmiento (1994) providing ratios of 1/16/117/170 for P/N/C/ $\Delta O_2$  for the global ocean. However, in the Mediterranean Sea, much higher N/P ratios of 26.9/1 and 22.1/1 were recorded in our study for the Eastern and Western basins, respectively, in agreement with previous reported values (Ribera d'Alcalà et al., 2003; Krom et al., 2010). Over the past 20 years, several studies attempted to resolve this Mediterranean stoichiometric anomaly (Béthoux et al., 1992, 1998, 2002; Sarmiento et al., 1988; Gruber and Sarmiento, 1997; Pantoja et al., 2002; Ribera d'Alcalà et al., 2003, Krom et al., 2004, 2010) and two hypotheses still persist. The older hypothesis was historically proposed by Béthoux et al. (1992) and suggests that all the nutrients inputs in the Mediterranean Sea have an N/P ratio equal to, or lower than the RR. It is then argued that intense N<sub>2</sub> fixation by seagrass and diazotroph phytoplankton is required to elucidate the the high N/P anomaly. A second hypothesis proposed by Krom et al., (2004) based on budget of nutrients inputs argued that all the nutrient sources (atmosphere, coastal and rivers) have an N/P ratio higher than the RR (Krom et al., 2004, Ludwig et al., 2009; MerMex group, 2011). Then, considering the oligotrophy of the Mediterranean Sea, the well oxygenation of deep water masses and the short residence time of the Mediterranean waters, the biogeochemical changes of the N/P ratio (through biological uptake, denitrification or anammox processes) could be restricted before the outflow across Sicily channel and Gibraltar strait, explaining the N/P anomaly. Consequently to the high N/P ratio observed in Mediterranean Sea, an overall P-limiting condition is assumed (Krom et al., 2010). However, surface P-limitation could shift into N-limitation especially during the winter (Marty el al., 2002).

Our investigations on nutrient particulate C/N/P stoichiometry in the surface waters (0-200 m) show a mean nutrient C/N/P ratio of 131/19/1 (normalized to P; n = 23) during the cruises, similarly to the ratio reported by Pujo-Pay et al. (2011). These observations suggest that the biological nutrient fractionation could not itself explain the N/P anomaly.

**Table 1:** Mean nutrients and cobalt stoichiometries in the particles collected in surface waters (0-100m) along the GA04-section.

Sector	sub-basin	mean C/N/P	mean Co/P (μmol/mol)	mean Co/C (μmol/mol)	Co/C estimated* (μmol/mol)
<b>Atlantic</b>	<i>Eastern Atlantic</i>	116/15/1 (n=5)	90.5 (n=5)	0.89 (n=5)	0.78
	<i>Alboran Sea</i>	82/14/1 (n=3)	241.7 (n=6)	4.60 (n=3)	2.95
<b>Western basin</b>	<i>Central Western basin</i>	181/18/1 (n=6)	246.5 (n=6)	1.59 (n=6)	1.36
	<i>Tyrrenhan Sea</i>	121/19/1 (n=1)	164.5 (n=5)	1.26 (n=1)	1.36
<b>Eastern Basin</b>	<i>Ionian Sea</i>	158/24/1 (n=3)	246.9 (n=7)	1.35 (n=3)	1.56
	<i>Levantine Basin</i>	128/15/1 (n=3)	567.1 (n=3)	5.16 (n=3)	4.43
<b>Black Sea</b>	<i>Western Gyre</i>	158/18/1 (n=1)	215.4 (n=3)	2.34 (n=1)	1.87

\* mean Co/P divided by mean C/P

Additionally we investigate the N/P ratio provided by the remineralization processes ( $\Delta N/\Delta P_{\text{remineralization}}$ ) that can be estimated following Equation (2). The value of  $\Delta N/\Delta P_{\text{remineralization}}$  estimated that way is equal to about 21.4 in the Western and 25.2 in the Eastern basins, suggesting preferential remineralization of N over P. These higher N/P ratio than that given by RR can be seen as a preferential remineralization of N compared to P (Figure 8). This preferential remineralization could explain the N/P anomaly in the western Basin but not in the eastern basin.

$$\Delta N/\Delta P_{\text{remineralization}} = \Delta N/\Delta AOU * (\Delta P/\Delta AOU)^{-1} \quad (2)$$

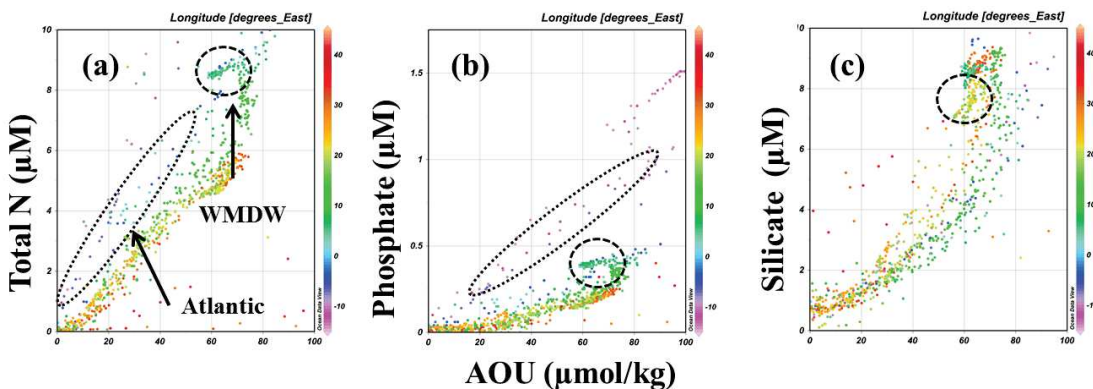


**Figure 8 :** Scatter plots of: **a)** nitrate + nitrite (Total N), **b)** phosphate, **c)** silicate concentrations versus the apparent utilization of oxygen (AOU). The color scale stands for the longitude of the sample (°E).

## *Chlorophyll a, nitrite and particulate nutrients stoichiometry*

Strong seasonal variability in the trophic and biogeochemical conditions is commonly observed in the Mediterranean Sea (Marty et al., 2002), as well as a high spatial biodiversity between and within the different sub-basins (Ignatiades et al., 2009). Additionally, meso-scale structures like eddies strongly impact the phytoplankton distributions (Vidussi et al., 2001). Indeed, the anti-cyclones commonly observed in the South-eastern Mediterranean (Millot and Taupier-Lepage, 2005) can maintain ultra-oligotrophic conditions by lowering the exchanges between intermediate and surface waters, hence they could impact the phytoplankton distributions and productivities (Vidussi et al., 2001). Differently, the cyclones in the North Ionian Sea observed during the winter can promote the nutrients availability to phytoplankton and increase the new production in this area (Vidussi et al., 2001).

At the time of sampling, the upper vertical distributions of Chl *a* and nitrite are presented on Figure 9. Mostly resulting from nitrification processes and considering its short life in oxygenated seawater, nitrite can be used as a tracer of the nitrate regeneration at depth, as well as to track the biological state of the system (pre/in/post bloom). The elemental P/N/C compositions of particulate matter collected in the Chl *a* maximum in the different basins are reported in Table 1 and provide indications on the possible dominant taxa.

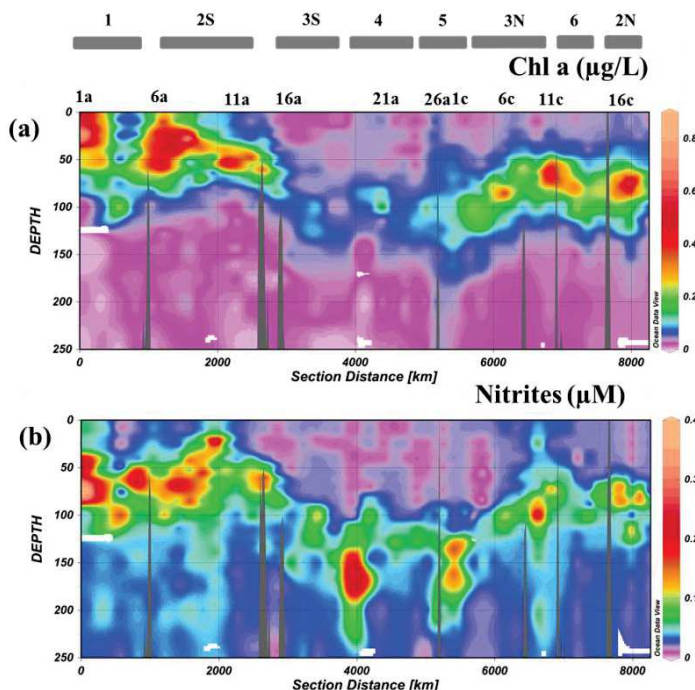


**Figure 9:** Vertical distributions in the top-250 m of: **a**) Chlorophyll a (fluorescence derived); **b**) nitrite concentrations along the section. Few stations numbers are labelled. The different sub-basins are labeled as indicated in Figure 6.

In the Western basin, the Alboran Sea and close to the Algerian coasts, Chl *a* maxima were significantly high and shallow (~50 m), generally exceeding 0.4 µg/L and up to 0.6 µg/L (Figure 9). There, Chl *a* and nitrite relative maxima did not correlate (Figure 9), which could reflect a productivity based on new production during the springtime over the period of sampling. During our sampling (late spring) the stratification was still smooth, thus nutrients availability could keep relatively enhanced, hence it could have sustain relatively high Chl *a* concentrations and new primary production. In the Alboran Sea, the relatively high Chl *a* concentrations in the top to 55 m (> 0.5 µg/L) were associated with stoichiometric P/N/C ratios of 1/20/125 in the first 10 m, and of 1/12/62 in the layer between 25 and 55 m depths. Those elemental ratios are similar to the elemental compositions of cyanobacteria and of estuarine diatoms, respectively (Ho et al., 2003; Bertilson et al., 2013), suggesting that two different communities of phytoplankton dominated the surface layer, with cyanobacteria located at the subsurface and diatoms deeper.

Offshore of the Algerian coasts (e.g. Station 11a), the depths of Chl *a* and nitrite maxima were similar (Figure 9). The dissolved Silicates concentrations were depleted, and the particulate elemental stoichiometric ratio of 1/14/87 was in excellent agreement with the elemental composition of the diatom *Thalassiosira weissflogii* (Ho et al., 2003). These features suggested that we may have sampled in a post diatoms bloom area, which is further supported by reported significant proportion of diatoms in this area (Ignatades et al., 2008). The Tyrrhenian Sea and the central part of the Western basin both sampled in summertime were marked by low and deep Chl *a* maxima (apart at Station 17c where Chl *a* = 0.7 µg/L), likely due to strong stratification of surface waters and low inputs of nutrients from below. Relative maxima of nitrite were observed in or just below Chl *a* maxima (Figure 9), suggesting regenerated production during this stratification period (as previously observed by Marty et al., 2002). The P/N/C stoichiometric ratio in the Chl *a* maxima were of 1/18/123 in the Tyrrhenian Sea, and 1/20/122 in the central of the Western basin (Table 1). These ratios are similar to those of dinoflagellates and cyanobacteria, respectively (Ho et al., 2003; Bertilson et al., 2013). Hence, dinoflagellates and cyanobacteria were likely dominating the micro- and nano-pico- plankton assemblages, respectively.

In the Eastern basin, the fluorescence maxima were generally observed around 75 meters depth. In the ultra-oligotrophic south-eastern basin (Figures 7 and 9) extremely low Chl *a* maxima were recorded (< 0.1 µg/L). Elemental P/N/C stoichiometry ratios of ~ 1/22/171 were recorded in the Chl *a* maxima at Stations 16 and 21, similar to the nano-

phytoplankton elemental composition (Ho et al., 2003). Nano-plankton is indeed abundant in this part of the Mediterranean Sea (Christaki et al., 2001; Vidussi et al., 2001). Differently, Station 18 was marked by a P/N/C elemental stoichiometry of 1/22/80, which is likely similar to the elemental composition of diazotrophs (Sañudo-Wilhelmy et al., 2001).

Near of Rhodes Island and in the Cretan Sea, low Chl a and higher nitrite concentrations compared to nitrate ( $\text{NO}_2 > \text{NO}_3$ ) were recorded, both suggesting that primary production could be dominated by regenerated production.

The northern Ionian Sea and the south Adriatic Sea were marked by Chl a maxima generally higher than 0.2  $\mu\text{g/L}$ , reaching up to 0.46  $\mu\text{g/L}$  near the Strait of Messine (Figures 7 and 9). The relatively high concentrations of nitrite recorded in this basin suggested that regenerated production can sustain the primary production there. Nano-plankton and cyanobacteria can be the dominant phytoplankton functional groups in these waters during summer (Rabitti et al., 1994).

### 4.3 Black Sea

The Black Sea is the widest anoxic basin on Earth, and it is a unique environment to study natural redox reactions of the different elements and their possible evolution along the ocean oxygenation modifications over the past.

#### *Surface biogeochemical features*

The surface waters of the Black Sea (0-40m) were marked by extremely low nutrients concentrations which likely resulted from strong phytoplankton assimilation. Maximum of Chl a ranged from 0.25  $\mu\text{g/L}$ , at the edge of the Batumi eddy, to 0.9  $\mu\text{g/L}$  in the center of the eastern gyre. These maxima were generally observed in the thermocline, just above the suboxic zone, and could mainly consist of biogenic debris (Tankeré et al., 2001). Dinoflagellates can be the dominant phytoplankton group in the Western part of the Black Sea during the summertime of the period of sampling (Uysal et al., 1998), whereas chlorophyceae can dominate in the Eastern basin during this period (Uysal et al., 2001). The surface P/N/C stoichiometric ratio normalized to phosphate of 1/18/156 recorded in the Western part of the Black Sea influenced by riverine inputs (Station 2b, Table 1) was similar to the elemental composition of the estuarine dinoflagellates specie *Amphidinium carterae* (Ho et al., 2003), in

good agreement with previous taxonomy studies in these waters (Uysal et al., 2001; Eker et al., 2000).

### *Oxic-anoxic transition layer and nutrients behaviors*

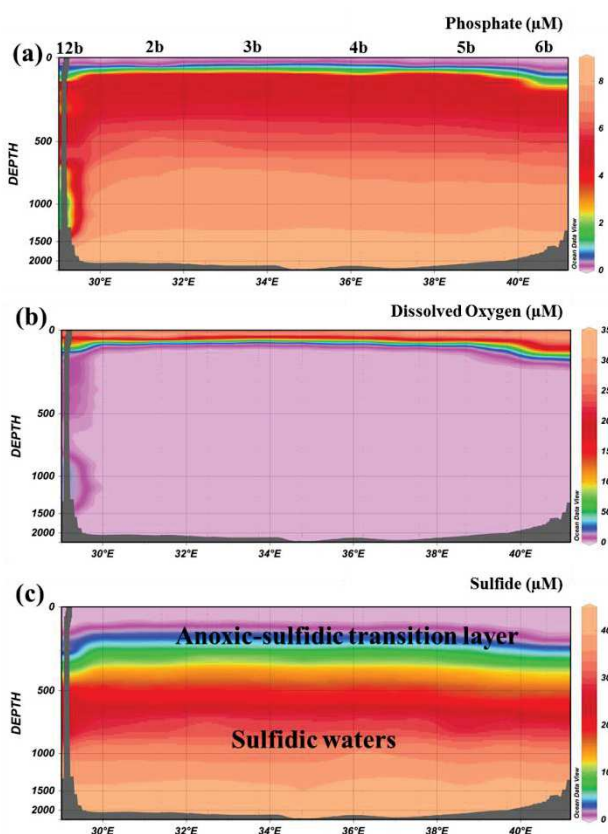


**Figure 10:** Vertical distributions of: a) phosphate, b) dissolved oxygen, c) sulfide concentrations in the Black Sea during the GA04 section. Anoxic-sulfidic transition layer and sulfidic reservoir are indicated. Few stations numbers are labelled.

Since we sampled mostly in the open Black Sea, each nutrient display a single behavior all along the Black Sea transect (Figure 10). In this basin, oxygen concentrations recorded were extremely low apart in the ventilated surface waters, and a deep sulfidic layer was observed below 200 meters. Silicate and phosphate concentrations recorded in the Black Sea were significantly higher than those observed in the Mediterranean Sea, on the contrary to nitrite and especially nitrate which were significantly lower in this Sea compared to the Mediterranean Sea. Strong stratification of the water column was observed due to a marked thermocline (20-50 m) and halocline (40-120 m, Figures 4b). The oxic-anoxic transition layer, also called the suboxic zone, was generally located

between 50 and 120 meters depth (Figure 10), except in the Batumi eddy where this layer was deeper probably resulting from the permanent anti-cyclonic circulation of this gyre (Figure 10). The depth of the upper boundary of the suboxic zone is determined by the balance between oxygen injected in surface by the convection and the oxygen consumed by oxidation of organic matter (Konovalov and Murray, 2001). The injection of oxygen into the upper sulfidic zone by the Bosphorus Plume can play a role to delimit the depth of the lower edge of the suboxic zone (Konovalov and Murray, 2001; Konovalov et al., 2003). Below 120 meters depth in the open Black Sea and below 200 meters depth in the Batumi gyre, the waters were anoxic, and the sulfide concentrations increased with depth (Figures 10-11).

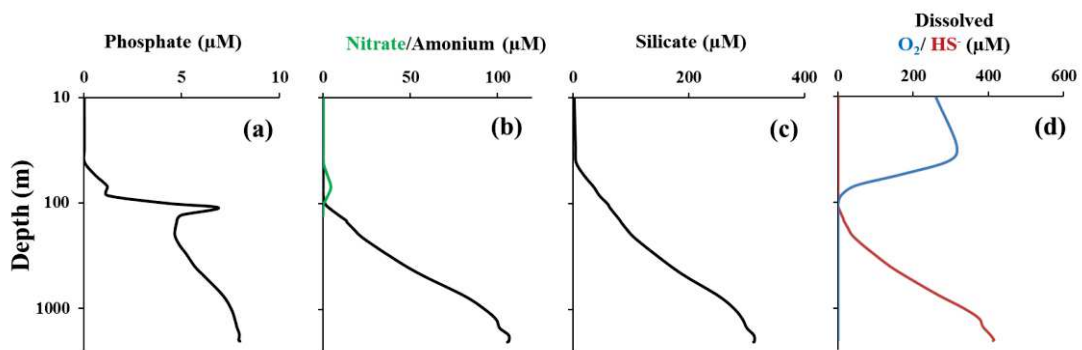


**Figure 11:** Vertical distributions of: **a)** phosphate, **b)** nitrate (green line) and ammonium (black line), **c)** silicate, **d)** dissolved oxygen ( $O_2$ , blue line) and sulfides ( $HS^-$ , red line) in the central Black Sea (Station 5b). Note: nitrate are reduced into ammonium in the anoxic-sulfidic transition layer located at 100 meters depth.

The macro-nutrients (Si, P, N) were depleted in surface waters (0-75m), and they increased with depth until the upper boundary of the suboxic layer. From this depth, silicate continuously increased with depth (Figure 11c) likely due to remineralization of sinking particulate material, whereas phosphate increased up to the bottom of the suboxic zone then decreased in the upper part of the anoxic layer before increasing again up to bottom (Figure 11a). The second increase generally occurs when sulfide concentrations reached values of about  $10 \mu\text{mol} \cdot \text{kg}^{-1}$ . Such distribution of phosphate has been previously observed in the Black Sea, and the decrease of phosphate concentrations in the upper anoxic layer could be due to scavenging of P onto manganese oxides (MnOx). The reduction of MnOx due to increasing sulfide concentrations (Shaffer, 1986) can then release phosphate deeper. The different chemical species of nitrogen ( $\text{NO}_3$ ,  $\text{NO}_2$ ,  $\text{NH}_4$ ) showed specific distributions (Figure 11b). Nitrate and Nitrites generally displayed maxima at the bottom of the suboxic layer, below which the concentration strongly decreased to reach undetectable value in deep waters. The reduction of nitrate and nitrite into ammonium is well known in the deep Black Sea due to their denitrification in the presence of sulfur. Ammonium is indeed accumulating in the deep anoxic basin (Figure 11b).

## 5 Cobalt biogeochemistry

### 5.1 Overview of vertical distributions

#### *Dissolved cobalt*

The distribution of DCo in the Atlantic sector of the section showed a nutrient like distribution in the upper waters (0-200m), an increase up to intermediate depth and a deep distribution which can be related to water masses circulation (Figure 12a, 13a, 14).

In the Mediterranean Sea the distribution was similar to that historically observed (Ngoc and Whitehead, 1986). High DCo concentrations (>100 pM) were observed in the surface waters, decreasing in the intermediate waters (~70 pM, Figure 12b). Deeper a nearly conservative distribution was observed with a quasi-constant concentration below 1000 m (~50 pM; Figure 12b).

The Black Sea was characterized by extremely high DCo concentrations and complex distribution likely representative of the different oxydo-reductive processes specific of this element (Figure 12c). High concentrations of DCo were recorded in the sub-surface waters (>400 pM), decreasing as low as 30pM in the suboxic waters (Figure 12c). In the top part of the sulfidic layer, the highest seawater concentrations recorded along the section were observed (up to 6.6 nM), quickly decreasing with depth to a nearly constant concentration below 1000 m (~330 pM).

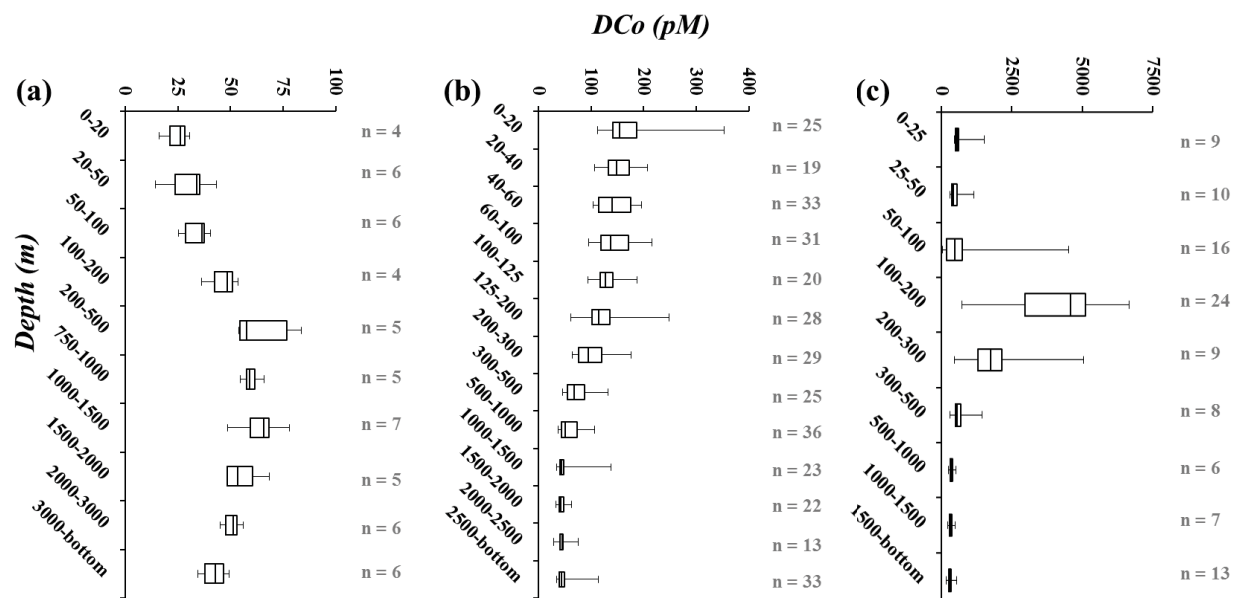


**Figure 12 :** Box plots of dissolved cobalt concentrations (DCo) versus depth in: **a)** the Atlantic sector, **b)** the Mediterranean Sea, **c)** the Black Sea. Number of observations is indicated.

### *Soluble cobalt*

Soluble cobalt (sCo) concentrations ranged from 11.7 to 256.4 pM. The distribution of sCo tightly followed the DCo distribution, (Figure 16a, b). However, sCo generally displayed a slight subsurface depletion, suggesting that sCo could have been biologically consumed. Unfortunately, no ultra-filtered data were available at date for the Black Sea.

### *Colloidal cobalt*

Colloidal cobalt (cCo) concentrations were significantly lower than that of DCo and sCo (Figure 16c). cCo concentrations ranged from undetectable values at several depths in the deep waters to 72 pM in the North-eastern Ionian Sea (e.g.; at Station 5c).

No clear typical behavior was observed for the colloidal cobalt vertical distribution, probably due to their very reactive properties. However, similar trends were observed apart at Station 5c where very high cCo were recorded (Figure 16c). Relatively high concentrations ( $> 15$  pM) were generally recorded at subsurface and near the Chl a maximum. The sub-surface maxima could be related to photo-oxydation of cobalt that forms insoluble Co(III) species (e.g.  $\text{Co(OH)}_3$ ) that agglomerate into cCo. Differently the Chl a maxima suggest biologically driven production of cCo by cell degradation and/or bio excretion. Deeper, cCo decreased with depth in the intermediate waters, with concentrations generally lower than 5 pM and suggest a removal pathway a DCo by adsorption of cCo onto settling particles. In the deep sea, cCo often increases again especially above the bottom depth to value  $> 10$  pM (Figure 16c) probably resulting from benthic input.

### *Particulate Cobalt*

The distribution of PCo was investigated at 15 selected stations (Figure 18a). PCo concentrations range from 0.27 pM in the deep Eastern Atlantic to 622.98 pM in the suboxic waters of the Black Sea. No typical PCo distribution was observed (Figure 18), probably resulting from the short residence time of this fraction in seawater (Dulaquais et al., in revivion). PCo were generally relatively high in the subsurface waters and below the Chl a maxima ( $> 5\text{-}10$  pM), that could be related to dust input and accumulation in settling organic matter, respectively. On the contrary, concentrations were low in the deep waters (0-5 pM), except near the seafloor where high PCo can be recorded (PCo  $> 20$  pM). The extremely high

PCo recorded in the Black Sea corresponded to low DCo, and thus they can be related to transfer between DCo and PCo depending of the oxygenation state of the water column.

**Table 2:** Average surface concentrations and standards deviations of dissolved (DCo), Soluble (SCo), colloidal (cCo) and particulate (PCo) cobalt in the different reservoirs of the Mediterranean Sea. Numbers in brackets are ranges of concentrations

Basin		Western Basin			Eastern Basin			
Sub-basin		Alboran Sea	Central	Tyrrhenian Sea	Ionian Sea	Levantine	Cretan	Aegean
<b>Surface (0-200m)</b>								
<b>DCo (pM)</b>		118.3 ± 15.5 n = 18 (88.3-151.4)	120.2 ± 20.9 n = 40 (61.3-174.9)	121.4 ± 24.6 n = 17 (76.3-163.9)	154.9 ± 40.8 n = 43 (104.0-353.3)	153.6 ± 22.9 n = 19 (107.1-184.8)	186.6 ± 27.1 n = 18 (118.7-248.1)	175.2 ± 12.3 n = 8 (149.6-192.5)
<b>SCo (pM)</b>		106.3 ± 21.1 n = 8 (79.4-136.6)	119.1 ± 11.8 n = 8 (105.1-136.9)	113.6 ± 24.3 n = 6 (90.9-155.2)	144.0 ± 31.0 n = 21 (103.3-326.4)	129.6 ± 14.8 n = 6 (100.3-139.8)	N.D.	N.D.
<b>cCo (pM)</b>		7.8 ± 5.0 n = 3 (2.8 - 14.4)	14.4 ± 8.2 n = 7 (3.4 - 25.5)	10.5 ± 7.0 n = 6 (0 - 18.7)	9.3 ± 11.3 n = 21 (0 - 39.1)	5.6 ± 2.4 n = 5 (1.9 - 8.0)	N.D.	N.D.
<b>PCo (pM)</b>		11.9 ± 8.3 n = 6 (2.7-22.9)	24.4 ± 50.6 n = 9 (1.2-158.5)	3.7 ± 1.5 n = 4 (2.1-5.2)	4.6 ± 7.2 n = 7 (1.0-20.0)	5.1 ± 0.9 n = 2 (4.5 - 5.8)	12.1 ± 17.2 n = 4 (1.7-37.7)	7.9 ± 3.6 n = 4 (4.2- 12.8)
<b>Intermediate (200-600m)</b>								
<b>DCo (pM)</b>		68.2 ± 20.7 n = 7 (48.0-98.4)	73.2 ± 22 n = 11 (47.8 - 126.5)	67.4 ± 8.5 n = 7 (52.5-78.2)	93.2 ± 23.6 n = 14 (53.4-143.2)	76.7 ± 13.7 n = 5 (60.9-94.1)	110.6 ± 43.5 n = 5 (34.3 - 93.3)	108.1 ± 22.1 n = 3 (86.8-130.8)
<b>SCo (pM)</b>		53.81 ± 9.2 n = 4 (46.2 - 66.2)	60.5 ± 6.2 n = 2 (56.1-64.9)	69.6 ± 7.74 n = 3 (63.3-78.2)	85.9 ± 21. 2 n = 7 (48.8 - 114.4)	60.1 ± 6.4 n = 2 (55.4-64.6)	N.D.	N.D.
<b>cCo (pM)</b>		0.19 ± 1.0 n = 1 (11.2 - 16.3)	13.7 ± 3.6 n = 2 (0 - 1.5)	0.5 ± 0.8 n = 3 (3.8 - 24.5)	10.4 ± 8.0 n = 7 (5.5 - 6.7)	6.1 ± 0.9 n = 2 (5.5 - 6.7)	N.D.	N.D.
<b>PCo (pM)</b>		13.3 ± 1.5 n = 2 (12.2 - 14.3)	4.3 ± 2.9 n = 2 (2.2-6.2)	1.26 ± 0.1 n = 1 (1.4 - 2.2)	5.25 ± 0.5 n = 1 (2.0-2.4)	2.3 ± 0.2 n = 4 (10.0-12.8)	11.4 ± 2.0 n = 2 (15.7- 20.3)	18.0 ± 3.3 n = 2 (15.7- 20.3)
<b>Deep (600-Bottom)</b>								
<b>DCo (pM)</b>		53.8 ± 15.7 n = 7 (38.4-85.6)	47.2 ± 8 n = 30 (38.9-76.3)	41.9 ± 7.7 n = 15 (32.6-60.0)	59.2 ± 24.6 n = 32 (34.8-137.0)	44.6 ± 11.2 n = 17 (28.8-75.7)	56.2 ± 20.8 n = 12 (34.3 - 93.3)	
<b>SCo (pM)</b>		51.5 ± 24.1 n = 7 (36.5-81.4)	44.9 ± 4.5 n = 6 (40.0-51.7)	41.8 ± 3.7 n = 7 (36.5-48.5)	44.2 ± 16.5 n = 14 (31.3-99.6)	44.4 ± 4.2 n = 5 (41.2-51.3)	N.D.	
<b>cCo (pM)</b>		3.1 ± 1.6 n = 2 (1.9 - 4.2)	10.3 ± 12.3 n = 6 (1.4 - 27.7)	BLD n = 6	17.2 ± 18.6 n = 14 (1.4 - 72.3)	1.5 ± 0.8 n = 5 (0.7 - 2.6)	N.D.	
<b>PCo</b>		18.6 ± 6.1 n = 4 (11.4-25.3)	7.2 ± 6.1 n = 4 (0.8-15.3)	3.2 ± 0.3 n = 1 (1.2-22.2)	7.4 ± 8.4 n = 7 (1.2-22.2)	2.3 ± 0.2 n = 4 (2.0-2.4)	6.0 ± 0.6 n = 1	

## 5.2 Geochemistry of cobalt in the intermediate and deep waters

### 5.2.1 From the Eastern Atlantic to the Alboran Sea

#### *Eastern Atlantic*

The Eastern Atlantic DCo profiles are similar in concentration and distribution to those observed at the same latitude in the Western Atlantic (Figure 13, Dulaquais et al., 2014) suggesting a similar cycling both side of the Atlantic at temperate latitudes.

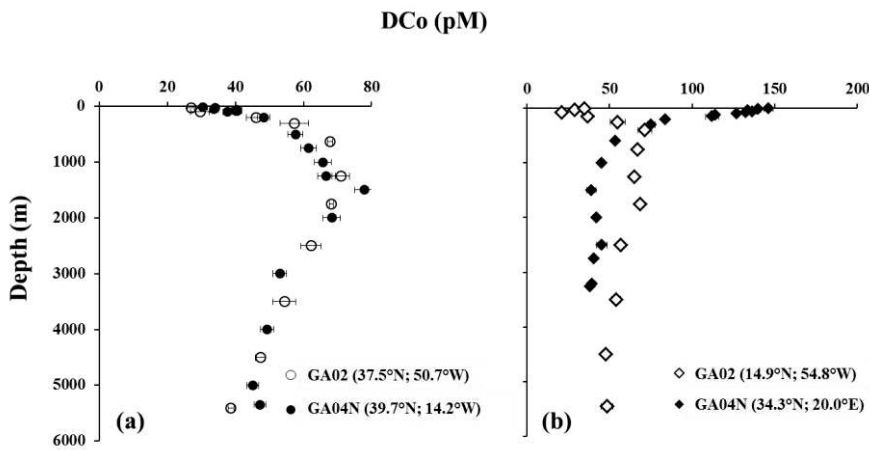


**Figure 13:** Comparison between the vertical distributions of dissolved cobalt (DCo) recorded in the Western Atlantic (section GA02; Dulaquais et al., 2014) and in the Eastern Atlantic (section GA04N, this study), **a)** at temperate latitudes, **b)** in oligotrophic domains. Note: the distributions are similar in the eastern (black dots) and western (open dots) temperate latitudes of the Atlantic Ocean, but different in the Sargasso Sea (open diamonds) and the oligotrophic areas of the Mediterranean Sea (dark diamonds).

The DCo distribution suggested biological assimilation in surface waters and remineralization in the relatively poor oxygenated intermediate waters. High DCo concentrations ( $> 75$  pM) were also recorded in the Atlantic Central Waters, probably resulting from cumulative enrichment of DCo through remineralization processes (Dulaquais et al., 2014). The MOW displayed also a typical DCo signature of  $\sim 50$  pM which increased westward, as a result of its mixing with DCo-enriched NEADW and NACW. Below 1500 meters, relatively high concentrations in the core of the young NEADW (Figure 14) likely due to the influence of the LSW (van Haken, 2001a), a water mass enriched in DCo (Dulaquais et al., 2014). Concentrations of PCo in surface ( $> 2$  pM) were slightly higher than those in the deep-waters ( $< 1$  pM), and the PCo maxima recorded in the Chl a, all suggested an assimilation of DCo by the biota at this latitude. The decreasing PCo concentrations in the deep-waters (to sub-picomolar levels) further suggested the absence of scavenging of DCo as previously suggested in the Western Atlantic (Dulaquais et al., 2014).

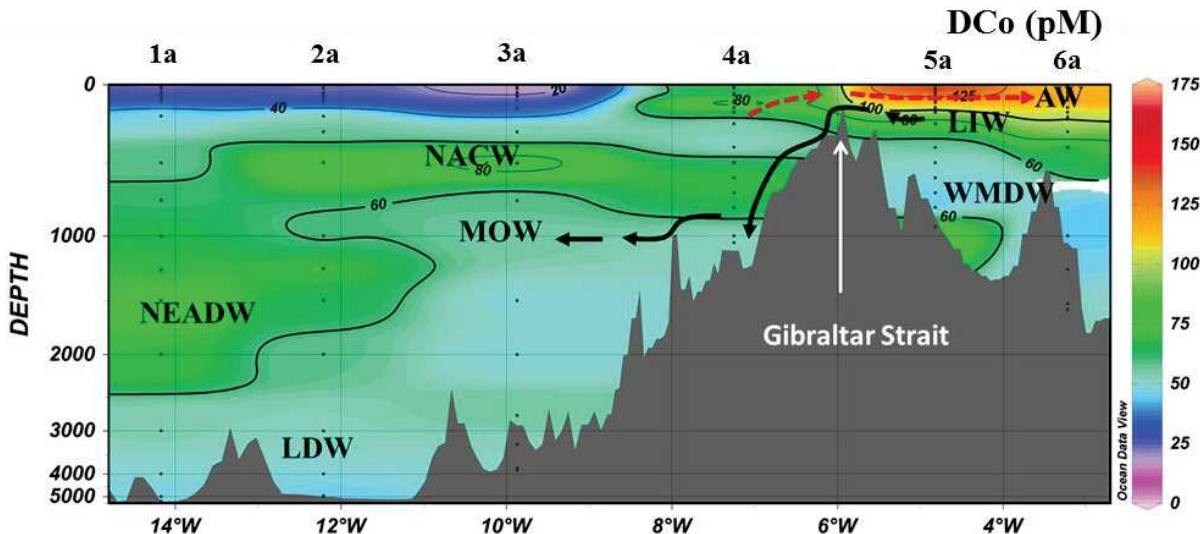


**Figure 14 :** Vertical distributions of dissolved cobalt (DCo) between Stations 1a and 6a along the GA04N-section. Sampling stations for DCo are labelled. Locations of North Atlantic Central Waters (NACW); Mediterranean Outflow waters (MOW); Lower Deep Waters (LDW); Atlantic inflowing Waters (AW); Levantine Intermediate Waters (LIW); Western Mediterranean Deep Waters (WMDW); North East Atlantic Deep Waters and Antarctic Intermediate Deep Waters (AAIW) are labeled. Arrows indicate water-flow direction at the Gibraltar Strait.

### Gibraltar Strait and Alboran Sea

On the West side of Gibraltar Strait (Station 4a), the vertical distribution of DCo was complex and impacted by the circulation of the different water masses (Figures 14, 15a). The 0-25 m layer was marked by relatively high DCo concentrations (~70 pM) potentially reflecting shelf influence. Deeper in the Chl a max (60 meters depth) DCo decreased to about 53 pM suggesting biological assimilation of DCo. The waters originated from the Gulf of Cadiz were depicted at 115 meters depth by their salinity (36.4) and temperature (16°C) signatures (Morley et al., 1997) display high DCo concentrations (> 100 pM). This DCo-enriched signal can be tracked up to Station 6a (Figure 16a), suggesting strong input of DCo to the Mediterranean Sea from the Gulf of Cadiz system like previously reported for other trace elements (Boyle et al., 1985; Van Geen et al., 1991; Elbaz Poulichet et al., 2001a). Deeper, typical DCo concentrations were recorded in the different water-masses, with a concentration of ~70 pM in the NACW and lower concentrations at the bottom in the MOW outflow (~50 pM).

Eastward of the Strait of Gibraltar (Station 5a), the DCo distribution dispatched very high concentrations in the whole upper 100m (> 140 pM, Figure 15a) compared to the Atlantic sector, with a slight depletion in surface which might result from biological

assimilation of cyanobacteria suspected to dominate the sub-surface waters (Dachs et al., 1998). These very high concentrations are related to a strong input of DCo by the shelf of the Gulf of Cadix. Additionally PCo concentrations recorded in the upper 60 meters at Station 5a (>17 pM, Figure 15b) were higher than those found in the surface Atlantic sector (3-5 pM), suggesting an input of particulate trace elements from the Gulf of Cadix. Alternatively this high PCo can also reflect a strong DCo assimilation by the cyanobacteria. In the central Alboran Sea (Station 6a), DCo and PCo surface concentrations were significantly lower in the upper 80 meters (~115 pM) than at Station 5a. This eastward surface decrease of DCo and PCo could be due to a biological assimilation and subsequent export of the biogenic material during the transportation of the AW. Indeed in this highly productive area (Bosc et al., 2004) where cyanobacteria can represent a significant portion of the biota (Dachs et al., 1998) assimilation of DCo and its export under PCo to the sediments, could be important (Table 4). On the other hand the adsorption of DCo onto MnO<sub>x</sub> surface during the lateral transport could be invoked since the high surface PMn concentrations (> 1.5 nM) recorded at Station 5a were not observed at Station 6a suggesting a removal of PMn during the eastward transport.

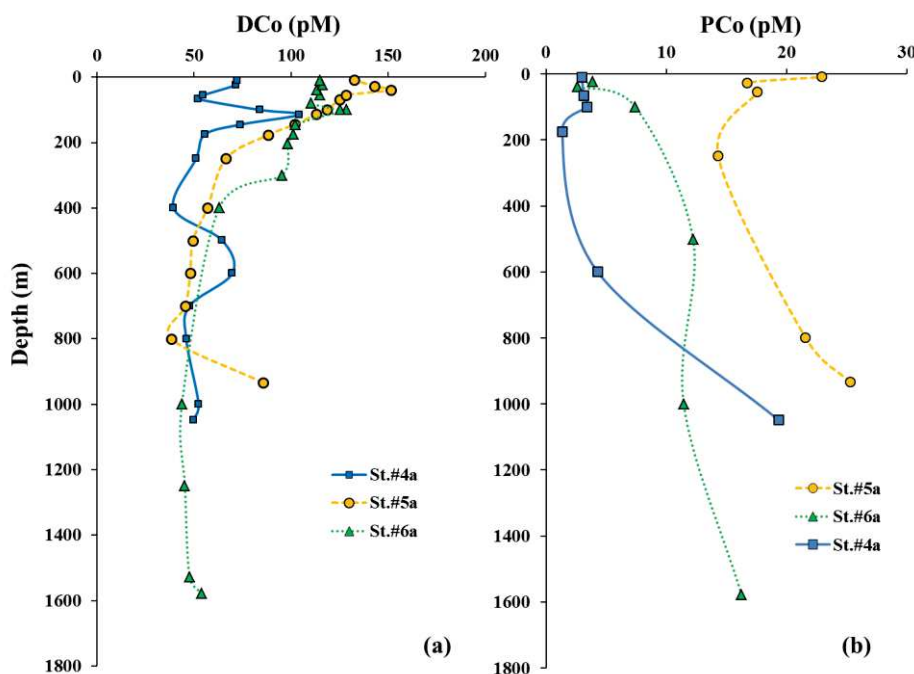


**Figure 15:** Vertical distributions of: a) dissolved cobalt (DCo), b) particulate cobalt (PCo) in the area of the Gibraltar Strait.

In the deep Alboran Sea, DCo concentrations decreased with depth, designing an apparent scavenged-like profile. Scavenging of DCo by MnO<sub>x</sub> could be invoked, since the higher PMn concentration recorded along the section were indeed observed in this area. However, the particulate Co-Mn correlation we observed in the deep Alboran Sea, was

weaker with a lower slope ( $\Delta\text{PCo}/\Delta\text{PMn} = 1.77\text{mmol/mol}$ ) when compared to the other areas of the Mediterranean Sea (Figure 17), both could suggest a restricted removal of DCo from the upper water column by MnOx in this area. Furthermore strong increases of DCo were observed at Station 5a and in a lesser extend at Station 6a close to the bottom depth (Figure 15a) together with high PCo concentrations (Figure 15b), both suggesting possible benthic remobilization of PCo and subsequent dissolution. This area being prone to high seafloor velocities due to the complex circulation and of the topography (Gascard and Richez, 1985), hence it further supports benthic resuspension of PCo. Alternatively in this productive sea, large amount of biogenic material could be buried and its degradation in the superficial sediments could have released Mn<sup>2+</sup> by diagenesis process (Price et al., 1999). Co and Mn often cycling together in sediments (Heggie and Lewis, 1984), DCo could have been also release by this diagenesis as Co<sup>2+</sup>. Shortly the sedimentary release of Mn<sup>2+</sup> could precipitate as MnOx in the water column and partially scavenged Co<sup>2+</sup> (Murray, 1975) creating the highest PMn concentration and the Co-Mn relationship observed. However a part of this Co<sup>2+</sup> could have been stabilized in solution under colloidal form, as suggested by relatively high cCo (cCo = 4.4 pM, Figure 16c) or by strong organic Co biding ligands released from by sediments (Bown et al., 2012). Both latter mechanisms prevent DCo adsorption onto MnOx and might explain the low particulate Co-Mn slope observed. Nevertheless, further investigations on the speciation of DCo and Mn are required to fully explain the distribution of Co in this area.

### 5.2.2 Mediterranean Sea

#### *Vertical distribution of cobalt*

In the Mediterranean Sea, DCo concentrations ranged from 28.8 pM in the deep Levantine basin to 353.3 pM in the sub-surface waters of the Otranto Strait (Table 2). The concentrations we measured were generally higher than those reported by Morley et al. (1997), probably due to the absence of UV digestion of their samples. The vertical distribution of DCo displayed an overall apparent scavenged like profile in the Mediterranean Sea (Figures 12b &16a), with very high concentrations in the surface layer (100 pM < DCo) that quickly decreased in the intermediate layer below the thermocline (200-500 m), creating a strong DCo stratification between the surface and deep reservoirs. Below 1000 m, a homogenous concentration of ~ 50 pM was recorded (Table 2, Figures 12b and 16a), probably resulting from a rapid mixing of the deep waters. Nevertheless, several stations were marked

by peaks of high DCo concentrations at the bottom or at intermediate depths near islands, which correlated with relatively high PCo concentrations and indicate the potential influence of benthic and margin inputs to the deep Mediterranean reservoir. Additionally, high DCo and PCo concentrations were measured at Station 9c located in the Otranto Strait (Figures 16a & 18a). The high concentrations observed at station 9c in the south Adriatic Sea can be related to the anthropogenic releases, riverine inputs (Pô River) and benthic remobilization occurring in the North Adriatic Sea and their advection to the north Ionian Sea by the Adriatic circulation (Tankéré et al., 2000).

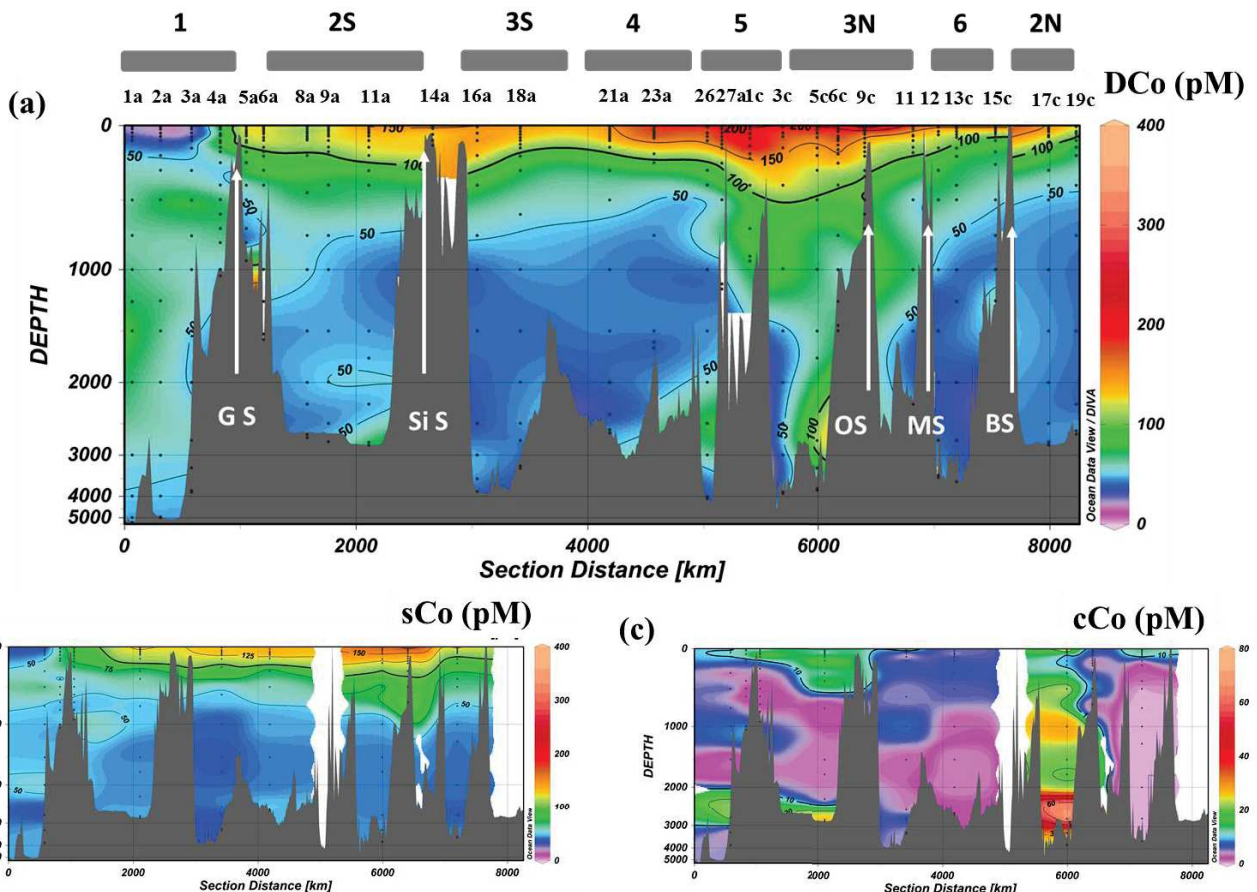


**Figure 16 :** Vertical distributions of: a) dissolved cobalt (DCo); b) Soluble cobalt (sCo); c) colloidal cobalt (cCo) along the section. Sampling stations for DCo are indicated and the different sub-basins are labeled as indicated in Figure 6.

The spatial distribution of PCo across the intermediate and deep waters of the Mediterranean Sea (Figure 18) suggests a strong influence of the benthic and margin inputs. While offshore PCo kept low (< 5 pM), the concentrations are high close to margins and in a lesser extend near the bottom depth (> 10 pM; Figure 18a). The increase of PCo concentrations recorded at the bottom depth and close to margins can be related to a benthic

remobilization. Other lithogenic tracers such as particulate manganese or aluminum also displayed relative increases above the seafloor, close to margins and at straits (Figure 18) suggesting that high slope currents can remobilize particles from shelf that could be transported along LIW circulation pathway (Figure 18). The advection of enriched-particulate trace metals can be exemplified at the bottom of the Sicily Strait (Figure 18), where the highest PCo (158.5 pM), PAI (1481 nM) and PFe (439 nM) concentrations encounter in the Mediterranean Sea were observed.

#### *Particulate Co-Mn relationship*

Significant correlations between PMn and PCo were observed in the Mediterranean Sea (Figure 18), however slopes of the PCo-PMn correlation vary and suggest different processes depending of the layers and of the sub-basins.

The high  $\Delta\text{PCo}/\Delta\text{PMn}$  slope observed in the mixed layer can represent the residual elemental Co/Mn ratio of aerosols ( $\text{RER}_{\text{Co}: \text{Mn}}$ ) after their deposition and dissolution (Equation 3). The crustal Co/Mn ratio is about 18 mmol/mol (Rudnick and Gao, 2003), but a mean Co/Mn ratio of 39 mmol/mol has been reported in Mediterranean aerosols (after Heimburger, 2010). Additionally, the fractional solubility of Co and Mn in seawater are different for Mediterranean aerosols (10% and 30-55% for Co and Mn, respectively; Guieu et al., 1997). Thus after the deposition of aerosols deposition and their partial dissolution in seawater, the Co/Mn ratio in marine lithogenic particles would range between 23 and 78 mmol/mol. In turn the PCo-PMn correlation we recorded in the mixed-layer (45 mmol/mol) could be related to the residual dust elemental Co/Mn ratio.

$$\text{RER}_{\text{Co}: \text{Mn}} = \text{Co/Mn}_{\text{dust}} * (1 - S_{\text{Co}} / 1 - S_{\text{Mn}})^{-1} \quad (3)$$

With  $S_{\text{Co}}$  and  $S_{\text{Mn}}$  the fractional solubilities of cobalt and manganese for Mediterranean aerosols set to 10% for cobalt and range between 30 and 55% for manganese (Guieu et al., 1997).

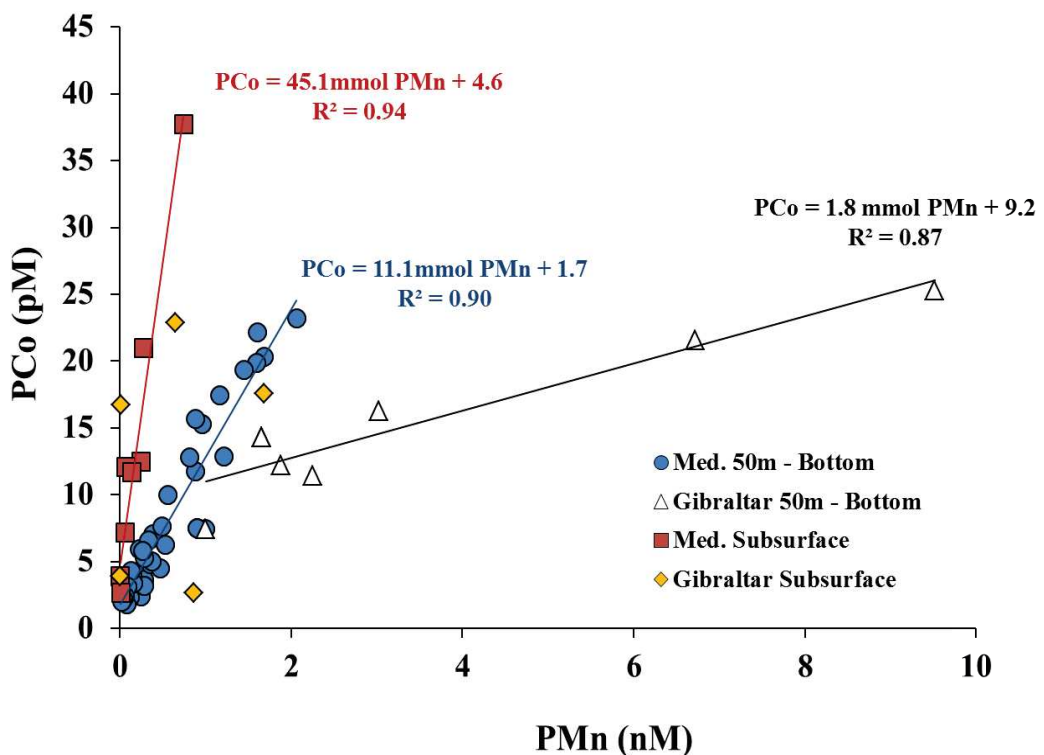


**Figure 17:** Plot of particulate cobalt concentrations (PCo) versus particulate manganese concentrations (PMn) measured in the Mediterranean Sea. The different relationships and colors stand for the area and water-layers depths.

In the bio-active layer (50-200) and the intermediate depth (200-500) the  $\Delta PCo/\Delta PMn$  slope decrease significantly to 11 mmol/mol (Figure 17), suggesting a preferential uptake of Mn by particles rather than Co. Deeper (500-4000m) PMn concentrations were extremely low (Figure 18b), with concentrations ranging from undetectable values at several depths to 0.96 nM, with a mean of  $0.32 \pm 0.33$  nM ( $n = 12$ ; excluding bottom depth). Thus, considering the low PMn concentrations, the scavenging of DCo by MnO<sub>x</sub> could be rather limited below 500 meters, by the low abundance of these species. Additionally, the PCo/PMn ratio, PCo and PMn concentrations did not increase throughout the water column, further suggesting that scavenging of DCo did not significantly occur in the deep sea. The conservative DCo deep distribution also suggested the absence of significant scavenging processes in the deep waters. In turn below the surface layer particles poorly interact with the dissolved fraction during their sink to sediments.

### Sediments and margin as sources of Co

The sediment remobilization could be a source of DCo to the Mediterranean intermediate and deep waters, as exemplified by concomitant peaks of DCo and PCo in the vertical distribution (Figure 16a, 18a). Assuming that the mean PCo concentration recorded at the bottom depths (mean PCo =  $9.7 \pm 8$  pM, n = 12, excluding the Sicily Strait station) is representative of the PCo concentration in the well mixed bottom nepheloid layer (10 meters high above the seafloor), 97 nM.m<sup>-2</sup> of PCo can be potentially subject to desorption. Since Co and Mn often bound cycle together in the superficial sediments (Heggie and Lewis, 1984), the partial release of Co from manganese oxides (MnOx) could be a source of DCo. It has been shown that after 5 h incubation of MnOx in solution, 3% of Co sorbed onto MnOx can be remobilized in solution (Backes et al., 1995). Thus, the remobilization of sediments near the seafloor or by margins might provide  $2.8 \pm 2.4$  nmol.m<sup>-2</sup>.d<sup>-1</sup> of DCo after sediments dissolution. This source of DCo could be then entrained by the fast deep circulation and feeds the entire deep water-column in DCo by mixing. However, if the DCo released is not stabilized in solution by organic complexation or under cCo the sedimentary inputs would only have local effects. Investigation on the chemical speciation of DCo would be required to further constrain the impact of the the sedimentary source.

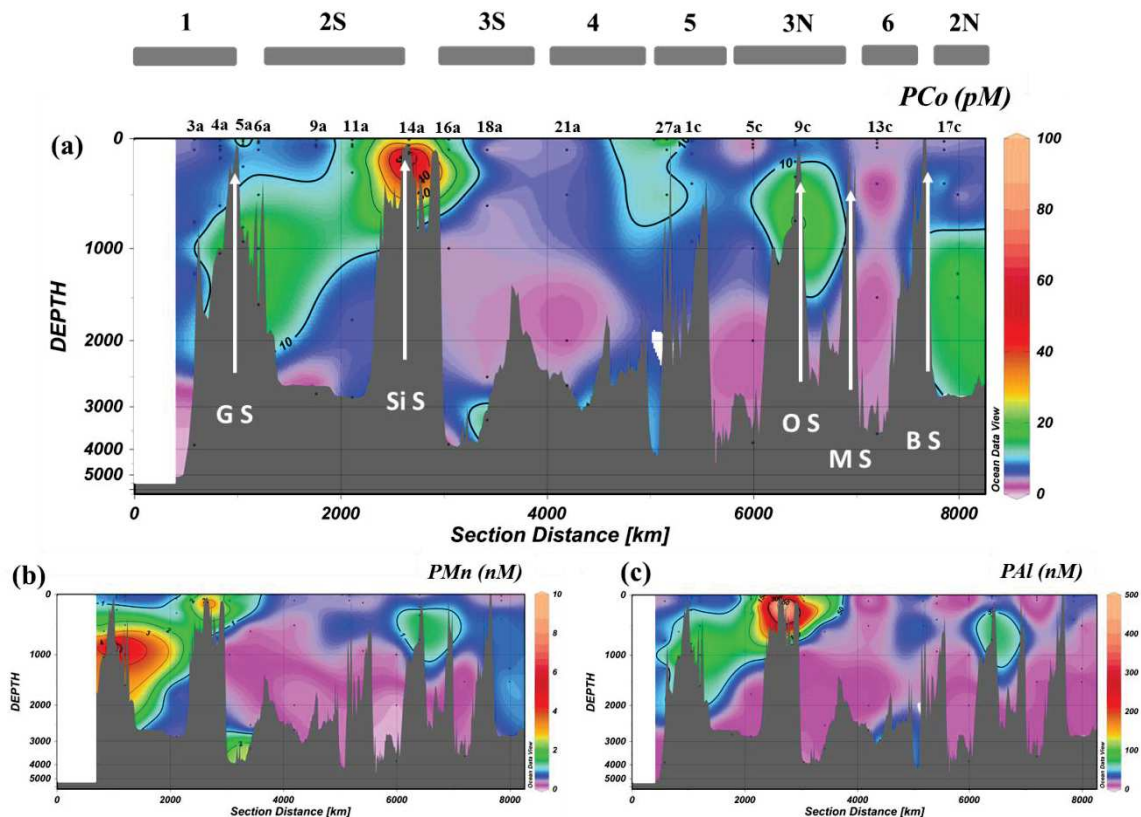


**Figure 18 :** Particulate concentrations of: a) cobalt (PCo), b) manganese (PMn), c) aluminum (PAI) measured along the section. Sampling stations for PCo are indicated and the different sub-basins are labeled as indicated in Figure 6.

### *A hydrothermal fluid contribution?*

In the North-eastern Ionian Sea (at Station 5c and in a lesser extend at Station 6c), high deep DCo concentrations were recorded compared to other sub-basins (Figure 16a, DCo > 70 pM). Particulate matter was collected at Station 5c, but it did not show enrichment in PCo in the deep waters. Thus, a benthic or margin origin can be discarded to explain the high DCo concentrations above the bottom. Additionally, the intermediate and deep northward circulation in this area plays against an input by the Adriatic waters that are enriched in DCo. The investigation of the size fractionation of DCo showed a specific signature at station 5c. Indeed, while DCo was mainly in the soluble fraction in the deep waters ( $s\text{Co} = \sim 43 \text{ pM}$ , representing about 85% of DCo, Figure 16a&b), at station 5c a significant portion of DCo was in the colloids phase ( $c\text{Co} > 50\% \text{ DCo}$ , Figure 16c). Hydrothermal fluids can release large amounts of metals under colloids phase (Sands et al., 2012), and the geological variation of cobalt concentrations in seawater has been recently linked to hydrothermal activity (Swanner et al., 2014). Thus, it is conceivable that hydrothermal fluids might be source of cCo. Despite the strong geological activity of the North Ionian Sea, there is no evidence of the presence of hydrothermal vents close to Station 5c. However, hydrothermal fluids can spread for hundred kilometers under the oceanic crust with residence times of days to years and significant part of the fluid emerged on flank ridge (Johnson et al., 2010). The Station 5c being close to the Mediterranean ridge, hydrothermal fluid input is conceivable to explain the high cCo observed in this area. Nevertheless the impact of this crustal DCo input should be restricted since this signature was mostly related to increase in cCo that can be quickly removed from the water column. Indeed, colloids are very reactive and their residence times very short (hours to day; Baskaran et al., 1992; Moran and Buesseler, 1992; Moran and Buesseler, 1993).

### *Deep convection of DCo*

In the Cretan Sea and the North Ionian Basin, high deep DCo concentrations were recorded ( $\text{DCo} > 80 \text{ pM}$ ) compared to other areas (Figure 16a). There, EMDW are formed by convection of intermediate waters (250-600 m) to the deep sea (Lascaratos et al., 1999). The intermediate waters consisting mainly of LIW and Cretan Intermediate waters were relatively enriched in DCo (Figure 17a, Table 2). The deep convection of these DCo rich waters feeds the entire Eastern basin in DCo. The Adriatic deep waters formation rate is 0.3 Sv (Roether and Schlitzer, 1991), and the Cretan Sea deep waters formation rate is estimated at about 0.9

Sv (Lascaratos et al., 1999). In the Adriatic and Cretan Seas intermediate waters displayed a mean DCo concentration of 110 pM (SD = 26, n = 14), and the mean DCo in the deep sea was estimated to 51 pM (SD = 17, n = 120), thus we estimated the input of DCo to the deep Eastern basin by convection of EMDW to  $6.1 \pm 3.2 \cdot 10^3$  mol DCo.d<sup>-1</sup> following Equation 4. Similarly, the convection rate of WMDW estimated to 2.4 Sv (Schroeder et al., 2008) could provide  $1.45 \pm 3.9 \cdot 10^3$  mol DCo.d<sup>-1</sup> considering the Western intermediate and deep waters DCo concentrations of 58 pM (SD = 9, n = 5) and 51 pM (SD = 17, n = 120), respectively.

$$F_{DCo\text{convection}} = ([DCo]_{IW} - [DCo]_{DW}) * F_{W\text{convection}} \quad (4)$$

Here [DCo]<sub>IW</sub> and [DCo]<sub>DW</sub> are the mean DCo concentrations in intermediate and deep waters ( $110 \pm 26$  pM and  $51 \pm 17$  pM respectively) F<sub>Wconvection</sub> is the convection rate of deep water masses in the eastern basin and is 1.2 Sv (CDW = 0.9 Sv; ADW = 0.3 Sv).

### *Vertical diffusion*

The sharp DCo gradient observed between the surface layer and the deep reservoir (Figures 12b & 16a) suggest potential vertical diffusion of DCo between the surface and the deep sea. Using an idealized vertical diffusivity (Figure 19) determined by Wu and Haines (1998) for the Mediterranean Sea, we calculated the vertical diffusion of DCo (F<sub>ZDiffDCO</sub>) across the different water-layers for the entire Mediterranean Sea and its sub-basins (Table 3) following Equation 5.

$$F_{ZDiffDCO} = -K_z * \partial[DCo]/\partial z \quad (5)$$

**Table 3** Vertical diffusive fluxes of DCo from the surface to the intermediate reservoirs (FzDCo at 200m), and from the intermediate to the deep reservoirs (FzDCo at 600m) in the different sub-basins of the Mediterranean Sea.

<b>Basin</b>	<b>Western Basin</b>			<b>Eastern Basin</b>		
	<i>Sub-basin</i>	<i>Alboran Sea</i>	<i>Central + Tyrrehnan Sea</i>	<i>Ionian</i>	<i>Levantine + Cretan Seas</i>	<i>Aegean</i>
F <sub>ZDiffDCO</sub> at 200m ( $10^{-3}$ nmol/m <sup>2</sup> /d)		5.1	6.2	14.1	23.0	38.2
F <sub>ZDiffDCO</sub> at 600m ( $10^{-3}$ nmol/m <sup>2</sup> /d)		0.4	0.4	0.3	0.3	0.1

The vertical diffusive fluxes of DCo were relatively homogenous within the different sub-basins at same depth (Figure 19c), allowing a general description of this process. Fluxes strongly decreased with depth (Figure 19b), with the higher diffusive inputs being estimated between the mixed-layer and the lower surface layer ( $1\text{-}5 \text{ nmol DCo.m}^{-2}\cdot\text{d}^{-1}$ ). This flux strongly decreased across the thermocline to reach values near of  $10^{-4} \text{ nmol DCo.m}^{-2}\cdot\text{d}^{-1}$  in the deep sea (Table 3). The vertical diffusive flux keeps relatively low at the interface between the surface, the intermediate layer and the deep sea, with a mean flux of  $1.3 \pm 0.7 \cdot 10^{-2} \text{ nmol DCo.m}^{-2}\cdot\text{d}^{-1}$  at  $200 \pm 50$  meters, and of  $4.7 \pm 1.1 \cdot 10^{-4} \text{ nmol DCo.m}^{-2}\cdot\text{d}^{-1}$  at  $600 \pm 100$  meters. Below 600 meters depth, the vertical input by diffusion can be considered negligible (Figure 19b&c).

Assuming DCo has a residence time equivalent to the conveyor belt ( $\sim 25$  years in the Western Basin and  $\sim 50$  years in the Eastern basin), the cumulative input of DCo by the vertical diffusion processes to the deep Mediterranean waters ( $F_{Z\text{Diff}}\text{DCo}$  at 600m) would be  $8.6 \pm 1.9 \text{ nmol DCo.m}^{-2}$  and  $4.3 \pm 0.6 \text{ DCo.m}^{-2}$  for the Eastern and Western basins, respectively. DCo concentration being of the order of  $50 \text{ nmol.m}^{-3}$  below 500 meters depth, this cumulative input could not recover the deep water DCo stock of  $50 \mu\text{mol.m}^{-2}$  (mean Mediterranean bottom depth  $\sim 1500$  meters) in the time scale of the deep Mediterranean circulation and likely accounts for less than 0.1% of the deep DCo reservoir. In turn, despite a sharp vertical DCo inverse gradient, the input by vertical diffusion to the deep reservoir keeps small, this is essentially due to the strong stratification of the Mediterranean Sea that induces low diffusivity.

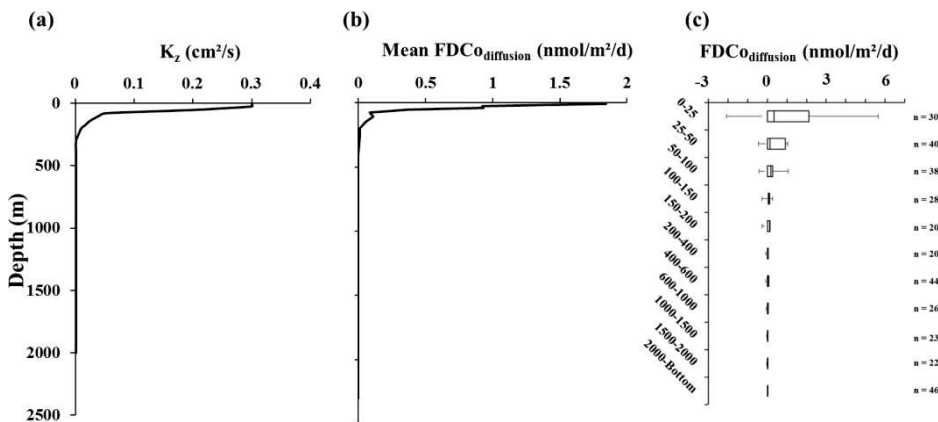


**Figure 19 :** Vertical distributions of: a) idealized diffusivity ( $K_z$ ) model after Wu and Haines (1998), b) mean vertical diffusion flux of dissolved cobalt to the deep sea, c) box-plots of vertical diffusion flux of dissolved cobalt to the deep sea estimated for the entire Mediterranean Sea (number of estimations per range of depth are indicated).

### *Absence of Co remineralization*

Interestingly, DCo and AOU did not correlate in the Mediterranean Sea on the contrary to other oceanic domains (Dulaquais et al., 2014). Indeed, no increase of DCo concentrations was observed with increasing AOU. This peculiar feature might result from a combination of the ultra-oligotrophy of this Sea and the short residence times of intermediate and deep waters. Indeed, the ultra-oligotrophy would lead to a low export of biogenic material to intermediate and deep waters, hence the export of organic material including biogenic PCo would keep relatively low and the remineralization also as exemplified by low the phosphate and nitrate concentrations in the intermediate waters. Secondly, since the residence times of deep water masses are short in the Mediterranean Sea (~25-50 years), the remineralization of organic matter can be less efficient than in other basins, as exemplified by the lower  $\Delta N/\Delta AOU$  or  $\Delta P/\Delta AOU$  observed in the Mediterranean Sea compared to the Eastern Atlantic (Figure 8). Furthermore, it has been suggested that P is preferentially remineralized compared to Co in oxygen-depleted waters (Dulaquais et al., 2014). Hence, it is conceivable that the absence of clear Co-AOU relationship in the intermediate waters of the Mediterranean Sea results from the absence of remineralization of Co because the time-scale of the remineralization of Co would be longer than the residence times of the water masses. Additionally, there was no significant correlation between PCo and AOU, further supporting that remineralization of PCo did not occur through oxygen consumption in the Mediterranean Sea.

### *Deep basin Co budgets*

As a result of the strong surface stratification of the Mediterranean Sea, the intermediate and deep reservoirs are almost isolated from the surface layer. In this condition, DCo entrained by the deep outflow at the Straits of Sicily would act as a sink of DCo for the deep Eastern basin since this outflow could not be compensated by surface inputs. However, the deep convection of DCo rich intermediate waters and the benthic and margins inputs provided by sediments resuspension and subsequent dissolution could constitute sources. Using a deep outflow of 1.2 Sv at the Sicily Strait (Béthoux; 1980) and a mean DCo concentration of  $59.2 \pm 6$  pM ( $n = 8$ ) in the 200-1300 meters layer recorded in the western part of the Eastern basin that feeds the deep outflow of the Eastern basin (Béthoux et al., 2002), we estimated a loss of  $6.1 \pm 0.7 \cdot 10^3$  molDCo.d<sup>-1</sup> in the deep Eastern basin. This

outflow is 30% higher than that estimated by Elbaz-Poulichet et al. (2001b) using non-UV DCo dataset. The loss of DCo at Sicily Strait could be recover by deep-waters convection ( $FDCo_{convection} = 6.1 \pm 3.2 \cdot 10^3 \text{ molDCo.d}^{-1}$ ). In addition considering the size of the Eastern basin ( $1.65 \cdot 10^{12} \text{ m}^2$ ), the basin scale sedimentary input of  $4.6 \pm 3.8 \cdot 10^3 \text{ molDCo.d}^{-1}$  could also participated to recover this loss.

Similarly, the Gibraltar Strait could be viewed as a sink of DCo to the Western Mediterranean Sea. Using the deep outflow of 1.6 Sv at Gibraltar Strait (Béthoux, 1980) and the mean DCo concentration in the modified LIW of Alboran Sea ( $DCo = 52.2 \pm 8.2 \text{ pM}$ ,  $n = 8$ ) that feed the Gibraltar outflow (Millot and Taupier-Letage, 2002b), we estimated a loss of  $7.2 \pm 1.2 \cdot 10^3 \text{ molDCo.d}^{-1}$  in the deep Western basin which is, as for the Sicilian budget, higher by 20% than estimated by Elbaz-Poulichet et al., (2001b). The loss at Gibraltar can be partially compensated by the input we determined at the Strait of Sicily, resulting in a net loss of  $1.1 \pm 1.4 \cdot 10^3 \text{ molDCo.d}^{-1}$ . This loss would be fully compensated by the deep convection of WMDW ( $1.45 \cdot 10^3 \text{ molDCo.d}^{-1}$ ) as well as by benthic inputs ( $2.4 \pm 1.9 \cdot 10^3 \text{ molDCo.d}^{-1}$  considering an area of  $0.85 \cdot 10^{12} \text{ m}^2$ ).

In turn, the distribution of DCo in the deep Mediterranean Sea could be mainly described by four processes: i) the fast deep circulation of the Mediterranean Sea that homogenizes the distribution of DCo below 500 meters depth, as exemplified by an apparent conservative behavior; ii) the deep convection of intermediate waters feeds the deep sea in DCo; iii) the benthic remobilization of PCo caused by relatively high slope currents, could be source of DCo to the deep sea, after dissolution of sediments; iii) the decoupling between the surface and the deep reservoirs caused by strong stratification, and the deep Mediterranean circulation, induce a loss of DCo from the Eastern basin through the Sicily Strait and from the Western basin through Gibraltar Strait; iv) the losses are compensated at basin scale by the deep convection of intermediate waters and by benthic sources. The vertical diffusion, remineralization and scavenging processes did not significantly impact the distribution of DCo in the deep Mediterranean Sea. The particulate Co originated from the surface layer (lithogenic and/or biogenic particles) would, thus, not significantly impact the deep DCo distribution in the Mediterranean Sea.

### 5.2.3 Black Sea

In the Black Sea, DCo concentrations range from 29 pM to 6.6 nM (Station 5b). It is the widest variation in concentration recorded at date in a water-column profile. In this Sea, the vertical distribution of DCo showed a specific profile similar to that previously observed (Landing and Lewis, 1991; Tankéré et al., 2001). However, the DCo concentrations we measured were higher than those reported in these previous studies. The ventilated surface waters displayed high sub-surface DCo concentrations ( $> 400$  pM), potentially due to the discharge of the Danube river (Tankéré et al., 2001) that feeds the surface waters of the Black Sea. Deeper, DCo decreased with decreasing oxygen concentrations (as low as 29 pM at Station 5b at 85 meters depth). Then, in the top of suboxic-sulfidic transition layer, DCo quickly increased to a relative maximum where extremely high concentrations (up to 6.6 nM) were depicted. Under this relative maximum, a sharp decrease of DCo was observed (Figure 20). Below 500 meters depth, DCo concentrations of 330 pM were measured. The complex distribution of DCo in the Black Sea might be mostly related to competitive geochemistry between oxydo-reductive processes and perhaps stabilization by organic ligands.

Decreases of DCo with depth and strong increases of PCo were observed in the suboxic-anoxic layer, where PCo and PMn were significantly correlating ( $R^2 > 0.99$  n = 6, Figure 21c). These observations suggested scavenging of DCo onto MnOx in the suboxic and anoxic zones. Deeper, DCo increased in the upper sulfidic waters, probably due to the release of Co caused by the reduction of MnOx. This process was further supported by the decreases of both PCo and PMn concentrations at these depths. Just below the DCo maximum the sharp DCo decrease observed with depth (Figure 20b) could be related to sorption of DCo to ferrihydrite. Indeed, in the top sulfidic layer, iron was rich (M. Rijkenberg, personal communication) and sorption of DCo to ferrihydrite could dominate scavenging (Konhauser et al., 2009; Swanner et al., 2014). This process initially proposed by Lewis and Landing (1992), was further supported by the significant correlation recorded between PCo and PFe ( $R^2 > 0.96$  n = 5; Figure 20d), and by the absence of a significant there correlation between PMn and PCo. In the deep Black Sea, DCo concentrations kept high compared to other oceanic basins, suggesting that a part of DCo can be prevented from scavenging processes. For instance, a competition ligands model has been proposed to estimate the partitioning of DCo between organically bound Co and  $\text{CoS}(\text{SH})^-$  (Landing and Lewis, 1991). According to this model, DCo would mostly occur as  $\text{CoS}(\text{SH})^-$  forms to account for the observed concentrations. However, the organic ligands represented in this model are nitrilotriacetic acid

and cysteine, which are not representative of Co organic ligands. Indeed, Co is suspected to be complexed by a corrin function in marine system (e.g., vitamin B12 and its derived products,) that could bind more strongly Co ( $\log K_{CoL} > 15$ ; Saito and Moffett, 2001; Bown et al., 2012) than cysteine ( $\log K_{CoCys} = 8.95$ , Landing and Lewis, 1991) and nitrilotriacetic ( $\log K_{CoNTA} = 10.53$ , Landing and Lewis, 1991). In turn, strong organic complexes of Co may have partially prevent the formation of  $CoS(SH)^-$  species in the deep Black Sea. Further investigations on the organic speciation of Co would be required to better assess the geochemical behavior of cobalt in this Sea.

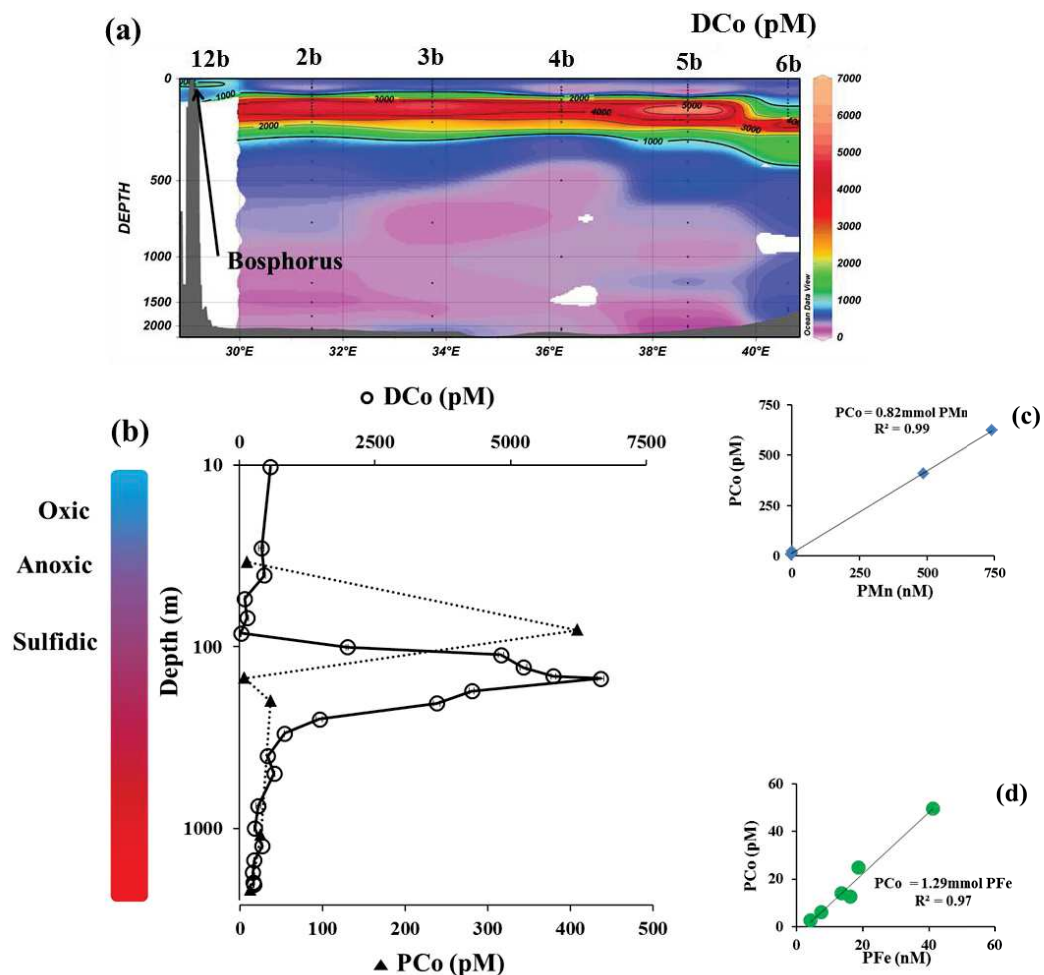


**Figure 20:** a) Vertical distribution of dissolved cobalt (DCo) in the Black Sea. Bosphorus location and sampling stations for DCo are indicated; b) vertical distribution of DCo and particulate cobalt (PCo) in the open Black Sea (at Station 5b). States of oxygenation of the water-column are indicated; c) relationship between PCo and particulate manganese (PMn) in the suboxic layer, d) relationship between PCo and particulate iron (PFe) in the sulfidic waters.

## 5.3 Surface spatial distribution of DCo

### 5.3.1 From the Eastern Atlantic to Gibraltar strait

The surface (0-200 m) distribution of DCo in the temperate surface Atlantic displayed relatively sub-surface low values (< 30 pM) similar to those recorded in the Western Atlantic at the same latitudes (Figure 13a, Dulaquais et al., 2014), which increased with depth in a nutrient like behavior. A significant correlation between DCo and P was observed in the surface waters at the most western side of the section (Stations 1a-3a) with a Co/P ratio of 77 µM/M ( $n = 18$ ,  $R^2 > 0.9$ ), suggesting similar surface cycles. A strong eastward increase of DCo was recorded, with sub-surface DCo concentrations reaching values > 70 pM (at Station 4a) and up to > 100 pM (at Station 5a). This eastward enrichment was likely due to shelf, margin and riverine inputs from the Gulf of Cadix, as observed for several other trace elements (Boyle et al., 1985; van Geen et al., 1997, Elbaz-Poulichet et al., 2001a). This high DCo signature was then entrained by the inflows of AW into the Mediterranean Sea, as described here above.

#### *DCo inputs at Gibraltar Strait*

As far as we know, the input of DCo to the Mediterranean Sea at Gibraltar Strait has been previously estimated only in one study (Elbaz-Poulichet et al., 2001b). This estimation was based on DCo concentrations determined in non-UV digested samples (Morley et al., 1997), probably leading to underestimations of the DCo concentrations and its inputs at Gibraltar. As we do not sample at the entrance of the strait, Here, we attempt to re-estimate these inputs, but since the entrance of the Strait was not sampled, the concentrations we reported in the different surface water-masses, especially in the GCW, might not be fully representative of the inflowing DCo concentrations. Thus, we assumed that the difference of DCo in the inflow waters between Stations 3a and 5a ( $\Delta\text{DCo}$ ) was representative of the surface enrichment by the different components of the inflowing AW (NASW, NACW, and GCW). The mean surface DCo concentrations recorded at Stations 3a being respectively of  $32.6 \pm 5.6$  and  $125.8 \pm 17.0$  pM, the resulting  $\Delta\text{DCo}$ , and thus the input of DCo to the Mediterranean Sea was estimated to  $93.2 \pm 17.9$  pM. Combining  $\Delta\text{DCo}$  with the water flux determined by Béthoux (1980), the net input of DCo to the Mediterranean Sea we estimated was about  $13.5 \pm 2.6 \cdot 10^3$  mol DCo.d<sup>-1</sup>. This estimation is two times higher than that of Elbaz-Poulichet et al. (2001b).

### 5.3.2 Mediterranean Sea

Previous studies suggested that DCo displays a nutrient-like P distribution in the oligotrophic seawaters (Saito and Moffett, 2002; Noble et al., 2008, 2012; Bown et al., 2011; Dulaquais et al., 2014b). This behavior has been related to the strong assimilation of DCo by cyanobacteria (Bown et al., 2011; Dulaquais et al., 2014b), caused by their absolute requirement for this element (Saito et al., 2002). Indeed, cyanobacteria represent a significant proportion of the phytoplankton assemblage in these domains (Agusti, 2004), just like in oligotrophic Mediterranean seawaters (Moutin and Rimbault, 2002; Casotti et al., 2003; Dash et al., 2004).

There, the surface DCo concentrations ( $> 100$  pM up to  $> 300$  pM in the Eastern Mediterranean Basin) were, however, significantly higher than those measured in the other oceanic oligotrophic areas (10-30 pM; Saito and Moffett, 2002; Noble et al., 2008; Bown et al., 2011; Dulaquais et al., 2014) (Figure 13b). Moreover, an overall scavenged-like profile was observed unlike the nutrient like-P DCo distribution reported in the oligotrophic oceans, and there was no clear DCo-P relationship in the surface waters of the Mediterranean Sea.

The sub-surface DCo concentrations (at 10 m depth) in the Mediterranean Sea ranged from 111.6 pM (at Station 8a off shore Algeria) to 353.3 pM (at Station 9c at the Otranto Strait). The spatial DCo distribution in sub-surface waters suggested the influences of the Black and Adriatic Seas (Figure 21a). Both Black sea surface waters (BSW) and Adriatic sea surface waters (ASW) dispatching DCo concentrations higher than 400 pM. Furthermore, the strong input of DCo provided by the advection of AW that has been enriched in metals in the Gulf of Cadix (Boyle et al., 1985; van Geen et al., 1997, Elbaz-Poulichet et al., 2001a) was still depicted in the Alboran Sea (Figure 16). These DCo-enriched surface waters are entrained across the Mediterranean Basins by the rapid surface circulation of AW.

In the Western Mediterranean basin, the DCo concentrations increased eastward with ageing of the AW (DCo from  $\sim 110$  pM in the Alboran Sea to  $\sim 160$  pM in the Tyrrhenian Sea) and decreased during the way back of the AW (from  $\sim 160$  pM in the Tyrrhenian Sea to  $\sim 130$  pM central Western Basin). In the Eastern Basin, sub-surface DCo concentrations increased eastward from the central Ionian Sea to the Levantine basin (from 140 pM to 180 pM). Considering the fast ventilation of the surface layer in this basin ( $\sim 20$  years), the absence of an homogenous DCo concentrations in the entire basin strongly suggest that biogeochemical processes like atmospheric inputs or biological assimilation impact the surface waters in the

time-scale of the surface ventilation. Thereafter, we will discuss the potential impact of these processes on the DCo distribution in the surface waters.

#### *The concept of $\Delta\text{DCo}_{\text{surface}}$*

With the aim to determine if an area is a sink or a source of DCo due to biogeochemical processes, we defined the concept of  $\Delta\text{DCo}_{\text{surface}}$ . For each station, the surface DCo was integrated over the top-200 m, representing the surface  $\text{DCo}_{\text{surface}}$ . Then, considering a simplistic AW circulation in the Mediterranean Sea (Figure 3a), the  $\Delta\text{DCo}_{\text{surface}}$  could be defined following equation 6

$$\Delta\text{DCo}_{\text{surface}} = \text{Downstream AW DCo}_{\text{surface}} - \text{Upstream AW DCo}_{\text{surface}} \quad (6)$$

In this condition if  $\Delta\text{DCo}_{\text{surface}} > 0$  the area between the two nearby stations is a source of DCo, and if  $\Delta\text{DCo}_{\text{surface}} < 0$  the area is a sink of DCo. Figure 21 shows the spatial distribution of (b)  $\text{DCo}_{\text{surface}}$  and (c)  $\Delta\text{DCo}_{\text{surface}}$  and allows identifying key areas of the DCo biogeochemical cycle of the Mediterranean Sea.

The spatial distribution of  $\text{DCo}_{\text{surface}}$  showed the same gradients than those observed for surface DCo (Figure 21b), with an eastward increase and lower surface DCo inventories in the Western Basin compared to the Eastern Basin. The higher  $\text{DCo}_{\text{surface}}$  were recorded in the Cretan Sea and close to Greek Islands, probably reflecting strong margin inputs. The influences of ASW and BSW on DCo surface inventories were not as marked as for subsurface DCo concentrations. Their low densities and their small contribution to the Eastern Mediterranean water budget both have probably limited their influence to the mixed layer.

The  $\Delta\text{DCo}_{\text{surface}}$  varied geographically (Figure 21c), and it suggested that the Gibraltar Strait, the center of the Western basin and the most eastern side of the Mediterranean Sea could act as sources of DCo. These two latter areas are prone to intensive dust events (Guerzoni et al., 1999; Guieu et al., 2010), hence the atmospheric deposition of Co could have led to these positive anomalies. In addition to this source, margins inputs near islands and low biological uptake of DCo due to ultra-oligotrophy (Bosc et al., 2004) could also contributed to the accumulation of DCo (e.g., positive  $\Delta\text{DCo}_{\text{surface}}$ ) in the Levantine Basin. By contrast, the negative anomalies estimated in the Alboran, south Adriatic, Aegean sea, and in the coastal Western Basin (Figure 21c; Bosc et al., 2004) suggested that those areas could act as sinks of

DCo, probably due to intensified biological assimilation of DCo in these productive waters (Figure 7, Bosc et al., 2004).

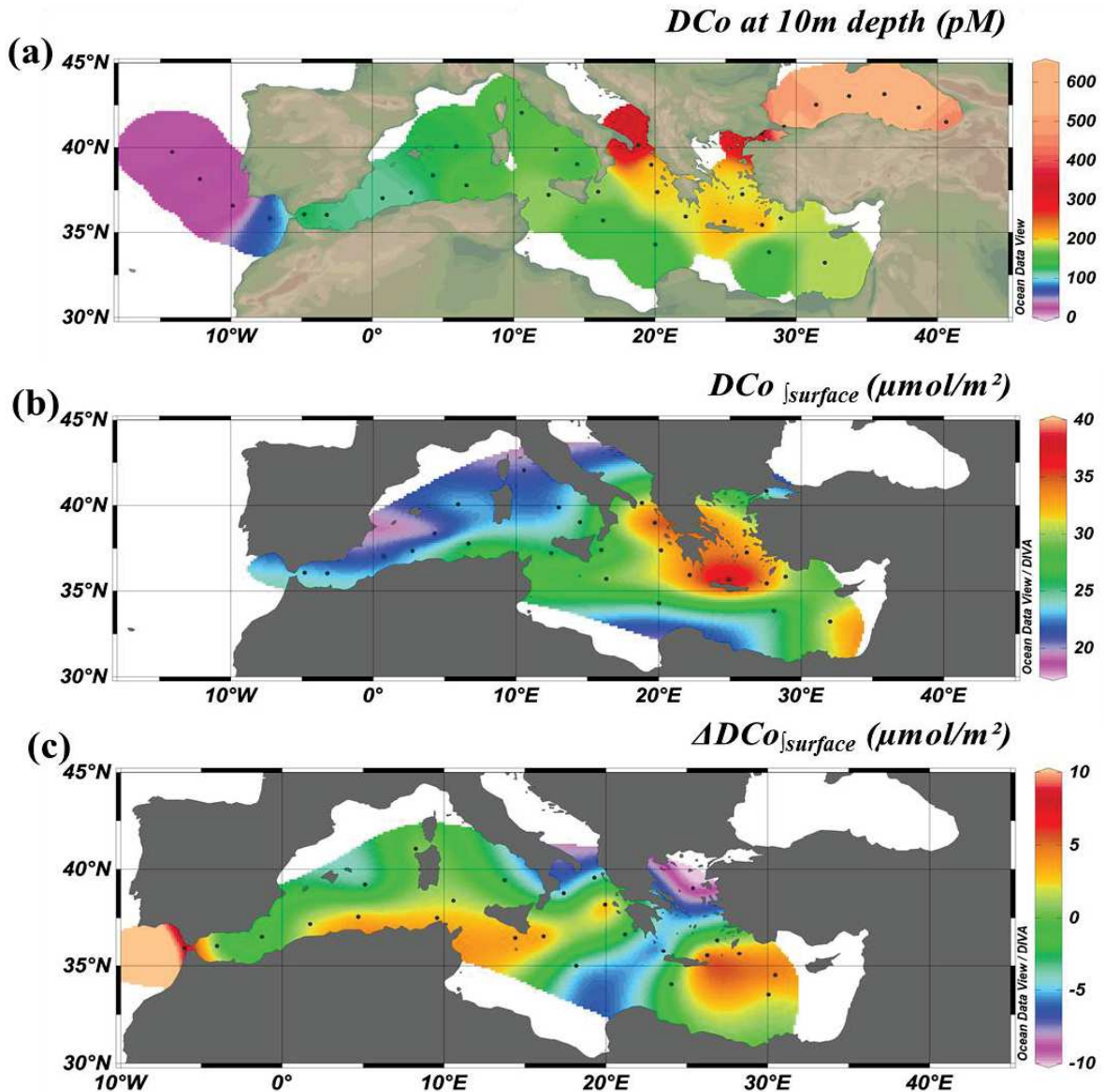


**Figure 21** : Spatial distribution of: **a)** dissolved cobalt (DCo) at 10 meters depth along the GA04N-section, **b)** integrated dissolved cobalt concentration ( $\text{DCo}_{\text{surface}}$ ), **c)** integrated dissolved cobalt anomaly ( $\Delta\text{DCo}_{\text{surface}}$ , see text for calculation), in the top-200 meters in the Mediterranean Sea.

### *Co-P biogenic ratio*

The particulate cobalt to particulate phosphorus ratios (Co/P) determined in the top-100 m at 17 stations in the Mediterranean Sea were used as a proxy of the biological utilization of DCo relative to phosphorus (Co/P; Table 1). The ratios varied from 70  $\mu\text{mol/mol}$  in the Sicily Strait to 700  $\mu\text{mol/mol}$  in the Levantine basin, with a mean ratio of  $277 \pm 200 \mu\text{mol/mol}$  ( $n = 37$ ), which is higher than the averaged ratio reported for culture experiments including a wide range of phytoplankton species (e.g.; Co/P =  $190 \pm 32 \mu\text{mol/mol}$ ; Ho et al., 2003). The high biodiversity in the different sub-basins of the Mediterranean Sea (Ignatiades et al., 2009) may account for this wide range of Co/P ratios.

In the Alboran Sea and the central Western Basin, Co/P ratios were high (~240  $\mu\text{mol.mol}^{-1}$ ), and similar to the Co/P cellular quota reported for cyanobacteria (~260  $\mu\text{mol/mol}$ ; Tovar-Sanchez et al., 2006). It suggested an important biological utilization of DCo by cyanobacteria in these areas.

Differently, low Co/P ratios (70-130  $\mu\text{mol/mol}$ ) were observed in the South-western Mediterranean Sea where diatoms probably represented a significant proportion of the phytoplankton assemblage. These ratios were also similar to the Co/P cellular quota of diatoms (~100  $\mu\text{mol/mol}$ ; Ho et al., 2003), reflecting their low requirement for this element.

In the Tyrrhenian Sea, dinoflagellates (nano-plankton) and cyanobacteria (pico-plankton) may have co-occurred. There, the Co/P ratios (~165  $\mu\text{mol/mol}$  in the central Western basin,  $n = 2$ ) ranged between the Co/P cellular quotas of dinoflagellates (~100  $\mu\text{mol/mol}$ ; Ho et al., 2003) and of cyanobacteria (~260  $\mu\text{mol/mol}$ ; Tovar-Sánchez et al., 2006).

The Ionian Sea was marked by Co/P ratios of about 250  $\mu\text{mol.mol}^{-1}$  ( $n = 7$ ), similar to the Co/P cellular ratio of cyanobacteria (Tovar-Sánchez et al., 2006) that were abundant in these oligotrophic waters (Rabitti et al., 1994; Casotti et al., 2003). Interestingly, low Co/P ratio (~80  $\mu\text{mol/mol}$ ) was observed in the South-eastern Ionian Sea (Station 18a) where diazotrophs were probably present. Those species can have relatively low Co/P cellular ratio (~31  $\mu\text{mol/mol}$ ; Tovar-Sánchez et al., 2006).

Extremely high Co/P ratios (> 500  $\mu\text{mol/mol}$ ) were recorded in the Aegean Sea (data not showed) and in the Levantine basin (Table 1), probably caused by nano-molar concentrations of P and extremely high surface DCo concentrations (> 200 pM) that would have promoted the biological uptake of DCo compared to P, and increased the cellular Co/P quotas as previously suggested in these conditions (Ji and Sherrell, 2008). Alternatively

enhanced dust deposition would have increase PCo concentration in this area, resulting in an apparent high Co/P ratio.

#### *Biological assimilation and export of Co*

The biological assimilation is a sink of DCo, but the regeneration of PCo in surface waters can significantly decrease the impact of this sink (Dulaquais et al., 2014b). In the oligotrophic Western Atlantic, it has been suggested that about 80% of the assimilated Co can be regenerated in surface waters (Dulaquais et al., 2014b). Here below, we estimated the uptake flux of DCo by using our PCo/POC measurements, and the primary production published in the literature for the different sub-basins of the Mediterranean Sea.

Assuming that the PCo/POC ratios recorded within the Chl a maxima in the different areas (Table 4) represented the cellular PCo/POC ratios of the biota in the surface waters, the biological uptake rate of DCo ( $FDCo_{uptake}$ ) can be determined following Equation 7. Published primary production rates (PPR) were used in the Western and Eastern Basins (Moutin and Rimbault, 2002) and in the Alboran Sea (Bosc et al., 2004).

$$FDCo_{uptake} = PCo/POC_{biogenic} * PPR \quad (7)$$

The higher DCo uptake flux ( $\sim 133 \text{ nmol.m}^{-2}.\text{d}^{-1}$ ) was estimated in the Alboran Sea (Table 4), consistent with the high productivity of this area and the presence of cyanobacteria which require DCo to grow (Saito et al., 2002). Much lower assimilation fluxes were estimated in the central Western basin and South Tyrrhenian Sea (36 and  $39 \text{ nmol.m}^{-2}.\text{d}^{-1}$ , respectively). In these areas, the biomass was relatively high (Figure 7), but the cyanobacteria may accounted only for a very small portion of the phytoplankton assemblage as reflected by the relatively low Co/P ratio we observed ( $160 \mu\text{M/M}$ ). The lowest DCo uptake flux was estimated in the South Ionian Sea ( $21-31 \text{ nmol.m}^{-2}.\text{d}^{-1}$ ), in line with these ultra-oligotrophic waters in which the productivity was limited by the nano-molar concentrations of macro-nutrients keeping the assimilation of DCo low. Interestingly, relatively high  $FDCo_{uptake}$  were estimated in the Levantine Basin and the Aegean Sea ( $\sim 70$  and  $100 \text{ nmol.m}^{-2}.\text{d}^{-1}$ , respectively), probably caused by the high PCo/POC ratios recorded in the Chl a maximum depth of these areas ( $3.86 \mu\text{mol/mol}$  and  $3.11 \mu\text{mol/mol}$ , respectively).

Recently, it has been evidenced that export of trace elements, including Co, is mainly driven by the settling of biogenic carbon production in the Mediterranean Sea, rather than atmospheric deposition (Heimburger, 2010; Heimburger et al., 2014). In that way, the export of Co from the surface waters could be estimated using PCo/POC ratios combined with the carbon export fluxes, following Equation 8. To estimate the latter fluxes, the PCo/POC ratios measured just below the Chl a maxima ( $\text{PCo}/\text{POC}_{10\% \text{Chla}}$ ; Table 4) were used, since the export of biogenic particles can mainly occur below the Chl a maxima (Buesseler, 1998). The export fluxes were then determined following Equation 9, using the primary production rates combined with local biological pumps efficiencies (BPE, Table 4) published for the Western and Eastern Basins (Moutin and Rimbault, 2002; Sanchez-Vidal et al., 2005).

$$\text{FPCo}_{\text{export}} = \text{PCo}/\text{POC}_{10\% \text{Chla}} * \text{POC export flux} \quad (8)$$

$$\text{POC export flux} = \text{PPR} * \text{BPE} \quad (9)$$

Most of the Mediterranean Sea displayed low export fluxes of Co ( $\leq 5 \text{ nmol.m}^{-2}.\text{d}^{-1}$ ; Table 4), suggesting that most of the assimilated DCo was regenerated in the surface waters. This result is in line with high proportion of regenerated production in this semi-enclosed Sea (up to 90% of primary production, Moutin and Rimbault, 2002). However, the Alboran Sea and the South Western Basin were marked by relatively more intense Co export fluxes ( $> 12 \text{ nmol.m}^{-2}.\text{d}^{-1}$ ). In these areas,  $\text{PCo}/\text{POC}_{10\% \text{Chla}}$  ratios were significantly higher than  $\text{PCo}/\text{POC}_{\text{biogenic}}$  ratios, causing the high export fluxes estimated. These high  $\text{PCo}/\text{POC}_{10\% \text{Chla}}$  ratios could be related to aggregation of lithogenic PCo onto biogenic settling particles, as observed for other trace elements in the mesotrophic North-western Mediterranean Sea (Heimburger et al., 2014).

**Table 4** Biological Co-uptake fluxes (**Fuptake**), and Co export fluxes on settling particles (**FCo export**) in the different sub-basins of the Mediterranean Sea (see text for the explanation of the other terms).

Basin	sub-basin	Station	longitude (°W)	latitude (°N)	PPR (mg/m <sup>2</sup> /d)	Co/C Chla max (μmol/mol)	Fuptake (nmol/m <sup>2</sup> /d)	Co/C 10% Chla (μmol:mol)	CP E (%)	FCo export (nmol/m <sup>2</sup> /d)
Western basin	Alboran Sea	5a	-4.82	36.06	52.51	2.53	132.85	6.67	4.13	14.47
	Central Western basin	11a	6.66	37.77	43.14	1.53	66.00	8.26	4.26	15.18
	Central Western basin	17c	5.95	40.07	39.33	1.00	39.33	2.24	5.80	5.11
	Tyrrenian Sea	13c	13.01	39.88	28.79	1.26	36.28	2.20	1.53	0.97
Eastern Basin	Ionian Sea	16a	16.33	35.71	27.38	1.12	30.66	1.12	4.05	1.24
	Ionian Sea	18a	20.02	34.28	21.38	1.00	21.38	1.00	1.76	0.38
	Levantine Basin	21a	28.08	33.84	18.00	3.86	69.48	3.86	4.35	3.02

### 5.3.3 Black Sea

High surface concentrations of DCo were recorded in the Black Sea (> 400 pM). Despite the strong influence of Danube River in this Sea as denoted by the low salinities (< 20), these high concentrations could not be directly related to the input of DCo by this river. Indeed, DCo concentrations reported in the fresh Danube waters (DCo = 266 pM; Guieu et al., 1998) are lower than those we recorded in surface waters of the Black Sea (> 400 pM). Alternatively, these high DCo concentrations may result from the discharge of PCo by Turkish rivers (Yiğiterhanand et al., 2011) and their dissolution along the salinity gradient (Gieu et al., 1998) or in the surface coastal Sea. Additionally the regeneration of DCo after its assimilation could lead to its accumulation in this basin.

## 5.4 Atmospheric deposition of cobalt in the Mediterranean Sea

### Dust deposition inferred by particulate aluminum surface concentration

We estimated the dust deposition of cobalt to the surface Mediterranean Sea by developing a new model, DIPA (Dust deposition Inferred by Particulate Aluminum seawater concentrations), based on the particulate aluminum concentrations (PAI) measured in the subsurface samples along the section and used as a proxy of the near real time dust deposition. For these estimates, we assumed,: i) an atmospheric origin of PAI in the top-10 m, ii) an homogeneity of PAI concentrations in the well-mixed top-10 m; iii) an absence of scavenging at these depths, iv) a residence time of PAI ( $\tau_{PAI}$ ) driven by the sinking velocity of dust.  $\tau_{PAI}$  was set to 2 days in the top-10 m.

Thus, in this model the integrated PAI in the top-10 meters represented the accumulation of two days of atmospheric input after dissolution of dust. The dust deposition was then estimated according to Equation 10. These assumptions are rather realistic, since PAI is known to have a short surface residence time in areas receiving high dust inputs (5-25 days in the upper 100 m; Dammshäuser et al., 2013), and since the scavenging of Al can be mainly driven by adsorption onto sinking biogenic particles (Moran and Moore, 1988; Middag et al., 2009) that would occur below the top-10 m and beneath the chlorophyll maxima (Damhausser et al., 2013).

$$\text{Dust Deposition} = \text{PAI}_{\int z} * M_{Al} * z * [(1-S_{Al}) * A_{bAl} * \tau_{PAIz}]^{-1} \quad (10)$$

Here  $\text{PAI}_{\int z}$  is the integrated particulate aluminium on a water column of  $z$  meters,  $M_{Al}$  is the molar mass of aluminum (27 g/mol),  $z$  is set to 10 meters,  $S_{Al}$  is the solubility of Al (set to 3%),  $A_{bAl}$  is the crustal abundance of Al (set to 7.7%, Rudnick and Gao, 2003),  $\tau_{PAIz}$  is the residence time of PAI in the water column of  $z$  meters ( $\tau_{PAI} = 2$  days when  $z = 10$  m).

Station 5a was excluded for our estimations because of the strong particulate inputs from the Gulf of Cadix that were not related to atmospheric deposition at this station. The dust deposition we estimated varied between < 10 and up to 156 mg.m<sup>-2</sup>.d<sup>-1</sup>, with a mean flux of 60 ± 50 mg.m<sup>-2</sup>.d<sup>-1</sup> (n = 16). The Eastern Atlantic received lower dust input (< 20 mg.m<sup>-2</sup>.d<sup>-1</sup>) than the Mediterranean Sea (Figure 22). High dust inputs (> 100 mg.m<sup>-2</sup>.d<sup>-1</sup>) were estimated offshore Algeria and in the Eastern Basin. The model clearly showed the influence of the Sahara over the Mediterranean Sea, since the South Mediterranean Sea received higher dust input than its Northern side, and the Eastern Atlantic received lower dust deposition than the Mediterranean Sea. Our estimations of the dust deposition were quantitatively and geographically in good agreement with previous estimations of dust delivery in the different basins of the Mediterranean Sea (Figure 22; Guieu et al., 1997, 2002 2010; Guerzoni et al., 1999), supporting the use of seawater PAI concentrations as a good tracer for dust deposition estimation. However, the sinking velocity of particles that drives the residence time of PAI can vary, depending on the size-distributions of the aerosols, the stratification and trophic conditions. Improvements are required to better constrain this parameter in the model.

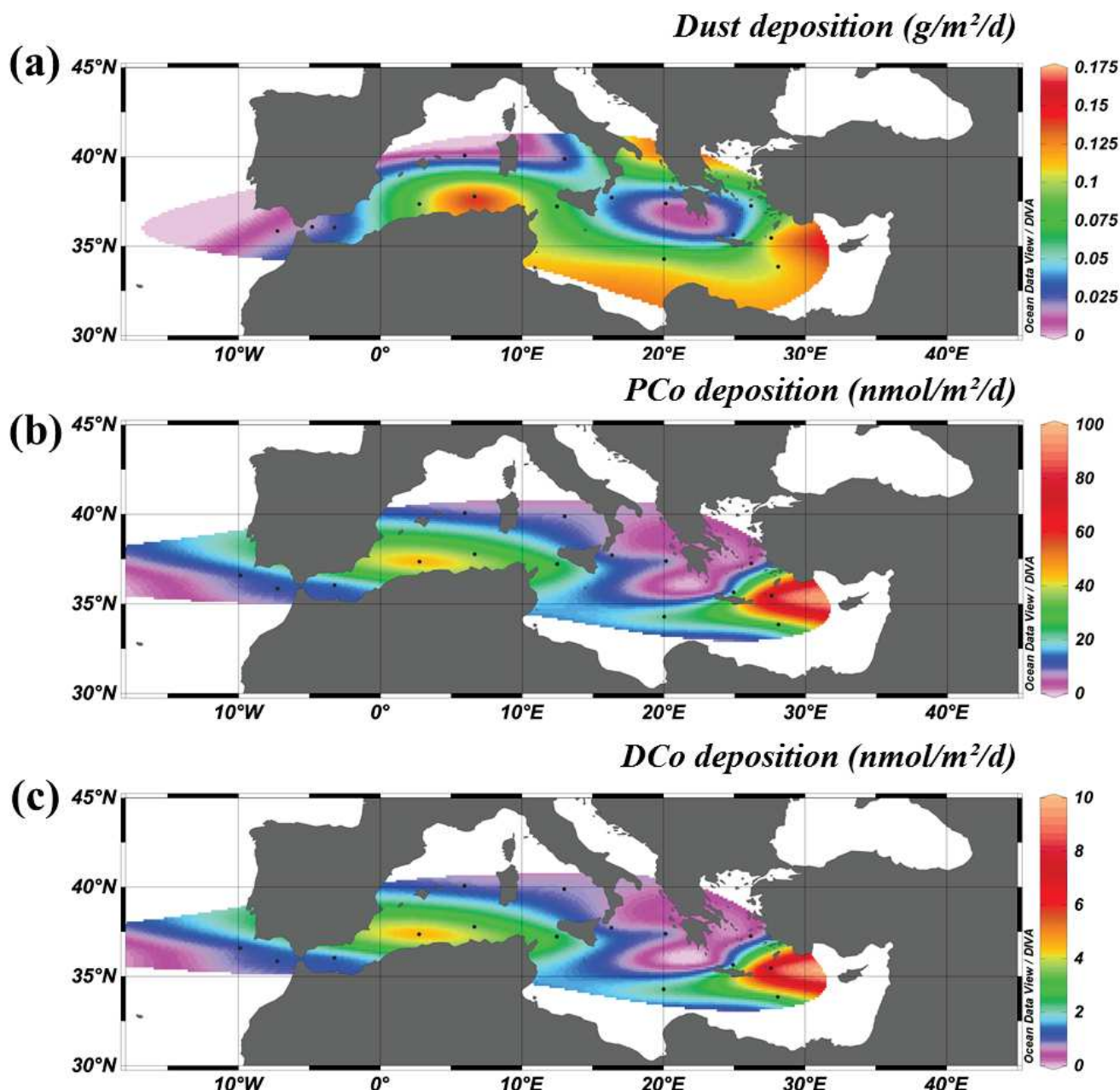


**Figure 22 :** Spatial distributions of: **a)** dust deposition, **b)** particulate cobalt deposition (PCo deposition) and **c)** dissolved cobalt deposition (DCo deposition) fluxes to the surface waters along the GA04N-section. Estimations are based on the DIPA model (see text for the explanation). Note: there is no estimation for those fluxes in the Black Sea.

### *Atmospheric deposition of cobalt*

Since Co is a micronutrient, PCo can be of biogenic origin in the subsurface waters, in addition to the atmospheric inputs. Thus, the biogenic and lithogenic proportions of PCo were estimated in the subsurface Mediterranean waters. To this end, the particulate phosphorus concentrations (PP) measured along the section were used to discriminate between biogenic and lithogenic origins of the particles, following Equations 11 and 12. Assuming the particulate Co/P ratios measured in the Chl a maxima ( $(PCo / PP)_{Chl\ a\ max}$ ) represented the biogenic ratios in subsurface waters, the biogenic PCo, and then the atmospheric PCo, were estimated following Equations 13 and 14. Finally, the atmospheric fluxes of PCo and DCo were calculated following Equations 15 and 16, respectively, by assuming the atmospheric deposition was the only source of lithogenic PCo.

$$PP_{lithogenic\int_z} = \text{Dust deposition} * Ab_p * EF_p * (1-S_p) * \tau_{PP} * M_p^{-1} \quad (11)$$

$$PP_{biogenic} = PP_{\int_z} - PP_{lithogenic\int_z} \quad (12)$$

$$PCo_{Biogenic} = PP_{biogenic} * (PCo / PP)_{Chl\ a\ max} \quad (13)$$

$$PCo_{lithogenic} = PCo_{\int_z} - PCo_{Biogenic} \quad (14)$$

$$PCo\ deposition = PCo_{lithogenic} * [\tau_{PCo_z} * (1-S_{Co})]^{-1} \quad (15)$$

$$DCo\ deposition = PCo\ deposition * S_{Co} \quad (16)$$

Here,  $Ab_p$  is the crustal abundance of phosphorus (set to 0.075%; Rudnick and Gao, 2003),  $EF_p$  is the enrichment factor of phosphorus in Mediterranean aerosols (set to 3; Ternon et al., 2011),  $S_p$  is the aerosol fractional solubility of P in seawater (set to 35%; Ternon et al., 2011),  $M_p$  is the molar mass of P (16 g.mol<sup>-1</sup>),  $PP_{\int_z}$  and  $PCo_{\int_z}$  are the integrated PP and PCo on a water-column of z meters, z is set to 10 meters,  $S_{Co}$  is the aerosol fractional solubility of Co in seawater (set to 10%; Guieu et al., 1997), and  $\tau_{PCo_z}$  and  $\tau_{PP}$  are the residence time of PCo and PP in the water column of z meters ( $\tau_{PCo} = \tau_{PP} = 2$  days with z= 10 m).

The atmospheric inputs of PCo ranged between 1.2 nmol.m<sup>-2</sup>.d<sup>-1</sup> in the Aegean Sea and 93.0 nmol.m<sup>-2</sup>.d<sup>-1</sup> in the Levantine Basin, with a mean of  $20.8 \pm 23.0$  nmol.m<sup>-2</sup>.d<sup>-1</sup> (Figure 22, Table 5). The atmospheric inputs of DCo after 10% dissolution of dust in the subsurface waters (Guieu et al., 1997) co-varied with those of PCo (Figure 22), accounting for 10% of the atmospheric PCo inputs. The eastern side of the Mediterranean Sea and the south-western basin received high atmospheric inputs of PCo ( $> 25$  nmol.m<sup>-2</sup>.d<sup>-1</sup>) and of DCo ( $> 2.5$  nmol.m<sup>-2</sup>.d<sup>-1</sup>), whereas these inputs kept relatively low in the Atlantic sector and in northern side of

the Mediterranean Sea ( $< 10 \text{ nmol.m}^{-2}.\text{d}^{-1}$  and  $1 \text{ nmol.m}^{-2}.\text{d}^{-1}$  for PCo and DCo, respectively). Interestingly, the areas receiving the higher atmospheric inputs of DCo fitted with the areas where positive  $\Delta\text{DCo}_{\text{surface}}$  anomalies were reported, suggesting that the inputs of DCo provide by dust deposition and subsequent dissolution of aerosols accounted for these anomalies.

**Table 5** Dust, PCo and DCo depositions and of the Co enrichment factor estimations in the different sub-basin of the Mediterranean Sea using the DIPA model (see text for calculation)

Basin	Sub - basin	Station	Longitude (°E)	Latitude (°N)	Dust deposition (g/m <sup>2</sup> /d)	PCo deposition (nmol/m <sup>2</sup> /d)	DCo Deposition (nmol/m <sup>2</sup> /d)	EFCo
Atlantic	<i>Eastern Atlantic</i>	3a	-9.87	36.57	n.d	9.52	0.95	n.d
	<i>Eastern Atlantic</i>	4a	-7.25	35.84	0.02	13.33	1.33	2.94
	<i>Alboran Sea</i>	6a	-3.22	36.04	0.02	11.40	1.14	1.92
	<i>Central Western basin</i>	9a	2.75	37.35	0.09	48.12	4.81	1.86
Western Basin	<i>Central Western basin</i>	11a	6.66	37.77	0.16	32.68	3.27	0.72
	<i>Tyrrhenian Sea</i>	13c	13.01	39.88	0.01	8.07	0.81	2.51
	<i>Central Western basin</i>	14a	12.47	37.22	0.07	27.54	2.75	1.30
	<i>Central Western basin</i>	17c	5.95	40.07	0.01	8.53	0.85	2.80
Eastern Basin	<i>Ionian Sea</i>	16a	16.33	37.71	0.04	5.16	0.52	0.44
	<i>Ionian Sea</i>	9c	18.22	40.15	0.13	6.99	0.70	0.19
	<i>Ionian Sea</i>	18a	20.02	34.28	0.10	23.30	2.33	0.90
	<i>Levantine Basin</i>	21a	28.08	33.84	0.10	27.42	2.74	0.91
	<i>Cretan Sea</i>	1c	24.92	35.64	0.01	3.60	0.36	0.84
	<i>Cretan Sea</i>	27a	27.59	35.45	0.13	92.98	9.30	2.43
	<i>Aegean Sea</i>	29a	26.17	37.24	0.05	1.18	0.12	0.09

#### *Enrichment factor of Co in aerosols*

The atmospheric inputs of PCo did not significantly correlated with the dust deposition fluxes (Figures 22a-b), potentially due to spatial variations of the concentrations of Co in aerosols that depend of the air mass origin (Dulaquais et al., 2014b). Thus, the enrichment factors of Co in Mediterranean aerosols ( $\text{EF} = [\text{Co}]_{\text{aerosols}}/[\text{Co}]_{\text{crust}}$ ) were estimated following Equation 17.

$$EF_{Co} = PCo \text{ deposition} * M_{Co} * (Ab_{Co} * \text{dust deposition})^{-1} \quad (17)$$

With  $M_{Co}$  is molar mass of cobalt ( $59 \text{ g.mol}^{-1}$ ),  $Ab_{Co}$  is the crustal abundance of Co (set to  $17.3 \mu\text{g.g}^{-1}$ ; Rudnick and Gao, 2003).

The estimated values of EF ranged between 0.1 and 4.3, with a mean of 1.6 (Table 5, Figure 25). Interestingly, EF were equal to 1 in the Mediterranean areas receiving the higher dust inputs (Figures 22-23), suggesting crustal origin of the aerosols. On the contrary, EF were significantly higher in the low dust delivery areas, up to 4.3 in the central Ionian Sea (Table 5; Figure 23). The air mass backward-trajectory provided by NOAA Hysplit model (Figure 23) showed that the North-western Mediterranean Sea was under the influence of European air masses at the time of sampling, whereas Saharan air-masses influenced the Southern Mediterranean Sea (Figure 23). In turn, European aerosols were enriched in Co (e.g., high EF) compared to Saharan aerosols (e.g., crustal EF) (Table 5), probably related to pollution from industrial smokes from European countries. Such differences in EF should be taken into account when estimating the atmospheric input of Co to surface waters.

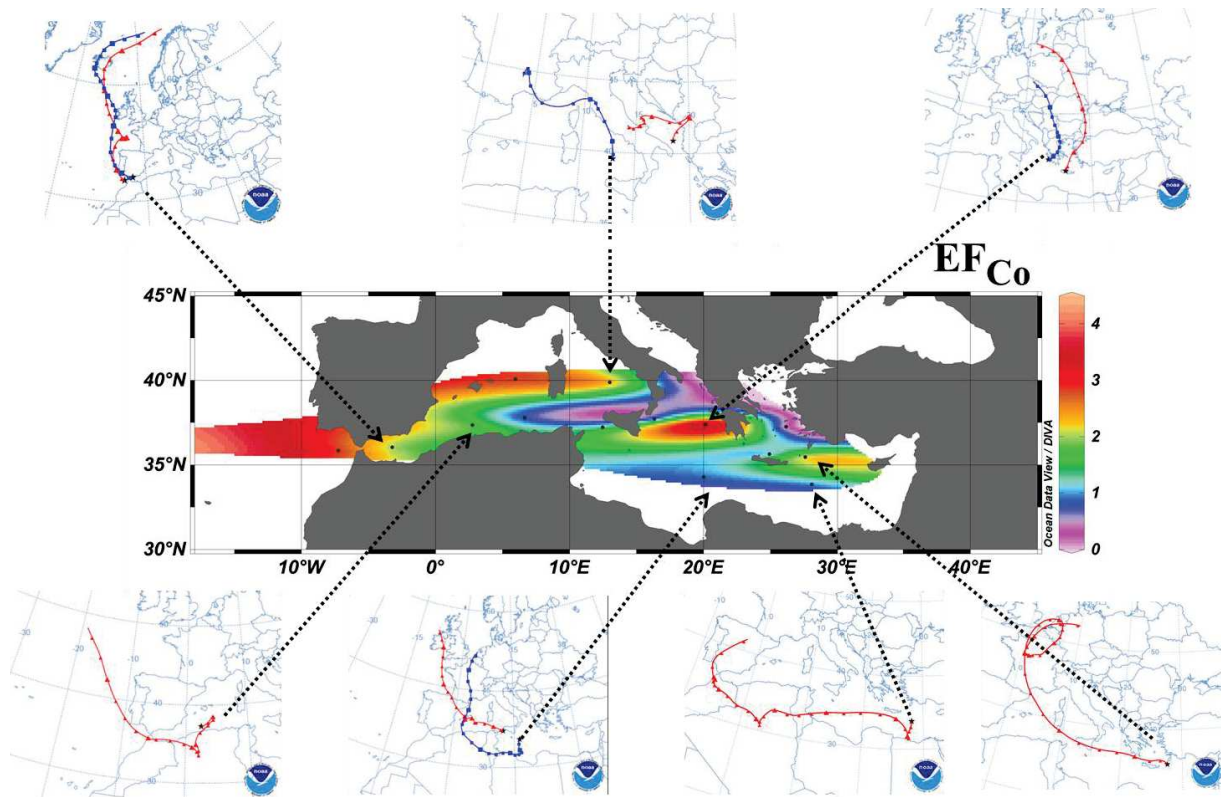


**Figure 23:** Spatial distribution of the enrichment factor of cobalt in aerosols ( $EF_{Co}$ ) estimated using the DIPA model (see text for the calculations). Air-flow directions from NOAA (Hysplit model) are reported for the 3-5 days before the sampling day.

*Comparison with the atmospheric Co inputs estimated in the Western Atlantic*

The mean atmospheric inputs of DCo we estimated in the Mediterranean Sea ( $2.1 \pm 2.3 \text{ nmol.m}^{-2}.\text{d}^{-1}$ ) were 5 times higher than those we estimated in the Western Atlantic ( $0.5 \pm 0.4 \text{ nmol.m}^{-2}.\text{d}^{-1}$ ; Dulaquais et al., 2014b; Table 6). These higher atmospheric inputs of Co to the Mediterranean Sea compared to the Western Atlantic probably result from the direct proximity of the Sahara (high dust delivery). Additionally, the high anthropogenic forcing of the Mediterranean Sea (high EF) compared to the Open Atlantic account for the difference of atmospheric Co delivery.

The higher atmospheric inputs in the Mediterranean Sea were also reflected by DCo concentrations in surface waters that were 3-5 higher (100-300 pM) than those recorded in the surface Western Atlantic (20-80 pM; Dulaquais et al., 2014). In a first order approach, the difference of subsurface DCo concentrations recorded between the different basins could be related to the atmospheric Co delivery.

**Table 6** Comparison of atmospheric inputs of PCo and DCo between the Western Atlantic (Dulaquais et al., 2014b) and the Mediterranean Sea (this study).

Domain	Mediterranean Sea	West Atlantic
Dust deposition ( $\text{mg/m}^2/\text{d}$ )	$60 \pm 50$ n = 14 (10- 156)	$4 \pm 4$ n = 55 (< 1 -16)
PCo deposition ( $\text{nmol/m}^2/\text{d}$ )	$20.8 \pm 23.0$ n = 15 (1.2 - 93.0)	$6.1 \pm 3.3$ n = 55 (0.9 -17.4)
DCo deposition ( $\text{nmol/m}^2/\text{d}$ )	$2.1 \pm 2.3$ n = 15 (0.1 - 9.3)	$0.5 \pm 0.4$ n = 55 (< 0.1 -1.3)

## 6 Conclusions

This study presented the first cobalt comprehensive datasets in the Mediterranean and Black Seas.

The Atlantic sector west of the Gibraltar Strait was marked by similar DCo distribution than that previously observed in the Western Atlantic at the same latitudes (Dulaquais et al., 2014). There, the vertical distribution of DCo was nutrient-like in surface waters due to its biological uptake, and increased in intermediate waters due to remineralization. The distribution of DCo in deep waters was related to the circulation of the different water-masses that dispatched characteristic DCo concentrations. The surface waters of the Gulf of Cadix that enter in the Mediterranean at the Gibraltar Strait were strongly enriched in DCo and feed the surface Mediterranean waters.

The deep distribution of DCo in the Mediterranean Sea was mainly controlled by the short transit times of deep waters, resulting in a quasi-constant DCo concentration below 1000 meters. In addition, the distribution PCo in these deep waters could be locally impacted by benthic and margins inputs. Due to strong stratification of the Mediterranean Sea, the exchange fluxes of DCo between the enriched surface waters and the deep waters were negligible, apart in the areas of deep-water formation that entrain and mix surface waters ( $\text{DCo} > 100 \text{ pM}$ ) with Levantine and Cretan Intermediate Waters ( $\text{DCo} < 60 \text{ pM}$ ). The Intermediate Mediterranean Waters (IMW) formed by this deep convection dispatched medium and constant DCo concentrations. Due to the specific deep circulation of the Mediterranean Sea, DCo was lost at the Strait of Sicily along the deep circulation in the Eastern Basin, and at the Strait of Gibraltar in the Western Basin. But these losses could be compensated by the convection of DCo-rich intermediate waters to the deep sea and by the remobilization of PCo from seafloor and margin sediments, and its subsequent dissolution. Remineralization, vertical diffusion and scavenging did not significantly impact the deep distribution of DCo in the deep Mediterranean Sea.

The spatial distribution of DCo in the surface Mediterranean waters displayed higher DCo concentrations in the Eastern Basin compared the Western Basin. This asymmetry probably resulted from several processes, including: i) a higher biological assimilation of DCo in the Western Basin due to the higher productivity compared to the Eastern Basin; ii) the higher export of Co on settling particles from the surface layer in the West than in the East; iii) the higher atmospheric inputs of DCo in the Eastern Basin; iv) the higher margins inputs

near the Greek Islands in the Eastern Basin; v) the surface DCo inputs from the Adriatic and Black Seas in the Eastern Basin.

In the Black Sea, the DCo and PCo concentrations recorded were extremely high compared to other marine systems. While the high surface DCo concentrations could be related to riverine inputs, the vertical distributions of DCo and PCo were mainly controlled by redox-processes. Scavenging by MnO<sub>x</sub> could indeed control their distributions in the transition layer between oxic-anoxic conditions. Below this layer, the reduction of MnO<sub>x</sub> in the upper sulfidic layer released Co into the dissolved phase that was marked by maxima and extremely high DCo concentrations (up to 6.6 nM). Below these maxima, scavenging of DCo onto ferrihydrite could cause the sharp decrease of DCo observed with depth. These chemical processes were further supported by the significant correlations found between PCo and PMn in the suboxic layer, and between PCo and PFe in the sulfidic waters. In the deep Black Sea, a fairly constant and relatively high DCo concentrations of 330 pM were recorded. Competitive complexation between strong organic Co-binding ligands and HS<sup>-</sup> may occur.

The determination of the dust deposition toward a new DIPA model based on particulate trace elements concentrations in seawater has allowed determining the PCo and DCo deposition fluxes in the different sub-basins of the Mediterranean Sea. The initial Co concentration in the aerosols has been estimated from measurements of surface marine particles composition. Results provide evidence of the strong influence of the Sahara dust delivery on surface DCo concentrations. Furthermore, estimated cobalt contents in aerosols were function of the air mass origin. Hence, we evidenced higher Co content in aerosols originating from Europe indicating an anthropogenic forcing on the atmospheric deposition of cobalt.

This study provided new keys on processes that govern the cobalt distribution in seawater, with evidence on the importance of size and time scales in the biogeochemical cycle of cobalt in marine system.

## Acknowledgements

We are indebted to the Captain, Officers and Crew Members of the *R.V. Pelagia*. We are most grateful to Loes Gerringa and Micha Rijkenberg, the Chief Scientists of the cruises. We warmly thank Jan van Ooijen, K. Bakker, E. van Weerlee, S. Ossebaar for the analyses of nutrients, as well as S. Ober, M. Laan, S. van Heuven, S. Asjes and L. Wuis for providing high quality CTD data. This investigation was supported by the GEOTRACES Med.&Black Seas project coordinated by M. Boye and funded by the LABEX-MER Program of the Ministère de l'Education Nationale, de l'Enseignement Supérieur et de la Recherche. The Université de Bretagne Occidentale and the Région Bretagne were supporting the PhD fellowship of G. Dulaquais. This investigation is a contribution to the international GEOTRACES program.

## References

- Achterberg, E. P., & Van Den Berg, C. M. (1997). Chemical speciation of chromium and nickel in the western Mediterranean. *Deep Sea Research Part II: Topical Studies in Oceanography*, 44(3), 693-720.
- Agustí, S. (2004). Viability and niche segregation of Prochlorococcus and Synechococcus cells across the Central Atlantic Ocean. *Aquatic microbial ecology*, 36(1), 53-59.
- Anderson, L. A., & Sarmiento, J. L. (1994). Redfield ratios of remineralization determined by nutrient data analysis. *Global biogeochemical cycles*, 8(1), 65-80.
- Aston, S., Chester, R., & Johnson, L. R. (1972). Uptake of cobalt from seawater by Aeolian dust. *Nature*, 235, 380-381.
- Backes, C. A., McLaren, R. G., Rate, A. W., & Swift, R. S. (1995). Kinetics of cadmium and cobalt desorption from iron and manganese oxides. *Soil Science Society of America Journal*, 59(3), 778-785.
- Baskaran, M., Santschi, P. H., Benoit, G., & Honeyman, B. D. (1992). Scavenging of thorium isotopes by colloids in seawater of the Gulf of Mexico. *Geochimica et cosmochimica Acta*, 56(9), 3375-3388.
- Bertilsson, S., O. Berglund, D. M. Karl, and S. W. Chisholm. (2003), Elemental composition of marine *Prochlorococcus* and *Synechococcus*: implications for the ecological stoichiometry of the sea. *Limnol. Oceanogr.*, 48, 1721-1731.
- Bethoux, J. P. (1980). Mean water fluxes across sections in the mediterranean-sea, evaluated on the basis of water and salt budgets and of observed salinities. *Oceanologica Acta*, 3(1), 79-88.
- Béthoux, J. P., Courau, P., Nicolas, E., & Ruizpino, D. (1990). Trace-metal pollution in the mediterranean-sea. *Oceanologica acta*, 13(4), 481-488.
- Bethoux, J. P., Morin, P., Madec, C., & Gentili, B. (1992). Phosphorus and nitrogen behaviour in the Mediterranean Sea. *Deep Sea Research Part A. Oceanographic Research Papers*, 39(9), 1641-1654.
- Bethoux, J. P., Morin, P., Chaumery, C., Connan, O., Gentili, B., & Ruiz-Pino, D. (1998). Nutrients in the Mediterranean Sea, mass balance and statistical analysis of concentrations with respect to environmental change. *Marine Chemistry*, 63(1), 155-169.
- Béthoux, J. P., Morin, P., & Ruiz-Pino, D. P. (2002). Temporal trends in nutrient ratios: chemical evidence of Mediterranean ecosystem changes driven by human activity. *Deep Sea Research Part II: Topical Studies in Oceanography*, 49(11), 2007-2016.

- Bethoux, J. P., El Boukhary, M. S., Ruiz-Pino, D., Morin, P., & Copin-Montégut, C. (2005). Nutrient, Oxygen and Carbon Ratios, CO<sub>2</sub> Sequestration and Anthropogenic Forcing in the Mediterranean Sea. In *The Mediterranean Sea* (pp. 67-86). Springer Berlin Heidelberg.
- Bonnet, S., Tovar-Sánchez, A., Panzeca, C., Duarte, C. M., Ortega-Retuerta, E., & Sanudo Wilhelmy, S. A. (2013). Geographical gradients of dissolved Vitamin B12 in the Mediterranean Sea. *Frontiers in microbiology*, 4.
- Bosc, E., Bricaud, A., & Antoine, D. (2004). Seasonal and interannual variability in algal biomass and primary production in the Mediterranean Sea, as derived from 4 years of SeaWiFS observations. *Global Biogeochemical Cycles*, 18(1).
- Boutov, D., Peliz, Á., Miranda, P., Soares, P. M., Cardoso, R. M., Prieto, L., Ruiz, J., & García-Lafuente, J. (2014). Inter-annual variability and long term predictability of exchanges through the Strait of Gibraltar. *Global and Planetary Change*, 114, 23-37.
- Boutron, C. F., Gorlach, U., Candelone, J.-P., Bolshov, M. A., and Delmas, R. J. (1991). Decrease in anthropogenic lead, cadmium and zinc in Greenland snows since the late 1960s. *Nature*, 353, 153-156.
- Bown, J., Boye, M., Baker, A., Duvieilbourg, E., Lacan, F., Le Moigne, F., Planchon, F., Speich, S., and Nelson, D. M. (2011). The biogeochemical cycle of dissolved cobalt in the Atlantic and the Southern Ocean south off the coast of South Africa. *Mar. Chem.*, 126, 193–206, doi:10.1016/j.marchem.2011.03.008, 2011.
- Bown, J., Boye, M., & Nelson, D. M. (2012). New insights on the role of organic speciation in the biogeochemical cycle of dissolved cobalt in the southeastern Atlantic and the Southern Ocean. *Biogeosciences*, 9, 2719-2736.
- Boyle, E. A., Chapnick, S. D., Bai, X. X., & Spivack, A. (1985). Trace metal enrichments in the Mediterranean Sea. *Earth and Planetary Science Letters*, 74(4), 405-419.
- Bryden, H. L., & Kinder, T. H. (1991). Steady two-layer exchange through the Strait of Gibraltar. *Deep Sea Research Part A. Oceanographic Research Papers*, 38, S445-S463.
- Bryden, H. L., Candela, J., & Kinder, T. H. (1994). Exchange through the Strait of Gibraltar. *Progress in Oceanography*, 33(3), 201-248.
- Buesseler, K. O. (1998). The decoupling of production and particulate export in the surface ocean. *Global Biogeochemical Cycles*, 12(2), 297-310.
- Casotti, R., Landolfi, A., Brunet, C., D'Ortenzio, F., Mangoni, O., Ribera d'Alcalà, M., & Denis, M. (2003). Composition and dynamics of the phytoplankton of the Ionian Sea (eastern Mediterranean). *Journal of Geophysical Research: Oceans (1978–2012)*, 108(C9).
- Chester, R., Baxter, G. G., Behairy, A. K. A., Connor, K., Cross, D., Elderfield, H., & Padgham, R. C. (1977). Soil-sized eolian dusts from the lower troposphere of the eastern Mediterranean Sea. *Marine Geology*, 24(3), 201-217.
- Chester, R., Murphy, K. J. T., Lin, F. J., Berry, A. S., Bradshaw, G. A., & Corcoran, P. A. (1993). Factors controlling the solubilities of trace metals from non-remote aerosols deposited to the sea surface by the 'dry' deposition mode. *Marine Chemistry*, 42(2), 107-126.
- Christaki, U., Giannakourou, A., Van Wambeke, F., & Grégori, G. (2001). Nanoflagellate predation on auto- and heterotrophic picoplankton in the oligotrophic Mediterranean Sea. *Journal of Plankton Research*, 23(11), 1297-1310.
- Codispoti, L. A. (1989). Phosphorus vs. nitrogen limitation of new and export production. *Productivity of the ocean: Present and past*, 44, 377-394.

- Cullen, J. T., & Sherrell, R. M. (1999). Techniques for determination of trace metals in small samples of size-fractionated particulate matter: phytoplankton metals off central California. *Marine Chemistry*, 67(3), 233-247.
- de Baar, H.J.W., K.R. Timmermans, P. Laan , H.H. De Porto, S. Ober, J.J. Blom, M.C. Bakker, J. Schilling, G. Sarthou, M.G. Smit and M. Klunder (2008), Titan: A new facility for ultraclean sampling of trace elements and isotopes in the deep oceans in the international GEOTRACES program. *Mar. Chem.*, 111 (1-2).
- Dammshäuser, A., Wagener, T., Garbe-Schönberg, D., & Croot, P. (2013). Particulate and dissolved aluminum and titanium in the upper water column of the Atlantic Ocean. *Deep Sea Research Part I: Oceanographic Research Papers*, 73, 127-139.
- Dachs, J., Bayona, J. M., Fowler, S. W., Miquel, J. C., & Albaiges, J. (1998). Evidence for cyanobacterial inputs and heterotrophic alteration of lipids in sinking particles in the Alboran Sea (SW Mediterranean). *Marine chemistry*, 60(3), 189-201.
- Dulaquais, G., Boye, M., Rijkenberg, M. J. A., & Carton, X. (2014), Physical and remineralization processes govern the cobalt distribution in the deep western Atlantic Ocean. *Biogeosciences*, 11(6), 1561-1580.
- Dulaquais, G., Boye, M., Middag, R., Owens, S., Puigcorbe, V., Buesseler, K., de Baar, H. & Carton, X. (2014). Contrasting biogeochemical cycles of cobalt in the surface western Atlantic Ocean. *Global Biogeochemical Cycles*, 28(12), 1387-1412.
- Dulaquais, G. and Boye, M., Atmospheric cobalt deposition along the surface west Atlantic and biogeochemical implications (in review), In review for publication in *Marine Chemistry*.
- Eker, E., Georgieva, L., Senichkina, L., & Kideys, A. E. (2000). Phytoplankton distribution in the western and eastern Black Sea in spring and autumn 1995. *ICES Journal of Marine Science*, 56, 15-22.
- Elbaz-Poulichet, F., Morley, N. H., Beckers, J. M., & Nomerange, P. (2001a). Metal fluxes through the Strait of Gibraltar: the influence of the Tinto and Odiel rivers (SW Spain). *Marine Chemistry*, 73(3), 193-213.
- Elbaz-Poulichet, F., Guieu, C., & Morley, N. H. (2001b). A reassessment of trace metal budgets in the western Mediterranean Sea. *Marine Pollution Bulletin*, 42(8), 623-627.
- Elbaz-Poulichet, F., Braungardt, C., Achterberg, E., Morley, N., Cossa, D., Beckers, J. M., Nomérang, P., Cruzado, A., & Leblanc, M. (2001c). Metal biogeochemistry in the Tinto–Odiel rivers (Southern Spain) and in the Gulf of Cadiz: a synthesis of the results of TOROS project. *Continental Shelf Research*, 21(18), 1961-1973.
- Gascard, J. C., & Richez, C. (1985). Water masses and circulation in the Western Alboran Sea and in the Straits of Gibraltar. *Progress in Oceanography*, 15(3), 157-216.
- Grasshoff, K. et al.: Methods of seawater analysis. Verlag Chemie GmbH, Weinheim. 419 pp., 1983.
- Gregg, M. C., Özsoy, E., & Latif, M. A. (1999). Quasi-steady exchange flow in the bosphorus. *Geophysical Research Letters*, 26(1), 83-86.
- Gruber, N., & Sarmiento, J. L. (1997). Global patterns of marine nitrogen fixation and denitrification. *Global Biogeochemical Cycles*, 11(2), 235-266.
- Guerzoni, S., Chester, R., Dulac, F., Herut, B., Loÿe-Pilot, M. D., Measures, C., Migon, C., Molinaroli, E., Moulin, C., Rossini, P., Saydam, C., & Ziveri, P. (1999). The role of atmospheric deposition in the biogeochemistry of the Mediterranean Sea. *Progress in Oceanography*, 44(1), 147-190.
- Guieu, C., Chester, R., Nimmo, M., Martin, J. M., Guerzoni, S., Nicolas, E., ... & Keyse, S. (1997). Atmospheric input of dissolved and particulate metals to the northwestern Mediterranean. *Deep Sea Research Part II: Topical Studies in Oceanography*, 44(3), 655-674.

- Guieu, C., Martin, J. M., Tankere, S. P. C., Mousty, F., Trincherini, P., Bazot, M., & Dai, M. H. (1998). On trace metal geochemistry in the Danube River and western Black Sea. *Estuarine, Coastal and Shelf Science*, 47(4), 471-485.
- Guieu, C., Loÿe-Pilot, M. D., Ridame, C., & Thomas, C. (2002). Chemical characterization of the Saharan dust end-member: Some biogeochemical implications for the western Mediterranean Sea. *Journal of Geophysical Research: Atmospheres (1984–2012)*, 107(D15), ACH-5.
- Guieu, C., Loÿe-Pilot, M. D., Benyahya, L., & Dufour, A. (2010). Spatial variability of atmospheric fluxes of metals (Al, Fe, Cd, Zn and Pb) and phosphorus over the whole Mediterranean from a one-year monitoring experiment: biogeochemical implications. *Marine Chemistry*, 120(1), 164-178.
- Haraldsson, C., & Westerlund, S. (1991). Total and suspended cadmium, cobalt, copper, iron, lead, manganese, nickel, and zinc in the water column of the Black Sea. In *Black Sea Oceanography* (pp. 161-172). Springer Netherlands.
- Heggie, D., & Lewis, T. (1984). Cobalt in pore waters of marine sediments. *Nature*, 311, 453-455.
- Heimbürger, L. E., (2010). Dynamics of Chemical contaminants in the open ocean, the Mediterranean Sea as an example. (Doctoral dissertation, University of Sofia Antipolis)
- Heimbürger, L. E., Migon, C., & Cossa, D. (2011). Impact of atmospheric deposition of anthropogenic and natural trace metals on Northwestern Mediterranean surface waters: A box model assessment. *Environmental Pollution*, 159(6), 1629-1634.
- Heimbürger, L. E., Migon, C., Losno, R., Miquel, J. C., Thibodeau, B., Stabholz, M., Dufour, A. & Leblond, N. (2014). Vertical export flux of metals in the Mediterranean Sea. *Deep Sea Research Part I: Oceanographic Research Papers*, 87, 14-23.
- Ho, T. Y., A. Quigg, Z. V. Finkel, A. J. Milligan, K. Wyman, P. G. Falkowski, and F. M. Morel. (2003), The elemental composition of some marine phytoplankton. *J. Phycol.* 39: 1145–1159.
- Ignatiades, L., Gotsis-Skretas, O., Pagou, K., & Krasakopoulou, E. (2009). Diversification of phytoplankton community structure and related parameters along a large-scale longitudinal east–west transect of the Mediterranean Sea. *Journal of plankton research*, 31(4), 411-428.
- Ji, Y., Sherrell, R.M., (2008), Differential effects of phosphorus limitation on cellular metals in Chlorella and Microcystis. *Limnol. Oceanogr.* 53, 1790–1804.
- Jickells, T.S., An, Z.A., Baker, A.R., Bergametti, G., Brooks, N., Boyd, P.W., Duce, R.A., Hunter, K.A., Junji, C., Kawahata, H., Kubilay, N., Andersen, K.K., La Roche, J., Liss, P.S., Mahowald, N., Prospero, J.M., Ridgwell, A.J., Tegen, I., Torres, R.,(2005), Global iron connections between desert dust, ocean biogeochemistry and climate. *Science*, 308, 67–71.
- Johnson, H. P., Tivey, M. A., Bjorklund, T. A., & Salmi, M. S. (2010). Hydrothermal circulation within the Endeavour segment, Juan de Fuca Ridge. *Geochemistry, Geophysics, Geosystems*, 11(5).
- Kinder, T. H., & Parrilla, G. (1987). Yes, some of the Mediterranean outflow does come from great depth. *Journal of Geophysical Research: Oceans (1978–2012)*, 92(C3), 2901-2906.
- Konhauser, K. O., Pecoits, E., Lalonde, S. V., Papineau, D., Nisbet, E. G., Barley, M. E., ... & Kamber, B. S. (2009). Oceanic nickel depletion and a methanogen famine before the Great Oxidation Event. *Nature*, 458(7239), 750-753.
- Konovalov, S. K., & Murray, J. W. (2001). Variations in the chemistry of the Black Sea on a time scale of decades (1960–1995). *Journal of Marine Systems*, 31(1), 217-243.

- Konovalov, S. K., Luther, G. W., Friederich, G. E., Nuzzio, D. B., Tebo, B. M., Murray, J. W., Oguz, T., Glazer, B., Trouwborst, R.E., Clement, B., Murray, K.J. & Romanov, A. S. (2003). Lateral injection of oxygen with the Bosphorus plume-fingers of oxidizing potential in the Black Sea. *Limnology and Oceanography*, 48(6), 2369-2376.
- Kremling, K., & Petersen, H. (1981). The distribution of zinc, cadmium, copper, manganese and iron in waters of the open Mediterranean Sea. *Meteor Forschungsergebnisse Reihe A/B*, (23), 5-14.
- Kress, N., & Herut, B. (2001). Spatial and seasonal evolution of dissolved oxygen and nutrients in the Southern Levantine Basin (Eastern Mediterranean Sea): chemical characterization of the water masses and inferences on the N: P ratios. *Deep Sea Research Part I: Oceanographic Research Papers*, 48(11), 2347-2372.
- Kress, N., Manca, B. B., Klein, B., & Deponte, D. (2003). Continuing influence of the changed thermohaline circulation in the eastern Mediterranean on the distribution of dissolved oxygen and nutrients: Physical and chemical characterization of the water masses. *Journal of Geophysical Research: Oceans (1978–2012)*, 108(C9).
- Krom, M. D., Kress, N., Brenner, S., & Gordon, L. I. (1991). Phosphorus limitation of primary productivity in the eastern Mediterranean Sea. *Limnology and Oceanography*, 36(3), 424-432.
- Krom, M. D., Herut, B., & Mantoura, R. F. C. (2004). Nutrient budget for the Eastern Mediterranean: Implications for phosphorus limitation. *Limnology and Oceanography*, 49(5), 1582-1592.
- Krom, M. D., Emeis, K. C., & Van Cappellen, P. (2010). Why is the Eastern Mediterranean phosphorus limited?. *Progress in Oceanography*, 85(3), 236-244.
- Landing, W. M., & Lewis, B. L. (1991). Thermodynamic modeling of trace metal speciation in the Black Sea. In *Black Sea Oceanography* (pp. 125-160). Springer Netherlands.
- Lascaratos, A., Roether, W., Nittis, K., & Klein, B. (1999). Recent changes in deep water formation and spreading in the eastern Mediterranean Sea: a review. *Progress in oceanography*, 44(1), 5-36.
- Lewis, B. L., & Landing, W. M. (1992). The investigation of dissolved and suspended particulate trace metal fractionation in the Black Sea. *Marine Chemistry*, 40(1), 105-141.
- L'Helguen, S., Chauvaud, L., Cuet, P., Frouin, P., Maguer, J. F., & Clavier, J. (2014). A novel approach using the  $^{15}\text{N}$  tracer technique and benthic chambers to determine ammonium fluxes at the sediment–water interface and its application in a back-reef zone on Reunion Island (Indian Ocean). *Journal of Experimental Marine Biology and Ecology*, 452, 143-151.
- Ludwig, W., Dumont, E., Meybeck, M., & Heussner, S. (2009). River discharges of water and nutrients to the Mediterranean and Black Sea: major drivers for ecosystem changes during past and future decades? *Progress in Oceanography*, 80(3), 199-217.
- Mantyla, A. W., & Reid, J. L. (1983). Abyssal characteristics of the World Ocean waters. *Deep Sea Research Part A. Oceanographic Research Papers*, 30(8), 805-833.
- Mariotti, A., Struglia, M. V., Zeng, N., & Lau, K. M. (2002). The hydrological cycle in the Mediterranean region and implications for the water budget of the Mediterranean Sea. *Journal of climate*, 15(13), 1674-1690.
- Marty, J. C., Chiavérini, J., Pizay, M. D., & Avril, B. (2002). Seasonal and interannual dynamics of nutrients and phytoplankton pigments in the western Mediterranean Sea at the DYFAMED time-series station (1991–1999). *Deep Sea Research Part II: Topical Studies in Oceanography*, 49(11), 1965-1985.
- McCartney, M. S. (1992). Recirculating components to the deep boundary current of the northern North Atlantic. *Progress in Oceanography*, 29(4), 283-383.

- MerMex group (2011). Marine ecosystems' responses to climatic and anthropogenic forcings in the Mediterranean. *Progress in Oceanography*, 91(2), 97-166.
- Middag, R., H. J. W. de Baar, P. Laan, and K. Bakker (2009), Dissolved aluminium and the silicon cycle in the Arctic Ocean, *Mar. Chem.*, 115, 176–195, doi:10.1016/j.marchem.2009.08.002.
- Millot, C. (1987). Circulation in the western Mediterranean-sea. *Oceanologica Acta*, 10(2), 143-149.
- Millot, C. (1999). Circulation in the western Mediterranean Sea. *Journal of Marine Systems*, 20(1), 423-442.
- Millot, C., Taupier-Letage, I., (2005a). Circulation in the Mediterranean Sea. In: Saliot, A. (Ed.), *The Handbook of Environmental Chemistry* 5 (K). Springer-Verlag, Heidelberg, pp. 29–66.
- Millot, C., Taupier-Letage, I., (2005b). Additional evidence of LIW entrainment across the Algerian Basin by mesoscale eddies and not by a permanent westward flowing vein. *Progress in Oceanography* , 66 (2-4), 231–250.
- Moran, S. B., and R. M. Moore (1988), Evidence from mesocosm studies for biological removal of dissolved aluminum from sea water, *Nature*, 335, 706–708, doi:10.1038/335706a0
- Moran, S. B., & Buesseler, K. O. (1992). Short residence time of colloids in the upper ocean estimated from  $^{238}\text{U}$ - $^{234}\text{Th}$  disequilibria. *Nature*, 359, 221-223
- Moran, S.B. & Buesseler, K. O. (1993). Size-fractionated  $^{234}\text{Th}$  in continental shelf waters off New England: Implications for the role of colloids in oceanic trace metal scavenging. *Journal of Marine Research*, 51(4), 893-922.
- Morley, N. H., Burton, J. D., Tankere, S. P. C., & Martin, J. M. (1997). Distribution and behaviour of some dissolved trace metals in the western Mediterranean Sea. *Deep Sea Research Part II: Topical Studies in Oceanography*, 44(3), 675-691.
- Moutin, T., & Raimbault, P. (2002). Primary production, carbon export and nutrients availability in western and eastern Mediterranean Sea in early summer 1996 (MINOS cruise). *Journal of Marine Systems*, 33, 273-288.
- Murphy, J. & Riley, J.P (1962), A modified single solution method for the determination of phosphate in natural waters. *Analytica Chim. Acta*, 27, 31-36.
- Murray, J. W. (1975). The interaction of cobalt with hydrous manganese dioxide. *Geochimica et Cosmochimica Acta*, 39(5), 635-647.
- Murray, J. W., Top, Z., & Özsoy, E. (1991). Hydrographic properties and ventilation of the Black Sea. *Deep Sea Research Part A. Oceanographic Research Papers*, 38, S663 S689
- Ngoc, L. H., & Whitehead, N. E. (1986). Nickel and cobalt determination in the north-western mediterranean by differential pulse cathodic stripping voltammetry. *Oceanologica acta*, 9(4), 433-438.
- Noble, A. E., Saito, M. A., Maiti, K., and Benitez-Nelson, C. R. (2008), Cobalt, manganese, and iron near the Hawaiian Islands: A potential concentrating mechanism for cobalt within a cyclonic eddy and implications for the hybrid-type trace metals. *Deep-Sea Res. artt. II*, 55, 1473–1490, doi:10.1016/j.dsr2.2008.02.010.
- Öguz, T., Latun, V. S., Latif, M. A., Vladimirov, V. V., Sur, H. I., Markov, A. A., Özsoy, E., Kotovshchikov,B.B., Eremeev, V.V. & Ünlüata, Ü. (1993). Circulation in the surface and intermediate layers of the Black Sea. *Deep Sea Research Part I: Oceanographic Research Papers*, 40(8), 1597-1612.
- Öguz, T., Malanotte-Rizzoli, P., & Aubrey, D. (1995). Wind and thermohaline circulation of the Black Sea driven by yearly mean climatological forcing. *Journal of Geophysical Research: Oceans (1978–2012)*, 100(C4), 6845-6863.

- Öguz, T. (2005). Hydraulic adjustments of the Bosphorus exchange flow. *Geophysical research letters*, 32(6).
- Özsoy, E., Top, Z., White, G., & Murray, J. W. (1991). Double diffusive intrusions, mixing and deep sea convection processes in the Black Sea. In *Black Sea Oceanography* (pp. 17-42). Springer Netherlands.
- Özsoy, E., Ünlüata, Ü., & Top, Z. (1993). The evolution of Mediterranean water in the Black Sea: interior mixing and material transport by double diffusive intrusions. *Progress in Oceanography*, 31(3), 275-320.
- Pantoja, S., Repeta, D. J., Sachs, J. P., & Sigman, D. M. (2002). Stable isotope constraints on the nitrogen cycle of the Mediterranean Sea water column. *Deep Sea Research Part I: Oceanographic Research Papers*, 49(9), 1609-1621.
- Planquette, H., & Sherrell, R. M. (2012). Sampling for particulate trace element determination using water sampling bottles: methodology and comparison to in situ pumps. *Limnology and Oceanography: Methods*, 10, 367-388.
- Price, N. B., Brand, T., Pates, J. M., Mowbray, S., Theocharis, A., Civitarese, G., Miserocchi, S., Heussner, S. & Lindsay, F. (1999). Horizontal distributions of biogenic and lithogenic elements of suspended particulate matter in the Mediterranean Sea. *Progress in Oceanography*, 44(1), 191-218.
- Pujo-Pay, M., Conan, P., Oriol, L., Cornet-Barthaux, V., Falco, C., Ghiglione, J. F., Goyet, C., Moutin, T. & Prieur, L. (2011). Integrated survey of elemental stoichiometry (C, N, P) from the western to eastern Mediterranean Sea. *Biogeosciences*, 8(4), 883-899.
- Rabitti, S., Bianchi, F., Boldrin, A., Daros, L., Socal, G., & Totti, C. (1994). Particulate matter and phytoplankton in the Ionian Sea. *Oceanologica Acta*, 17(3), 297-307.
- Redfield, A. C. (1963). The influence of organisms on the composition of sea water. *The sea*, 26-77.
- Ribera d'Alcalà, M., Civitarese, G., Conversano, F., & Lavezza, R. (2003). Nutrient ratios and fluxes hint at overlooked processes in the Mediterranean Sea. *Journal of Geophysical Research: Oceans (1978–2012)*, 108(C9).
- Rijkenberg, M. J., Middag, R., Laan, P., Gerrings, L. J., van Aken, H. M., Schoemann, V., de Jong, J. & de Baar, H. J. (2014). The Distribution of Dissolved Iron in the West Atlantic Ocean. *PloS one*, 9(6), e101323.
- Roether, W., & Schlitzer, R. (1991). Eastern Mediterranean deep water renewal on the basis of chlorofluoromethane and tritium data. *Dynamics of Atmospheres and Oceans*, 15(3), 333-354.
- Rudnick, R. L., & Gao, S. (2003). Composition of the continental crust. *Treatise on geochemistry*, 3, 1-64.
- Ruiz Pino, D. P., Jeandel, C., Bethoux, J. P., & Minster, J. F. (1990). Are the trace metal cycles balanced in the Mediterranean Sea?. *Palaeogeography, Palaeoclimatology, Palaeoecology*, 82(3), 369-388.
- Ruiz-Pino, D. P., Nicolas, E., Bethoux, J. P., & Lambert, C. E. (1991). Zinc budget in the Mediterranean Sea: a hypothesis for non-steady-state behavior. *Marine Chemistry*, 33(1), 145-169.
- Saager, P. M., Schijf, J., & de Baar, H. J. (1993). Trace-metal distributions in seawater and anoxic brines in the eastern Mediterranean Sea. *Geochimica et cosmochimica acta*, 57(7), 1419-1432.
- Saito, M. A. and Moffett, J. W. (2001). Complexation of cobalt by natural organic ligands in the Sargasso Sea as determined by a new high sensitivity electrochemical cobalt speciation method suitable for open ocean work. *Mar. Chem.*, 75, 49-68.
- Saito, M. A. and Moffett, J. W. (2002). Temporal and spatial variability of cobalt in the Atlantic Ocean. *Geochim. Cosmochim. Acta*, 66, 1943-1953.

- Saito, M. A., Moppett, J. W., Chisholm, S. W., & Waterbury, J. B. (2002). Cobalt limitation and uptake in Prochlorococcus. *Limnol. and Oceanogr.*, 47(6), 1629-1636..
- Sanchez-Vidal, A., Calafat, A., Canals, M., Frigola, J., & Fabres, J. (2005). Particle fluxes and organic carbon balance across the Eastern Alboran Sea (SW Mediterranean Sea). *Continental shelf research*, 25(5), 609-628.
- Sands, C. M., Connelly, D. P., Statham, P. J., & German, C. R. (2012). Size fractionation of trace metals in the Edmond hydrothermal plume, Central Indian Ocean. *Earth and Planetary Science Letters*, 319, 15-22.
- Sañudo-Wilhelmy, S. A., Kustka, A. B., Gobler, C. J., Hutchins, D. A., Yang, M., Lwiza, K., Burns, J., Capone, D.G., Raven, J.A., & Carpenter, E. J. (2001). Phosphorus limitation of nitrogen fixation by Trichodesmium in the central Atlantic Ocean. *Nature*, 411(6833), 66-69.
- Sarmiento, J. L., Herbert, T., & Toggweiler, J. R. (1988). Mediterranean nutrient balance and episodes of anoxia. *Global Biogeochemical Cycles*, 2(4), 427-444.
- Schmitz, W. J., & McCartney, M. S. (1993). On the north Atlantic circulation. *Reviews of Geophysics*, 31(1), 29-49.
- Schroeder, K., Ribotti, A., Borghini, M., Sorgente, R., Perilli, A., & Gasparini, G. P. (2008). An extensive western Mediterranean deep water renewal between 2004 and 2006. *Geophysical Research Letters*, 35(18).
- Shapiro, G. I. (2009). Black Sea Circulation. *Ocean currents: a derivative of the encyclopedia of ocean sciences*, 1, 318-331.
- Shaffer, G. (1986). Phosphate pumps and shuttles in the Black Sea. *Nature*, 321, 515-517.
- Shelley, R. U., Zachhuber, B., Sedwick, P. N., Worsfold, P. J., and Lohan, M. C. (2010), Determination of total dissolved cobalt in UV-irradiated seawater using flow injection with chemiluminescence detection. *Limnol. Oceanogr.*, 8, 352-362, doi:10.1029/2009JC005880.
- Sherrell, R. M., & Boyle, E. A. (1988). Zinc, chromium, vanadium and iron in the Mediterranean Sea. *Deep Sea Research Part A. Oceanographic Research Papers*, 35(8), 1319-1334.
- Spencer, D. W., & Brewer, P. G. (1971). Vertical advection diffusion and redox potentials as controls on the distribution of manganese and other trace metals dissolved in waters of the Black Sea. *Journal of Geophysical Research*, 76(24), 5877-5892.
- Spencer, D. W., Brewer, P. G., & Sachs, P. L. (1972). Aspects of the distribution and trace element composition of suspended matter in the Black Sea. *Geochimica et Cosmochimica Acta*, 36(1), 71-86.
- Spivack, A. J., Huested, S. S., & Boyle, E. A. (1983). Copper, nickel and cadmium in the surface waters of the Mediterranean. In *Trace metals in sea water* (pp. 505-512). Springer US.
- Strickland, J.D.H. and Parsons, T.R. (1968), A practical handbook of seawater analysis. First Edition, Fisheries Research Board of Canada, Bulletin. No 167, p.65.
- Swanner, E. D., Planavsky, N. J., Lalonde, S. V., Robbins, L. J., Bekker, A., Rouxel, O. J., ... & Konhauser, K. O. (2014). Cobalt and marine redox evolution. *Earth and Planetary Science Letters*, 390, 253-263.
- Tankere, S. P. C. (1998). *The biogeochemistry of some trace metals in some eutrophic areas: the Adriatic sea and the North-Western black sea* (Doctoral dissertation, University of Southampton).
- Tankéré, S. P. C., Price, N. B., & Statham, P. J. (2000). Mass balance of trace metals in the Adriatic Sea. *Journal of Marine systems*, 25(3), 269-286.

- Tankere, S. P. C., Muller, F. L. L., Burton, J. D., Statham, P. J., Guieu, C., & Martin, J. M. (2001). Trace metal distributions in shelf waters of the northwestern Black Sea. *Continental Shelf Research*, 21(13), 1501-1532.
- Ternon, E., Guieu, C., Ridame, C., L'Helguen, S., & Catala, P. (2011). Longitudinal variability of the biogeochemical role of Mediterranean aerosols in the Mediterranean Sea. *Biogeosciences*, 8, 1067-1080.
- Tovar-Sanchez, A., Sanudo-Wilhelmy, S. A., Kustka, A. B., Agusti, S., Dachs, J., Hutchins, D. A., Capone, D. G., Duarte, C. M. (2006). Effects of dust deposition and river discharges on trace metal composition of *Trichodesmium* spp. in the tropical and subtropical North Atlantic Ocean. *Limnol. Oceanogr.*, 51(4), 1755–1761.
- Tsuchiya, M., Talley, L. D., & McCartney, M. S. (1992). An eastern Atlantic section from Iceland southward across the equator. *Deep Sea Research Part A. Oceanographic Research Papers*, 39(11), 1885-1917.
- Ünlülata, Ü., Oğuz, T., Latif, M. A., & Özsoy, E. (1990). On the physical oceanography of the Turkish Straits. In *The physical oceanography of sea straits* (pp. 25-60). Springer Netherlands.
- Uysal, Z. (2001). Chroococcoid cyanobacteria *Synechococcus* spp. in the Black Sea: pigments, size, distribution, growth and diurnal variability. *Journal of plankton research*, 23(2), 175-190.
- Uysal, Z., Kideys, A., Unsal, M., & Altukhov, D. (1998). Long-term changes in the Black Sea zooplankton: the role of natural and anthropogenic factors. *Ecosystem Modeling as a Management Tool for the Black Sea:[Proceedings of the NATO TU Black Sea Project, Ecosystem Modeling as a Management Tool for the Black Sea, Zori Rossii, Ukraine, 15-19 June, 1997]*, 1, 221.
- van Aken, H. M. (2000a). The hydrography of the mid-latitude northeast Atlantic Ocean: I: The deep water masses. *Deep Sea Research Part I: Oceanographic Research Papers*, 47(5), 757-788.
- van Aken, H. M. (2000b). The hydrography of the mid-latitude Northeast Atlantic Ocean: II: The intermediate water masses. *Deep Sea Research Part I: Oceanographic Research Papers*, 47(5), 789-824.
- van Geen, A., Rosener, P., & Boyle, E. (1988). Entrainment of trace-metal-enriched Atlantic shelf water in the inflow to the Mediterranean Sea. *Nature*, 331, 4.
- van Geen, A., & Boyle, E. (1990). Variability of trace-metal fluxes through the Strait of Gibraltar. *Global and Planetary Change*, 3(1), 65-79.
- van Geen, A., Boyle, E. A., & Moore, W. S. (1991). Trace metal enrichments in waters of the Gulf of Cadiz, Spain. *Geochimica et Cosmochimica Acta*, 55(8), 2173-2191.
- van Geen, A., Adkins, J. F., Boyle, E. A., Nelson, C. H., & Palanques, A. (1997). A 120-yr record of widespread contamination from mining of the Iberian pyrite belt. *Geology*, 25(4), 291-294.
- Vega, M., van den Berg, C.M.G.: Determination of cobalt in seawater by catalytic adsorptive cathodic stripping voltammetry. *Analytical Chemistry* 69 (5), 874–881. 1997.
- Vidussi, F., Claustre, H., Manca, B. B., Luchetta, A., & Marty, J. C. (2001). Phytoplankton pigment distribution in relation to upper thermocline circulation in the eastern Mediterranean Sea during winter. *Journal of Geophysical Research: Oceans (1978-2012)*, 106(C9), 19939-19956.
- Wu, P., & Haines, K. (1998). The general circulation of the Mediterranean Sea from a 100 year simulation. *Journal of Geophysical Research: Oceans (1978–2012)*, 103(C1), 1121-1135.

- Yığiterhan, O., Murray, J. W., & Tuğrul, S. (2011). Trace metal composition of suspended particulate matter in the water column of the Black Sea. *Marine Chemistry*, 126(1), 207-228.
- Zhang, H., Wollast, R., Vire, J. C., & Patriarche, G. J. (1989). Simultaneous determination of cobalt and nickel in sea water by adsorptive cathodic stripping square-wave voltammetry. *Analyst*, 114(12), 1597-1602.
- Zhang, H., and Wollast, R.: Distributions of dissolved cobalt and nickel in the Rhone and the Gulf of Lions, Commission of the European Communities, Blanes, Spain20, 397-414, 1990.



# **Conclusion générale**



# Conclusion générale

Ce travail de doctorat est une contribution majeure aux études en cours visant à déterminer les processus impliqués dans le cycle biogéochimique du cobalt en milieu marin. Les objectifs visés étaient : i) d'évaluer la faisabilité de combiner des jeux de données de cobalt dissous provenant de différents laboratoires utilisant différentes techniques; ii) d'améliorer les résolutions spatiale et verticale des concentrations en cobalt en milieu océanique; iii) d'identifier et de quantifier les processus qui contrôlent la distribution du cobalt dans les océans en intégrant les échelles spatiale et temporelle ; iv) de progresser sur l'étude des interactions existantes entre le cobalt et le phytoplancton marin.

Afin de répondre à ces objectifs, ces travaux se sont basés sur l'observation en milieu océanique. Des échantillons d'eau de mer et de particules marines provenant de domaines océaniques contrastés géographiquement, et en termes de ventilation et de fonctionnement biogéochimique.

## 1) Efforts analytiques

### 1.1 Exercices GEOTRACES d'inter-calibration et d'inter-comparaison

Dans le cadre des exercices d'inter-calibration menés par le programme international GEOTRACES, nos analyses du cobalt dissous dans les eaux de références SAFE et GEOTRACES après UV oxydation sont comprises dans les rangs d'incertitudes des valeurs de consensus fournies par différents laboratoires utilisant différentes techniques d'analyse. Ces exercices valident donc notre méthode d'analyse, et montrent que différentes techniques peuvent être utilisées pour l'analyse de DCo dans un même échantillon acidifié et traité aux UV.

En revanche, les exercices de comparaison des concentrations de DCo aux stations conjointes des sections GEOTRACES révèlent des écarts significatifs ( $0 < \sigma < 35\%$ , avec  $\sigma_{moyen} \sim 15\%$ ) entre les mesures des différents laboratoires (Chapitre 1). Ces différences peuvent intégrées des différences d'instrumentation utilisée dans le prélèvement des échantillons, de mode de filtration des échantillons, et/ou de leur mode de conservation. Elles peuvent aussi être liées à une variabilité temporelle de la distribution de DCo, puisque les stations ont été prélevées à différentes saisons ou années au cours des différentes campagnes

océanographiques qui ont lieu dans le cadre de GEOTRACES depuis 2008. Nos travaux ont montré effectivement que la saisonnalité est un facteur important dans la distribution du cobalt dissous en surface (Dulaquais et al., 2014b) et en profondeur (Dulaquais et al., 2014) dans l'Atlantique Nord-Ouest. Cette saisonnalité a aussi été récemment reportée en Atlantique Sud-Est (Wyatt, 2014).

Sous couvert d'un regard critique quant aux saisons et aux domaines étudiés, l'inter-comparaison entre les différents jeux de données de cobalt dissous provenant des différents laboratoires impliqués dans le programme international GEOTRACES est envisageable.

### *1.2 Une cartographie du cobalt dans les eaux marines*

Ces travaux ont considérablement augmenté la résolution spatiale et verticale du cobalt dissous et particulaire en milieu océanique. Ces travaux rapportent l'un des jeux de données le plus important, comptabilisant 1261 analyses d'échantillons de cobalt dissous (DCo), 310 analyses de cobalt particulaire (PCo), 211 analyses de cobalt soluble (sCo) et 211 analyses de cobalt colloïdal (cCo). En Atlantique Ouest le long de la section GEOTRACES-A02, 47 profils de DCo et 15 profils de PCo ont été analysés au sein de 5 domaines biogéochimiques différents couvrant ainsi la totalité de ce bassin en terme de latitudes (64°N à 50°S) ainsi qu'en terme de profondeurs (8 à 5810 m). Par ailleurs, 5 profils de surface (0-300 m) ont été analysés le long de la dérive Nord Atlantique, ainsi que 4 profils de DCo et 2 profils de PCo en Atlantique Est sur la section GEOTRACES-A04N. En Mer Méditerranée le long de la section GEOTRACES-A04N, 25 profils de DCo et 15 profils de PCo ont été analysés couvrant ainsi l'ensemble des différents bassins, à l'exception de la Mer Adriatique. En Mer Noire, les concentrations ont été déterminées pour 6 profils de DCo et 2 profils de PCo, le long de la section GEOTRACES-A04N, du Bosphore à la partie la plus orientale du bassin.

Le fractionnement en tailles du DCo a été déterminé pour la première fois dans l'Atlantique Nord en surface, et en Mer Méditerranée sur toute la colonne d'eau. Les fractions solubles ( $sCo < 0.02 \mu\text{m}$ ) et colloïdales ( $0.02 \mu\text{m} < cCo < 0.2 \mu\text{m}$ ) ont été analysées à 25 stations.

Avec cet effort analytique considérable, ces travaux constituent une contribution importante au programme international GEOTRACES.

## **2) Distribution et comportement du cobalt dans les eaux profondes**

A l'issus de ces travaux, l'ensemble des analyses a révélé que le DCo adopte différentes distributions verticales dans les différents domaines biogéochimiques étudiés (Figure 1).

### 2.1 Distribution verticale

Aux hautes latitudes de l'Atlantique Ouest, le profil de DCo est de type conservatif, alors que dans les gyres subtropicaux il est de type nutritif à tendance hybride (Figure 1). Dans le domaine équatorial, la distribution verticale de DCo est de type hybride avec des concentrations élevées dans la couche du minimum d'oxygène (Figure 1). Aux latitudes tempérées ( $40^{\circ}\text{N}$ ), la distribution du DCo est également hybride à l'Ouest et l'Est du Bassin Atlantique (Figure 1). Les concentrations de DCo varient de 14 à 94 pM en Atlantique Ouest. La distribution verticale de PCo dans l'Atlantique Ouest (0-19 pM) montre généralement des concentrations plus élevées dans les eaux de surface et au dessus des sédiments que dans les eaux intermédiaires et profondes qui sont extrêmement pauvres en PCo. Les concentrations de surface en DCo et PCo varient selon les domaines biogéochimiques traversés dans l'Atlantique Ouest.

En Mer Méditerranée, la distribution verticale de DCo est de type scavengé dans l'ensemble du bassin (Figure 1), avec des concentrations en DCo variant de 28 à 353 pM. Ainsi, à l'inverse de l'Atlantique Ouest, les concentrations en DCo y sont plus élevées en surface qu'en profondeur. Les concentrations de DCo dans les eaux profondes sont homogènes dans l'ensemble du Bassin Méditerranéen, contrairement à celles des eaux de surface qui décrivent un gradient Ouest-Est. L'étude de la fraction particulaire ( $1 < \text{PCo} < 159$  pM) a quant-à-elle mis en évidence, comme en Atlantique, des concentrations plus élevées en surface et au-dessus du sédiment qu'en eaux profondes caractérisées par de très faibles concentrations. Les plus fortes concentrations de PCo ont été enregistrées aux abords des marges continentales et au niveau des détroits.

En Mer Noire, la distribution de DCo (29 pM-6.6 nM) montre un profil de type « anoxique » (Figure 1). Des concentrations extrêmement élevées en DCo ont été enregistrées en Mer Noire, avec des maxima dans la partie supérieure de la couche sulfidique ( $> 4$  nM). Les concentrations en PCo sont elles aussi élevées ( $5 < \text{PCo} < 623$  pM) en Mer Noire, à la différence de DCo les maxima de PCo sont observés dans la couche anoxique.

L'ensemble de notre étude concernant le fractionnement en tailles du DCo révèle que le cobalt dissous existe majoritairement ( $> 85\%$ ) sous forme soluble en Méditerranée, et également dans les eaux de surface de l'Atlantique Nord. La fraction colloïdale n'est significative en Méditerranée qu'en surface et proche du fond.

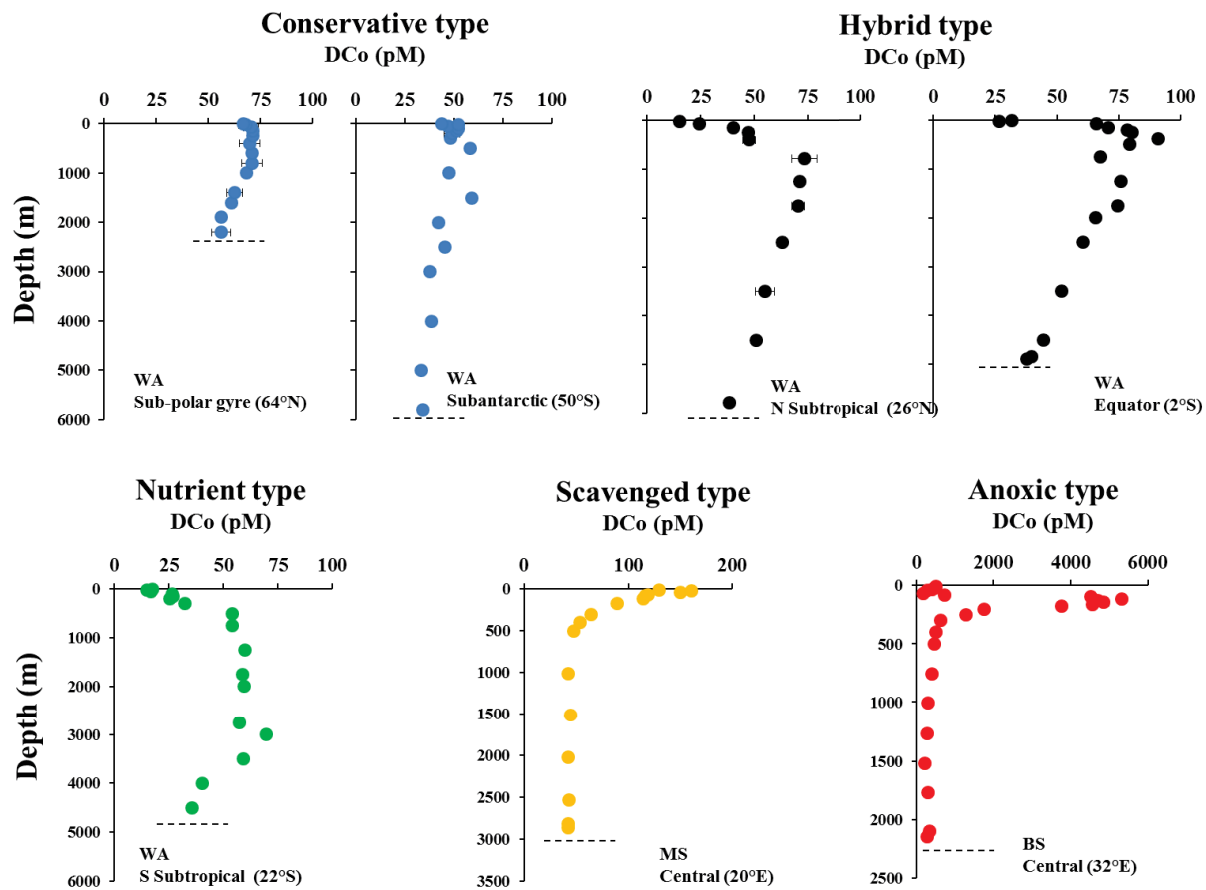


**Figure 1:** Typical vertical distributions of DCo observed during this study  
(WA = West Atlantic, MS = Mediterranean Sea, BS = Black Sea)

## 2.2 Processus contrôlants la distribution verticale dans les eaux intermédiaires et profondes

Ces travaux mettent en évidence l'importance de la circulation océanique et des processus de mélange de grande échelle sur la distribution verticale du cobalt dissous dans les eaux intermédiaires et profondes des bassins oxygénés. Ils montrent aussi l'importance des processus chimiques d'adsorption-désorption du cobalt à la surface des oxydes de fer et de manganèse dans les eaux anoxique et sulfidique.

### 2.2.1 Océan Atlantique

Les eaux intermédiaires et profondes de l'Atlantique sont caractérisées par des signatures spécifiques en DCo (Figure 2 ; Dulaquais et al., 2014). Grâce à celles-ci et à la quantification des mélanges le long de la circulation des masses d'eau, nous avons pu montrer que la diminution des concentrations en DCo observée le long de la circulation thermohaline résulte de mélanges entre les Eaux Profondes Nord Atlantique riches en DCo et les Eaux Antarctiques de Fond pauvres en DCo, plutôt que de processus de scavenging (Figure 2 ; Dulaquais et al., 2014).

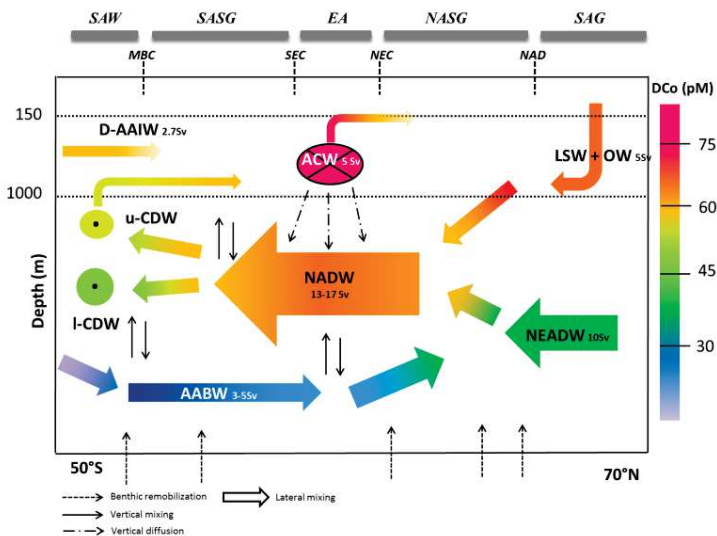


**Figure 2:** Conceptual schema of the DCo transportation along the large-scale circulation in the western Atlantic. In Dulaquais et al., 2014

En effet, les très faibles concentrations et l'absence d'augmentation de PCo dans les eaux intermédiaires et profondes, suggèrent que le scavenging ne serait pas un processus significatif. L'absence de corrélation entre le DCo et le manganèse dissous (DMn, Figure 3) vient appuyer cette idée en montrant que l'adsorption de DCo à la surface des oxydes de manganèse n'est pas significative dans les eaux profondes de l'Atlantique Ouest (Dulaquais et al., 2014). Des travaux très récents montrent d'ailleurs que la cinétique de formation des oxydes de manganèse dans l'Atlantique profond est lente, et également indépendante de l'activité bactérienne (Wu et al., 2014).

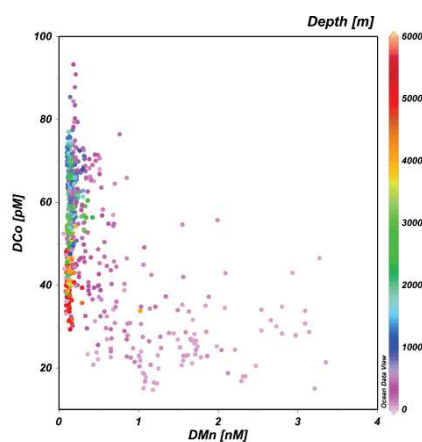


**Figure 3:** Scatter plot of DCo vs DMn in the West Atlantic. Colorbar as depth. DMn from Rob Middag pers. Comm.

Nos travaux montrent aussi que l'advection des Eaux Centrales Atlantiques enrichies en DCo sur les bords Est de l'Atlantique, et la minéralisation du matériel détritique biogénique le long de leur transport, seraient une source importante de DCo pour les eaux intermédiaires de Atlantique Ouest (Dulaquais et al., 2014). Les concentrations en DCo sont plus élevées dans ces eaux qu'en profondeur, générant le profil de type hybride observé dans la zone équatoriale de l'Atlantique Ouest.

### 2.2.2 Mer Méditerranée

La circulation contrôlerait principalement la distribution du DCo dans les eaux intermédiaires et profondes Méditerranéennes (Figure 4). Due à une rapide ventilation du bassin profond, les concentrations de DCo sont y quasi-constantes, dessinant un profil type conservatif au-dessous de 1000 mètres. Par ailleurs, résultant d'une forte stratification, les eaux de surface riches en DCo et les eaux profondes appauvries interagissent peu, à l'exception des zones de formation d'eaux intermédiaires et profondes. Les concentrations en DCo dans les eaux intermédiaires sont relativement constantes et élevées, résultant de son processus de formation. Ces eaux se forment en effet par convection du bord inférieur des eaux de surface ( $\text{DCo} > 100 \text{ pM}$ ) qui se mélangent au bord supérieur des eaux profondes ( $\text{DCo} < 60 \text{ pM}$ ). Le découplage entre la surface et les réservoirs profonds, ainsi que la circulation profonde induisent une perte de DCo dans le Bassin Oriental qui se produit au passage du détroit de Sicile, ainsi que dans le Bassin Occidental au passage de Gibraltar (Figure 4). De ce fait, le DCo ne s'accumule pas dans les eaux profondes de Méditerranée. En estimant les flux, nous avons pu montrer que les pertes de DCo aux détroits seraient compensées par la convection des eaux intermédiaires plus riches en DCo vers les eaux profondes ainsi que par remobilisation sédimentaire de PCo et sa dissolution. Nous avons aussi montré que la minéralisation, la diffusion verticale et le scavenging n'impactent pas de manière significative la distribution de DCo en profondeur.

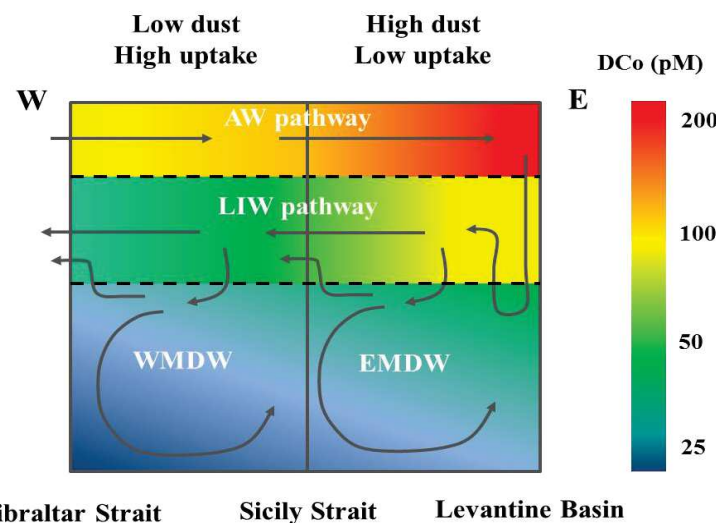


**Figure 4:** Conceptual schema of the DCo transportation in the Mediterranean Sea. Colorbar as the DCo concentration. Arrows represent a simplistic marine circulation of the basin

Dans les eaux de fond Méditerranéennes, la distribution du PCo serait principalement régie par des apports sédimentaires au-dessus des fonds et des marges. En effet, les concentrations très élevées en PCo ( $> 20$  pM) sont enregistrées près des plateaux et des fonds marins, alors qu'en bassin ouvert les concentrations sont faibles ( $< 5$  pM). Nous avons d'autre part observé de fortes corrélations entre le cobalt et le manganèse dans la phase particulaire, mais qui ne sont pas observées dans la phase dissoute (Rob Middag, communication personnelle). Les rapports PCo/PMn diminuent de plus avec la profondeur. L'état d'avancement des travaux ne permet de déterminer si ces découplages résultent de différentes assimilations biologiques dans les eaux de surface ou de réactions physico-chimiques dans la colonne d'eau.

### 2.2.3 Mer Noire

Dans la Mer Noire, les concentrations en DCo et PCo enregistrées étaient extrêmement élevées par rapport aux autres systèmes marins. A l'inverse des Bassins de l'Atlantique Ouest et de la Méditerranée, la circulation ne semble que très peu impacter la distribution verticale de DCo. La distribution verticale de DCo (Figure 5) et celle de PCo sont principalement dirigées par des processus oxydo-reductifs et de transfert entre ces deux phases. La dissolution de particules terrigènes drainées par les apports fluviaux pourrait également être une source de DCo dans les eaux de surface. En se basant sur la forte augmentation conjointe et proportionnelle des concentrations en PCo et PMn, et sur la diminution associée en DCo, nous avons suggéré que les processus d'adsorption à la surface des oxydes de manganèse contrôleraient la distribution de DCo dans les couches suboxique et anoxique. Ces oxydes de manganèse sont réduits dans la couche supérieure sulfidique et libèrent du DCo. Le DCo s'accumule dans cette couche stable, ce qui est à l'origine des plus fortes concentrations en DCo relevées dans cette étude. En dessous de ce maximum, les équilibres chimiques montrent que le DCo est stabilisé par complexation avec les sulfures, et la corrélation PCo-PFe que nous avons observé suggère qu'il est aussi soustrait par adsorption sur les oxydes de fer. L'utilisation d'un modèle chimique (Minteq®) laisse penser qu'il y aurait une compétition entre les sulfures et des ligands organiques pour complexer le DCo. L'état d'avancement actuel de ces travaux ne permet cependant pas de le vérifier.

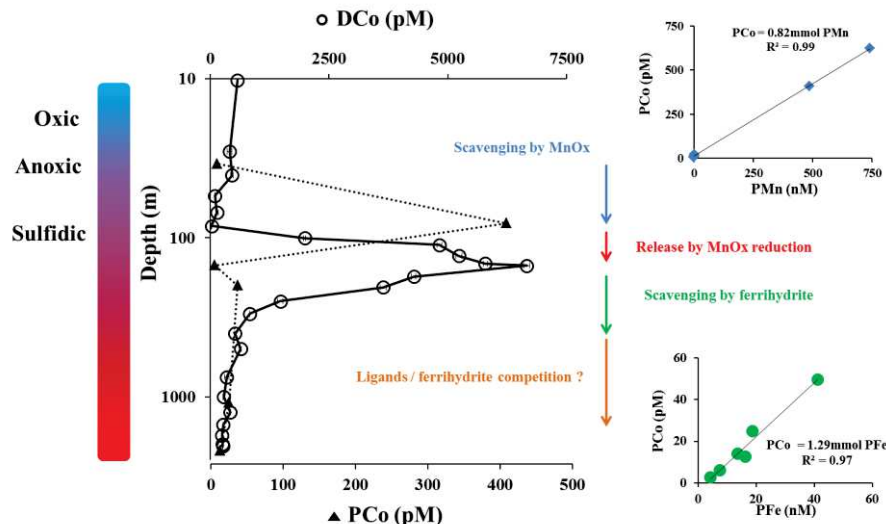


**Figure 5 :** The vertical distribution of DCo (open dots) and PCo (Dark triangles) in the Black Sea is function of the state of oxygenation (colorbar). DCo is scavenged by MnOx in anoxic waters and by FeOx in Sulfidic waters

### 2.3 Minéralisation préférentielle

La corrélation  $\Delta\text{DCo}-\Delta\text{P}$  que nous avons observé dans la zone de minéralisation en Atlantique Ouest est significativement inférieure aux quotas cellulaires phytoplanctoniques (Ho et al., 2003 ; Twining and Baines, 2013), suggérant une minéralisation préférentielle du phosphore par rapport au cobalt. En Méditerranée, l'absence de corrélation DCo-UAO alors que P est corrélé à l'UAO, suggère aussi une minéralisation préférentielle du phosphore, et indique de plus que le cobalt particulaire détritique n'est pas minéralisé dans ce bassin.

La minéralisation préférentielle du phosphore par rapport au cobalt pourrait expliquer l'enrichissement en Co par rapport au P observé dans les particules sédimentantes (Sherell and Boyle, 1992, Dulaquais et al., 2014), ainsi que le découplage entre les cycles de ces deux éléments dans les eaux profondes (Dulaquais et al., 2014).

## 3) Cycle biogéochimique dans les eaux de surface

### 3.1 Océan Atlantique

En Atlantique Ouest, nous avons réalisé la première tentative de budget du DCo à l'échelle d'un océan. Ce budget a mis en évidence que l'assimilation biologique est le principal facteur contrôlant la distribution de surface du DCo, comme l'indique aussi son profil nutritif en surface. De plus, les différentes corrélations stœchiométriques entre DCo et P, et ce budget, nous ont aussi permis de montrer que le flux d'assimilation dépendait des

espèces phytoplanctoniques les plus abondantes. Ainsi dans les eaux oligotrophes de la Mer des Sargasses peuplée de cyanobactéries, l'assimilation de DCo ( $\sim 65 \text{ nmol.m}^{-2}.\text{j}^{-1}$ ) est plus importante que dans les eaux mésotrophes du Bassin Argentin ( $\sim 20 \text{ nmol.m}^{-2}.\text{j}^{-1}$ ) peuplée de diatomées. L'assimilation du cobalt plus importante dans les eaux oligotrophes que mésotrophes indique, de plus, qu'elle n'est pas proportionnelle à la biomasse ce qui est une particularité de ce micro-nutritif (Dulaquais and Boye, *in review*). D'autre part, l'estimation des fractions biogénique et lithogénique du PCo indique une origine biogénique du PCo dans la couche de mélange des gyres oligotrophes ( $\sim 90 \%$ ) contrairement aux autres domaines où PCo serait majoritairement d'origine lithogénique (Dulaquais and Boye, *in review*).

Les corrélations stœchiométriques entre DCo et P ont souvent été décrites dans la littérature comme représentatives de l'assimilation biologique du cobalt par rapport à celle du P (Saito and Moffett, 2002 ; Noble et al., 2008 ; Saito et al., 2010 ; Bown et al., 2011). Cependant nous avons suggéré que ces pentes ne représenteraient pas l'assimilation réelle mais l'assimilation nette (assimilation - régénération), masquant ainsi le flux d'assimilation biologique du DCo par rapport à P. Ceci est par ailleurs illustré par la différence entre les corrélations stœchiométriques DCo:P enregistrées dans les eaux de surface Atlantique (22 - 65  $\mu\text{M:M}$  ; Dulaquais et al., 2014b) et les mesures de composition élémentaires du phytoplancton océanique (100-500  $\mu\text{mol:mol}$ ; Twining and Baines, 2013).

Nos travaux suggèrent ainsi de considérer l'ensemble des flux impliqués dans les cycles de DCo et P pour interpréter les corrélations DCo-P ( $\Delta\text{DCo}/\Delta\text{P} = \Sigma\text{FluxDCo}/\Sigma\text{FluxP}$ ), plutôt que seuls les flux biologiques (Dulaquais et al., 2014b). Ceci nous a permis de quantifier pour la première fois, sous conditions de non-équilibre, le flux de régénération dans les différents domaines biogéochimiques de l'Atlantique Ouest (Dulaquais et al., 2014b). Ce flux représente près de 80% du taux d'assimilation dans les gyres subtropicaux, alors qu'aux hautes latitudes il représente moins de 30%.

Si les cycles biogéochimiques du DCo et du PCo peuvent être globalement décrits dans les eaux de surface de l'Atlantique Ouest par les processus d'assimilation et de régénération ; et par l'assimilation, la régénération et l'export, respectivement, les sources externes (Amazone, apport atmosphériques) dans l'hémisphère nord, et les apports induits par la circulation (advection-diffusion latérale et verticale) aux hautes latitudes et dans la zone équatoriale, sont aussi à prendre en compte dans le budget du cobalt en surface. L'apport en DCo par l'Amazone en est un exemple, puisqu'il représente jusqu'à 50% de l'inventaire de

DCo présent dans la couche de mélange, y compris à des centaines de kilomètres de son embouchure (Dulaquais et al., 2014b).

L'estimation de l'ensemble des sources et des puits nous a permis de déterminer les temps de résidence du DCo et du PCo dans les premiers 100 mètres, en prenant pour la première fois en compte le recyclage biologique cet élément (Dulaquais et al., 2014b). Aux hautes latitudes, le temps de résidence du DCo est court et gouverné par des processus physiques ( $\sim 0.7$  ans), au contraire des gyres subtropicaux où il est plus long ( $\sim 1.5$  ans) du fait de la régénération du cobalt dans la couche de surface (représentant  $>80\%$  du taux d'assimilation). Par ailleurs, ces estimations ont indiqué que le temps de résidence du DCo n'est pas régi par l'apport atmosphérique en Atlantique Ouest (Dulaquais and Boye, *in review*).

Les budgets que nous avons établis indiquent qu'aucun domaine biogéochimique n'est à l'état d'équilibre ( $\Sigma\text{Flux} \neq 0$ ). Cependant à l'échelle du Bassin Atlantique Ouest, le budget est équilibré (Dulaquais et al., 2014b). Ce résultat souligne l'importance du transport méso-(tourbillons) et grande échelle (eaux intermédiaires) dans les échanges de DCo des domaines sources (hautes latitudes) aux domaines puits (gyres subtropicaux).

### 3.2 Mer Méditerranée

Nous avons montré que l'une des principales sources de DCo au Bassin méditerranéen est l'apport au niveau du détroit de Gibraltar par l'entrée des Eaux Atlantique, lesquelles sont enrichies en DCo par l'apport des eaux du Golfe de Cadix. Les eaux du Golfe de Cadix sont en effet alimentées par les fleuves espagnols Rio Tinto et Rio Odiel qui s'écoulent sur le bassin versant de l'*« Iberian Pyrite belt »*, particularité géologique du Dévonien dont la teneur en cobalt est importante (Marcoux et al., 1996). Le lessivage et l'exploitation minière de ce système nourrissent ainsi indirectement les eaux de surfaces Méditerranéennes en cobalt. Nous avons estimé que cet apport fournit une quantité importante de DCo à la couche de surface ( $+ 70 \text{ pmol.l}^{-1}$ ). Ce DCo « préformé » est ensuite redistribué à l'ensemble du bassin par la circulation des eaux de surface.

La distribution spatiale du DCo en Mer Méditerranée montre une asymétrie entre l'est et l'ouest, avec un gradient de concentrations Ouest-Est. Nous avons suggéré que cette asymétrie serait due à une combinaison de plusieurs processus: i) une intensification de l'oligotrophie induisant une diminution de l'assimilation biologique du DCo, vers l'Est; ii) une régénération du cobalt biogénique plus importante à l'Est; iii) un dépôt atmosphérique

plus élevé dans le Bassin Oriental qu'Occidental; iv) des apports par les marges plus intenses dans l'Est, en particulier près de l'archipel Grec ; v) un apport de type estuaire dans le Bassin Oriental, des Mers Adriatique et Noire enrichies en DCo.

### 3.3 Le fractionnement en taille de DCo

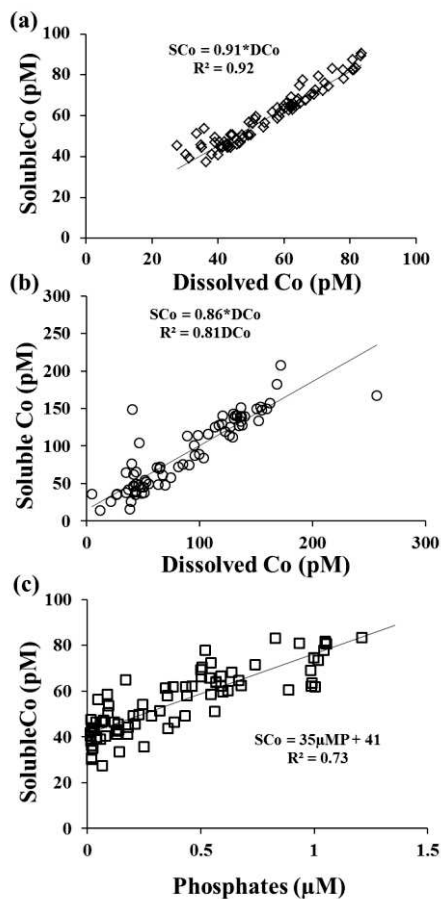


**Figure 6 :** Soluble cobalt (DCo) versus dissolved cobalt (sCo) (a) in the surface North Atlantic Ocean; (b) in the Mediterranean Sea. (c) sCo –P correlation observed in the North Atlantic

L'étude pionnière du fractionnement en taille de DCo réalisée dans ces travaux indique que le cobalt dissous est principalement sous la forme soluble (< 0.02 µm ; Figure 6). Le sCo pourrait être la fraction bio-assimilable, comme le suggère la corrélation sCo-P que nous avons enregistrée en Atlantique Nord (Figure 6c).

La fraction colloïdale n'est significative qu'en sub-surface, dans le maximum de chlorophylle, ainsi que, dans une moindre mesure, au dessus du sédiment profond. L'oxydation photochimique de Co(II) en Co(III) (peu soluble) en sub-surface pourrait conduire à la formation du cobalt colloïdal. Dans le maximum de chlorophylle, la dégradation de résidus cellulaires, les produits d'excrétion cellulaire et la désorption pourraient constituer des sources de cobalt colloïdal. De plus, les diminutions de cCo observés avec la profondeur au-dessous du maximum de chlorophylle suggèrent une voie d'export de cobalt dissous de la couche de surface par agrégation et/ou adsorption des colloïdes à la surface des particules sédimentantes. Les maxima relatifs de cCo enregistrés au dessus du sédiment pourraient être liés au relargage de Co<sup>2+</sup> issus de la diagénèse du sédiment de surface, et sa rapide complexation sous forme d'agrégats ou d'oxyde avec le Mn<sup>2+</sup> produit aussi par diagénèse.

colloïdes à la surface des particules sédimentantes. Les maxima relatifs de cCo enregistrés au dessus du sédiment pourraient être liés au relargage de Co<sup>2+</sup> issus de la diagénèse du sédiment de surface, et sa rapide complexation sous forme d'agrégats ou d'oxyde avec le Mn<sup>2+</sup> produit aussi par diagénèse.

## 4) Apports atmosphériques

### 4.1 Développement de nouveaux modèles

L'apport atmosphérique est généralement considéré comme une source majeure des éléments traces à l'océan ouvert. Dans ces travaux, un effort important sur la quantification du dépôt de poussières atmosphériques et des apports atmosphériques en cobalt a été apporté. Nous avons proposé des améliorations du modèle MADCOW développé par Measures and Vink (2000). Ce modèle basé sur les concentrations en aluminium dissous dans les eaux de surface présentait en effet de grandes différences par rapport à d'autres simulations basées sur des mesures de terrain du dépôt atmosphérique (Figure 7). Notre optimisation qui a consisté à inclure des facteurs clefs tels que la variabilité spatiale des taux de dissolution et des temps de résidences, a ainsi permis de diminuer considérablement ces écarts (Figure 7).

Nous avons également développé un nouveau modèle pour estimer l'apport atmosphérique à partir des concentrations particulières en éléments traces dans les eaux de surface. Ce nouveau modèle DIPA (Dust Inferred by Particulate Aluminum seawater concentration) permet non seulement d'estimer l'apport atmosphérique « near real time » (échelle du jour), mais aussi de déterminer l'une des caractéristiques importantes de l'aérosol, sa composition en éléments traces.

Ces modèles ont été utilisés pour estimer les apports atmosphériques en poussières et en cobalt en Atlantique Ouest (MADCOW-modified) et en Méditerranée (DIPA).

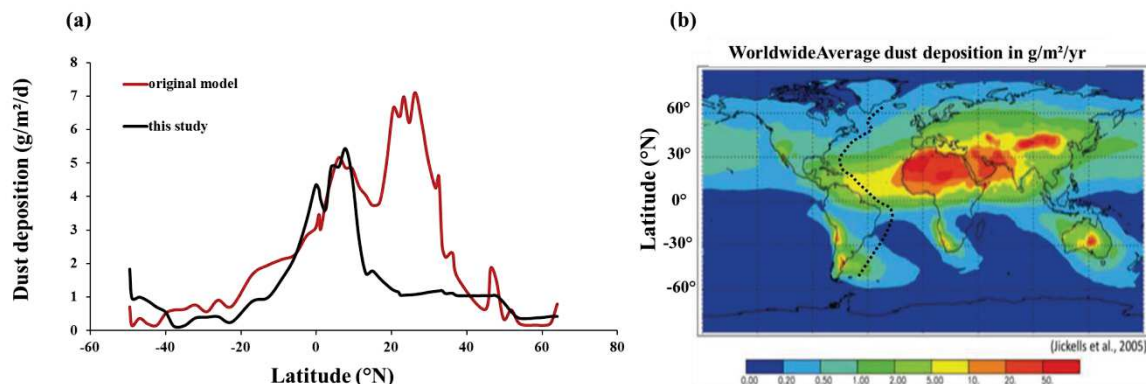


**Figure 7:** (a) Comparison of dust deposition estimation using modified MADCOW model (dark line; Dulaquais et al., 2014b) and historical MADCOW model (red line; Measures and Vink, 2000) using the same dissolved aluminum concentration recorded along the GA02 section (Rob Middag, pers. comm.). (b) Actual most popular dust deposition model (Mahowald et al., 2005; Jickells et al., 2005). Dashed line represent the GA02 cruise track

#### 4.2 Apport atmosphérique de cobalt dissous

Nos estimations montrent que l'apport atmosphérique en cobalt dissous dans les eaux de surface varie de  $< 0.05 \text{ nmol.m}^{-2}.\text{j}^{-1}$  en Atlantique Sud-Ouest à plus de  $9 \text{ nmol.m}^{-2}.\text{j}^{-1}$  dans le Bassin Oriental de la Mer Méditerranée, soit plus de deux ordres de grandeur. L'apport moyen en DCo au Bassin Atlantique est 4 à 5 fois plus faible qu'en Méditerranée, ce qui est également reflété par les concentrations de DCo 4 à 5 fois plus faibles dans les eaux oligotrophes Atlantiques ( $\sim 30 \text{ pM}$  au Nord,  $\sim 25 \text{ pM}$  au Sud) qu'en Méditerranée ( $\sim 150 \text{ pM}$ ) (Figure 8). Par ailleurs, nous avons montré que l'apport atmosphérique de DCo pouvait varier au sein d'un même bassin (Chapitres 3-4-5).

Le dépôt atmosphérique est une source de DCo dont l'intensité comparée aux autres flux est variable selon le domaine biogéochimique et le réservoir considéré. Nous avons vu par exemple que cette source est peu significative à l'échelle de la colonne d'eau ou de la couche de surface par rapport à l'intensité des processus biologiques, et qu'au contraire elle peut se révéler importante à l'échelle de la couche de mélange.

Nous avons estimé que l'apport atmosphérique et la dissolution des aérosols représentaient moins de 10% de l'inventaire de DCo dans la couche de mélange de l'Atlantique Sud, alors qu'ils compteraient jusqu'à 80% de celui du gyre subtropical de l'Atlantique Nord (Chapitre 4). En réalisant une compilation des données de cobalt dissous actuellement disponibles pour les eaux de surface (Figure 8), l'influence des alizés transportant du matériel lithogénique au nord de la convergence intertropicale peut être détectée par de plus fortes concentrations en DCo.

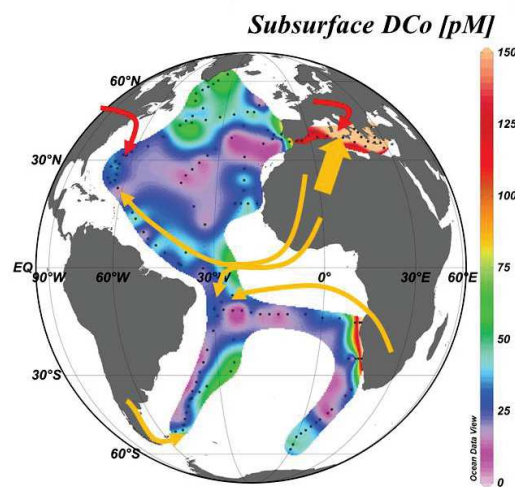


**Figure 8 :** Actual surface available UV-DCo database. Orange arrows indicate natural dust input. Red arrows indicate anthropogenic dust inputs.

#### 4.3 Interactions biogéochimiques

En comparant les abondances des cyanobactéries de type *Synechococcus* avec la spéciation organique du cobalt (Olson et al., 1990 ; Partensky et al., 1999 ; Saito et al., 2004 ; 2005), nous avons proposé que ces espèces résideraient principalement dans la couche de mélange des zones présentant de forts apports en cobalt inorganique dissous  $\text{Co}^{2+}$  (Dulaquais

and Boye, in review). D'autre part, nous avons montré que l'apport atmosphérique pouvait être la source principale de cobalt inorganique en bassin ouvert, en dehors des zones d'upwelling (Dulaquais and Boye, in review). Ainsi, nous suggérons que l'apport atmosphérique de cobalt pourrait en partie contrôler l'abondance de *Synechococcus* en océan ouvert. En effet, les forts apports atmosphériques que nous avons estimés dans le gyre subtropical Nord Atlantique sont associés à des concentrations élevées en  $\text{Co}^{2+}$  et à une population importante de *Synechococcus*, et les faibles apports dans le gyre subtropical Sud correspondent à des concentrations en  $\text{Co}^{2+}$  extrêmement faibles et à une faible abondance des *Synechococcus*. En revanche, ces relations ne sont pas observées pour les cyanobactéries de type *Prochlorococcus* dont l'abondance est similaire dans les deux gyres subtropicaux (Dulaquais and Boye, in review). La capacité des espèces *Prochlorococcus* à assimiler du cobalt organiquement lié (Saito et al., 2002) pourrait favoriser leur croissance dans les régions de faibles apports atmosphériques, pauvres en  $\text{Co}^{2+}$  (Dulaquais and Boye, in review).

Les *Synechococcus* sont capables de synthétiser et de sécréter de grandes quantités de vitamine  $\text{B}_{12}$ , essentielle pour une majorité d'eucaryotes (Bonnet et al., 2010). La biodisponibilité de la  $\text{B}_{12}$ , dans les eaux pourrait contrôler le taux de croissance et la distribution spatiale de beaucoup d'eucaryotes en milieu marin (Sañudo-Wilhelmy et al., 2006; Panzeca et al., 2006; Bertrand et al., 2007; Gobler et al., 2007, Koch et al., 2011). De plus, il a été montré que de forts apports en cobalt inorganique dissous augmentaient la synthèse de cette vitamine (Panceza et al., 2008). Ainsi, sur la base de ces travaux, nous avons proposé que l'apport en  $\text{Co}^{2+}$  par dissolution des aérosols dans la couche de surface pourrait contrôler non seulement l'abondance des *Synechococcus*, mais également la diversité écologique dans certains domaines biogéochimiques par un effet en cascade poussière- $\text{Co}^{2+}$ -*Synechococcus*- $\text{B}_{12}$ -eucaryotes (Figure 9 ; Dulaquais and Boye, in review).

Les concentrations en  $\text{B}_{12}$  plus élevées en Mer Méditerranée qu'en Atlantique (Bertrand et al., 2013) sont associées à une abondance de *Synechococcus* plus élevées en Méditerranée qu'en Atlantique (Agawin et al., 1998 ; Agusti et al., 2004), et comme nous l'avons vu, à des apports atmosphériques plus intenses en Méditerranée qu'en Atlantique (Chapitres 3-4-5). Ces observations viennent souligner les liens entre les apports atmosphériques en cobalt, l'abondance des *Synechococcus* et la disponibilité en  $\text{B}_{12}$ .

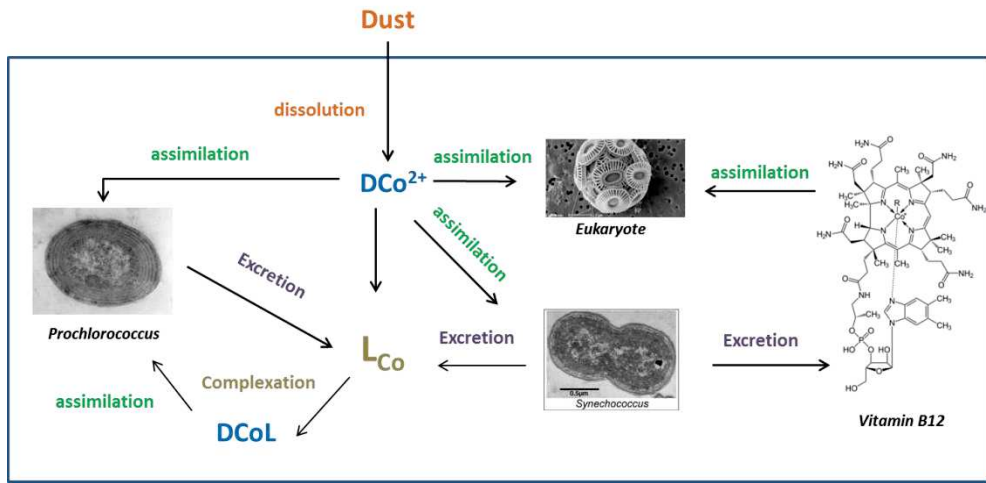


**Figure 9:** Conceptual schema of the possible interaction between the phytoplankton and the DCo provided by dust dissolution

## 5) Vue d'ensemble et perspectives

### 5.1 Représentation 0D

Dans une représentation des interactions biogéochimiques du cobalt en 0D (Figure 10), les échanges entre les différentes phases physiques et chimiques du cobalt, les processus mis en jeux dans ces interactions (biologiques, géochimiques) et leurs intensités dépendent des conditions physico-chimiques ( $h\nu$ , S,  $T^\circ$ , P) et de l'état d'oxygénation du milieu ( $O_2$ ,  $H_2S$ ), ainsi que des conditions écologiques. Ces dernières sont-elles mêmes dépendantes des conditions biogéochimiques (nutritifs,  $O_2$ ,  $h\nu$ ,  $T^\circ$ , S, P).

Dans cette représentation 0D, nous avons mis en évidence que les équilibres thermodynamiques contrôlaient les interactions de phases dans un système marin réducteur à forte pression, tel que dans les eaux profondes de la Mer Noire. En revanche, dans les eaux de surface oxygénées de l'Atlantique Ouest, ceux sont les processus biologiques qui contrôlaient ces échanges. L'intensité de ces processus biologiques dépendait de l'assemblage phytoplanctonique (i.e., cyanobactéries vs diatomées). En Méditerranée, les interactions sont contrôlées par les processus biologiques dans cette représentation 0D qui n'intègre pas de source externe de cobalt. Cependant, le forçage engendré par des apports externes intenses augmente l'importance des interactions géochimiques dans le cycle de cet élément.

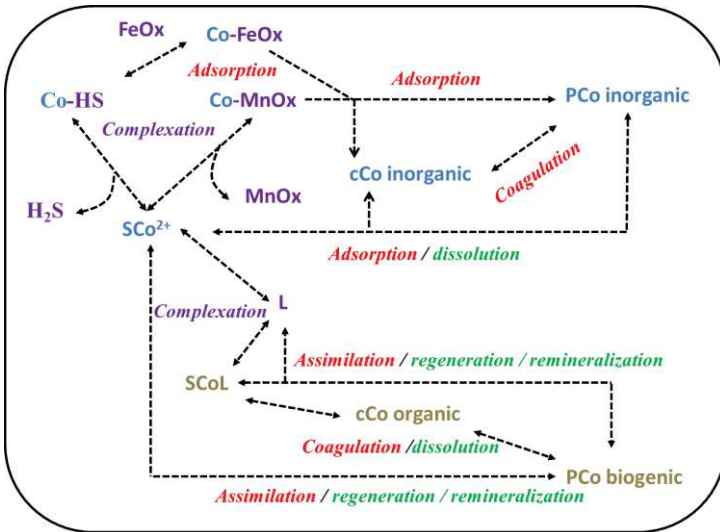


**Figure 10:** 0 dimensional conceptual schema of the interactions occurring between the different fractions in the cobalt biogeochemical cycle.

### 5.2 Représentation 1D

En intégrant la profondeur, la représentation 1D du cycle du Co (Figure 11) tient compte des sources externes et de ses puits à une profondeur donnée. En 1D, les concentrations en DCo et PCo de chaque réservoir sont contrôlées par les processus bio-géochimiques (0D), par les sources et puits dans ce réservoir, ainsi que par les processus physiques entre les différents réservoirs (advection-diffusion verticale, sédimentation). Ainsi, dans l'Atlantique Ouest, l'export est un puits de PCo pour la couche de surface (Dulaquais et al., 2014b), alors qu'il est une source de DCo pour les eaux intermédiaires et profondes par le biais du processus de minéralisation de la matière détritique (Dulaquais et al., 2014). Dans cette représentation, l'unique puits de cobalt devient l'enfouissement sédimentaire.

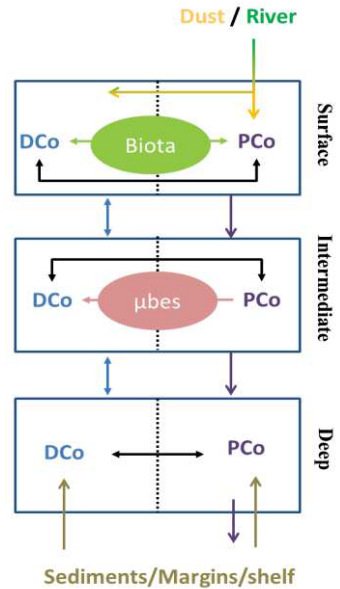


**Figure 11:** Simplistic 1 dimensional conceptual schema of the interactions occurring between the DCo and PCo pools in a 3 layers marine system. Each layer is a 0 D model

### 5.3 Représentation 3D

Dans une représentation spatiale en trois dimensions, l'advection latérale est alors intégrée dans le cycle du cobalt. Ainsi, les distributions de DCo et PCo ne sont plus uniquement régies par les échanges de phases (0D) ou par les échanges entre les différents réservoirs de la colonne d'eau (1D) mais aussi par des processus qui peuvent avoir lieu à des distances de l'ordre de  $10^3$  km. La distribution à un endroit donné peut alors être impactée par des processus biogéochimiques ayant eu lieu dans d'autres domaines après transport méso-échelle (tourbillons) à travers les fronts, ou grande échelle (circulation générale) à travers les

bassins. Nos travaux ont mis en évidence que l'étude du cycle biogéochimique du cobalt en milieu marin ne peut être détachée de la dynamique et de la circulation océanique (vision 3D), à l'exception des eaux profondes de la Mer Noire.

Grâce à une vision lagrangienne en Atlantique Ouest (section GA02), nous avons pu montrer que le profil de type hybride du DCo observé en Atlantique Ouest ne serait pas du à des processus de scavenging (1D) mais résulterait de l'advection et du mélange des masses d'eaux Arctiques et Intermédiaires enrichies en DCo avec les Eaux Antarctiques de Fond pauvres en DCo (3D ; Figure 12 ; Dulaquais et al., 2014).

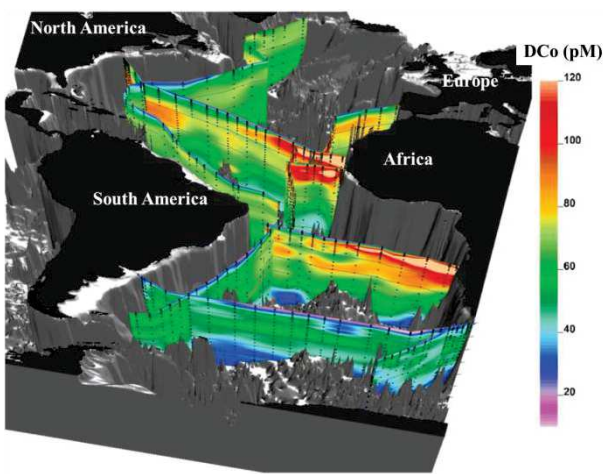


**Figure 12:** Distribution of dissolved cobalt in the Atlantic Ocean. Including data from Bown et al., 2011; Noble et al., 2012; Dulaquais et al., 2014 ; Lohan Laboratory (unpublished) and Saito laboratory (unpublished). Plot generated by Reiner Schlitzer

du programme international GEOTRACES illustrent ce transport des Eaux Intermédiaires Atlantiques enrichies en DCo (Figure 12). De plus, nous avons pu observer la remontée d'eaux intermédiaires enrichies en DCo par le biais de tourbillons cycloniques le long de la dérive Nord Atlantique (Figure 13) illustrant ainsi le transfert de DCo entre les eaux intermédiaires et la surface.

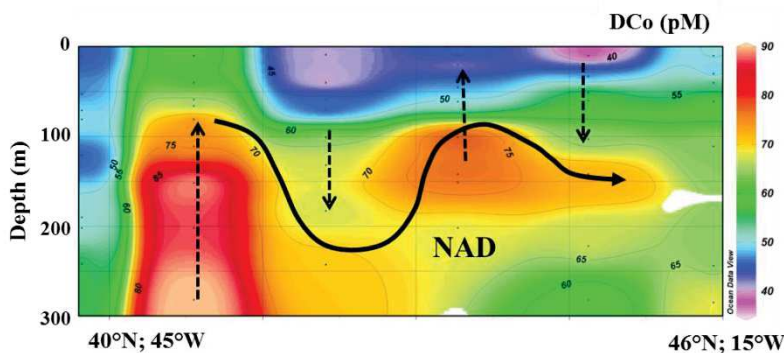


**Figure 13:** Vertical distribution of dissolved cobalt along the North Atlantic Drift (NAD). Dashed arrows indicate the direction of the vertical advection. Filled arrow indicates the pathway of the NAD

Nos travaux soulignent également la capacité d'un processus local du cycle du cobalt à impacter sa distribution à grande échelle. Le profil de type scavengé du DCo observé dans l'ensemble du Bassin Méditerranéen (grande échelle) en est un exemple puisqu'il résulte en partie du lessivage de l'Iberian Pyrite Belt (échelle locale) combiné aux particularités de la circulation Méditerranéenne.

#### 5.4 Perspectives

L'approche physique-biogéochimique intégrant les échanges aux interfaces est nécessaire pour comprendre le cycle du cobalt à grande échelle. Cependant, elle est actuellement limitée par le peu de connaissance que nous avons des processus de transferts de phases (vision 0D). La prise en compte de l'ensemble des paramètres biologiques (taxonomie, production primaire), géochimiques (spéciation, cinétique, composition multi-élémentaire, diagénèse) et physiques (export, diffusivité, advection) combinée à des études expérimentales des processus (dissolution, adsorption, assimilation biologique, régénération) permettrait d'améliorer notre compréhension du cycle de cet élément.

Un effort particulier devrait être porté à l'étude de la spéciation organique dans l'ensemble du spectre de taille du cobalt pour mieux comprendre les interactions du cobalt avec les espèces phytoplanctoniques (biodisponibilité), et les échanges entre les différentes phases (solubilité, temps de résidence). Les études expérimentales permettront de recueillir les informations indispensables sur les processus d'échanges entre les phases dissoute et particulaire, biotique et lithogénique (vision 0D). Des études conduites en incubateur en flux continu permettraient aussi de caractériser les cinétiques d'échange (adsorption, dissolution), pour différents types de matrices solides (aérosols, sédiments) de composition variée (matière organique, minéral, anthropogénique). Elles permettraient ainsi de progresser sur la caractérisation des sources et des puits de cobalt dans l'océan.

Ces études complémentaires sont indispensables pour la conception d'un modèle biogéochimique océanique tridimensionnel qui intègrerait les compétitions cinétiques de transferts de phases.

L'ensemble de ces travaux met en évidence que le cycle biogéochimique du cobalt est régi par une combinaison de phénomènes locaux et de grande échelle dont les effets peuvent être directs et indirects. Dans ce sens, le cycle du cobalt en milieu marin semble destiné à être perturbé en raison des changements environnementaux locaux (pressions anthropogéniques) ou de grande échelle (modification de la Meridional Overturning Circulation).

## Références complémentaires

- Agawin, N. S., Duarte, C. M., & Agustí, S. (1998). Growth and abundance of *Synechococcus* sp. in a Mediterranean Bay: seasonality and relationship with temperature. *Marine Ecology Progress Series*, 170, 45-53.
- Agustí, S. (2004). Viability and niche segregation of Prochlorococcus and *Synechococcus* cells across the Central Atlantic Ocean. *Aquatic microbial ecology*, 36(1), 53-59.
- Aston, S., Chester, R., & Johnson, L. R. (1972). Uptake of cobalt from seawater by Aeolian dust. *Nature*, 235, 380-381.
- Baars, O., Abouchami, W., Galer, S. J., Boye, M., & Croot, P. L. (2014). Dissolved cadmium in the Southern Ocean: Distribution, speciation, and relation to phosphate. *Limnology and oceanography*, 59(2), 385-399.
- Baeyens, W., Bowie, A. R., Buesseler, K., Elskens, M., Gao, Y., Lamborg, C., Leermakers, M., Remenyi & Zhang, H. (2011). Size-fractionated labile trace elements in the Northwest Pacific and Southern Oceans. *Marine Chemistry*, 126(1), 108-113.
- Baker, A.R., K. Weston, S.D. Kelly, M. Voss, P. Streu, J.N. Cape (2007) Dry and wet deposition of nutrients from the tropical Atlantic atmosphere: Links to primary productivity and nitrogen fixation. *Deep Sea Res. Part I*, 54, 1704 - 1720.
- Banerjee, R., & Ragsdale, S. W. (2003). The Many Faces of Vitamin B12: Catalysis by Cobalamin-Dependent Enzymes 1. *Annual review of biochemistry*, 72(1), 209-247.
- Bertrand, E. M., Saito, M. A., Rose, J. M., Riesselman, C. R., Lohan, M. C., Noble, A. E., Lee, P.A., & DiTullio, G. R. (2007). Vitamin B<sub>12</sub> and iron colimitation of phytoplankton growth in the Ross Sea. *Limnology and Oceanography*, 52(3), 1079.
- Bown, J., Boye, M., Baker, A., Duvieilbourg, E., Lacan, F., Le Moigne, F., Planchon, F., Speich, S., and Nelson, D. M. (2011), The biogeochemical cycle of dissolved cobalt in the Atlantic and the Southern Ocean south off the coast of South Africa. *Mar. Chem.*, 126, 193–206, doi:10.1016/j.marchem.2011.03.008, 2011.
- Bown, J., Boye, M., & Nelson, D. M. (2012a). New insights on the role of organic speciation in the biogeochemical cycle of dissolved cobalt in the southeastern Atlantic and the Southern Ocean. *Biogeosciences*, 9, 2719-2736.
- Bown, J., Boye, M., Laan, P., Bowie, A. R., Park, Y. H., Jeandel, C., & Nelson, D. M. (2012b). Imprint of a dissolved cobalt basaltic source on the Kerguelen Plateau. *Biogeosciences*, 9, 5279-5290.
- Bonnet, S., Webb, E. A., Panzeca, C., Karl, D. M., Capone, D. G., & Sañudo-Wilhelmy, S. A. (2010). Vitamin B12 excretion by cultures of the marine cyanobacteria *Crocospheara* and *Synechococcus*. *Limnol. & Oceanogr.*, 55(5), 1959.
- Bonnet, S., Tovar-Sanchez, A., Panzeca, C., Duarte, C. M., Ortega-Retuerta, E., & Sanudo Wilhelmy, S. A. (2013). Geographical gradients of dissolved Vitamin B12 in the Mediterranean Sea. *Frontiers in microbiology*, 4.
- Bowie, A. R., Whitworth, D. J., Achterberg, E. P., Mantoura, R. F. C., & Worsfold, P. J. (2002). Biogeochemistry of Fe and other trace elements (Al, Co, Ni) in the upper Atlantic Ocean. *Deep Sea Research Part I: Oceanographic Research Papers*, 49(4), 605-636.
- Bowie, A. R., Townsend, A. T., Lannuzel, D., Remenyi, T. A., & Van der Merwe, P. (2010). Modern sampling and analytical methods for the determination of trace elements in marine particulate material using magnetic sector inductively coupled plasma–mass spectrometry. *Analytica chimica acta*, 676(1), 15-27.
- Boyle, E. A., Slater, F., & Edmond, J. M. (1976). On the marine geochemistry of cadmium. *Nature*, 263(5572), 42-44.

- Bruland, K. W. (1980). Oceanographic distributions of cadmium, zinc, nickel, and copper in the North Pacific. *Earth and Planetary Science Letters*, 47(2), 176-198.
- Bruland, K. W. and M. C. Lohan.: Controls of trace metals in seawater, p. 23–47. In H.D. Holland and K. K. Turekian [eds.], Treatise on geochemistry, v. 6. Elsevier, 2003.
- Burns, R.G. (1965) Formation of cobalt in the amorphous FeOOH-nH<sub>2</sub>O phase of manganese nodules. *Nature* 205, 999.
- Coale, H. Buck, Distribution of dissolved trace metals at time-series sites in the Sargasso Sea. Ocean Science Meeting, Honolulu, 2014
- Ćosović, B., Degobbis, D., Bilinski, H., & Branica, M. (1982). Inorganic cobalt species in seawater. *Geochimica et Cosmochimica Acta*, 46(2), 151-158.
- Cullen, J. T., & Sherrell, R. M. (1999). Techniques for determination of trace metals in small samples of size-fractionated particulate matter: phytoplankton metals off central California. *Marine Chemistry*, 67(3), 233-247.
- Cullen, J. T., Chase, Z., Coale, K. H., Fitzwater, S. E., & Sherrell, R. M. (2003). Effect of iron limitation on the cadmium to phosphorus ratio of natural phytoplankton assemblages from the Southern Ocean.
- de Baar, H.J.W., K.R. Timmermans, P. Laan , H.H. De Porto, S. Ober, J.J. Blom, M.C. Bakker, J. Schilling, G. Sarthou, M.G. Smit and M. Klunder (2008), Titan: A new facility for ultraclean sampling of trace elements and isotopes in the deep oceans in the international GEOTRACES program. *Mar. Chem.*, 111 (1-2).
- Dyrssen, D., & Kremling, K. (1990). Increasing hydrogen sulfide concentration and trace metal behavior in the anoxic Baltic waters. *Marine Chemistry*, 30, 193-204.
- Dulaquais, G., Boye, M., Rijkenberg, M. J. A., & Carton, X. (2014), Physical and remineralization processes govern the cobalt distribution in the deep western Atlantic Ocean. *Biogeosciences*, 11(6), 1561-1580.
- Dulaquais, G., Boye, M., Middag, R., Owens, S., Puigcorbe, V., Buesseler, K., de Baar, H. & Carton, X. (2014). Contrasting biogeochemical cycles of cobalt in the surface western Atlantic Ocean. *Global Biogeochemical Cycles*, 28(12), 1387-1412.
- Dulaquais, G. and Boye, M., Atmospheric cobalt deposition along the surface west Atlantic and biogeochemical implications (in review), In review for publication in *Marine Chemistry*.
- Elbaz-Poulichet, F., Guieu, C., & Morley, N. H. (2001b). A reassessment of trace metal budgets in the western Mediterranean Sea. *Marine Pollution Bulletin*, 42(8), 623-627.
- Ellwood, M.J. and C.M.G. van den Berg, (2001). Determination of organic complexation of cobalt in seawater by cathodic stripping voltammetry, *Mar. Chem.*, 75, 33-47.
- Ellwood, M. J., van den Berg, C. M., Boye, M., Veldhuis, M., de Jong, J. T., de Baar, H. J., Croot, P.L. & Kattner, G. (2005). Organic complexation of cobalt across the Antarctic Polar Front in the Southern Ocean. *Marine and freshwater research*, 56(8), 1069-1075.
- Gaiero, D.M., Probst, J. -L., Depetris, P. J., Bidart, S. M. and Leleyter, L., (2003). Iron and other transition metals in Patagonian riverborne and windborne materials: geochemical control and transport to the southern South Atlantic Ocean. *Geochimica & Cosmochimica Acta*, 67 (19), 3603-3623.
- Gobler, C. J., Norman, C., Panzeca, C., Taylor, G. T., & Sañudo-Wilhelmy, S. A. (2007). Effect of B-vitamins (B1, B12) and inorganic nutrients on algal bloom dynamics in a coastal ecosystem. *Aquatic Microbial Ecology*, 49(2), 181-194.
- Goldberg E. D. (1954) Marine geochemistry. 1. Chemical scavengers of the sea. *J. Geol.* 62, 249-265.
- Goldberg E. D. (1961) Chemistry in the oceans. In: Oceanography, pp. 583-597.
- Guieu, C., Loÿe-Pilot, M. D., Ridame, C., & Thomas, C. (2002). Chemical characterization of the Saharan dust end-member: Some biogeochemical implications for the western

- Mediterranean Sea. *Journal of Geophysical Research: Atmospheres (1984–2012)*, 107(D15), ACH-5.
- Heimbürger, L. E., Migon, C., & Cossa, D. (2011). Impact of atmospheric deposition of anthropogenic and natural trace metals on Northwestern Mediterranean surface waters: A box model assessment. *Environmental Pollution*, 159(6), 1629-1634.
- Haraldsson, C., & Westerlund, S. (1991). Total and suspended cadmium, cobalt, copper, iron, lead, manganese, nickel, and zinc in the water column of the Black Sea. In *Black Sea Oceanography* (pp. 161-172). Springer Netherlands.
- Ho, T. Y., A. Quigg, Z. V. Finkel, A. J. Milligan, K. Wyman, P. G. Falkowski, and F. M. Morel. (2003), The elemental composition of some marine phytoplankton. *J. Phycol.* 39: 1145–1159.
- Jakuba, R.W., Moffett, J.W., Dyhrman, S.T. (2008), Evidence for the linked biogeochemical cycling of zinc, cobalt, and phosphorus in the western North Atlantic Ocean. *Global Biogeochem. Cycles*, 22 (4) , doi: 10.1029/2007GB003119.
- Jickells, T.S., An, Z.A., Baker, A.R., Bergametti, G., Brooks, N., Boyd, P.W., Duce, R.A., Hunter, K.A., Junji, C., Kawahata, H., Kubilay, N., Andersen, K.K., La Roche, J., Liss, P.S., Mahowald, N., Prospero, J.M., Ridgwell, A.J., Tegen, I., Torres, R., Global iron connections between desert dust, ocean biogeochemistry and climate. *Science*, 308, 67–71, 2005
- Koch, F., Alejandra Marcoval, M., Panzeca, C., Bruland, K. W., Sanudo-Wilhelmy, S. A., & Gobler, C. J. (2011). The effect of vitamin B12 on phytoplankton growth and community structure in the Gulf of Alaska. *Limnology and oceanography*, 56(3), 1023-1034.
- Knauer, G.A., Martin, J.H., Gordon, R.M.: Cobalt in Northeast Pacific Waters. *Nature* 297 (5861), 49–51, 1982.
- Kremling, K. (1983). The behavior of Zn, Cd, Cu, Ni, Co, Fe, and Mn in anoxic Baltic waters. *Marine Chemistry*, 13(2), 87-108.
- Kuss, J., & Kremling, K. (1999). Particulate trace element fluxes in the deep northeast Atlantic Ocean. *Deep-Sea Research Part I*, 46(1), 149-169.
- Landing, W. M., & Lewis, B. L. (1991). Thermodynamic modeling of trace metal speciation in the Black Sea. In *Black Sea Oceanography* (pp. 125-160). Springer Netherlands.
- Lane, T. W., and F. M. M. Morel (2000), Regulation of carbonic anhydrase expression by zinc, cobalt, and carbon dioxide in the marine diatom *Thalassiosira weissflogii*. *Plant Physiol.*, 123, 345–352, doi:10.1104/pp.123.1.345.
- Lane, T. W., Saito, M. A., George, G. N., Pickering, I. J., Prince, R. C., & Morel, F. M. (2005). Biochemistry: a cadmium enzyme from a marine diatom. *Nature*, 435(7038), 42-42.
- Lewis, B. L., & Landing, W. M. (1992). The investigation of dissolved and suspended particulate trace metal fractionation in the Black Sea. *Marine Chemistry*, 40(1), 105–141.
- L'Helguen, S., Chauvaud, L., Cuet, P., Frouin, P., Maguer, J. F., & Clavier, J. (2014). A novel approach using the  $^{15}\text{N}$  tracer technique and benthic chambers to determine ammonium fluxes at the sediment–water interface and its application in a back-reef zone on Reunion Island (Indian Ocean). *Journal of Experimental Marine Biology and Ecology*, 452, 143-151.
- Marcoux, E., Moëlo, Y., & Leistel, J. M. (1996). Bismuth and cobalt minerals as indicators of stringer zones to massive sulphide deposits, Iberian Pyrite Belt. *Mineralium Deposita*, 31(1-2), 1-26.

- Martin, J.H., Gordon, R.M., Fitzwater, S., Broenkow, W.W., (1989), Vertex — phytoplankton iron studies in the Gulf of Alaska. *Deep-Sea Res. Part a—Oceanographic Research Papers* 36 (5), 649.
- Martin, J.H., Fitzwater, S.E., Gordon, R.M., Hunter, C.N., Tanner, S.J., (1993), Iron, primary production and carbon nitrogen flux studies during the JGOFS North-Atlantic Bloom Experiment. *Deep-Sea Res. Part I — Topical Studies in Oceanography* 40 (1–2), 115–134.
- Martin, J. M., & Windom, H. L. (1991). Present and future roles of ocean margins in regulating marine biogeochemical cycles of trace elements. *Ocean margin processes in global change*, 45-67.
- Measures, C. I., & Vink, S. (2000). On the use of dissolved aluminum in surface waters to estimate dust deposition to the ocean. *Global biogeochemical cycles*, 14(1), 317-327.
- Moffett, J.W., Ho, J.(1996), Oxidation of cobalt and manganese in seawater via a common microbially catalyzed pathway. *Geochimica and Cosmochimica Acta*, 60 (18), 3415-3424.,
- Morel, F. M. M., & Reinfelder, R. (1994). of marine phytoplankton. *Nature*, 369.
- Morel, F.M.M., Milligan, A.J. & Saito M.A. (2003), Marine Bioinorganic Chemistry: The role of trace metals in the oceanic cycles of major nutrients In H.D.Holland and K. K. Turekian [eds.], Treatise on geochemistry, v. 6. Elsevier, 2003.
- Murray D. J., Healy T. W. and Fuerstenau D. W. (1968) The adsorption of aqueous metal on colloidal hydrous manganese oxide. *Adv. Chem. Ser.* 79, 74-81.
- Murray, J. W. (1975). The interaction of cobalt with hydrous manganese dioxide. *Geochimica et Cosmochimica Acta*, 39(5), 635-647.
- Murray, J. W., & Dillard, J. G. (1979). The oxidation of cobalt (II) adsorbed on manganese dioxide. *Geochimica et Cosmochimica Acta*, 43(5), 781-787.
- Murray, K. J., Webb, S. M., Bargar, J. R., & Tebo, B. M. (2007). Indirect oxidation of Co (II) in the presence of the marine Mn (II)-oxidizing bacterium *Bacillus* sp. strain SG-1. *Applied and environmental microbiology*, 73(21), 6905-6909.
- Ngoc, L. H., & Whitehead, N. E. (1986). Nickel and cobalt determination in the north-western mediterranean by differential pulse cathodic stripping voltammetry. *Oceanologica acta*, 9(4), 433-438.
- Noble, A. E., Saito, M. A., Maiti, K., and Benitez-Nelson, C. R. (2008). Cobalt, manganese, and iron near the Hawaiian Islands: A potential concentrating mechanism for cobalt within a cyclonic eddy and implications for the hybrid-type trace metals. *Deep-Sea Res. Part II*, 55, 1473-1490, doi:10.1016/j.dsr2.2008.02.010.
- Noble, A. E., Lamborg, C. H., Ohnemus, D. C., Lam, P. J., Goepfert, T. J., Measures, C. I., Frame, C. H., Casciotti, K. L., DiTullio, G. R., Jennings, J., and Saito, M. A. (2012). Basin scale inputs of cobalt, iron, and manganese from the Benguela-Angola front to the South Atlantic Ocean. *Limnol. & Oceanogr.*, 57, 989-1010.
- Noble, A. E., Moran, D. M., Allen, A. E., & Saito, M. A. (2013). Dissolved and particulate trace metal micronutrients under the McMurdo Sound seasonal sea ice: basal sea ice communities as a capacitor for iron. *Frontiers in chemistry*, 1.
- Panzeca, C., Beck, A. J., Leblanc, K., Taylor, G. T., Hutchins, D. A., & Sañudo-Wilhelmy, S. A. (2008). Potential cobalt limitation of vitamin B12 synthesis in the North Atlantic Ocean. *Global Biogeochemical Cycles*, 22(2).
- Planquette, H., & Sherrell, R. M. Sampling for particulate trace element determination using water sampling bottles: methodology and comparison to in situ pumps. *Limnology and Oceanography: Methods*, 10, 367-388, 2012
- Pohl, C., Croot, P.L., Hennings, U., Daberkow, T., Budeus, G., von der Loeff, M.R., 2011. Synoptic transects on the distribution of trace elements (Hg, Pb, Cd, Cu, Ni, Zn, Co,

- Mn, Fe, and Al) in surface waters of the Northern- and Southern East Atlantic. *Journal of Marine Systems* 84 (1–2), 28–41, 2011.
- Price, N. M., & Morel, F. M. M. (1990). Cadmium and cobalt substitution for zinc in a marine diatom. *Nature*, 344(6267), 658–660.
- Quigg, A., Finkel, Z. V., Irwin, A. J., Rosenthal, Y., Ho, T. Y., Reinfelder, J. R., Schofield O. , Morel F.M.M. & Falkowski, P. G. (2003). The evolutionary inheritance of elemental stoichiometry in marine phytoplankton. *Nature*, 425(6955), 291-294.
- Reid, E.A., Reid, J.S., Meier, M.M., Dunlap, M.R., Cliff, S.S., Broumas, A., (2003), Characterization of African dust transported to Puerto Rico by individual particle and size segregated bulk analysis. *J. Geophys. Res. D: Atmos.* 19, 108.
- Rijkenberg, M. J., Middag, R., Laan, P., Gerringsa, L. J., van Aken, H. M., Schoemann, V., de Jong, J.T.M. & de Baar, H. J. The Distribution of Dissolved Iron in the West Atlantic Ocean. *PloS one*, 9(6), e101323, 2014
- Rudnick, R. L., & Gao, S. (2003). Composition of the continental crust. *Treatise on geochemistry*, 3, 1-64.
- Saito, M. A. and Moffett, J. W. (2001), Complexation of cobalt by natural organic ligands in the Sargasso Sea as determined by a new highsensitivity electrochemical cobalt speciation method suitable for open ocean work. *Mar. Chem.*, 75, 49–68.
- Saito, M. A. and Moffett, J. W. (2002), Temporal and spatial variability of cobalt in the Atlantic Ocean. *Geochim. Cosmochim. Acta*, 66, 1943–1953.
- Saito, M. A., Moppett, J. W., Chisholm, S. W., & Waterbury, J. B. (2002), Cobalt limitation and uptake in Prochlorococcus. *Limnol. and Oceanogr.*, 47(6), 1629-1636..
- Saito, M. A., Sigman, D. M., & Morel, F. M. (2003). The bioinorganic chemistry of the ancient ocean: the co-evolution of cyanobacterial metal requirements and biogeochemical cycles at the Archean–Proterozoic boundary?. *Inorganica Chimica Acta*, 356, 308-318.
- Saito, M. A., Moffett, J. W., and DiTullio, G. R. (2004), Cobalt and nickel in the Peru upwelling region: A major flux of labile cobalt utilized as a micronutrient. *Global Biogeochem. Cycles*, 18, GB4030, doi:10.1029/2003GB002216.
- Saito M. A., G. Rocap, and J. W. Moffett (2005); Production of cobalt binding ligands in a Synechococcus feature at the Costa Rica Upwelling Dome. *Limnol. Oceanogr.*, 50, 279–290, doi:10.4319/lo.2005.50.1.0279.
- Saito, M. A., Goepfert, T. J., & Ritt, J. T. (2008). Some thoughts on the concept of colimitation: three definitions and the importance of bioavailability. *Limnology & Oceanography*, 53(1), 276.
- Saito, M. A., Goepfert, T. J., Noble, A. E., Bertrand, E. M., Sedwick, P. N., and DiTullio, G. R. (2010), A seasonal study of dissolved cobalt in the Ross Sea, Antarctica: micronutrient behavior, absence of scavenging, and relationships with Zn, Cd, and P. *Biogeosciences*, 7, 4059–4082, doi:10.5194/bg-7-4059-2010.
- Santelli, C. M., Edgcomb, V. P., Bach, W., & Edwards, K. J. (2009). The diversity and abundance of bacteria inhabiting seafloor lavas positively correlate with rock alteration. *Environmental microbiology*, 11(1), 86-98.
- Sañudo-Wilhelmy, S. A., Gobler, C. J., Okbamichael, M., & Taylor, G. T. (2006). Regulation of phytoplankton dynamics by vitamin B12. *Geophysical Research Letters*, 33(4), L04604.
- Shelley, R. U., Zachhuber, B., Sedwick, P. N., Worsfold, P. J., and Lohan, M. C. (2010), Determination of total dissolved cobalt in UV-irradiated seawater using flow injection

- with chemiluminescence detection. *Limnol. Oceanogr.*, 8, 352–362, doi:10.1029/2009JC005880.
- Shelley, R. U., Sedwick, P. N., Bibby, T. S., Cabedo-Sanz, P., Church, T. M., Johnson, R. J., Macey, A. I., Marsay, C. M., Sholkovitz, E. R., Ussher, S. J., Worsfold, P. J., and Lohan, M. C. (2012). Controls on dissolved cobalt in surface waters of the Sargasso Sea: Comparisons with iron and aluminum. *Global Biogeochem. Cycles*, 26 (2) GB2020.
- Sherrell, R. M., & Boyle, E. A. (1992). The trace metal composition of suspended particles in the oceanic water column near Bermuda. *Earth and Planetary Science Letters*, 111(1), 155-174.
- Sunda, W.G., and S.A. Huntsman (1995). Cobalt and zinc inter-replacement in marine phytoplankton: biological and geochemical implications. *Limnol. & Oceanogr.*, 40, 1404-1417.
- Sundby, B., Anderson, L. G., Hall, P. O., Iverfeldt, Å., van der Looff, M. M., & Westerlund, S. F. (1986). The effect of oxygen on release and uptake of cobalt, manganese, iron and phosphate at the sediment-water interface. *Geochimica et Cosmochimica Acta*, 50(6), 1281-1288.
- Spencer, D. W., & Brewer, P. G. (1971). Vertical advection diffusion and redox potentials as controls on the distribution of manganese and other trace metals dissolved in waters of the Black Sea. *Journal of Geophysical Research*, 76(24), 5877-5892.
- Spencer, D. W., Brewer, P. G., & Sachs, P. L. (1972). Aspects of the distribution and trace element composition of suspended matter in the Black Sea. *Geochimica et Cosmochimica Acta*, 36(1), 71-86.
- Swanner, E. D., Planavsky, N. J., Lalonde, S. V., Robbins, L. J., Bekker, A., Rouxel, O. J., ... & Konhauser, K. O. (2014). Cobalt and marine redox evolution. *Earth and Planetary Science Letters*, 390, 253-263.
- Tebo, B. M., Nealson, K. H., Emerson, S., & Jacobs, L. (1984). Microbial mediation of Mn (II) and Co (II) precipitation at the O/H, S interfaces in two anoxic fjords1. *Limnol. Oceanogr.*, 29(6), 1247-1258.
- Thuróczy, C. E., Boye, M., & Losno, R. (2010). Dissolution of cobalt and zinc from natural and anthropogenic dusts in seawater. *Biogeosciences*, 7(6), 1927-1936.
- Tovar-Sánchez, A., Sanudo-Wilhelmy, S. A., Kustka, A. B., Agustí, S., Dachs, J., Hutchins, D. A., Capone, D. G., Duarte, C. M. (2006). Effects of dust deposition and river discharges on trace metal composition of *Trichodesmium spp.* in the tropical and subtropical North Atlantic Ocean. *Limnol. & Oceanogr.*, 51(4), 1755–1761.
- Tovar-Sánchez, A. and Sanudo-Wilhelmy, S. A. (2011). Influence of the Amazon River on dissolved and intra-cellular metal concentrations in *Trichodesmium* colonies along the western boundary of the sub-tropical North Atlantic Ocean. *Biogeosciences*, 8, 217–225, doi:10.5194/bg-8-217-2011.
- Trapp, J. M., F. J. Millero, and J. M. Prospero (2010), Temporal variability of the elemental composition of African dust measured in trade wind aerosols at Barbados and Miami, *Mar. Chem.*, 120(1–4), 71–82, doi:10.1016/j.marchem.2008.10.004
- Twining, B. S., Baines, S. B., Bozard, J. B., Vogt, S., Walker, E. A., & Nelson, D. M. (2011). Metal quotas of plankton in the equatorial Pacific Ocean. *Deep Sea Research Part II: Topical Studies in Oceanography*, 58(3), 325-341.
- Twining, B. S., & Baines, S. B. (2013). The trace metal composition of marine phytoplankton. *Annual review of marine science*, 5, 191-215.
- Xia, L., & Gao, Y. (2010). Chemical composition and size distributions of coastal aerosols observed on the US East Coast. *Mar. Chem.*, 119(1), 77-90.

- Xu, Y., Feng, L., Jeffrey, P. D., Shi, Y., & Morel, F. M. (2008). Structure and metal exchange in the cadmium carbonic anhydrase of marine diatoms. *Nature*, 452(7183), 56-61.
- Vega, M., van den Berg, C.M.G.: Determination of cobalt in seawater by catalytic adsorptive cathodic stripping voltammetry. *Analytical Chemistry* 69 (5), 874–881. 1997.
- Wu, J., Roshan, S., & Chen, G. (2014). The distribution of dissolved manganese in the tropical-subtropical North Atlantic during US GEOTRACES 2010 and 2011 cruises. *Marine Chemistry*.
- Wyatt, N. (2014). The biogeochemistry of iron, zinc and cobalt in the Atlantic Ocean: the Atlantic meridional transect and UK GEOTRACES sections. *PhD Thesis*. University of Plymouth, 292pp.
- Zhang, H., Van Den Berg, C. M., & Wollast, R. The determination of interactions of cobalt (II) with organic compounds in seawater using cathodic stripping voltammetry. *Marine Chemistry*, 28(4), 285-300, 1990.



## **Annexes**



## **Annexe 1: Supplément au chapitre 3**

Auxiliary Material for

### **HOW TO CONSTRAIN THE BIOGEOCHEMICAL CYCLE OF COBALT IN THE SURFACE WESTERN ATLANTIC OCEAN?**

Gabriel Dulaquais

Laboratoire des Sciences de l'Environnement Marin UMR6539, Institut Universitaire Européen de la Mer, Technopôle Brest Iroise, Place Nicolas Copernic, 29280 Plouzané, France

Marie Boye

Laboratoire des Sciences de l'Environnement Marin UMR6539, Institut Universitaire Européen de la Mer, Technopôle Brest Iroise, Place Nicolas Copernic, 29280 Plouzané, France

Rob Middag

Department of Marine Chemistry and Geology, Royal Netherlands Institute for Sea Research, P.O. Box 59, 1790 AB Den Burg, The Netherlands  
Now at Department of Chemistry, University of Otago, P.O. Box 56, Dunedin 9054, New Zealand

Stephanie Owens

Woods Hole Oceanographic Institution, Woods Hole, MA 02543-1050, USA

Viena Puigcorbé

Institut de Ciencia i Tecnologia Ambientals & Department of Physics, Universitat Atonoma de Barcelona, 08193 Bellaterra, Spain

Ken Buesseler

Woods Hole Oceanographic Institution, Woods Hole, MA 02543-1050, USA

Pere Masqué

Institut de Ciencia i Tecnologia Ambientals & Department of Physics, Universitat Atonoma de Barcelona, 08193 Bellaterra, Spain

Hein de Baar

Department of Marine Chemistry and Geology, Royal Netherlands Institute for Sea Research, P.O. Box 59, 1790 AB Den Burg, The Netherlands

Xavier Carton

Laboratoire de Physique des Océans, Université de Bretagne Occidentale - UFR Sciences, 6 avenue Le Gorgeu, C.S. 93837, 29238 Brest Cedex 3, France

### *Global Biogeochemical cycles*

#### **Introduction**

The auxiliary material contains one text file, one table and two figures. S1 gives the methods of modified MADCOW model and its application to Co in order to constrain the impact of dust deposition on Co distribution in seawater (see section 4.2 in chapter 4). Figure S1 displays results of our modified madcow model for dust deposition ( $\text{g/m}^2/\text{yr}$ ) compare to other model estimations at the surface West Atlantic Ocean. Figure S2 displays results of our modified MADCOW model for residence time (yr) compare to other model estimations at the surface West Atlantic Ocean.

# Estimation of the atmospheric deposition of soluble cobalt along the GEOTRACES-A02 section

## 1) Estimation of the dust deposition

The dust deposition was inferred from the concentrations of dissolved aluminium measured in seawater along the section, following a modified version of the MADCOW model (*de Jong et al.*, 2007).

### Model:

$$\text{Dust deposition rate (g.m}^{-2}.\text{year}^{-1}) = \text{DAL} * z * M_{\text{Al}} * (\text{Ab. Al} * S_{\text{Al}} * \tau_{\text{Al}})^{-1} \quad \text{Equation 1}$$

$$\tau_{\text{Al}} = \text{DAL} * z * (\text{Scav. Al})^{-1} \quad \text{Equation 2}$$

In steady state condition  $dP_{\text{Al}}/dt = 0$ ; Scav. Al = Dust dissolution; Scav. Al can be rewritten:

$$\text{Scav. Al} = F_{\text{POC}} * (\text{PAL:POC}) * S_{\text{Al}} \quad \text{Equation 3}$$

### Conditions:

- Assuming dissolved (DAL) and particulate (PAL) aluminium are at steady state in the mixed layer, and thus that their stocks are constant.
- Assuming the dissolution of dust is the only source of DAL in the mixed layer\* and scavenging on particles its only sink; and that the sum of both is equal to zero.

\*except in the subantarctic waters where input of  $6 \text{ nmol.m}^{-2}.\text{yr}^{-1}$  is attributed to lateral advection using DAL gradient between  $40^{\circ}\text{S}$  and  $50^{\circ}\text{S}$  ( $\text{Grad}_{40^{\circ}\text{S} \rightarrow 50^{\circ}\text{S}} \text{DAL} = 4 \cdot 10^{-12} \text{ mol.m}^{-3}.\text{m}^{-1}$ ), an advection of  $30 \text{ cm.s}^{-1}$  in this area for the upper 100 meters [*Vivier and Provost, 1999*] and an area of  $0.5 \cdot 10^{12} \text{ m}^{-2}$

### Parameters:

**DAL** : mean concentration of dissolved aluminium measured in the mixed layer (in  $\text{mol.m}^{-3}$ ; Appendix 1) [R. Middag, unpublished data]

**z** : depth of the mixed layer derived from CTD data (in m; supplement 2)

**M Al** : molar mass of aluminium ( $27 \text{ g.mol}^{-1}$ )

**Ab. Al** : crustal abundance of aluminium ( $0.077 \text{ g.g}^{-1}$ ; *Rudnick and Gao [2003]*)

**S Al** : solubility of aluminium from dust (3 to 15% *Baker et al. [2013]*; supplement 2)

**τ Al** : residence time of aluminium in the mixed layer calculated using Equation 2 (in year; 0.03 - 3.6 years, supplement 2).

**Scav. Al** : scavenging of dissolved aluminium on settling particles calculated using Equation 3 (in  $\text{mol.m}^{-2}.\text{year}^{-1}$ ; supplement 2)

**F<sub>POC</sub>** : exported flux of organic carbon on settling particles (*Owens [2013]* in the southern section; *Puigcorbé et al., [in prep.]* in the northern section)

**Al:POC** : Aluminum to organic carbon ratio in particles used in the model were estimated after determination of Al:POC ratio in particles collected in the eastern Atlantic (Al:POC ~ 1-3 mmol/mol) and the Mediterranean Sea (Al:POC ~ 10mmol/mol) for low and intensive dust input areas respectively [Dulaquais *et al.*, unpublished data]. Data used are in accordance with *Sherrel and Boyle* [1992] dataset in the Sargasso Sea area

## 2) Estimation of the atmospheric deposition rate of soluble cobalt

The deposition of soluble cobalt from dust was inferred from the dust deposition rate (Equation 1) and the abundance of cobalt in dusts.

### Model

$$FCo_{atm.} = \text{Dust deposition rate} * [Co]_{dust} \quad \text{Equation 4}$$

$$FSCo = FCo_{atm.} * SCo \quad \text{Equation 5}$$

### Parameters:

**[Co]<sub>dust</sub>** : mean concentration of cobalt reported in aerosols of the West Atlantic (in g.g<sup>-1</sup>; 17 10<sup>-6</sup> - 170 10<sup>-6</sup> g.g<sup>-1</sup>; [Gaiero *et al.*, 2003; Reid *et al.*, 2003; Rudnick and Gao, 2003; Baker *et al.*, 2007; Trapp *et al.* 2010; Xia & Gao, 2010; Shelley *et al.*, 2012; Shelley *et al.*, subm.]; supplement2)

**FCo<sub>atm.</sub>** : Atmospheric deposition flux of cobalt calculated using Equation 4 (in mol.m<sup>-2</sup>.d<sup>-1</sup> using the molar mass of Co (59 g.mol<sup>-1</sup>) and the number of days per year (1 year = 365.25 d); supplement 2)

**SCo** : Cobalt fractional solubility of atmospheric particles in seawater. Without data available at date it is assumed that S Al = S Co (supplement 2). Values used are in the range of reported data [Gaiero *et al.*, 2003; Baker *et al.*, 2007; Turoczy *et al.*, 2010; Shelley *et al.*, 2012]

**F SCo** : dust deposition rate of soluble cobalt calculated using Equation 5 (in mol.m<sup>-2</sup>.d<sup>-1</sup>; supplement 2)

**Table S1:** Parameterization and output of modified MADCOW model.

Latitude (°N)	longitude (°E)	D Al (nM)	z (m)	S Al	Ab Al (g/g)	Al:POC (mmol/mol)	FPOC (mmol/m <sup>2</sup> /d)	τ DAL (yr)	F Dust (g/m <sup>2</sup> /yr)	[Co] dust (μg/g)	S Co	F Co (nmol/m <sup>2</sup> /d)	F SCo (nmol/m <sup>2</sup> /d)
64.00	-34.25	5.44	60	0.15	0.08	2	1.5	1.98	0.42	170	0.15	3.33	0.5
62.35	-36.00	1.62	40	0.15	0.08	2	1.5	0.39	0.42	170	0.15	3.33	0.5
60.43	-37.91	1.07	40	0.15	0.08	2	1.4	0.28	0.39	170	0.15	3.11	0.47
58.60	-39.71	1.12	30	0.15	0.08	2	1.35	0.23	0.38	170	0.15	3	0.45
54.06	-45.84	1.38	40	0.15	0.08	2	1.3	0.39	0.37	170	0.15	2.89	0.43
51.82	-45.73	4.21	35	0.15	0.08	2	2	0.67	0.56	170	0.15	4.45	0.67
49.72	-42.45	2.41	45	0.15	0.08	2	3	0.33	0.85	170	0.15	6.67	1
47.80	-39.40	10.33	40	0.15	0.08	2	3.7	1.02	1.04	170	0.15	8.22	1.23
46.31	-39.66	12.74	25	0.15	0.08	2	3.7	0.79	1.04	170	0.15	8.22	1.23
44.84	-42.53	4.29	20	0.15	0.08	2	3.7	0.21	1.04	170	0.15	8.22	1.23
37.53	-50.74	10.81	25	0.15	0.08	2	3.7	0.67	1.04	170	0.15	8.22	1.23
36.21	-53.29	15.81	18	0.14	0.08	2.14	3.7	0.7	1.12	170	0.14	8.81	1.23

34.33	-55.43	14.98	20	0.13	0.08	2.31	3.4	0.8	1.11	165.88	0.13	8.51	1.11
33.43	-58.05	17.32	18	0.11	0.08	2.73	3.1	0.92	1.19	160.41	0.11	8.87	0.98
32.55	-61.10	31.46	10	0.1	0.08	3	2.8	1.03	1.18	155.01	0.1	8.51	0.85
31.67	-64.17	29.13	12.5	0.09	0.08	3.33	2.5	1.33	1.17	149.6	0.09	8.15	0.73
29.62	-66.53	35.19	10	0.08	0.08	3.68	2.2	1.46	1.14	137.05	0.08	7.26	0.59
28.09	-67.50	42.18	10	0.08	0.08	3.57	2.2	1.75	1.11	127.72	0.08	6.57	0.55
26.24	-67.80	48.63	10	0.09	0.08	3.48	2.2	2.02	1.08	116.38	0.09	5.83	0.5
24.72	-67.07	42.46	15	0.09	0.08	3.43	2.2	2.64	1.06	107.06	0.09	5.29	0.46
23.28	-65.55	47.77	15	0.09	0.08	3.41	2.2	2.97	1.06	98.24	0.09	4.82	0.42
22.34	-63.58	43.89	20	0.09	0.08	3.41	2.2	3.64	1.06	92.53	0.09	4.54	0.4
21.78	-61.84	43.75	20	0.09	0.08	3.41	2.4	3.33	1.15	89.08	0.09	4.77	0.42
20.45	-59.53	45.45	20	0.09	0.08	3.43	2.5	3.32	1.21	86.54	0.09	4.85	0.42
18.57	-57.61	33.78	25	0.09	0.08	3.49	2.8	2.75	1.38	80.14	0.09	5.12	0.44
16.83	-56.27	26.19	25	0.08	0.08	3.58	3.1	1.93	1.56	74.23	0.08	5.38	0.45
14.88	-54.80	25.61	25	0.08	0.08	3.73	3.4	1.72	1.78	67.59	0.08	5.6	0.45
13.16	-53.42	23.64	25	0.08	0.08	3.56	3.4	1.74	1.7	61.75	0.08	4.88	0.38
11.37	-52.05	25.41	35	0.07	0.08	5.68	3.4	1.74	2.72	55.67	0.07	7.03	0.51
9.55	-50.47	25.12	55	0.07	0.08	9.5	3.4	1.74	4.55	49.46	0.07	10.44	0.7
7.77	-48.88	25.25	60	0.06	0.08	11.34	3.4	1.74	5.43	43.4	0.06	10.94	0.68
5.98	-46.42	27.35	45	0.06	0.08	10.51	3.3	1.74	4.88	37.33	0.06	8.46	0.47
3.97	-43.75	26.88	40	0.05	0.08	10.52	3.3	1.74	4.89	34	0.05	7.71	0.38
2.54	-41.70	22.41	30	0.04	0.08	7.8	3.3	1.64	3.62	34	0.04	5.72	0.25
1.15	-39.69	16.64	32.5	0.04	0.08	8.42	3.3	1.39	3.91	34	0.04	6.17	0.24
0.72	-38.97	19.72	27	0.04	0.08	9.06	3.3	1.33	4.21	34	0.04	6.65	0.24
-0.18	-32.88	16.96	30	0.03	0.08	9.33	3.3	1.3	4.34	34	0.03	6.84	0.24
-2.64	-28.91	15.3	40	0.04	0.08	7.22	3.2	1.65	3.26	34	0.04	5.14	0.23
-5.68	-28.46	11.52	60	0.05	0.08	5.41	2.9	2.2	2.21	17	0.05	1.74	0.1
-9.15	-28.00	10.53	60	0.07	0.08	4.38	2.5	2.39	1.54	17	0.07	1.22	0.08
-12.89	-29.22	9.35	50	0.08	0.08	3.67	1.9	2.4	0.98	29.65	0.08	1.35	0.1
-17.02	-30.59	7.44	40	0.08	0.08	3.09	2	1.57	0.87	47.68	0.08	1.93	0.16
-22.47	-32.73	0.94	40	0.09	0.08	0.86	2.1	0.64	0.26	71.53	0.09	0.85	0.07
-26.09	-34.28	2.21	40	0.09	0.08	1.65	1.8	0.95	0.42	87.35	0.09	1.7	0.15
-29.06	-35.78	1.2	40	0.08	0.08	1.52	2	0.53	0.4	100.34	0.08	1.86	0.15
-32.09	-37.46	1.24	40	0.08	0.08	1.22	2.2	0.65	0.38	113.56	0.08	1.99	0.15
-35.01	-39.44	0.36	40	0.07	0.08	0.48	2.2	0.54	0.15	126.33	0.07	0.87	0.06
-37.84	-41.13	0.2	50	0.07	0.08	0.28	3.3	0.44	0.13	138.71	0.07	0.85	0.06
-39.97	-42.49	0.34	40	0.06	0.08	0.6	6.4	0.15	0.54	148.02	0.06	3.74	0.23
-42.38	-44.02	0.34	35	0.06	0.08	2.2	5.8	0.04	0.7	158.56	0.06	5.15	0.29
-44.70	-45.55	0.23	40	0.05	0.08	1.31	4.8	0.08	0.88	168.71	0.05	6.91	0.36
-46.93	-47.22	0.07	40	0.05	0.08	0.23	4.1	0.17	1	178.46	0.05	8.28	0.38
-48.97	-48.88	0.15	50	0.04	0.08	1.47	4.7	0.07	0.97	187.35	0.04	8.43	0.35
-49.55	-52.69	1.2	50	0.04	0.08	2.46	5.3	0.31	1.83	189.89	0.04	16.17	0.65

**Figure S1:** Comparison of dust deposition in the Atlantic between this study and other published models. Dashed line indicates the GA02 section. Note the different color scales.

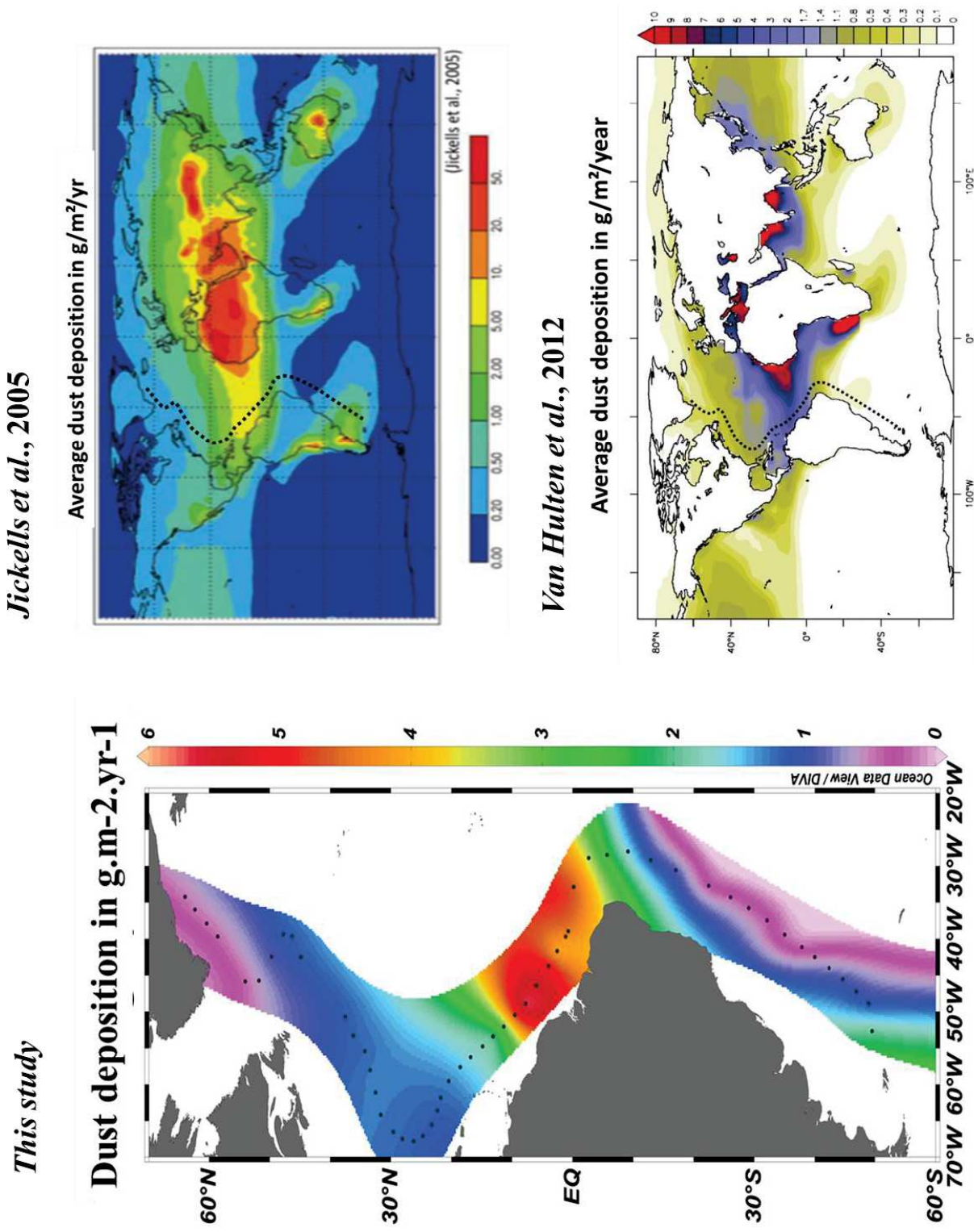
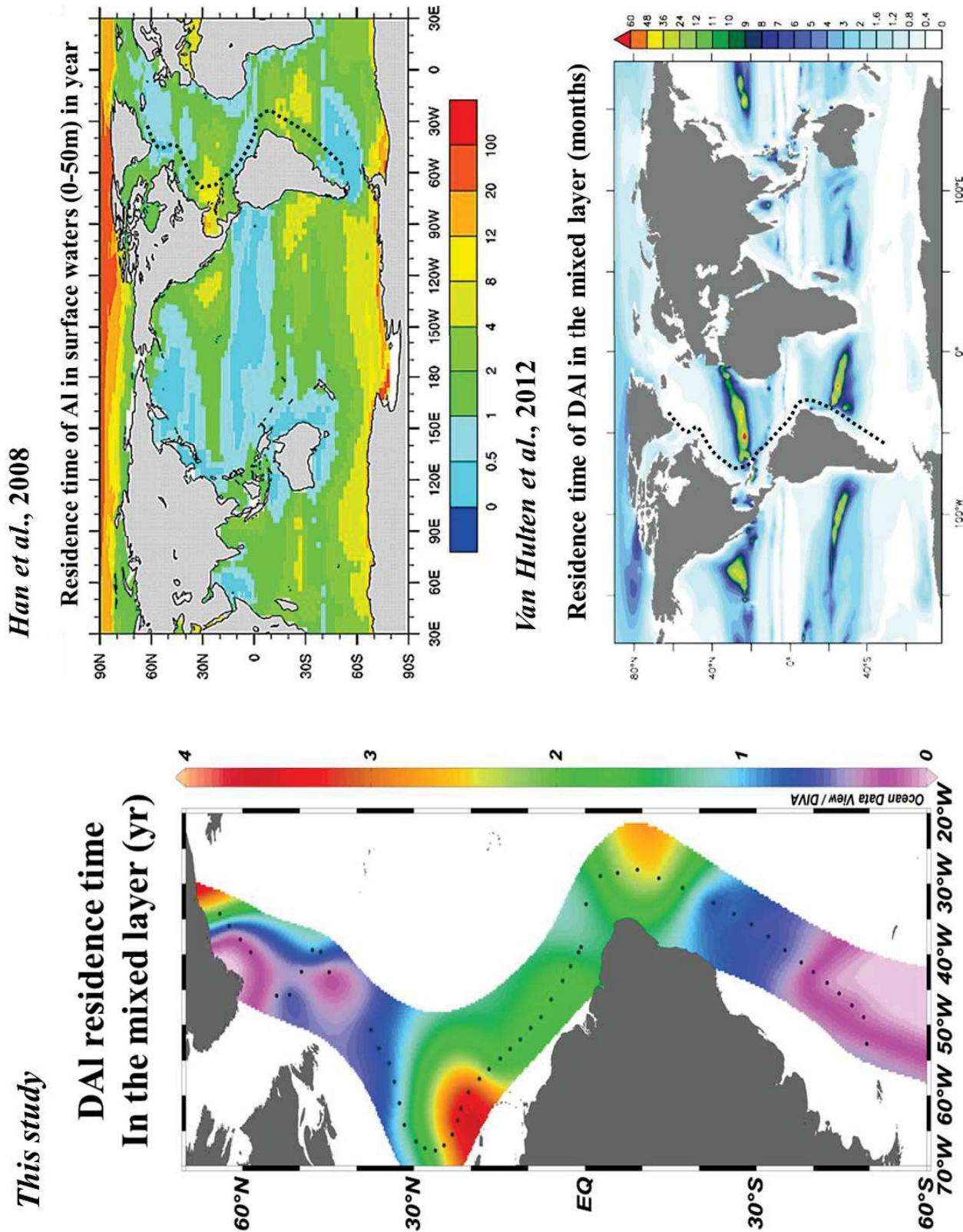


**Figure S2:** Comparison of dissolved Aluminum surface residence time in the Atlantic between this study and other published models. Dashed line indicates the GA02 section. Note the different color scales.



## Annexe 2 Performance analytiques relatives au chapitre 5

**Table 1:** Comparison of dissolved cobalt analyses obtained in the UV-oxidized samples by the FIA-Chemiluminescence method used in the chapter 6 with consensus values reported by the Sampling and Analysis of iron (SAFe) and GEOTRACES programs

Sample	DCo measured	Consensus DCo Value
SAFe D2	45.0 ± 1.9 (n = 25)	45.7 ± 2.9
SAFe D1	41.4 ± 2.1 (n = 25)	45.4 ± 4.7
GEOTRACES S	33.1 ± 3.2 (n = 25)	31.8 ± 1.1
GEOTRACES D	67.1 ± 4.3 (n=25)	65.2 ± 1.2

**Table 2:** Analytical performance of SF-ICP-MS measurements for particulate trace elements

### Total particulate trace metals (pTM) quality control data

Element	Al	P	Mn	Fe	Co
Isotope measured (for ICP-MS)	27	31	55	56	59
Resolution used	MR	MR	MR	MR	MR
<b>Instrument Blank (pmol/mL)</b>					
mean value	4.36	4.20	0.146	1.00	0.054
standard deviation	0.188	0.782	0.021	0.264	0.002
instrument detection limit	0.565	2.34	0.064	0.791	0.007
replicate number	10	10	10	10	10
<b>Digest Blank (pmol/digest)</b>					
mean	763	729	21.0	190	4.41
std dev	311	201.5	9.00	53.8	1.64
replicate number	7	7	7	7	7
<b>Unused Blank (pmol/digest)</b>					
mean	4314	1695	45.1	2614	7.27
std dev	2054	678	16.1	1656	2.19
replicate number	9	9	9	9	9
<b>Process Blank (pmol/digest)</b>					
mean	4599	4413	325	2172	8.15
std dev	1541	1892	95.3	853.1	1.86
replicate number	21	21	21	21	21

### Certified Reference Material (CRM)--BCR-414

ug/g after correction for digest blank	GeoReM	GeoReM	BCR-Certified	BCR-Indicative	BCR-Indicative
BCR 414 value	2154.3	12840	299	1850	1.43
BCR 414 uncertainty	803.4	4978	13	190	0.06
BCR 414 RSD	37.3%	38.8%	4.3%	10.3%	4.2%
mean	2392.6	13837	265	1745	1.22
uncertainty	355.1	1879	43	279	0.21
RSD	14.8%	13.6%	16.4%	16.0%	17.5%
recovery	111%	108%	89%	94%	85%
					250



# Cycle biogéochimique du cobalt en domaines océaniques contrastés : l'Atlantique Ouest, la Mer Méditerranée et la Mer Noire.

Gabriel Dulaquais

## Résumé :

Le cobalt est un métal de transition essentiel pour la croissance du phytoplancton, et en particulier pour les cyanobactéries qui ont un besoin absolu pour cet élément. En étant l'atome central de la cobalamine (vitamine B12), le cobalt est aussi indirectement essentiel aux eucaryotes marins qui ne synthétisent pas cette vitamine. Cet élément peut se substituer au zinc et au cadmium au sein de la carbonique anhydrase, l'enzyme permettant la fixation du dioxyde de carbone dans la cellule phytoplanctonique. Il pourrait intervenir également dans l'activation de l'acaline phosphatase. De part ses implications biologiques, le cobalt pourrait jouer un rôle important dans le cycle océanique du carbone. Cependant, les connaissances du cycle biogéochimique du cobalt en milieu marin sont encore largement limitées.

Ce travail de thèse de doctorat s'inscrit dans le cadre du programme international GEOTRACES au sein duquel le cobalt y est désigné comme un élément clé de la biogéochimie marine.

Au cours de ces travaux, l'un des plus larges jeux de données, rapporté à ce jour, incluant les différentes fractions du cobalt (soluble, dissous, particulaire, spéciation organique) a été produit. Les données recueillies proviennent d'échantillons collectés au sein de domaines océaniques contrastés. Une stratégie de prélèvement à haute résolution et à grande échelle a été mise en place dans diverses régions océaniques du monde lors de campagnes à la mer. Ainsi pour la première fois, une cartographie du cobalt dissous (DCo) et particulaire (PCo) a pu être définie pour l'ensemble de l'Atlantique Ouest, ainsi que des bassins Méditerranéens et de la Mer Noire.

Ce jeu de données a pu être produit par l'utilisation de différentes techniques d'analyses (Flow-Injection-Analysis and Chemiluminescence detection ; Voltamétrie, SF-ICP-MS) aux limites de détections basses permettant la détermination de cet élément, présent dans l'eau de mer à des concentrations de l'ordre du pico-molaire (10-12 M). Le cobalt est en effet l'un des micro-nutritifs le moins abondant dans l'eau de mer.

Les concentrations les plus faibles en DCo ont été observées dans les eaux oligotrophes de l'Atlantique Ouest (< 15 pM) alors que les plus élevées sont enregistrées dans la couche supérieure des eaux sulfidiques de la Mer Noire (> 5 nM). La distribution verticale du cobalt dissous variait selon les systèmes biogéochimiques. Ainsi, le profil vertical est de type nutritif comme les phosphates dans les eaux de surface de l'océan Atlantique. Les concentrations y augmentent avec la profondeur, jusqu'à un maximum relatif dans les eaux intermédiaires, puis décroissent dans l'océan profond. Ce comportement contraste avec le profil observé pour l'ensemble des bassins de la Mer Méditerranée. Dans cette mer, les fortes concentrations en DCo mesurées en surface (100-300 pM) diminuent en effet avec la profondeur. En Mer Noire, la distribution verticale varie selon les conditions d'oxygénéation des eaux. Les concentrations y sont extrêmement élevées par comparaison aux autres systèmes marins.

L'étude approfondie de l'ensemble de ces résultats a mis en évidence l'importance de la circulation à grande échelle dans la distribution du cobalt en milieu océanique. Ainsi, les circulations intermédiaires et profondes semblent régir la distribution profonde du cobalt dissous en Atlantique Ouest, ainsi qu'en Mer Méditerranée. De plus, le processus de minéralisation de la matière particulaire est une source importante de DCo dans les eaux de minimum d'oxygène de l'Atlantique Ouest impactant ainsi sa distribution. Cependant, la minéralisation n'est pas significative en Mer Méditerranée. Dans le bassin Méditerranéen, l'apport sédimentaire identifié par des traceurs lithogéniques, est une source importante en DCo et en PCo. Les processus d'adsorption/désorption à la surface des oxydes de manganèse et de fer pourraient contrôler la distribution verticale du DCo dans les eaux anoxiques et sulfidiques de la Mer Noire.

Une forte collaboration internationale au cours de ces travaux a permis d'établir le premier budget en cobalt dans les eaux de surface à l'échelle d'un océan. Ainsi, l'ensemble des flux du cycle biogéochimique du cobalt dissous et particulaire a été paramétré dans les eaux de surface de l'Atlantique Ouest. Ce budget met en évidence des cycles contrastés entre les domaines biogéochimiques, et souligne l'importance de l'assimilation biologique du cobalt dans les zones oligotrophes. Dans ces zones où les cyanobactéries sont abondantes, le processus de régénération du cobalt soutiendrait le besoin absolu en cobalt de ces espèces.

Lors de ces travaux, un effort particulier a été apporté sur la quantification des apports externes en cobalt (atmosphère, rivière) le long de l'Atlantique Ouest et en Mer Méditerranée par le développement de modèles. Ainsi, les implications biogéochimiques des apports atmosphériques ont été estimées en Atlantique Ouest. Elles suggèrent un possible effet cascade entre l'apport atmosphérique, le développement des cyanobactéries de type *Synechococcus* et la production de vitamine B12.

Ces travaux sont une contribution majeure aux études en cours qui visent à comprendre et estimer les interactions biologiques et géochimiques du cycle du cobalt en milieu marin. Ce type d'étude permettra de développer des représentations en 4 dimensions (échelle de temps inclue) du cycle biogéochimique du cobalt en milieu marin.

**Mots clés :** cobalt, océan, élément trace, micro-nutritif, biogéochimie, GEOTRACES, modélisation.